January 2015

CHARACTERIZATION OF THE FUNCTION OF THE DEAD-BOX RNA HELICASE DBP2

Wai Kit Ma
Purdue University

Graduate School Form 30
Updated 1/15/2015

PURDUE UNIVERSITY
GRADUATE SCHOOL
Thesis/Dissertation Acceptance

This is to certify that the thesis/dissertation prepared

By Wai Kit Ma

Entitled

CHARACERIZATION OF THE FUNCTION OF THE DEAD-BOX RNA HELICASE DBP2

For the degree of Doctor of Philosophy

Is approved by the final examining committee:

Elizabeth Tran
Chair

Barbara Golden

Mark Hall

Robert Geahlen

To the best of my knowledge and as understood by the student in the Thesis/Dissertation Agreement, Publication Delay, and Certification Disclaimer (Graduate School Form 32), this thesis/dissertation adheres to the provisions of Purdue University's "Policy of Integrity in Research" and the use of copyright material.

Approved by Major Professor(s): Elizabeth Tran

Approved by: Andy Mesecar 11/16/2015

Head of the Departmental Graduate Program Date

CHARACTERIZATION OF THE FUNCTION OF THE DEAD-BOX RNA HELICASE DBP2

A Dissertation

Submitted to the Faculty

Of

Purdue University

By

Wai Kit Ma

In Partial Fulfillment of the

Requirements for the Degree

of

Doctor of Philosophy

December 2015

Purdue University

West Lafayette, Indiana

To my parents, brother and sister

ACKNOWLEDGEMENTS

First, I would like to thank my major advisor Dr. Elizabeth Tran for her guidance and patience throughout my graduate career. I learned a lot from her. I sincerely appreciate her training and career advice to mold me as the independent scientist that I am today. I would also like to thank my committee members for their critical direction and help in my thesis project. Dr. Mark Hall encouraged me when I was down and offered suggestions on how to be a great scientist. Dr. Barbara Golden constantly challenged me to think critically about science. Dr. Robert Geahlen taught me to look at the big picture of my project.

I would also like to thank all the current and past members of the Tran laboratory that I have worked with, including Sara Cloutier, Luyen Nguyen, Siwen Wang, Christopher Petell, Zheng (Cindy) Xing, and Yu-Hsuan (Karen) Lai. We all shared some memories together. Those are the memories that I will never forget.

Last but not least, I would like to thank my father Ma Kam Ho, mother Tse Chung Man, brother Ma Wai Lun, and sister Ma Yuen To for their support and understanding throughout these years. They definitely made my graduate school career easier. I could not finish this thesis without their support.

TABLE OF CONTENTS

Page

Page

Page

Page

Page

Page

LIST OF FIGURES

Figure Page

Figure Page

Figure Page

LIST OF TABLES

Table Page

LIST OF ABBREVIATIONS

RNA	Ribonucleic acid
RNP	Ribonucleoprotein
ATP	Adenosine triphosphate
ADP	Adenosine diphosphate
AMP	Adenosine monophosphate
ADP-BeF_3	Adenosine diphosphate beryllium fluoride
P_i	Inorganic phosphate
UTP	Uridine triphosphate
GTP	Guanosine triphosphate
CTP	Cytidine triphosphate
mRNA	Messenger ribonucleic acid
DNA	Dexoyribonucleic acid
snRNP	Small nuclear ribonucleic protein
NTP	Nucleoside triphosphate
SF	Superfamily
NMD	Nonsense-mediated decay
bp	Base pair
nt	Nucleotide

ss	Single-stranded
ds	Double-stranded
siRNA	Small interfering ribonucleic acid
miRNA	Micro ribonucleic acid
EJC	Exon junction complex
LSU	Large subunit
SSU	Small subunit
rRNA	Ribosomal ribonucleic acid
PIC	Preinitiation complex
PTC	Premature termination codon

ABSTRACT

Ma, Wai Kit. Ph.D., Purdue University, December 2015. Characterization of the Function of the DEAD-box RNA Helicase Dbp2. Major Professor: Elizabeth Tran.

In eukaryotes, there are highly coupled mechanisms that require RNA-binding proteins to facilitate gene expression. Proper RNA structure and ribonucleoprotein (RNP) complex formation are critical for gene expression. DEAD-box proteins are the largest class of RNA helicases that play fundamental roles in RNA and RNP structure remodeling. However, the precise biological role of the vast majority of the ~ 40 members in this family has not been completely described. Therefore, my research focused on characterizing the role of the DEAD-box RNA helicase Dbp2 during gene expression in *S. cerevisiae*.

To decipher the biological roles of DEAD-box proteins, I first demonstrated that the *S. cerevisiae* DEAD-box protein Dbp2 is an active RNA dependent ATPase and RNA helicase that unwinds RNA duplexes *in vitro*. Furthermore, I found that Dbp2 associates with actively transcribing genes via RNA and functions as a co-transcriptional RNA chaperone to promote efficient assembly of the mRNA binding proteins, Yra1, Nab2, and Mex67, onto poly(A)+RNA. This assembly is critical for 3’ end processing and mRNA export. I also showed that Yra1 interacts directly with Dbp2 and inhibits its unwinding

activity by reducing single-stranded RNA-binding activity. This inhibition prevents over-accumulation of Dbp2 on mRNA and stabilization of a subset of RNA Pol II transcripts. Collectively, my work shows that Dbp2 is recruited to nascent RNA to unwind aberrant structures and facilitate assembly of RNA-binding proteins, including Yra1, Nab2, and Mex67, during transcription. Yra1 then prevents further cycles of unwinding by inhibiting the ability of Dbp2 to associate with single-stranded RNA. This sequential order of events involving regulation of a DEAD-box RNA helicase is critical for efficient mRNP assembly and proper gene expression. These findings provide ideas on how DEAD-box proteins are regulated and insights on the role of DDX5, which is the human ortholog of Dbp2 and is often overexpressed in cancer cells.

CHAPTER 1. INTRODUCTION

1.1 mRNP biogenesis is critical for proper gene expression

The cell is the basic unit of all living organisms. The survival and functions of a cell is dictated by proper gene expression, which is a highly complicated and regulated process that involves numerous interconnected steps to convert genetic information from DNA to RNA to protein. During transcription, different processing steps including addition of a 5' methylguanosine cap, removal of introns, and 3' end formation occur on the nascent RNA while it is being synthesized (Lee and Tarn 2013; Zorio and Bentley 2004; Cramer et al. 2001). After the RNA is properly processed, it is exported out to the cytoplasm for translation. Throughout all of these maturation steps, the RNA is associated with different RNA-binding proteins to form distinct ribonucleoprotein complexes (RNPs) via a process called RNP assembly (Chen and Shyu 2014).

RNA structure is one of the major factors that influence the efficiency of RNP assembly (Gosai et al. 2015). Several studies have demonstrated that secondary structures are found in mRNA *in vivo* and are overlapped with regulatory sites (Ding et al. 2014; Rouskin et al. 2014; Wan et al. 2014). Strong secondary structures tend to associate with alternative polyadenylation and splicing, suggesting that secondary structures regulate cleavage and splicing pre-mRNA. In contrast, start codons, stop codons, microRNA-

binding sites and 5’ splice sites tend to have less structure (Ding et al. 2014; Wan et al. 2014). This indicates that structural elements on RNA could potentially play a role in gene expression regulation. Furthermore, genome wide analyses have revealed that the pattern of RNA-protein interactions and RNA secondary structure in Arabidopsis displays an anti-correlative relationship (Gosai et al. 2015). This suggests that RNA unwinding is required for proper RNP assembly. Consistent with this idea, a stem-loop structure downstream of the 5’ splice site of the human *tau* exon 10 regulates alternative splicing (Kar et al. 2011). Remodeling of the stem-loop is necessary for U1 snRNP to access the 5’ splice site of exon 10, which promotes exon inclusion (Kar et al. 2011). Interestingly, mis-regulation of splicing in the *tau* gene is associated with dementia (Hutton et al. 1998; Hasegawa et al. 1999). This suggests that RNA remodeling is necessary to prevent human diseases. Similarly, the splicing of Troponin T (TNNT2) pre-mRNA also requires remodeling of a stem-loop structure to promote association of the splicing factor MBNL1 (Warf and Berglund 2007). Resolving the stem-loop structure promotes binding of MBNL1 and facilitates alternative splicing of TNNT2 pre-mRNA (Laurent et al. 2012). These examples suggest that RNA structural rearrangement constitutes a mechanism for gene regulation.

1.2 Helicases

Helicases are a class of P-loop NTPases that contain the typical Walker A and B sites for NTP binding and hydrolysis (Abdelhaleem 2010). As the name implies, these enzymes usually function as molecular motors that convert energy from NTP binding and/or hydrolysis to perform mechanical work on nucleic acid, such as translocation

along nucleic acid, double-stranded nucleic acid unwinding and disruption of protein-nucleic acid complex (Durr et al. 2006; Szczelkun 2000; Kawaoka and Pyle 2005; Guenther et al. 2009; Jankowsky et al. 2001). Helicases are ubiquitously expressed in every organism and are catagorized into six different superfamilies, SF1 – SF6, based on amino acid sequence (Singleton et al. 2007). Helicases are classified into DNA and RNA helicases depended on the nucleic acid that the enzymes target. In humans, there are 95 helicsaes of which 31 are DNA helicases and 64 are RNA helicases (Umate et al. 2011). DNA helicases are found in all six superfamilies and have been implicated in genome maintenance processes including replication, DNA repair and homologous recombination (Singleton et al. 2007; Labib et al. 2000; Manosas et al. 2013; Pakotiprapha et al. 2012; West 1996).

Unlike DNA, RNA is a dynamic macromolecule that tends to form mis-folded, local secondary structures that are long-lived and require large amounts of energy to transition between alternative structural conformations (Herschlag 1995; Pan and Russell 2010). In addition, RNA polymerase II synthesizes approximately 2000 RNA bases per minute in yeast and the newly synthesized RNA can fold co-transcriptionally (Mason and Struhl 2005; Wong et al. 2005; Pan et al. 1999). This allows the nascent RNA to grow at a rapid pace and fold into different local secondary structures, providing a narrow window of opportunity for RNP formation. Therefore, there is a great need of RNA helicases to accelerate the structural conversion of RNA in order to overcome these challenges *in vivo* (Jarmoskaite and Russell 2014; Leitão et al. 2015).

RNA helicases are found in all domains of life and some have even been identified in viruses. Unlike DNA helicases, RNA helicases are only found in SF1 – SF5

(Singleton et al. 2007). Besides the predominant role in RNA biology, some RNA helicases are also able to utilize DNA for NTP hydrolysis and unwind DNA/RNA hybrids and/or DNA duplexes (Kim et al. 1999; Guenther et al. 2009; Bhattacharya et al. 2000; Lee and Hurwitz 1992; Bayliss and Smith 1996; Kawaoka and Pyle 2005; Pang et al. 2002; Shu et al. 2004; Brennan et al. 1990). Furthermore, RNA helicases do not necessarily display unwinding activity *in vitro* or function to unwind duplexes in cells. Some RNA helicases have been reported to function as annealers, nucleotide sensors, RNA clamps and NTP-driven translocases (Leitão et al. 2015; Putnam and Jankowsky 2013b).

1.2.1 SF3 – SF5 RNA helicases

The SF3 – SF5 superfamilies consist of both DNA and RNA helicases. They all contain one helicase core with only one RecA-like domain that can oligomerize and form a hexameric ring structure. The hexameric ring structure is formed around the central channel from six individual protomers (Fig 1.1, (Mancini et al. 2004; Enemark and Joshua-Tor 2006)). Six identical ATP binding sites are located at the interface between two adjacent protomers. Nucleic acid-binding sites are found within the central channel of the ring (Skordalakes and Berger 2003). This architecture allows the hexameric helicase to unwind duplex by translocating along the nucleic acid that is bound within the central channel while excluding the complementary strand from the ring (Rabhi et al. 2010; Patel and Picha 2000). Thus far, only three RNA helicases have been identified in SF3 – SF5 (Jankowsky et al. 2011). They are Simian virus 40 (SV40) large T antigen (TAg) in SF3, P4 in SF4, and Rho in SF5. These hexameric RNA helicases are involved

in numerous functions ranging from transcription termination to viral replication and assembly (Table 1.1).

SV40 is the founding member of the *Polyomaviridae*, a family of small dsDNA viruses. TAg of SV40 is a well-characterized helicase that oligomerizes into hexamers in the presence of ATP and magnesium ions (Uhlmann-Schiffler et al. 2002). TAg plays a key role in hijacking the cellular replication machinery for viral replication inside the host-cell nucleus (Ahuja et al. 2005). TAg binds to the viral origin of replication and unwinds the DNA duplex by translocating along one of the DNA strands in the 3' to 5' direction in an ATP-dependent manner (Stahl et al. 1986). This provides a template for the cellular DNA polymerase machinery to replicate the viral genome. In addition to DNA duplex unwinding activity, TAg also unwinds RNA duplexes with a 3' overhang in a processive manner (Scheffner et al. 1989; Uhlmann-Schiffler et al. 2002). However, the function of the RNA unwinding activity of TAg during the viral life cycle is still not clear. Unlike DNA unwinding, TAg cannot utilize ATP to unwind RNA duplexes efficiently. Instead, TAg uses UTP, CTP or GTP to unwind RNA duplexes (Scheffner et al. 1989). Thus, the bound nucleotide might be the decisive factor for TAg to act as a DNA helicase or as a RNA helicase.

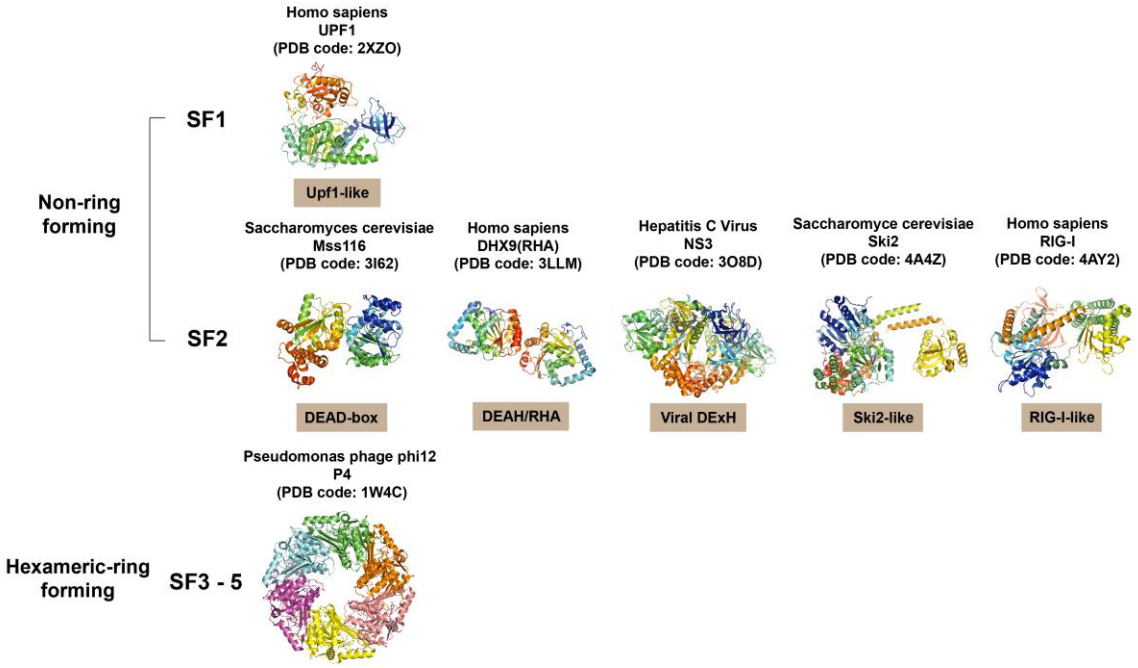

Figure 1.1. RNA helicases from SF1 – SF5. Superfamilies 1 and 2 (SF1 and SF2) consist of non-ring forming RNA helicases that are found in all living organisms and viruses. RNA helicases in SF1 are grouped into the Upf1-like family. A structure of UPF1ΔCH (PDB ID: 2XZO) is shown. RNA helicases in SF2 can be divided into five different groups, including DEAD-box protein, DEAH/RHA protein, viral DExH protein, Ski2-like protein, and RIG-I-like protein. Structures of the DEAD-box protein Mss116ΔC-terminal tail (PDB ID: 3I62), the DExH/RHA protein DHX9-DEIH domain (PDB ID: 3LLM), the viral DExH protein NS3 (PDB ID: 3O8D), the Ski2-like protein Ski2ΔN (PDB ID: 4A4Z), and the RIG-I-like protein RIG-IΔCARD (PDB ID: 4AY2) are shown. SF3 – SF5 consist of mainly viral RNA helicases that generally form a hexameric-ring structure. A structure of P4 (PDB ID: 1W4C) from SF4 is shown (Figure is modified from Leitão et al. 2015).

Table 1.1. Summary of the biological functions and biochemical properties of RNA helicases

Superfamily	Class/e.g. in the superfamily	Biological functions	Nucleic acid preference	NTP specificity	Unwinding polarity/ Translocation
SF1	Upf1-like	NMD[a], splicing[b], translation termination[c], miRNA processing[d],	RNA, DNA	A	5' to 3'
SF2	DEAD-box	Transcription[e], splicing[f], RNA export[g], translation[h], RNA decay[i], ribosome biogenesis[j], mitochondrial RNA processing[k]	RNA, DNA/RNA	A	Non-directional, Do not translocate
	DEAH/RHA	Transcription[e], splicing[f], translation[l], RNA decay[m], ribosome biogenesis[j]	RNA, DNA*	A, U, G, C	3' to 5'
	Viral DExH	Transcription termination[n], RNA transport[o], viral replication[p]	RNA, DNA	A, U, G, C	3' to 5'
	Ski2-like	RNA processing[q], mitochondrial translation[r], RNA decay[s]	RNA, DNA**	A	3' to 5' 5' to 3'**
	RIG-I-like	Innate immune system[t], miRNA and siRNA processing[u]	RNA	A	3' to 5'
SF3	TAg	Viral replication[v]	DNA, RNA	A for DNA U, G, C for RNA	3' to 5'
SF4	P4	Genome packaging[v]	RNA	A	5' to 3'
SF5	Rho	Transcription termination[w]	RNA, DNA/RNA	A, U, G, C	5' to 3'

References: [a]Fiorini et al. 2012, [b]Molnar et al. 1997, [c]Czaplinski et al. 1999, [d]Chendrimada et al. 2007, [e]Fuller-Pace 2006, [f]Liu and Cheng 2015, [g]Luo et al. 2001, [h]Sen et al. 2015, [i]Swisher and Parker 2010, [j]Strunk and Karbstein 2009, [k]Huang et al. 2005, [l]Hartman et al. 2006, [m]Tran et al. 2004, [n]Gross and Shuman 1996, [o]Shuman 1993, [p]Speroni et al. 2008, [q]Small et al. 2006, [r]Dziembowski et al. 1998, [s]Wang et al. 2005, [t]Yoneyama et al. 2005, [u]Meister and Tuschl 2004, [v]Uhlmann-Schiffler et al. 2002, [w]Rabhi et al. 2011

* DNA can stimulate RHA, but not DEAH, proteins

** Suv3 has been demonstrated to unwind both RNA and DNA duplexes from both polarities (Shu et al. 2004)

Another viral RNA helicase is P4 from dsRNA bacteriophages in the *Cystoviridae* family (Φ6 – Φ14) (Poranen and Tuma 2004). P4 is a 35 kDa packaging motor protein that assembles into hexamers in the presence of adenosine di/triphosphate and magnesium ions (Juuti et al. 1998). The hexameric P4 functions as a structural protein to promote capsid assembly for virus to enclose genetic material (Kainov et al. 2003). Unlike TAg, the NTPase activity of P4 can only be stimulated by RNA, but not DNA (Kainov et al. 2003, 2004). In addition, P4 translocates from the 5' end to the 3' end of RNA to unwind duplex regions (Kainov et al. 2003). These activities are crucial for the dsRNA bacteriophage to package their replicated genomic RNA into the capsid of virus (Poranen et al. 2008).

Besides viral RNA helicases, hexameric RNA helicases can also be found in bacteria. Rho is a bacterial transcription termination factor that is responsible for disrupting the transcription elongation complex at the termini of specific loci within the bacterial genome (Rabhi et al. 2010). Rho is an active NTPase that can hydrolyze all four NTPs in an RNA-dependent manner (Lowery-Goldhammer and Richardson 1974). However, ATP appears to be the most efficient nucleotide co-factor for the helicase activity of Rho (Brennan et al. 1990). Rho translocates towards the 3' end of the RNA, where the RNA polymerase is bound, at the expense of ATP, to trigger the release of the RNA polymerase (Rabhi et al. 2010). Consistent with this, Rho is also able to displace proteins from RNA (Schwartz et al. 2007). Moreover, Rho also shows ATP-dependent RNA duplex and DNA/RNA hybrid unwinding activities *in vitro* (Brennan et al. 1987, 1990). The latter is proposed to resolve toxic R-loops, which are usually formed upon

hybridization of the newly synthesized transcript with the complementary template stranded behind elongating RNA polymerases.

1.2.2 SF1 RNA helicases

Like other helicase families, SF1 contains both RNA and DNA helicases (Gilhooly et al. 2013). All SF1 helicases have a structurally conserved helicase core that consists of two highly similar domains, arranged in tandem. These domains fold independently and are termed RecA-like domains, due to their resemblance to the bacterial Recombinase A (RecA) protein (Fig 1.1; (Caruthers and McKay 2002)). There are at least 12 characteristic sequence motifs throughout these two domains (Fairman-Williams et al. 2010). Within these 12 motifs, the motif III sequence (GDxxQ) is the hallmark of an SF1 helicase (Gilhooly et al. 2013). Another major characteristic of SF1 RNA helicases is that they contain large inserts within the RecA-like domains (Gilhooly et al. 2013). These inserts are up to hundreds of amino acids long and adopt independent folds that are often essential for enzyme functions (Saikrishnan et al. 2008; Brendza et al. 2005). SF1 helicases are divided into three families, Uvrd/Rep-like helicase, Pif1-like enzymes and the Upf1-like family (Fairman-Williams et al. 2010). While all three families consists of DNA helicases, RNA helicases can only be found in the Upf1-like family (Jankowsky et al. 2011). SF1 DNA helicases have been identified in all three kingdoms of life and viruses. They are involved in DNA repair, replication, and recombination (Iyer et al. 2006; Bruand and Ehrlich 2000; Baharoglu et al. 2010; Cromie 2009; Mendonca et al. 1995).

In contrast, SF1 RNA helicases have only been identified in eukaryotes and viruses, but not in bacteria (Jankowsky et al. 2011). SF1 RNA helicases have been implicated in nonsense-mediated mRNA decay (NMD), pre-mRNA splicing, translation termination and miRNA processing (Table 1.1; (Fiorini et al. 2012; Molnar et al. 1997; Czaplinski et al. 1999; Chendrimada et al. 2007)). Among the SF1 RNA helicases, Upf1, Sen1, and IGHMBP2 (immunoglobulin μ-binding protein 2) are the most well characterized enzymes and they all share similar biochemical characteristics. Upf1 is an RNA-dependent ATPase with low basal ATPase activity in the absence of RNA (Bhattacharya et al. 2000). Though the ATPase activity of Upf1 is dependent on RNA, ATP binding decreases the affinity of Upf1 with RNA (Czaplinski et al. 1995; Weng et al. 1998). Nonetheless, ATP is required for Upf1 to unwind RNA duplexes from the 5' – 3' end. The latter activity is essential for NMD, a mRNA surveillance pathway that degrades aberrant mRNAs containing premature termination codons (Bhattacharya et al. 2000; Czaplinski et al. 1995; Weng et al. 1996; Lejeune and Maquat 2005). However, the precise role of the RNA unwinding activity of Upf1 in NMD remains unknown.

Unlike Upf1, the low basal ATPase activity of Sen1 can be stimulated by both ssRNA and ssDNA (Porrua and Libri 2013; Kim et al. 1999). Besides the ATPase activity, Sen1 has also been shown to unwind RNA and DNA duplexes from 5' – 3' end in an ATP-dependent fashion (Kim et al. 1999). Studies have demonstrated that Sen1 in yeast is implicated in transcription termination of snRNAs, mRNAs and snoRNAs (Rasmussen and Culbertson 1998; Steinmetz et al. 2001). The helicase activity of Sen1 is suggested to facilitate the removal of RNA Pol II from the transcript during transcription termination (Kim et al. 2006; Rasmussen and Culbertson 1998; Steinmetz et al. 2001).

Similar to other SF1 RNA helicases, IGHMBP2 in humans also has low basal ATPase activity (Guenther et al. 2009). The ATPase activity can either be stimulated by RNA or DNA (Guenther et al. 2009). Furthermore, IGHMBP2 also displays ATP-dependent, 5' – 3' RNA and DNA unwinding activity (Guenther et al. 2009). It has been proposed that IGHMBP2 plays role in transcription activation and pre-mRNA splicing (Molnar et al. 1997; Shieh et al. 1995). However, how the biochemical activities of IGHMBP2 contribute to its biological role remains to be explored.

1.2.3 SF2 RNA helicases

SF2 is the largest superfamily (Fairman-Williams et al. 2010). SF2 can be subdivided into 10 families, 5 of which are families of DNA helicases including RecG-like proteins, RecQ-like proteins, Rad3/XPD family, Type 1 restriction enzymes, and the Swi/Snf family. The other 5 families contain RNA helicases, which are often referred as DExH/D RNA helicases, including the DEAH/RHA family, viral DExH proteins, Ski2-like proteins, Rig-I-like proteins, and the DEAD-box proteins (Linder and Jankowsky 2011). SF2 DNA helicases are implicated in DNA related processes such as DNA repair, chromatin rearrangement, telomere maintenance, and replication (Lucic et al. 2011; Gaymes et al. 2002; Kasten et al. 2011; Opresko et al. 2005; Eller et al. 2006; McGlynn et al. 1997). SF2 RNA helicases are involved in every aspect of RNA maturation (Fuller-Pace 2006; Liu and Cheng 2015;Cordin et al. 2006; Jarmoskaite and Russell 2014; Strunk and Karbstein 2009). Similar to SF1 helicases, SF2 helicases also contain one helicase core that consists of at least 12 characteristics motifs throughout the two RecA-like domains. There is high sequence conservation in the characteristic motifs within the

family, but not across different families. Furthermore, not all motifs are shared between these two superfamilies (Fairman-Williams et al. 2010). The only motifs that share high sequence conservation across both superfamilies are motif I (Walker A) and motif II (Walker B), which are involved in binding and hydrolysis of the nucleotide triphosphate (Fairman-Williams et al. 2010). Despite sequence differences in the characteristic motifs between superfamilies, the position and the molecular function of the characteristic motifs in SF1 and SF2 are very similar. For example, motifs Ic and V in both superfamilies are involved in nucleic acid binding and are located at similar positions in the helicase core (Fairman-Williams et al. 2010). In addition, both superfamilies, except some SF2 RNA helicases, contain the Q-motif, which provides nucleotide specificity towards adenosine triphosphates (Tanner et al. 2003).

1.2.3.1 DEAH/RHA family

The DEAH/RHA family is the second largest family in the SF2 helicase group with 15 members in humans, 7 in yeast and 2 in bacteria (Jankowsky et al. 2011). This family is subdivided into two groups. DEAH proteins are named after the single letter amino acid code (D-E-A-H) that is found in their conserved motif II. The other group is referred to as RHA-like proteins because they display high similarity to RNA helicase A (RHA), and their motif II does not always contain alanine in the D-E-A-H. RNA helicases from DEAH/RHA family do not contain the Q-motif that is found in some other RNA helicases. Thus, they do not show specificity towards adenine and are able to hydrolyze all NTPs (Tanner et al. 2003; Wang et al. 1998; Tanaka and Schwer 2005, 2006). The basal NTPase activity of most DEAH/RHA family members in the absence of

any nucleic acid is relatively high compare to other RNA helicases (Wang et al. 1998; Tanaka and Schwer 2005, 2006). Both RNA and DNA can stimulate the NTPase activity of RHA, but only RNA is able to stimulate the NTPase activity of DEAH proteins (Wang et al. 1998; Tanaka and Schwer 2005, 2006). The DEAH/RHA family helicases are further differentiated from the rest of the SF2 RNA helicases in that they share two highly conserved stretches of amino acids located C-terminal to the helicase core of DEAH/RHA proteins (Sanjuán and Marín 2001). Although this C-terminal region is essential for viability for some organisms, the exact function of this region is not fully characterized (Edwalds-Gilbert et al. 2004; Wang and Guthrie 1998; Martin et al. 2002).

DEAH/RHA proteins are implicated in many different RNA biology steps including transcription, pre-mRNA splicing, translation, RNA decay and ribosome biogenesis (Table 1.1; (Fuller-Pace 2006; Liu and Cheng 2015; Hartman et al. 2006; Strunk and Karbstein 2009)). The majority of members in this family are involved in pre-mRNA splicing and ribosome biogenesis (Liu and Cheng 2015; Strunk and Karbstein 2009). Four out of the seven members in yeast (e.g. Prp2, Prp16, Prp22 and Prp43) are involved in pre-mRNA splicing and three out of the seven members (Dhr1, Dhr2 and Prp43) are involved in ribosome biogenesis. The NTPase activity of all yeast spliceosomal DEAH helicases are stimulated by RNA (Wagner et al. 1998; Schwer and Guthrie 1991; O'Day et al. 1996b; Kim et al. 1992; Xu et al. 1996). In addition, all splcieosomal DEAH helicases, but not Prp2, display RNA unwinding activity in the presence of NTP (Kim et al. 1992; Wang et al. 1998; Tanaka and Schwer 2005, 2006). It is plausible that other factors from cells are required to activate the unwinding activity of Prp2. Prp16 and Prp22 prefer unwinding from 3' – 5', whereas Prp43 can unwind from

both polarities (Wang et al. 1998; Tanaka and Schwer 2005, 2006). The helicase activities of these spliceosomal DEAH helicases are critical for efficient pre-mRNA splicing (Cordin and Beggs 2013; Koodathingal and Staley 2014).

We have known for a while that both the DEAH/RHA proteins, Dhr1 and Dhr2, are implicated in rRNA maturation (Colley et al. 2000). Nevertheless, the precise role of these two enzymes was not clear. A recent study has now demonstrated that Dhr1 is an active RNA-dependent ATPase that exhibits ATP-dependent RNA unwinding activity (Sardana et al. 2015). The latter activity is required for the removal of the U3 snoRNA from the 18S rRNA to promote rRNA folding and processing (Sardana et al. 2015). Given that other members of DEAH/RHA family can hydrolyze all NTPs and unwind in a 3' – 5' direction, it would be interesting to determine if Dhr1 can hydrolyze other NTPs and unwind RNA duplexes with a polarity.

Without a doubt, the most well-studied RNA helicase from the RHA-like group is RHA. RHA in humans plays a role in transcription, translation and miRNA biogenesis (Nakajima et al. 1997; Hartman et al. 2006; Robb and Rana 2007). RHA unwinds RNA duplexes, DNA duplexes and DNA/RNA hybrid from 3' – 5' *in vitro* (Lee and Hurwitz 1992). However, how the unwinding activity relates to the biological roles remains to be determined.

1.2.3.2 Viral DExH RNA helicases

Viral DExH RNA helicases are closely related to DEAH/RHA proteins, but they are not the same. Two highly conserved stretches of amino acids are found in the C-terminal of DEAH/RHA proteins, but not the DExH helicases (Walbott et al. 2010;

Sanjuán and Marín 2001). Like DEAH/RHA family, viral DExH helicases do not contain the Q-motif. Therefore, DExH helicases can hydrolyze all NTPs (Table 1.1; (Jankowsky et al. 2010)). In addition, all DExH helicases show high basal NTPase activity that is stimulated by both RNA and DNA (Laín et al. 1991; Shuman 1992, 1993). DExH helicases are named because of the single amino acid code in the conserved helicase motif II that reads D-E-x-H, where x stands for a variable amino acid (Jankowsky and Jankowsky 2000). The two most prominent members of DExH helicases are the nucleoside triphosphate phosphohydrolase II (NPH-II) from vaccinia virus and the nonstructural protein 3 (NS3) from flaviviridae. Therefore, DExH helicases are sometime referred as the NS3/NPH-II family. NPH-II displays NTP-dependent unidirectional unwinding (3' – 5') *in vitro* on both RNA and DNA (Bayliss and Smith 1996; Kawaoka and Pyle 2005). Unlike most other RNA helicases, NPH-II is able to unwind long duplexes (~ 90 bp) (Gross and Shuman 1996). In addition to the helicase activity, NPH-II was the first helicase shown to displace proteins from RNA duplexes and unstructured RNA *in vitro* (Jankowsky et al. 2001; Fairman et al. 2004). The latter suggests that NPH-II is able to displace RNA-binding proteins from RNA without unwinding RNA duplexes. It has been proposed that NPH-II is involved in transcription termination during viral gene expression and transport of viral transcripts out of the virion (Gross and Shuman 1996; Shuman 1993). Nevertheless, the exact RNA targets of NPH-II remain to be identified.

Flaciciridae viruses encode a single poly-protein that is cleaved into 3 structural and 7 nonstructural proteins (Harris et al. 2006). Among the nonstructural proteins, the DExH protein NS3 is the largest and is essential for viral replication (Matusan et al.

2001; Gu et al. 2000; Kolykhalov et al. 2000). *In vitro* studies have demonstrated that NS3 unwinds RNA and DNA that contains a 3' overhang in a NTP-dependent fashion (Gwack et al. 1997). ATP binding weakens the affinity of NS3 for single-stranded nucleic acid (Levin et al. 2005). This regulation is proposed to be critical for NS3 to translocate along DNA or RNA. Several studies have demonstrated that the NTPase and helicase activities of NS3 are essential for replication of many viruses, but it is not clear which stage in the viral life cycle requires duplexes unwinding during viral replication (Wengler et al. 1991; Speroni et al. 2008; Suzich et al. 1993; Gwack et al. 1999).

1.2.3.3 Ski2-like proteins

Comparing to the rest of the DExH/D RNA helicases, there are relatively fewer RNA helicases in the Ski2-like protein family, which is comprised of 8 members in humans and 6 members in yeast (Jankowsky et al. 2011). Unlike other DExH/D RNA helicases, the Ski-2 like protein family also consists of DNA helicases that participate in the repair of dsDNA breaks and meiotic recombination (McCaffrey et al. 2006; Nakagawa et al. 2001). Ski2-like proteins contain a helicase core with highly conserved sequence motifs. One of these motifs is the Q-motif that provides specificity towards ATP as an energy source (Tanner et al. 2003). One distinct feature of the Ski2-like proteins is their large size (Johnson and Jackson 2013). Members of this family contain multiple accessory domains that flank the helicase core (Johnson and Jackson 2013). The molecular weight of all members in the Ski2-like proteins is at least 100 kDa. RNA helicases in this family function in different RNA maturation steps including RNA

processing, mitochondrial translation and RNA degradation (Table 1.1; (Small et al. 2006; Dziembowski et al. 1998; Wang et al. 2005)).

Ski2-like proteins are named after the founding member Ski2 in yeast. Ski2 associates with Ski3 and Ski8 to form the Ski complex (Anderson and Parker 1998; Brown et al. 2000). The Ski complex functions with the cytoplasmic exosome, a multisubunit complex that contains 3' – 5' exonuclease activity, to promote RNA turnover (Anderson and Parker 1998; Araki et al. 2001; van Hoof et al. 2000). Although all components in the Ski complex are necessary for exosome-dependent RNA turnover (Anderson and Parker 1998), only Ski2 exhibits enzymatic activities. Ski2 is a RNA-dependent ATPase and unwinds 3' overhang RNA duplexes (Halbach et al. 2013). These enzymatic activities are necessary for the Ski complex to transfer the unwound RNA to exosome for RNA degradation in the cytoplasm (Wang et al. 2005; Halbach et al. 2013).

In the nucleus, the TRAMP complex adds the short poly(A) tails to nuclear RNAs that are subjected to degradation by the nuclear exosome (Kong et al. 2014; Vanacova and Stefl 2007; Houseley and Tollervey 2009). The Ski2-like RNA helicase Mtr4, the poly (A) polymerase (Trf4/5p) and the putative RNA-binding protein (Air1/2p) are the components of the TRAMP complex (Lebreton and Séraphin 2008). Mtr4 displays RNA-dependent ATPase activity and unwinds RNA duplexes through translocation from 3' – 5' end in the presence of ATP (Bernstein et al. 2008). The helicase activity of Mtr4 is suggested to displace RNA-binding proteins and resolve the RNA secondary structures to promote delivery of ssRNA to exosome (Houseley and Tollervey 2009; Lykke-Andersen et al. 2009). Consistent with this, Mtr4 displays unwinding preference for substrates with a 3' overhang containing a poly(A) tail (Jia et al. 2012). Ski2-like proteins are multi-

domains proteins (Johnson and Jackson 2013). The ratchet helix domain of Mtr4 is responsible for providing the selectivity towards poly(A) substrates (Taylor et al. 2014).

The Ski2-like protein Brr2 is a component of the U5 snRNP and also contains the ratchet helix domain (Laggerbauer et al. 1998). A point mutation within the ratchet helix domain abolishes its unwinding activity and confers a slow growth phenotype (Zhang et al. 2009). Studies have shown that Brr2 unwinds 3' overhang RNA duplexes and implicated in pre-mRNA splicing (Pena et al. 2009; Mozaffari-Jovin et al. 2012; Small et al. 2006). This helicase activity allows Brr2 to unwind the U4/U6 duplex in the U4/U6-U5 tri-snRNP complex to promote spliceosomal assembly (Kim and Rossi 1999; Raghunathan and Guthrie 1998). In addition to U4/U6 unwinding, Brr2 also functions in spliceosomal disassembly after spliced mRNA is released (Small et al. 2006). RNA binding and/or unwinding activities of Brr2 are crucial for this function. Other components of the U5 snRNP, Prp8 and Snu114, have been shown to regulate the enzymatic activities of Brr2 to ensure the appropriate timing for the activation and disassembly of the spliceosome (Brow 2002; Small et al. 2006; Grainger and Beggs 2005; Brenner and Guthrie 2005; Mozaffari-Jovin et al. 2013).

In addition to cytoplasmic and nuclear RNA decay, RNA degradation also occurs in the mitochondria (Rorbach and Minczuk 2012). The Ski2-like protein Suv3p is one of the components of the yeast mitochondrial degradosome (Malecki et al. 2007). The degradosome have been implicated in RNA degradation and translation of mitochondrial RNAs (Dziembowski et al. 1998, 2003). Consistent with this, depletion of the *Drosophila* ortholog DmSUB3 severely reduced mitochondrial mRNAs and tRNAs levels (Clemente et al. 2015). Biochemical studies have revealed that Suv3p alone shows RNA-stimulated

ATPase activity, but low RNA unwinding activity *in vitro* (Min et al. 1993; Malecki et al. 2007). However, RNA unwinding activity of Suv3p is needed for RNA degradation, which suggests that the unwinding activity of Suv3 needs to be stimulated in cells. This is accomplished by another component of the mitochondrial degradosome Dss1, who increases the unwinding activity of Suv3p (Malecki et al. 2007).

The human ortholog of Suv3p (Suv3) is also implicated in mitochondrial RNA degradation (Szczesny et al. 2010; Borowski et al. 2013). Consistent with this, Suv3 is predominately localized in the mitochondria, but a small fraction is also found in the nucleus (Pereira et al. 2001). Furthermore, Suv3 associates with WRN and BLM helicases, which are proteins that function in recombination and DNA repair and are required for genomic stability (Pereira et al. 2001), suggesting that Suv3 in human may also play a role in recombination or replication. Supporting this idea, down-regulation of Suv3 enhances homologous recombination (Pereira et al. 2001). In addition, Suv3 is able to unwind both RNA and DNA duplexes from both polarities (Shu et al. 2004).

1.2.3.4 RIG-I-like proteins

RIG-I-like proteins have the least members in SF2. There are six members in this family, five of which are found in humans and one in fungi (Jankowsky et al. 2011). RIG-I-like proteins contain all twelve characteristic motifs of SF2, with the Q-motif providing nucleotide specificity towards adenosine triphosphate (Tanner et al. 2003). One unique characteristic of RIG-I-like proteins is the large, well-conserved, independently folded insert that forms between the two RecA-like domains. Most members including RIG-I, MDA5 and LGP2, function in the innate immune system in response to pathogens

(Table 1.1; (Yoneyama et al. 2005)). This response requires highly specific receptors to sense foreign molecules and pathogen-associated molecular patterns (PAMPs) to trigger the host response to pathogens. One of the major challenges for these sensors is to distinguish self from non-self-components. RIG-I and MDA5 can act as a sensor to detect different PAMPs from different viruses (Kato et al. 2006; Gitlin et al. 2006; McCartney et al. 2008; Loo et al. 2008). RIG-I and MDA5 are able to distinguish viral RNAs from cellular RNAs by the fact that cellular RNAs are usually processed and capped at the 5' end (Banerjee 1980). RNA that contains a 5' triphosphate, which is usually generated by viral RNA polymerases, activates RIG-I to trigger an interferon-α response (Hornung et al. 2006). In contrast, 5' mono or diphosphate RNAs show no stimulation (Hornung et al. 2006; Pichlmair et al. 2006; Plumet et al. 2007). Moreover, transcriptional modifications that are usually found in cellular RNAs, including 7-methylguanosine caps, pseudouridine, or 2-thiouridine abolish activation (Hornung et al. 2006). This suggests that the 5' end and modified bases of cellular RNAs are critical for RIG-I to sense self from non-self.

Unlike RIG-I, 5' triphosphates do not activate MDA5. Instead a long nonphysiological double-stranded RNA mimic stimulates MDA5 (Kato et al. 2006; Gitlin et al. 2006). This suggests that RIG-I and MDA5 use different mechanisms for detecting viral RNAs. Several biochemical studies have demonstrated that both RIG-I and MDA5 are RNA-dependent ATPases, but RNA unwinding activity has only been showed in RIG-I (Takahasi et al. 2008; Cui et al. 2008).

Unlike other RIG-I-like RNA helicases, Dicer is the only member that does not primarily function in anti-pathogen innate immunity. Dicer plays a major role in

microRNAs (miRNAs) and small-interfering RNAs (siRNAs) processing (Meister and Tuschl 2004). Dicer is a dsRNA-stimulated ATPase, whose activity is necessary for processing long dsRNA to siRNA and primary miRNAs (pri-miRNAs) to miRNAs (Cenik et al. 2011; Flores-Jasso et al. 2009; Feng et al. 2012). However, there is currently no evidence showing that Dicer possesses unwinding activity. Whether Dicer functions as an unwinder or not remains to be elucidated.

1.2.3.5 DEAD-box proteins

DEAD-box proteins are the largest class of enzymes in the RNA helicase family. This class consists of 36 members in humans, 25 in yeast and 9 in bacteria. Similar to other SF2 RNA helicases, DEAD-box proteins contain twelve highly conserved motifs throughout the signature RecA-like domains in the helicase core that are responsible for recognizing RNA and binding and/or hydrolyzing ATP (Putnam and Jankowsky 2013b). The name DEAD-box proteins originates from the single letter amino acid codes Asp (D)-Glu (E)-Ala (A)-Asp (D) that are present at the highly conserved motif II in the helicase core. DEAD-box proteins are RNA-dependent ATPases and cannot recognize other NTPs due to the presence of the Q-motif (Linder and Fuller-Pace 2013; Tanner et al. 2003). In addition to ATPase activity, numerous studies have also demonstrated that DEAD-box proteins can function as RNA clamps, biosensors to detect nucleotide metabolites and RNP chaperones (Ballut et al. 2005; Young et al. 2013; Putnam and Jankowsky 2013b; Jarmoskaite and Russell 2014).

The term “RNA clamp” refers to a RNA-binding protein that is stably locked on the RNA for an extended period of time and functions as a scaffold for proteins to

assemble on RNA. It is well established that the DEAD-box protein eIF4A-III is a clamp that can act as a protein assembly platform for assembly of the multicomponent exon junction complex (EJC) upstream of exon-exon junctions on mRNA (Ballut et al. 2005). EJC components Y14 and Magoh prevent eIF4A-III from releasing inorganic phosphate (P_i) and ADP after hydrolyzing ATP (Nielsen et al. 2009). This ADP-P_i-bound state of eIF4A-III can stably bind to RNA because of its conformation (Nielsen et al. 2009) (For further detail, please see section 1.2.3.5.3).

The vast majority of DEAD-box proteins exhibit a cooperative binding with RNA and ATP (Banroques et al. 2008; Lorsch and Herschlag 1998; Polach and Uhlenbeck 2002; Theissen et al. 2008; Samatanga and Klostermeier 2014). Moreover, several reports have shown that the ATPase cycle of DEAD-box proteins is highly associated with their RNA binding affinity (Tran et al. 2007; Cao et al. 2011; Henn et al. 2008, 2010). In the ATPase cycle of DEAD-box proteins, ADP-P_i-bound DEAD-box proteins exhitit the highest RNA binding affinity followed by ATP-bound. ADP-bound DEAD-box proteins tend to have the lowest RNA-binding affinity (Cao et al. 2011; Henn et al. 2008, 2010). Though AMP is not part of the ATPase cycle, DEAD-box proteins can also bind to AMP (Rudolph et al. 2006; Putnam and Jankowsky 2013a; Hogbom et al. 2007). Interestingly, binding of AMP inhibits the RNA binding and unwinding activities of certain DEAD-box proteins (Putnam and Jankowsky 2013a). The concentration of AMP *in vivo* is increased upon metabolic stress (Wilson et al. 1996; Dudley et al. 1987). The AMP-dependent regulation of the enzymatic properties of DEAD-box proteins in RNA metabolism is intriguing, as it suggests that DEAD-box proteins can function as biosensors of cellular stress (Putnam and Jankowsky 2013a). Along with this idea, the DEAD-box protein

DDX41 is able to sense bacterial secondary messengers cyclic di-GMP and cyclic di-AMP to activate the innate immune response (Parvatiyar et al. 2012).

One of the major functions of DEAD-box proteins is to act as RNP chaperones to promote structural rearrangement and remodel RNPs (Jarmoskaite and Russell 2014). This includes displacing RNA-binding proteins from RNA, assembling RNA-binding proteins on RNA, and facilitating the folding of RNA. Numerous studies have shown that DEAD-box proteins are involved in displacing RNA-binding proteins from RNA to facilitate RNA maturation (Chen et al. 2001; Kistler and Guthrie 2001; Tran et al. 2007; Perriman et al. 2003). In addition, there is direct biochemical evidence demonstrating that DEAD-box proteins utilize a different mechanism from the viral DExH RNA helicase NPH-II to remove proteins from RNA in an ATP-dependent manner (Fairman et al. 2004; Bowers et al. 2006). In addition to protein displacement, DEAD-box helicases also promote loading of RNA-binding proteins onto RNA (Kar et al. 2011; Laurent et al. 2012; Ma et al. 2013). This is presumably accomplished by remodeling RNA structure to expose binding sites for RNA-binding proteins. To promote structural rearrangement of RNA, RNA annealers and RNA unwinders are needed. An RNA annealer is a protein that speeds up the annealing process of two strands of RNA that are complementary with each other. Several DEAD-box proteins display annealing activity independent of ATP (Rössler et al. 2001; Yang and Jankowsky 2005; Halls et al. 2007; Ma et al. 2013; Young et al. 2013; Uhlmann-Schiffler et al. 2006). The DEAD-box protein Rok1 appears to function solely as an annealer to facilitate the formation of a duplex during early ribosome biogenesis steps (Young et al. 2013). However, the mechanism of annealing is not fully understood.

Similar to other RNA helicases, DEAD-box proteins can also unwind RNA duplexes. However, DEAD-box proteins utilize a different unwinding mechanism from canonical RNA helicases (Rudolph and Klostermeier 2015). Most other RNA helicases use a translocation-based duplex unwinding mechanism, where the helicase first binds to a single-stranded region next to the duplex and then translocates in a unidirectional manner (Jankowsky et al. 2000; Fiorini et al. 2015). This separates the helicase-bound strand from the complementary strand. The two RecA-like domains in the helicase core are bound on the single-stranded region of the RNA duplex. Translocation happens when ATP is bound to the helicase core to shorten the distance between the two RecA-like domains on the bound RNA. Then, ATP hydrolysis and product release increase the distance between the two RecA-like domains, and one of the domains is now released from the RNA while the other domain remains stably bound (Myong et al. 2007; Dumont et al. 2006). The released domain then seeks binding to a new position that is one nucleotide away from the previous binding site, which generates the forward movement by one nucleotide. Once a new ATP binds to the helicase core, a new cycle begins (Fig 1.2; (Myong and Ha 2010; Pyle 2008; Patel and Donmez 2006)). This allows the two domains to translocate across the ssRNA one nucleotide at a time in an inchworm-like fashion (Jankowsky 2011). Thus, a series of ATP hydrolysis cycles and a single-stranded region are both necessary for canonical RNA helicases to unwind in a translocation-based manner.

DEAD-box proteins do not unwind in a translocation-based fashion, but rather load directly onto the duplex region and separate the two strands in an ATP-dependent manner (Yang and Jankowsky 2006; Yang et al. 2007). This is possible because DEAD-

box proteins can disrupt RNA duplexes locally by bending one of the RNA strands (Rudolph and Klostermeier 2015). Although some DEAD-box proteins show more efficient unwinding with an overhang region next to the duplex, DEAD-box proteins can still unwind blunt end duplexes (Yang et al. 2007; Ma et al. 2013; Halls et al. 2007). Moreover, a single cycle of ATP binding and hydrolysis is sufficient to completely unwind a short RNA helix (~6 base pairs)(Chen et al. 2008). This suggests that ATP-binding is sufficient for DEAD-box proteins to unwind RNA duplexes. Consistent with this finding, a non-hydrolysable ATP analog, ADP-BeF_3, is able to promote duplex unwinding (Liu et al. 2008).

Multiple X-ray crystallographic studies of DEAD-box helicases have demonstrated that DEAD-box proteins contain a structurally conserved helicase core that consists of two globular RecA-like domains (RecA_N, RecA_C). The two domains are connected by a flexible linker to form a characteristic "dumbbell-like" core (Fig 1.1). The RecA_N alone is sufficient to interact with ATP, but both RecA domains are required for ATP hydrolysis (Mallam et al. 2012; Samatanga and Klostermeier 2014). During RNA unwinding, the helicase core binds to the dsRNA. Closing of the two domains upon binding of the dsRNA and ATP bends one strand of the RNA so that it is incompatible with the geometry of an A-form RNA duplex (Sengoku et al. 2006; Andersen et al. 2006; Del Campo and Lambowitz 2009; von Moeller et al. 2009). The bending is achieved by an α-helix in the RecA_N domain that hinders a straight path of the RNA backbone. This allows DEAD-box proteins to destabilize RNA duplexes locally and release the unbent RNA strand when the base pairs in the duplex are disrupted (Rudolph and Klostermeier 2015). Upon ATP hydrolysis, the inorganic phosphate is released, which is the rate-

limiting step in the ATPase cycle (Henn et al. 2008). The resulting ADP-bound helicase has a weaker affinity for RNA and thus dissociates from single-stranded RNA, terminating a single round of the unwinding cycle. The DEAD-box helicase then can either recycle back on the same RNA substrate or find a new target (Fig 1.3; (Rudolph and Klostermeier 2015)). Since each ATP hydrolysis cycle can only unwind ~ 6 base pairs of the RNA duplex (Chen et al. 2008), multiple cycles of unwinding are required to completely separate longer duplexes. A recent study has revealed that the DEAD-box protein Ded1 oligomerizes into a trimer to promote duplex unwinding (Putnam et al. 2015). Similar to Ded1, another DEAD-box helicase Mss116 also shows cooperativity during unwinding (Yang et al. 2007). This suggests that oligomerization maybe a common theme for DEAD-box proteins during duplex unwinding. Consistent with this idea, oligomerization has been observed in several DEAD-box proteins (Rudolph et al. 2006; Ogilvie et al. 2003; Minshall and Standart 2004).

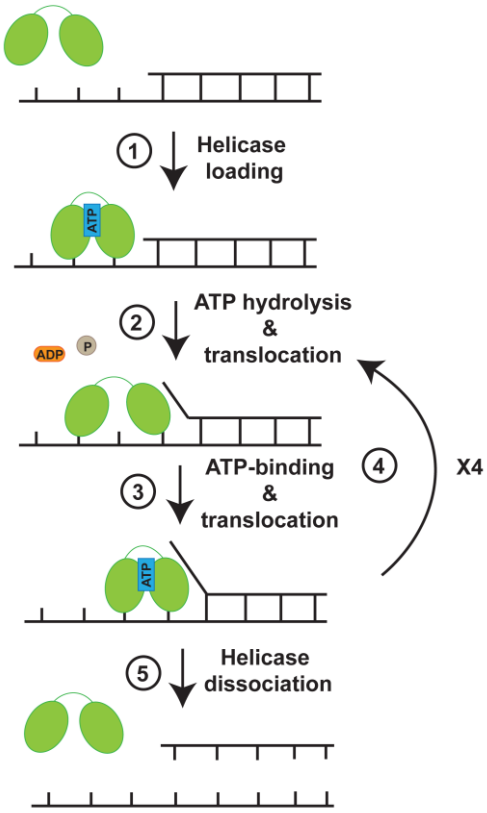

Figure 1.2. Canonical RNA helicases unwind duplexes by translocation. Lines represent RNA strands and the two ovals represent the two RecA-like domains. First, a RNA helicase binds to the single-stranded region adjacent to the duplex in the presence of ATP. The RNA helicase then translocates along the bound strand towards the duplex region to unwind the duplex 1 nt at a time upon each ATP hydrolysis cycle. (Figure is modified from Myong and Ha 2010).

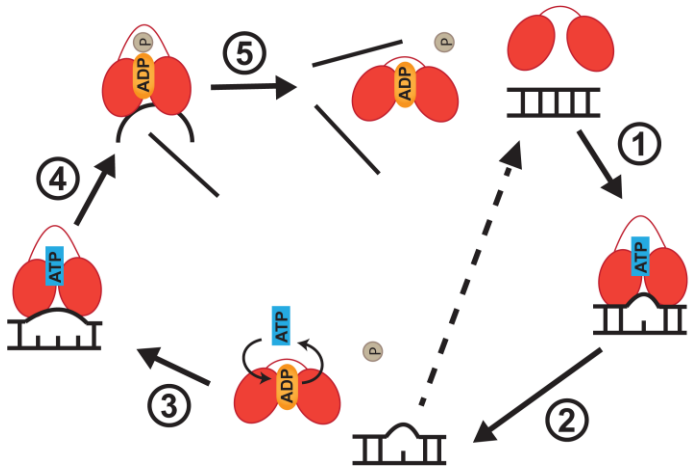

Figure 1.3. DEAD-box proteins unwind duplexes non-processively via local strand separation. Lines represent RNA strands and the two ovals represent the two RecA-like domains that are connected by a flexible linker. In the absence of any nucleotide and RNA, the two RecA-like domains are farther apart and exhibit a flexible "opened uproductive" conformation. During unwinding, the two RecA-like domains come closer together to form a "closed productive" conformation upon binding to the double-stranded RNA (dsRNA) and ATP (step 1). Closing of the two domains bends one strand of the dsRNA and results in local duplex destabilization (~ 6 bp). Duplexes longer than 6 bp require multiple cycles of unwinding. ATP hydrolysis and inorganic phosphate release convert the two RecA-like domains back to the "opened" conformation (step 2). This causes dissociation of the helicase core from the partially opened dsRNA. The partially opened dsRNA can potentially snap back to produce a non-productive unwinding cycle (dotted arrow) or is subjected to another round of local duplex destabilization (step 3). Another round of local duplex destabilization happens after the ADP is exchanged to ATP in the DEAD-box protein or a new ATP-bound DEAD-box protein recognizes the partially opened dsRNA. This allows the DEAD-box protein to fully disrupt the partially opened duplex. Upon ATP hydrolysis, the ADP-P_i bound DEAD-box protein still associates with the bent strand whereas the non-bent strand is released (step 4). The bent strand is eventually dissociated from the DEAD-box protein once the inorganic phosphate is released (step 5) (Figure is modified from Rudolph and Klostermeier 2015).

DEAD-box proteins recognize the phosphate backbone of RNA instead of the nucleotide bases (Sengoku et al. 2006; Andersen et al. 2006; Del Campo and Lambowitz 2009; von Moeller et al. 2009), suggesting that DEAD-box proteins bind to RNA substrates in a sequence non-specific manner. Consistent with this, numerous biochemical studies have shown that DEAD-box proteins are able to unwind RNA duplexes with random sequences (Putnam and Jankowsky 2013a; Halls et al. 2007; Ma et al. 2013). This could potentially be an advantage for DEAD-box proteins to act as general RNA chaperones to target many different misfolded RNAs (Jarmoskaite and Russell 2014). However, accessory domains of some DEAD-box proteins do confer substrate specificity (for further detail, please see section 1.2.3.5.2)

1.2.3.5.1 Biological functions of DEAD-box proteins

DEAD-box proteins are involved in every aspect of RNA biology ranging from transcription to RNA decay (Table 1.2; Cordin et al. 2006; Jarmoskaite and Russell 2014). Transcription regulation in eukaryotes is highly associated with chromatin structure and transcription factors (Venkatesh and Workman 2015; Lee and Young 2013). Numerous studies have demonstrated that long non-coding RNAs (lncRNAs), transcripts that are longer than 200 nucleotides and do not exhibit protein-coding potential, regulate transcription through modulating chromatin structure (Cloutier et al. 2013; Martianov et al. 2007; Rinn and Chang 2012; Tsai et al. 2010; Spitale et al. 2011; Geisler and Coller 2013). Furthermore, recent studies have also suggested that RNA alters transcription factor occupancy (Sigova et al. 2015; Vance and Ponting 2014). These studies indicate

that RNAs play a role in transcription. Thus, DEAD-box RNA helicases can potentially involve in transcription through RNA.

1.2.3.5.1.1 Transcription

Several DEAD-box proteins have been implicated in transcription. DDX20 functions as a repressor to suppress the transcriptional activity of the orphan nuclear receptor steroidogenic factor 1 (SF-1) and the transcription factor early growth response 2 (Egr2/Krox-20) (Yan et al. 2003; Gillian and Svaren 2004). The DEAD-box protein DDX3 activates the promoter of interferon β (IFN β) and $p21^{WAF1/CIP1}$ and represses the E-cadherin promoter (Soulat et al. 2008; Chao et al. 2006; Botlagunta et al. 2008).

Numerous lines of evidence indicate that the DEAD-box protein DDX5 (p68) acts as a co-activator of several transcription factors and nuclear receptors, including the estrogen receptor alpha (ERα), the androgen receptor (AR), the tumor suppressor p53, and a transcription factor for osteoblast development Runx2 (Endoh et al. 1999; Clark et al. 2008; Bates et al. 2005; Jensen et al. 2008). Interestingly, these studies demonstrated that the DDX5 ATPase deficient mutants (D248N and K114R) that presumably abolish its helicase activity is still able to activate transcription (Endoh et al. 1999; Clark et al. 2008; Bates et al. 2005; Jensen et al. 2008). Nonetheless, no biochemical study has verified if the DDX5 mutant exhibits any RNA-binding activity. Reports have also revealed that DDX5 and the noncoding RNA SRA together act as a co-activator in skeletal muscule differentiation and the Notch signaling pathway (Caretti et al. 2006; Jung et al. 2013). This suggests that DDX5 might not function as an unwinder to remodel RNA structures, but may act as a protein scaffold on RNA for other factors similar to

eIF4A-III and the EJC. Thus, it will be important to determine whether the ATPase deficient mutants also retain RNA binding activity. This would elucidate if there were an RNA-dependent role for previous observations. In addition to its function as a co-activator, DDX5 also acts as a co-repressor with histone deacetylase 1 (HDAC1) at certain promoters (Wilson et al. 2004).

1.2.3.5.1.2 Pre-mRNA splicing

Pre-mRNA splicing requires proper spliceosome formation on structurally resolved pre-mRNA. Spliceosome formation is accomplished by the assembly of 5 snRNPs (U1, U2, U4, U5 and U6) onto pre-mRNA in an orderly fashion (Liu and Cheng 2015; Ding et al. 2014; Wan et al. 2014). Each snRNP contains a snRNA that can fold and form base pairs with pre-mRNA. Once the spliceosome is properly assembled, structural rearrangements occur to activate the spliceosome and catalyze two consecutive transesterification steps. After the reaction is completed, the spliced mRNA is released and the spliceosome is disassembled (Fig 1.4; (Liu and Cheng 2015)). These processes require eight RNA helicases including three DEAD-box proteins (Sub2, Prp5 and Prp28), four DEAH/RHA helicases (Prp2, Prp16, Prp22 and Prp43) and one Ski2-like protein (Brr2) (Kistler and Guthrie 2001; Wang et al. 2008; Perriman and Ares 2007; Staley and Guthrie 1999; Chen and Lin 1990; Burgess et al. 1990; Schwer and Guthrie 1991; Company et al. 1991; Tanaka et al. 2007; Arenas and Abelson 1997; Raghunathan and Guthrie 1998; Small et al. 2006). The three DEAD-box proteins are particularly important for spliceosome assembly and activation. During spliceosome assembly, U1 snRNA recognizes the 5’ splice site by RNA base pairing. The branch point binding

protein BBP initially binds to the branch site and interacts with U1 snRNP proteins Prp40 and Mud2 to join the 5’ splice site and the 3’ splice site together (Abovich et al. 1994; Berglund et al. 1997). Sub2 removes Mud2 from the branch site, which opens up the site for U2 snRNP to bind (Kistler and Guthrie 2001; Wang et al. 2008). In order for U2 snRNA to form base pairs with the branch site, Prp5 is required to convert U2 snRNP into its functional form by removing Cus2 from U2 snRNP in an ATP-dependent manner (Perriman et al. 2003; Perriman and Ares 2007). When U1 and U2 snRNPs are bound to the pre-mRNA, the pre-formed U4/U6.U5 tri-snRNP is recruited to form a properly assembled spliceosome (Huang et al. 2014; Cheng and Abelson 1987; Roscigno and Garcia-Blanco 1995). The spliceosome then undergoes structural rearrangements. This promotes the dissociation of U1 and U4 so U6 can form new base pairs with the 5’ splice site and U2 can form a new interaction with U6 (Brow 2002). Prp28 resolves the six base pair helix between U1 and the 5’ splice site to release U1 from the spliceosome (Staley and Guthrie 1999). Meanwhile, Brr2 destabilizes the U4/U6 base pairs to promote the dissociation of U4 (Raghunathan and Guthrie 1998). The rearranged spliceosome is now active to perform transesterification catalysis for splicing to occur.

1.2.3.5.1.3 Mitochrondrial RNA processing

Mitochondria contain their own genome, the mitochondrial DNA (mtDNA), that is separated from the genome in the nucleus (Taanman 1999). The mtDNA encodes tRNAs, mRNAs and rRNAs (Falkenberg et al. 2007). Several studies have shown that DEAD-box proteins are also involved in mitochondrial RNA processing (Huang et al. 2005; Del Campo et al. 2007; Valgardsdottir et al. 2001). For instance, the DEAD-box

protein Mss116 facilitates folding of all mitochondrial group I and group II introns (Huang et al. 2005). Moreover, Mss116 is required for splicing of the mitochondrial introns (Solem et al. 2006; Del Campo et al. 2007; Mohr et al. 2008). In addition to Mss116, another DEAD-box RNA helicase DDX28 has shown to be localized in mitochondria, suggesting that it is also involved in mitochondrial functions (Valgardsdottir et al. 2001).

1.2.3.5.1.4 mRNA export

Unlike prokaryotes, eukaryotes have a nucleus where mRNA is synthesized and processed. The processed mRNA is then exported to the cytoplasm through the nuclear pore complex (Okamura et al. 2015). mRNA export requires proper mRNP assembly prior to the mRNA being transported from the nucleus to the cytoplasm. Multiple DEAD-box proteins, such as DDX19/Dbp5, UAP56/Sub2, and DDX5 have been shown to play roles in this process (Zhao et al. 2002; Luo et al. 2001; Strässer and Hurt 2001; Zonta et al. 2013). The DEAD-box protein DDX19/Dbp5 is localized at the cytoplasmic face of the nuclear pore complex through interacting with NUP214/ Nup159 (Zhao et al. 2002; Weirich et al. 2004). This allows DDX19/Dbp5 to release export factors from mRNA by mRNP remodeling to promote mRNA export through the nuclear pore complex (Lund and Guthrie 2005; Tran et al. 2007). DDX3 and DDX1 have been implicated in viral RNA export in mammalian cells (Fullam and Schröder 2013).

1.2.3.5.1.5 Ribosome biogenesis

Ribosome biogenesis also involves many structural rearrangements (Martin et al. 2013). It is well established that ribosome biogenesis is a highly complicated process that

involves many RNA helicases and other factors. There are 19 RNA helicases, ~ 200 ribosome assembly factors, and 75 small nucleolar RNAs (snoRNAs) involved in ribosome biogenesis in *S. cerevisiae* (Watkins and Bohnsack 2012; Martin et al. 2013; Thomson et al. 2013). During transcription of the ribosomal DNA repeat in the nucleolus, the nascent pre-ribosomal RNA (pre-rRNA) associates with ribosomal proteins and RNA helicases. This promotes the pre-rRNA to undergo different processing and modification steps to form the 40S and 60S subunits prior to cytoplasmic export (Mougey et al. 1993; Miller and Beatty 1969; Henras et al. 2014). Each mature ribosome consists of a large subunit (LSU) and a small subunit (SSU). In *S. cerevisiae*, the LSU contains three rRNAs (25S, 5.8S and 5S) and the SSU has only one rRNA (18S). All of these rRNAs, except the 5S rRNA, are originated from one long transcript (35S) that is generated by polymerase I and processed at specific sites (Goetze et al. 2010). RNA polymerase III is responsible for synthesizing the 5S rRNA (Costanzo et al. 2001).

DEAD-box proteins Dbp3, Dbp7, Dbp2, Dbp6, Dbp9, Mak5, Drs1, Dbp10 and Sbp4 are required for LSU biogenesis (Weaver et al. 1997; Daugeron and Linder 1998; Ripmaster et al. 1993; de la Cruz et al. 1998; Kressler et al. 1998; Burger et al. 2000; Bond et al. 2001; Bernstein et al. 2006) while Dbp8, Rok1, Fal1, Rrp3 and Dbp4 are necessary for SSU biogenesis (O'Day et al. 1996a; Liang et al. 1997; Venema et al. 1997; Daugeron and Linder 2001; Granneman et al. 2006; Kressler et al. 1997). In addition, Has1 is involved in both LSU and SSU biogenesis (Liang and Fournier 2006; Bernstein et al. 2006; Emery et al. 2004). These DEAD-box proteins are usually involved in structural changes on pre-rRNAs for proper processing (Weaver et al. 1997; Young et al. 2013; Lamanna and Karbstein 2011).

Table 1.2. List of DEAD-box proteins involved in different RNA biology processes

Biological function	DEAD-box protein	
	Mammalian	**Yeast**
Transcription	DDX20(Gemin3)[a, b], DDX3[c, d, e], DDX5[f, g, h, i, j, k, l]	Dbp2[ddd, eee ,fffff]
Splicing	UAP56[ggg, hhh], DDX5[q, r], DDX3[s]	Sub2[m, n], Prp5[o], Prp28[p]
RNA export	UAP56[v], DDX5[x], DDX3[y]	Dbp5[t, u], Sub2[w]
Translation	eIF4A[z], DDX4(VASA)[bb, cc]	Tif1[aa], Ded1[aa], Dbp5[dd]
RNA decay	eIF4A-III[hh]	Dhh1[ee, ff, gg]
Ribosome biogenesis	DDX5[iii], DDX50[uu], DDX21[vv],	Dbp3[ii], Dbp7[jj], Dbp2[kk], Dbp6[ll], Spb4[mm], Dbp10[nn], Has1[oo, pp], Rok1[qq], Rrp3[rr], Dbp8[ss], Drs1[tt], Dbp4[ww], Fal1[xx], Dbp9[yy], Mak5[zz]
Mitochondrial RNA processing	DDX28[bbb]	Mss116[aaa], Mrh4[ccc]

References: [a]Yan et al. 2003, [b]Gillian and Svaren 2004, [c]Soulat et al. 2008, [d]Chao et al. 2006, [e]Botlagunta et al. 2008, [f]Endoh et al. 1999, [g]Clark et al. 2008, [h]Bates et al. 2005, [i]Jensen et al. 2008, [j]Caretti et al. 2006, [k]Jung et al. 2013, [l]Wilson et al. 2004, [m]Kistler and Guthrie 2001, [n]Wang et al. 2008, [o]Perriman and Ares 2007, [p]Staley and Guthrie 1999, [q]Kar et al. 2011, [r]Dardenne et al. 2014, [s]Schröder 2010, [t]Zhao et al. 2002, [u]Weirich et al. 2004, [v]Luo et al. 2001, [w]Strässer and Hurt 2001, [x]Zonta et al. 2013, [y]Fullam and Schröder 2013, [z]Svitkin et al. 2001, [aa]Sen et al. 2015, [bb]Carrera et al. 2000, [cc]Lasko 2013, [dd]Gross et al. 2007, [ee]Fischer and Weis 2002, [ff]Coller et al. 2001, [gg]Sheth and Parker 2003, [hh]Ferraiuolo et al. 2004, [ii]Weaver et al. 1997, [jj]Daugeron and Linder 1998, [kk]Bond et al. 2001, [ll]Kressler et al. 1998, [mm]de la Cruz et al. 1998, [nn]Burger et al. 2000, [oo]Bernstein et al. 2006, [pp]Liang and Fournier 2006, [qq]Venema et al. 1997, [rr]O'Day et al. 1996, [ss]Daugeron and Linder 2001, [tt]Ripmaster et al. 1993, [uu]Henning et al. 2003, [vv]Calo et al. 2015, [ww]Liang et al. 1997, [xx]Kressler et al. 1997, [yy]Daugeron et al. 2001, [zz]Zagulski et al. 2003, [aaa]Huang et al. 2005, [bbb]Valgardsdottir et al. 2001, [ccc]Schmidt et al. 2002, [ddd]Cloutier et al. 2012, [eee]Cloutier et al. 2013, [fff]Beck et al. 2014, [ggg]Shen et al. 2008, [hhh]Fleckner et al. 1997, [iii]Jalal et al. 2007

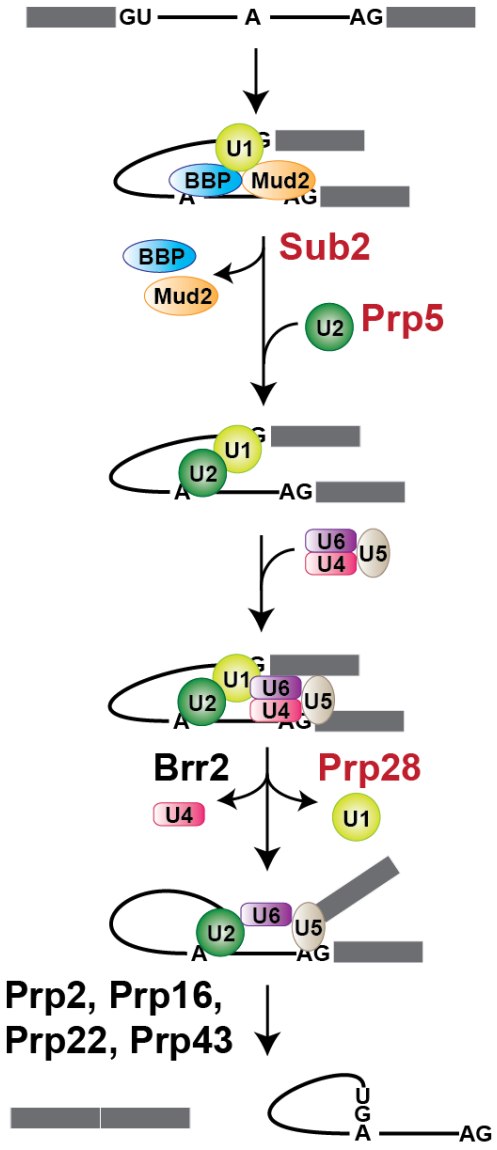

Figure 1.4. DEAD-box proteins are heavily involved in spliceosome assembly and activation. During spliceosome assembly, Sub2 removes Mud2 from the branch site while Prp5 dissociates Cus2 from U2 and switches U2 to a functional conformation. This allows U2 snRNP to bind to the branch site and interact with U1 snRNP. The pre-formed U4/U6.U5 complex is then recruited and forms a properly assembled spliceosome. To activate the spliceosome, Prp28 removes U1 snRNP from the spliceosome while the Ski2-like protein Brr2 promotes the release of U4 from U6. The spliceosome undergoes drastic structural rearrangements and is ready for a splicing reaction (Figure is modified from Liu and Cheng 2015).

1.2.3.5.1.6 Translation

Translation initiation requires the preinitiation complex (PIC) to load and scan from 5' to 3' along the 5' UTR seeking the start codon. Both of these processes require disruption of RNA structures within the 5' UTR, which is facilitated by the DEAD-box helicases eIF4A and Ded1 (Svitkin et al. 2001; Sen et al. 2015). The initiation factor eIF4A is part of the eIF4F complex that promotes the recruitment of the PIC to the 5' cap (Svitkin et al. 2001). Once the PIC is loaded, Ded1 helps the PIC to scan for the start codon through secondary structures within the 5' UTR (Sen et al. 2015). Several reports have also revealed that the human DEAD-box protein DDX4 (Vasa in Drosophila) facilitates eIF5B loading to the PIC and promotes translation of mRNAs encoding proteins that play roles in embryogenesis and germline development (Carrera et al. 2000; Lasko 2013; Johnstone and Lasko 2004).

1.2.3.5.1.7 RNA decay

RNA degradation plays a huge role in maintaining the cellular RNA homeostasis (Parker 2012; Houseley and Tollervey 2009). Cytoplasmic mRNA degradation in yeast occurs by two general pathways, both of which are initiated by deadenylation (Decker and Parker 1993). After deadenylation, the mRNA is either subjected to 3' to 5' degradation by the cytoplasmic exosome or decapped by the decapping enzyme followed by 5' to 3' degradation by Xrn1 (Anderson and Parker 1998; Steiger et al. 2003; Van Dijk et al. 2002; Hsu and Stevens 1993; Muhlrad et al. 1994). In yeast, the DEAD-box protein Dhh1 associates with mRNA deadenylation factors Pop2/Caf1 and Ccr4, the mRNA degradation factor Pat1 and the exonuclease Xrn1 (Hata et al. 1998).

Furthermore, Dhh1 induces mRNA decapping activity and is associated with 3’ to 5’ degradation in the cytoplasm (Fischer and Weis 2002; Coller et al. 2001; Sheth and Parker 2003). This suggests that Dhh1 plays a role in mRNA decay. The surveillance mechanism NMD degrades mRNAs that carry a premature termination codon (PTC). Genomomic mutation or errors occur during RNA processing could result a PTC in a transcript (Brogna and Wen 2009; Christiano et al. 1997). In yeast, pre-mRNAs that contain a stop codon in the intron or mRNAs with an atypically long 3’ UTR are considered transcripts with PTC (Kebaara and Atkin 2009). In mammals, a stop codon is considered premature when it is located upstream of an EJC on a mRNA (Mendell et al. 2004; Isken and Maquat 2008). The EJC contains the DEAD-box protein eIF4A-III, which has been shown to play a role in NMD (Ferraiuolo et al. 2004; Palacios et al. 2004; Shibuya et al. 2004).

1.2.3.5.2 Specificity of DEAD-box proteins

Given that DEAD-box proteins specifically function in different biological processes and the helicase core of DEAD-box proteins recognize RNA in a non-specific manner, the cellular specificity needs to arise from outside the helicase core. This specificity is provided by accessory domains flanking the helicase core and/or protein co-factors. Numerous studies have revealed that the C-terminal domain of DbpA and YxiN provide specificity towards the hairpin 92 in 23S rRNA (Kossen et al. 2002; Karginov et al. 2005; Diges and Uhlenbeck 2001; Tsu et al. 2001). Similarly, the C-terminal domain of Hera promotes recognition of RNAs with a single-stranded GGXY stretch adjacent to a duplex region (Morlang et al. 1999; Linden et al. 2008). Moreover, the C-terminal

domain of DDX20 is required to interact with survival of motor neurons (SMN) to facilitate assembly of snRNP particles (Charroux et al. 1999). Besides substrate specificity, accessory domains can also modulate the enzymatic activities of DEAD-box proteins. This has been observed with the N-terminal helix of DDX19/Dbp5 that folds between the two RecA-like domains. This helix inhibits the intrinsic ATPase activity of DDX19/Dbp5 in the absence of RNA (Collins et al. 2009). The C-terminus of CYT-19 has also been shown to enhance the unwinding activity via tethering of the helicase to structured RNA (Grohman et al. 2007). Further evidence has also demonstrated that the C-terminus of Ded1 contains an RGG-rich motif that is important for its annealing activity (Yang and Jankowsky 2005).

1.2.3.5.3 Protein co-factors and DEAD-box proteins

Protein co-factors have also been shown to regulate the enzymatic activities of DEAD-box proteins (Table 1.3). The DEAD-box protein eIF4A is one of the most well-studied examples of regulation by protein co-factors. The initiation factor eIF4G interacts with eIF4A and guides the conformational change on the helicase core. This stimulates the ATPase activity and decreases the RNA, ATP and ADP binding affinity of eIF4A (Montpetit et al. 2011; Schutz et al. 2008; Hilbert et al. 2011). Another initiation factor, eIF4B, has also been shown to stimulate both the ATPase and unwinding activities of eIF4A by increasing its affinity towards RNA and ATP (Abramson et al. 1988; Rogers Jr. et al. 2001; Rozen et al. 1990; Bi et al. 2000). These translation factors work together to regulate the enzymatic activity of eIF4A and promote efficient translation initiation. In contrast, the tumor suppressor Pdcd4 inhibits the unwinding and ATPase

activities of eIF4A by occluding the RNA-binding site to decrease its RNA-binding affinity (Chang et al. 2009; Loh et al. 2009). This inhibition reduces translation initiation efficiency.

Another well-known example is observed when the mRNA export protein Gle1, together with chemical compound inositol hexaphosphate (IP_6), promote ATP binding of the DEAD-box protein DDX19/Dbp5 to potentiate its ATPase activity (Alcazar-Roman et al. 2006; Weirich et al. 2006; Noble et al. 2011). In contrast, the cytoplasmic nucleoporin Nup159/NUP214 inhibits the ATPase and RNA binding activities of DDX19/Dbp5 by occupying the RNA binding site and sterically preventing the helicase core from folding into its active state (von Moeller et al. 2009; Montpetit et al. 2011). These protein co-factors together regulate DDX19/Dbp5 at the cytoplasmic side of the nuclear pore complex to maintain unidirectional movement of the mRNP during nuclear export (Tran et al. 2007).

Table 1.3. Effects of protein co-factors on DEAD-box proteins

DEAD-box protein	Protein co-factor	Protein co-factor effects			
		Substrate binding	**ATPase activity**	**Unwinding activity**	**Annealing activity**
Rok1	Rrp5	RNA: Increase[a]	N/D	No effect[a]	Increase[a]
eIF4A-III	MLN51	RNA: Increase[b] ATP: Increase[c]	Increase[b, c]	Increase[c]	N/D
eIF4A-III	MAGOH-Y14	RNA: No effect[b], but increase when associate with MLN51)[d] P_i release: Decrease[d]	Abolish MLN51-dependent stimulation[b, c]	Increase (when associate with MLN51)[c]	N/D
eIF4A-III	CWC22	RNA: Decrease[e]	Decrease[e]	N/D	N/D
DDX6	CNOT1	N/D	Increase[f]	N/D	N/D
Dbp5	Gle1:IP_6	RNA: Decrease[k] ATP:Increase[i]	Increase[g, h]	N/D	N/D
DDX19/Dbp5	NUP214/Nup159	ADP: Decrease[i] RNA:Decrease[j, k]	Decrease[j]	N/D	N/D
Dbp8	Esf2	N/D	Increase[l]	N/D	N/D
eIF4A	PDCD4	RNA: Decrease[m]	Decrease[n]	Decrease[m, n]	N/D
eIF4A	eIF4G	RNA: Decrease[k] ATP: Decrease[o] ADP: Decrease[o] P_i release: Increase[o]	Increase[o, p]	N/D	N/D
eIF4A	eIF4B	RNA: Increase[q] ATP: Increase[r] P_i release: Increase[r]	Increase[q, s, t]	Increase[u]	N/D
Dhh1	Pat1 and Edc3	RNA: Decrease[v]	N/D	N/D	N/D
Ded1	Gle1	N/D	Decrease[w]	N/D	N/D
Ded1	eIF4G	RNA: Increase[x]	N/D	Decrease[x]	N/D
Dbp2	Yra1	RNA: Decrease*	Increaese[y]	Decrease[y]	N/D

References: [a]Young et al. 2013, [b]Ballut et al. 2005, [c]Noble and Song 2007, [d]Nielsen et al. 2009, [e]Barbosa et al. 2012, [f]Mathys et al. 2014, [g]Weirich et al. 2006, [h]Alcazar-Roman et al. 2006, [i]Noble et al. 2011, [j]von Moeller et al. 2009, [k]Montpetit et al. 2011, [l]Granneman et al. 2006, [m]Chang et al. 2009, [n]Loh et al. 2009, [o]Hilbert et al. 2011, [p]Schutz et al. 2008, [q]Abramson et al. 1988, [r]Bi et al. 2000, [s]Grifo et al. 1984, [t]Rogers Jr. et al. 2001, [u]Rozen et al. 1990, [v]Sharif et al. 2013, [w]Bolger and Wente 2011, [x]Putnam et al. 2015, [y]Ma et al. 2013

N/D indicates not determine

*indicates unpublished data from the Tran lab

The DEAD-box protein eIF4A-III is stably locked onto RNA to act as a RNA clamp by interacting with the other components of the EJC, including MLN51, MAGOH and Y14 (Ballut et al. 2005). Though MLN51 stimulates the ATPase and unwinding activities of eIF4A-III, addition of MAGOH and Y14 to the complex inhibits the stimulation and further reduces phosphate release of eIF4A-III. This increases the affinity of eIF4A-III towards RNA (Noble and Song 2007; Ballut et al. 2005; Nielsen et al. 2009). It has also been demonstrated that the ribosomal protein Rrp5 provides substrate specificity for the DEAD-box protein Rok1 and increases its annealing activity (Young et al. 2013). This regulation is critical to promote efficient ribosome biogenesis. In contrast, some protein cofactors do not modulate the activity of DEAD-box proteins. For example, the stem loop binding protein (SLBP)-binding protein 1 (SLIP1), which activates the translational activity of SLBP bound histone mRNAs, interacts with the DEAD-box protein DDX19/Dbp5. However, this interaction does not appear to modulate the enzymatic activity of this helicase (von Moeller et al. 2009). Similarly, another DEAD-box protein, UAP56, interacts directly with the mRNA export factor ALY (Luo et al. 2001). ALY also does not affect the catalytic activity of UAP56 (Shen et al. 2007).

1.2.3.5.4 DEAD-box proteins and diseases

Regulation of DEAD-box proteins is critical for cells to perform their physiological functions. Mis-regulation of DEAD-box RNA helicases has been implicated in numerous diseases (Steimer and Klostermeier 2012). For instance, upregulation of UAP56 has been reported in Alzheimer's patients and reduction of DDX5 is found in skeletal muscle biopsies of myotonic dystrophy type 1 and type 2 patients

(Wong et al. 2003; Jones et al. 2015). Studies have also revealed that many DEAD-box proteins are aberrantly expressed in cancer (Fuller-Pace 2013; Hashimoto et al. 2001; Miyaji et al. 2003; Botlagunta et al. 2008). This includes DDX1, which is upregulated in neuroblastoma and retinoblastoma (Godbout et al. 1998; Godbout and Squire 1993; George et al. 1996). Overexpression of DDX39 is found in lung squamous cell cancer and pancreatic cancer (Sugiura et al. 2007; Kuramitsu et al. 2013). Furthermore, DDX5 is uprregulated in a range of cancers including colorectal, colon, prostate, breast, and glioma (Causevic et al. 2001; Shin et al. 2007; Clark et al. 2008; Wortham et al. 2009; Wang et al. 2012). Several reports have also indicated that eIF4A is downregulated in glioma, lung, colon and breast cancer (Wen et al. 2007; Chen et al. 2003; Gao et al. 2007; Mudduluru et al. 2007). To alleviate or even cure these diseases, it is important to understand how DEAD-box proteins are being regulated.

1.3 Summary

RNA helicases are a class of enzymes that function in all steps of RNA biology. Research in the past 30 years has demonstrated a wide range of biochemical properties of RNA helicases. One of the long-standing questions in the RNA helicase field is how these properties dictate cellular functions. For example, many biochemical studies have demonstrated that some RNA helicases exhibit unwinding activity *in vitro*. However, whether these RNA helicases unwind RNA substrates *in vivo* remains to be addressed. If they do unwind RNA targets in cells, when and where do they unwind? In addition, how is this activity regulated so the RNA helicase can perform this function at the correct time and location? These questions also apply to biochemical activities other than unwinding.

Progress in answering these questions has been hindered in the past mainly due to lack of information on the cellular RNA targets of the RNA helicases. With recent rapid advancements in sequencing technology, it has become easier to identify the RNA targets and binding sites of RNA helicases. It is expected that more and more cellular RNA targets of RNA helicases will be identified in the near future. This allows biochemical analysis to be conducted using the endogenous RNA targets to study the precise role of the RNA helicase.

Given the importance of RNA helicases in almost all RNA related cellular processes, mis-regulation of RNA helicases have been implicated in numerous human diseases and pathogen infections (Steimer and Klostermeier 2012). Protein co-factors and accessory domains have been demonstrated to regulate the enzymatic properties of RNA helicases. However, it is not well understood that how these factors modulate the enzymatic activities of most RNA helicases on a molecular level. Understanding the precise mechanism of regulation on RNA helicases might shed light on targets for drug design for diseases that involve mis-regulated DEAD-box proteins. In the following years, it will be exciting to learn more about the precise role and the regulation mechanism of RNA helicases.

1.4 References

Abdelhaleem M. 2010. Helicases: an overview. *Methods Mol Biol* **587**: 1–12.

Abovich N, Liao XC, Rosbash M. 1994. The yeast MUD2 protein: an interaction with PRP11 defines a bridge between commitment complexes and U2 snRNP addition. *Genes Dev* **8**: 843–854.

Abramson RD, Dever TE, Merrick WC. 1988. Biochemical evidence supporting a mechanism for cap-independent and internal initiation of eukaryotic mRNA. *J Biol Chem* **263**: 6016–6019.

Ahuja D, Sáenz-Robles MT, Pipas JM. 2005. SV40 large T antigen targets multiple cellular pathways to elicit cellular transformation. *Oncogene* **24**: 7729–7745.

Alcazar-Roman AR, Tran EJ, Guo S, Wente SR. 2006. Inositol hexakisphosphate and Gle1 activate the DEAD-box protein Dbp5 for nuclear mRNA export. *Nat Cell Biol* **8**: 711–716.

Andersen CB, Ballut L, Johansen JS, Chamieh H, Nielsen KH, Oliveira CL, Pedersen JS, Seraphin B, Le Hir H, Andersen GR. 2006. Structure of the exon junction core complex with a trapped DEAD-box ATPase bound to RNA. *Science (80-)* **313**: 1968–1972.

Anderson J, Parker R. 1998. The 3’ to 5' degradation of yeast mRNAs is a general mechanism for mRNA turnover that requires the SKI2 DEVH box protein and 3' to 5' exonucleases of the exosome complex. *EMBO J* **17**: 1497–1506.

Araki Y, Takahashi S, Kobayashi T, Kajiho H, Hoshino S, Katada T. 2001. Ski7p G protein interacts with the exosome and the Ski complex for 3’-to-5' mRNA decay in yeast. *EMBO J* **20**: 4684–93.

Arenas JE, Abelson JN. 1997. Prp43: An RNA helicase-like factor involved in spliceosome disassembly. *Proc Natl Acad Sci U S A* **94**: 11798–11802.

Baharoglu Z, Lestini R, Duigou S, Michel B. 2010. RNA polymerase mutations that facilitate replication progression in the rep uvrD recF mutant lacking two accessory replicative helicases. *Mol Microbiol* **77**: 324–36.

Ballut L, Marchadier B, Baguet A, Tomasetto C, Seraphin B, Le Hir H. 2005. The exon junction core complex is locked onto RNA by inhibition of eIF4AIII ATPase activity. *Nat Struct Mol Biol* **12**: 861–869.

Banerjee AK. 1980. 5’-terminal cap structure in eucaryotic messenger ribonucleic acids. *Microbiol Rev* **44**: 175–205.

Banroques J, Cordin O, Doere M, Linder P, Tanner NK. 2008. A conserved phenylalanine of motif IV in superfamily 2 helicases is required for cooperative, ATP-dependent binding of RNA substrates in DEAD-box proteins. *Mol Cell Biol* **28**: 3359–3371.

Barbosa I, Haque N, Fiorini F, Barrandon C, Tomasetto C, Blanchette M, Le Hir H. 2012. Human CWC22 escorts the helicase eIF4AIII to spliceosomes and promotes exon junction complex assembly. *Nat Struct Mol Biol* **19**: 983–990.

Barta I, Iggo R. 1995. Autoregulation of expression of the yeast Dbp2p “DEAD-box” protein is mediated by sequences in the conserved DBP2 intron. *EMBO J* **14**: 3800–3808.

Bates GJ, Nicol SM, Wilson BJ, Jacobs AM, Bourdon JC, Wardrop J, Gregory DJ, Lane DP, Perkins ND, Fuller-Pace F V. 2005. The DEAD box protein p68: a novel transcriptional coactivator of the p53 tumour suppressor. *EMBO J* **24**: 543–553.

Bayliss CD, Smith GL. 1996. Vaccinia virion protein I8R has both DNA and RNA helicase activities: implications for vaccinia virus transcription. *J Virol* **70**: 794–800.

Beck ZT, Cloutier SC, Schipma MJ, Petell CJ, Ma WK, Tran EJ. 2014. Regulation of Glucose-Dependent Gene Expression by the RNA Helicase Dbp2 in Saccharomyces cerevisiae. *Genetics* **198**: 1001–14.

Berglund J a, Chua K, Abovich N, Reed R, Rosbash M. 1997. The splicing factor BBP interacts specifically with the pre-mRNA branchpoint sequence UACUAAC. *Cell* **89**: 781–787.

Bernstein J, Patterson DN, Wilson GM, Toth E a. 2008. Characterization of the essential activities of Saccharomyces cerevisiae Mtr4p, a 3’ to 5' helicase partner of the nuclear exosome. *J Biol Chem* **283**: 4930–4942.

Bernstein KA, Granneman S, Lee A V, Manickam S, Baserga SJ. 2006. Comprehensive mutational analysis of yeast DEXD/H box RNA helicases involved in large ribosomal subunit biogenesis. *Mol Cell Biol* **26**: 1195–208.

Bhattacharya a, Czaplinski K, Trifillis P, He F, Jacobson a, Peltz SW. 2000. Characterization of the biochemical properties of the human Upf1 gene product that is involved in nonsense-mediated mRNA decay. *RNA* **6**: 1226–1235.

Bi X, Ren J, Goss DJ. 2000. Wheat germ translation initiation factor eIF4B affects eIF4A and eIFiso4F helicase activity by increasing the ATP binding affinity of eIF4A. *Biochemistry* **39**: 5758–65.

Bolger TA, Wente SR. 2011. Gle1 is a multifunctional DEAD-box protein regulator that modulates Ded1 in translation initiation. *J Biol Chem* **286**: 39750–39759.

Bond a T, Mangus D a, He F, Jacobson a. 2001. Absence of Dbp2p alters both nonsense-mediated mRNA decay and rRNA processing. *Mol Cell Biol* **21**: 7366–79.

Borowski LS, Dziembowski A, Hejnowicz MS, Stepien PP, Szczesny RJ. 2013. Human mitochondrial RNA decay mediated by PNPase-hSuv3 complex takes place in distinct foci. *Nucleic Acids Res* **41**: 1223–1240.

Botlagunta M, Vesuna F, Mironchik Y, Raman A, Lisok A, Winnard P, Mukadam S, Van Diest P, Chen JH, Farabaugh P, et al. 2008. Oncogenic role of DDX3 in breast cancer biogenesis. *Oncogene* **27**: 3912–3922.

Bowers HA, Maroney PA, Fairman ME, Kastner B, Lührmann R, Nilsen TW, Jankowsky E. 2006. Discriminatory RNP remodeling by the DEAD-box protein DED1. *RNA* **12**: 903–12.

Brendza KM, Cheng W, Fischer CJ, Chesnik M a, Niedziela-Majka A, Lohman TM. 2005. Autoinhibition of Escherichia coli Rep monomer helicase activity by its 2B subdomain. *Proc Natl Acad Sci U S A* **102**: 10076–10081.

Brennan C a, Dombroski a J, Platt T. 1987. Transcription termination factor rho is an RNA-DNA helicase. *Cell* **48**: 945–952.

Brennan CA, Steinmetz EJ, Spear P, Platt T. 1990. Specificity and efficiency of rho-factor helicase activity depends on magnesium concentration and energy coupling to NTP hydrolysis. *J Biol Chem* **265**: 5440–7.

Brenner TJ, Guthrie C. 2005. Genetic analysis reveals a role for the C terminus of the Saccharomyces cerevisiae GTPase Snu114 during spliceosome activation. *Genetics* **170**: 1063–1080.

Brogna S, Wen J. 2009. Nonsense-mediated mRNA decay (NMD) mechanisms. *Nat Struct Mol Biol* **16**: 107–113.

Brow D a. 2002. Allosteric cascade of spliceosome activation. *Annu Rev Genet* **36**: 333–360.

Brown JT, Bai X, Johnson a W. 2000. The yeast antiviral proteins Ski2p, Ski3p, and Ski8p exist as a complex in vivo. *RNA* **6**: 449–457.

Bruand C, Ehrlich SD. 2000. UvrD-dependent replication of rolling-circle plasmids in Escherichia coli. *Mol Microbiol* **35**: 204–210.

Burger F, Daugeron MC, Linder P. 2000. Dbp10p, a putative RNA helicase from Saccharomyces cerevisiae, is required for ribosome biogenesis. *Nucleic Acids Res* **28**: 2315–23.

Burgess S, Couto JR, Guthrie C. 1990. A putative ATP binding protein influences the fidelity of branchpoint recognition in yeast splicing. *Cell* **60**: 705–17.

Calo E, Flynn RA, Martin L, Spitale RC, Chang HY, Wysocka J. 2015. RNA helicase DDX21 coordinates transcription and ribosomal RNA processing. *Nature* **518**: 249–53.

Cao W, Coman MM, Ding S, Henn A, Middleton ER, Bradley MJ, Rhoades E, Hackney DD, Pyle AM, De La Cruz EM. 2011. Mechanism of Mss116 ATPase reveals functional diversity of DEAD-Box proteins. *J Mol Biol* **409**: 399–414.

Caretti G, Schiltz RL, Dilworth FJ, Di Padova M, Zhao P, Ogryzko V, Fuller-Pace F V., Hoffman EP, Tapscott SJ, Sartorelli V. 2006. The RNA Helicases p68/p72 and the Noncoding RNA SRA Are Coregulators of MyoD and Skeletal Muscle Differentiation. *Dev Cell* **11**: 547–560.

Carrera P, Johnstone O, Nakamura a, Casanova J, Jäckle H, Lasko P. 2000. VASA mediates translation through interaction with a Drosophila yIF2 homolog. *Mol Cell* **5**: 181–187.

Caruthers JM, McKay DB. 2002. Helicase structure and mechanism. *Curr Opin Struct Biol* **12**: 123–133.

Causevic M, Hislop RG, Kernohan NM, Carey FA, Kay RA, Steele RJ, Fuller-Pace F V. 2001. Overexpression and poly-ubiquitylation of the DEAD-box RNA helicase p68 in colorectal tumours. *Oncogene* **20**: 7734–7743.

Cenik ES, Fukunaga R, Lu G, Dutcher R, Wang Y, Tanaka Hall TM, Zamore PD. 2011. Phosphate and R2D2 Restrict the Substrate Specificity of Dicer-2, an ATP-Driven Ribonuclease. *Mol Cell* **42**: 172–184.

Chang JH, Cho YH, Sohn SY, Choi JM, Kim A, Kim YC, Jang SK, Cho Y. 2009. Crystal structure of the eIF4A-PDCD4 complex. *Proc Natl Acad Sci U S A* **106**: 3148–3153.

Chao C-H, Chen C-M, Cheng P-L, Shih J-W, Tsou A-P, Lee Y-HW. 2006. DDX3, a DEAD box RNA helicase with tumor growth-suppressive property and transcriptional regulation activity of the p21waf1/cip1 promoter, is a candidate tumor suppressor. *Cancer Res* **66**: 6579–88.

Charroux B, Pellizzoni L, Perkinson R a., Shevchenko A, Mann M, Dreyfuss G. 1999. Gemin3: A novel DEAD box protein that interacts with SMN, the spinal muscular atrophy gene product, and is a component of gems. *J Cell Biol* **147**: 1181–1193.

Chen CYA, Shyu A Bin. 2014. Emerging mechanisms of mRNP remodeling regulation. *Wiley Interdiscip Rev RNA* **5**: 713–22.

Chen J, Lu G, Lin J, Davidson AL, Quiocho FA. 2003. A tweezers-like motion of the ATP-binding cassette dimer in an ABC transport cycle. *Mol Cell* **12**: 651–661.

Chen JH, Lin RJ. 1990. The yeast PRP2 protein, a putative RNA-dependent ATPase, shares extensive sequence homology with two other pre-mRNA splicing factors. *Nucleic Acids Res* **18**: 6447.

Chen JYF, Stands L, Staley JP, Jackups RR, Latus LJ, Chang TH. 2001. Specific alterations of U1-C protein or U1 Small nuclear RNA can eliminate the requirement of Prp28p, an essential DEAD Box splicing factor. *Mol Cell* **7**: 227–232.

Chen Y, Potratz JP, Tijerina P, Del Campo M, Lambowitz AM, Russell R. 2008. DEAD-box proteins can completely separate an RNA duplex using a single ATP. *Proc Natl Acad Sci U S A* **105**: 20203–20208.

Chendrimada TP, Finn KJ, Ji X, Baillat D, Gregory RI, Liebhaber S a, Pasquinelli AE, Shiekhattar R. 2007. MicroRNA silencing through RISC recruitment of eIF6. *Nature* **447**: 823–828.

Cheng SC, Abelson J. 1987. Spliceosome assembly in yeast. *Genes Dev* **1**: 1014–1027.

Christiano AM, Amano S, Eichenfield LF, Burgeson RE, Uitto J. 1997. Premature termination codon mutations in the type VII collagen gene in recessive dystrophic epidermolysis bullosa result in nonsense-mediated mRNA decay and absence of functional protein. *J Invest Dermatol* **109**: 390–394.

Clark EL, Coulson A, Dalgliesh C, Rajan P, Nicol SM, Fleming S, Heer R, Gaughan L, Leung HY, Elliott DJ, et al. 2008. The RNA helicase p68 is a novel androgen receptor coactivator involved in splicing and is overexpressed in prostate cancer. *Cancer Res* **68**: 7938–7946.

Clemente P, Pajak A, Laine I, Wibom R, Wedell A, Freyer C, Wredenberg A. 2015. SUV3 helicase is required for correct processing of mitochondrial transcripts. *Nucleic Acids Res* **43**: 7398–413.

Cloutier SC, Ma WK, Nguyen LT, Tran EJ. 2012. The DEAD-box RNA helicase Dbp2 connects RNA quality control with repression of aberrant transcription. *J Biol Chem* **287**: 26155–26166.

Cloutier SC, Wang S, Ma WK, Petell CJ, Tran EJ. 2013. Long Noncoding RNAs Promote Transcriptional Poising of Inducible Genes. *PLoS Biol* **11**.

Coller JM, Tucker M, Sheth U, Valencia-Sanchez MA, Parker R. 2001. The DEAD box helicase, Dhh1p, functions in mRNA decapping and interacts with both the decapping and deadenylase complexes. *RNA* **7**: 1717–27.

Colley A, Beggs JD, Tollervey D, Lafontaine DL. 2000. Dhr1p, a putative DEAH-box RNA helicase, is associated with the box C+D snoRNP U3. *Mol Cell Biol* **20**: 7238–46.

Collins R, Karlberg T, Lehtio L, Schutz P, van den Berg S, Dahlgren L-G, Hammarstrom M, Weigelt J, Schuler H. 2009. The DEXD/H-box RNA Helicase DDX19 Is Regulated by an -Helical Switch. *J Biol Chem* **284**: 10296–10300.

Company M, Arenas J, Abelson J. 1991. Requirement of the RNA helicase-like protein PRP22 for release of messenger RNA from spliceosomes. *Nature* **349**: 487–493.

Cordin O, Banroques J, Tanner NK, Linder P. 2006. The DEAD-box protein family of RNA helicases. *Gene* **367**: 17–37.

Cordin O, Beggs JD. 2013. RNA helicases in splicing. *RNA Biol* **10**: 83–95.

Costanzo G, Camier S, Carlucci P, Burderi L, Nucleici A. 2001. RNA Polymerase III Transcription Complexes on Chromosomal 5S rRNA Genes In Vivo : TFIIIB Occupancy and Promoter Opening. *Mol Cell Biol* **21**: 3166–3178.

Cramer P, Srebrow A, Kadener S, Werbajh S, de la Mata M, Melen G, Nogues G, Kornblihtt AR. 2001. Coordination between transcription and pre-mRNA processing. *FEBS Lett* **498**: 179–182.

Cromie GA. 2009. Phylogenetic ubiquity and shuffling of the bacterial RecBCD and AddAB recombination complexes. *J Bacteriol* **191**: 5076–84.

Cui S, Eisenächer K, Kirchhofer A, Brzózka K, Lammens A, Lammens K, Fujita T, Conzelmann KK, Krug A, Hopfner KP. 2008. The C-Terminal Regulatory Domain Is the RNA 5′-Triphosphate Sensor of RIG-I. *Mol Cell* **29**: 169–179.

Czaplinski K, Ruiz-Echevarria MJ, González CI, Peltz SW. 1999. Should we kill the messenger? The role of the surveillance complex in translation termination and mRNA turnover. *BioEssays* **21**: 685–696.

Czaplinski K, Weng Y, Hagan KW, Peltz SW. 1995. Purification and characterization of the Upf1 protein: a factor involved in translation and mRNA degradation. *RNA* **1**: 610–23.

Dardenne E, PolayEspinoza M, Fattet L, Germann S, Lambert MP, Neil H, Zonta E, Mortada H, Gratadou L, Deygas M, et al. 2014. RNA Helicases DDX5 and DDX17 Dynamically Orchestrate Transcription, miRNA, and Splicing Programs in Cell Differentiation. *Cell Rep* **7**: 1900–1913.

Daugeron MC, Kressler D, Linder P. 2001. Dbp9p, a putative ATP-dependent RNA helicase involved in 60S-ribosomal-subunit biogenesis, functionally interacts with Dbp6p. *RNA* **7**: 1317–34.

Daugeron MC, Linder P. 2001. Characterization and mutational analysis of yeast Dbp8p, a putative RNA helicase involved in ribosome biogenesis. *Nucleic Acids Res* **29**: 1144–1155.

Daugeron MC, Linder P. 1998. Dbp7p, a putative ATP-dependent RNA helicase from Saccharomyces cerevisiae, is required for 60S ribosomal subunit assembly. *RNA* **4**: 566–81.

de la Cruz J, Kressler D, Rojo M, Tollervey D, Linder P. 1998. Spb4p, an essential putative RNA helicase, is required for a late step in the assembly of 60S ribosomal subunits in Saccharomyces cerevisiae. *RNA* **4**: 1268–1281.

Decker CJ, Parker R. 1993. A turnover pathway for both stable and unstable mRNAs in yeast: Evidence for a requirement for deadenylation. *Genes Dev* **7**: 1632–1643.

Del Campo M, Lambowitz AM. 2009. Structure of the Yeast DEAD box protein Mss116p reveals two wedges that crimp RNA. *Mol Cell* **35**: 598–609.

Del Campo M, Tijerina P, Bhaskaran H, Mohr S, Yang Q, Jankowsky E, Russell R, Lambowitz AM. 2007. Do DEAD-box proteins promote group II intron splicing without unwinding RNA? *Mol Cell* **28**: 159–66.

Diges CM, Uhlenbeck OC. 2001. Escherichia coli DbpA is an RNA helicase that requires hairpin 92 of 23S rRNA. *EMBO J* **20**: 5503–5512.

Ding Y, Tang Y, Kwok CK, Zhang Y, Bevilacqua PC, Assmann SM. 2014. In vivo genome-wide profiling of RNA secondary structure reveals novel regulatory features. *Nature* **505**: 696–700.

Dudley G a., Tullson PC, Terjung RL. 1987. Influence of mitochondrial content on the sensitivity of respiratory control. *J Biol Chem* **262**: 9109–9114.

Dumont S, Cheng W, Serebrov V, Beran RK, Tinoco I, Pyle AM, Bustamante C. 2006. RNA translocation and unwinding mechanism of HCV NS3 helicase and its coordination by ATP. *Nature* **439**: 105–108.

Durr H, Flaus A, Owen-Hughes T, Hopfner K-P. 2006. Snf2 family ATPases and DExx box helicases: differences and unifying concepts from high-resolution crystal structures. *Nucleic Acids Res* **34**: 4160–4167.

Dziembowski A, Malewicz M, Minczuk M, Golik P, Dmochowska A, Stepien PP. 1998. The yeast nuclear gene DSS1, which codes for a putative RNase II, is necessary for the function of the mitochondrial degradosome in processing and turnover of RNA. *Mol Gen Genet* **260**: 108–14.

Dziembowski A, Piwowarski J, Hoser R, Minczuk M, Dmochowska A, Siep M, van der Spek H, Grivell L, Stepien PP. 2003. The yeast mitochondrial degradosome. Its composition, interplay between RNA helicase and RNase activities and the role in mitochondrial RNA metabolism. *J Biol Chem* **278**: 1603–11.

Edwalds-Gilbert G, Kim DH, Silverman E, Lin RJ. 2004. Definition of a spliceosome interaction domain in yeast Prp2 ATPase. *RNA* **10**: 210–220.

Eller MS, Liao X, Liu S, Hanna K, Bäckvall H, Opresko PL, Bohr V a, Gilchrest B a. 2006. A role for WRN in telomere-based DNA damage responses. *Proc Natl Acad Sci U S A* **103**: 15073–8.

Emery B, De La Cruz J, Rocak S, Deloche O, Linder P. 2004. Has1p, a member of the DEAD-box family, is required for 40S ribosomal subunit biogenesis in Saccharomyces cerevisiae. *Mol Microbiol* **52**: 141–158.

Endoh H, Maruyama K, Masuhiro Y, Kobayashi Y, Goto M, Tai H, Yanagisawa J, Metzger D, Hashimoto S, Kato S. 1999. Purification and identification of p68 RNA helicase acting as a transcriptional coactivator specific for the activation function 1 of human estrogen receptor alpha. *Mol Cell Biol* **19**: 5363–72.

Enemark EJ, Joshua-Tor L. 2006. Mechanism of DNA translocation in a replicative hexameric helicase. *Nature* **442**: 270–275.

Fairman ME, Maroney PA, Wang W, Bowers HA, Gollnick P, Nilsen TW, Jankowsky E. 2004. Protein displacement by DExH/D “RNA helicases” without duplex unwinding. *Science (80-)* **304**: 730–734.

Fairman-Williams ME, Guenther UP, Jankowsky E. 2010. SF1 and SF2 helicases: family matters. *Curr Opin Struct Biol* **20**: 313–324.

Falkenberg M, Larsson N-G, Gustafsson CM. 2007. DNA replication and transcription in mammalian mitochondria. *Annu Rev Biochem* **76**: 679–699.

Feng Y, Zhang X, Graves P, Zeng Y. 2012. A comprehensive analysis of precursor microRNA cleavage by human Dicer. *Rna* **18**: 2083–2092.

Ferraiuolo MA, Lee C-S, Ler LW, Hsu JL, Costa-Mattioli M, Luo M-J, Reed R, Sonenberg N. 2004. A nuclear translation-like factor eIF4AIII is recruited to the mRNA during splicing and functions in nonsense-mediated decay. *Proc Natl Acad Sci U S A* **101**: 4118–23.

Fiorini F, Bagchi D, Le Hir H, Croquette V. 2015. Human Upf1 is a highly processive RNA helicase and translocase with RNP remodelling activities. *Nat Commun* **6**: 7581.

Fiorini F, Bonneau F, Le Hir H. 2012. Biochemical characterization of the RNA Helicase UPF1 involved in nonsense-mediated mRNA decay. *Methods Enzymol* **511**: 255–274.

Fischer N, Weis K. 2002. The DEAD box protein Dhh1 stimulates the decapping enzyme Dcp1. *EMBO J* **21**: 2788–2797.

Fleckner J, Zhang M, Valcarcel J, Green MR. 1997. U2AF65 recruits a novel human DEAD box protein required for the U2 snRNP-branchpoint interaction. *Genes Dev* **11**: 1864–1872.

Flores-Jasso CF, Arenas-Huertero C, Reyes JL, Contreras-Cubas C, Covarrubias A, Vaca L. 2009. First step in pre-miRNAs processing by human Dicer. *Acta Pharmacol Sin* **30**: 1177–1185.

Fullam A, Schröder M. 2013. DExD/H-box RNA helicases as mediators of anti-viral innate immunity and essential host factors for viral replication. *Biochim Biophys Acta* **1829**: 854–65.

Fuller-Pace F V. 2013. DEAD box RNA helicase functions in cancer. *RNA Biol* **10**: 121–32.

Fuller-Pace F V. 2006. DExD/H box RNA helicases: multifunctional proteins with important roles in transcriptional regulation. *Nucleic Acids Res* **34**: 4206–4215.

Gao F, Zhang P, Zhou C, Li J, Wang Q, Zhu F, Ma C, Sun W, Zhang L. 2007. Frequent loss of PDCD4 expression in human glioma: possible role in the tumorigenesis of glioma. *Oncol Rep* **17**: 123–128.

Gaymes TJ, North PS, Brady N, Hickson ID, Mufti GJ, Rassool F V. 2002. Increased error-prone non homologous DNA end-joining--a proposed mechanism of chromosomal instability in Bloom's syndrome. *Oncogene* **21**: 2525–33.

Geisler S, Coller J. 2013. RNA in unexpected places: long non-coding RNA functions in diverse cellular contexts. *Nat Rev Mol Cell Biol* **14**: 699–712.

George R, Kenyon R, McGuckin A, Malcolm A, Pearson A, Lunec J. 1996. Investigation of co-amplification of the candidate genes ornithine decarboxylase, ribonucleotide reductase, syndecan-1 and a DEAD box gene, DDX1, with N-myc in neuroblastoma. United Kingdom Children's Cancer Study Group. *Oncogene* **12**: 1583–1587.

Gilhooly NS, Gwynn EJ, Dillingham MS. 2013. Superfamily 1 helicases . *Front Biosci (Schol Ed)* **5**: 206–16.

Gillian AL, Svaren J. 2004. The Ddx20/DP103 Dead Box Protein Represses Transcriptional Activation by Egr2/Krox-20. *J Biol Chem* **279**: 9056–9063.

Gitlin L, Barchet W, Gilfillan S, Cella M, Beutler B, Flavell R a, Diamond MS, Colonna M. 2006. Essential role of mda-5 in type I IFN responses to polyriboinosinic:polyribocytidylic acid and encephalomyocarditis picornavirus. *Proc Natl Acad Sci U S A* **103**: 8459–8464.

Godbout R, Packer M, Bie W. 1998. Overexpression of a DEAD box protein (DDX1) in neuroblastoma and retinoblastoma cell lines. *J Biol Chem* **273**: 21161–21168.

Godbout R, Squire J. 1993. Amplification of a DEAD box protein gene in retinoblastoma cell lines. *Proc Natl Acad Sci U S A* **90**: 7578–7582.

Goetze H, Wittner M, Hamperl S, Hondele M, Merz K, Stoeckl U, Griesenbeck J. 2010. Alternative chromatin structures of the 35S rRNA genes in Saccharomyces cerevisiae provide a molecular basis for the selective recruitment of RNA polymerases I and II. *Mol Cell Biol* **30**: 2028–2045.

Gosai SJ, Foley SW, Wang D, Silverman IM, Selamoglu N, Nelson ADL, Beilstein MA, Daldal F, Deal RB, Gregory BD. 2015. Global analysis of the RNA-protein interaction and RNA secondary structure landscapes of the Arabidopsis nucleus. *Mol Cell* **57**: 376–88.

Grainger RJ, Beggs JD. 2005. Prp8 protein: at the heart of the spliceosome. *RNA* **11**: 533–57.

Granneman S, Lin C, Champion EA, Nandineni MR, Zorca C, Baserga SJ. 2006. The nucleolar protein Esf2 interacts directly with the DExD/H box RNA helicase, Dbp8, to stimulate ATP hydrolysis. *Nucleic Acids Res* **34**: 3189–3199.

Grifo J a, Abramson RD, Satler C a, Merrick WC. 1984. RNA-stimulated ATPase activity of eukaryotic initiation factors. *J Biol Chem* **259**: 8648–8654.

Grohman JK, Del Campo M, Bhaskaran H, Tijerina P, Lambowitz AM, Russell R. 2007. Probing the mechanisms of DEAD-box proteins as general RNA chaperones: the C-terminal domain of CYT-19 mediates general recognition of RNA. *Biochemistry* **46**: 3013–22.

Gross CH, Shuman S. 1996. Vaccinia virions lacking the RNA helicase nucleoside triphosphate phosphohydrolase II are defective in early transcription. *J Virol* **70**: 8549–57.

Gross T, Siepmann A, Sturm D, Windgassen M, Scarcelli JJ, Seedorf M, Cole CN, Krebber H. 2007. The DEAD-box RNA helicase Dbp5 functions in translation termination. *Science* **315**: 646–649.

Gu B, Liu C, Lin-Goerke J, Maley DR, Gutshall LL, Feltenberger C a, Del Vecchio a M. 2000. The RNA helicase and nucleotide triphosphatase activities of the bovine viral diarrhea virus NS3 protein are essential for viral replication. *J Virol* **74**: 1794–1800.

Guenther UP, Handoko L, Laggerbauer B, Jablonka S, Chari A, Alzheimer M, Ohmer J, Plöttner O, Gehring N, Sickmann A, et al. 2009. IGHMBP2 is a ribosome-associated helicase inactive in the neuromuscular disorder distal SMA type 1 (DSMA1). *Hum Mol Genet* **18**: 1288–1300.

Gwack Y, Kim DW, Han JH, Choe J. 1997. DNA helicase activity of the hepatitis C virus nonstructural protein 3. *Eur J Biochem* **250**: 47–54.

Gwack Y, Yoo H, Song I, Choe J, Han JH. 1999. RNA-Stimulated ATPase and RNA helicase activities and RNA binding domain of hepatitis G virus nonstructural protein 3. *J Virol* **73**: 2909–2915.

Halbach F, Reichelt P, Rode M, Conti E. 2013. The yeast ski complex: Crystal structure and rna channeling to the exosome complex. *Cell* **154**: 814–826.

Halls C, Mohr S, Del Campo M, Yang Q, Jankowsky E, Lambowitz AM. 2007. Involvement of DEAD-box proteins in group I and group II intron splicing. Biochemical characterization of Mss116p, ATP hydrolysis-dependent and -independent mechanisms, and general RNA chaperone activity. *J Mol Biol* **365**: 835–855.

Harris E, Holden KL, Edgil D, Polacek C, Clyde K. 2006. Molecular biology of flaviviruses. *Novartis Found Symp* **277**: 23–39; discussion 40, 71–3, 251–3.

Hartman TR, Qian S, Bolinger C, Fernandez S, Schoenberg DR, Boris-Lawrie K. 2006. RNA helicase A is necessary for translation of selected messenger RNAs. *Nat Struct Mol Biol* **13**: 509–516.

Hasegawa M, Smith MJ, Iijima M, Tabira T, Goedert M. 1999. FTDP-17 mutations N279K and S305N in tau produce increased splicing of exon 10. *FEBS Lett* **443**: 93–96.

Hashimoto K, Nakagawa Y, Morikawa H, Niki M, Egashira Y, Hirata I, Katsu K, Akao Y. 2001. Co-overexpression of DEAD box protein rck/p54 and c-myc protein in human colorectal adenomas and the relevance of their expression in cultured cell lines. *Carcinogenesis* **22**: 1965–70.

Hata H, Mitsui H, Liu H, Bai Y, Denis CL, Shimizu Y, Sakai A. 1998. Dhh1p, a putative RNA helicase, associates with the general transcription factors Pop2p and Ccr4p from Saccharomyces cerevisiae. *Genetics* **148**: 571–579.

Henn A, Cao W, Hackney DD, De La Cruz EM. 2008. The ATPase cycle mechanism of the DEAD-box rRNA helicase, DbpA. *J Mol Biol* **377**: 193–205.

Henn A, Cao W, Licciardello N, Heitkamp SE, Hackney DD, De La Cruz EM. 2010. Pathway of ATP utilization and duplex rRNA unwinding by the DEAD-box helicase, DbpA. *Proc Natl Acad Sci U S A* **107**: 4046–4050.

Henning D, So RB, Jin R, Lau LF, Valdez BC. 2003. Silencing of RNA helicase II/Gualpha inhibits mammalian ribosomal RNA production. *J Biol Chem* **278**: 52307–14.

Henras AK, Plisson-Chastang C, O'Donohue M-F, Chakraborty A, Gleizes P-E. 2014. An overview of pre-ribosomal RNA processing in eukaryotes. *Wiley Interdiscip Rev RNA* **6**: 225–242.

Herschlag D. 1995. RNA chaperones and the RNA folding problem. *J Biol Chem* **270**: 20871–20874.

Hilbert M, Kebbel F, Gubaev A, Klostermeier D. 2011. eIF4G stimulates the activity of the DEAD box protein eIF4A by a conformational guidance mechanism. *Nucleic Acids Res* **39**: 2260–2270.

Hogbom M, Collins R, van den Berg S, Jenvert RM, Karlberg T, Kotenyova T, Flores A, Karlsson Hedestam GB, Schiavone LH. 2007. Crystal structure of conserved domains 1 and 2 of the human DEAD-box helicase DDX3X in complex with the mononucleotide AMP. *J Mol Biol* **372**: 150–159.

Hornung V, Ellegast J, Kim S, Brzózka K, Jung A, Kato H, Poeck H, Akira S, Conzelmann K-K, Schlee M, et al. 2006. 5’-Triphosphate RNA is the ligand for RIG-I. *Science (80-)* **314**: 994–997.

Houseley J, Tollervey D. 2009. The many pathways of RNA degradation. *Cell* **136**: 763–76.

Hsu CL, Stevens A. 1993. Yeast cells lacking 5’ to 3' exoribonuclease 1 contain mRNA species that are poly(A) deficient and partially lack the 5' cap structure. *Mol Cell Biol* **13**: 4826–35.

Huang H-R, Rowe CE, Mohr S, Jiang Y, Lambowitz AM, Perlman PS. 2005. The splicing of yeast mitochondrial group I and group II introns requires a DEAD-box protein with RNA chaperone function. *Proc Natl Acad Sci U S A* **102**: 163–8.

Huang Y-H, Chung C-S, Kao D-I, Kao T-C, Cheng S-C. 2014. Sad1 counteracts Brr2-mediated dissociation of U4/U6.U5 in tri-snRNP homeostasis. *Mol Cell Biol* **34**: 210–20.

Hutton M, Lendon CL, Rizzu P, Baker M, Froelich S, Houlden H, Pickering-Brown S, Chakraverty S, Isaacs A, Grover A, et al. 1998. Association of missense and 5’-splice-site mutations in tau with the inherited dementia FTDP-17. *Nature* **393**: 702–705.

Isken O, Maquat LE. 2008. The multiple lives of NMD factors: balancing roles in gene and genome regulation. *Nat Rev Genet* **9**: 699–712.

Iyer RR, Pluciennik A, Burdett V, Modrich PL. 2006. DNA mismatch repair: Functions and mechanisms. *Chem Rev* **106**: 302–323.

Jalal C, Uhlmann-Schiffler H, Stahl H. 2007. Redundant role of DEAD box proteins p68 (Ddx5) and p72/p82 (Ddx17) in ribosome biogenesis and cell proliferation. *Nucleic Acids Res* **35**: 3590–3601.

Jankowsky A, Guenther UP, Jankowsky E. 2011. The RNA helicase database. *Nucleic Acids Res* **39**: 1–4.

Jankowsky E. 2011. RNA helicases at work: binding and rearranging. *Trends Biochem Sci* **36**: 19–29.

Jankowsky E, Gross CH, Shuman S, Pyle AM. 2001. Active disruption of an RNA-protein interaction by a DExH/D RNA helicase. *Science (80-)* **291**: 121–125.

Jankowsky E, Gross CH, Shuman S, Pyle AM. 2000. The DExH protein NPH-II is a processive and directional motor for unwinding RNA. *Nature* **403**: 447–51.

Jankowsky E, Jankowsky A. 2000. The DExH/D protein family database. *Nucleic Acids Res* **28**: 333–4.

Jankowsky E, Margaret E, Fairman-Williams. 2010. *Chapter 1: An Introduction to RNA Helicase: Superfamilies, Families, and Major Themes*. ed. E. Jankowsky. Royal Society of Chemistry, Cambridge.

Jarmoskaite I, Russell R. 2014. RNA helicase proteins as chaperones and remodelers. *Annu Rev Biochem* **83**: 697–725.

Jensen ED, Niu L, Caretti G, Nicol SM, Teplyuk N, Stein GS, Sartorelli V, van Wijnen AJ, Fuller-Pace F V, Westendorf JJ. 2008. p68 (Ddx5) interacts with Runx2 and regulates osteoblast differentiation. *J Cell Biochem* **103**: 1438–1451.

Jia H, Wang X, Anderson JT, Jankowsky E. 2012. RNA unwinding by the Trf4/Air2/Mtr4 polyadenylation (TRAMP) complex. *Proc Natl Acad Sci* **109**: 7292–7297.

Johnson SJ, Jackson RN. 2013. Ski2-like RNA helicase structures: common themes and complex assemblies. *RNA Biol* **10**: 33–43.

Johnstone O, Lasko P. 2004. Interaction with eIF5B is essential for Vasa function during development. *Development* **131**: 4167–78.

Jones K, Wei C, Schoser B, Meola G, Timchenko N, Timchenko L. 2015. Reduction of toxic RNAs in myotonic dystrophies type 1 and type 2 by the RNA helicase p68/DDX5. *Proc Natl Acad Sci U S A* **112**: 8041–5.

Jung C, Mittler G, Oswald F, Borggrefe T. 2013. RNA helicase Ddx5 and the noncoding RNA SRA act as coactivators in the Notch signaling pathway. *Biochim Biophys Acta - Mol Cell Res* **1833**: 1180–1189.

Juuti JT, Bamford DH, Tuma R, Thomas Jr. GJ. 1998. Structure and NTPase activity of the RNA-translocating protein (P4) of bacteriophage phi 6. *J Mol Biol* **279**: 347–359.

Kainov DE, Lísal J, Bamford DH, Tuma R. 2004. Packaging motor from double-stranded RNA bacteriophage phi12 acts as an obligatory passive conduit during transcription. *Nucleic Acids Res* **32**: 3515–21.

Kainov DE, Pirttimaa M, Tuma R, Butcher SJ, Thomas GJ, Bamford DH, Makeyev E V. 2003. RNA packaging device of double-stranded RNA bacteriophages, possibly as simple as hexamer of P4 protein. *J Biol Chem* **278**: 48084–91.

Kar A, Fushimi K, Zhou X, Ray P, Shi C, Chen X, Liu Z, Chen S, Wu JY. 2011. RNA helicase p68 (DDX5) regulates tau exon 10 splicing by modulating a stem-loop structure at the 5' splice site. *Mol Cell Biol* **31**: 1812–1821.

Karginov F V, Caruthers JM, Hu Y, McKay DB, Uhlenbeck OC. 2005. YxiN is a modular protein combining a DEx(D/H) core and a specific RNA-binding domain. *J Biol Chem* **280**: 35499–505.

Kasten MM, Clapier CR, Cairns BR. 2011. SnapShot: Chromatin remodeling: SWI/SNF. *Cell* **144**: 310.e1.

Kato H, Takeuchi O, Sato S, Yoneyama M, Yamamoto M, Matsui K, Uematsu S, Jung A, Kawai T, Ishii KJ, et al. 2006. Differential roles of MDA5 and RIG-I helicases in the recognition of RNA viruses. *Nature* **441**: 101–5.

Kawaoka J, Pyle AM. 2005. Choosing between DNA and RNA: the polymer specificity of RNA helicase NPH-II. *Nucleic Acids Res* **33**: 644–9.

Kebaara BW, Atkin AL. 2009. Long 3'-UTRs target wild-type mRNAs for nonsense-mediated mRNA decay in Saccharomyces cerevisiae. *Nucleic Acids Res* **37**: 2771–8.

Kim DH, Rossi JJ. 1999. The first ATPase domain of the yeast 246-kDa protein is required for in vivo unwinding of the U4/U6 duplex. *RNA* **5**: 959–71.

Kim H-D, Choe J, Seo Y-S. 1999. The sen1 + Gene of Schizosaccharomyces pombe , a Homologue of Budding Yeast SEN1, Encodes an RNA and DNA Helicase †. *Biochemistry* **38**: 14697–14710.

Kim M, Vasiljeva L, Rando OJ, Zhelkovsky A, Moore C, Buratowski S. 2006. Distinct Pathways for snoRNA and mRNA Termination. *Mol Cell* **24**: 723–734.

Kim S, Smith J, Claude A, Lin R. 1992. The purified yeast pre-mRNA splicing factor PRP2 is an RNA-dependent NTPase. *EMBO J* **1**: 2319–2326.

Kistler AL, Guthrie C. 2001. Deletion of MUD2, the yeast homolog of U2AF65, can bypass the requirement for Sub2, an essential spliceosomal ATPase. *Genes Dev* **15**: 42–49.

Kolykhalov AA, Mihalik K, Feinstone SM, Rice CM. 2000. Hepatitis C virus-encoded enzymatic activities and conserved RNA elements in the 3' nontranslated region are essential for virus replication in vivo. *J Virol* **74**: 2046–51.

Kong K-YE, Tang H-MV, Pan K, Huang Z, Lee T-HJ, Hinnebusch AG, Jin D-Y, Wong C-M. 2014. Cotranscriptional recruitment of yeast TRAMP complex to intronic sequences promotes optimal pre-mRNA splicing. *Nucleic Acids Res* **42**: 643–60.

Koodathingal P, Staley JP. 2014. Splicing fidelity. *RNA Biol* **10**: 1073–1079.

Kossen K, Karginov F V, Uhlenbeck OC. 2002. The carboxy-terminal domain of the DExDH protein YxiN is sufficient to confer specificity for 23S rRNA. *J Mol Biol* **324**: 625–36.

Kressler D, de la Cruz J, Rojo M, Linder P. 1998. Dbp6p is an essential putative ATP-dependent RNA helicase required for 60S-ribosomal-subunit assembly in Saccharomyces cerevisiae. *Mol Cell Biol* **18**: 1855–65.

Kressler D, de la Cruz J, Rojo M, Linder P. 1997. Fal1p is an essential DEAD-box protein involved in 40S-ribosomal-subunit biogenesis in Saccharomyces cerevisiae. *Mol Cell Biol* **17**: 7283–94.

Kuramitsu Y, Suenaga S, Wang Y, Tokuda K, Kitagawa T, Tanaka T, Akada J, Maehara S-I, Maehara Y, Nakamura K. 2013. Up-regulation of DDX39 in human pancreatic cancer cells with acquired gemcitabine resistance compared to gemcitabine-sensitive parental cells. *Anticancer Res* **33**: 3133–6.

Labib K, Tercero J a, Diffley JF. 2000. Uninterrupted MCM2-7 function required for DNA replication fork progression. *Science* **288**: 1643–1647.

Laggerbauer B, Achsel T, Lührmann R. 1998. The human U5-200kD DEXH-box protein unwinds U4/U6 RNA duplices in vitro. *Proc Natl Acad Sci U S A* **95**: 4188–92.

Laín S, Martín MT, Riechmann JL, García JA. 1991. Novel catalytic activity associated with positive-strand RNA virus infection: nucleic acid-stimulated ATPase activity of the plum pox potyvirus helicaselike protein. *J Virol* **65**: 1–6.

Lamanna AC, Karbstein K. 2011. An RNA conformational switch regulates pre-18S rRNA cleavage. *J Mol Biol* **405**: 3–17.

Lamm GM, Nicol SM, Fuller-Pace F V., Lamond AL. 1996. P72: A human nuclear DEAD box protein highly related to p68. *Nucleic Acids Res* **24**: 3739–3747.

Lasko P. 2013. The DEAD-box helicase Vasa: evidence for a multiplicity of functions in RNA processes and developmental biology. *Biochim Biophys Acta* **1829**: 810–6.

Laurent FX, Sureau A, Klein AF, Trouslard F, Gasnier E, Furling D, Marie J. 2012. New function for the RNA helicase p68/DDX5 as a modifier of MBNL1 activity on expanded CUG repeats. *Nucleic Acids Res* **40**: 3159–3171.

Lebreton A, Séraphin B. 2008. Exosome-mediated quality control: Substrate recruitment and molecular activity. *Biochim Biophys Acta - Gene Regul Mech* **1779**: 558–565.

Lee CG, Hurwitz J. 1992. A new RNA helicase isolated from HeLa cells that catalytically: Translocates in the 3’ to 5' direction. *J Biol Chem* **267**: 4398–4407.

Lee K-M, Tarn W-Y. 2013. Coupling pre-mRNA processing to transcription on the RNA factory assembly line. *RNA Biol* **10**: 380–90.

Lee TI, Young RA. 2013. Transcriptional regulation and its misregulation in disease. *Cell* **152**: 1237–51.

Leitão AL, Costa MC, Enguita FJ. 2015. Unzippers, resolvers and sensors: a structural and functional biochemistry tale of RNA helicases. *Int J Mol Sci* **16**: 2269–93.

Lejeune F, Maquat LE. 2005. Mechanistic links between nonsense-mediated mRNA decay and pre-mRNA splicing in mammalian cells. *Curr Opin Cell Biol* **17**: 309–15.

Levin MK, Gurjar M, Patel SS. 2005. A Brownian motor mechanism of translocation and strand separation by hepatitis C virus helicase. *Nat Struct Mol Biol* **12**: 429–435.

Liang WQ, Clark JA, Fournier MJ. 1997. The rRNA-processing function of the yeast U14 small nucleolar RNA can be rescued by a conserved RNA helicase-like protein. *Mol Cell Biol* **17**: 4124–32.

Liang X-H, Fournier MJ. 2006. The helicase Has1p is required for snoRNA release from pre-rRNA. *Mol Cell Biol* **26**: 7437–7450.

Linden MH, Hartmann RK, Klostermeier D. 2008. The putative RNase P motif in the DEAD box helicase Hera is dispensable for efficient interaction with RNA and helicase activity. *Nucleic Acids Res* **36**: 5800–5811.

Linder P, Fuller-Pace F V. 2013. Looking back on the birth of DEAD-box RNA helicases. *Biochim Biophys Acta - Gene Regul Mech* **1829**: 750–755.

Linder P, Jankowsky E. 2011. From unwinding to clamping - the DEAD box RNA helicase family. *Nat Rev Mol Cell Biol* **12**: 505–516.

Liu F, Putnam A, Jankowsky E. 2008. ATP hydrolysis is required for DEAD-box protein recycling but not for duplex unwinding. *Proc Natl Acad Sci U S A* **105**: 20209–20214.

Liu Y-C, Cheng S-C. 2015. Functional roles of DExD/H-box RNA helicases in Pre-mRNA splicing. *J Biomed Sci* **22**: 54.

Loh PG, Yang HS, Walsh MA, Wang Q, Wang X, Cheng Z, Liu D, Song H. 2009. Structural basis for translational inhibition by the tumour suppressor Pdcd4. *EMBO J* **28**: 274–285.

Loo YM, Fornek J, Crochet N, Bajwa G, Perwitasari O, Martinez-Sobrido L, Akira S, Gill MA, Garcia-Sastre A, Katze MG, et al. 2008. Distinct RIG-I and MDA5 signaling by RNA viruses in innate immunity. *J Virol* **82**: 335–345.

Lorsch JR, Herschlag D. 1998. The DEAD box protein eIF4A. 2. A cycle of nucleotide and RNA-dependent conformational changes. *Biochemistry* **37**: 2194–2206.

Lowery-Goldhammer C, Richardson JP. 1974. An RNA-dependent nucleoside triphosphate phosphohydrolase (ATPase) associated with rho termination factor. *Proc Natl Acad Sci U S A* **71**: 2003–7.

Lucic B, Zhang Y, King O, Mendoza-Maldonado R, Berti M, Niesen FH, Burgess-Brown N a., Pike ACW, Cooper CDO, Gileadi O, et al. 2011. A prominent beta-hairpin structure in the winged-helix domain of RECQ1 is required for DNA unwinding and oligomer formation. *Nucleic Acids Res* **39**: 1703–1717.

Lund MK, Guthrie C. 2005. The DEAD-box protein Dbp5p is required to dissociate Mex67p from exported mRNPs at the nuclear rim. *Mol Cell* **20**: 645–651.

Luo ML, Zhou Z, Magni K, Christoforides C, Rappsilber J, Mann M, Reed R. 2001. Pre-mRNA splicing and mRNA export linked by direct interactions between UAP56 and Aly. *Nature* **413**: 644–647.

Lykke-Andersen S, Brodersen DE, Jensen TH. 2009. Origins and activities of the eukaryotic exosome. *J Cell Sci* **122**: 1487–1494.

Ma WK, Cloutier SC, Tran EJ. 2013. The DEAD-box protein Dbp2 functions with the RNA-binding protein Yra1 to promote mRNP assembly. *J Mol Biol* **425**: 3824–3838.

Malecki M, Jedrzejczak R, Stepien PP, Golik P. 2007. In vitro Reconstitution and Characterization of the Yeast Mitochondrial Degradosome Complex Unravels Tight Functional Interdependence. *J Mol Biol* **372**: 23–36.

Mallam AL, Del Campo M, Gilman B, Sidote DJ, Lambowitz AM. 2012. Structural basis for RNA-duplex recognition and unwinding by the DEAD-box helicase Mss116p. *Nature* **490**: 121–125.

Mancini EJ, Kainov DE, Grimes JM, Tuma R, Bamford DH, Stuart DI. 2004. Atomic snapshots of an RNA packaging motor reveal conformational changes linking ATP hydrolysis to RNA translocation. *Cell* **118**: 743–755.

Manosas M, Perumal SK, Bianco P, Ritort F, Benkovic SJ, Croquette V. 2013. RecG and UvsW catalyse robust DNA rewinding critical for stalled DNA replication fork rescue. *Nat Commun* **4**: 2368.

Martianov I, Ramadass A, Serra Barros A, Chow N, Akoulitchev A. 2007. Repression of the human dihydrofolate reductase gene by a non-coding interfering transcript. *Nature* **445**: 666–670.

Martin A, Schneider S, Schwer B. 2002. Prp43 is an essential RNA-dependent ATPase required for release of lariat-intron from the spliceosome. *J Biol Chem* **277**: 17743–17750.

Martin R, Straub AU, Doebele C, Bohnsack MT. 2013. DExD/H-box RNA helicases in ribosome biogenesis. *RNA Biol* **10**: 4–18.

Mason PB, Struhl K. 2005. Distinction and relationship between elongation rate and processivity of RNA polymerase II in vivo. *Mol Cell* **17**: 831–840.

Mathys H, Basquin J, Ozgur S, Czarnocki-Cieciura M, Bonneau F, Aartse A, Dziembowski A, Nowotny M, Conti E, Filipowicz W. 2014. Structural and biochemical insights to the role of the CCR4-NOT complex and DDX6 ATPase in microRNA repression. *Mol Cell* **54**: 751–65.

Matusan AE, Pryor MJ, Davidson AD, Wright PJ. 2001. Mutagenesis of the Dengue virus type 2 NS3 protein within and outside helicase motifs: effects on enzyme activity and virus replication. *J Virol* **75**: 9633–9643.

McCaffrey R, St Johnston D, González-Reyes A. 2006. Drosophila mus301/spindle-C encodes a helicase with an essential role in double-strand DNA break repair and meiotic progression. *Genetics* **174**: 1273–85.

McCartney S a, Thackray LB, Gitlin L, Gilfillan S, Virgin HW, Virgin Iv HW, Colonna M. 2008. MDA-5 recognition of a murine norovirus. *PLoS Pathog* **4**: e1000108.

McGlynn P, Al-Deib a a, Liu J, Marians KJ, Lloyd RG. 1997. The DNA replication protein PriA and the recombination protein RecG bind D-loops. *J Mol Biol* **270**: 212–221.

Meister G, Tuschl T. 2004. Mechanisms of gene silencing by double-stranded RNA. *Nature* **431**: 343–349.

Mendell JT, Sharifi N a, Meyers JL, Martinez-Murillo F, Dietz HC. 2004. Nonsense surveillance regulates expression of diverse classes of mammalian transcripts and mutes genomic noise. *Nat Genet* **36**: 1073–1078.

Mendonca VM, Klepin HD, Matson SW. 1995. DNA helicases in recombination and repair: construction of a delta uvrD delta helD delta recQ mutant deficient in recombination and repair. *J Bacteriol* **177**: 1326–35.

Miller OL, Beatty BR. 1969. Visualization of nucleolar genes. *Science* **164**: 955–957.

Min J, Heuertz RM, Zassenhaus HP. 1993. Isolation and characterization of an NTP-dependent 3'-exoribonuclease from mitochondria of Saccharomyces cerevisiae. *J Biol Chem* **268**: 7350–7.

Minshall N, Standart N. 2004. The active form of Xp54 RNA helicase in translational repression is an RNA-mediated oligomer. *Nucleic Acids Res* **32**: 1325–1334.

Miyaji K, Nakagawa Y, Matsumoto K, Yoshida H, Morikawa H, Hongou Y, Arisaka Y, Kojima H, Inoue T, Hirata I, et al. 2003. Overexpression of a DEAD box/RNA helicase protein, rck/p54, in human hepatocytes from patients with hepatitis C virus-related chronic hepatitis and its implication in hepatocellular carcinogenesis. *J Viral Hepat* **10**: 241–8.

Mohr G, Del Campo M, Mohr S, Yang Q, Jia H, Jankowsky E, Lambowitz AM. 2008. Function of the C-terminal domain of the DEAD-box protein Mss116p analyzed in vivo and in vitro. *J Mol Biol* **375**: 1344–1364.

Molnar GM, Crozat A, Kraeft SK, Dou QP, Chen LB, Pardee AB. 1997. Association of the mammalian helicase MAH with the pre-mRNA splicing complex. *Proc Natl Acad Sci U S A* **94**: 7831–6.

Montpetit B, Thomsen ND, Helmke KJ, Seeliger M a, Berger JM, Weis K. 2011. A conserved mechanism of DEAD-box ATPase activation by nucleoporins and InsP6 in mRNA export. *Nature* **472**: 238–242.

Morlang S, Weglöhner W, Franceschi F. 1999. Hera from Thermus thermophilus: the first thermostable DEAD-box helicase with an RNase P protein motif. *J Mol Biol* **294**: 795–805.

Mougey EB, O'Reilly M, Osheim Y, Miller OL, Beyer A, Sollner-Webb B. 1993. The terminal balls characteristic of eukaryotic rRNA transcription units in chromatin spreads are rRNA processing complexes. *Genes Dev* **7**: 1609–1619.

Mozaffari-Jovin S, Santos KF, Hsiao HH, Will CL, Urlaub H, Wahl MC, Lührmann R. 2012. The Prp8 RNase H-like domain inhibits Brr2-mediated U4/U6 snRNA unwinding by blocking Brr2 loading onto the U4 snRNA. *Genes Dev* **26**: 2422–2434.

Mozaffari-Jovin S, Wandersleben T, Santos KF, Will CL, Lührmann R, Wahl MC. 2013. Inhibition of RNA helicase Brr2 by the C-terminal tail of the spliceosomal protein Prp8. *Science* **341**: 80–4.

Mudduluru G, Medved F, Grobholz R, Jost C, Gruber A, Leupold JH, Post S, Jansen A, Colburn NH, Allgayer H. 2007. Loss of programmed cell death 4 expression marks adenoma-carcinoma transition, correlates inversely with phosphorylated protein kinase B, and is an independent prognostic factor in resected colorectal cancer. *Cancer* **110**: 1697–707.

Muhlrad D, Decker CJ, Parker R. 1994. Deadenylation of the unstable mRNA encoded by the yeast MFA2 gene leads to decapping followed by 5' to 3' digestion of the transcript. *Genes Dev* **8**: 855–866.

Myong S, Bruno MM, Pyle AM, Ha T. 2007. Spring-Loaded Mechanism of DNA Unwinding by Heptitis C Virus NS3 Helicase. *Science* **317**: 513–516.

Myong S, Ha T. 2010. Stepwise translocation of nucleic acid motors. *Curr Opin Struct Biol* **20**: 121–127.

Nakagawa T, Flores-Rozas H, Kolodner RD. 2001. The MER3 helicase involved in meiotic crossing over is stimulated by single-stranded DNA-binding proteins and unwinds DNA in the 3’ to 5' direction. *J Biol Chem* **276**: 31487–93.

Nakajima T, Uchida C, Anderson SF, Chee-Gun L, Hurwitz J, Parvin JD, Montminy M. 1997. RNA helicase A mediates association of CBP with RNA polymerase II. *Cell* **90**: 1107–1112.

Nielsen KH, Chamieh H, Andersen CB, Fredslund F, Hamborg K, Le Hir H, Andersen GR. 2009. Mechanism of ATP turnover inhibition in the EJC. *RNA* **15**: 67–75.

Noble CG, Song H. 2007. MLN51 stimulates the RNA-helicase activity of eIF4AIII. *PLoS One* **2**: e303.

Noble KN, Tran EJ, Alcazar-Roman AR, Hodge CA, Cole CN, Wente SR. 2011. The Dbp5 cycle at the nuclear pore complex during mRNA export II: nucleotide cycling and mRNP remodeling by Dbp5 are controlled by Nup159 and Gle1. *Genes Dev* **25**: 1065–1077.

O’Day CL, Chavanikamannil F, Abelson J. 1996a. 18S rRNA processing requires the RNA helicase-like protein Rrp3. *Nucleic Acids Res* **24**: 3201–7.

O’Day CL, Dalbadie-McFarland G, Abelson J. 1996b. The Saccharomyces cerevisiae Prp5 protein has RNA-dependent ATPase activity with specificity for U2 small nuclear RNA. *J Biol Chem* **271**: 33261–33267.

Ogilvie VC, Wilson BJ, Nicol SM, Morrice NA, Saunders LR, Barber GN, Fuller-Pace F V. 2003. The highly related DEAD box RNA helicases p68 and p72 exist as heterodimers in cells. *Nucleic Acids Res* **31**: 1470–1480.

Okamura M, Inose H, Masuda S. 2015. RNA Export through the NPC in Eukaryotes. *Genes (Basel)* **6**: 124–49.

Opresko PL, Mason P a., Podell ER, Lei M, Hickson ID, Cech TR, Bohr V a. 2005. POT1 stimulates RecQ helicases WRN and BLM to unwind telomeric DNA substrates. *J Biol Chem* **280**: 32069–32080.

Pakotiprapha D, Samuels M, Shen K, Hu JH, Jeruzalmi D. 2012. Structure and mechanism of the UvrA–UvrB DNA damage sensor. *Nat Struct Mol Biol* **19**: 291–298.

Palacios IM, Gatfield D, Johnston DS, Izaurralde E. 2004. An eIF4AIII-containing complex required for mRNA localization and nonsense-mediated mRNA decay. *Nature* **427**: 753–757.

Pan C, Russell R. 2010. Roles of DEAD-box proteins in RNA and RNP Folding. *RNA Biol* **7**: 667–676.

Pan T, Artsimovitch I, Fang XW, Landick R, Sosnick TR. 1999. Folding of a large ribozyme during transcription and the effect of the elongation factor NusA. *Proc Natl Acad Sci U S A* **96**: 9545–9550.

Pang PS, Jankowsky E, Planet PJ, Pyle AM. 2002. The hepatitis C viral NS3 protein is a processive DNA helicase with cofactor enhanced RNA unwinding. *EMBO J* **21**: 1168–1176.

Parker R. 2012. RNA degradation in Saccharomyces cerevisae. *Genetics* **191**: 671–702.

Parvatiyar K, Zhang Z, Teles RM, Ouyang S, Jiang Y, Iyer SS, Zaver SA, Schenk M, Zeng S, Zhong W, et al. 2012. The helicase DDX41 recognizes the bacterial secondary messengers cyclic di-GMP and cyclic di-AMP to activate a type I interferon immune response. *Nat Immunol* **13**: 1155–61.

Patel SS, Donmez I. 2006. Mechanisms of helicases. *J Biol Chem* **281**: 18265–18268.

Patel SS, Picha KM. 2000. Structure and function of hexameric helicases. *Annu Rev Biochem* **69**: 651–697.

Pena V, Jovin SM, Fabrizio P, Orlowski J, Bujnicki JM, Lührmann R, Wahl MC. 2009. Common Design Principles in the Spliceosomal RNA Helicase Brr2 and in the Hel308 DNA Helicase. *Mol Cell* **35**: 454–466.

Pereira M, Mason P, Szczesny RJ, Maddukuri L, Dziwura S, Jedrzejczak R, Paul E, Wojcik A, Dybczynska L, Tudek B, et al. 2001. Interaction of human SUV3 RNA/DNA helicase with BLM helicase; loss of the SUV3 gene results in mouse embryonic lethality. *Mech Ageing Dev* **128**: 609–17.

Perriman R, Barta I, Voeltz GK, Abelson J, Ares Jr. M. 2003. ATP requirement for Prp5p function is determined by Cus2p and the structure of U2 small nuclear RNA. *Proc Natl Acad Sci U S A* **100**: 13857–13862.

Perriman RJ, Ares M. 2007. Rearrangement of competing U2 RNA helices within the spliceosome promotes multiple steps in splicing. *Genes Dev* **21**: 811–20.

Pichlmair A, Schulz O, Tan CP, Naslund TI, Liljestrom P, Weber F, Reis e Sousa C, Näslund TI, Liljeström P. 2006. RIG-I-mediated antiviral responses to single-stranded RNA bearing 5'-phosphates. *Science (80-)* **314**: 997–1001.

Plumet S, Herschke F, Bourhis J-M, Valentin H, Longhi S, Gerlier D. 2007. Cytosolic 5'-triphosphate ended viral leader transcript of measles virus as activator of the RIG I-mediated interferon response. *PLoS One* **2**: e279.

Polach KJ, Uhlenbeck OC. 2002. Cooperative binding of ATP and RNA substrates to the DEAD/H protein DbpA. *Biochemistry* **41**: 3693–702.

Poranen MM, Butcher SJ, Simonov VM, Laurinmäki P, Bamford DH. 2008. Roles of the minor capsid protein P7 in the assembly and replication of double-stranded RNA bacteriophage phi6. *J Mol Biol* **383**: 529–38.

Poranen MM, Tuma R. 2004. Self-assembly of double-stranded RNA bacteriophages. *Virus Res* **101**: 93–100.

Porrua O, Libri D. 2013. A bacterial-like mechanism for transcription termination by the Sen1p helicase in budding yeast. *Nat Struct Mol Biol* **20**: 884–91.

Putnam AA, Gao Z, Liu F, Jia H, Yang Q, Jankowsky E. 2015. Division of Labor in an Oligomer of the DEAD-Box RNA Helicase Ded1p. *Mol Cell* **59**: 541–52.

Putnam AA, Jankowsky E. 2013a. AMP sensing by DEAD-box RNA helicases. *J Mol Biol* **425**: 3839–3845.

Putnam AA, Jankowsky E. 2013b. DEAD-box helicases as integrators of RNA, nucleotide and protein binding. *Biochim Biophys Acta* **1829**: 884–893.

Pyle AM. 2008. Translocation and unwinding mechanisms of RNA and DNA helicases. *Annu Rev Biophys* **37**: 317–336.

Rabhi M, Gocheva V, Jacquinot F, Lee A, Margeat E, Boudvillain M. 2011. Mutagenesis-based evidence for an asymmetric configuration of the ring-shaped transcription termination factor Rho. *J Mol Biol* **405**: 497–518.

Rabhi M, Tuma R, Boudvillain M. 2010. RNA remodeling by hexameric RNA helicases. *RNA Biol* **7**: 655–666.

Raghunathan PL, Guthrie C. 1998. RNA unwinding in U4/U6 snRNPs requires ATP hydrolysis and the DEIH-box splicing factor Brr2. *Curr Biol* **8**: 847–55.

Rasmussen TP, Culbertson MR. 1998. The putative nucleic acid helicase Sen1p is required for formation and stability of termini and for maximal rates of synthesis and levels of accumulation of small nucleolar RNAs in Saccharomyces cerevisiae. *Mol Cell Biol* **18**: 6885–96.

Rinn JL, Chang HY. 2012. Genome regulation by long noncoding RNAs. *Annu Rev Biochem* **81**: 145–166.

Ripmaster TL, Vaughn GP, Woolford JL. 1993. DRS1 to DRS7, novel genes required for ribosome assembly and function in Saccharomyces cerevisiae. *Mol Cell Biol* **13**: 7901–7912.

Robb GB, Rana TM. 2007. RNA Helicase A Interacts with RISC in Human Cells and Functions in RISC Loading. *Mol Cell* **26**: 523–537.

Rogers Jr. GW, Richter NJ, Lima WF, Merrick WC. 2001. Modulation of the helicase activity of eIF4A by eIF4B, eIF4H, and eIF4F. *J Biol Chem* **276**: 30914–30922.

Rorbach J, Minczuk M. 2012. The post-transcriptional life of mammalian mitochondrial RNA. *Biochem J* **444**: 357–373.

Roscigno RF, Garcia-Blanco MA. 1995. SR proteins escort the U4/U6.U5 tri-snRNP to the spliceosome. *RNA* **1**: 692–706.

Rössler OG, Straka A, Stahl H. 2001. Rearrangement of structured RNA via branch migration structures catalysed by the highly related DEAD-box proteins p68 and p72. *Nucleic Acids Res* **29**: 2088–2096.

Rouskin S, Zubradt M, Washietl S, Kellis M, Weissman JS. 2014. Genome-wide probing of RNA structure reveals active unfolding of mRNA structures in vivo. *Nature* **505**: 701–705.

Rozen F, Edery I, Meerovitch K, Dever TE, Merrick WC, Sonenberg N. 1990. Bidirectional RNA helicase activity of eucaryotic translation initiation factors 4A and 4F. *Mol Cell Biol* **10**: 1134–1144.

Rudolph MG, Heissmann R, Wittmann JG, Klostermeier D. 2006. Crystal structure and nucleotide binding of the Thermus thermophilus RNA helicase Hera N-terminal domain. *J Mol Biol* **361**: 731–743.

Rudolph MG, Klostermeier D. 2015. When core competence is not enough: functional interplay of the DEAD-box helicase core with ancillary domains and auxiliary factors in RNA binding and unwinding. *Biol Chem* **396**: 849–65.

Saikrishnan K, Griffiths SP, Cook N, Court R, Wigley DB. 2008. DNA binding to RecD: role of the 1B domain in SF1B helicase activity. *EMBO J* **27**: 2222–2229.

Samatanga B, Klostermeier D. 2014. DEAD-box RNA helicase domains exhibit a continuum between complete functional independence and high thermodynamic coupling in nucleotide and RNA duplex recognition. *Nucleic Acids Res* **42**: 1–11.

Sanjuán R, Marín I. 2001. Tracing the origin of the compensasome: evolutionary history of DEAH helicase and MYST acetyltransferase gene families. *Mol Biol Evol* **18**: 330–343.

Sardana R, Liu X, Granneman S, Zhu J, Gill M, Papoulas O, Marcotte EM, Tollervey D, Correll CC, Johnson AW. 2015. The DEAH-box helicase Dhr1 dissociates U3 from the pre-rRNA to promote formation of the central pseudoknot. *PLoS Biol* **13**: e1002083.

Scheffner M, Knippers R, Stahl H. 1989. RNA unwinding activity of SV40 large T antigen. *Cell* **57**: 955–963.

Schmidt U, Lehmann K, Stahl U. 2002. A novel mitochondrial DEAD box protein (Mrh4) required for maintenance of mtDNA in Saccharomyces cerevisiae. *FEMS Yeast Res* **2**: 267–76.

Schröder M. 2010. Human DEAD-box protein 3 has multiple functions in gene regulation and cell cycle control and is a prime target for viral manipulation. *Biochem Pharmacol* **79**: 297–306.

Schutz P, Bumann M, Oberholzer AE, Bieniossek C, Trachsel H, Altmann M, Baumann U. 2008. Crystal structure of the yeast eIF4A-eIF4G complex: an RNA-helicase controlled by protein-protein interactions. *Proc Natl Acad Sci U S A* **105**: 9564–9569.

Schwartz A, Margeat E, Rahmouni a R, Boudvillain M. 2007. Transcription termination factor rho can displace streptavidin from biotinylated RNA. *J Biol Chem* **282**: 31469–31476.

Schwer B, Guthrie C. 1991. PRP16 is an RNA-dependent ATPase that interacts transiently with the spliceosome. *Nature* **349**: 494–9.

Sen ND, Zhou F, Ingolia NT, Hinnebusch AG. 2015. Genome-wide analysis of translational efficiency reveals distinct but overlapping functions of yeast DEAD-box RNA helicases Ded1 and eIF4A. *Genome Res* **25**: 1196–205.

Sengoku T, Nureki O, Nakamura A, Kobayashi S, Yokoyama S. 2006. Structural basis for RNA unwinding by the DEAD-box protein Drosophila Vasa. *Cell* **125**: 287–300.

Sharif H, Ozgur S, Sharma K, Basquin C, Urlaub H, Conti E. 2013. Structural analysis of the yeast Dhh1-Pat1 complex reveals how Dhh1 engages Pat1, Edc3 and RNA in mutually exclusive interactions. *Nucleic Acids Res* **41**: 8377–90.

Shen H, Zheng X, Shen J, Zhang L, Zhao R, Green MR. 2008. Distinct activities of the DExD/H-box splicing factor hUAP56 facilitate stepwise assembly of the spliceosome. *Genes Dev* **22**: 1796–803.

Shen J, Zhang L, Zhao R. 2007. Biochemical characterization of the ATPase and helicase activity of UAP56, an essential pre-mRNA splicing and mRNA export factor. *J Biol Chem* **282**: 22544–22550.

Sheth U, Parker R. 2003. Decapping and decay of messenger RNA occur in cytoplasmic processing bodies. *Science* **300**: 805–8.

Shibuya T, Tange TØ, Sonenberg N, Moore MJ. 2004. eIF4AIII binds spliced mRNA in the exon junction complex and is essential for nonsense-mediated decay. *Nat Struct Mol Biol* **11**: 346–51.

Shieh S-Y, Stellrecht CMM, Tsai M-J. 1995. Molecular Characterization of the Rat Insulin Enhancer-binding Complex 3b2. *J Biol Chem* **270**: 21503–21508.

Shin S, Rossow KL, Grande JP, Janknecht R. 2007. Involvement of RNA helicases p68 and p72 in colon cancer. *Cancer Res* **67**: 7572–7578.

Shu Z, Vijayakumar S, Chen C-F, Chen P-L, Lee W-H. 2004. Purified human SUV3p exhibits multiple-substrate unwinding activity upon conformational change. *Biochemistry* **43**: 4781–4790.

Shuman S. 1992. Vaccinia virus RNA helicase: an essential enzyme related to the DE-H family of RNA-dependent NTPases. *Proc Natl Acad Sci U S A* **89**: 10935–10939.

Shuman S. 1993. Vaccinia virus RNA helicase. Directionality and substrate specificity. *J Biol Chem* **268**: 11798–11802.

Sigova AA, Abraham BJ, Ji X, Molinie B, Hannett NM, Guo YE, Jangi M, Giallourakis CC, Sharp PA, Young RA. 2015. Transcription factor trapping by RNA in gene regulatory elements. *Science (80-).*

Singleton MR, Dillingham MS, Wigley DB. 2007. Structure and mechanism of helicases and nucleic acid translocases. *Annu Rev Biochem* **76**: 23–50.

Skordalakes E, Berger JM. 2003. Structure of the Rho transcription terminator: mechanism of mRNA recognition and helicase loading. *Cell* **114**: 135–46.

Small EC, Leggett SR, Winans AA, Staley JP. 2006. The EF-G-like GTPase Snu114p regulates spliceosome dynamics mediated by Brr2p, a DExD/H box ATPase. *Mol Cell* **23**: 389–99.

Solem A, Zingler N, Pyle AM. 2006. A DEAD protein that activates intron self-splicing without unwinding RNA. *Mol Cell* **24**: 611–617.

Soulat D, Bürckstümmer T, Westermayer S, Goncalves A, Bauch A, Stefanovic A, Hantschel O, Bennett KL, Decker T, Superti-Furga G. 2008. The DEAD-box helicase DDX3X is a critical component of the TANK-binding kinase 1-dependent innate immune response. *EMBO J* **27**: 2135–2146.

Speroni S, De Colibus L, Mastrangelo E, Gould E, Coutard B, Forrester NL, Blanc S, Canard B, Mattevi A. 2008. Structure and biochemical analysis of Kokobera virus helicase. *Proteins* **70**: 1120–3.

Spitale RC, Tsai MC, Chang HY. 2011. RNA templating the epigenome: Long noncoding RNAs as molecular scaffolds. *Epigenetics* **6**: 539–543.

Stahl H, Dröge P, Knippers R. 1986. DNA helicase activity of SV40 large tumor antigen. *EMBO J* **5**: 1939–1944.

Staley JP, Guthrie C. 1999. An RNA switch at the 5' splice site requires ATP and the DEAD box protein Prp28p. *Mol Cell* **3**: 55–64.

Steiger M, Carr-Schmid A, Schwartz DC, Kiledjian M, Parker R. 2003. Analysis of recombinant yeast decapping enzyme. *RNA* **9**: 231–8.

Steimer L, Klostermeier D. 2012. RNA helicases in infection and disease. *RNA Biol* **9**: 751–771.

Steinmetz EJ, Conrad NK, Brow DA, Corden JL. 2001. RNA-binding protein Nrd1 directs poly(A)-independent 3'-end formation of RNA polymerase II transcripts. *Nature* **413**: 327–31.

Strässer K, Hurt E. 2001. Splicing factor Sub2p is required for nuclear mRNA export through its interaction with Yra1p. *Nature* **413**: 648–652.

Strunk BS, Karbstein K. 2009. Powering through ribosome assembly. *RNA* **15**: 2083–2104.

Sugiura T, Nagano Y, Noguchi Y. 2007. DDX39, upregulated in lung squamous cell cancer, displays RNA helicase activities and promotes cancer cell growth. *Cancer Biol Ther* **6**: 957–964.

Suzich J a, Tamura JK, Palmer-Hill F, Warrener P, Grakoui a, Rice CM, Feinstone SM, Collett MS. 1993. Hepatitis C virus NS3 protein polynucleotide-stimulated nucleoside triphosphatase and comparison with the related pestivirus and flavivirus enzymes. *J Virol* **67**: 6152–8.

Svitkin Y V, Pause a, Haghighat a, Pyronnet S, Witherell G, Belsham GJ, Sonenberg N. 2001. The requirement for eukaryotic initiation factor 4A (elF4A) in translation is in direct proportion to the degree of mRNA 5' secondary structure. *RNA* **7**: 382–394.

Swisher KD, Parker R. 2010. Localization to, and effects of Pbp1, Pbp4, Lsm12, Dhh1, and Pab1 on stress granules in Saccharomyces cerevisiae. *PLoS One* **5**: e10006.

Szczelkun MD. 2000. How to proteins move along DNA? Lessons from type-I and type-III restriction endonucleases. *Essays Biochem* **35**: 131–143.

Szczesny RJ, Borowski LS, Brzezniak LK, Dmochowska A, Gewartowski K, Bartnik E, Stepien PP. 2010. Human mitochondrial RNA turnover caught in flagranti: involvement of hSuv3p helicase in RNA surveillance. *Nucleic Acids Res* **38**: 279–298.

Taanman JW. 1999. The mitochondrial genome: structure, transcription, translation and replication. *Biochim Biophys Acta* **1410**: 103–123.

Takahasi K, Yoneyama M, Nishihori T, Hirai R, Kumeta H, Narita R, Gale Jr. M, Inagaki F, Fujita T, Gale M. 2008. Nonself RNA-sensing mechanism of RIG-I helicase and activation of antiviral immune responses. *Mol Cell* **29**: 428–440.

Tanaka N, Aronova A, Schwer B. 2007. Ntr1 activates the Prp43 helicase to trigger release of lariat-intron from the spliceosome. *Genes Dev* **21**: 2312–2325.

Tanaka N, Schwer B. 2005. Characterization of the NTPase, RNA-binding, and RNA helicase activities of the DEAH-box splicing factor Prp22. *Biochemistry* **44**: 9795–9803.

Tanaka N, Schwer B. 2006. Mutations in PRP43 that uncouple RNA-dependent NTPase activity and pre-mRNA splicing function. *Biochemistry* **45**: 6510–6521.

Tanner NK, Cordin O, Banroques J, Doère M, Linder P. 2003. The Q motif: a newly identified motif in DEAD box helicases may regulate ATP binding and hydrolysis. *Mol Cell* **11**: 127–138.

Taylor LL, Jackson RN, Rexhepaj M, King AK, Lott LK, van Hoof A, Johnson SJ. 2014. The Mtr4 ratchet helix and arch domain both function to promote RNA unwinding. *Nucleic Acids Res* 1–12.

Theissen B, Karow AR, Köhler J, Gubaev A, Klostermeier D. 2008. Cooperative binding of ATP and RNA induces a closed conformation in a DEAD box RNA helicase. *Proc Natl Acad Sci U S A* **105**: 548–553.

Thomson E, Ferreira-Cerca S, Hurt E. 2013. Eukaryotic ribosome biogenesis at a glance. *J Cell Sci* **126**: 4815–21.

Tran EJ, Zhou Y, Corbett AH, Wente SR. 2007. The DEAD-box protein Dbp5 controls mRNA export by triggering specific RNA:protein remodeling events. *Mol Cell* **28**: 850–859.

Tran H, Schilling M, Wirbelauer C, Hess D, Nagamine Y. 2004. Facilitation of mRNA Deadenylation and Decay by the Exosome-Bound, DExH Protein RHAU. *Mol Cell* **13**: 101–111.

Tsai M-C, Manor O, Wan Y, Mosammaparast N, Wang JK, Lan F, Shi Y, Segal E, Chang HY. 2010. Long noncoding RNA as modular scaffold of histone modification complexes. *Science* **329**: 689–693.

Tsu CA, Kossen K, Uhlenbeck OC. 2001. The Escherichia coli DEAD protein DbpA recognizes a small RNA hairpin in 23S rRNA. *RNA* **7**: 702–709.

Uhlmann-Schiffler H, Jalal C, Stahl H. 2006. Ddx42p--a human DEAD box protein with RNA chaperone activities. *Nucleic Acids Res* **34**: 10–22.

Uhlmann-Schiffler H, Seinsoth S, Stahl H. 2002. Preformed hexamers of SV40 T antigen are active in RNA and origin-DNA unwinding. *Nucleic Acids Res* **30**: 3192–201.

Umate P, Tuteja N, Tuteja R. 2011. Genome-wide comprehensive analysis of human helicases. *Commun Integr Biol* **4**: 1–20.

Valgardsdottir R, Brede G, Eide LG, Frengen E, Prydz H. 2001. Cloning and characterization of MDDX28, a putative dead-box helicase with mitochondrial and nuclear localization. *J Biol Chem* **276**: 32056–63.

Van Dijk E, Cougot N, Meyer S, Babajko S, Wahle E, Séraphin B. 2002. Human Dcp2: A catalytically active mRNA decapping enzyme located in specific cytoplasmic structures. *EMBO J* **21**: 6915–6924.

van Hoof A, Staples RR, Baker RE, Parker R. 2000. Function of the ski4p (Csl4p) and Ski7p proteins in 3’-to-5' degradation of mRNA. *Mol Cell Biol* **20**: 8230–43.

Vanacova S, Stefl R. 2007. The exosome and RNA quality control in the nucleus. *EMBO Rep* **8**: 651–657.

Vance KW, Ponting CP. 2014. Transcriptional regulatory functions of nuclear long noncoding RNAs. *Trends Genet* **30**: 348–355.

Venema J, Bousquet-Antonelli C, Gelugne JP, Caizergues-Ferrer M, Tollervey D. 1997. Rok1p is a putative RNA helicase required for rRNA processing. *Mol Cell Biol* **17**: 3398–3407.

Venkatesh S, Workman JL. 2015. Histone exchange, chromatin structure and the regulation of transcription. *Nat Rev Mol Cell Biol* **16**: 178–189.

von Moeller H, Basquin C, Conti E. 2009. The mRNA export protein DBP5 binds RNA and the cytoplasmic nucleoporin NUP214 in a mutually exclusive manner. *Nat Struct Mol Biol* **16**: 247–254.

Wagner JD, Jankowsky E, Company M, Pyle AM, Abelson JN. 1998. The DEAH-box protein PRP22 is an ATPase that mediates ATP-dependent mRNA release from the spliceosome and unwinds RNA duplexes. *EMBO J* **17**: 2926–37.

Walbott H, Mouffok S, Capeyrou R, Lebaron S, Humbert O, van Tilbeurgh H, Henry Y, Leulliot N. 2010. Prp43p contains a processive helicase structural architecture with a specific regulatory domain. *EMBO J* **29**: 2194–2204.

Wan Y, Qu K, Zhang QC, Flynn R a, Manor O, Ouyang Z, Zhang J, Spitale RC, Snyder MP, Segal E, et al. 2014. Landscape and variation of RNA secondary structure across the human transcriptome. *Nature* **505**: 706–9.

Wang L, Lewis MS, Johnson AW. 2005. Domain interactions within the Ski2/3/8 complex and between the Ski complex and Ski7p. *RNA* **11**: 1291–302.

Wang Q, Zhang L, Lynn B, Rymond BC. 2008. A BBP-Mud2p heterodimer mediates branchpoint recognition and influences splicing substrate abundance in budding yeast. *Nucleic Acids Res* **36**: 2787–2798.

Wang R, Jiao Z, Li R, Yue H, Chen L. 2012. p68 RNA helicase promotes glioma cell proliferation in vitro and in vivo via direct regulation of NF-κB transcription factor p50. *Neuro Oncol* **14**: 1116–24.

Wang Y, Guthrie C. 1998. PRP16, a DEAH-box RNA helicase, is recruited to the spliceosome primarily via its nonconserved N-terminal domain. *RNA* **4**: 1216–29.

Wang Y, Wagner JD, Guthrie C. 1998. The DEAH-box splicing factor Prp16 unwinds RNA duplexes in vitro. *Curr Biol* **8**: 441–51.

Warf MB, Berglund JA. 2007. MBNL binds similar RNA structures in the CUG repeats of myotonic dystrophy and its pre-mRNA substrate cardiac troponin T. *RNA* **13**: 2238–2251.

Watkins NJ, Bohnsack MT. 2012. The box C/D and H/ACA snoRNPs: key players in the modification, processing and the dynamic folding of ribosomal RNA. *Wiley Interdiscip Rev RNA* **3**: 397–414.

Weaver PL, Sun C, Chang TH. 1997. Dbp3p, a putative RNA helicase in Saccharomyces cerevisiae, is required for efficient pre-rRNA processing predominantly at site A3. *Mol Cell Biol* **17**: 1354–65.

Weirich CS, Erzberger JP, Berger JM, Weis K. 2004. The N-terminal domain of Nup159 forms a beta-propeller that functions in mRNA export by tethering the helicase Dbp5 to the nuclear pore. *Mol Cell* **16**: 749–60.

Weirich CS, Erzberger JP, Flick JS, Berger JM, Thorner J, Weis K. 2006. Activation of the DExD/H-box protein Dbp5 by the nuclear-pore protein Gle1 and its coactivator InsP6 is required for mRNA export. *Nat Cell Biol* **8**: 668–676.

Wen YH, Shi X, Chiriboga L, Matsahashi S, Yee H, Afonja O. 2007. Alterations in the expression of PDCD4 in ductal carcinoma of the breast. *Oncol Rep* **18**: 1387–1393.

Weng Y, Czaplinski K, Peltz SW. 1998. ATP is a cofactor of the Upf1 protein that modulates its translation termination and RNA binding activities. *RNA* **4**: 205–14.

Weng Y, Czaplinski K, Peltz SW. 1996. Identification and characterization of mutations in the UPF1 gene that affect nonsense suppression and the formation of the Upf protein complex but not mRNA turnover. *Mol Cell Biol* **16**: 5491–5506.

Wengler G, Czaya G, Färber PM, Hegemann JH. 1991. In vitro synthesis of West Nile virus proteins indicates that the amino-terminal segment of the NS3 protein contains the active centre of the protease which cleaves the viral polyprotein after multiple basic amino acids. *J Gen Virol* **72 (Pt 4)**: 851–8.

West SC. 1996. The RuvABC proteins and Holliday junction processing in Escherichia coli. *J Bacteriol* **178**: 1237–41.

Wilson BJ, Bates GJ, Nicol SM, Gregory DJ, Perkins ND, Fuller-Pace F V. 2004. The p68 and p72 DEAD box RNA helicases interact with HDAC1 and repress transcription in a promoter-specific manner. *BMC Mol Biol* **5**: 11.

Wilson WA, Hawley SA, Hardie DG. 1996. Glucose repression/derepression in budding yeast: SNF1 protein kinase is activated by phosphorylation under derepressing conditions, and this correlates with a high AMP:ATP ratio. *Curr Biol* **6**: 1426–1434.

Wong AM-L, Allcock RJN, Cheong KYM, Christiansen FT, Price P. 2003. Alleles of the proximal promoter of BAT1, a putative anti-inflammatory gene adjacent to the TNF cluster, reduce transcription on a disease-associated MHC haplotype. *Genes Cells* **8**: 403–12.

Wong T, Sosnick TR, Pan T. 2005. Mechanistic insights on the folding of a large ribozyme during transcription. *Biochemistry* **44**: 7535–7542.

Wortham NC, Ahamed E, Nicol SM, Thomas RS, Periyasamy M, Jiang J, Ochocka AM, Shousha S, Huson L, Bray SE, et al. 2009. The DEAD-box protein p72 regulates ERalpha-/oestrogen-dependent transcription and cell growth, and is associated with improved survival in ERalpha-positive breast cancer. *Oncogene* **28**: 4053–4064.

Xu D, Nouraini S, Field D, Tang SJ, Friesen JD. 1996. An RNA-dependent ATPase associated with U2/U6 snRNAs in pre-mRNA splicing. *Nature* **381**: 709–13.

Yan X, Mouillet J-F, Ou Q, Sadovsky Y. 2003. A Novel Domain within the DEAD-Box Protein DP103 Is Essential for Transcriptional Repression and Helicase Activity. *Mol Cell Biol* **23**: 414–423.

Yang Q, Del Campo M, Lambowitz AM, Jankowsky E. 2007. DEAD-box proteins unwind duplexes by local strand separation. *Mol Cell* **28**: 253–263.

Yang Q, Jankowsky E. 2005. ATP- and ADP-dependent modulation of RNA unwinding and strand annealing activities by the DEAD-box protein DED1. *Biochemistry* **44**: 13591–13601.

Yang Q, Jankowsky E. 2006. The DEAD-box protein Ded1 unwinds RNA duplexes by a mode distinct from translocating helicases. *Nat Struct Mol Biol* **13**: 981–986.

Yoneyama M, Kikuchi M, Matsumoto K, Imaizumi T, Miyagishi M, Taira K, Foy E, Loo Y-M, Gale M, Akira S, et al. 2005. Shared and unique functions of the DExD/H-box helicases RIG-I, MDA5, and LGP2 in antiviral innate immunity. *J Immunol* **175**: 2851–8.

Young CL, Khoshnevis S, Karbstein K. 2013. Cofactor-dependent specificity of a DEAD-box protein. *Proc Natl Acad Sci U S A* **110**: E2668–76.

Zagulski M, Kressler D, Bécam A-M, Rytka J, Herbert CJ. 2003. Mak5p, which is required for the maintenance of the M1 dsRNA virus, is encoded by the yeast ORF YBR142w and is involved in the biogenesis of the 60S subunit of the ribosome. *Mol Genet Genomics* **270**: 216–24.

Zhang L, Xu T, Maeder C, Bud L-O, Shanks J, Nix J, Guthrie C, Pleiss J a, Zhao R. 2009. Structural evidence for consecutive Hel308-like modules in the spliceosomal ATPase Brr2. *Nat Struct Mol Biol* **16**: 731–9.

Zhao J, Jin SB, Björkroth B, Wieslander L, Daneholt B. 2002. The mRNA export factor Dbp5 is associated with Balbiani ring mRNP from gene to cytoplasm. *EMBO J* **21**: 1177–1187.

Zonta E, Bittencourt D, Samaan S, Germann S, Dutertre M, Auboeuf D. 2013. The RNA helicase DDX5/p68 is a key factor promoting c-fos expression at different levels from transcription to mRNA export. *Nucleic Acids Res* **41**: 554–564.

Zorio DA, Bentley DL. 2004. The link between mRNA processing and transcription: communication works both ways. *Exp Cell Res* **296**: 91–97.

CHAPTER 2. The DEAD-BOX RNA HELICASE DBP2 CONNECTS RNA QUALITY CONTROL WITH REPRESSION OF ABERRANT TRANSCRIPTION

2.1 Introduction

Essential cellular processes, such as growth, organ development and differentiation, require precise spatial and temporal control of gene expression. Eukaryotic gene expression involves highly complex and coordinated events including transcription, pre-messenger RNA (pre-mRNA) processing, mRNA transport to the cytoplasm, translation and decay. During synthesis, RNA-binding proteins and complexes dynamically associate with the RNA to form a mature, translationally competent mRNP complex (mRNP) (Moore and Proudfoot 2009). These factors promote proper pre-mRNA processing and transport as well as couple upstream and downstream steps in the gene expression network. In addition to protein coding mRNAs, the eukaryotic genome also encodes numerous non-coding RNAs (Neil et al. 2009; van Dijk et al. 2011; Cabili et al. 2011). These include well known members such as transfer RNAs, ribosomal RNAs and spliceosomal RNAs, as well as a more recently recognized class of heterogeneous long non-coding RNAs (lncRNAs) (Berretta and Morillon 2009). The latter class has recently gained importance due to the conserved nature of this widespread transcription and connections between specific members and epigenetic gene regulatory mechanisms (Wang and Chang 2011).

In the budding yeast *Saccharomyces cerevisiae*, lncRNAs are very low in abundance and have been classically defined based on the inhibited RNA-decay mechanism used for detection. This has resulted in numerous names as cryptic unstable transcripts (CUTs), stable untranslated transcripts (SUTs) and Xrn1-dependent transcripts (XUTs) (Berretta and Morillon 2009). Whereas the precise function of these molecules is still hotly debated, it is clear that regulation is accomplished through the same mechanisms as those utilized for protein-coding mRNAs. In fact, lncRNAs are substrates for the nuclear exosome, a multiprotein complex responsible for maturation and degradation of numerous non-coding RNAs and aberrantly processed mRNAs (Schmid and Jensen 2010). This suggests that the signature of a non-coding or aberrant mRNA lies within the targeted RNA molecule itself. Consistent with this, numerous studies have underscored the importance of RNP composition as failure to properly assemble mRNPs results in selective retention and subsequent nuclear degradation (Schmid and Jensen 2010; Libri et al. 2002; Rougemaille et al. 2007; Galy et al. 2004). However, the molecular basis for discrimination of aberrant versus mature mRNPs is not fully understood.

One class of enzymes that function as critical regulators of RNP assembly are the DEAD-box RNA helicases. DEAD-box proteins are RNA-dependent ATPases that function in all aspects of RNA biology including transcription, mRNA export, and ribosome biogenesis. DEAD-box proteins are the largest group within the RNA helicase superfamily with ~25 members in the budding yeast *Saccharomyces cerevisiae* and ~40 in humans (Linder and Jankowsky 2011). Numerous studies have shown that DEAD-box proteins display a wide variety of biochemical activities *in vitro*, which includes RNA

duplex unwinding, RNA folding and RNP remodeling (Fairman et al. 2004; Del Campo et al. 2009; Bhaskaran and Russell 2007). In contrast to *in vitro* analyses, however, little is known regarding the precise biological function of individual DEAD-box protein family members.

One largely uncharacterized DEAD-box protein in *S. cerevisiae* is Dbp2. In mammalian cells, the ortholog of Dbp2, termed DDX5, functions in ribosome biogenesis as well as numerous transcriptional and co-transcriptional processes with RNA polymerase II (RNA Pol II) (Janknecht 2010). Dbp2, on the other hand, has only been linked to ribosome biogenesis and nonsense mediated decay in *S. cerevisiae* despite the fact that human DDX5 functionally complements loss of *DBP2* (Bond et al. 2001; Nissan et al. 2002; Barta and Iggo 1995). This suggests that a role in transcriptional processes is either not conserved or that Dbp2 plays an as-of-yet uncharacterized function in budding yeast.

In this study, we undertook a directed approach to define the role of Dbp2 in budding yeast. Our studies now provide documentation that Dbp2 functions at the interface of chromatin and RNA structure to represses expression of aberrant transcripts. We suggest that Dbp2 is a missing link in the gene expression network that functions as a cotranscriptional RNA chaperone. This would provide a model RNA modulation during transcription with broad implications to other aspects of RNA biology.

2.2 Materials and methods

Strains, plasmids and oligos are detailed in Tables 2.1-2.6 .

Plasmids and Cloning

All plasmids were constructed by standard molecular biology techniques and are listed in Table 2.1. DBP2 was expressed in yeast using the intronless pDBP2-PL-ADH-p415 (Banroques et al. 2008) to avoid splicing-dependent changes in expression level. ATPase-deficient variants were constructed by site-directed mutagenesis using Pfu polymerase. The pET28a-DBP2 was generated by subcloning techniques from pDBP2-PL-ADH-p415.

Yeast Manipulations - Yeast strains were constructed using classical yeast genetic techniques and are listed in Table 2.2. DBP2-deletion strains (dbp2Δ) were constructed by PCR-based gene replacement using pUG6 as a template. DBP2-3XFLAG strains were constructed similarly using the p3X-FLAG plasmid. 6AU studies were conducted with yeast strains grown in synthetic media -uracil (-URA) + 2% glucose and spotted onto -URA plates with or without 100 µg/mL 6-azauracil (Sigma). For all RNA analyses, yeast strains were grown in rich YPD media (YP+2% glucose) at either 35 or 30˚C as indicated to an OD of 0.4-0.5 prior to cell harvesting and RNA isolation. Transcriptional induction was performed by shifting yeast cells from YPD to YP+1% raffinose for 1 hour, to induce a derepressed state, and then to YP-Gal (YP+2% galactose) for 5 hours prior to cell harvesting.

Recombinant Protein Purification

Expression of pET28a 6xHIS-DBP2 in Rosetta E. coli (DE3) cells (Novagen) was induced by 0.2mM IPTG overnight at 16 °C. Cells were lysed in 20mM Tris at pH 7.9, 100mM NaCl, 5mM imidazole. Recombinant proteins were purified from the soluble fraction using nickel affinity chromatography according to the manufacturer's instructions (Ni-NTA, Qiagen).

In vitro ATPase Assays

In vitro ATP hydrolysis assays were performed using a PK/LDH enzyme-coupled absorbance assay as described previously (Noble et al. 2011) but with 440 nM Dbp2 and total yeast RNA (Sigma) or purchased DNA or RNA oligonucleotides (IDT). k_{obs} were calculated using the following formula: $V_0 = (OD_{340}/\text{min} \times 2.5)/(6.22 \times 10^{-3}\ \mu M)$, $k_{obs}(\text{min}^{-1}) = V_0/\text{protein concentration}$ and the EC_{50} was determined using GraphPad Prism software. Vo was normalized to background NADH loss in buffer alone for each condition. Presented data is the average of three independent experiments.

Cellular Microscopy

Wild type (BY4741) or DBP2-GFP strains were grown at 30˚C in YPD and were subsequently fixed with 10% formaldehyde, washed with PBS and stained with 2µg/mL DAPI (Sigma) for visualization of DNA. Images were collected using an Olympus BX51 fluorescent microscope and Metamorph TL software (Olympus America).

Chromatin Immunoprecipitation - Chromatin immunoprecipitation experiments were conducted as previously described with the following changes (Johnson et al. 2009).

Input represents 2.5% of lysate. Anti-FLAG antibodies (M2, Sigma) were pre-incubated with protein G Dynabeads (Invitrogen) prior to incubation with crosslinked, sheared lysate. Immunoprecipitated DNA was eluted 400µL elution buffer (1% SDS, 0.1M $NaHCO_3$) followed by reversal of crosslinks by addition 16uL of 5M NaCl and 65˚C overnight incubation. Resulting DNA was incubated with RNAse A and proteinase K, phenol extracted and ethanol precipitated. Samples were resuspended in 50µL of TE and 1/50 was used for qPCR using Primetime assay probes listed in Table 2.5 (IDT) and Taqman qPCR mix (Life Technologies). All ChIP experiments were conducted with 3 biological replicates with 4 technical repeats and are shown as the fold increase above wild type signal relative to input.

RT-qPCR and 5'RACE

RNA was isolated from cells standard acid phenol purification. Complementary DNA (cDNA) was prepared using the Quantitect Reverse Transcriptase kit (Qiagen) according to manufacturer's instructions using random hexamer primers provided. Primer pairs for qPCR were designed using default parameters in Primer Express 3.0 (Life Technologies) and are listed in Table 2.3. PCR reactions were performed in the BioRad CFX96 system. Fold changes were calculated using the Pfaffl method (Pfaffl 2001), and are reported as three biological replicates with three technical repeats each with standard error of the mean (SEM). 5' RACE of GAL7 mRNA was conducted according to manufacturer's protocol (Life Technologies). GAL7 gene-specific primers (GSP primers) are listed in Table 2.5. Resulting 5'RACE products were cloned using a UA cloning kit (Qiagen) and precise 5' ends were determined by DNA sequencing.

Northern Blotting

20 to 50µg of total RNA was resolved on a 1.2% formaldehyde agarose gel followed by transfer to a nylon membrane (Brightstar Hybond N+, Life Technologies). Northern blotting was conducted using standard methods. Radiolabeled double-stranded DNA probes were generated using PCR products from a plasmid template (see Table 2.6) and the Decaprime II kit according to manufacturer's instructions (Life Technologies). Transcripts were visualized using a PhosphorImager (Molecular Dynamics) and quantified by densitometry (ImageQuant, Molecular Dynamics)

2.3 Results

2.3.1 Dbp2 is an RNA-dependent ATPase *in vitro*

Dbp2 is a member of the DEAD-box family of RNA-dependent ATPases in *S. cerevisiae* based on the presence of 10 conserved sequence motifs organized into two, distinct structural domains ((Linder and Jankowsky 2011), Fig. 2.1A). Dbp2 also contains a C-terminal RGG motif and a unique N-terminus implicated in high affinity RNA and protein binding *in vivo*, respectively (Barta and Iggo 1995; Banroques et al. 2011).

Whereas studies from other laboratories have utilized genetic manipulations to assess the enzymatic function of Dbp2 *in vivo* (Bond et al. 2001; Barta and Iggo 1995; Banroques et al. 2011), Dbp2 has not been biochemically characterized to date. To determine if Dbp2 is a functional RNA-dependent ATPase, we established *in vitro* ATPase assays with recombinant, purified Dbp2 and increasing amounts of total RNA as previously described (Noble et al. 2011). Consistent with other DEAD-box enzymes, our results demonstrate that Dbp2 is an active ATPase *in vitro* with a 50% effective

concentration (EC_{50}) of 26 µg/ml for RNA (Fig. 2.1B). Next, we used site directed mutagenesis to incorporate amino acid substitutions in Motif I or II and assayed ATP hydrolysis of the resulting purified proteins to verify the origin of wild type Dbp2 activity (Fig. 2.1A). This revealed that both the K136N (Motif I) and E268Q (Motif II) substitutions abolish enzymatic activity at RNA concentrations one and three-fold above the EC_{50}, consistent with mutations of other DEAD-box enzymes (Fig. 2.1C). Thus, Dbp2 is a functional RNA-dependent ATPase *in vitro.*

To determine if the enzymatic activity of Dbp2 is required for normal cell growth, we utilized a plasmid complementation assay (Fig. 2.1D). To this end, we generated a *dbp2*Δ strain and analyzed the ability of wild type or ATPase-deficient *dbp2* alleles, p*dbp2-K136N* and p*dbp2-E268Q* to confer cell growth as compared to vector alone. Consistent with previous reports, loss of *DBP2* results in slow growth and cold sensitivity with an optimal growing temperature of 35˚C (Barta and Iggo 1995; Banroques et al. 2008, 2011). Importantly, neither point mutant restored wild type growth, paralleling the growth of the *dbp2*Δ strain with vector alone (Fig. 2.1D). This is in contrast to ectopic expression of the wild-type *DBP2* (*pDBP2*), which enabled growth at all temperatures. Immunoblotting analysis verified that the inability of the mutant plasmids to rescue the *dbp2*Δ strain is not due to expression differences between the wild type (p*DBP2*) and mutant *dbp2* vectors (data not shown). Thus, substitutions that impair enzymatic activity also impair cell growth, underscoring a requirement for enzymatically active Dbp2 in budding yeast.

2.3.2 Dbp2 is a dsRNA-directed ATPase

Given that the ATPase activity of Dbp2 is required for growth, we next asked if Dbp2 preferred specific RNAs for stimulation of ATP hydrolysis. This would indicate a preference for specific RNAs *in vivo*. To test this, we conducted *in vitro* ATPase assays as above in the presence of single-stranded RNA molecules (ssRNA) of different lengths (16 or 37mer) or dsRNA with a GNRA tetraloop (ΔG=-34 kcal/mol; Fig. 2.2A). Strikingly, this revealed that Dbp2 strongly prefers dsRNA for activation of ATP hydrolysis with a resulting EC_{50} of $10^{-6.5}$ or ~0.3μM (Fig. 2.2B). This is near the concentration of Dbp2 (0.2μM), suggesting that the affinity is likely higher with the EC_{50} representing the upper limit of the dissociation constant. Strikingly, a longer, 37mer ssRNA is also able to stimulate RNA-dependent ATPase activity but to a significantly lower extent that impairs affinity measurement. This was in contrast to the shorter, 16 nucleotide ssRNA, which was unable to activate Dbp2 at any concentration. Importantly, Dbp2 displayed no DNA-directed ATPase activity (Fig. 2.2C). This suggests that Dbp2 displays dsRNA-dependent ATPase activity, an enzymatic parameter that parallels human DDX5 but is not common among other DEAD-box family members (Huang and Liu 2002; Cordin et al. 2006). Furthermore, preliminary studies show that Dbp2 is a functional RNA helicase (Ma et al. 2013). This suggests that Dbp2 is a dsRNA-directed ATPase, which targets structured RNA elements *in vivo*.

2.3.3 Dbp2 is a predominantly nuclear protein whose loss is suppressed by 6-Azauracil

Studies of Dbp2 in budding yeast have provided conflicting evidence regarding the precise localization of Dbp2 ranging from nuclear/nucleolar to predominantly

cytoplasmic (Bond et al. 2001; Huh et al. 2003). To understand the cellular function(s) of Dbp2, we asked where Dbp2 is localized at steady state by conducting fluorescent microscopy of a fluorescently tagged *DBP2-GFP* strain harboring a GFP fusion at the endogenous locus. This revealed that Dbp2-GFP is a predominantly nucleoplasmic protein, colocalizing with DAPI-stained DNA, with accumulation in the nucleolus (Fig. 2.3A). This is consistent with the role of Dbp2 in ribosome biogenesis and suggestive of an additional nuclear function.

To pinpoint a role for Dbp2 in the nucleoplasm, we subsequently asked if loss of *DBP2* renders cells sensitive to transcriptional stress by conducting growth assays of wild type and *dbp2*Δ cells with or without 100 µg/ml 6-azauracil (6AU) (Fig. 2.3B). 6AU is a transcriptional inhibitor that has been widely utilized to identify genes whose products positively regulate transcription elongation (Riles et al. 2004). Surprisingly, 6AU partially rescues the slow growth defects of the *dbp2*Δ strain at semi-permissive temperatures of 30˚C and 32˚C, suggesting that reduction of transcription improves the growth of *DBP2*-deficient strains.

2.3.4 *DBP2* represses cryptic initiation within the *FLO8* locus

Interestingly, 6AU resistance or suppression phenotypes have been noted in only a few published reports and correlate with loss of gene products that negatively regulate transcription. This includes the transcriptional regulator/mRNA processing factor, *SSU72*, as well as chromatin modifying enzymes like the histone methyltransferase *SET2* (Keogh et al. 2005; Dichtl et al. 2002; Du and Briggs 2010). To further characterize the biological role of Dbp2, we asked if *dbp2*Δ strains exhibit transcriptional defects similar

to those associated with impaired repression. One type of transcriptional defect is cryptic initiation whereby failure to properly assemble chromatin results in initiation at non-cognate sites either within (intragenic) or outside of (intergenic) transcribed genomic loci (Cheung et al. 2008; Kaplan et al. 2003; Quan and Hartzog 2010). To determine if *DBP2* is required for repression of intragenic cryptic initiation, we utilized a previously characterized p*GAL-FLO8:HIS3* reporter construct for identification of initiation defects through a simple growth assay (Cheung et al. 2008; Kaplan et al. 2003). We constructed *dbp2*Δ *pGAL-FLO8:HIS3* strains and subsequently analyzed growth of two, independent isolates with respect to wild type and *spt6-1004* strains as negative and positive controls, respectively. *SPT6* encodes a transcriptional elongation factor whose mutation results in characterized cryptic initiation defects (Cheung et al. 2008; Kaplan et al. 2003). Strikingly, loss of *DBP2* also results in cryptic, intragenic initiation (Fig. 2.3D). Unlike *spt6-1004* strains, however, *dbp2*Δ strains require transcriptional induction for detection of cryptic initiation. This suggests that Dbp2 is needed only in the context of active transcriptional activity. Next, we conducted Northern blotting of *FLO8* transcripts from wild type, *dbp2*Δ and *spt6-1004* strains to determine if *dbp2*Δ strains also display cryptic initiation at the endogenous *FLO8* gene (Fig. 2.3E). This revealed a small, ~4-fold increase in short *FLO8* products in the *dbp2*Δ strain as compared to wild type (4% to 16%). Thus, *DBP2* is required for repression of cryptic, intragenic initiation in the *FLO8* reporter and within the endogenous locus.

2.3.5 *GAL7* transcripts are overabundant in the absence of *DBP2*

Given that *DBP2*-deficient cells display defects associated with active transcription, we asked if *DBP2* is required for normal expression levels of endogenous genes (Fig. 2.3F). To this end, we selected a panel of genes and assessed transcript abundance in wild type and *dbp2*Δ cells using quantitative PCR of reverse transcribed RNA (RT-qPCR). These genes were chosen based on the characterized role of the mammalian Dbp2 ortholog, DDX5, in cell cycle progression, cell differentiation and response to extracellular cues (Janknecht 2010). This revealed that *GAL7* transcripts are specifically overabundant in *dbp2*Δ cells as compared to wild type, in contrast to other gene products (Fig. 2.3F). Notably, this increase occurs under typically transcriptionally repressive conditions, suggesting that the *GAL7* gene is aberrantly derepressed in *dbp2*Δ cells. Furthermore, there was no detectible difference in *GAL7* transcript levels under induced conditions (+galactose) between wild type and *dbp2*Δ cells. This suggests that Dbp2 is required for both repression of cryptic, intragenic initiation and of normal promoter elements of protein-coding genes.

2.3.6 Dbp2 associates directly with chromatin, correlating with transcriptional activity

The *GAL* cluster is a well-established model for dissection of gene regulatory mechanisms in *S. cerevisiae*. Briefly, the *GAL* genes are considered to have three transcriptional states: active (+galactose), derepressed (+raffinose), and repressed (+glucose) (Sellick et al. 2008). In the presence of galactose, transcriptional activation proceeds via the transcription factor Gal4. In the repressed state, transcriptional

repressors Nrg1, and Mig1/Mig2 are responsible for promoting glucose-dependent repression (Sellick et al. 2008; Zhou and Winston 2001).

Our results suggest that *DBP2* is required for proper repression of *GAL7* under transcriptionally repressive conditions, drawing parallels between Dbp2 and glucose-dependent repressors. If this is the case, this would suggest that Dbp2 functions at the *GAL7* and *FLO8* loci through distinctly different mechanisms. To test this, we utilized chromatin immunoprecipitation (ChIP) to determine if a 3X-FLAG-tagged Dbp2 is directly bound to *GAL7* under transcriptionally repressive conditions. Strikingly, this resulted in detection of Dbp2 at the *GAL7* locus under transcriptionally active conditions, in contrast to our predictions (Fig. 2.4A). Dbp2-3XFLAG associates with similar levels ~5-fold above background across the *GAL7* open reading frame with slightly lower association at the promoter region, suggesting recruitment throughout the transcriptional unit (Fig. 2.4A). We were not able to detect appreciable accumulation of Dbp2 at any tested region under repressive conditions (Fig. 2.4B, glucose). Thus, Dbp2 is associated with chromatin in a transcriptionally dependent manner, suggestive of association with the transcriptional machinery and/or nascent RNAs. This also indicates the *GAL7* derepression defect in *dbp2*Δ cells may be due to either an indirect effect or to transcriptional activity, which is below the ChIP detection limit for Dbp2.

2.3.7 *DBP2*-deficient cells display expression defects across *GAL10-GAL7*

The *GAL7* gene is a member of the *GAL1-GAL10-GAL7* gene cluster (Fig. 2.5A). In addition to proteinaceous transcription factors, the *GAL* cluster is also associated with overlapping long non-coding RNAs (lncRNAs) with estimated levels as low as one

molecule in 14 cells (Houseley et al. 2008). These include the well-characterized *GAL10* lncRNA (Houseley et al. 2008; Geisler et al. 2012; Pinskaya et al. 2009) and a recently identified, sense oriented *GAL10s* lncRNA (termed *XUT 109-2m* in (van Dijk et al. 2011)).

To determine the origin of the *GAL7* transcriptional product in *dbp2*Δ cells under repressive conditions, we conducted a high resolution RT-qPCR analysis by positioning qPCR primer pairs at the 5' end of *GAL1*, 5', middle, and 3' end of *GAL10*, intragenic region between *GAL10*-*GAL7* and the 5', middle and 3' region of *GAL7* (Fig. 2.5A, #1-8). Consistent with our original RT-qPCR analysis above, we detected a 2.5-fold increase at the 5' end of *GAL7* in *dbp2*Δ (Fig. 2.5B, #6) and similar increases across the *GAL7* open reading frame indicative of low level expression of the *GAL7* protein-coding gene. Unexpectedly, we also detected a two-fold increase in transcript abundance upstream of *GAL7*. This is in contrast to the 5' ends of *GAL1* and *GAL10*, which were not significantly different in wild type versus *dbp2*Δ (Fig. 2.5B, #1). Next, we conducted RT-qPCR analysis at the *dbp2*Δ semi-permissive temperature of 30˚C with the idea that growth at lower temperatures would thermodynamically 'trap' Dbp2-dependent substrates (Fig. 2.5C). Strikingly, this revealed a sharp increase in transcript abundance to ~5-fold above wild type across the same genomic region. This pattern is consistent with aberrant expression across the *GAL7* and *GAL10s* lncRNA coding regions, the latter of which is indicative of a defect in RNA quality control (van Dijk et al. 2011).

2.3.8 *DBP2*-deficient cells accumulate aberrant *GAL7* RNAs

To further characterize the role of Dbp2 at the *GAL7* locus, we conducted Northern blotting to visualize *GAL7* transcripts under repressive conditions in wild type and *dbp2*Δ cells at 30˚C (Fig. 2.6A). This revealed a weak but detectible accumulation of transcripts corresponding to both the *GAL7* protein-coding gene and a weak ~2.5kb product in the *dbp2*Δ strain (Fig.2.6A, lanes 4-6). The latter product most likely corresponds to a 3' extended *GAL10s* lncRNA that terminates at the end of the *GAL7* gene. This is suggestive of aberrant expression of two *GAL* cluster gene products in *dbp2*Δ cells under normally repressive conditions.

Next, we analyzed the *GAL7* transcripts produced during transcriptional activation in *dbp2*Δ cells at 30˚C (Fig. 2.6B). Strikingly, in addition to abundant expression of *GAL7* mRNA transcripts, which accumulated to similar levels between wild type and *dbp2*Δ, we also detected an ~4kb product in *DBP2*-deficient cells (Fig. 2.6B, lanes 4-6). The 4kb transcript is consistent with expression of a *GAL10-GAL7* bicistronic mRNA that results from aberrant pre-mRNA processing in other mutant yeast strains (Greger and Proudfoot 1998; Rondón et al. 2009; Kaplan et al. 2005). Interestingly, we did not detect defects in *dbp2*Δ cells grown at 35˚C, suggesting that higher temperatures partially bypasses the requirement for Dbp2 (Fig. 2.2F and data not shown). This is consistent with a general role for Dbp2 in cotranscriptional RNA folding and/or assembly.

2.3.9 *GAL7* transcripts are a result of cryptic initiation in *DBP2*-deficient cells

Given that *GAL7* transcription is induced by the action of a galactose-dependent transcription factor, Gal4 (Sellick et al. 2008), we were surprised at our detection of

GAL7 mRNAs in repressive conditions when Gal4 is inactive. To determine if the *GAL7* transcripts originate from the normal +1 transcriptional start site, we utilized 5'RACE to map the 5' ends of *GAL7* sense transcripts in *DBP2*-deficient cells. Strikingly, this revealed that the *GAL7* transcripts are aberrant with respect to the wild type initiation site (Fig. 2.6C). Whereas transcriptional induction in wild type cells by addition of galactose results in a single PCR product of ~500bp, transcripts in the *dbp2*Δ cells are distinct from normal *GAL7* mRNAs (Fig. 2.6C, lanes 1 and 2). Sequencing of the resulting PCR products revealed three distinct transcriptional start sites in the *dbp2*Δ strain: one intergenic site at -50bp upstream of the +1 start site, corresponding to two PCR products due to 5'RACE efficiency and two, intragenic sites within the open reading frame of *GAL7* (Fig. 2.6D). In contrast, 5'RACE analysis of *GAL7* mRNAs under activated conditions revealed identical transcriptional start sites between wild type and *dbp2*Δ cells (data not shown). Thus, the *GAL7* transcripts in *dbp2*Δ cells under repressive conditions are a result of cryptic intragenic initiation with respect to the *GAL10s* lncRNA, consistent with the requirement for *DBP2* at the *FLO8* locus. We speculate that the cryptic initiation defects in *DBP2*-deficient cells are an indirect result of failure to 'clear' aberrant RNAs rather than a direct role in chromatin assembly, given the recent connections between RNA quality control and chromatin architecture (see Discussion).

2.3.10 simultaneous loss of *DBP2* and *RRP6* results in a lethal growth phenotype

Major factors in RNA quality control are the nuclear exosome component, *RRP6* and the cytoplasmic exonuclease, *XRN1* (Neil et al. 2009; van Dijk et al. 2011). To gain further insight into the biochemical pathway for *DBP2* function, we conducted synthetic

genetic analysis of *dbp2*Δ and *xrn1*Δ or *rrp6*Δ alleles using a plasmid shuffle assay (Fig. 2.7). Briefly, this assay exploits the toxic effects of 5-fluoroorotic acid (5-FOA) in strains that cannot grow in the absence of a plasmid encoding the uracil biosynthesis gene *(URA3)* and wild type *DBP2* (p*DBP2*). Strikingly, this revealed that *rrp6*Δ and *dbp2*Δ are synthetic lethal at all growth temperatures (Fig. 2.7). This genetic interaction is specific, as a *dbp2*Δ *xrn1*Δ strain grows well in the absence of the p*DBP2*. This supports a role for Dbp2 in RNA quality control steps in the nucleus. More importantly, this shows that Dbp2 is a major factor in RNA quality control that likely plays roles at multiple genes outside of the *GAL7* and *FLO8.* Taken together, we provide a model whereby the DEAD-box protein Dbp2 functions at the interface of chromatin and RNA quality control to modulate RNA structure in a manner that promotes both downstream processing steps and reassembly of chromatin in the wake of active transcription (Fig. 2.8). This suggests that Dbp2 is a co-transcriptional RNA chaperone, central to fidelity of the gene expression network.

2.4 Discussion

A major challenge to the RNA biology field is understanding how RNA and RNP structure contributes to cellular processes. The DEAD-box RNA helicases are central players in RNP dynamics, functioning in all aspects of RNA metabolism through ATP-dependent modulation of RNA structures (Linder and Jankowsky 2011). These include the DEAD-box proteins Sub2 and Dbp5, which are required for mRNP packing and nuclear export, respectively (Tran et al. 2007; Strasser et al. 2002; Fasken and Corbett 2009). Our studies now elucidate Dbp2 as a central player in transcriptional fidelity,

adding to the complement of DEAD-box proteins associated with maintenance of the transcriptome. Furthermore, our studies provide provocative evidence that Dbp2 functions as a cotranscriptional RNA chaperone. This would be consistent with current models for DEAD-box proteins as ATP-dependent chaperones and with elegant in vitro studies which support this mechanism (Bhaskaran and Russell 2007; Jarmoskaite and Russell 2011; Sinan et al. 2011).

With elucidation of Dbp2 as a key player in this process, several tantalizing questions now emerge regarding the precise biochemical mechanism in gene regulation. Our results suggest that Dbp2 is a dsRNA-dependent ATPase recruited to chromatin during transcription. Furthermore, our studies show that *DBP2* is genetically linked to the nuclear exosome component, *RRP6*. It is well established that Rrp6-dependent decay of numerous non-coding RNAs is dependent on transcription termination mechanisms (Rougemaille and Libri 2011). The primary mechanism for termination of short, non-coding transcripts is through the Nrd1-Sen1 pathway whereby RNA-binding proteins, Nrd1 and Nab3, recognize specific RNA sequences in nascent RNA transcripts (Kuehner et al. 2011; Steinmetz et al. 2006, 2001). Thus, it is tempting to speculate that Dbp2 promotes loading of RNA binding proteins, such as Nrd1 and Nab3, by resolving inhibitory RNA structures. This is consistent with accumulation of a putative *GAL10-GAL7* read-through transcript in *dbp2*Δ cells and with identification of a Nrd1-dependent termination mechanism at the *GAL10* gene (Rondón et al. 2009). However, given the pattern of Dbp2 gene association and the requirement for repression of initiation, the role of Dbp2 is not likely limited to recruitment these two factors. Interestingly, studies have also shown that the genes within the *GAL* cluster are associated with gene looping events

between promoters and terminators (O'Sullivan et al. 2004; Lainé et al. 2009; Ansari and Hampsey 2005). These gene loops have been shown to influence the rate of transcriptional reactivation in a process termed 'transcriptional memory' (Brickner 2009). It will be interesting to determine if Dbp2 and/or RNA folding influence higher order chromatin architecture.

Because loss of *DBP2* results in cryptic transcription indicative of aberrant chromatin architecture, we suggest that the activity of *DBP2* is necessary to promote clearance of nascent RNAs from genomic loci. Furthermore, we speculate that this requirement is due to the presence of RNA structures within nascent transcripts, which would be predicted to impair RNA processing and RNP complex assembly. In line with this model, strains deficient in cotranscriptional mRNP processing and packaging accumulate RNA:DNA hybrids in structures termed R-loops, which induce multiple defects associated with aberrant chromatin architecture (Kim et al. 1999; Mischo et al. 2011; Skourti-Stathaki et al. 2011; Aguilera and García-Muse 2012; Gómez-González et al. 2011). For example, simultaneous loss of the TRAMP component Trf4 and histone deacetylase Sir2 results in severe ribosomal DNA instability, underscoring an intimate connection between maintenance of the genome and transcriptome (Houseley et al. 2007).

It is well understood that the activity of RNA polymerases is dependent on the chromatin environment. Moreover, loss of chromatin remodeling or histone modification machinery results in aberrant transcription including cryptic transcriptional initiation both between and within gene loci (Cheung et al. 2008; Kaplan et al. 2003; Yadon et al. 2010). To the best of our knowledge, however, no RNA decay or processing factors have been

linked specifically to repression of cryptic initiation. Instead, genes encode histones, histone-modifying enzymes, and chromatin remodeling factors as well as transcription factors have been linked to this activity, supporting the fact that aberrant transcriptional initiation is a result of altered chromatin structure (Cheung et al. 2008). This suggests that either Dbp2 plays a distinct role as a bridging factor between nascent RNAs and chromatin, or that roles in repressing cryptic initiation have not been defined thus far for other RNA processing factors.

In mammals, DDX5 has been linked to numerous cotranscriptional processing steps and has been suggested to associate with dsRNA both *in vitro* and *in vivo*, consistent with the idea that Dbp2 cotranscriptionally modulates RNA structures (Huang and Liu 2002; Kar et al. 2011; Suzuki et al. 2009). Thus, the role of Dbp2 is likely evolutionarily conserved with future studies providing key insights into the biochemical mechanisms in eukaryotic gene regulation. More importantly, however, numerous studies have shown that DDX5 is a potent oncogene whose overexpression results in chemotherapeutic resistance (Cohen et al. 2008; Fuller-Pace and Moore 2011). In summary, our studies uncover a role for Dbp2 at the interface of RNA surveillance and chromatin architecture as a missing link in quality control of the transcriptome.

2.5 References

Aguilera A, García-Muse T. 2012. R Loops: From Transcription Byproducts to Threats to Genome Stability. *Mol Cell* **46**: 115–124.

Ansari A, Hampsey M. 2005. A role for the CPF 3' -end processing machinery in RNAP II-dependent gene looping. *Genes Dev* **19**: 2969–2978.

Banroques J, Cordin O, Doere M, Linder P, Tanner NK. 2008. A conserved phenylalanine of motif IV in superfamily 2 helicases is required for cooperative, ATP-dependent binding of RNA substrates in DEAD-box proteins. *Mol Cell Biol* **28**: 3359–3371.

Banroques J, Cordin O, Doère M, Linder P, Tanner NK. 2011. Analyses of the functional regions of DEAD-box RNA "helicases" with deletion and chimera constructs tested in vivo and in vitro. *J Mol Biol* **413**: 451–472.

Barta I, Iggo R. 1995. Autoregulation of expression of the yeast Dbp2p "DEAD-box" protein is mediated by sequences in the conserved DBP2 intron. *EMBO J* **14**: 3800–3808.

Berretta J, Morillon A. 2009. Pervasive transcription constitutes a new level of eukaryotic genome regulation. *EMBO Rep* **10**: 973–982.

Bhaskaran H, Russell R. 2007. Kinetic redistribution of native and misfolded RNAs by a DEAD-box chaperone. *Nature* **449**: 1014–1018.

Bond a T, Mangus D a, He F, Jacobson a. 2001. Absence of Dbp2p alters both nonsense-mediated mRNA decay and rRNA processing. *Mol Cell Biol* **21**: 7366–79.

Brickner JH. 2009. Transcriptional memory at the nuclear periphery. *Curr Opin Cell Biol* **21**: 127–33.

Cabili MN, Trapnell C, Goff L, Koziol M, Tazon-Vega B, Regev A, Rinn JL. 2011. Integrative annotation of human large intergenic noncoding RNAs reveals global properties and specific subclasses. *Genes Dev* **25**: 1915–1927.

Cheung V, Chua G, Batada NN, Landry CR, Michnick SW, Hughes TR, Winston F. 2008. Chromatin- and transcription-related factors repress transcription from within coding regions throughout the Saccharomyces cerevisiae genome. *PLoS Biol* **6**: 2550–2562.

Cohen AA, Geva-Zatorsky N, Eden E, Frenkel-Morgenstern M, Issaeva I, Sigal A, Milo R, Cohen-Saidon C, Liron Y, Kam Z, et al. 2008. Dynamic proteomics of individual cancer cells in response to a drug. *Science (80-)* **322**: 1511–1516.

Cordin O, Banroques J, Tanner NK, Linder P. 2006. The DEAD-box protein family of RNA helicases. *Gene* **367**: 17–37.

Del Campo M, Mohr S, Jiang Y, Jia H, Jankowsky E, Lambowitz AM. 2009. Unwinding by local strand separation is critical for the function of DEAD-box proteins as RNA chaperones. *J Mol Biol* **389**: 674–693.

Dichtl B, Blank D, Ohnacker M, Friedlein A, Roeder D, Langen H, Keller W. 2002. A role for SSU72 in balancing RNA polymerase II transcription elongation and termination. *Mol Cell* **10**: 1139–1150.

Du HN, Briggs SD. 2010. A nucleosome surface formed by histone H4, H2A, and H3 residues is needed for proper histone H3 Lys36 methylation, histone acetylation, and repression of cryptic transcription. *J Biol Chem* **285**: 11704–11713.

Fairman ME, Maroney PA, Wang W, Bowers HA, Gollnick P, Nilsen TW, Jankowsky E. 2004. Protein displacement by DExH/D “RNA helicases” without duplex unwinding. *Science (80-)* **304**: 730–734.

Fasken MB, Corbett AH. 2009. Mechanisms of nuclear mRNA quality control. *RNA Biol* **6**: 237–41.

Fuller-Pace F V, Moore HC. 2011. RNA helicases p68 and p72: multifunctional proteins with important implications for cancer development. *Future Oncol* **7**: 239–51.

Galy V, Gadal O, Fromont-Racine M, Romano A, Jacquier A, Nehrbass U. 2004. Nuclear Retention of Unspliced mRNAs in Yeast Is Mediated by Perinuclear Mlp1. *Cell* **116**: 63–73.

Geisler S, Lojek L, Khalil AM, Baker KE, Coller J. 2012. Decapping of Long Noncoding RNAs Regulates Inducible Genes. *Mol Cell* **45**: 279–291.

Gelbart ME, Rechsteiner T, Richmond TJ, Tsukiyama T. 2001. Interactions of Isw2 chromatin remodeling complex with nucleosomal arrays: analyses using recombinant yeast histones and immobilized templates. *Mol Cell Biol* **21**: 2098–106.

Gómez-González B, García-Rubio M, Bermejo R, Gaillard H, Shirahige K, Marín A, Foiani M, Aguilera A. 2011. Genome-wide function of THO/TREX in active genes prevents R-loop-dependent replication obstacles. *EMBO J* **30**: 3106–19.

Greger IH, Proudfoot NJ. 1998. Poly(A) signals control both transcriptional termination and initiation between the tandem GAL10 and GAL7 genes of Saccharomyces cerevisiae. *EMBO J* **17**: 4771–4779.

Güldener U, Heck S, Fiedler T, Beinhauer J, Hegemann JH. 1996. A new efficient gene disruption cassette for repeated use in budding yeast. *Nucleic Acids Res* **24**: 2519–2524.

Hartzog GA, Wada T, Handa H, Winston F. 1998. Evidence that Spt4, Spt5, and Spt6 control transcription elongation by RNA polymerase II in Saccharomyces cerevisiae. *Genes Dev* **12**: 357–369.

Houseley J, Kotovic K, El Hage A, Tollervey D. 2007. Trf4 targets ncRNAs from telomeric and rDNA spacer regions and functions in rDNA copy number control. *EMBO J* **26**: 4996–5006.

Houseley J, Rubbi L, Grunstein M, Tollervey D, Vogelauer M. 2008. A ncRNA modulates histone modification and mRNA induction in the yeast GAL gene cluster. *Mol Cell* **32**: 685–695.

Huang Y, Liu ZR. 2002. The ATPase, RNA unwinding, and RNA binding activities of recombinant p68 RNA helicase. *J Biol Chem* **277**: 12810–12815.

Huh W-K, Falvo J V, Gerke LC, Carroll AS, Howson RW, Weissman JS, O'Shea EK. 2003. Global analysis of protein localization in budding yeast. *Nature* **425**: 686–691.

Janknecht R. 2010. Multi-talented dead-box proteins and potential tumor promoters: P68 RNA helicase (DDx5) and its paralog, p72 RNA helicase (DDx17). *Am J Transl Res* **2**: 223–234.

Jarmoskaite I, Russell R. 2011. DEAD-box proteins as RNA helicases and chaperones. *Wiley Interdiscip Rev RNA* **2**: 135–152.

Johnson SA, Cubberley G, Bentley DL. 2009. Cotranscriptional recruitment of the mRNA export factor Yra1 by direct interaction with the 3' end processing factor Pcf11. *Mol Cell* **33**: 215–226.

Kaplan CD, Holland MJ, Winston F. 2005. Interaction between transcription elongation factors and mRNA 3'-end formation at the Saccharomyces cerevisiae GAL10-GAL7 locus. *J Biol Chem* **280**: 913–22.

Kaplan CD, Laprade L, Winston F. 2003. Transcription elongation factors repress transcription initiation from cryptic sites. *Science* **301**: 1096–1099.

Kar A, Fushimi K, Zhou X, Ray P, Shi C, Chen X, Liu Z, Chen S, Wu JY. 2011. RNA helicase p68 (DDX5) regulates tau exon 10 splicing by modulating a stem-loop structure at the 5' splice site. *Mol Cell Biol* **31**: 1812–1821.

Keogh MC, Kurdistani SK, Morris S a., Ahn SH, Podolny V, Collins SR, Schuldiner M, Chin K, Punna T, Thompson NJ, et al. 2005. Cotranscriptional set2 methylation of histone H3 lysine 36 recruits a repressive Rpd3 complex. *Cell* **123**: 593–605.

Kim H-D, Choe J, Seo Y-S. 1999. The sen1 + Gene of Schizosaccharomyces pombe , a Homologue of Budding Yeast SEN1, Encodes an RNA and DNA Helicase †. *Biochemistry* **38**: 14697–14710.

Kuehner JN, Pearson EL, Moore C. 2011. Unravelling the means to an end: RNA polymerase II transcription termination. *Nat Rev Mol Cell Biol* **12**: 283–294.

Lainé JP, Singh BN, Krishnamurthy S, Hampsey M. 2009. A physiological role for gene loops in yeast. *Genes Dev* **23**: 2604–2609.

Libri D, Dower K, Boulay J, Thomsen R, Rosbash M, Jensen TH. 2002. Interactions between mRNA export commitment, 3'-end quality control, and nuclear degradation. *Mol Cell Biol* **22**: 8254–66.

Linder P, Jankowsky E. 2011. From unwinding to clamping - the DEAD box RNA helicase family. *Nat Rev Mol Cell Biol* **12**: 505–516.

Ma WK, Cloutier SC, Tran EJ. 2013. The DEAD-box protein Dbp2 functions with the RNA-binding protein Yra1 to promote mRNP assembly. *J Mol Biol* **425**: 3824–3838.

Mischo HE, Gómez-González B, Grzechnik P, Rondón AG, Wei W, Steinmetz L, Aguilera A, Proudfoot NJ. 2011. Yeast Sen1 helicase protects the genome from transcription-associated instability. *Mol Cell* **41**: 21–32.

Moore MJ, Proudfoot NJ. 2009. Pre-mRNA Processing Reaches Back toTranscription and Ahead to Translation. *Cell* **136**: 688–700.

Nagalakshmi U, Wang Z, Waern K, Shou C, Raha D, Gerstein M, Snyder M. 2008. The transcriptional landscape of the yeast genome defined by RNA sequencing. *Science* **320**: 1344–9.

Neil H, Malabat C, d'Aubenton-Carafa Y, Xu Z, Steinmetz LM, Jacquier A. 2009. Widespread bidirectional promoters are the major source of cryptic transcripts in yeast. *Nature* **457**: 1038–42.

Nissan TA, Bassler J, Petfalski E, Tollervey D, Hurt E. 2002. 60S pre-ribosome formation viewed from assembly in the nucleolus until export to the cytoplasm. *EMBO J* **21**: 5539–47.

Noble KN, Tran EJ, Alcazar-Roman AR, Hodge CA, Cole CN, Wente SR. 2011. The Dbp5 cycle at the nuclear pore complex during mRNA export II: nucleotide cycling and mRNP remodeling by Dbp5 are controlled by Nup159 and Gle1. *Genes Dev* **25**: 1065–1077.

O'Sullivan JM, Tan-Wong SM, Morillon A, Lee B, Coles J, Mellor J, Proudfoot NJ. 2004. Gene loops juxtapose promoters and terminators in yeast. *Nat Genet* **36**: 1014–8.

Pfaffl MW. 2001. A new mathematical model for relative quantification in real-time RT-PCR. *Nucleic Acids Res* **29**: e45.

Pinskaya M, Gourvennec S, Morillon A. 2009. H3 lysine 4 di- and tri-methylation deposited by cryptic transcription attenuates promoter activation. *EMBO J* **28**: 1697–1707.

Prather D, Krogan NJ, Emili A, Greenblatt JF, Winston F. 2005. Identification and characterization of Elf1, a conserved transcription elongation factor in Saccharomyces cerevisiae. *Mol Cell Biol* **25**: 10122–10135.

Quan TK, Hartzog GA. 2010. Histone H3K4 and K36 methylation, Chd1 and Rpd3S oppose the functions of Saccharomyces cerevisiae Spt4-Spt5 in transcription. *Genetics* **184**: 321–34.

Riles L, Shaw RJ, Johnston M, Reines D. 2004. Large-scale screening of yeast mutants for sensitivity to the IMP dehydrogenase inhibitor 6-azauracil. *Yeast* **21**: 241–8.

Rondón AG, Mischo HE, Kawauchi J, Proudfoot NJ. 2009. Fail-Safe Transcriptional Termination for Protein-Coding Genes in S. cerevisiae. *Mol Cell* **36**: 88–98.

Rougemaille M, Gudipati RK, Olesen JR, Thomsen R, Seraphin B, Libri D, Jensen TH. 2007. Dissecting mechanisms of nuclear mRNA surveillance in THO/sub2 complex mutants. *EMBO J* **26**: 2317–26.

Rougemaille M, Libri D. 2011. Control of cryptic transcription in eukaryotes. *Adv Exp Med Biol* **702**: 122–131.

Schmid M, Jensen TH. 2010. Nuclear quality control of RNA polymerase II transcripts. *Wiley Interdiscip Rev RNA* **1**: 474–485.

Sellick C a., Campbell RN, Reece RJ. 2008. Galactose Metabolism in Yeast-Structure and Regulation of the Leloir Pathway Enzymes and the Genes Encoding Them. *Int Rev Cell Mol Biol* **269**: 111–150.

Sikorski RS, Hieter P. 1989. A system of shuttle vectors and yeast host strains designed for efficient manipulation of DNA in Saccharomyces cerevisiae. *Genetics* **122**: 19–27.

Sinan S, Yuan X, Russell R. 2011. The Azoarcus group I intron ribozyme misfolds and is accelerated for refolding by ATP-dependent RNA chaperone proteins. *J Biol Chem* **286**: 37304–12.

Skourti-Stathaki K, Proudfoot NJ, Gromak N. 2011. Human senataxin resolves RNA/DNA hybrids formed at transcriptional pause sites to promote Xrn2-dependent termination. *Mol Cell* **42**: 794–805.

Steinmetz EJ, Conrad NK, Brow DA, Corden JL. 2001. RNA-binding protein Nrd1 directs poly(A)-independent 3'-end formation of RNA polymerase II transcripts. *Nature* **413**: 327–31.

Steinmetz EJ, Warren CL, Kuehner JN, Panbehi B, Ansari AZ, Brow DA. 2006. Genome-wide distribution of yeast RNA polymerase II and its control by Sen1 helicase. *Mol Cell* **24**: 735–746.

Strasser K, Masuda S, Mason P, Pfannstiel J, Oppizzi M, Rodriguez-Navarro S, Rondon AG, Aguilera A, Struhl K, Reed R, et al. 2002. TREX is a conserved complex coupling transcription with messenger RNA export. *Nature* **417**: 304–308.

Suzuki HI, Yamagata K, Sugimoto K, Iwamoto T, Kato S, Miyazono K. 2009. Modulation of microRNA processing by p53. *Nature* **460**: 529–533.

Tajima M, Nogi Y, Fukasawa T. 1986. Duplicate upstream activating sequences in the promoter region of the Saccharomyces cerevisiae GAL7 gene. *Mol Cell Biol* **6**: 246–256.

Tran EJ, Zhou Y, Corbett AH, Wente SR. 2007. The DEAD-box protein Dbp5 controls mRNA export by triggering specific RNA:protein remodeling events. *Mol Cell* **28**: 850–859.

van Dijk EL, Chen CL, D'Aubenton-Carafa Y, Gourvennec S, Kwapisz M, Roche V, Bertrand C, Silvain M, Legoix-Ne P, Loeillet S, et al. 2011. XUTs are a class of Xrn1-sensitive antisense regulatory non-coding RNA in yeast. *Nature* **475**: 114–117.

Wang KC, Chang HY. 2011. Molecular Mechanisms of Long Noncoding RNAs. *Mol Cell* **43**: 904–914.

Yadon AN, Van de Mark D, Basom R, Delrow J, Whitehouse I, Tsukiyama T. 2010. Chromatin remodeling around nucleosome-free regions leads to repression of noncoding RNA transcription. *Mol Cell Biol* **30**: 5110–22.

Yassour M, Kaplan T, Fraser HB, Levin JZ, Pfiffner J, Adiconis X, Schroth G, Luo S, Khrebtukova I, Gnirke A, et al. 2009. Ab initio construction of a eukaryotic transcriptome by massively parallel mRNA sequencing. *Proc Natl Acad Sci U S A* **106**: 3264–9.

Zhou H, Winston F. 2001. NRG1 is required for glucose repression of the SUC2 and GAL genes of Saccharomyces cerevisiae. *BMC Genet* **2**: 5.

Zuker M. 2003. Mfold web server for nucleic acid folding and hybridization prediction. *Nucleic Acids Res* **31**: 3406–3415.

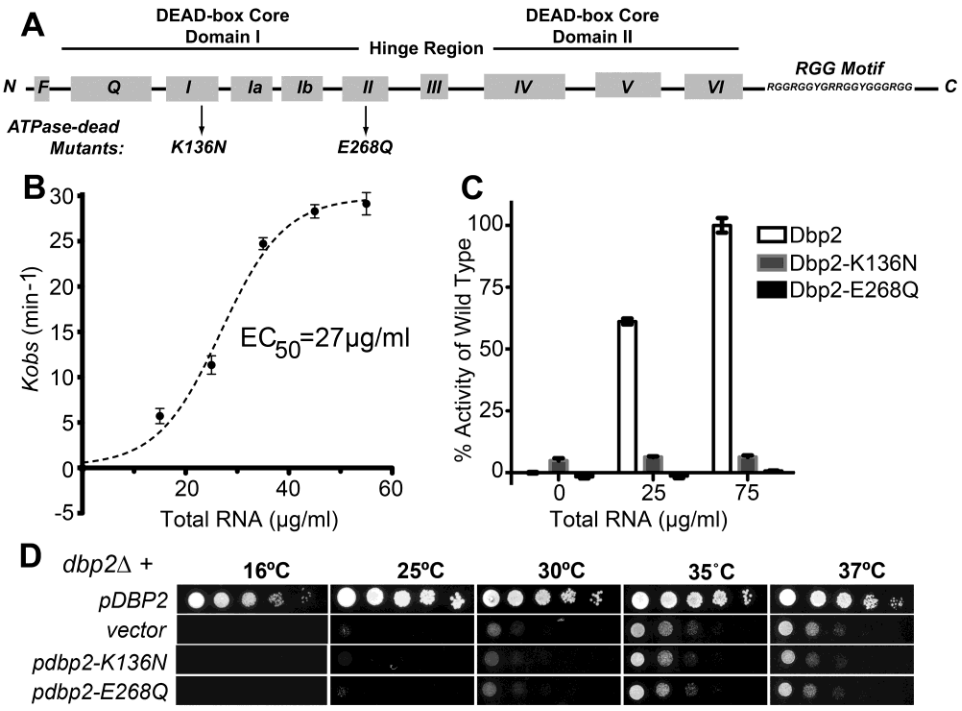

(Data from figure 2.1D were provided by Sara Cloutier.)

Figure 2.1. Dbp2 is an RNA-dependent ATPase *in vitro* whose activity is required for normal cell growth. *(A) Schematic representation of Dbp2 primary sequence and conserved DEAD-box protein motifs.* Core domains and the 10 sequence motifs are indicated (Linder and Jankowsky 2011). Dbp2 also contains a C-terminal RGG accessory domain predicted to enhance RNA binding activity (Banroques et al. 2011). Arrows denote amino acid substitutions in Motif I or Motif II. *(B) Dbp2 is an enzymatically active, RNA-dependent ATPase in vitro.* The ability of Dbp2 to hydrolyze ATP was assessed using an absorbance-based *in vitro* ATPase assay as previously described which measures ATP hydrolysis indirectly through a linear depletion of NADH (Noble et al. 2011). Assays were conducted with 400nM of recombinant, purified 6XHIS-tagged Dbp2 and increasing amounts of total yeast RNA. ATP turnover numbers (k_{obs}) were calculated from initial velocities of each assay conducted in triplicate. The EC_{50} for RNA was determined through non-linear regression analysis and is reflective of the concentration of RNA needed to activate ATP hydrolysis to a half-maximal rate. All data is normalized to background signal that results from very low levels of NADH depletion in buffer alone ($V_0 = 1.01 \pm 0.5$ min^{-1}). The observed ATPase rate of Dbp2 in the absence of RNA is 0.98 ± 0.4 min^{-1}, which is equivalent to buffer alone. *(C) Mutation of residues within motif I and II impair enzymatic activity.* Recombinant, purified 6XHIS-tagged variants Dbp2-K136N or Dbp2-E268Q were assayed for ATP hydrolysis as above using RNA concentrations equal to or 3-fold above the wild type EC_{50} concentration. Enzymatic activities are reported as a percentage of the initial velocity of ATP hydrolysis of wild type Dbp2 with 75 µg/mL RNA. *(D) DBP2-deficient strains display a slow growth and cold sensitive phenotype.* Yeast growth was analyzed using serial dilution analysis of *dbp2*Δ strains transformed with either empty vector alone or CEN plasmids encoding wild type (*pDBP2*) or ATPase-deficient mutants (*pdbp2-K136N* or *pdbp2-E268Q*) as indicated. Strains were subsequently spotted in 5 fold serial dilutions onto selective media and grown for 3-5 days at the indicated temperatures.

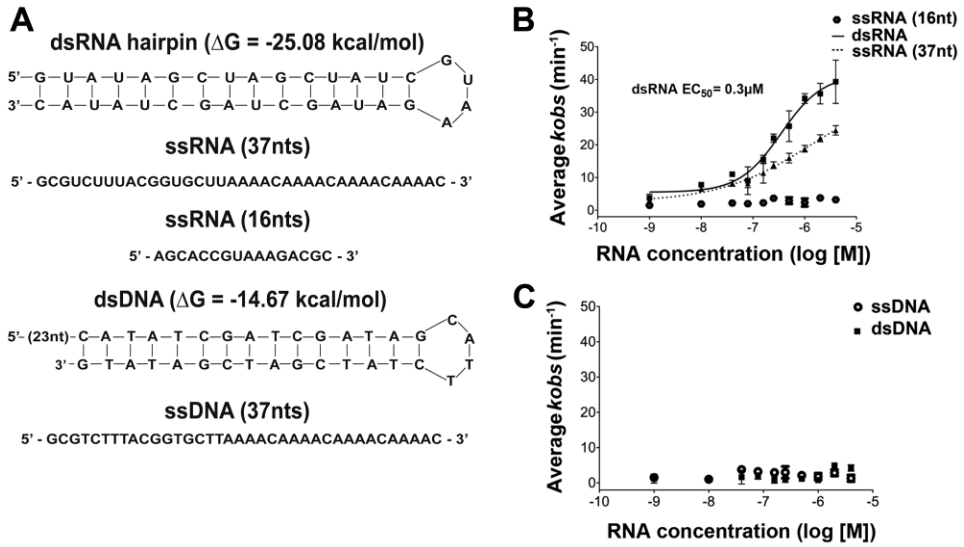

Figure 2.2. Dbp2 is a dsRNA-directed ATPase *in vitro*. *(A) Sequence and schematic representation of RNA and DNA molecules used below.* ΔG parameters were calculated using the MFOLD web server (http://mfold.rna.albany.edu/?q=mfold, (Zuker 2003)). (B) *Dbp2 displays a preference for dsRNA in stimulation of ATP hydrolysis.* ATPase assays were conducted as above using purchased, single strand or double stranded RNA molecules in (A) at varying concentrations from 1nM to 4μM and purified Dbp2 (0.2μM). ATP hydrolysis activity was determined in triplicate for each nucleic acid concentration and is plotted on a semi-logarithmic graph as *kobs* versus log[M] concentration of RNA. The resulting EC_{50} from the dsRNA hairpin was determined through non-linear regression analysis. EC_{50} values could not be determined for the single stranded RNA molecules due to low levels of ATPase stimulation. *(C) The ATPase activity of Dbp2 is not stimulated by DNA.* In vitro ATPase assays were conducted as above with the DNA molecules indicated in (A) using purchased DNA molecules.

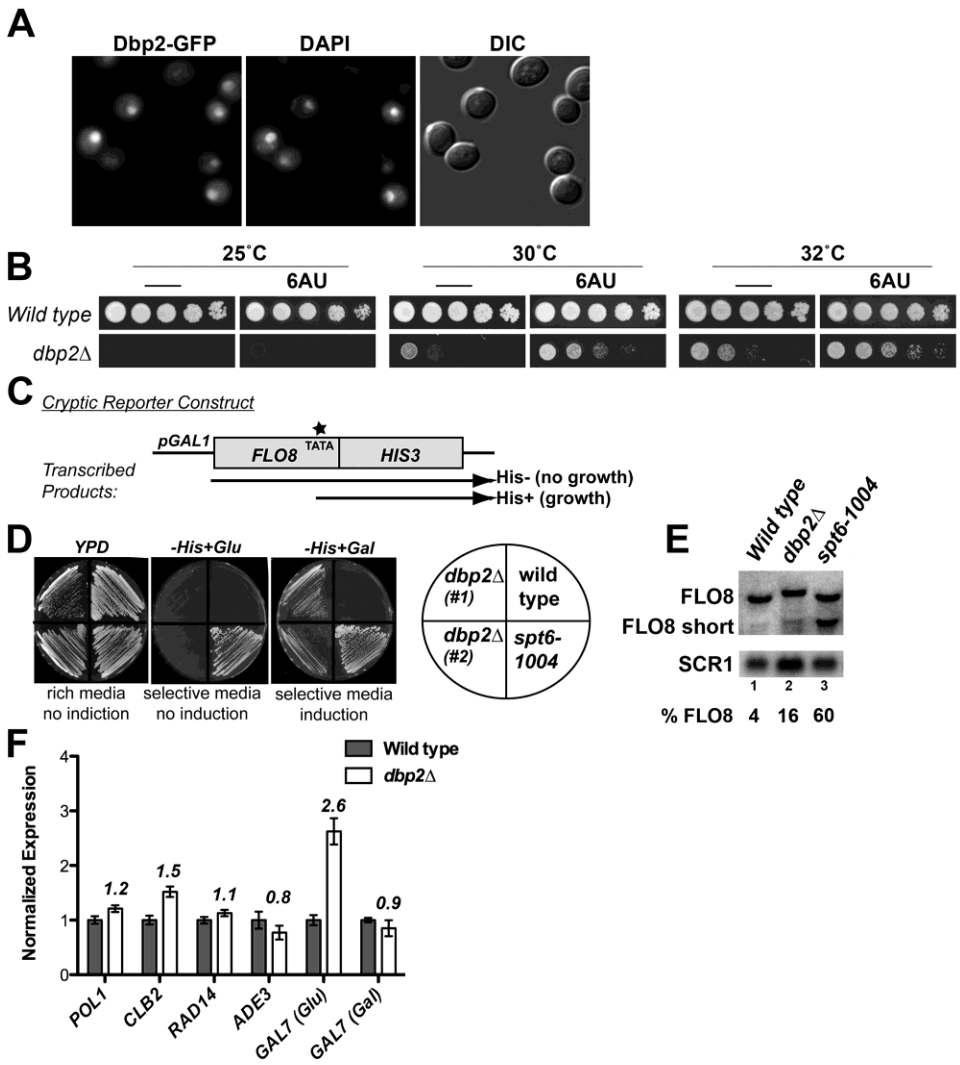

(Data from figure 2.3A and E were provided by Dr. Elizabeth Tran and data from figure 2.3B, D, and F were provided by Sara Cloutier.)

Figure 2.3. Dbp2 is a predominantly nuclear protein required for repression of cryptic, intragenic initiation within *FLO8* and expression of *GAL7*. *(A) Live cell imaging reveals whole cell distribution of Dbp2 with a predominantly nuclear localization at steady state.* Fluorescent microscopy was conducted with exponentially growing *DBP2-GFP* strains grown at 30˚C. Cells were fixed for 1 hour with formaldehyde in rich growth media, washed extensively, and stained with DAPI for visualization of DNA. Differential contrast (DIC) images are presented in the right-most panel. *(B) The transcriptional elongation inhibitor, 6-azauracil (6AU), partially rescues dbp2Δ growth defects.* Wild type (BY4741) or *dbp2*Δ strains were analyzed for 6AU sensitivity using serial dilution analysis of strains onto -URA+ 2%glucose plates with or without 100 µg/mL 6AU at the indicated temperatures. *(C) Schematic diagram of the FLO8:HIS3 cryptic initiation reporter (adapted from* (Cheung et al. 2008). TATA (*) indicates the approximate position of the cryptic, internal start site within the *FLO8* open reading frame. Following induction with galactose (+Gal), transcription in wild type cells

proceeds through the internal TATA, resulting in out of frame *HIS3* mRNA, and failure to grow on media lacking histidine (-His+Gal). Defects in chromatin structure or assembly are correlated with aberrant initiation at the internal TATA site, which results in grown on -His media due to production of an in frame *HIS3* mRNA. *(D) DBP2 is required for repression of cryptic, intragenic initiation within the FLO8:HIS3 reporter gene.* Cryptic initiation defects were assessed following construction of *dbp2*Δ strains encoding a chromosomally integrated *pGAL-FLO8:HIS3* reporter. Two, independent *dbp2*Δ strain isolates are shown compared to *DBP2* wild type and an *spt6-1004* mutant strain as negative and positive controls, respectively (Prather et al. 2005; Cheung et al. 2008). *(E) Loss of DBP2 results in an ~4-fold increase in aberrant FLO8 transcripts from the endogenous FLO8 locus.* Briefly, total RNA was isolated from wild type, *dbp2*Δ, and *spt6-1004* strains and subjected to Northern blotting. 30µg of total RNA was resolved on a 1.2% formaldehyde/agarose gel, transferred to a nylon membrane and probed with a double stranded, radiolabeled DNA probe corresponding to both the full-length and short 3' transcript product. *SCR1* transcripts are shown as a loading control. *(F) DBP2 is required to maintain endogenous levels of GAL7 under transcriptionally repressive conditions (+glucose).* The transcript abundance of individual gene products was determined by RT-qPCR analysis of RNA isolated from wild type or *dbp2*Δ strains grown at 35˚C. Transcript levels were determined by quantitative PCR using the BioRad CFX system and SYBR green with the indicated primer sets (Table 2.2). Gene product annotations are as follows: *POL1* (DNA Primase 1), *CLB2* (cyclin B2), *RAD14* (DNA repair), *ADE3* (nucleotide biosynthesis) and *GAL7* (carbon source metabolism). *GAL7* primers correspond to set #6 in subsequent figures. Differences were calculated using the Pfaffl method (Pfaffl 2001) and are normalized to the level of *ACT1*. Error bars represent the standard error of the mean (SEM).

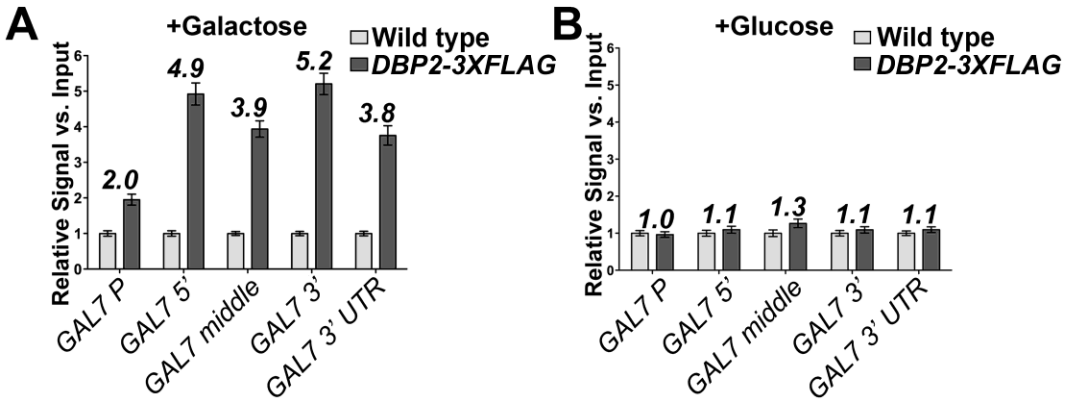

(Data from figure 2.4 were provded by Luyen Nguyen.)

Figure 2.4. Dbp2-3XFLAG is recruited to the *GAL7* open reading frame in a transcriptionally dependent manner. *(A) Dbp2 associates with the GAL7 locus, predominantly within the coding region and 3'UTR.* Chromatin immunoprecipitation (ChIP) experiments were conducted with strains expressing untagged or C-terminally 3XFLAG-tagged Dbp2 from the endogenous locus grown in rich media after a 5-hour transcriptional induction (+galactose). Bound DNA was detected by quantitative PCR (qPCR) using primer sets corresponding to the indicated genomic locations (see Table 2.5). Resulting signals are reported as the relative signal above an untagged, wild type strain with respect to input and are the result of 3 independent, biological replicates with 3 technical repeats. Numbers above each bar represent the average difference above background (untagged strain). Error bars indicate SEM as above. *(B) Dbp2-3XFLAG is not detectibly associated with GAL7 under transcriptionally repressive conditions*. ChIP-qPCR analysis was conducted as in A with yeast strains grown in glucose (repressive) conditions.

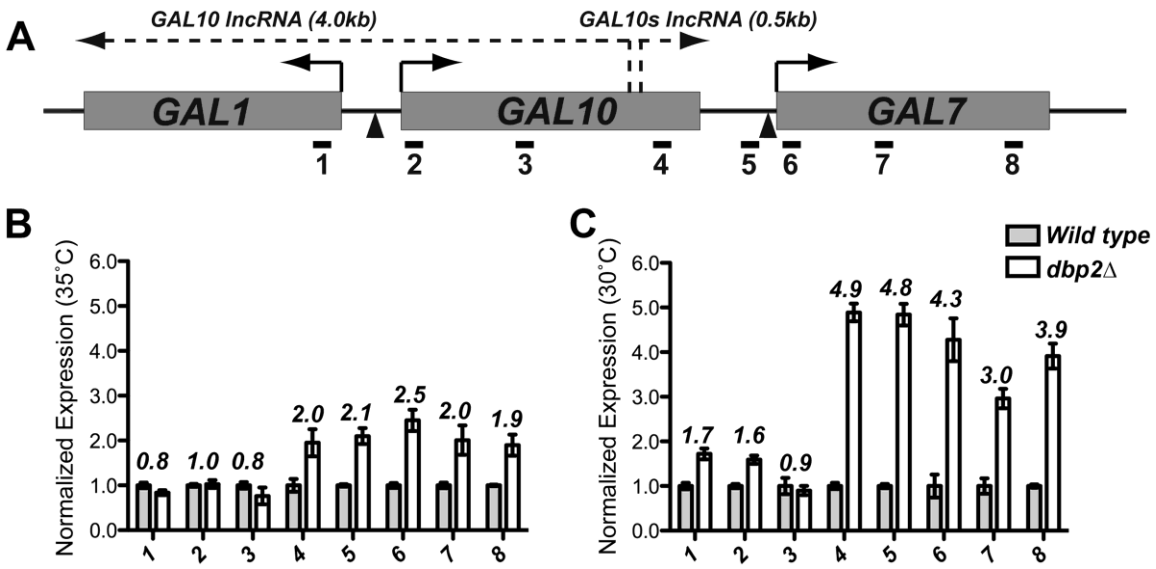

(Data from figure 2.5 were provided by Sara Cloutier.)

Figure 2.5. *GAL7* Expression is a result of transcriptional defects across the *GAL10-GAL7* genomic region in *DBP2*-deficient cells. *(A) Schematic representation of the GAL operon in S. cerevisiae denoting the three galactose-dependent genes (GAL1, GAL10 and GAL7) and previously identified non-coding RNAs* (van Dijk et al. 2011; Houseley et al. 2008). Short solid-line arrows denote the direction of protein-coding (sense) transcription whereas lncRNA transcription is represented by a dotted line. Triangles below the genes denote approximate positions of promoter elements whereas short horizontal lines demonstrate positions of primer sets utilized in qPCR (Table 2.2). Set #6 is the same set used for detection of *GAL7* in Fig. 2.2. *(B) High resolution RT-qPCR reveals accumulation of the GAL10s lncRNA and transcription through the GAL7 ORF.* RT-qPCR was conducted as in Fig. 2.2 using higher resolution qPCR primer pairs (Table 2.2) with strains grown at 35˚C. *(C) Growth at the dbp2Δ semi-permissive temperature of 30˚C exacerbates GAL7 expression defects.* High resolution RT-qPCR was conducted as above using wild type or *dbp2*Δ strains grown at 30˚C.

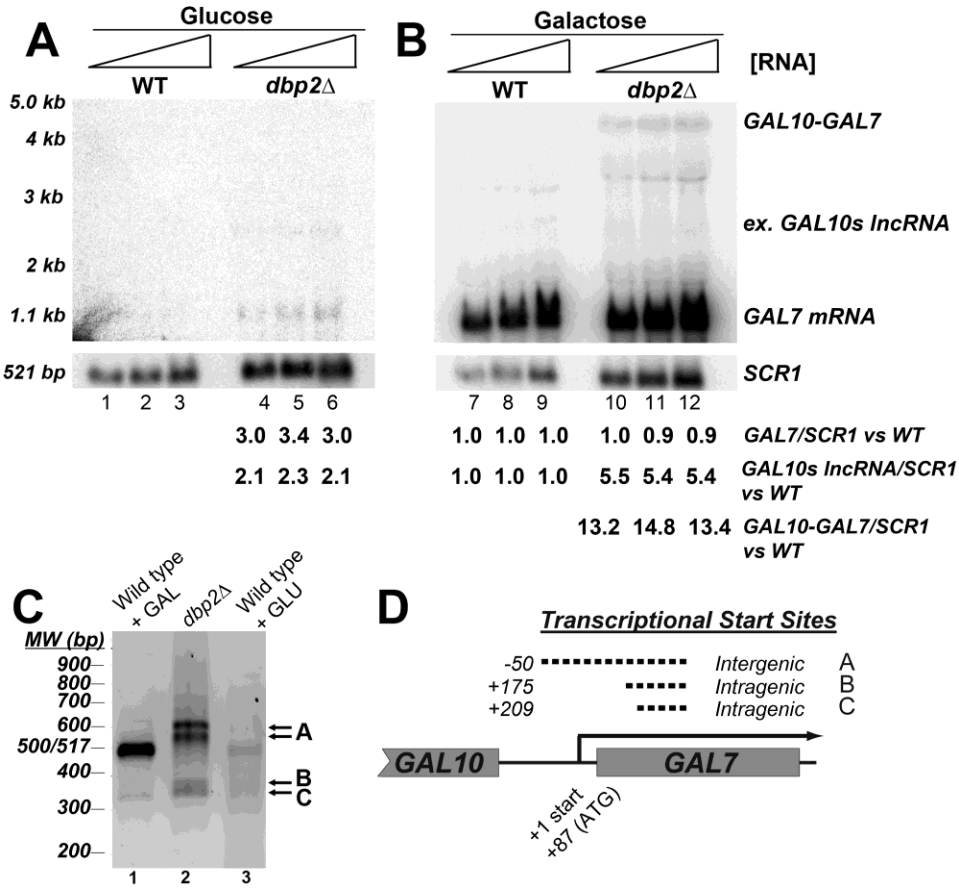

(Data from figure 2.6 were provided by Sara Cloutier.)
Figure 2.6. Loss of *DBP2* results in cryptic initiation at *GAL7* and termination defects within the *GAL10-GAL7* region under repressed and activated conditions, respectively. (A) *Northern blotting of total RNA from wild type and dbp2*Δ *cells reveals expression of GAL7 and a 3' extended GAL10s lncRNA under typically repressive conditions.* Northern blotting was conducted with increasing amounts of total RNA (20-50µg) from indicated strains grown at the semi-permissive *dbp2*Δ temperature of 30˚C in glucose (repressive) conditions (lanes 1-6). Accumulation of *GAL7* mRNA and a 2.5kb transcript, likely corresponding to a 3' extended *GAL10s* lncRNA, is evident in lanes 4-6. Other products at ~ 2kb and 3.5kb are background detection of 18S and 25S rRNA. Quantification is provided below each lane and corresponds to the quantity of the indicated transcript versus wild type normalized to levels of SCR1 for each lane. In lanes with no detectible product, quantities were normalized to background. *(B) Transcriptional induction of the GAL genes results in expression of GAL7 and appearance of a GAL10-GAL7 transcript.* Northern blotting was conducted as above following a 5-hour shift to galactose-containing media. Under transcriptionally induced conditions, GAL7 mRNA is induced along with an ~4kb product which most likely corresponds to a *GAL10-GAL7* bicistronic mRNA (lanes 10-12). *(C) GAL7 mRNA transcripts in dbp2*Δ *strains are aberrant with respect to wild type GAL7 products.* Resulting 5' RACE products of aberrant *dbp2*Δ transcripts (lane 2) are shown with respect to the induced, wild type GAL7 transcript (lane 1) and basal transcriptional

products (lane 3) shown following resolution on a 1.3% agarose gel and visualization by ethidium bromide staining. The three most prominent 5' RACE products in the *dbp2*Δ cells are denoted A, B, C to the right of the gel. The two 'A' bands correspond to the same transcription initiation site (as determined by sequencing) and are likely due to differences in the cDNA 'tailing' efficiency in the 5'RACE. Note that these experiments are not quantitative and do not reflect relative transcript abundance between strains or conditions. (D) *GAL7 transcripts are the result of cryptic initiation events in the dbp2*Δ *strain under typically repressive conditions.* Schematic representation of *GAL7* transcriptional start sites in *DBP2*-deficient cells as determined following cloning and sequencing of resulting 5'RACE products. Dotted lines denote cryptic transcriptional elements between (inter) or within (intra) an open reading frame with respect to the normal +1 start site in transcriptionally induced, wild type cells ((Tajima et al. 1986); solid line).

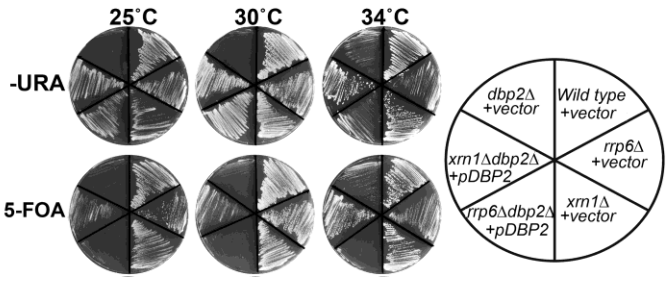

(Data from figure 2.7 were provided by Sara Cloutier.)
Figure 2.7. Simultaneous loss of *DBP2* and the nuclear RNA decay factor, *RRP6*, results in synthetic lethality. Synthetic growth defects were measured using a plasmid shuffle assay, which exploits the ability of yeast to grow in the absence of a *URA3*-encoding plasmid (vector or p*DBP2*). Indicated strains were constructed using standard yeast manipulations and resulting transformants were streaked on either -URA or 5-FOA media to demonstrate growth in the presence or absence of plasmid-encoded *DBP2*, respectively.

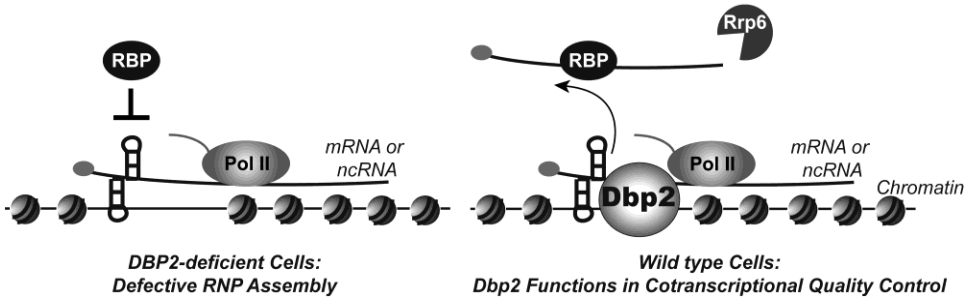

Figure 2.8. Dbp2 is a dsRNA-directed DEAD-box enzyme that functions in cotranscriptional RNA quality control. Our results document a previously unrecognized role for Dbp2 in transcriptional quality control. We suggest that Dbp2 is recruited during transcription to promote clearance of newly transcribed RNA from genomic loci, whose presence interferes with both chromatin and mRNP assembly. This activity may involve direct modulation of RNA or RNP structures to promote association of RNA-binding proteins (RBPs) such as factors required for RNA processing and/or decay. This activity would also be predicted to inhibit further synthesis of aberrant cryptic transcripts through reformation of chromatin architecture, consistent with recent studies of other cotranscriptional RNA processing/assembly factors (Mischo et al. 2011; Aguilera and García-Muse 2012).

Table 2.1: Yeast and Bacterial Plasmids

Name	Description	Source/Reference
pUG6	KanMx disruption cassette plasmid	(Güldener et al. 1996)
BTP13	pET28a-*DBP2*	This study
BTP18	pET28a-*dbp2-E268Q*	This study
BTP21	pet28a-*dbp2-K136N*	This study
pDBP2	*DBP2*-PL-ADH-P415	(Banroques et al. 2008)
BTP24	*pdbp2-K136N/CEN/LEU2*	This study
BTP25	*pdbp2-E268Q/CEN/LEU2*	This study
pCEN/URA3	pRS316	(Sikorski and Hieter 1989)
pCEN/LEU2	pRS315	(Sikorski and Hieter 1989)
p3XFLAG	p3XFLAG:KanMx	(Gelbart et al. 2001)
pGAL1-GAL10-GAL7	pYGPM11l14	Open Biosystems (Genomic Tiling)
pFLO8	pGAL-YER109C	Open Biosystems (Yeast ORF Collection)
pSCR1	YGPM29b01	Open Biosystems (Genomic Tiling)

Table 2.2: Yeast Strains

Strain	Genotype	Source
Wild Type (BY4741)	MATa *his3Δ1 leu2Δ0 met15Δ0 ura3Δ0*	Open Biosystems
DBP2-GFP	MATa *DBP2-GFP:HIS3 his3D1 leu2D0 met15D0 ura3D0*	Invitrogen
xrn1Δ	MATa *xrn1::KanMx his3D1 leu2D0 met15D0 ura3D0*	Open Biosystems
dbp2Δ (BTY115)	MATa *dbp2::KanMx ura3Δ0 leu2Δ0 his3Δ0 TRP1 met- lys?*	This study
dbp2-K136N (BTY166)	MATa *dbp2::KanMx ura3Δ0 leu2Δ0 his3Δ0 TRP1 met- lys? + pdbp2-K136N/CEN/LEU2*	This study
dbp2-E268Q (BTY180)	MATa *dbp2::KanMx ura3Δ0 leu2Δ0 his3Δ0 TRP1 met- lys? pdbp2-E268Q/CEN/LEU2*	This study
Wild type (FY120)	MATa *his4-912∂ lys2-128∂ leu2Δ1 ura3-52*	(Hartzog et al. 1998)
prGAL-FLO8:HIS3 (FY2393)	MATa *lys2-128∂ his3Δ200 ura3-52 leu2Δ1 trp1Δ63 prGAL1-FLO8-HIS3:KanR*	(Prather et al. 2005)
spt6-1004 (FY2139)	*MATα FLAG-spt6-1004 ura3-52 leu2Δ1 lys2-128∂*	(Prather et al. 2005)
spt6-1004 prGAL-FLO8:HIS3 (BTY217)	MATα *spt6-1004-FLAG prGAL-FLO8-HIS3::KanMx ura3-52 leu2Δ1 lys2-128∂ his4-912∂ trp?*	Reconstructed from (Cheung et al. 2008)
dbp2Δ prGAL-FLO8:HIS3 (BTY124)	MATα *dbp2::KanR prGAL1-FLO8-HIS3::KanMx ura3 leu2 his3 trp? lys? met?*	This study
rrp6Δ	MATa *rrp6::KanMx his3D1 leu2D0 met15D0 ura3D0*	Open Biosystems
DBP2-3XFLAG (BTY200)	MATa *DBP2-3XFLAG:KanMx his3Δ1 leu2Δ0 met15Δ0 ura3Δ0*	This study
Wild type FT4 (JOU538)	*MATa ura3-52 trp1-Δ63 his3-Δ200 leu2::PET56*	(Houseley et al. 2008)
FT4 + Reb1BSΔ (JOU811)	*MATa ura3-52 trp1-Δ63 his3-Δ200 leu2::PET56 gal10::URA3::pMV12 (EcoRI/XhoI-Reb1 BSΔ with BS2 silent)*	(Houseley et al. 2008)
dbp2Δ FT4 (BTY219)	*MATa ura3-52 trp1-Δ63 his3-Δ200 leu2::PET56 dbp2::KanMx*	This study
dbp2Δ FT4+Reb1BSΔ (BTY220)	*MATa ura3-52 trp1-Δ63 his3-Δ200 leu2::PET56 gal10::URA3::pMV12 (EcoRI/XhoI-Reb1 BSΔ with BS2 silent) dbp2::KanMx*	This study

Table 2.3: RT-qPCR Oligos

1 F	TGAGTTCAATTCTAGCGCAAAGG
1 R	TTCTTAATTATGCTCGGGCACTT
2 F	GAGGTCTTGACCAAGCATCACA
2 R	TTCCAGACCTTTTCGGTCACA
3 F	AAATGAAGGTTTGTGTCGTGA
3 R	AAGCTTTGCAGAATGCATGA
4 F	TGAACAAGCCATATGGAGACA
4 R	CGACGATATTACCCGTAGGAA
5 F	CAAAAAGCGCTCGGACAACT
5 R	GCTTGGCTATTTTGTGAACACTGT
6 F (or GAL7 F)	CAA AAA GCG CTC GGA CAA CT
6R (or GAL7 R)	GCT TGG CTA TTT TGT GAA CAC TGT
7 F	TCAACAGGAGGCTGCTTACAAG
7 R	CCAGGACATAGATAGCATTTTGGA
8 F	CCATTCCACAAATGAAACAATC
8 R	ACAACCCATGGCTGTACCTT
CLB2 F	GCGAATAATCCAGCCCTAAC
CLB2 R	CGGCTGTTGATCTTGATACG
POL1 F	CAGAAAGCGCCAGGAATTG
POL1 R	CGTAGCCTACACCATCGTCATC
RAD 14 F	CCGGCCTCTCGCAGTTACTA
RAD14 R	GCGGCTGCTGCATTATCAT
ACT1 F	TGGATTCCGGTGATGGTGTT
ACT1 R	TCAAAATGGCGTGAGGTAGAGA
ADE 3 F	CCCGTGATATCGCATCATACTTAC
ADE3 R	GGCCGATGGCAACGACTA

Table 2.4: 5'RACE Primers

GAL7-GSP1	GTCCTCCTTCACCATTTGG
GAL7-GSP2	GGCCCAGTATGGAACAACAAC
GAL7-GSP3	CGTCAGTCAATGCTTGCCAAG

Table 2.5: Oligos for Chromatin Immunoprecipitation

Name	Forward	Reverse	Probe	Relative to +1 Start	+1 Start References
GAL7 P	GCGCTCGGACAACTGTTG	TTTCCGACCTGCTTTTATATCTTTG	CCGTGATCCGAAGGACTGGCTATACA	-66	(Greger and Proudfoot 1998)
GAL7 5'	ATCATACAATGGAGCTGTGGG	CTAGCCATTCCCATAGACGTTAC	AAGCAGCCTCCTGTTGACCTAACC	+190	(Greger and Proudfoot 1998)
GAL7 middle	TGCGAAACTTCACTAGGGATG	CCAGAGAAGCAAAGAAAATCATAAG	CAACCCATGGCTGTACCTTTGTTTTCA	+587	(Greger and Proudfoot 1998)
GAL7 3'	GCATTTCTACCCACCTTTACTGAG	CAGCTTGTTCCGAAGTTAAATCTC	AGGCTCACCTAACAATTCAAAACCAACC	+1079	(Greger and Proudfoot 1998)
GAL7 3' UTR	GGACCACTCTTACATAACTAGAATAGC	TTTTCTATTAACTGCCTGGTTTCTTT	TGTCACTCCGTTCAAGTCGACAACC	+1259	(Greger and Proudfoot 1998; Nagalakshmi et al. 2008)
POL1 5'	AGAATACAGGGCCAGAAAGC	GTAGCCTACACCATCGTCATC	ACAACAAATCGTCATGCAGCAATTCCT	+125	(Nagalakshmi et al. 2008)
RAD14 5'	TGTGTTTGTATTTTAACCGTGGG	GATTCAATTGGTCGCTACTCAG	TGTTAGCCTCCTGCACAGCTCATC	+211	(Nagalakshmi et al. 2008)
CLB2 5'	TCCAGCCCTAACAAATTTCAAATC	GCTGTTGATCTTGATACGCTTTC	TCCGACTTCCCTCCTTCTTTACTGAGTT	+1634	(Yassour et al. 2009)
ADE3 5'	TGGCTGGTCAAGTGTTGG	TGGTCTGTTGCCTACTTGAATG	TCAAAAGCATTCAAGGTCACGTGCC	+100	(Nagalakshmi et al. 2008)

Table 2.6: Oligos for Northern Blotting (dsDNA probes)

FLO8 F	CTGTATCCAGTCCATTATCTTCAG
FLO8 R	TCAGCCTTCCCAATTAATAAAATTG
SCR1 F	GGATACGTTGAGAATTCTGGCCGAGG
SCR1 R	AATGTGCGAGTAAATCCTGATGGCACC
GAL7 F	CCTTGGTTAGGTCAACAGGAG
GAL7 R	AGTCGCATTCAAAGGAGCC

CHAPTER 3. THE DEAD-BOX PROTEIN DBP2 FUNCTIONS WITH THE RNA-BINDING PROTEIN YRA1 TO PROMOTE mRNP ASSEMBLY

3.1 Introduction

Over the last several decades, major advances have been made in our understanding of RNA structures and the parameters for RNA folding *in vivo* and *in vitro* (Zemora and Waldsich 2010; Wan et al. 2012). Unlike DNA, cellular RNAs have a high propensity to form intramolecular helices and tertiary contacts that are central to the functionality of the given RNA molecule (Zemora and Waldsich 2010; Woodson 2010; Treiber and Williamson 1999; Wilson et al. 2005). Proper folding is not only critical for small ribozymes to form active sites but also to enable highly efficient catalysis (Zemora and Waldsich 2010; Woodson 2010; Wilson et al. 2005). This is also the case for more complex RNAs, such as the 18 and 28S ribosomal (r)RNAs, which also assemble with RNA-binding proteins to form a fully functional translational apparatus (Woodson 2008; Stern et al. 1989).

Strikingly, while it is now common knowledge that cellular RNAs such as rRNAs, transfer RNAs (t)RNAs and spliceosomal (sn)RNAs are all highly structured and intrinsically dynamic, our knowledge regarding messenger RNA (mRNA) structure has lagged behind (Rajkowitsch et al. 2007). One possible explanation for this discrepancy is

that, unlike other RNAs, mRNAs are highly heterogeneous in sequence, length and assembly with RNA-binding proteins. Moreover, both the structure and composition of a given messenger ribonucleoprotein complex (mRNP) changes at different steps during synthesis, maturation and translation (Moore 2005; Schmid and Jensen 2010). Computational predictions and genome-wide *in vivo* analyses demonstrate that mRNAs have significant secondary structure and this characteristic is likely a critical aspect of gene regulation (Wan et al. 2012; Gaspar et al. 2013; Kertesz et al. 2010). However, key mechanistic questions regarding the factors that are required for proper folding of mRNAs and subsequent assembly of the mRNA into an mRNP have not been fully addressed.

One class of enzymes that controls cellular RNA structures is the DEAD-box RNA helicase family. DEAD-box helicases are the largest class of enzymes within the RNA helicase superfamily, functioning in all aspects of RNA metabolism from transcription to translation (Putnam and Jankowsky 2013; Linder and Jankowsky 2011). DEAD-box RNA helicases are unique among other helicase enzyme families in that they are non-directional and non-processive, with maximal unwinding on duplexes that are one to one and a half turns of an A-form RNA helix. This activity makes DEAD-box proteins well suited for cellular RNAs, which rarely contain helices longer than 12 base pairs in length (Linder and Jankowsky 2011). Furthermore, DEAD-box proteins exhibit a wide array of biochemical activities including duplex unwinding, RNA-binding protein displacement from single stranded RNA, and RNA strand annealing (Putnam and Jankowsky 2013; Linder and Jankowsky 2011). Thus, although classically defined as

helicases, these enzymes are more likely to function as cellular RNA chaperones that conduct a variety of biochemically distinct steps to properly assemble RNPs *in vivo.*

Three DEAD-box proteins, namely Sub2, Dbp5 and Dbp2, have been implicated in nuclear gene expression steps in the budding yeast *Saccharomyces cerevisiae* (Linder and Jankowsky 2011). The least well understood DEAD-box protein, however, is Dbp2. In multicellular eukaryotes, the Dbp2 ortholog DDX5 functions in multiple gene expression steps including pre-mRNA splicing, microRNA processing, and regulation of transcription initiation (Janknecht 2010; Fukuda et al. 2007; Caretti et al. 2006). This factor has also recently been linked to nuclear mRNA export and RNA quality control in yeast and metazoan cells (Cloutier et al. 2012; Zonta et al. 2013; Buszczak and Spradling 2006). Moreover, recent studies from our laboratory determined that Dbp2 is directly associated with transcriptionally active chromatin (Cloutier et al. 2012). This suggests that Dbp2 may function as a co-transcriptional mRNA chaperone by facilitating proper mRNA folding, and likely messenger ribonucleoprotein (mRNP) formation, in the nucleus.

To shed light on the mechanisms governing mRNP structure and assembly, we focused on the biological and biochemical mechanism of Dbp2. Our results now show that Dbp2 is an efficient RNA helicase that promotes assembly of the RNA-binding proteins Yra1, Nab2 and the export receptor Mex67 onto newly synthesized mRNA. We also demonstrate that Dbp2 interacts directly with Yra1 and that Yra1 inhibits the duplex unwinding activity of Dbp2. We speculate that this may be a common mode of regulation for other DEAD-box RNA helicases and provide a model whereby Dbp2 duplex

unwinding and subsequent enzymatic inhibition is necessary to properly assemble mRNPs.

3.2 Materials and methods

Yeast strains, yeast plasmids and bacterial plasmids

Listed in Table 1 and Table 2.

Recombinant Protein Expression and Purification

Expression of pMAL MBP-TEV-DBP2 in BL21 *E. coli* (DE3) cells (New England Bio Labs) was induced with 1 mM isopropyl 1-thio-β-D-galactopyranoside (IPTG) at 37 °C for 3 hours and was subsequently purified from the soluble fraction using amylose resin according to the manufacturer's instructions (New England Bio Labs). The MBP tag was then cleaved with 50 U of TEV protease (Invitrogen) overnight at 16 °C. The cleaved Dbp2 was then subjected to cation exchange chromatography with SP sepharose (Sigma). Dbp2 was eluted in 50 mM Tris-HCl at pH 8 with 600 mM NaCl, and 20% glycerol and stored at -80 °C until usage. Expression of pET28a His_6-*DBP2* in Rosetta *E. coli* (DE3) cells (Novagen) was induced by 0.2 mM IPTG at 16 °C and purified as previously described (Cloutier et al. 2012). Two consecutive TEV sites were inserted between the GST-tag and the coding sequence of Yra1 by PCR using pFS1853 GST-Yra1 as a template, a set of primer pairs that contain the TEV sites coding sequence flanked next to the GST-tag and Yra1 coding sequence. Forward primer: 5'-GAAAACCTGTACTTCCAGGGAATGTCTGCTAACTTAGATAAATCCTTAGAC-3'

and a reverse primer: 5'-TCCCTGGAAGTACAGGTTTTCCTCGAGATGGTCGCCACCACCAAACGTGGC-3'. Expression of the GST-TEV-YRA1 in Rosetta *E. coli* (DE3) cells (Novagen) was induced by 0.2 mM IPTG overnight at 16 °C and was subsequently purified from the soluble fraction using glutathione sepharose according to the manufacturer's instructions (GE healthcare). The GST tag was then cleaved with 50 U of TEV protease (Invitrogen) overnight at 16 °C. The cleaved purified recombinant proteins were subsequently subjected to SP sepharose (Sigma). Yra1 were eluted in 50 mM Tris-HCl at pH 8 with 600 mM NaCl, and 20% glycerol and stored at -80 °C until usage. Expression of the pET21 GST-Yra1C and pET21 GST-Yra1 RRM+C in Rosetta *E. coli* (DE3) cells (Novagen) was induced by 0.2 mM IPTG overnight at 16 °C and was subsequently purified from the soluble fraction using glutathione sepharose according to the manufacturer's instructions (GE healthcare). The purified proteins were eluted with 20mM glutathione, 150 mM NaCl, 20% glycerol and 20 mM HEPES at pH 7.5 and stored at -80 °C until usage.

Unwinding Assays

RNA oligonucleotides were purchased from Integrated DNA Technologies (IDT), and duplex substrates were prepared as previously described (Yang and Jankowsky 2005; Jankowsky and Putnam 2010). The blunt end RNA duplex sequences are: (top strand) 5'-AGCACCGUAAAGACGC-3' + (bottom strand) 5'-GCGUCUUUACGGUGCU-3'. The overhang RNA duplex sequences are: (top strand) 5'-AGCACCGUAAAGACGC-3' + (bottom strand) 5'-GCGUCUUUACGGUGCUUAAAACAAAACAAAACAAAAC-3'.

The blunt end RNA/DNA duplex sequences are: (top strand) 5'-GGCACGGUGGGGACCG-3' + (bottom strand) 5'-CGGTCCCCACCGTGCC-3'. The top strand of the RNA duplex was 5' end-labeled with [γ^{32}P]-ATP using T4 polynucleotide kinase according to standard methods. *In vitro* unwinding assays were conducted as previously described (Yang and Jankowsky 2005) except for using 0.1 nM ^{32}P labeled duplex in a 30 µl reaction mixture containing 40 mM TrisHCl (pH 8), 50 mM NaCl, 2.5 mM $MgCl_2$, 2 mM DTT, 60 U Superase-in (Life Technologies) and 600 nM Dbp2 and 600 nM or 1200 nM of Yra1 where indicated. The reaction mixture was incubated in a 19 °C water bath for 10 min prior to the reaction. All reactions were performed at 19 °C. Unwinding reactions were initiated by adding ATP (2 mM or 0.1 mM as indicated). At the times indicated, 3 µl aliquots were removed and the reaction was stopped with a buffer containing 1% SDS, 50 mM EDTA, 0.1% xylene cyanol, 0.1% bromophenol blue and 20% glycerol. Aliquots were subsequently resolved on a 10% nondenaturing PAGE. The gels were dried and radiolabeled RNAs were quantified using ImageQuant software. The data from each time point was calculated using the formula: fraction of single stranded = (single stranded RNA / total RNA). The integrated form of a homogenous first order rate law equation was used to fit the data to determine the $k_{obs}^{(unw)}$.

The rate constants for unwinding k_{unw} and k_{ann} were determined using Frac ss =**k**unw(**k**unw + **k**ann)-1(1 – exp(-(**k**unw + **k**ann)**t)**) as described in [26].

Annealing assays

In vitro annealing assays were performed in the presence of 2 mM or 0.1 mM ATP with

the same reaction mixture as unwinding assays without the 10 min pre-incubation. The RNA duplex was denatured at 95 °C for 2 min to generate single-stranded RNAs. All the reactions were conducted in a 19 °C water bath and were initiated by addition of 0.1 nM of the denatured substrate strands. Aliquots of the reactions were treated as described in the unwinding assays. The data from each time point was calculated as described in the unwinding assays. The integrated rate law for the bimolecular annealing reaction equation was used to fit the data to determine the $k_{obs}^{(ann)}$.

Cellular Microscopy

In situ hybridization was performed on cells that were grown to mid-log phase at the permissive temperature (25 °C) with -URA+2% glucose and then shifted to -URA+2% galactose for a 1-hour induction of *DBP2* overexpression. Cells were subsequently harvested, fixed with formaldehyde and mounted on glass slides. Poly(A)+ RNA was then visualized by microscopy following hybridization with digoxygenin-conjugated oligodT_{50} and detection with FITC-conjugated anti-digoxygenin secondary antibody (Roche) as previously described (Tran et al. 2007). DAPI staining was utilized to visualize DNA (Tran et al. 2007). Images were collected using an Olympus BX51 microscope using Metamorph software.

TAP-tag immunoprecipitation

Cells expressing genomically encoded Dbp2-TAP or untagged Dbp2 (BY4741) were grown in YPD at 30 °C to an OD_{600} of 0.6. Harvested cells were pelleted and injected into liquid nitrogen. The frozen cells were then lysed in the solid phase by milling, using

a planetary ball mill. The lysed cells were subsequently resuspended in 15ml of extraction buffer (20mM HEPES at pH7.4, 110 mM KoAc, 0.5% Triton X-100, 0.1% Tween-20 and 70 mM NaCl) in the presence of 1X protease inhibitor cocktail tablets (Roche) followed by centrifugation at 4700 RPM at 4 °C for 15 min as previously described (Carmody et al. 2010). The soluble fraction of the lysate was incubated with IgG-conjugated dynabeads at 4 °C for 30 min. The unbound protein was washed away with extraction buffer. The bound protein was eluted with 10 U of AcTEV protease (Life Technologies) followed by TCA precipitation. The proteins were then resolved by SDS-PAGE and detected by Western blotting analysis. Western blotting analysis was conducted with standard molecular biology techniques rabbit anti-Yra1 (Johnson et al. 2009), rabbit anti-Protein A and horseradish peroxidase conjugated goat anti-rabbit antibody (Sigma).

In vitro binding (pull down) assays

20 µg of recombinant, purified GST-Yra1, GST-Yra1 RRM+C, GST- Yra1 C, GST-Dbp5, His-Dbp2, Dbp5 or Dbp2 were incubated with the glutathione sepharose in 20 mM HEPES pH 7.5, 150 mM NaCl and 20% glycerol at room temperature for 10min as indicated following removal of 20% of the protein mixture for input. Bound proteins were eluted with 50 mM reduced glutathione in 20 mM HEPES pH 7.5, 150 mM NaCl and 20% glycerol and were resolved by SDS-PAGE followed by Coomassie staining.

In vitro ATPase assays

In vitro ATP hydrolysis assays were performed using a PK/lactate dehydrogenase enzyme-coupled absorbance assay as previously described (Cloutier et al. 2012), but with 200 nM Dbp2 and increasing amounts of recombinant purified Yra1, total yeast RNA (Sigma) or ATP as indicated. Presented data is the average of three independent experiments and the error bars represent the standard deviation.

In vivo UV cross-linking assays

Wild type and *dbp2Δ* yeast cells were grown in YPD at 30 °C. Mid-log phase cells were harvested and resuspended into 50 ml of 10 mM Tris-HCl at pH 7.5, 500 mM NaCl and 1 mM EDTA. The resuspended cells were then subjected to UV light with 180,000 μJ/cm^2 on ice for 2.5 minutes using UV Stratalinker 1800. The UV treatment was conducted twice with 45-second pause in between each treatment. The cells were then centrifuged at 4000 rpm for 10 minutes at 4 °C. The pelleted cells were resuspended into 10 ml of 10 mM Tris-HCl at pH 7.5, 500 mM NaCl, 1 mM EDTA, 500 U of Superase-in (Life Technologies), 1 mM PMSF and 0.5 X of protease inhibitor cocktail tablets (Roche). The cells were then lysed by bead beating, cleared by centrifugation and then subjected to poly(A)+ RNA pull down using oligo dT cellulose (Life Technologies). The RNA concentration from the eluted fraction was determined by measuring the absorbance at 260 nm. RNase treatment and TCA precipitation were then performed to recover bound proteins. Fractions were then resolved by SDS-PAGE and proteins were detected by western blotting with rabbit anti-Nab2 (Tran et al. 2007), rabbit anti-Mex67 (Gwizdek et al. 2006), rabbit anti-Yra1 (Johnson et al. 2009) and horseradish peroxidase conjugated goat anti-rabbit antibodies (Promega).

RT-qPCR analysis

RNA was isolated from oligo dT-purified RNPs (see UV crosslinking) by standard acid phenol purification. Equal fractions from the elution were then reverse transcribed into complementary DNA (cDNA) (Qiagen) and the quantity of *ACT1* RNA was measured by quantitative PCR using BioRad CFX96 system. The sequences for *ACT1* primers were: (Forward primer) 5'-TGGATTCCGGTGATGGTGTT3' and (Reverse primer) 5'-TCAAAATGGCGTGAGGTAGAGA-3'. The fold change of *ACT1* transcript abundance was calculated by normalizing the signal from each sample to the signal obtained from wild type without UV treatment and are reported as the average of three technical repeats with standard error from the mean (S.E.).

Serial dilution growth assay

Indicated strains were grown in -URA+2% glucose or YPD liquid cultures and then harvested at mid-log phase. Cells were then spotted in 5-fold serial dilutions onto -URA+2% glucose, -URA+2% galactose, or YPD plates and incubated at temperatures ranging from 16°C-37°C as indicated.

3.3 Results

3.3.1 Dbp2 catalyzes RNA duplex unwinding on blunt end and single-strand overhang substrates

Previous studies from our laboratory established that Dbp2 is an enzymatically active ATPase associated with transcribing genes (Cloutier et al. 2012). Moreover, we found that loss of *DBP2* in budding yeast results in RNA quality control and termination

defects, suggesting that Dbp2 may function in proper assembly of mRNPs in the nucleus. To shed light on the role of Dbp2 in gene expression, we first asked if Dbp2 is a *bona fide* RNA helicase *in vitro* and if this enzyme shows any preference for specific RNA duplex substrates. It is well established that DEAD-box proteins, with the exception of DbpA, show no sequence-specific association with RNA (Putnam and Jankowsky 2013). However, individual members display preferences for pure RNA duplexes and/or RNA-binding 'platforms' for duplex unwinding (Yang et al. 2007; Halls et al. 2007; Tijerina et al. 2006; Turner et al. 2007). To this end, we conducted an analysis of *in vitro* strand unwinding under pre-steady state conditions with three different nucleic acid substrates and 2 mM ATP:Mg^{2+} in the presence of recombinant, purified Dbp2 (Fig. 3.1 and Fig. 3.2). These substrates include a 16 base pair (bp) blunt ended RNA duplex, a 16-bp duplex of identical sequence with a 21 nucleotide (nt) single-stranded overhang and a 16-bp RNA-DNA duplex with a different sequence but similar stability (Fig. 3.1A). The latter was chosen to account for the fact that RNA-DNA duplexes are less stable than their RNA-RNA counterparts and that the ability of DEAD-box RNA helicases to unwind a given substrate is inversely proportional to duplex stability (Stampfl et al. 2013). The unwinding assays were then conducted with 600 nM of Dbp2 and preformed duplexes over a 30 min time frame (Fig. 3.1 and Fig. 3.3).

Consistent with other DEAD-box proteins, Dbp2 is able to unwind all three nucleic acid substrates with a preference for an RNA-RNA duplex (Fig. 3.1B-D). Importantly, we observed no ATP-independent unwinding activity, as evidenced from a lack of duplex destabilization after a 30 min incubation (Fig. 3.3A-C, lane 10). Unlike Ded1, which exhibits unwinding rate constants of ~0.1 min^{-1} or ~3.8 min^{-1} on blunt end

or single strand overhang duplexes, respectively (Yang et al. 2007), Dbp2 shows no preferential unwinding of a duplexed RNA with a single stranded region. This is evidenced by observed unwinding rates that are dependent upon the presence of Dbp2 and ATP (Fig. 3.1B-D, bottom; Fig. 3.3).

DEAD-box proteins also exhibit RNA-strand annealing activity *in vitro* (Putnam and Jankowsky 2013)[13]. To measure annealing activity, we conducted the same assay as above but with the single strand components for each substrate. This showed that the substrates have no spontaneous annealing activity whereas Dbp2 exhibits some annealing activity on all three substrates at 2 mM ATP (Fig. 3.1B-D, Fig. 3.3D-F). To determine the precise biochemical mechanism of Dbp2, we subsequently calculated rate constants for both unwinding an annealing because the observed unwinding rate does not distinguish between these two parameters. Initial attempts to measure observed annealing rates at 2mM ATP were complicated due to substantial unwinding activity. This results in a poor curve fit for annealing (open circles, Fig. 3.1B-D, Fig. 3.3), However, when this RNA-strand annealing activity is taken into account according to the steady-state equation in (Yang and Jankowsky 2005), both the unwinding and annealing rate constants were accurately determined (Fig. 3.1E). The similar unwinding rate constants of ~0.2 min^{-1} for both blunt end and overhang substrates further demonstrate that Dbp2 does not require a single stranded overhang for duplex destabilization (Fig. 3.1E). This is consistent with our previous studies demonstrating dsRNA-directed ATPase activity (Cloutier et al. 2012), and is similar to another DEAD-box protein, Mss116, whose activity is not enhanced by the presence of a single-stranded region within the RNA substrate (Halls et al. 2007). This suggests that Dbp2 recognizes duplexed RNAs directly.

3.3.2 Dbp2 preferentially anneals RNA duplexes with single-stranded regions at low ATP concentrations

Studies of the human ortholog of Dbp2, termed DDX5, have shown that this enzyme promotes efficient annealing under ATP-limiting conditions (Rössler et al. 2001). As mentioned above, DEAD-box proteins also facilitate strand annealing and, in some cases, this activity is biologically relevant (Halls et al. 2007; Yang and Jankowsky 2005; Zingler et al. 2010; Fedorova et al. 2010; Liebeg et al. 2010). To determine if the annealing activity of Dbp2 is enhanced by reduced ATP concentrations, we conducted our unwinding and annealing assays again but with 20-fold less ATP (0.1 mM ATP). Consistent with previous studies of Ded1 and Mss116 (Halls et al. 2007; Yang and Jankowsky 2005), Dbp2 efficiently annealed all three nucleic acid substrates at low ATP concentrations with little to no detectible unwinding activity (Fig. 3.4A-C and Fig. 3.5). Moreover, Dbp2 can anneal overhang and blunt end RNA substrates in the absence of ATP (data not shown). In contrast to other DEAD-box proteins, however, Dbp2 exhibits a strong annealing preference for RNA substrates with a single stranded overhang, resulting in a $k_{obs}^{(ann)}$ of 3.60 ± 0.50 min^{-1} (Fig. 3.4D). This is approximately four-fold higher than the 0.8 min^{-1} rate observed for the blunt end RNA-RNA and RNA-DNA duplexes. To the best of our knowledge, this preference has not been observed for any other DEAD-box protein to date, suggesting that Dbp2 has a unique ability to preferentially anneal structured RNAs with single stranded regions. In general, this is the type of secondary structure we expect to find in mRNAs, sporadic regions of duplex RNA flanked by single stranded regions. We would therefore speculate that this activity

might make Dbp2 a more effective chaperone for secondary structure formation of cellular mRNAs under specific growth conditions with limited ATP (see Discussion).

3.3.3 *DBP2* genetically interacts with mRNA export factors *YRA1* and *MEX67*

Given the biochemical activity of Dbp2, we would speculate that Dbp2 functions as an RNA chaperone for newly synthesized mRNA. Previous studies from our laboratory have provided evidence that Dbp2 is required for early gene expression steps including termination and RNA quality control (Cloutier et al. 2012), two processes intimately connected to mRNP assembly and export (Schmid and Jensen 2010; Moore and Proudfoot 2009; Fasken and Corbett 2009; Qu et al. 2009). To pinpoint the precise biological role of Dbp2, we first conducted a series of genetic studies with a plasmid that overexpresses *DBP2* via a galactose-inducible promoter (*pGAL-DBP2*), and strains harboring mutations in genes linked to 3' end formation and/or mRNA export. To this end, we selected yeast strains with mutations in the polyadenylation/cleavage factor *PCF11* (Birse et al. 1998; Amrani et al. 1997), the pre-mRNA splicing and export factor *SUB2* (Strässer and Hurt 2001; Kistler and Guthrie 2001), the RNA-binding protein gene *YRA1* (Stutz et al. 2000), and the mRNA export receptor *MEX67* (Segref et al. 1997), with the idea that overexpression of *DBP2* might either rescue or enhance the growth defects of specific mutant strains. Yeast strains were transformed with either vector alone or with a *pGAL-DBP2* high copy, overexpression vector and then plated as five-fold serial dilutions onto either transcriptionally-repressive (GLU) or inducing (GAL) media at multiple temperatures. Strikingly, whereas wild type, *pcf11-2, sub2-85* and *yra1*Δ*N*

mutant strains displayed no obvious growth differences, overexpression of *DBP2* was lethal in *mex67-5* cells at all temperatures (Fig.3.6A, bottom).

Because Mex67 is required for mRNA exit from the nucleus, we then asked if *DBP2* overexpression results in a perturbation of mRNA transport. This was addressed by conducting *in situ* hybridization assays to visualize the cellular localization of poly(A)+ RNAs by indirect immunofluorescence in wild type or *mex67-5* cells with vector only or overexpressed *DBP2*. Importantly, these experiments were conducted at the permissive temperature for *mex67-5*, which does not typically result in accumulation of poly(A)+ RNAs in nucleus (Segref et al. 1997). Whereas both wild type and *mex67-5* cells showed diffuse, whole cell staining in the presence of vector alone, *mex67-5* cells with overexpressed *DBP2* exhibited a striking accumulation of poly(A)+ RNA in the nucleus (Fig. 3.6B). We also observed a detectible accumulation of mRNA in the nucleus of wild type cells upon overexpression of *DBP2* (Fig. 3.6B), even though we did not previously observe any growth defects in wild type cells (Fig. 3.6A). It is of note that this nuclear poly(A)+ RNA accumulation is not as great as when the *mex67-5* cells are grown at the non-permissive temperature of 37˚C ((Segref et al. 1997) and data not shown) suggesting that the export block is modest or is a result of a secondary effect. Consistent with the latter, we observed no mRNA transport defects in a *dbp2*Δ strain (data not shown). Thus, *DBP2* overexpression induces a slight mRNA export defect in *mex67-5* cells, suggesting a role for this enzyme during or immediately prior to mRNA transport.

Mex67 is recruited to nascent mRNPs during transcription through protein-protein interactions with RNA-binding proteins Npl3, Yra1 and Nab2 (Strasser and Hurt 2000; Iglesias et al. 2010; Gilbert and Guthrie 2004). Interestingly, recent studies have

documented an interaction between DDX5 and Aly, the human ortholog of Yra1 (Zonta et al. 2013). This suggests that Dbp2 may be functionally connected to Mex67 recruitment through Yra1. To test this, we asked if loss of *DBP2* results in synthetic genetic interactions with *mex67-5* or *yra1*Δ*N* alleles by constructing double mutant strains and analyzing growth defects as above. Both the *mex67-5* and *yra1*Δ*N* strains failed to grow at 37˚C whereas the *dbp2*Δ exhibits a previously documented cold sensitive growth at 25˚C and below (Cloutier et al. 2012; Segref et al. 1997; Zenklusen et al. 2001). However, the *yra1*Δ*N dbp2*Δ strain displayed severely retarded growth at the permissive temperature for both single mutants alone (30˚C), suggesting that *DBP2* and *YRA1* are functionally linked (Fig. 3.6C). Loss of *DBP2* also results in a synthetic growth defect with *mex67-5*, albeit much weaker than with *yra1*Δ*N* (Fig. 3.6C). This suggests that Dbp2 and Yra1 function in a similar pathway and that Dbp2 is not directly required for mRNA export.

3.3.4 *DBP2* is required for efficient association of Yra1, Nab2 and Mex67 with poly(A)+ RNA

Messenger RNA is assembled with 12-30 different RNA-binding proteins to form co-transcriptionally assembled mRNPs (Hogan et al. 2008). Given the genetic interactions between *DBP2*, *YRA1* and *MEX67* above, we asked if *DBP2* is required for efficient association of these RNA-binding proteins with mRNA. To test this, we conducted *in vivo* UV crosslinking and subsequently isolated poly(A)+RNA from wild type or *dbp2*Δ cells. We then analyzed the association of Yra1 and Mex67 by western blotting the isolated fractions. We also analyzed Nab2, a nuclear poly(A)-RNA-binding

protein that interacts directly with both Yra1 and Mex67 (Iglesias et al. 2010; Anderson et al. 1993). Strikingly, this analysis revealed that all three proteins, Yra1, Nab2 and Mex67, exhibit reduced association with poly(A)+ RNA in *dbp2*Δ cells (Fig. 3.7A-C). This decrease is not due to differences in UV-independent, nonspecific binding, as evidenced by a representative western blot (Fig. 3.7D). Furthermore, analysis of *ACT1* transcript abundance by reverse transcription-quantitative PCR (RT-qPCR) revealed that this reduction in *dbp2*Δ cells is not due to mRNA isolation efficiency (Fig. 3.7E). Thus, Dbp2 is required for efficient association of Yra1, Nab2 and Mex67 with poly(A)+ RNA, consistent with a role in nuclear mRNP assembly.

3.3.5 Dbp2 physically interacts with Yra1 *in vivo* and *in vitro*

Many DEAD-box proteins associate with protein co-factors that either regulate the enzymatic activity or direct the biological role of a given DEAD-box enzyme (Jankowsky 2011). Two independent studies have identified Dbp2 as a component of Yra1-bound protein complexes, suggesting that Dbp2 may interact directly with Yra1 (Oeffinger et al. 2007; Kashyap et al. 2005). To test this, we first confirmed the previous interaction by asking if Yra1 copurifies with a genomically-encoded, TAP-tagged Dbp2 in yeast cells, which consists of two IgG-binding units of Protein A, a TEV cleavage site and the calmodulin-binding peptide that is fused to Dbp2 (Fig. 3.8A). An untagged wild type strain was utilized as a negative control for background association of Yra1 with the IgG-bound magnetic beads. Consistent with the previous studies, selection of Dbp2-TAP results in co-purification of Yra1 (Fig. 3.8A). No Yra1 was detected in our background control, indicating that the interaction is Dbp2-dependent. Next, we asked if the

association between Dbp2 and Yra1 is direct by conducting protein pull downs with recombinant, purified proteins expressed in *E. coli*. Dbp2 and Yra1 were expressed as N-terminal HIS-tag or GST-tag fusion proteins, respectively, and then purified to homogeneity by standard affinity chromatography methods. The proteins were then incubated together, selected on glutathione resin selection, resolved by SDS-PAGE electrophoresis and visualized by Coomassie staining (Fig. 3.8B). Dbp5 is another DEAD-box protein was used as negative control for non-specific interactions. Whereas Dbp2 does not interact beads alone or with Dbp5 (Fig. 3.8B, lanes 2 and 8), Dbp2 was co-purified with GST-tagged Yra1 (Fig. 3.8B, lane 4). Dbp5, on the other hand, did not co-purify with GST-Yra1 (Fig. 3.8B, lane 6), further demonstrating the specificity of the interaction with Dbp2. Thus, Dbp2 interacts directly with Yra1.

Yra1 is an evolutionarily conserved RNA-binding protein and export factor (REF) (Stutz et al. 2000). Like other members of the REF protein family, Yra1 contains a central RNA recognition motif (RRM), two variable spacer regions, and highly conserved N- and C-termini (REF-N and REF-C, respectively)((Stutz et al. 2000), Fig. 3.8C). Previous studies have shown that Mex67 interacts with the N-terminus (a.a. 1-77) and C-variable spacer region (a.a. 167-210) of Yra1, whereas the N-variable spacer region (a.a. 14-77) and C-variable spacer region (a.a. 167-210) of this protein are each sufficient to interact with RNA (Zenklusen et al. 2001). To determine what region of Yra1 is necessary for Dbp2 binding, we obtained bacterial expression plasmids for expression of two GST-tagged Yra1 truncation mutations that express either the RRM and C-terminal region (RRM+C) or the C-terminal region alone (yra1C) (Fig. 3.8C, (Johnson et al. 2009)). We then purified the truncation mutants and conducted pull down assays as

above. Interestingly, Dbp2 interacted with all three proteins, full length Yra1, Yra1 RRM+C and the C-terminus alone (Fig. 3.8D, lanes 6 and 8), suggesting that the C-terminus constitutes the Dbp2-binding domain. We then attempted to determine if the C-terminus is necessary for this interaction, however, we were unable to express the GST-yra1ΔC mutant in bacteria. Regardless, these studies suggest that Dbp2 interacts with the C-terminus of Yra1.

3.3.6 Yra1 inhibits the helicase activity of Dbp2

Many DEAD-box protein factors also regulate the enzymatic activity of their respective RNA helicase. This includes the translation initiation factor eIF4A, whose helicase activity is activated by eIF4B, 4H and 4F, and eIF4AIII, whose ATPase activity is inhibited by Y14 and MAGOH (Oberer et al. 2005; Rogers Jr. et al. 2001; Ballut et al. 2005; Nielsen et al. 2009). Thus, we asked if Yra1 modulates the helicase activity of Dbp2. To test this, we first conducted *in vitro* unwinding assays with Dbp2 in the presence of full length Yra1. However, we were unable to accurately measure the unwinding activity of Dbp2 due to the previously documented strand annealing activity of Yra1 ((Portman et al. 1997) and data not shown). To resolve this problem, we then analyzed the annealing activity of the minimal Dbp2-interacting domain, yra1C, which has previously been shown to have severely impaired RNA-binding activity *in vitro* (Zenklusen et al. 2001). Importantly, this revealed that the yra1C protein has no intrinsic annealing activity *in vitro* at the tested concentrations (Fig. 3.9E-F). To test the effect of yra1C on the unwinding activity of Dbp2, we conducted unwinding assays as above with the blunt end RNA duplex either with Dbp2 alone or with equimolar or two-fold excess

of Yra1 (Fig. 3.10). Strikingly, we found that yra1C decreased both the unwinding rate ($k_{obs}^{(unw)}$) and the amplitude of duplex unwinding by Dbp2 (Fig. 3.10A-B; Fig. 3.9A-C). In fact, the decreased unwinding rate is almost a full order of magnitude lower with yra1C (Fig. 3.10B). We also tested the unwinding activity of Dbp2 in the presence of two-fold molar excess of BSA to show that the unwinding inhibition effect is specific to Yra1. Interestingly, this revealed a slight increase in the *kobs* for unwinding most likely due to molecular crowding (Fig. 3.10A-B; Fig. 3.9D). This suggests that the inhibition of Dbp2 is specific to Yra1.

To elucidate the mechanism of inhibition, we then asked if Yra1 alters the ATPase activity of Dbp2 by conducting *in vitro* ATP hydrolysis assays with increasing concentrations of full length Yra1 or BSA (Fig. 3.10C). Consistent with our previous studies, Dbp2 exhibited an observed ATP hydrolysis rate (k_{obs}) of 21 min^{-1} with saturating RNA (250 □g/ml of total yeast RNA) and 1 mM ATP (Fig. 3.10C). Whereas addition of BSA resulted in a slight enhancement of the k_{obs} from 21 to 25 min^{-1}, Yra1 gave a greater stimulation at each tested concentration. Thus, Yra1 slightly enhances the ATPase activity of Dbp2.

To determine if Yra1 enhances the ATPase rate by increasing the ATP-binding affinity of Dbp2, we measured the K_M for ATP with or without a two-fold excess of Yra1 or BSA (Fig. 3.10D). This revealed that Yra1 reduces the K_M for ATP by ~30%, from 2.3 to 1.6 mM. This modest effect is similar to the observed increase in ATPase rate. Although moderate, this increase is specific for Yra1 as addition of BSA resulted in an ATPase curve that was superimposable with Dbp2 alone. This suggests that Yra1 stimulates the ATPase activity of Dbp2 through increasing the affinity for ATP. We

suggest that this decrease in the K_M is biologically relevant because it occurs within the physiological range of cellular ATP concentrations.

Finally, we asked if Yra1 alters the effective RNA-binding activity of Dbp2. Thus, we measured the ATPase activity of Dbp2 as above but with a range of RNA concentrations from 1 ng/ml to 1 mg/ml (Fig. 3.10E). It is of note that the EC_{50} of Dbp2 alone is lower than our previous studies (Cloutier et al. 2012), due to a more refined purification method for enzymatically-active Dbp2 that increases its specific activity. Interestingly, inclusion of Yra1 increased the amount of RNA necessary for ATP hydrolysis by Dbp2 by ~50% (Fig. 3.10E). This suggests that Yra1 slightly reduces the RNA-binding affinity of Dbp2, while increasing the ATP binding and hydrolysis rate. We suggest that these subtle changes on the enzymatic parameters of Dbp2 result in release of Dbp2 from RNA, thereby inhibiting helicase activity *in vitro.* It is also possible that inhibition could also be due to Yra1 blocking initial association of Dbp2 with RNA. However, if this were the case, we would expect that Yra1 would reduce the RNA-dependent ATPase activity (Fig. 3.10C). Because we do not observe a decrease in RNA-dependent ATPase activity, this suggests that Yra1 inhibits duplex unwinding of Dbp2 through an as-of-yet uncharacterized mode distinct from other DEAD-box RNA helicase-interacting proteins.

Taken together, we provide a model whereby Yra1 controls the enzymatic activity of Dbp2 to promote proper mRNP formation in gene expression (Fig. 3.11). During transcription, Dbp2 unwinds aberrant structures on the nascent transcript that are refractory to RNA-binding protein assembly. This facilitates the loading of Yra1, Mex67 and Nab2 and likely other RNA-binding proteins onto the mRNA. The interaction of

Yra1 with Dbp2 then inhibits duplex unwinding and possibly also promotes Dbp2 release. Alternatively, Dbp2 may remain bound to the mRNA as part of a Yra1-Dbp2 complex. If this were the case, Dbp2 would function similarly to eIF4AIII, which acts as an RNA clamp for an ribonucleoprotein complex (Ballut et al. 2005). With either scenario, we predict that inhibition of Dbp2 helicase activity by Yra1 prevents further remodeling of the properly assembled mRNP, as DEAD-box proteins can also efficiently remodel ribonucleoprotein complexes (Tran et al. 2007; Jankowsky et al. 2001; Fairman et al. 2004). This constitutes a previously unknown mechanism for regulation of RNA helicases as well as the first biochemical mechanism for co-transcriptional assembly of a mRNP complex.

3.4 Discussion

Proper nuclear mRNP assembly is crucial for co-transcriptional and post-transcriptional processing steps including removal of introns by splicing, 3' end cleavage and polyadenylation, as well as formation of a translationally competent mRNA (Schmid and Jensen 2010; Kallehauge et al. 2012). During each of these steps, the evolving mRNP must assemble with a complement of RNA-binding proteins to direct the next step in the gene expression process. Our studies now provide evidence that the DEAD-box RNA helicase, Dbp2, plays a critical role in mRNP assembly in the nucleus. The human ortholog of Dbp2, termed DDX5, has been implicated in numerous transcriptional and post-transcriptional events, including transcriptional regulation, alternative splicing and microRNA processing (Janknecht 2010; Caretti et al. 2006; Kar et al. 2011; Salzman et al. 2007). The fact that ectopic expression of human DDX5 in yeast fully complements

the growth defects of *dbp2*Δ cells suggests that these roles are evolutionarily conserved (Barta and Iggo 1995). Given the multifaceted role, it is likely that DDX5 and Dbp2 are major players in the structural assembly of the transcriptome in all eukaryotes.

Our studies establish that Dbp2 is a *bona fide* RNA helicase, with efficient duplex unwinding activity on blunt ended duplexes. This suggests that Dbp2 recognizes secondary structure directly, without the need for a single stranded region for initial "loading" of the enzyme. This activity is consistent with a subset of DEAD-box family members with highly efficient duplex unwinding, such as CYT-19 and Mss116 (Halls et al. 2007; Chen et al. 2008; Del Campo et al. 2009; Yang and Jankowsky 2006). Moreover, it is consistent with our previous observation that Dbp2 displays dsRNA-directed ATPase activity (Cloutier et al. 2012). Interestingly, whereas the core sequence is conserved among all DEAD-box protein family members, these three enzymes also contain a C-terminal RGG extension. In fact, a recent biochemical and structural analysis of CYT-19 demonstrated that the RGG motif of this enzyme functions as a 'tether" to enable multiple rounds of duplex unwinding (Mallam et al. 2011).

Several DEAD-box proteins have been shown to utilize protein cofactors to trigger duplex unwinding by increasing the ATP binding or RNA-binding affinities of an inefficient DEAD-box enzyme (Rogers Jr. et al. 2001; Granneman et al. 2006; Alcazar-Roman et al. 2006; Weirich et al. 2006). Given the high duplex unwinding activity of Dbp2, however, inhibition may be the more important mode of regulation. In support of this, we find that Yra1 inhibits the helicase activity of Dbp2. The human ortholog of Dbp2, DDX5, was recently shown to interact with Aly, the human counterpart to Yra1 (Zonta et al. 2013), suggesting that this regulation is conserved in higher eukaryotes. We

speculate that *in vivo* the modulation of Dbp2 helicase activity by Yra1 is utilized to prevent further remodeling of the assembled mRNP. If this is the case, this would constitute a previously unrecognized mechanism for temporal regulation of DEAD-box enzymes *in vivo.* Although we do not know the mechanism for inhibition of duplex unwinding by Yra1, a recent study of Mss116 revealed that DEAD-box proteins are modular enzymes (Mallam et al. 2012). In fact, the C-terminal domain provides direct recognition of double-stranded RNA duplexes whereas the N-terminal domain interacts with ATP (Mallam et al. 2012). The ability to couple ATP hydrolysis with duplex unwinding lies in the formation of a closed helicase with juxtaposed N and C-terminal domains (Mallam et al. 2012). Because our studies suggest that Yra1 uncouples ATP hydrolysis from duplex unwinding, it will be interesting to determine the precise mechanism for Yra1-dependent inhibition of Dbp2 given this insight.

Our studies show that Dbp2 is required for assembly of Yra1, Nab2 and Mex67 onto Poly(A)+ RNA. It is well established that proper termination and 3' end formation is required for mRNA export, as defects in these processes result in impaired recruitment of Mex67 to newly synthesized mRNAs and RNA decay (Qu et al. 2009; Schmid et al. 2012; Saguez et al. 2008). The fact that loss of *DBP2* results in reduced association of Mex67 as well as the poly(A)+ RNA-binding protein Nab2, suggests that Dbp2 functions concert with termination and 3' end formation. In support of this, loss of *DBP2* results in transcription of a bicistronic *GAL10-GAL7* mRNA, a characteristic phenotype of termination defects (Cloutier et al. 2012). This idea is also consistent with our genetic analysis and the fact that *DBP2* overexpression resulted in lethality of *mex67-5* strains but not *sub2-85* or *pcf11-2* strains. This suggests that Dbp2 functions upstream of Mex67

but downstream or independent of Sub2 and Pcf11. Interestingly, Yra1 also interacts directly with all three of these proteins (Strässer and Hurt 2001; Strasser and Hurt 2000; Johnson et al. 2009), indicating that this small protein acts as a coupling factor for multiple co-transcriptional processing and assembly steps. Furthermore, recent studies from the Bentley laboratory have demonstrated that Pcf11 is required for recruitment of Yra1 to chromatin, which then functions to modulate poly(A) site selection (Johnson et al. 2009, 2011). Thus, the order of events for this process and role of Dbp2 in termination is an intriguing question for future studies.

In addition to canonical duplex unwinding, our studies also show that Dbp2 displays strong RNA strand-annealing activity. This is not unprecedented as the DEAD-box protein Mss116 utilizes both annealing and duplex unwinding activities to promote folding of the ai5□ group II intron in mitochondria (Zingler et al. 2010; Fedorova et al. 2010; Liebeg et al. 2010). This would suggest that Dbp2 could function similarly, however, in contrast to Mss116, Dbp2 only displays significant annealing under ATP-limiting conditions. Interestingly, recent work from the Parker laboratory revealed that, under conditions of glucose starvation, the sub-cellular localization of numerous RNA-binding proteins is drastically altered (Mitchell et al. 2013). This suggests that cellular ribonucleoprotein complexes undergo dynamic alterations in nutrient-limited conditions when cellular ATP concentrations are low. Thus, it will be interesting to determine the function of Dbp2 under specific physiological growth conditions, which may promote strand annealing.

Our studies now add Dbp2 to the complement of DEAD-box proteins that function in nuclear mRNP assembly in *S. cerevisiae*. This includes Sub2, which

functions in both splicing and formation of an export competent mRNP, and Dbp5, which promotes nuclear release of exporting transcripts (Linder and Jankowsky 2011). When considering that rRNA biogenesis requires 21 of the 25 DEAD-box proteins in budding yeast (Linder and Jankowsky 2011; Cordin et al. 2006), one might ask why there aren't more DEAD-box RNA helicases associated with mRNP biogenesis. Unlike other cellular RNAs such as snRNAs, tRNAs and rRNAs, mRNAs stand out as distinct as tertiary structure does not appear to play a large role in the functionality of these RNAs in eukaryotes. Given the propensity for RNAs to fold and misfold in solution (Zemora and Waldsich 2010), the prevailing model is that co-transcriptional association of RNA-binding proteins maintains primarily linear structure of a nascent transcript (Schmid and Jensen 2010). Although the average length of an mRNA is 1kb, pre-mRNA transcripts can range from a 3 Kb to ~2.5 Mb, making it likely that DEAD-box helicases function as key structural modulators of the transcriptome. The challenge then will be defining the precise molecular rearrangements that require DDX5/Dbp2 or other members of the DEAD-box protein family given the highly coupled nature of nuclear gene expression steps. With the advancement in RNA sequence and target identification coupled with structural studies of mRNAs (Wan et al. 2011), these questions can be addressed in the very near future.

3.5 References

Alcazar-Roman AR, Tran EJ, Guo S, Wente SR. 2006. Inositol hexakisphosphate and Gle1 activate the DEAD-box protein Dbp5 for nuclear mRNA export. *Nat Cell Biol* **8**: 711–716.

Amrani N, Minet M, Wyers F, Dufour ME, Aggerbeck LP, Lacroute F. 1997. PCF11 encodes a third protein component of yeast cleavage and polyadenylation factor I. *Mol Cell Biol* **17**: 1102–1109.

Anderson JT, Wilson SM, Datar K V, Swanson MS. 1993. NAB2: a yeast nuclear polyadenylated RNA-binding protein essential for cell viability. *Mol Cell Biol* **13**: 2730–2741.

Ballut L, Marchadier B, Baguet A, Tomasetto C, Seraphin B, Le Hir H. 2005. The exon junction core complex is locked onto RNA by inhibition of eIF4AIII ATPase activity. *Nat Struct Mol Biol* **12**: 861–869.

Barta I, Iggo R. 1995. Autoregulation of expression of the yeast Dbp2p "DEAD-box" protein is mediated by sequences in the conserved DBP2 intron. *EMBO J* **14**: 3800–3808.

Birse CE, Minvielle-Sebastia L, Lee BA, Keller W, Proudfoot NJ. 1998. Coupling termination of transcription to messenger RNA maturation in yeast. *Science* **280**: 298–301.

Buszczak M, Spradling AC. 2006. The Drosophila P68 RNA helicase regulates transcriptional deactivation by promoting RNA release from chromatin. *Genes Dev* **20**: 977–989.

Caretti G, Schiltz RL, Dilworth FJ, Di Padova M, Zhao P, Ogryzko V, Fuller-Pace F V., Hoffman EP, Tapscott SJ, Sartorelli V. 2006. The RNA Helicases p68/p72 and the Noncoding RNA SRA Are Coregulators of MyoD and Skeletal Muscle Differentiation. *Dev Cell* **11**: 547–560.

Carmody SR, Tran EJ, Apponi LH, Corbett AH, Wente SR. 2010. The mitogen-activated protein kinase Slt2 regulates nuclear retention of non-heat shock mRNAs during heat shock-induced stress. *Mol Cell Biol* **30**: 5168–5179.

Chen Y, Potratz JP, Tijerina P, Del Campo M, Lambowitz AM, Russell R. 2008. DEAD-box proteins can completely separate an RNA duplex using a single ATP. *Proc Natl Acad Sci U S A* **105**: 20203–20208.

Cloutier SC, Ma WK, Nguyen LT, Tran EJ. 2012. The DEAD-box RNA helicase Dbp2 connects RNA quality control with repression of aberrant transcription. *J Biol Chem* **287**: 26155–26166.

Cordin O, Banroques J, Tanner NK, Linder P. 2006. The DEAD-box protein family of RNA helicases. *Gene* **367**: 17–37.

Del Campo M, Mohr S, Jiang Y, Jia H, Jankowsky E, Lambowitz AM. 2009. Unwinding by local strand separation is critical for the function of DEAD-box proteins as RNA chaperones. *J Mol Biol* **389**: 674–693.

Fairman ME, Maroney PA, Wang W, Bowers HA, Gollnick P, Nilsen TW, Jankowsky E. 2004. Protein displacement by DExH/D "RNA helicases" without duplex unwinding. *Science (80-)* **304**: 730–734.

Fasken MB, Corbett AH. 2009. Mechanisms of nuclear mRNA quality control. *RNA Biol* **6**: 237–41.

Fedorova O, Solem A, Pyle AM. 2010. Protein-Facilitated Folding of Group II Intron Ribozymes. *J Mol Biol* **397**: 799–813.

Fukuda T, Yamagata K, Fujiyama S, Matsumoto T, Koshida I, Yoshimura K, Mihara M, Naitou M, Endoh H, Nakamura T, et al. 2007. DEAD-box RNA helicase subunits of the Drosha complex are required for processing of rRNA and a subset of microRNAs. *Nat Cell Biol* **9**: 604–611.

Gaspar P, Moura G, Santos MAS, Oliveira JL. 2013. MRNA secondary structure optimization using a correlated stem-loop prediction. *Nucleic Acids Res* **41**.

Gilbert W, Guthrie C. 2004. The Glc7p Nuclear Phosphatase Promotes mRNA Export by Facilitating Association of Mex67p with mRNA. *Mol Cell* **13**: 201–212.

Granneman S, Lin C, Champion EA, Nandineni MR, Zorca C, Baserga SJ. 2006. The nucleolar protein Esf2 interacts directly with the DExD/H box RNA helicase, Dbp8, to stimulate ATP hydrolysis. *Nucleic Acids Res* **34**: 3189–3199.

Gwizdek C, Iglesias N, Rodriguez MS, Ossareh-Nazari B, Hobeika M, Divita G, Stutz F, Dargemont C. 2006. Ubiquitin-associated domain of Mex67 synchronizes recruitment of the mRNA export machinery with transcription. *Proc Natl Acad Sci U S A* **103**: 16376–16381.

Halls C, Mohr S, Del Campo M, Yang Q, Jankowsky E, Lambowitz AM. 2007. Involvement of DEAD-box proteins in group I and group II intron splicing. Biochemical characterization of Mss116p, ATP hydrolysis-dependent and -independent mechanisms, and general RNA chaperone activity. *J Mol Biol* **365**: 835–855.

Hogan DJ, Riordan DP, Gerber AP, Herschlag D, Brown PO. 2008. Diverse RNA-binding proteins interact with functionally related sets of RNAs, suggesting an extensive regulatory system. *PLoS Biol* **6**: 2297–2313.

Iglesias N, Tutucci E, Gwizdek C, Vinciguerra P, Von Dach E, Corbett AH, Dargemont C, Stutz F. 2010. Ubiquitin-mediated mRNP dynamics and surveillance prior to budding yeast mRNA export. *Genes Dev* **24**: 1927–1938.

Janknecht R. 2010. Multi-talented dead-box proteins and potential tumor promoters: P68 RNA helicase (DDx5) and its paralog, p72 RNA helicase (DDx17). *Am J Transl Res* **2**: 223–234.

Jankowsky E. 2011. RNA helicases at work: binding and rearranging. *Trends Biochem Sci* **36**: 19–29.

Jankowsky E, Gross CH, Shuman S, Pyle AM. 2001. Active disruption of an RNA-protein interaction by a DExH/D RNA helicase. *Science (80-)* **291**: 121–125.

Jankowsky E, Putnam A. 2010. Duplex unwinding with DEAD-box proteins. *Methods Mol Biol* **587**: 245–264.

Johnson SA, Cubberley G, Bentley DL. 2009. Cotranscriptional recruitment of the mRNA export factor Yra1 by direct interaction with the 3’ end processing factor Pcf11. *Mol Cell* **33**: 215–226.

Johnson SA, Kim H, Erickson B, Bentley DL. 2011. The export factor Yra1 modulates mRNA 3’ end processing. *Nat Struct Mol Biol* **18**: 1164–1171.

Kallehauge TB, Robert MC, Bertrand E, Jensen TH. 2012. Nuclear Retention Prevents Premature Cytoplasmic Appearance of mRNA. *Mol Cell* **48**: 145–152.

Kar A, Fushimi K, Zhou X, Ray P, Shi C, Chen X, Liu Z, Chen S, Wu JY. 2011. RNA helicase p68 (DDX5) regulates tau exon 10 splicing by modulating a stem-loop structure at the 5’ splice site. *Mol Cell Biol* **31**: 1812–1821.

Kashyap AK, Schieltz D, Yates 3rd J, Kellogg DR. 2005. Biochemical and genetic characterization of Yra1p in budding yeast. *Yeast* **22**: 43–56.

Katahira J, Strasser K, Podtelejnikov A, Mann M, Jung JU, Hurt E. 1999. The Mex67p-mediated nuclear mRNA export pathway is conserved from yeast to human. *EMBO J* **18**: 2593–2609.

Kertesz M, Wan Y, Mazor E, Rinn JL, Nutter RC, Chang HY, Segal E. 2010. Genome-wide measurement of RNA secondary structure in yeast. *Nature* **467**: 103–107.

Kistler AL, Guthrie C. 2001. Deletion of MUD2, the yeast homolog of U2AF65, can bypass the requirement for Sub2, an essential spliceosomal ATPase. *Genes Dev* **15**: 42–49.

Liebeg A, Mayer O, Waldsich C. 2010. DEAD-box protein facilitated RNA folding in vivo. *RNA Biol* **7**: 803–11.

Linder P, Jankowsky E. 2011. From unwinding to clamping - the DEAD box RNA helicase family. *Nat Rev Mol Cell Biol* **12**: 505–516.

Mallam AL, Del Campo M, Gilman B, Sidote DJ, Lambowitz AM. 2012. Structural basis for RNA-duplex recognition and unwinding by the DEAD-box helicase Mss116p. *Nature* **490**: 121–125.

Mallam AL, Jarmoskaite I, Tijerina P, Del Campo M, Seifert S, Guo L, Russell R, Lambowitz AM. 2011. Solution structures of DEAD-box RNA chaperones reveal conformational changes and nucleic acid tethering by a basic tail. *Proc Natl Acad Sci U S A* **108**: 12254–12259.

Mitchell SF, Jain S, She M, Parker R. 2013. Global analysis of yeast mRNPs. *Nat Struct Mol Biol* **20**: 127–133.

Moore MJ. 2005. From birth to death: the complex lives of eukaryotic mRNAs. *Science (80-)* **309**: 1514–1518.

Moore MJ, Proudfoot NJ. 2009. Pre-mRNA Processing Reaches Back toTranscription and Ahead to Translation. *Cell* **136**: 688–700.

Nielsen KH, Chamieh H, Andersen CB, Fredslund F, Hamborg K, Le Hir H, Andersen GR. 2009. Mechanism of ATP turnover inhibition in the EJC. *RNA* **15**: 67–75.

Oberer M, Marintchev A, Wagner G. 2005. Structural basis for the enhancement of eIF4A helicase activity by eIF4G. *Genes Dev* **19**: 2212–2223.

Oeffinger M, Wei KE, Rogers R, DeGrasse JA, Chait BT, Aitchison JD, Rout MP. 2007. Comprehensive analysis of diverse ribonucleoprotein complexes. *Nat Methods* **4**: 951–956.

Portman DS, O'Connor JP, Dreyfuss G. 1997. YRA1, an essential Saccharomyces cerevisiae gene, encodes a novel nuclear protein with RNA annealing activity. *RNA* **3**: 527–537.

Putnam AA, Jankowsky E. 2013. DEAD-box helicases as integrators of RNA, nucleotide and protein binding. *Biochim Biophys Acta* **1829**: 884–893.

Qu X, Lykke-Andersen S, Nasser T, Saguez C, Bertrand E, Jensen TH, Moore C. 2009. Assembly of an export-competent mRNP is needed for efficient release of the 3'-end processing complex after polyadenylation. *Mol Cell Biol* **29**: 5327–5338.

Rajkowitsch L, Chen D, Stampfl S, Semrad K, Waldsich C, Mayer O, Jantsch MF, Konrat R, Blasi U, Schroeder R. 2007. RNA chaperones, RNA annealers and RNA helicases. *RNA Biol* **4**: 118–130.

Rogers Jr. GW, Richter NJ, Lima WF, Merrick WC. 2001. Modulation of the helicase activity of eIF4A by eIF4B, eIF4H, and eIF4F. *J Biol Chem* **276**: 30914–30922.

Rössler OG, Straka A, Stahl H. 2001. Rearrangement of structured RNA via branch migration structures catalysed by the highly related DEAD-box proteins p68 and p72. *Nucleic Acids Res* **29**: 2088–2096.

Saguez C, Schmid M, Olesen JR, Ghazy MAEH, Qu X, Poulsen MB, Nasser T, Moore C, Jensen TH. 2008. Nuclear mRNA Surveillance in THO/sub2 Mutants Is Triggered by Inefficient Polyadenylation. *Mol Cell* **31**: 91–103.

Salzman DW, Shubert-Coleman J, Furneaux H. 2007. P68 RNA helicase unwinds the human let-7 microRNA precursor duplex and is required for let-7-directed silencing of gene expression. *J Biol Chem* **282**: 32773–32779.

Schmid M, Jensen TH. 2010. Nuclear quality control of RNA polymerase II transcripts. *Wiley Interdiscip Rev RNA* **1**: 474–485.

Schmid M, Poulsen MB, Olszewski P, Pelechano V, Saguez C, Gupta I, Steinmetz LM, Moore C, Jensen TH. 2012. Rrp6p Controls mRNA Poly(A) Tail Length and Its Decoration with Poly(A) Binding Proteins. *Mol Cell* **47**: 267–280.

Segref A, Sharma K, Doye V, Hellwig A, Huber J, Lührmann R, Hurt E. 1997. Mex67p, a novel factor for nuclear mRNA export. Binds to both poly(A)+ RNA and nuclear pores. *EMBO J* **16**: 3256–3271.

Stampfl S, Doetsch M, Beich-Frandsen M, Schroeder R. 2013. Characterization of the kinetics of RNA annealing and strand displacement activities of the E. coli DEAD-box helicase CsdA. *RNA Biol* **10**: 149–56.

Stern S, Powers T, Changchien LM, Noller HF. 1989. RNA-protein interactions in 30S ribosomal subunits: folding and function of 16S rRNA. *Science* **244**: 783–790.

Strasser K, Hurt E. 2000. Yra1p, a conserved nuclear RNA-binding protein, interacts directly with Mex67p and is required for mRNA export. *EMBO J* **19**: 410–420.

Strässer K, Hurt E. 2001. Splicing factor Sub2p is required for nuclear mRNA export through its interaction with Yra1p. *Nature* **413**: 648–652.

Strasser K, Masuda S, Mason P, Pfannstiel J, Oppizzi M, Rodriguez-Navarro S, Rondon AG, Aguilera A, Struhl K, Reed R, et al. 2002. TREX is a conserved complex coupling transcription with messenger RNA export. *Nature* **417**: 304–308.

Stutz F, Bachi A, Doerks T, Braun IC, Seraphin B, Wilm M, Bork P, Izaurralde E. 2000. REF, an evolutionary conserved family of hnRNP-like proteins, interacts with TAP/Mex67p and participates in mRNA nuclear export. *RNA* **6**: 638–650.

Sugimoto N, Nakano S, Katoh M, Matsumura A, Nakamuta H, Ohmichi T, Yoneyama M, Sasaki M. 1995. Thermodynamic parameters to predict stability of RNA/DNA hybrid duplexes. *Biochemistry* **34**: 11211–11216.

Tijerina P, Bhaskaran H, Russell R. 2006. Nonspecific binding to structured RNA and preferential unwinding of an exposed helix by the CYT-19 protein, a DEAD-box RNA chaperone. *Proc Natl Acad Sci U S A* **103**: 16698–16703.

Tran EJ, Zhou Y, Corbett AH, Wente SR. 2007. The DEAD-box protein Dbp5 controls mRNA export by triggering specific RNA:protein remodeling events. *Mol Cell* **28**: 850–859.

Treiber DK, Williamson JR. 1999. Exposing the kinetic traps in RNA folding Daniel K Treiber* and James R Williamson~. *Curr Opin Struct Biol* **9**: 339–345.

Turner A-MW, Love CF, Alexander RW, Jones PG. 2007. Mutational analysis of the Escherichia coli DEAD box protein CsdA. *J Bacteriol* **189**: 2769–2776.

Turner DH, Mathews DH. 2009. NNDB: The nearest neighbor parameter database for predicting stability of nucleic acid secondary structure. *Nucleic Acids Res* **38**.

Wan Y, Kertesz M, Spitale RC, Segal E, Chang HY. 2011. Understanding the transcriptome through RNA structure. *Nat Rev Genet* **12**: 641–655.

Wan Y, Qu K, Ouyang Z, Kertesz M, Li J, Tibshirani R, Makino DL, Nutter RC, Segal E, Chang HY. 2012. Genome-wide Measurement of RNA Folding Energies. *Mol Cell* **48**: 169–181.

Weirich CS, Erzberger JP, Flick JS, Berger JM, Thorner J, Weis K. 2006. Activation of the DExD/H-box protein Dbp5 by the nuclear-pore protein Gle1 and its coactivator InsP6 is required for mRNA export. *Nat Cell Biol* **8**: 668–676.

Wilson TJ, Nahas M, Ha T, Lilley DM. 2005. Folding and catalysis of the hairpin ribozyme. *Biochem Soc Trans* **33**: 461–465.

Woodson SA. 2010. Compact intermediates in RNA folding. *Annu Rev Biophys* **39**: 61–77.

Woodson SA. 2008. RNA folding and ribosome assembly. *Curr Opin Chem Biol* **12**: 667–673.

Yang Q, Del Campo M, Lambowitz AM, Jankowsky E. 2007. DEAD-box proteins unwind duplexes by local strand separation. *Mol Cell* **28**: 253–263.

Yang Q, Jankowsky E. 2005. ATP- and ADP-dependent modulation of RNA unwinding and strand annealing activities by the DEAD-box protein DED1. *Biochemistry* **44**: 13591–13601.

Yang Q, Jankowsky E. 2006. The DEAD-box protein Ded1 unwinds RNA duplexes by a mode distinct from translocating helicases. *Nat Struct Mol Biol* **13**: 981–986.

Zemora G, Waldsich C. 2010. RNA folding in living cells. *RNA Biol* **7**: 634–641.

Zenklusen D, Vinciguerra P, Strahm Y, Stutz F. 2001. The yeast hnRNP-Like proteins Yra1p and Yra2p participate in mRNA export through interaction with Mex67p. *Mol Cell Biol* **21**: 4219–4232.

Zingler N, Solem A, Pyle AM. 2010. Dual roles for the Mss116 cofactor during splicing of the ai5gamma group II intron. *Nucleic Acids Res* **38**: 6602–6609.

Zonta E, Bittencourt D, Samaan S, Germann S, Dutertre M, Auboeuf D. 2013. The RNA helicase DDX5/p68 is a key factor promoting c-fos expression at different levels from transcription to mRNA export. *Nucleic Acids Res* **41**: 554–564.

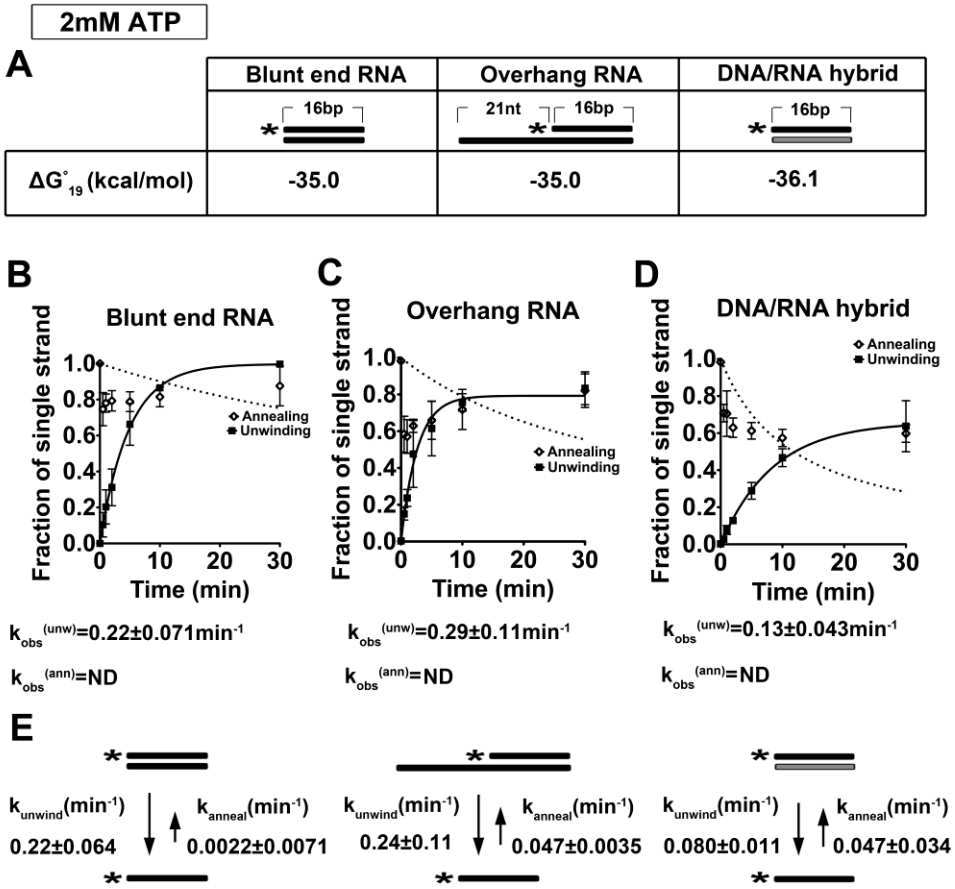

Figure 3.1. Dbp2 displays ATP-dependent duplex unwinding on multiple RNA substrates at 2 mM ATP:Mg2+. (A) Schematic representation and thermodynamic stability of RNA duplex substrates. All RNA substrates were designed with similar stability, which was calculated using the Nearest-Neighbor Database and converting to ΔG°19 using ΔG°= ΔH°-T ΔS° (Sugimoto et al. 1995; Turner and Mathews 2009). Black or gray coloring denotes RNA or DNA strands, respectively, whereas asterisks mark the position of the 32P-radiolabeled 5' end. (B) Graphical representations of unwinding and annealing assays using radiolabeled 16-bp blunt end RNA duplexes, (C) 21-nt overhang that is 3' to the 16-bp RNA duplexes and (D) 16-bp blunt end DNA/RNA hybrids. Reactions were performed at 19 °C with 2 mM ATP:Mg2+, 0.1 nM radiolabeled duplex, and 600 nM recombinant, purified Dbp2. The fraction of the single stranded substrate at each time point is plotted as the average of three independent reactions with standard deviations from the mean. The integrated form of a homogenous first order rate law equation was used to fit the data to determine the kobs(unw). kobs(ann) was determined using the integrated rate law for the bimolecular annealing reaction as previously described (Yang and Jankowsky 2005). N.D. = not determined. Representative non-denaturing gels are shown in Fig 3.3. (E) Kinetic parameters for Dbp2 unwinding and annealing at 2 mM ATP. The rate constants for Dbp2 unwinding and annealing were

calculated as previously described (Yang and Jankowsky 2005). This reveals that Dbp2 preferentially unwinds RNA-RNA duplexes irrespective of the presence of a single-stranded overhang region. Dbp2 exhibits RNA-DNA duplex unwinding but with a lower activity than RNA-RNA substrates of similar overall stability.

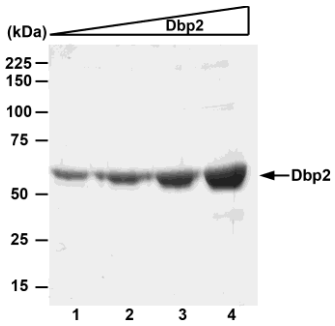

Figure 3.2. Coomassie gel of recombinant, purified Dbp2 used in *in vitro* assays. *A coomassie stained SDS-PAGE gel of purified Dbp2.* Increasing amounts of Dbp2 (5 μg, 10 μg, 15 μg, and 20 μg) is loaded in lane 1 to lane 4, respectively. This purification shows that Dbp2 is >95% pure as estimated by staining.

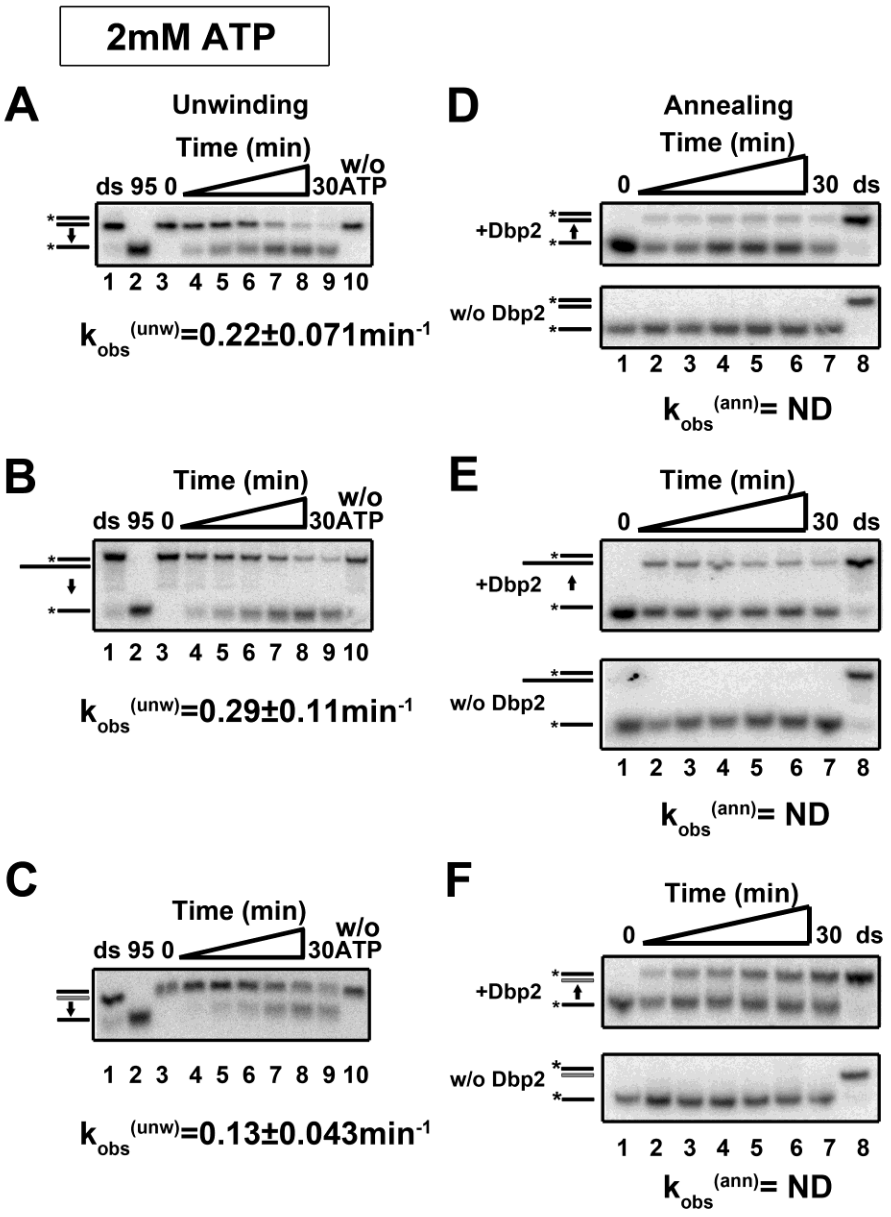

Figure 3.3. Dbp2 displays both unwinding and annealing activities at 2 mM ATP. *(A) Representative non-denaturing gels of RNA unwinding reaction in Fig 3.1 using the blunt end RNA duplexes, (B) the overhang RNA duplexes and (C) the DNA/RNA hybrids. The corresponding single stranded substrates from the denatured duplex were used in the annealing reaction (D-F, respectively).* Double stranded RNA (ds) and denatured duplex at 95°C (95) were used as double stranded and singled stranded RNA positional markers, respectively. For the unwinding reactions (A-C), the 0 time point (lane 3) represents reactions before addition of 2 mM ATP and no unwinding activity was observed in the

absence of ATP in 30 min (lane 10). Time points from 0.5 min to 30 min were collected and shown that the duplex substrate was unwound to single stranded substrate (lane 4-9). For annealing reactions (D-F), the 0 time point (lane 1) represents the single stranded substrate before the reaction begins. In addition, no spontaneous annealing of the RNA substrate was observed as shown in the spontaneous annealing reaction (without Dbp2). During the annealing reaction in the presence of Dbp2, aliquots were removed from time 0.5 min to 30 min and shown that single stranded substrate was annealed to double stranded substrate (lane 4-9).

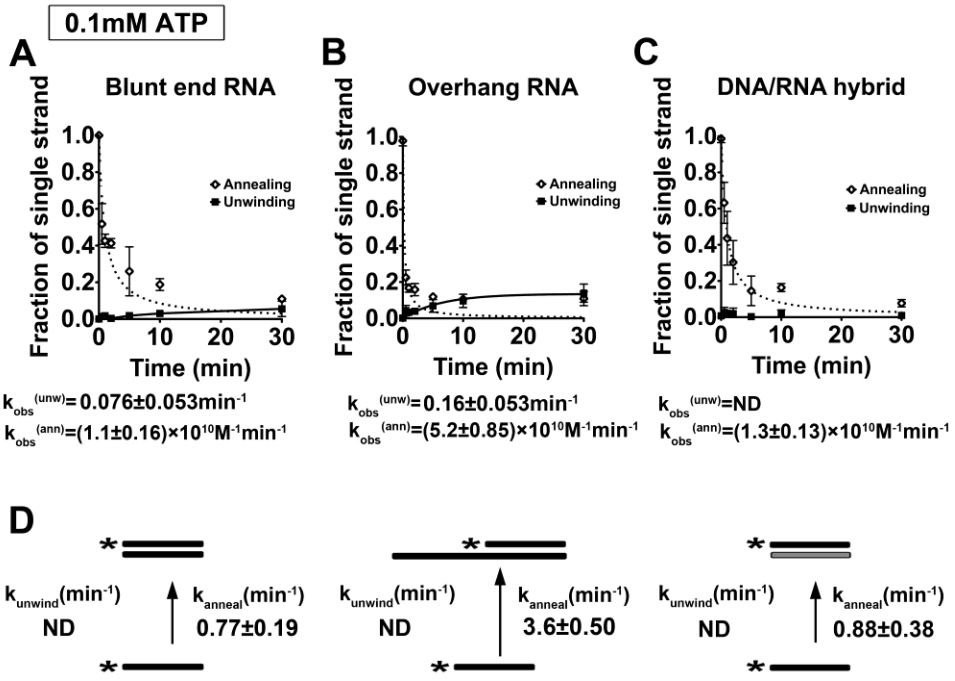

Figure 3.4. Dbp2 exhibits a preference for strand annealing with single stranded overhang RNA substrates at low ATP concentration. *(A-C) Graphical representation of unwinding and annealing assays with 0.1 mM ATP using (A) the blunt end RNA duplex, (B) the RNA duplex with 3' single strand overhang or (C) the blunt end RNA-DNA hybrid.* Unwinding and annealing assays were conducted as above but with 0.1 mM ATP and 2 mM $MgCl_2$. Data from the unwinding and annealing assays were fitted as above. Representative non-denaturing gels are shown in Fig 3.5. (D) *Kinetic parameters for Dbp2 unwinding at 0.1 mM ATP*. Since there is little or no observable unwinding, the unwinding data cannot be fitted with the steady state equation as mentioned above and are listed as ND (not determined). Therefore, we assumed the $k_{obs}^{(ann)}$ is the same as k_{anneal} and converted the reported $k_{obs}^{(ann)}$ to the first-order rate constant as described (Yang and Jankowsky 2005). This reveals that Dbp2 exhibits higher annealing on RNA duplexes with single stranded overhangs at low ATP.

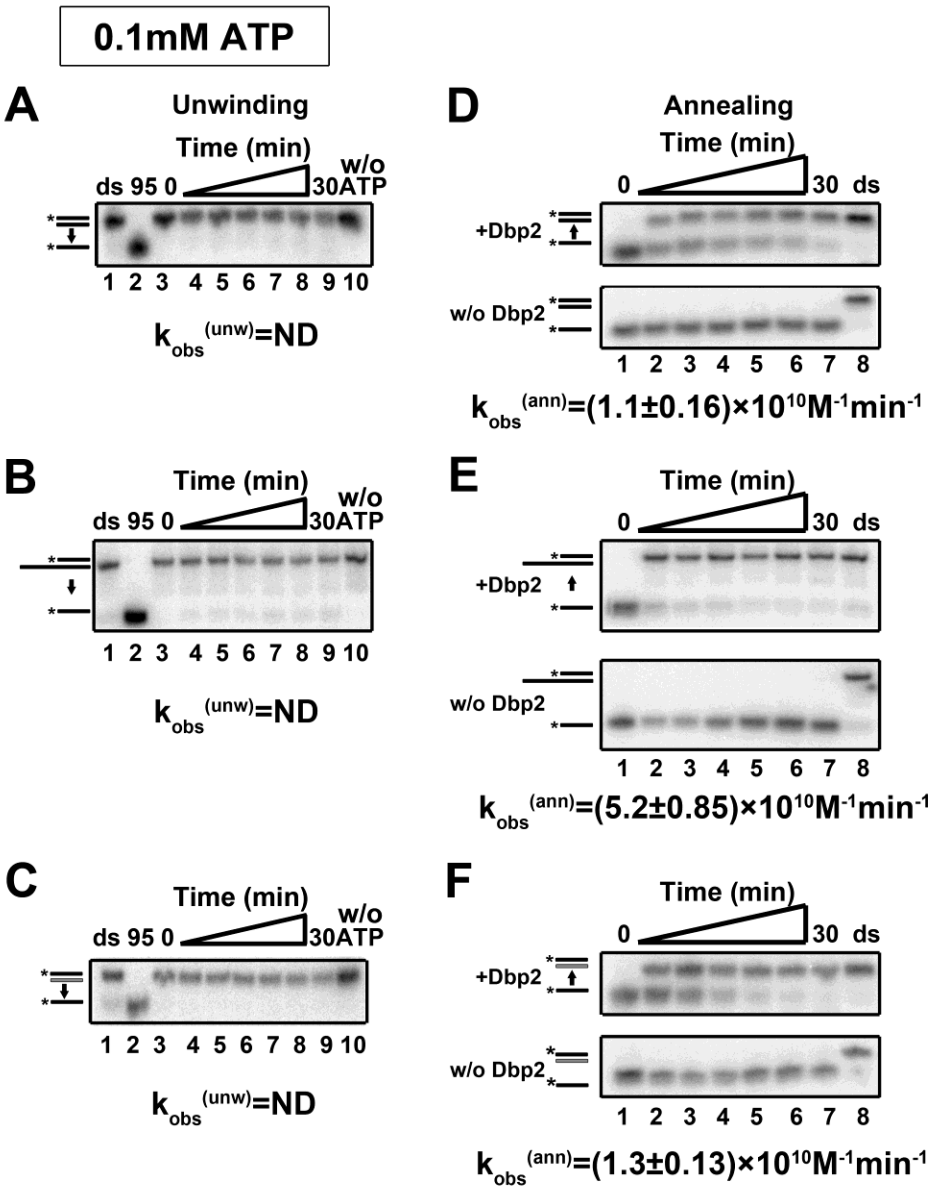

Figure 3.5. Dbp2 prefers annealing over unwinding at 0.1 mM ATP. *(A-F) Representative non-denaturing gels are shown as in Fig. 3.3 but with 0.1 mM ATP and saturating $MgCl_2$ (2 mM)*. This reveals that Dbp2 has little or no observable unwinding activity at 0.1 mM ATP and displays stronger annealing activity with substrate that has single stranded region. Note that the increased signal in the absence of ATP in all three gels (lane 10) is due to loading 10% more substrate per lane as compared to time course fractions (lanes 3-9).

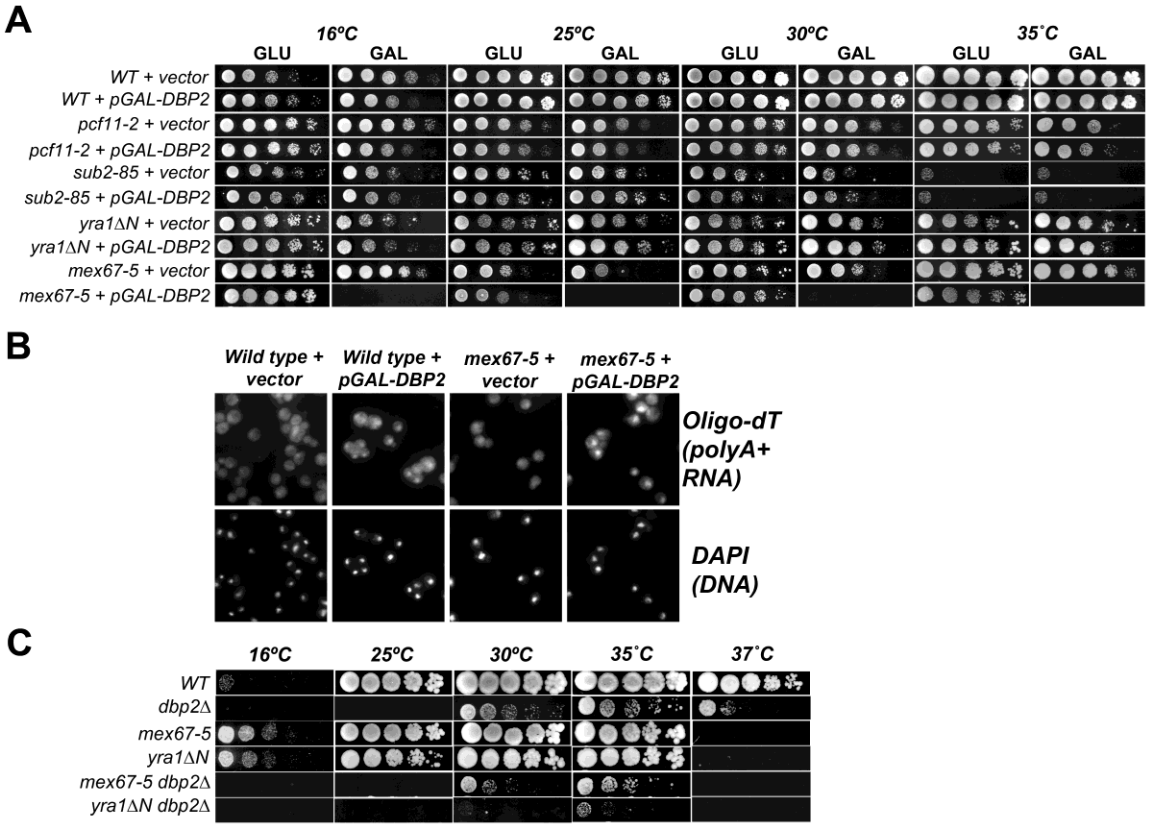

(Data from figure 3.6A and figure 3.6B were provided by Sara Cloutier and Dr. Elizabeth Tran, respectively.)

Figure 3.6. *DBP2* displays genetic interactions with mRNA export factor mutants *mex67-5* and *yra1ΔN*. *(A) Overexpression of DBP2 is lethal in mex67-5 strains.* Indicated strains were transformed with empty vector or galactose-inducible pGAL-*DBP2*. Resulting transformants were then spotted in 5-fold serial dilutions onto transcriptionally repressive (glucose) or inducing (galactose) media and subsequently grown at the indicated temperatures from 25-35 °C. *(B) Overexpression of DBP2 in the mex67-5 strain induces a mRNA export defect at the mex67-5 permissive temperature.* Briefly, yeast strains were grown at 25 ˚C to mid log phase in selective media and then shifted to galactose-containing media for 1 hour to induce *DBP2* overexpression. Cells were then harvested and *in situ* hybridization was conducted with oligodT_{30} to visualize accumulation of total poly(A)+ RNA. DAPI staining of DNA shows the position of the nucleus. *(C) Loss of DBP2 in yra1ΔN strain results in a synthetic sick growth defect.* The indicated double mutant strains were constructed using standard methods and were analyzed for growth defects as above by serial dilution analysis onto rich media. The *dbp2*Δ displays a cold sensitive phenotype as previously described (Cloutier et al. 2012).

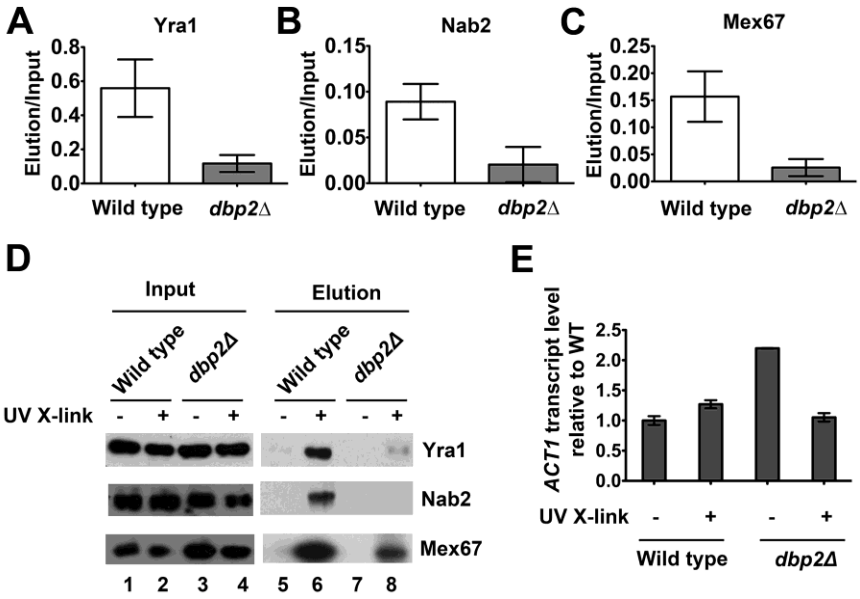

(Data from figure 3.7 were collected by Sara Cloutier and myself.)

Figure 3.7. Loss of *DBP2* results in reduced association of Yra1, Nab2 and Mex67 with poly(A)$^+$ RNA. *In vivo UV crosslinking reveals reduced association of (A) Yra1, (B) Nab2 and (C) Mex67 with poly(A)$^+$ RNA in dbp2Δ cells.* Wild type and *dbp2Δ* cells were subjected to UV crosslinking followed by poly(A)+ RNA isolation as previously described (Tran et al. 2007). The eluted fraction of wild type and *dbp2Δ* cells were normalized to equal RNA concentration using equivalent A260nm absorbance units. Proteins from the eluted fractions were detected by Western blotting. The relative quantity of poly(A)+ RNA-bound proteins was determined following quantification of the resulting isolated proteins from three independent biological replicates and is reported as the amount of isolated protein relative to total (input). (D) *Representative western blot of in vivo UV crosslinking.* The total protein abundance (input) is shown along with the amount of isolated proteins with and without UV crosslinking. The latter serves as a background control to show that proteins isolated following UV crosslinking are not due to non-specific interactions. (E) *Reverse-transcriptase, quantitative PCR (RT-qPCR) shows efficient isolation of ACT1 mRNA from both wild type and dbp2Δ cells following oligo-dT selection.* Equal fractions of eluted RNA were reverse transcribed and subjected to qPCR with ACT1-specific primers as previously described (Cloutier et al. 2012). Transcript levels were normalized by setting the wild type elution without UV crosslinking to 1 and are a result of three technical replicates from one biological sample per strain.

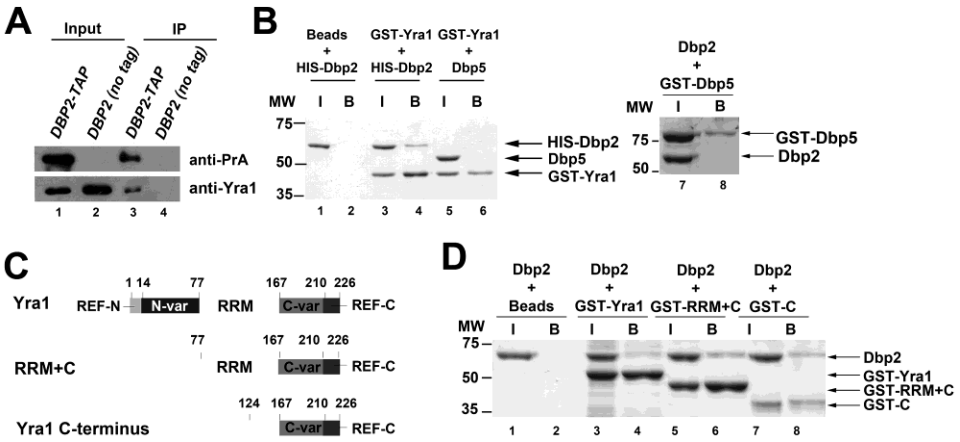

(Data from figure 3.8A and B were provided by Dr. Elizabeth Tran.)

Figure 3.8. Dbp2 physically interacts with Yra1 *in vivo* and *in vitro.* *(A) Yra1 co-immunoprecipitates with Dbp2.* Immunoprecipitation assays were performed from wild type (*DBP2* no tag) and *DBP2-TAP* strains using IgG-conjugated dynabeads. 10% lysate was used as input. Proteins from the input and immunoprecipitated fractions were resolved by SDS-PAGE and detected by Western blotting analysis. *(B) Dbp2 interacts directly with Yra1. In vitro* pull down assays were performed with recombinant, purified 6XHIS-tagged Dbp2 and GST-tagged Yra1. Briefly, recombinant, purified proteins were incubated together, 20% of the protein mix was removed as input ('I') and interacting proteins were selected on glutathione sepharose resin (bound 'B' proteins). Proteins were resolved by SDS-PAGE electrophoresis and visualized by Coomassie staining. Neither GST-Yra1 nor Dbp2 co-elute with an unrelated DEAD-box protein Dbp5 (lane 6 and 8), demonstrating that this interaction is specific. *(C) Schematic representation of the primary sequence of Yra1, functional motifs and truncation mutants.* Yra1 is composed of evolutionarily conserved RNA Export Factor (REF) domains at the N and C terminus separated by variable regions (Stutz et al. 2000; Strasser and Hurt 2000; Zenklusen et al. 2001; Johnson et al. 2009). Yra1 also contains a central RNA recognition motif (RRM) that does not appear to harbor RNA binding activity (Zenklusen et al. 2001). (*D) The C-terminal half of Yra1 (aa 124-226) is sufficient to interact with Dbp2.* GST-tagged Yra1 and truncation mutants were purified as recombinant proteins from *E. coli* and subjected to *in vitro* pull downs as above.

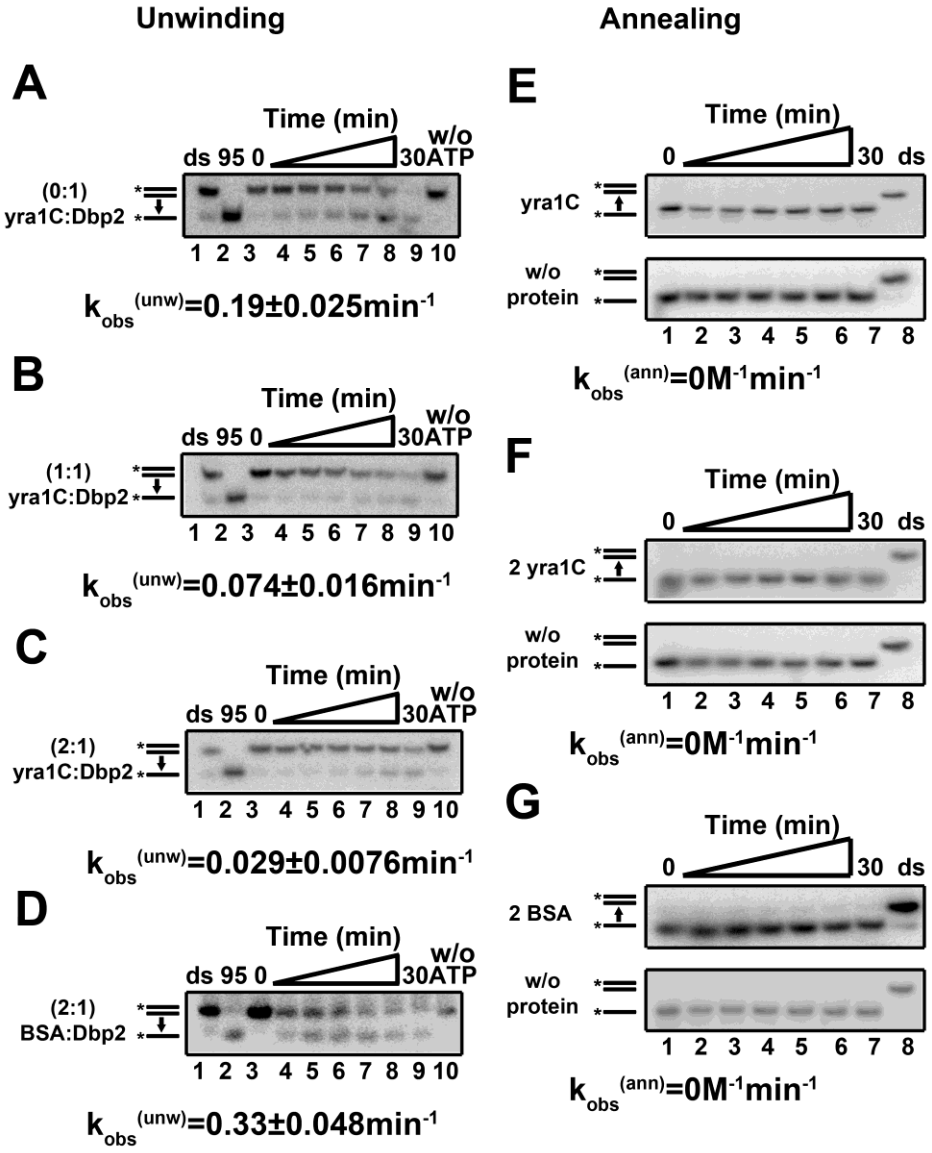

Figure 3.9. The C-terminus of Yra1, yra1C, inhibits the unwinding activity of Dbp2. *(A) Representative non-denaturing gels of RNA unwinding in Fig 3.10A using 600 nM Dbp2 alone, (B) 600 nM yra1C with 600 nM Dbp2, and (C) 1200 nM yra1C with 600 nM Dbp2*. This indicates that yra1C reduces the unwinding activity of Dbp2. *(D-E) Representative non-denaturing gels of RNA annealing using 600 nM yra1C or 1200 nM yra1C, respectively.* Importantly, no spontaneous annealing was observed with the single-stranded RNAs in the absence of protein. This reveals that yra1C does not display RNA annealing activity, demonstrating that the inhibition of the unwinding activity of Dbp2 is direct.

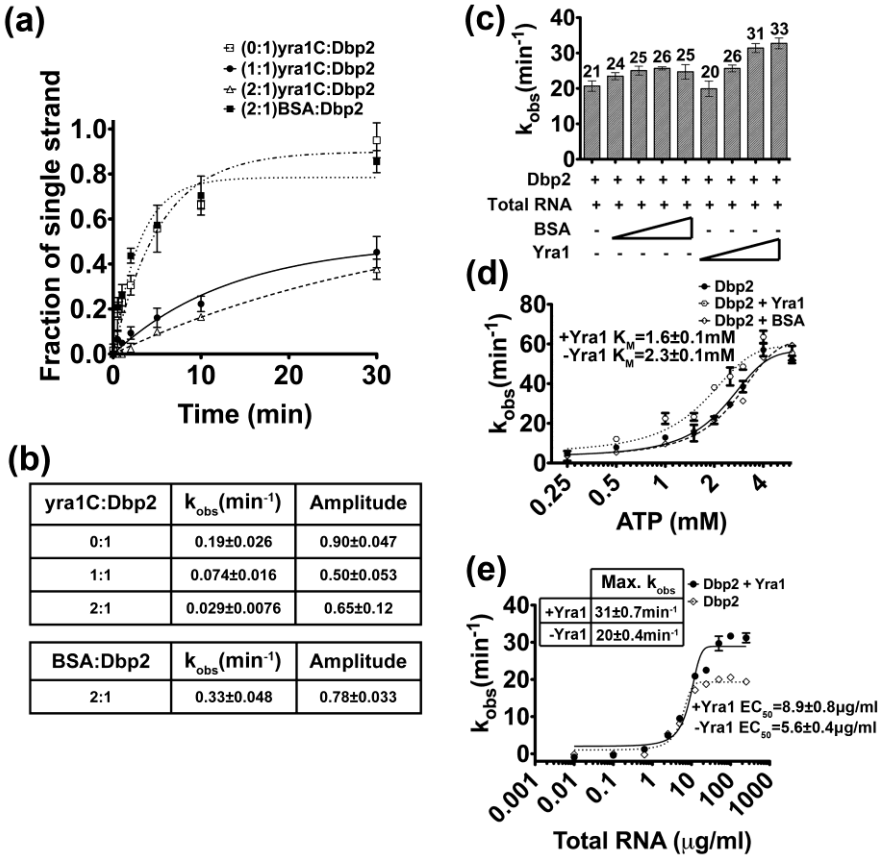

yra1C:Dbp2	k_{obs}(min^{-1})	Amplitude
0:1	0.19±0.026	0.90±0.047
1:1	0.074±0.016	0.50±0.053
2:1	0.029±0.0076	0.65±0.12

BSA:Dbp2	k_{obs}(min^{-1})	Amplitude
2:1	0.33±0.048	0.78±0.033

Figure 3.10. Yra1 modulates the enzymatic activity of Dbp2. *(A) Graphical representation of Dbp2 duplex unwinding with yra1C.* Unwinding assays were conducted with the blunt end RNA duplex and either Dbp2 alone (600 nM) or with yra1C (600 nM, 1200 nM) or BSA (1200 nM). Representative non-denaturing gels are shown in Fig 3.9 and demonstrate that yra1C and BSA do not have intrinsic annealing activity. *(B) The $k_{obs}^{(unw)}$ and the amplitude of the unwinding reaction*. The $k_{obs}^{(unw)}$ and the amplitude are determined using the integrated rate law for a homogeneous first-order reaction as previously described (Yang and Jankowsky 2005). *(C) Full length Yra1 moderately enhances ATP hydrolysis activity of Dbp2. In vitro* ATPase assays were conducted with 200 nM of recombinant, purified Dbp2 and 250 µg/ml of total yeast RNA using a PK/lactate dehydrogenase enzyme-coupled absorbance based detection method as previously described (Cloutier et al. 2012). Recombinant, purified Yra1 was included where indicated at final concentrations from 100-600 nM. Equal concentrations of BSA were also tested to account for non-specific interactions. The ATPase activity of Dbp2 alone is similar to previous publications and has already been characterized (Cloutier et al. 2012). *(D) Yra1 moderately enhances the ATP binding affinity of Dbp2*. *In vitro* ATPase assays were conducted as above with constant amounts of Dbp2, Yra1, total RNA (10 µg/mL), increasing amounts of ATP and constant $MgCl_2$ (2 mM). Assays were also conducted with BSA in place of Yra1 to account for non-specific effects. The K_M is the indicative of the ATP binding affinity of Dbp2. *(E) Yra1 slightly increases the amount of RNA necessary for activation of ATP hydrolysis*. *In vitro* ATPase assays were

conducted as above with 200 nM Dbp2, 400 nM Yra1 and increasing amounts of total yeast RNA. The amount of RNA necessary for 50% stimulation of maximum ATPase activity (EC_{50}) is reflective of the RNA binding affinity of Dbp2.

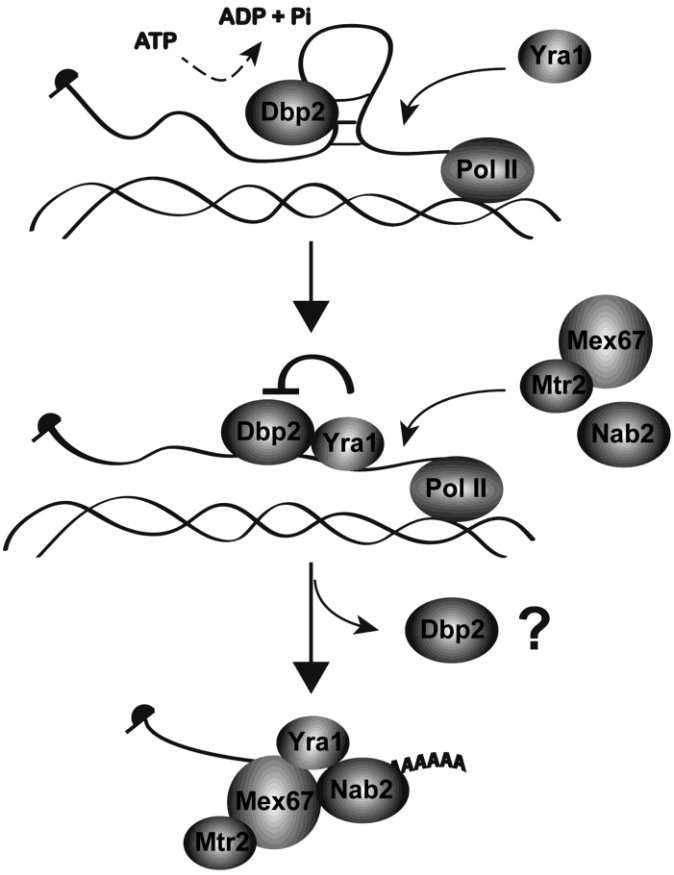

Figure 3.11. Model for Dbp2-dependent loading of RNA-binding proteins onto mRNA. Yra1 is recruited to the actively transcribing loci through interacting with Sub2 or Pcf11 on the C-terminal domain of the RNA polymerase II (Johnson et al. 2009; Strasser et al. 2002). However, structures of the nascent mRNA prevent association with Yra1. Dbp2 unwinds these structures co-transcriptionally in an ATP-dependent manner. This promotes mRNP assembly by facilitating loading of Yra1, Nab2, and Mex67 onto nascent mRNA. Mex67 is shown interacting with its heterodimerization partner, Mtr2 (Katahira et al. 1999). Yra1 then inhibits the helicase activity of Dbp2 to prevent further remodeling of the assembled mRNP and may also promote release of Dbp2 from the RNA. This constitutes a biochemical mechanism of RNA helicase unwinding and subsequent inhibition during co-transcriptional assembly of mRNAs in the nucleus.

Table 3.1. Yeast and bacterial plasmids

Name	Description	Source/Reference
BTP13	pET28a-DBP2	Cloutier et al. 2012
pCEN/URA3	pRS316	Sikorski and Hieter 1989
pGAL1-GAL10-GAL7	pYGPM11714	Open biosystems (Genomic Tiling)
BTP22	pMAL-TEV-Dbp2	This study
BTP27	GST-TEV-Yra1	This study
pSW3319	GST-Dbp5	Alcazar-Roman et al. 2006
pRS426	pURA3/2μ	Christianson et al. 1992
pGAL-DBP2	pGAL-DBP2/2μ/URA3	Open Biosystems
GST-Yra1 C	pET21GST-Yra1 C	Johnson et al., 2009
GST-Yra1 RRM+C	pET21GST-Yra1 RRM+C	Johnson et al., 2009
psub2-85	psub2-85/CEN/TRP1	Strasser and Hurt 2001

Table 3.2. Yeast strains

Strain	Genotype	Source
Wild type (BY4741)	MATa *his3Δ1 leu2Δ0 met15Δ0 ura3Δ0*	Open Biosystems
*dbp2*Δ (BTY115)	MATa *dbp2*::*KanMx ura3Δ0 leu2Δ0 his3Δ0 TRP1 met- lys?*	Cloutier et al. 2012
DBP2-TAP	MATa *DBP2-TAP:HIS3 his3Δ1 leu2Δ0 met15Δ0 ura3Δ0*	Open Biosystems
mex67-5	MATa *mex67::HIS3 ura3 ade2 his3 leu2 trp1 pTRP/CEN/mex67-5*	Stutz et al. 2000
Wild type (W303)	MATa *ura3-1 ade2-1 his3-11, 15 leu2-1 trp1-1 can1-100*	R. Rothstein
yra1ΔN + Yra1	MATα *yra1::HIS3 ura3 ade2 ade3 leu2-1 trp1 pRS314-yra1ΔN +pHT4467*Δ*-YRA1 (with intron)*	Strasser and Hurt 2001
pcf11-2	MATa *ura3-1 trp*Δ *ade2-1 leu2-3, 112 his3-11, 15 pcf11-2*	Amrani et al. 1997
SUB2 shuffle	MATa *sub2::HIS3 ade2 leu, ura3, trp1 pCG788*	Kistler and Guthrie 2001

CHAPTER 4. MEASURING HELICASE INHIBITION OF THE DEAD-BOX PROTEIN DBP2 BY YRA1

4.1 Introduction

DEAD-box RNA helicases are the largest class of enzymes within the helicase family and can be found in all domains of life (Linder and Fuller-Pace 2013). All DEAD-box proteins share at least 12 conserved motifs in the helicase core spread throughout two RecA-like domains, including the eponymic Asp-Glu-Ala-Asp (D-E-A-D) sequence in the Walker B motif (Putnam and Jankowsky 2013).

Several studies have revealed that individual DEAD-box proteins display diverse biochemical activities *in vitro*, including RNA-protein complex (RNP) remodeling, RNA-dependent ATP hydrolysis and ATP-dependent unwinding of RNA duplexes (Jankowsky 2011; Jarmoskaite and Russell 2011). A major question in the field is how this diversity of function is achieved among the ~25 different DEAD-box proteins in yeast (40 in humans), given the high degree of sequence and structural identity in the helicase core. Studies have shown that unique N- and/or C-terminus extensions can provide substrate specificity to individual family members (Klostermeier and Rudolph 2009; Tsu et al., 2001). For example, the C-terminus of DbpA provides specificity to target 23S rRNA (Fuller-Pace et al., 1993; Nicol and Fuller-Pace 1995; Hardin et al.,

2010). Moreover, the flanking regions can also provide non-specific RNA tethers. This has been described for Mss116 and CYT-19 (Mohr et al., 2008; Mallam et al., 2011).

In addition to unique flanking regions, specificity can also be conferred by protein cofactors that regulate the enzymatic activity of individual DEAD-box proteins (Bolger and Wente 2011; Granneman et al., 2006). For instance, the translation initiation factor eIF4G stimulates the weak ATPase activity of eIF4A (Hilbert et al., 2011). This is believed to allow eIF4A to unwind secondary structures in 5'UTR and facilitate the small ribosomal subunit to scan for the start codon during translation. Recently, our laboratory showed that the *S. cerevisiae* DEAD-box protein Dbp2 interacts directly with the mRNA binding protein Yra1 (Ma et al., 2013). Furthermore, we found that Yra1 inhibits the unwinding activity of Dbp2 without significantly altering the ATPase activity, suggesting specific regulation of duplex unwinding (Ma et al., 2013). Here, we describe a method to evaluate the effect of Yra1 on the unwinding activity of Dbp2. This method is widely applicable to the analysis of other protein binding cofactors for RNA helicases.

4.2 Materials

4.2.1 Expression and purification of recombinant Dbp2 and Yra1 (C-terminus domain) in E. coli

1. LB Broth: 10 g bacto tryptone, 5 g yeast extract and 10 g NaCl. Adjust the pH to ~ 7.0. Bring up to a final volume of 1 L with water. Autoclave the media.
2. LB agar: 10 g bacto tryptone, 5 g yeast extract, 10 g NaCl, and 20 g agar. Adjust the pH to ~ 7.0. Bring up to a final volume of 1 L with water. Autoclave the media and pour the plate after adding appropriate antibiotic.
3. LB Broth + 1% glucose: 10 g bacto tryptone, 5 g yeast extract, 10 g NaCl and 10 g glucose. Adjust the pH to ~ 7.0. Bring up to a final volume of 1 L with water. Autoclave the media.
4. Ampicillin: Dissolve ampicillin sodium salt in water to a final concentration of 75 mg/mL. Filter sterilize with a 0.2 μm syringe filter and store at -20°C in 1 mL aliquots.
5. Chloramphenicol: Dissolve chloramphenicol in 100% ethanol to a final concentration of 34 mg/mL and store at -20°C in 1 mL aliquots.
6. 20% glycerol stock of *Escherichia coli* Rosetta (DE3). Store at -80°C.
7. 20% glycerol stock of *Escherichia coli* BL21 (DE3). Store at -80°C.
8. pMAL-TEV-Dbp2 plasmid (Ma et al., 2013)
9. pET21GST-yra1C plasmid (Johnson et al., 2009)
10. IPTG solution: Dissolve Isopropyl β-d-thiogalactopyranoside (Amresco) in water to a final concentration of 1 M and store at -20°C.

11. Protease inhibitors that inhibits serine and cysteine proteases in bacterial extracts. *Ad hoc* protease inhibitors can be obtained from various commercial sources.
12. 7000 units/mL of RNase A
13. 100 U/μL of RNase I **(Note 1)**
14. Empty 0.7 X 15 cm and 1.5 X 10 cm chromatography columns for gravity flow separations.
15. Lysis buffer (Dbp2): 50 mM CHES, 100 mM NaCl, pH 9.0
16. Wash buffer (Dbp2): 50 mM CHES, 500 mM NaCl, pH 9.0
17. Elution buffer (Dbp2): 50 mM Tris-HCl, 10 mM maltose, 0.5 mM EDTA, 1 mM DTT, pH 8.0
18. Lysis buffer (yra1C): 20 mM HEPES, 1 mM EDTA, 20% (v/v) glycerol, pH 7.5
19. Wash buffer I (yra1C): 20 mM HEPES, 150 mM NaCl, 20% (v/v) glycerol, pH 7.5
20. Wash buffer II (yra1C): 20 mM HEPES, 500 mM NaCl, 20% (v/v) glycerol, pH 7.5
21. Elution buffer (yra1C): 20 mM HEPES, 20 mM glutathione, 150 mM NaCl, 20% (v/v) glycerol, pH 7.5 **(Note 2)**
22. 10 U/μL of TEV protease
23. Amylose resin
24. Glutathione sepharose resin (GE Healthcare)
25. SP sepharose resin
26. SP equilibration buffer: 50 mM Tris-HCl, pH 8.0
27. SP wash buffer: 50 mM Tris-HCl, 200 mM NaCl, pH 8.0
28. SP elution buffer: 50 mM Tris-HCl, 600 mM NaCl, 20% (v/v) glycerol, pH 8.0

4.2.2 Preparation of RNA duplexes

1. Adjustable height electrophoresis sequencer, 20 cm wide
2. RNA oligo: Top strand (5'- AGCACCGUAAAGACGC-3'), Bottom strand (5'-GCGUCUUUACGGUGCU-3') (Yang et al., 2007)
3. 3000 Ci/mmol, 10 mCi/mL of γ^{32}P-ATP
4. 10,000 untis/mL of T4 Polynucleotide Kinase (PNK)
5. 10X T4 Polynucleotide Kinase buffer
6. 10X TBE: 890 mM Tris base, 890 mM boric acid, 20 mM EDTA
7. Denaturing polyacrylamide gel: 20% acrylamide:bis 19:1, 7 M urea, 1X TBE
8. Non-denaturing polyacrylamide gel: 15% acrylamide:bis 19:1, 0.5X TBE
9. 5X Denaturing gel loading dye: 80% formamide, 0.1% bromophenol blue (BPB), 0.1% xylene cyanol (XC)
10. 5X Non-denaturing gel loading dye: 50% glycerol, 0.1% BPB, 0.1% XC
11. X-ray films for autoradiography (e.g., Kodak X-OMAT LS, Fuji RX, etc.)
12. 20 mg/mL glycogen
13. Gel elution buffer: 1 mM EDTA, 0.5% SDS, 300 mM NaOAc, pH 5.2
14. 10X duplex annealing buffer: 100 mM MOPS, 10 mM EDTA, 0.5 M KCl, pH 6.5
15. RNA substrate storage buffer: 50 mM MOPS, 50 mM KCl, pH 6.0

4.2.3 Unwinding and annealing assays

1. 10X Helicase reaction buffer (10X HRB): 400 mM Tris-HCl, 5 mM $MgCl_2$, 0.1% NP-40, 20 mM DTT, pH 8.0
2. 20 U/μL of Superase-in (Ambion)

3. 20 mM equimolar ATP/$MgCl_2$ (prepare from 100mM ATP)
4. Purified DEAD-box proteins and protein binding cofactors (see 4.3.1)
5. 1 nM radiolabeled RNA duplex
6. 12% Non-denaturing polyacrylamide gel: 12% acrylamide:bis 19:1, 0.5X TBE, 3% glycerol
7. 2X Helicase reaction stop buffer (2X HRSB): 50 mM EDTA, 1% SDS, 0.1% BPB, 0.1% XC, 20% glycerol
8. Whatman chromatography paper
9. Gel dryer
10. PhosphorImager screen/PhoshorImager

4.3 Methods

4.3.1 Preparation of active purified Dbp2 and yra1C

Dbp2 can bind *E. coli* RNA during expression of recombinant protein, resulting in copurification of contaminating RNA. To solve this problem, a high salt wash step and two RNase treatments are utilized during purification. Ion-exchange chromatography is needed to remove the RNAses and the affinity tags after TEV cleavage. The resulting protein preparations should be tested for RNAse contamination by incubating the proteins with a radioactively labeled single stranded RNA (ssRNA) and then resolving the RNA onto a non-denaturing polyacrylamide gel. A non-incubated, labeled RNA should be run in an adjacent well for comparison. The presence of RNA in the purified protein preparation can be determined by the ratio of A_{260nm}:A_{280nm} **(Note 3)**.

4.3.1.1 Expression of Dbp2 and production of cell paste

1. Transform the pMAL-TEV-Dbp2 plasmid into BL21 (DE3) and plate onto LB agar + Ampicillin (75 μg/mL). Incubate the plate at 37°C overnight.
2. Inoculate a single colony into a 4 mL LB + Ampicillin (75 μg/mL) culture and incubate at 37°C with shaking at 200 RPM overnight.
3. Inoculate a 1 L LB + 1% glucose + Ampicillin (75 μg/mL) with all of the 4 mL culture and grow the bacteria at 37°C with shaking at 200 RPM to an OD_{600nm} of 0.4-0.5 **(Note 4).**
4. Induce MBP-TEV-Dbp2 expression by adding a final concentration of 1 mM IPTG to the culture. Express for 3 hours at 37°C with 200 RPM shaking.
5. Pellet cells at 11,100xg for 15 min at 4°C in pre-weighed bottles and then weigh the cell pellet by subtracting the empty bottle weight.
6. Store cell pellet at -20°C or proceed to purification.

4.3.1.2 Purification of Dbp2

1. Resuspend the cell pellet with 6 mL of ice-cold Lysis buffer (Dbp2) per gram of cell pellet and put on ice during preparation.
2. Add protease inhibitor, RNase A and RNase I to a final concentration of 1X, 7 U/mL and 10 U/mL, respectively.
3. Lyse cells with a probe sonicator (Branson digital sonifier) on an ice bath three times for 30 seconds using 30% amplitude with 1 min cooling in between rounds. Utilization of a distinct sonifier may require re-optimization of these parameters.

4. Clear the lysate by centrifugation at 13,300xg for 30 min at 4°C. Step 5-13 are all performed at 4°C.
5. Equilibrate 4 mL of 50% slurry amylose resin (2 mL final packed volume) in a 1.5 X 10 cm chromatography column with 20 mL of Lysis buffer (Dbp2).
6. Incubate the cleared lysate with the equilibrated resin in a capped chromatography column for 1 hour at 4°C with gentle rocking.
7. Wash the column with 25 mL of Lysis buffer (Dbp2) followed by washing with 25 mL of Wash buffer (Dbp2).
8. Shut off the column when wash buffer has flowed through but column is still wet.
9. Add 5 mL of Wash buffer (Dbp2) to the column along with 35 U RNase A and 50 U RNase I.
10. Mix the resin by pipetting and incubate for at least 10 min at 4°C.
11. Let the remaining buffer flow through and wash the column with 25 mL of Lysis buffer (Dbp2).
12. Elute MBP-TEV-Dbp2 with Elution buffer (Dbp2) in a 15 mL RNase-free conical tube until the A_{280nm} ~ 0.3 O.D. **(Note 5).**
13. Add 50 U of TEV protease per 1 mL of MBP-TEV-Dbp2 elution to the eluted fraction and mix it by inverting the conical tube gently for several times.
14. Incubate at 16°C for 12 hours **(Note 6).**
15. Equilibrate 400 µL of 50% slurry SP sepharose (200 µL packed) with 5 mL SP equilibration buffer in a 0.7 X 15 cm chromatography column. The following purification steps (Step 17-19) are all performed at 4°C.

16. Apply the cleaved sample to the column at 4°C. Let the unbound sample flow through.
17. Wash the column with 10 mL of SP equilibration buffer and then 10 mL of SP wash buffer.
18. Elute with 3-5 column volumes of SP elution buffer. Store the purified Dbp2 protein at -80°C in small aliquots as Dbp2 is not compatible with multiple freeze-thaw cycles. The purified protein can be stored at -80°C up to four months.

4.3.1.3 Expression of yra1C and purification of yra1C

1. Expression and preparation of the cell pellet is as in Section 3.1.1 with the following exceptions: Transform the pET21GST-yra1C plasmid into Rosetta (DE3) cells, select with Ampicillin (75 μg/mL) + Chloramphenicol (34 μg/mL), and induce yra1C expression at 16°C overnight **(Note 7)**.
2. GST-yra1C lysate is prepared as in step 1-4 from section 3.1.2. except using lysis buffer (yra1C). Step 5-13 are all performed at 4°C.
3. Equilibrate 6 mL of 50% slurry glutathione sepharose (3 mL final packed volume) in a 1.5 X 10 cm chromatography column with 20 mL of Lysis buffer (yra1C).
4. Incubate the cleared lysate with the equilibrated resin in a capped chromatography column for 1.5 hours at 4°C with gentle rocking **(Note 8).**
5. Wash the column with 25 mL of Wash buffer I (yra1C) and then 25 mL of Wash buffer II (yra1C).
6. Shut off the column when vast majority of the wash buffer has flowed through but the column is still wet.

7. Add 5 mL of Wash buffer II (yra1C) along with 35 U RNase A and 50 U RNase I**.**
8. Mix the resin with pipet and incubate for at least 10 min at 4°C.
9. Let the remaining buffer flow through and wash the column with 50 mL of Wash buffer I (yra1C).
10. Elute the GST-yra1C protein with 9 mL Elution buffer (yra1C). Store the protein at -80°C in small aliquots to avoid freeze-thaw cycles. The purified protein is stable for up to four months at -80°C.

4.3.2. Preparation of RNA duplexes for unwinding and annealing assays

DEAD-box proteins can only unwind one to one-and-a-half turns of an RNA duplex (Yang et al., 2007; Chen et al., 2008), therefore, the RNA duplexes that are used in the assays are relatively short. Here, the 5' end of the top strand of the RNA duplex is labeled with γ^{32}P-ATP using T4 polynucleotide kinase. Alternatively, the substrate can also be labeled with a fluorophore, either internally or at the 5' or 3' end. Because some fluorophore dyes affect duplex stability, it is critical to define differences between radiolabeled and fluorescently labeled duplexes prior to analysis (Moreira et al., 2005).

4.3.2.1 Labeling and isolation of RNA duplexes

1. Mix 1 µL of 100 µM top strand RNA, 1 µL of 10X T4 PNK buffer, 1.5 µL of T4 PNK, 6 µL of 10 mCi/mL γ^{32}P-ATP and 1.5 µL of water.
2. Incubate the mixture at 37°C for 1 hour.
3. Inactivate the kinase by adding 2 µL of denaturing gel loading dye and heating at 95°C for 2 min **(Note 9)**.
4. Pre-run a 20% denaturing gel for 30 min at 30 V/cm in 1X TBE running buffer.

5. Load the labeled, top strand RNA and run at 30 V/cm for 2 hours at room temperature.
6. Expose the gel to film or a phosphorimager screen to localize the labeled RNA **(Note 10)**.
7. Cut out the labeled strand with a razor blade and crush the gel slice into smaller pieces by passing through a 3 mL syringe into a 1.5 mL eppendorf tube.
8. Add 600 μL of gel elution buffer to the gel pieces and incubate the sample overnight at 4°C with gentle shaking.
9. Spin down the gel debris for 1 min at room temperature at 3,000xg.
10. Transfer the aqueous fraction into two 1.5 mL tubes and add 3X volume of 100% ethanol and 1 μL of 20 mg/mL glycogen to each tube **(Note 11).**
11. Precipitate the labeled RNA for 1 hour at -20°C and centrifuge at 14,000xg for 30 min at 4°C.
12. Remove the supernatant and dry the pellet on the bench or in a speed vacuum.
13. Resuspend the two RNA pellets into a combined volume of 16 μL of water.
14. Add 2 μL of 100 μM unlabeled bottom strand RNA and 2 μL of 10X duplex annealing buffer to the 16 μL of labeled top strand RNA.
15. Heat the mixture at 95°C for 2 min and cool the substrate at room temperature for 30 min.
16. Pre-run a 15% non-denaturing gel for 30 min at 20 V/cm in 0.5X TBE running buffer.
17. Add 5 μL of non-denaturing gel loading dye to the labeled duplex mixture and load the labeled duplex on a 15% non-denaturing gel.

18. Run the gel at 20 V/cm for 1 hour with a cold water, cooling system or in a cold room to prevent duplex from denaturing.
19. Repeat steps 6-12 to extract the labeled duplex RNA from the gel.
20. Dissolve the pellet in 30 µL of RNA substrate storage buffer.
21. Measure the cpm of the labeled duplex by scintillation counting. It should be around 150,000 cpm/µL.
22. Use the cpm measured from scintillation counting and calculate the RNA duplex using an equation as described (Young and Karbstein 2012) :

$$\frac{\mathbf{X\ cpm}}{\mathbf{1\ \mu L}} \times \frac{\mathbf{3\ dpm}}{\mathbf{1\ cpm}} \times \frac{\mathbf{1\ \mu Ci}}{\mathbf{2220000\ dpm}} \times \frac{\mathbf{0.00001\ Ci}}{\mathbf{1\ \mu Ci}} \times \frac{\mathbf{1\ mmol}}{\mathbf{Z\ Ci}} \times \frac{\mathbf{10000000\ \mu L}}{\mathbf{1\ L}} = \mathbf{Y\ mM}$$

Where Z = the specific activity of γ^{32}P-ATP

23. Aliquot the isolated, labeled RNA duplex into 10 µL aliquots and store at -20°C for up to a month **(Note 12)**.

4.3.3 Unwinding and annealing assays

To study the effect of a protein cofactor on the unwinding activity of a DEAD-box protein, proper experimental controls are required. For instance, any unwinding and annealing activities of the cofactor in the absence of the helicase must be determined. If the protein cofactor can unwind and/or anneal an RNA substrate *in vitro*, these activities would need to be taken into account when assaying in the presence of an RNA helicase. Yra1 exhibits annealing activity *in vitro* (Portman et al., 1997), complicating analysis of Dbp2 helicase inhibition. However, deletion of the N-terminus abolishes annealing activity but preserves interaction with Dbp2 (Fig 4.1D-E, (Ma et al., 2013)). Thus, we measured the inhibition of Dbp2 in the presence of the C-terminal Yra1 domain (yra1C)

(Fig 4.1A-C). Bovine serum albumin (BSA) is used as a control to show specificity (Fig 4.2). A step-by-step schematic diagram for analysis of protein cofactors on a helicase is provided (Fig 4.3).

4.3.3.1 Unwinding assays

1. Mix 3.3 µL of 10X Helicase reaction buffer (HRB), 3.3 µL of 20 U/µL Superase-in, helicase and/or protein binding cofactor (dilute with protein storage buffer) to desired protein concentration (600 nM for Dbp2 and 1200 nM for yra1C), labeled RNA duplex to final concentration of 0.1 nM, and water to a final volume of 33 µL **(Note 13)**.
2. Incubate the mixture at 19°C for 5 min to facilitate Dbp2 binding to the RNA duplex **(Note 14).**
3. Aliquot 3 µL of the reaction mixture into 3 µL 2X Helicase reaction stop buffer (HRSB) for the zero time point (Fig 4.1A-C, lane 3) and place the sample on ice.
4. Aliquot another 3 µL of the reaction mixture to an empty tube and incubate at 19°C for 30 min. After 30 min, add 3 µL 2X HRSB to the reaction. This is the reaction without ATP (Fig. 4.1A-C, lane 10).
5. Add 3 µL of 20 mM ATP/$MgCl_2$ to initiate the unwinding reaction.
6. Aliquot 3 µL of the reaction mixture into 3 µL 2X HRSB at the desired time points and place on ice.
7. Mix 3 µL of 0.1 nM labeled RNA duplex with 3 µL 2X HRSB as a dsRNA loading marker (Fig. 4.1A-C, lane 1).

8. Prepare the ssRNA loading marker (Fig 4.1A-C, lane 2) by mixing 3 μL of 0.1 nM labeled RNA duplex with 3 μL 2X HRSB and heating the mixture at 95°C for 2 min.
9. Pre-run a 12% non-denaturing polyacrylamide gel for 30 min at 10 V/cm in 0.5X TBE running buffer and rinse the wells with the running buffer.
10. Load fractions on the gel and run for 1 hour at 10 V/cm as in step 18 from section 3.2.1.
11. Remove the glass plates, put the gel on Whatman chromatography paper and dry gel on a gel dryer.
12. Expose gel to a PhosphorImager screen or film.
13. Quantify the intensity of radioactivity in dsRNA (I^{ds}) and intensity of radioactivity in ssRNA (I^{ss}) of each time point using a PhosphorImager and ImageQuant software.
14. The fraction of ssRNA at each time point is calculated using: Fraction of ssRNA = $I^{ss}/(I^{ss} + I^{ds})$. The representative gels are shown in (Fig 4.1A-C).
15. Plot the fraction of ssRNA as a function of time and fit the integrated form of a homogenous first-order rate law equation to the data as described (Fig 4.2 and Yang et al., 2005): Fraction of ssRNA = Amplitude × $(1\text{-}e^{-kobs\times time})$, where k_{obs} is the observed rate for the unwinding reaction.

4.3.3.2 Annealing assays

1. Mix 3 μL of 10X HRB, 3 μL of 20 U/μL Superase-in, 3 μL of ATP/$MgCl_2$, helicase and/or protein binding cofactor (dilute with protein storage buffer) to desired protein concentration (600 nM for Dbp2 and 1200 nM for yra1C) and water to a final volume of 28.5 μL.

2. At the same time, prepare another mixture as in step 1 except in the absence of any protein.
3. Incubate the two individual mixtures at 19°C for 5 min.
4. Denature 10 μL of 2 nM labeled RNA duplex at 95°C for 2 min to generate substrates for the annealing assays **(Note 15)**.
5. Add 1.5 μL of the denatured, labeled RNA into a 28.5 μL mixture prepared in step 2.
6. Aliquot 3 μL of the mixture from step 5 into 3 μL 2X HRSB for a zero time point (Fig 4.1D-E, lane 1). Place on ice.
7. Initiate the annealing reaction by adding 1.5 μL of the denatured RNA into the mixture prepared in step 1.
8. Aliquot 3 μL of the reaction mixture into 3 μL 2X HRSB at desired time points and place on ice.
9. Mix 3 μL of 0.1 nM labeled RNA duplex with 3 μL 2X HRSB for dsRNA loading marker (Fig 4.1D-E, lane 8) as in step 7 from Section 3.3.1.
10. Follow steps 9-15 in section 3.3.1 to visualize and quantify the fraction of ssRNA in the annealing assay. The representative gels are shown in (Fig 4.1D-E).
11. Plot the fraction of ssRNA over time and fit the integrated form of a bimolecular annealing reaction equation to the data (Yang and Jankowsky 2005): Fraction of ssRNA = 1/(1+RNA concentration at time 0 × $k_{obs}^{(ann)}$ × Time).

4.4 Notes

1. RNase I cleaves after all four bases of ssRNA efficiently, whereas, RNase A only cleaves after C and U bases (Spahr and Hollingworth 1961; Grossman et al., 1998).
2. Adding glutathione decreases the pH of the buffer. Check the pH of the buffer again after the glutathione is fully dissolved and adjust the pH with a solution of 10M NaOH.
3. An A_{260nm}:A_{280nm} ratio of less than 0.5 suggests that there is no significant RNA contamination. This can be further verified by conducting ATPase assays in the absence of RNA.
4. Addition of glucose to the media can reduce basal expression level in the pET system. This is important if the protein is toxic in *E. coli* (Grossman et al., 1998).
5. Elute the MBP-TEV-Dbp2 protein until A_{280nm} reaches 0.3 O.D. Do not exceed this O.D. because Dbp2 will precipitate during TEV cleavage if the concentration exceeds 30 μM.
6. Vigorous rocking during the incubation with TEV protease will cause Dbp2 to precipitate.
7. yra1C expression is induced at 16°C overnight to promote soluble protein production.
8. Since the binding kinetics between GST and glutathione are relatively slow, it is necessary to allow sufficient time to obtain maximum binding capacity.
9. Denaturing gel-loading dye contains EDTA, which chelates magnesium ions and prevents heat-induced degradation of RNA.

10. Spotting radioactive ink (or sticking phosphorescent label) onto the gel for film orientation prior to gel slicing is highly recommended.
11. Glycogen acts as a carrier to increase the efficiency of nucleic acids precipitation.
12. ^{32}P has a half-life of around 14 days. Furthermore, RNA is subjected to radiolysis over time.
13. The protein concentration should be empirically determined using a Bradford assay for protein stocks.
14. Reaction temperatures may vary for different helicases and need to be determined experimentally.
15. Experimentally verify that the denatured substrate does not spontaneously anneal during the reaction (bottom panel, Fig 4.1D-E).

4.5 References

Bolger TA, Wente SR. 2011. Gle1 is a multifunctional DEAD-box protein regulator that modulates Ded1 in translation initiation. *J Biol Chem* **286**: 39750–39759.

Chen Y, Potratz JP, Tijerina P, Del Campo M, Lambowitz AM, Russell R. 2008. DEAD-box proteins can completely separate an RNA duplex using a single ATP. *Proc Natl Acad Sci U S A* **105**: 20203–20208.

Fuller-Pace F V, Nicol SM, Reid AD, Lane DP. 1993. DbpA: a DEAD box protein specifically activated by 23s rRNA. *EMBO J* **12**: 3619–3626.

Granneman S, Lin C, Champion EA, Nandineni MR, Zorca C, Baserga SJ. 2006. The nucleolar protein Esf2 interacts directly with the DExD/H box RNA helicase, Dbp8, to stimulate ATP hydrolysis. *Nucleic Acids Res* **34**: 3189–3199.

Grossman TH, Kawasaki ES, Punreddy SR, Osburne MS. 1998. Spontaneous cAMP-dependent derepression of gene expression in stationary phase plays a role in recombinant expression instability. *Gene* **209**: 95–103.

Hardin JW, Hu YX, McKay DB. 2010. Structure of the RNA binding domain of a DEAD-box helicase bound to its ribosomal RNA target reveals a novel mode of recognition by an RNA recognition motif. *J Mol Biol* **402**: 412–427.

Hilbert M, Kebbel F, Gubaev A, Klostermeier D. 2011. eIF4G stimulates the activity of the DEAD box protein eIF4A by a conformational guidance mechanism. *Nucleic Acids Res* **39**: 2260–2270.

Jankowsky E. 2011. RNA helicases at work: binding and rearranging. *Trends Biochem Sci* **36**: 19–29.

Jankowsky E, Putnam A. 2010. Duplex unwinding with DEAD-box proteins. *Methods Mol Biol* **587**: 245–264.

Jarmoskaite I, Russell R. 2011. DEAD-box proteins as RNA helicases and chaperones. *Wiley Interdiscip Rev RNA* **2**: 135–152.

Johnson SA, Cubberley G, Bentley DL. 2009. Cotranscriptional recruitment of the mRNA export factor Yra1 by direct interaction with the 3’ end processing factor Pcf11. *Mol Cell* **33**: 215–226.

Klostermeier D, Rudolph MG. 2009. A novel dimerization motif in the C-terminal domain of the Thermus thermophilus DEAD box helicase Hera confers substantial flexibility. *Nucleic Acids Res* **37**: 421–430.

Linder P, Fuller-Pace F V. 2013. Looking back on the birth of DEAD-box RNA helicases. *Biochim Biophys Acta - Gene Regul Mech* **1829**: 750–755.

Ma WK, Cloutier SC, Tran EJ. 2013. The DEAD-box protein Dbp2 functions with the RNA-binding protein Yra1 to promote mRNP assembly. *J Mol Biol* **425**: 3824–3838.

Mallam AL, Jarmoskaite I, Tijerina P, Del Campo M, Seifert S, Guo L, Russell R, Lambowitz AM. 2011. Solution structures of DEAD-box RNA chaperones reveal conformational changes and nucleic acid tethering by a basic tail. *Proc Natl Acad Sci U S A* **108**: 12254–12259.

Mohr G, Del Campo M, Mohr S, Yang Q, Jia H, Jankowsky E, Lambowitz AM. 2008. Function of the C-terminal domain of the DEAD-box protein Mss116p analyzed in vivo and in vitro. *J Mol Biol* **375**: 1344–1364.

Moreira BG, You Y, Behlke MA, Owczarzy R. 2005. Effects of fluorescent dyes, quenchers, and dangling ends on DNA duplex stability. *Biochem Biophys Res Commun* **327**: 473–484.

Nicol SM, Fuller-Pace F V. 1995. The "DEAD box" protein DbpA interacts specifically with the peptidyltransferase center in 23S rRNA. *Proc Natl Acad Sci U S A* **92**: 11681–11685.

Portman DS, O'Connor JP, Dreyfuss G. 1997. YRA1, an essential Saccharomyces cerevisiae gene, encodes a novel nuclear protein with RNA annealing activity. *RNA* **3**: 527–537.

Putnam AA, Jankowsky E. 2013. DEAD-box helicases as integrators of RNA, nucleotide and protein binding. *Biochim Biophys Acta* **1829**: 884–893.

Tsu CA, Kossen K, Uhlenbeck OC. 2001. The Escherichia coli DEAD protein DbpA recognizes a small RNA hairpin in 23S rRNA. *RNA* **7**: 702–709.

Yang Q, Del Campo M, Lambowitz AM, Jankowsky E. 2007. DEAD-box proteins unwind duplexes by local strand separation. *Mol Cell* **28**: 253–263.

Yang Q, Jankowsky E. 2005. ATP- and ADP-dependent modulation of RNA unwinding and strand annealing activities by the DEAD-box protein DED1. *Biochemistry* **44**: 13591–13601.

Young C, Karbstein K. 2012. Analysis of cofactor effects on RNA helicases. *Methods Enzym* **511**: 213–237.

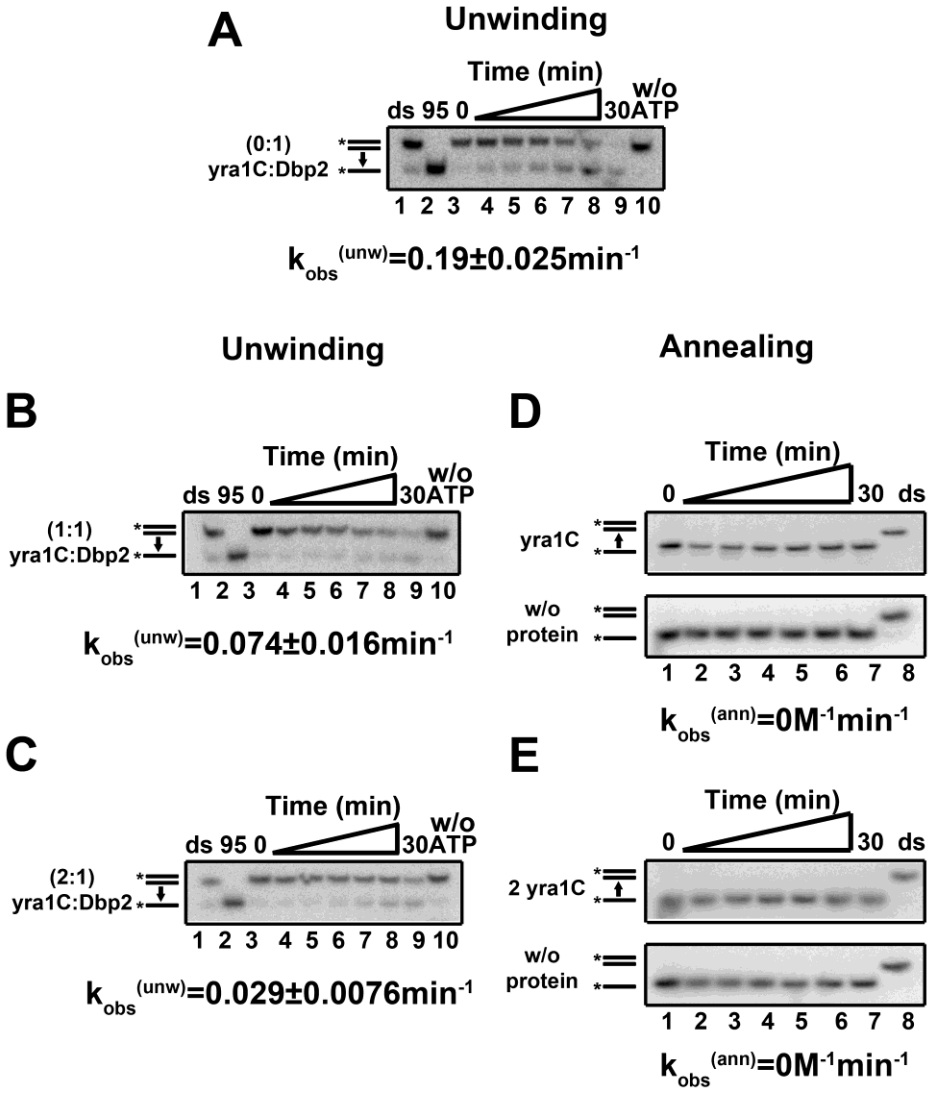

Figure 4.1. The C-terminus of Yra1, yra1C, inhibits the unwinding activity of Dbp2. (A-C) Representative non-denaturing polyacrylamide gels of RNA unwinding assays using 600 nM Dbp2 alone (A) or with equimolar (B) or two fold excess of yra1C (C). (D-E) Representative non-denaturing polyacrylamide gels of RNA annealing assays using 600 nM (D) or 1200 nM yra1C alone (E). This figure is reproduced from (Ma et al., 2013), with permission from Elsevier.

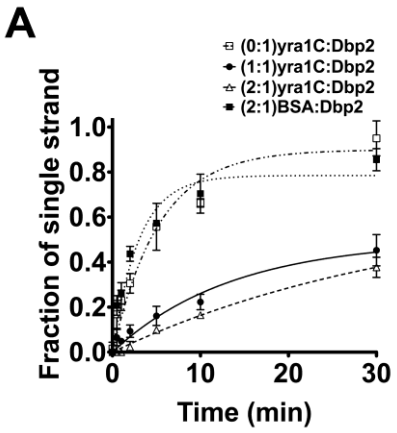

B

yra1C:Dbp2	k_{obs}(min^{-1})	Amplitude
0:1	0.19±0.026	0.90±0.047
1:1	0.074±0.016	0.50±0.053
2:1	0.029±0.0076	0.65±0.12

BSA:Dbp2	k_{obs}(min^{-1})	Amplitude
2:1	0.33±0.048	0.78±0.033

Figure 4.2. Yra1 inhibits the unwinding activity of Dbp2. (A) A graphical representation of Dbp2 unwinding time course in the presence or absence of the C-terminus of Yra1 (yra1C). The unwinding assays were performed with 0.1 nM blunt end RNA duplex and either Dbp2 alone (600 nM) or in the presence of a 1:1 or 1:2 ratio of yra1C (600nM, 1200 nM) or in the presence of BSA (1200 nM) at 19°C. (B) The kinetic parameters of the unwinding reaction. The $k_{obs}^{(unw)}$ and the amplitude of the unwinding reaction were determined using the integrated rate law for a homogenous first-order reaction as described (Yang and Jankowsky 2005). This figure is reproduced from (Ma et al., 2013), with permission from Elsevier.

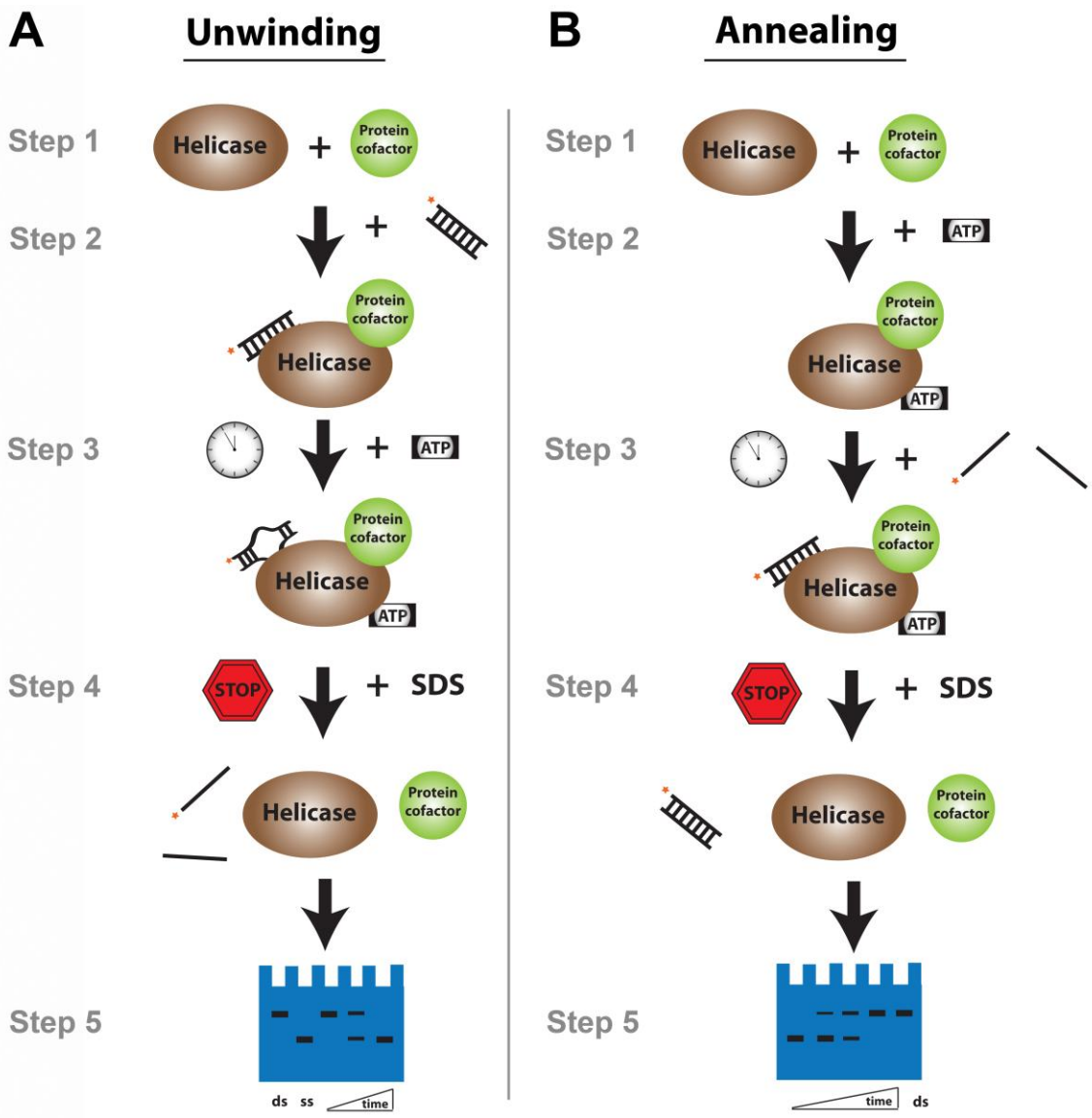

Figure 4.3. Schematic flowchart of the unwinding and annealing assays. (A) For unwinding assays, Step 1: incubate the helicase and the protein cofactor at room temperature for 5 min. Step 2: add the radiolabeled dsRNA and incubate at the appropriate reaction temperature for 5 min. Step 3: start the reaction with equimolar concentration of ATP and $MgCl_2$. Step 4: remove aliquots at different time points and mix with SDS and EDTA to stop the reaction. Step 5: resolve the labeled RNA on a non-denaturing gel and visualize the products by autoradiography. (B) For annealing assays, Step 1: incubate the helicase and the protein cofactor at room temperature for 5 min. Step 2: add an equimolar concentration of ATP and $MgCl_2$ and incubate at reaction temperature for at least 5 min. Step 3: denature the labeled dsRNA at 95°C before adding to the reaction mixture to start the reaction. Step 4-5: remove aliquots over time, resolve and visualize product as above.

CHAPTER 5. RECRUITMENT, DUPLEX UNWINDING AND PROTEIN-MEDIATED INHIBITION OF THE DEAD-BOX RNA HELICASE DBP2 AT ACTIVELY TRANSCRIBED CHROMATIN

5.1 Introduction

Gene expression is an extremely complex process that involves numerous, highly choreographed steps (Zorio and Bentley 2004). During transcription in eukaryotes, the newly synthesized messenger RNA (mRNA) undergoes a variety of intimately linked processing events, including 5' capping, splicing, and 3' end formation, prior to nuclear export and translation (Rouskin et al. 2014; Cramer et al. 2001; Zorio and Bentley 2004). Throughout each of these steps, the mRNA is bound by RNA-binding proteins to form messenger ribonucleoprotein complexes (mRNP), the composition of which is constantly changing at each maturation stage (Chen and Shyu 2014). Proper mRNP formation is critical for gene expression and requires correctly structured mRNA at the appropriate biological time point (Rouskin et al. 2014; Laurent et al. 2012). Given the physical properties of RNA, this molecule tends to form stable secondary structures that are long-lived and require large amounts of energy to unfold and refold to alternative conformations (Herschlag 1995; Pan and Russell 2010). This results in a need for proteins to accelerate RNA structural conversions inside the cell. MRNA in the budding

yeast *S. cerevisiae* appears to be largely unstructured *in vivo*, in contrast to thermodynamic predictions (Rouskin et al. 2014), suggesting the involvement of active mechanisms to prevent formation of aberrant structures. Consistently, ATP-depletion in budding yeast results in increased formation of secondary structure in mRNA (Rouskin et al. 2014). Moreover, recent genome wide analyses of mRNA secondary structure have found a striking correlation between single nucleotide polymorphisms and altered RNA structure within regulatory regions (i.e. miRNA-binding sites), indicating that structural abberations alters gene regulation (Wan et al. 2014; Ramos and Laederach 2014).

Likely candidates for structural rearrangement of cellular mRNAs are ATP-dependent RNA helicases, which act as RNA unwinding or RNA-protein (RNP) remodeling enzymes (Jarmoskaite and Russell 2014; Putnam and Jankowsky 2013b). DEAD-box proteins make up the largest class of enzymes in the RNA helicase family with around 40 members in human cells (25 in yeast). Members of this class are ubiquitously present in all domains of life from bacteria to mammals and are involved in every aspect of RNA metabolism, including pre-mRNP assembly (Linder and Fuller-Pace 2013). For example, alternative splicing of the pre-mRNA that encodes the human Tau protein is regulated by a stem-loop structure downstream of the 5' splice site of exon 10 (Kar et al. 2011). In order for U1 snRNP to access the 5' splice site of *tau* exon 10, this stem-loop needs to be resolved by the DEAD-protein DDX5 (Kar et al. 2011). Mis-regulation of splicing in the *tau* gene is highly associated with dementia, underscoring the importance of remodeling for proper gene expression (Hutton et al. 1998; Hasegawa et al. 1999). However, our understanding of the biochemical mechanism(s) of pre-mRNA/mRNA remodeling has been hampered due to the complex and highly

interdependent nature of co-transcriptional processes. Moreover, individual DEAD-box protein family members exhibit a wide variety of biochemically distinct activities including RNA annealing, nucleotide sensing, and RNP remodeling, with further diversification of biological functions conferred by regulatory accessory proteins (Yang and Jankowsky 2005; Ma et al. 2013; Putnam and Jankowsky 2013b; Tran et al. 2007)

The *S. cerevisiae* ortholog of DDX5 is Dbp2 (Barta and Iggo 1995). Our laboratory previously established that Dbp2 is an active ATPase and RNA helicase that associates with transcribing chromatin (Ma et al. 2013; Cloutier et al. 2012). Moreover, Dbp2 is required for assembly of the mRNA binding proteins Yra1 and Nab2, as well as the mRNA export receptor Mex67, onto mRNA (Ma et al. 2013). Interestingly, Yra1 interacts directly with Dbp2 and this interaction inhibits Dbp2 unwinding in multiple cycle, bulk assays, demonstrating that Yra1 restricts unwinding by Dbp2 (Ma et al. 2013). Nevertheless, the mechanism and the biological role of Yra1-dependent inhibition were not understood.

By utilizing a combination of biochemical, molecular biology and biophysical methods, we now provide compelling evidence that Yra1 constrains the activity of Dbp2 to co-transcriptional mRNP assembly steps. This inhibition is important for maintenance of transcript levels *in vivo*. Single molecule (sm) FRET and fluorescent anisotropy studies show that Yra1 inhibits Dbp2 unwinding by preventing association of Dbp2 with RNA without altering the kinetics of duplex unwinding. Consistently, loss of the Yra1-Dbp2 interaction in yeast cells causes post-transcriptional accumulation of Dbp2 on mRNA. Taken together, this suggests that Yra1 terminates a cycle of Dbp2-dependent mRNP assembly *in vivo*.

5.2 Materials and methods

Plasmids and Yeast Strains

Please see Table 5.1 and Table 5.2 for all the plasmids and yeast strains that were used in this study.

Chromatin Immunoprecipitation Assays (ChIP)

ChIP analysis was performed as described previously (Cloutier et al. 2012), with the following modifications. Sheared chromatin with or without RNase treatment was used in ChIP. Isolated DNA was then subjected to qPCR using primers listed (Table 5.3). All ChIP experiments were conducted with at least three biological replicates and three technical repeats. Error bars indicate the SEM of the biological replicates.

Protein Immunoprecipitation Assays

Cells were harvested at mid-log phase and lysed with glass beads using a mini-bead beater (BioSpec Products) in cold lysis buffer containing 20 mM Tris pH 6.5, 5 mM $MgCl_2$, 0.5% Triton X-100, 70 mM NaCl, 1Xprotease inhibitor (Complete, EDTA-free protease inhibitor cocktail tablet) (Roche), and 1 mM PMSF. Lysate was subjected to immunoprecipitation. Proteins were resolved by SDS-PAGE and detected by western blotting.

RNA Immunoprecipitation (RIP) Assays

RNA-IP was performed as described (Gilbert and Svejstrup 2006) with the following modifications and the isolated RNA was detected by RT-qPCR (for primers, see Table

5.4). All RNA-IP experiments were performed with three biological and three technical repeats. Error bars indicate the SEM of the biological replicates.

Glycerol Gradient Centrifugation

Cells were harvested at mid log phase and lysed. Lysate in the presence or absence of 70 U of RNase A and 1000 U of RNase I was subjected to 10-30% glycerol gradients in 20 mM HEPES pH 7.4, 110 mM KOAc, 0.5% Triton X-100 and 0.1% Tween. After centrifugation in an SW41 rotor using Beckman Coulter Optima L-90K Ultracentifuge at 35, 000 rpm for 18 hours at 4°C, 600 µl fractions were collected from the top of the gradient and analyzed for the presence of the proteins by SDS-PAGE followed by western blotting analysis. 0.6% of the lysate was used to serve as an input (T). Molecular weights from each fraction in the glycerol gradients were determined using a standard curve that was generated by resolving the molecular weight standards comprising catalase (250 kDa), apoferritin (480 kDa), and thyroglobulin (670 kDa).

TAP tag Immunoprecipitation

Immunoprecipitation was conducted as described previously (Ma et al. 2013) in the presence or absence of 70 U of RNase A and 1000 U of RNase I. Protein were resolved by SDS-PAGE and detected by Western blotting analysis using indicated antibodies.

Recombinant Protein Expression and Purification

Expression and purification of pMAL MBP-TEV-DBP2, GST-TEV-YRA1, and pET21GST-YRA1C in *E. coli* cells was conducted as previously described (Ma et al. 2013).

Single Molecule FRET

dsRNA hairpin was purchased from Integrated DNA technologies (IDT) and labeled as described (Wood et al. 2012). Single molecule experiments were carried out as previously described (Mundigala et al. 2014). Hexokinase treatment was conducted by incubating 10 nM Dbp2 with 100 μM hexokinase and 1 mM glucose in the imaging buffer for 10 minutes before imaging.

Gel Shift Assays

10 μL reactions containing 2 mM ADP-BeF_X/$MgCl_2$, 20 U of Superase-in (Ambion), 0.5 mM $MgCl_2$, 0.01% NP-40, 2 mM DTT, 40 mM Tris-HCl, pH 8, 10 nM labeled ssRNA (16 nt, 5'-AGC ACC GUA AAG ACG C-3'), and 400 nM of recombinant, purified Dbp2 in the presence or absence of varying amounts of recombinant, purified yra1C. Varying amounts of BSA with 400 nM of recombinant, purified Dbp2 was used to serve as specificity control. Components were added in the order as indicated and incubated at 4°C for indicated time. Reaction mixtures were resolved on a non-denaturing gel and signal was detected by densitometry.

Fluorescence Anisotropy Assays

40 μL reactions containing 40 mM Tris-HCl (pH 8), 30 mM NaCl, 2.5 mM $MgCl_2$, 2 mM ADP-BeFx, 2 mM DTT, 40 U Superase-in (Ambion), and varying amounts of Dbp2 in the presence or absence of 150 nM yra1C. Dbp2 and yra1C were first incubated in the reaction buffer at 25°C for 15 min, then 10 nM fluorescently labeled ssRNA (5'-6-FAM-AGC ACC GUA AAG ACG C-3') was added and incubated at 25°C for another 100 min to reach equilibrium binding. Fluorescence anisotropy signals of 6-FAM (λ_{ex} = 495 nm and λ_{em} = 520 nm) was measured using the BioTek Synergy 4 plate reader. The data were fitted to the following equation: $Y=B_{max}*X^h/(K_d{}^h+X^h)$ in Prism.

Transcriptional Shut Off Assays

Transcriptional shut off assays were conducted as described (Coller 2008). Cells were grown at 25°C in glucose to log phase then shift to galactose for 10 hours to induce the *GAL* genes expression followed by a shift to glucose to repress transcription. RNA was isolated at indicated time points, subjected to Northern Blotting analysis, and detected by densitometry. RNA half-lives were determined by measuring the amount of GAL10 or GAL7 transcript over time with respect to the stable scR1 transcript. All experiments were performed with three biological replicates.

5.3 Results

5.3.1 Dbp2 is recruited to chromatin via nascent RNA

The DEAD-box RNA helicase Dbp2 is predominately localized in the nucleus in association with actively transcribed genes (Cloutier et al. 2012; Johnson et al. 2011;

Zenklusen et al. 2001; Beck et al. 2014). To determine if Dbp2 is recruited to chromatin via nascent RNA, we conducted chromatin immunoprecipitation (ChIP) assays with or without RNase treatment (Abruzzi et al. 2004). Briefly, yeast cells harboring a 3XFLAG epitope tag fused to the 3' end of the endogenous *DBP2* coding region were grown in the presence of galactose to induce transcription of the *GAL* genes, known gene targets for Dbp2 association (Ma et al. 2013). *DBP2* untagged strains were used to serve as a background control. Chromatin was then isolated and incubated with a mixture of RNase A and RNase I or buffer alone prior to ChIP with the anti-FLAG antibody. The eluted fractions were then subjected to quantitative (q)PCR with probes across the *GAL10* and *GAL7* genes (Fig. 5.1A). Consistent with previous studies, this revealed that Dbp2 is evenly distributed across the coding regions of both *GAL10* and *GAL7* with little to no association with promoters (Fig. 5.1B). Interestingly, RNase treatment drastically reduced Dbp2 occupancy across the entire locus for both the *GAL10* and *GAL7* genes to levels that were not statistically different (p-value >0.05) from background (Fig. 5.1B). This suggests that Dbp2 is recruited to chromatin by interacting with newly transcribed RNA. The low level of RNase-resistant Dbp2 could be due to trace amounts of RNA still present after enzymatic digestion or an alternative recruitment mechanism, such as interaction with RNA Polymerase II (RNA Pol II).

Dbp2 is required for efficient assembly of mRNA-binding proteins and export factors, including Nab2, Mex67 and Yra1, and interacts directly with the C-terminal half of Yra1 (Ma et al. 2013). Yra1 is co-transcriptionally recruited to chromatin through interaction with Pcf11, an essential component of the cleavage and polyadenylation factor IA complex involved in 3'-end formation (Johnson et al. 2009). To determine if the

Dbp2-Yra1 interaction modulates recruitment of Dbp2 to chromatin, we conducted ChIP as above in either wild type or *yra1*Δ*C* strains, the latter of which lacks the ability to associate with Dbp2 *in vivo* (Fig. 5.1C – 5.1D). This revealed no difference in the recruitment pattern of level of Dbp2 to the *GAL10* and *GAL7* genes (Fig. 5.1E). Thus, Yra1 does not mediate recruitment of Dbp2 to chromatin.

5.3.2 Yra1 prevents accumulation of Dbp2 on RNA Pol II transcripts

To determine if the Dbp2-Yra1 interaction modulates the association of Dbp2 with RNA, we conducted RNA immunoprecipitation (RIP) of a *DBP2-3xFLAG* strain. Since Dbp2 associates with the *GAL10*, *GAL7*, *ACT1*, and *ADE3* genes shown by ChIP (Cloutier et al. 2012), we selected these four gene transcripts as candidates whereas 18S rRNA serves as a negative control. Analysis of the levels of immunoprecipitated transcripts by RT-qPCR revealed that Dbp2 associates with all four, candidate mRNAs at levels ~7-fold above an untagged background control strain. Furthermore, loss of the Dbp2-Yra1 interaction in the *yra1*Δ*C* strain increased the association of Dbp2 with RNA Pol II transcripts by ~3 to 5 – fold (Fig. 5.2A), suggesting that Yra1 prevents accumulation of Dbp2 on mRNA. Interestingly, the Dbp2-Yra1 interaction also affects the abundance of Dbp2 protein, with the *yra1*Δ*C* strain exhibiting two-fold more Dbp2 than wild type (Fig. 5.3A). To determine if the accumulation of Dbp2 on RNA in the *yra1*Δ*C* strain is due to overexpression of *DBP2*, we transformed wild type cells with a 2 micron plasmid encoding *DBP2* under the control of the highly active *GAL1/10* promoter or with empty vector and conducted RIP as above. Under this condition, Dbp2 protein level is at least two-fold more abundant in *pGAL-DBP2* than the wild type cells with

empty vector (Fig. 5.3B). Furthermore, this revealed co-precipitation of similar amounts of the GAL10, GAL7, ACT1 and ADE3 transcripts regardless of the levels of Dbp2 protein (Fig. 5.3C). This suggests that the accumulation of Dbp2 on mRNA is not simply due to overexpression but is specific to the *yra1ΔC* strain. Furthermore, the fact that Dbp2 accumulates on RNA not chromatin (Fig. 5.1E) suggests this accumulation occurs after the transcript is released from the site of synthesis in *yra1ΔC* strains.

Prior studies have shown that loss of the C-terminal half of Yra1 in *yra1ΔC* results in a mild but detectible mRNA export defect (Zenklusen et al. 2001). To determine if the accumulation of Dbp2 on RNA is caused by a block to mRNA export, we conducted RIP in *rat7-1* strains, which harbor a mutation in the *NUP159* gene required for mRNA export and has been shown to induce export defects at the non-permissive temperature (37°C) (Krebber et al. 1999; Gorsch et al. 1995; Del Priore et al. 1996). Interestingly, this revealed slightly lower levels of Dbp2 on mRNA at the non-permissive temperature (37°C) in *rat7-1* strain as compared to wild type (Fig. 5.2B), indicating that the accumulation of Dbp2 on mRNA is not due to a block in mRNA export.

5.3.3 Dbp2 is found in a large RNA-dependent complex *in vivo*

To determine if Dbp2 is found in a large complex *in vivo*, we subjected wild type whole cell lysate to gradient fractionation followed by western blotting for detection of Dbp2, mRNA binding protein Yra1, Mex67, and Nab2, and the DEAD-box helicase Dbp5. Approximate molecular weights were then determined from the fractionation pattern relative to a molecular weight standard for each protein. Interestingly, Dbp2, Yra1

and Mex67 co-migrated in a large ~1.2 MDa complex, with no detectible free Dbp2 (Fig. 5.4A, fractions 14 – 17). This corresponds to approximately 70% of the Dbp2 and Yra1 across all fractions and 40% of Mex67. The presence of Dbp2 in a large complex is not an inherent property of DEAD-box proteins in general as the mRNA export factor and DEAD-box RNA helicase Dbp5 migrated at a significantly smaller size (Fig. 5.4A, fraction 2 – 4). The remaining fraction of Mex67 migrated at a smaller position corresponding to fractions 5-10, partially overlapping the migration pattern of Nab2 (Fig. 5.4A fractions 4 – 6). Approximately 3% of the total Yra1 co-migrated with Nab2 and Mex67, suggesting that the vast majority of Yra1 is also found in a large complex. This suggests that there is little to no free Dbp2 in the cell and that Dbp2 may be in a large complex in association with Yra1 and Mex67 *in vivo*.

To determine if the migration pattern of Dbp2 is dependent on RNA, we subjected yeast cell lysate to RNase treatment prior to gradient fractionation. Interestingly, RNase treatment shifted the migration pattern of Dbp2, Yra1 and Mex67 to lower gradient fractions in the absence of RNA (Fig. 5.4B, fractions 6 – 8). Whereas the migration pattern of Nab2 was not significantly changed, Dbp2, Yra1 and Mex67 were detected across multiple smaller fractions with a larger portion of Mex67 (75%) co-fractionating with Nab2 than above (Fig. 5.4B, Lanes 3-6). This suggests that Dbp2, Yra1 and a fraction of Mex67 all form large RNA-dependent complexes *in vivo*.

To determine if Dbp2, Yra1 and Mex67 form a complex, we performed immunoprecipitation assays with *DBP2-TAP* strains with and without RNase treatment. *DBP2* untagged strains were used to serve as a background control. Though a faint band was observed at the size that equivalents to Dbp2 in the elution fraction of *DBP2*

untagged strains (Fig. 5.4C, lane 2), the signal of Dbp2 from *DBP2-TAP* strains was much stronger in either the presence or absence of RNase treatment (Fig. 5.4C, lanes 4 and 5). This suggests that Dbp2 was successfully precipitated. Consistent with *in vitro* studies, Yra1 was efficiently co-purified with Dbp2 regardless of RNase treatment (Fig. 5.4C, lanes 4 and 5). In addition, Mex67 was also co-purified with Dbp2 independent RNA (Fig. 5.4C, lanes 4 and 5). This suggests that the large 1.2 MDa complex contains all three proteins and that formation of the Dbp2-Yra1-Mex67 complex is not dependent on RNA. Consistent with gradient fractionation, Nab2 did not co-purify with Dbp2 regardless of RNase treatment (Fig. 5.4C, lanes 4 and 5). Together with the glycerol gradient assays, this suggests that Yra1 does not maintain a free pool of Dbp2 but rather may restrict the location of Dbp2 association with mRNA *in vivo*. As loss of Yra1-Dbp2 interaction accumulates Dbp2 on RNA, but not chromatin, and Nab2 does not associate with Dbp2 (Fig. 5.1E and 5.4C), suggesting that the Yra1-dependent restriction happens at a point after mRNA is released from chromatin but before association of Nab2 and subsequent mRNA export.

5.3.4 Yra1 does not alter the kinetics of Dbp2-dependent unwinding by smFRET

Our prior studies used bulk, multiple cycle assays to show that Yra1 inhibits Dbp2-dependent unwinding *in vitro* (Ma et al. 2013). A limitation of these assays was the inability to distinguish between kinetic effects of Yra1 on duplex unwinding rates or thermodynamic effects on association of Dbp2 with RNA targets. To determine if Yra1 inhibits Dbp2 by decreasing the duplex unwinding rate, we first established single molecule fluorescence resonance energy transfer (smFRET) assays for Dbp2-dependent

unwinding using a fluorescently labeled dsRNA stem-loop molecule. Although the precise substrates for Dbp2-dependent unwinding are unknown, a stem-loop is the most common secondary structure identified in cellular mRNAs to date (Svoboda and Di Cara 2006; Rouskin et al. 2014; Ding et al. 2014; Wan et al. 2014), and, thus, represents a likely physiological target for Dbp2 *in vivo.*

Briefly, a 39 nt hairpin dsRNA labeled with FRET pair fluorophores Cy3 and Cy5 was surface-immobilized onto a pegylated microscopic quartz slide through biotin-neutravidin linkage (Fig. 5.5A). The FRET pair fluorophores are close together and exhibit a high FRET state (0.9) when the dsRNA forms a closed hairpin whereas the FRET pair fluorophores are farther apart when the dsRNA is unwound with a low FRET state (0.1) (Fig. 5.5A). A threshold of 0.6 FRET was used to distinguish between the open (0.1 FRET) and closed (0.9 FRET) states of the hairpin. To study Dbp2-dependent unwinding at the single molecule level, we initially established smFRET assays in the presence of low salt (30 mM NaCl) to parallel previous bulk *in vitro* assay experiments (Ma et al. 2013). Under these conditions, 98% of the hairpin RNA molecules exhibit a high FRET state (0.9) in the absence of any protein or nucleotide (Fig. 5.6A and Fig. 5.6B), indicative of a stable dsRNA hairpin. In the presence of 10 nM Dbp2, we found that 27% showed a single transition from a closed to open state within the course of the experiment (Fig. 5.6A and Fig. 5.6B). This indicates that Dbp2 can unwind a dsRNA substrate in the absence of ATP, an unexpected observation not seen in our previous *in vitro* bulk unwinding assays (Ma et al. 2013). Addition of 100 μM ATP and equimolar magnesium increased the percentage of these molecules molecules to 61%, suggesting that more molecules are acted upon by Dbp2 in the presence of ATP. This is consistent

with the thermodynamic coupling of ATP and RNA-binding in DEAD-box family members (Samatanga and Klostermeier 2014; Banroques et al. 2008; Theissen et al. 2008). However, we were unable to monitor the kinetics of duplex unwinding in these conditions because only ~15% of the RNA molecules exhibited dynamic cycles of opening and closing (Fig. 5.6B).

To remedy this and to make our analyses more physiologically relevant, we conducted smFRET in the presence of 150mM NaCl. The representative FRET time trajectory of RNA alone shows that the hairpin dsRNA is stable at 150 mM NaCl (Fig. 5.5B). This resulted in 45% of the molecules exhibiting dynamic behavior in the presence of Dbp2 and ATP (Fig. 5.5B – 5.5C). This increased dynamics was not due to a less stable RNA substrate as the smFRET molecule remained stable throughout the timecourse (Fig. 5.5B). Interestingly, and consistent with our low salt studies, the addition of Dbp2 alone also resulted in dynamic cycles of opening and closing, albeit with less RNA molecules showing dynamic behavior in the absence of ATP (Fig. 5.5B-5.5C). ATP-independent unwinding was not due to contaminating ATP in the Dbp2 purification as dsRNA hairpins still exhibited dynamic opening and closing cycles in the presence of hexokinase and glucose (Fig. 5.5C). Interestingly, smFRET studies of the mitochondrial group II intron also demonstrated an ATP-independent role for the DEAD-box protein Mss116 in RNA folding, a process that requires both folding and unwinding steps ((Karunatilaka et al. 2010) and see Discussion).

To determine if ATP alters the opening and closing rates of the RNA molecules, numerous (~100) trajectories were used to build dwell time histograms. Measurement of the dwell time distribution in the presence of Dbp2 alone (no ATP) revealed opening and

closing rate constants of 4.1 s^{-1} and 3.3 s^{-1}, respectively (Table 5.5). Interestingly, addition of ATP and equimolar magnesium did not appreciably increase either the opening (6.3 s^{-1}) or closing (5.9 s^{-1}) rates of the RNA duplex (Table 5.5). Together, this indicates that ATP does not affect the unwinding rate but rather increases the population of dsRNA molecules acted upon by Dbp2.

Having established the unwinding behavior of Dbp2 at the single molecule level, we then asked if Yra1 affects the rate of duplex unwinding by incorporating a GST-tagged C-terminal half of Yra1 (yra1C) into our smFRET assays. Yra1C is the minimal Dbp2-interacting region in Yra1, which is sufficient for inhibition of helicase activity and also lacks intrinsic RNA-binding activity that would complicate experimental interpretation (Ma et al. 2013). Interestingly, addition of a two-fold molar excess of yra1C, consistent with the ratio of Dbp2 and Yra1 proteins in yeast cells (Chong et al. 2015), did not appreciably reduce the opening (4.8 s^{-1}) and closing (5.5 s^{-1}) rate of the hairpin (Table 5.5). However, yra1C did decrease the percentage of unwound molecules (both dynamic and closed to opened) across the population in a dose-dependent manner, to levels similar to Dbp2 without ATP (Fig. 5.5C). This suggests that Yra1 does not alter the kinetics of Dbp2-dependent unwinding of the RNA duplex.

5.3.5 Yra1 prevents Dbp2 from associating with ssRNA *in vitro*

ATP promotes high affinity RNA-binding by DEAD-box proteins (Rudolph and Klostermeier 2015). The population effects seen in our smFRET studies suggest that Yra1 decreases the affinity of Dbp2 for RNA, similar to the absence of ATP. To test this, we performed fluorescence anisotropy assays with Dbp2, 6-FAM-labeled ssRNA and the

pre-hydrolysis ATP analog ADP-BeFx (Fig. 5.7A). We also utilized low salt conditions (30 mM NaCl) as the increased dynamics would be predicted to reduce RNA-binding and the ability to form a stable complex. ADP-BeFx was utilized to promote stable binding of Dbp2 RNA (Liu et al. 2014). To ensure that our assays were performed under equilibrium conditions, we first conducted a time course and monitored the change in anisotropy over time. This revealed that equilibrium is established within 100 min (Fig. 5.8). Next, we conducted fluorescence anisotropy with Dbp2 in the presence or absence of ADP-BeFx. This revealed that ADP-BeFx decreased the dissociation constant (K_d) of Dbp2 for ssRNA from 237 to 38 nM (Fig. 5.7A), similar to other DEAD-box proteins (Cao et al. 2011; Henn et al. 2008). Interestingly, inclusion of 150nM yra1C increased the K_d by 7-fold to 271 nM (Fig. 5.7A). This suggests that Yra1 inhibits Dbp2 by reducing the affinity for RNA.

To determine if Yra1 prevents initial RNA-binding by Dbp2, we exploited the slow on rate of the ADP-BeFx-bound Dbp2 to RNA (Fig. 8; (Liu et al. 2014)) and asked if Yra1 reduces the RNA-binding affinity of Dbp2 by performing an order of addition experiment under pre-equilibrium conditions for the Dbp2-ADP-BeFx-RNA complex. Briefly, Dbp2 and yra1C or BSA were pre-incubated for 15 min in the presence of ADP-BeFx followed by addition of a radiolabeled, 16 nucleotide ssRNA for an additional 15 min prior to resolution of RNA-bound complexes on a native gel (Fig. 5.7B). Consistent with the reduced RNA-binding affinity above (Fig. 5.7A), pre-incubation of Dbp2 with yra1C resulted in a concentration-dependent reduction of Dbp2 binding to ssRNA, from 100% bound to 58% (Fig. 5.7B, lanes 6-10). The reduction is specific to yra1C, as BSA had no effect on the RNA-binding by Dbp2 (Fig. 5.7B, lanes 12-16). Moreover, this is

not due to competition between Yra1 and Dbp2 for RNA as yra1C does not exhibit appreciable RNA binding activity ((Ma et al. 2013) and Fig. 5.7B, lanes 2-5). Yra1 also reduced ssRNA binding by Dbp2 at physiological (150 mM) salt concentrations (Fig. 5.9). This indicates that Yra1 inhibits the unwinding activity of Dbp2 by reducing the affinity for RNA. Because Yra1 and Dbp2 exist in a 2:1 ratio in yeast cells (Chong et al. 2015) and Yra1 prevents overaccumulation of Dbp2 on cellular mRNAs (Fig. 5.2A), this suggests that Yra1 functions similarly to regulate Dbp2 *in vivo*.

5.3.6 Loss of the Dbp2-Yra1 interaction increases the half-life of GAL7 mRNA

To determine if Yra1-dependent inhibition of Dbp2 is necessary for proper gene expression, we analyzed Dbp2-bound targets for expression defects in wild type and *yra1*Δ*C* strains. We also analyzed the *DBP2* transcript itself since the *yra1*Δ*C* strain shows higher Dbp2 protein levels than wild type cells (Fig. 5.3A). Interestingly, this revealed that both the DBP2 and GAL7 transcripts and resulting proteins are significantly upregulated in *yra1*Δ*C* strains (Fig. 5.10A-B). In contrast, none of the other Dbp2-associated transcripts exhibited altered abundance (Fig. 5.10A). We were also unable to detect a change in protein level for *GAL10* (Fig. 5.10B). This suggests that the accumulation of Dbp2 results in a transcript-specific effect on gene expression.

To determine the mechanism for increased GAL7 mRNA abundance in *yra1*Δ*C* strains, we asked if the increase occurred at transcription or decay. To this end, we conducted ChIP of RNA Pol II and transcriptional shut off assays to compare the transcription and mRNA decay efficiencies, respectively. ChIP using anti-Rpb3 revealed similar levels and patterns of RNA Pol II occupancy in both wild type and *yra1*Δ*C* strains

across both *GAL7* and *GAL10*, suggesting that Dbp2 accumulation does not alter transcription efficiency (Fig. 5.10C). In contrast, however, transcriptional shut off assays using glucose addition to the media and subsequent northern blotting revealed that the half-life of the GAL7 mRNA is approximately two times longer in *yra1ΔC* strains as compared to wild type (Fig. 5.10D). This was not the case for the GAL10 mRNA, whose half-life was unchanged. This suggests that Dbp2 accumulation prevents efficient degradation of a subset of transcripts. Although it is currently unclear what renders GAL7 mRNAs sensitive to Dbp2 accumulation, it is likely that this specificity is dictated by the mRNA sequence and/or structure itself. Regardless, this demonstrates that Yra1-dependent inhibition of Dbp2 alters mRNA metabolism *in vivo*. Taken together, and in conjunction with our prior work and the current state of the mRNP assembly field (Ma et al. 2013; Oeffinger and Montpetit 2015; Babour et al. 2012) we propose a model whereby Dbp2 promotes efficient assembly of mRNA binding proteins including Yra1 onto mRNA during transcription which, in turn, prevent recycling of Dbp2 onto the properly formed mRNP (Fig. 5.11 and Discussion).

5.4 Discussion

The human genome encodes approximately 100 helicases, of which ~60% are RNA-dependent (Umate et al. 2011). DEAD-box proteins are the largest class in the RNA helicase family and have been implicated in all aspects of RNA biology. However, there is a large gap in our knowledge regarding the precise biochemical role(s) of individual DEAD-box protein family members in the cell. Our studies provide evidence that Dbp2 associates with transcribed chromatin via RNA, facilitates loading of RNA

binding proteins most likely by resolving RNA secondary structure, and is then released by one of the assembled proteins, Yra1. Yra1 is recruited to chromatin through direct interactions with the mRNA 3' end processing factor Pcf11, which associates with the CTD of RNA Pol II (Abruzzi et al. 2004; Johnson et al. 2009). Since Dbp2 is required for efficient assembly of Yra1 onto mRNA (Ma et al. 2013), this suggests that Yra1 is brought to the chromatin through interactions with the transcriptional apparatus and is subsequently transferred to mRNA by Dbp2. A recent study on the distribution of RNA-protein interactions and secondary structure in Arabidopsis has revealed an anti-correlative relationship (Gosai et al. 2015). Given that Dbp2 unwinds RNA duplexes efficiently *in vitro* (Ma et al. 2013) and that Yra1 is presumably a single-stranded RNA-binding protein, we envision that this transfer occurs because Dbp2 has remodeled secondary structures that are refractory to mRNP assembly. With the new advances in mRNA structural analysis in living cells (Ding et al. 2014; Rouskin et al. 2014; Wan et al. 2014), it may be possible to determine specific RNA sequences that depend on Dbp2 or other DEAD-box proteins in living cells.

The enzymatic activities of many DEAD-box proteins are regulated by protein co-factors (Hilbert et al. 2011; Ma et al. 2013; Schutz et al. 2008; Granneman et al. 2006; Alcazar-Roman et al. 2006). For example, the human tumor suppressor Pdcd4 inhibits both the unwinding and the ATPase activities of the human DEAD-box protein eIF4A (Chang et al. 2009; Loh et al. 2009). This allows Pdcd4 to inhibit translation resulting in suppression of neoplastic transformation and tumorigenesis in a mouse model (Yang et al. 2003; Cmarik et al. 1999; Jansen et al. 2005). In contrast, the translation initiation factor eIF4B stimulates both the unwinding and ATPase activities of rabbit eIF4A to

promote efficient translation (Rozen et al. 1990; Rogers Jr. et al. 2001, 1999). This suggests that individual DEAD-box proteins may have both activators and inhibitors *in vivo*, resulting in fine tuned control of enzymatic activity. This phenomenon has been seen in the Ski2-like RNA helicase Brr2 during spliceosome maturation whereby the spliceosomal protein Prp8 both stimulates and inhibits the unwinding activity of Brr2 (Pena et al. 2009; Maeder et al. 2009; Mozaffari-Jovin et al. 2012, 2013).

Prior studies from our laboratory showed that Yra1 interacts directly with Dbp2 and inhibits duplex unwinding activity without affecting the efficiency of ATP hydrolysis (Ma et al. 2013). Using smFRET, we now show that Yra1 reduces the number of dynamic molecules across a population and decreases the rate of unwinding of single dsRNAs. Moreover, Yra1 decreases the ssRNA-binding affinity of Dbp2, an activity that is essential for duplex unwinding (Rudolph and Klostermeier 2015). DEAD-box RNA helicases exhibit structurally distinct conformations based on association with ATP and RNA (Sengoku et al. 2006b; Andersen et al. 2006; Aregger and Klostermeier 2009). In the absence of either, these enzymes exist in a largely open confirmation, whereas binding of ATP and RNA induces formation of a closed state with the RecA domains coming together and bending the RNA into a structure that is incompatible with an A-form helix (Sengoku et al. 2006b; Andersen et al. 2006). The DEAD-box protein remains bound to the bent ssRNA until ATP hydrolysis promotes release.

Our data suggests that Yra1 does not inhibit Dbp2 from hydrolyzing ATP but prevents stable association of Dbp2 with ssRNA (Ma et al. 2013). This likely occurs through an Yra1-dependent structural rearrangement of Dbp2 which causes reduced RNA-binding affinity. To the best of our knowledge, eIF4A and Ded1 are the only two

DEAD-box proteins whose inhibition mechanisms have been determined (Chang et al. 2009; Loh et al. 2009; Putnam et al. 2015). Pdcd4 inhibits both the ATPase and unwinding activity of eIF4A through blocking RNA binding, whereas eIF4G inhibits the unwinding activity of Ded1 via interfering oligomerization of Ded1, and increases the affinity towards RNA. Since Yra1 inhibits Dbp2 helicase activity by reducing ssRNA-binding activity without abolishing ATP hydrolysis, this suggests that Yra1 utilizes a distinct inhibition mechanism from Pdcd4 and eIF4G. Although it is not known how this occurs, the fact that Yra1 prevents accumulation of Dbp2 on mRNA transcripts suggests that Yra1 functions similarly *in vivo* as *in vitro.*

By using gradient fractionation, we found that Yra1 and Dbp2 co-migrate at a position that corresponds to a large, RNA-dependent macromolecular complex. We speculate that this migration reflects association with assembled mRNPs in the cell, consistent with the biological roles of these two proteins. Although we cannot conclude that Yra1 and Dbp2 are present on the same mRNA molecule simultaneously, the fact that these two proteins interact directly regardless of the presence of RNA indicates that this is the case ((Ma et al. 2013)and Fig. 5.3). The question then is how Yra1 can both interact with Dbp2 and promote release from RNA simultaneously. One possible scenario is that Yra1 and/or Dbp2 is post-translationally modified to control protein-protein interactions between these two molecules. In line with this, ubiquitination of Yra1, Nab2 and Mex67 has been shown to modulate the interactions between these three RNA-binding proteins and mRNA export factors in a manner that controls the timing of pre-mRNP assembly in the nucleus (Iglesias et al. 2010). The fact that yra1ΔC does not exhibit increased Dbp2 accumulation on chromatin suggests that inhibition occurs post-

transcriptionally following release of the mRNA from the site of synthesis. Consistent with this, accumulation of Dbp2 causes stabilization of a subset of transcripts, a process that is predominantly post-transcriptional (Bevilacqua et al. 2003; Anderson and Kedersha 2009). Furthermore, both over-expression of *DBP2* and *yra1*Δ*C* lead to mild mRNA export defects (Zenklusen et al. 2001; Ma et al. 2013), suggesting that Yra1 acts immediately prior to mRNA transport from the nucleus.

Our results show that Dbp2 loads Yra1 onto poly(A)+ RNA (Ma et al. 2013), a role previously assigned to the DECD-box protein Sub2 (Taniguchi and Ohno 2008; Luo et al. 2001). Although this may seem redundant at first glance, the precise sites for Dbp2 and Sub2-dependent assembly are not yet known. Moreover, Dbp2 and Sub2 exhibit vastly different duplex unwinding activities *in vitro* with Sub2 exhibiting very weak activity (Ma et al. 2013; Putnam and Jankowsky 2013a). Thus, Dbp2 may be specifically recruited to RNA structures for mRNP assembly whereas Sub2 may function as an ATP-dependent binding protein more similar to eIF4AIII within the exon junction complex (EJC) (Ballut et al. 2005; Barbosa et al. 2012). This suggests that Dbp2 and Sub2 perform distinct biochemical activities in gene expression which both influence co-transcriptional loading of Yra1. Consistent with this, Sub2 has been proposed to disassemble Yra1-Pcf11 complexes by promoting assembly of a Sub2-Yra1 complex on RNA (Johnson et al. 2011). Thus, is possible that Dbp2 functions at the interface of this process to ensure that the structure of the nascent RNA is amenable to assembly.

The mammalian ortholog of Dbp2, termed DDX5, is a well known oncogene whose product is involved in numerous processes requiring modulation of RNA structure including pre-mRNA splicing (Kar et al. 2011; Liu 2002; Guil et al. 2003) and rRNA

processing (Jalal et al. 2007). Interestingly, the mammalian counterpart of Yra1, Aly, also interacts with DDX5 (Zonta et al. 2013). This suggests that the inhibition mechanism for Dbp2 may be conserved in multicellular eukaryotes. Several drugs have been successfully developed to target the DEAD-box RNA helicase eIF4A, which alter the enzymatic activity of this enzyme by manipulating RNA-binding activity and/or ATP hydrolysis activity (Eberle et al. 1997; Shuda et al. 2000; Gao et al. 2007; Wen et al. 2007; Bordeleau et al. 2006, 2008, 2005; Low et al. 2005). Thus far, the eIF4A inhibitors Silvestrol and Paetamine A have proven useful therapeutic tools for uncontrolled cell growth (Bordeleau et al. 2005, 2008), suggesting that inhibition of individual DEAD-box enzymes is a successful strategy for cancer intervention. Thus, understanding the mechanisms for enzymatic modulation of helicases *in vivo* is crucial for designing novel drug therapies.

5.5 References

Abruzzi KC, Lacadie S, Rosbash M. 2004. Biochemical analysis of TREX complex recruitment to intronless and intron-containing yeast genes. *EMBO J* **23**: 2620–2631.

Alcazar-Roman AR, Tran EJ, Guo S, Wente SR. 2006. Inositol hexakisphosphate and Gle1 activate the DEAD-box protein Dbp5 for nuclear mRNA export. *Nat Cell Biol* **8**: 711–716.

Andersen CB, Ballut L, Johansen JS, Chamieh H, Nielsen KH, Oliveira CL, Pedersen JS, Seraphin B, Le Hir H, Andersen GR. 2006. Structure of the exon junction core complex with a trapped DEAD-box ATPase bound to RNA. *Science (80-)* **313**: 1968–1972.

Anderson P, Kedersha N. 2009. RNA granules: post-transcriptional and epigenetic modulators of gene expression. *Nat Rev Mol Cell Biol* **10**: 430–436.

Aregger R, Klostermeier D. 2009. The DEAD box helicase YxiN maintains a closed conformation during ATP hydrolysis. *Biochemistry* **48**: 10679–10681.

Ballut L, Marchadier B, Baguet A, Tomasetto C, Seraphin B, Le Hir H. 2005. The exon junction core complex is locked onto RNA by inhibition of eIF4AIII ATPase activity. *Nat Struct Mol Biol* **12**: 861–869.

Barbosa I, Haque N, Fiorini F, Barrandon C, Tomasetto C, Blanchette M, Le Hir H. 2012. Human CWC22 escorts the helicase eIF4AIII to spliceosomes and promotes exon junction complex assembly. *Nat Struct Mol Biol* **19**: 983–990.

Beck ZT, Cloutier SC, Schipma MJ, Petell CJ, Ma WK, Tran EJ. 2014. Regulation of Glucose-Dependent Gene Expression by the RNA Helicase Dbp2 in Saccharomyces cerevisiae. *Genetics* **198**: 1001–14.

Bevilacqua A, Ceriani MC, Capaccioli S, Nicolin A. 2003. Post-transcriptional regulation of gene expression by degradation of messenger RNAs. *J Cell Physiol* **195**: 356–372.

Bordeleau ME, Cencic R, Lindqvist L, Oberer M, Northcote P, Wagner G, Pelletier J. 2006. RNA-mediated sequestration of the RNA helicase eIF4A by Pateamine A inhibits translation initiation. *Chem Biol* **13**: 1287–1295.

Bordeleau ME, Matthews J, Wojnar JM, Lindqvist L, Novac O, Jankowsky E, Sonenberg N, Northcote P, Teesdale-Spittle P, Pelletier J. 2005. Stimulation of mammalian translation initiation factor eIF4A activity by a small molecule inhibitor of eukaryotic translation. *Proc Natl Acad Sci U S A* **102**: 10460–10465.

Bordeleau ME, Robert F, Gerard B, Lindqvist L, Chen SM, Wendel HG, Brem B, Greger H, Lowe SW, Porco Jr. JA, et al. 2008. Therapeutic suppression of translation initiation modulates chemosensitivity in a mouse lymphoma model. *J Clin Invest* **118**: 2651–2660.

Brykailo MA, McLane LM, Fridovich-Keil J, Corbett AH. 2007. Analysis of a predicted nuclear localization signal: implications for the intracellular localization and function of the Saccharomyces cerevisiae RNA-binding protein Scp160. *Nucleic Acids Res* **35**: 6862–6869.

Cao W, Coman MM, Ding S, Henn A, Middleton ER, Bradley MJ, Rhoades E, Hackney DD, Pyle AM, De La Cruz EM. 2011. Mechanism of Mss116 ATPase reveals functional diversity of DEAD-Box proteins. *J Mol Biol* **409**: 399–414.

Chang JH, Cho YH, Sohn SY, Choi JM, Kim A, Kim YC, Jang SK, Cho Y. 2009. Crystal structure of the eIF4A-PDCD4 complex. *Proc Natl Acad Sci U S A* **106**: 3148–3153.

Chen CYA, Shyu A Bin. 2014. Emerging mechanisms of mRNP remodeling regulation. *Wiley Interdiscip Rev RNA* **5**: 713–22.

Cloutier SC, Ma WK, Nguyen LT, Tran EJ. 2012. The DEAD-box RNA helicase Dbp2 connects RNA quality control with repression of aberrant transcription. *J Biol Chem* **287**: 26155–26166.

Cmarik JL, Min H, Hegamyer G, Zhan S, Kulesz-Martin M, Yoshinaga H, Matsuhashi S, Colburn NH. 1999. Differentially expressed protein Pdcd4 inhibits tumor promoter-induced neoplastic transformation. *Proc Natl Acad Sci U S A* **96**: 14037–14042.

Coller J. 2008. Chapter 14 Methods to Determine mRNA Half-Life in Saccharomyces cerevisiae. *Methods Enzymol* **448**: 267–284.

Cramer P, Srebrow A, Kadener S, Werbajh S, de la Mata M, Melen G, Nogues G, Kornblihtt AR. 2001. Coordination between transcription and pre-mRNA processing. *FEBS Lett* **498**: 179–182.

Del Priore V, Snay CA, Bahr A, Cole CN. 1996. The product of the Saccharomyces cerevisiae RSS1 gene, identified as a high-copy suppressor of the rat7-1 temperature-sensitive allele of the RAT7/NUP159 nucleoporin, is required for efficient mRNA export. *Mol Biol Cell* **7**: 1601–1621.

Ding Y, Tang Y, Kwok CK, Zhang Y, Bevilacqua PC, Assmann SM. 2014. In vivo genome-wide profiling of RNA secondary structure reveals novel regulatory features. *Nature* **505**: 696–700.

Eberle J, Krasagakis K, Orfanos CE. 1997. Translation initiation factor eIF-4A1 mRNA is consistently overexpressed in human melanoma cells in vitro. *Int J Cancer* **71**: 396–401.

Gao F, Zhang P, Zhou C, Li J, Wang Q, Zhu F, Ma C, Sun W, Zhang L. 2007. Frequent loss of PDCD4 expression in human glioma: possible role in the tumorigenesis of glioma. *Oncol Rep* **17**: 123–128.

Geisberg J V., Moqtaderi Z, Fan X, Ozsolak F, Struhl K. 2014. Global analysis of mRNA isoform half-lives reveals stabilizing and destabilizing elements in yeast. *Cell* **156**: 812–824.

Gilbert C, Svejstrup JQ. 2006. RNA immunoprecipitation for determining RNA-protein associations in vivo. *Curr Protoc Mol Biol* **Chapter 27**: Unit 27 4.

Gorsch LC, Dockendorff TC, Cole CN. 1995. A conditional allele of the novel repeat-containing yeast nucleoporin RAT7/NUP159 causes both rapid cessation of mRNA export and reversible clustering of nuclear pore complexes. *J Cell Biol* **129**: 939–955.

Gosai SJ, Foley SW, Wang D, Silverman IM, Selamoglu N, Nelson ADL, Beilstein MA, Daldal F, Deal RB, Gregory BD. 2015. Global analysis of the RNA-protein interaction and RNA secondary structure landscapes of the Arabidopsis nucleus. *Mol Cell* **57**: 376–88.

Granneman S, Lin C, Champion EA, Nandineni MR, Zorca C, Baserga SJ. 2006. The nucleolar protein Esf2 interacts directly with the DExD/H box RNA helicase, Dbp8, to stimulate ATP hydrolysis. *Nucleic Acids Res* **34**: 3189–3199.

Guil S, Gattoni R, Carrascal M, Abian J, Stevenin J, Bach-Elias M. 2003. Roles of hnRNP A1, SR proteins, and p68 helicase in c-H-ras alternative splicing regulation. *Mol Cell Biol* **23**: 2927–2941.

Hasegawa M, Smith MJ, Iijima M, Tabira T, Goedert M. 1999. FTDP-17 mutations N279K and S305N in tau produce increased splicing of exon 10. *FEBS Lett* **443**: 93–96.

Henn A, Cao W, Hackney DD, De La Cruz EM. 2008. The ATPase cycle mechanism of the DEAD-box rRNA helicase, DbpA. *J Mol Biol* **377**: 193–205.

Henn A, Cao W, Licciardello N, Heitkamp SE, Hackney DD, De La Cruz EM. 2010. Pathway of ATP utilization and duplex rRNA unwinding by the DEAD-box helicase, DbpA. *Proc Natl Acad Sci U S A* **107**: 4046–4050.

Herschlag D. 1995. RNA chaperones and the RNA folding problem. *J Biol Chem* **270**: 20871–20874.

Hilbert M, Kebbel F, Gubaev A, Klostermeier D. 2011. eIF4G stimulates the activity of the DEAD box protein eIF4A by a conformational guidance mechanism. *Nucleic Acids Res* **39**: 2260–2270.

Hutton M, Lendon CL, Rizzu P, Baker M, Froelich S, Houlden H, Pickering-Brown S, Chakraverty S, Isaacs A, Grover A, et al. 1998. Association of missense and 5'-splice-site mutations in tau with the inherited dementia FTDP-17. *Nature* **393**: 702–705.

Iglesias N, Tutucci E, Gwizdek C, Vinciguerra P, Von Dach E, Corbett AH, Dargemont C, Stutz F. 2010. Ubiquitin-mediated mRNP dynamics and surveillance prior to budding yeast mRNA export. *Genes Dev* **24**: 1927–1938.

Jalal C, Uhlmann-Schiffler H, Stahl H. 2007. Redundant role of DEAD box proteins p68 (Ddx5) and p72/p82 (Ddx17) in ribosome biogenesis and cell proliferation. *Nucleic Acids Res* **35**: 3590–3601.

Jansen AP, Camalier CE, Colburn NH. 2005. Epidermal expression of the translation inhibitor programmed cell death 4 suppresses tumorigenesis. *Cancer Res* **65**: 6034–6041.

Jarmoskaite I, Russell R. 2014. RNA helicase proteins as chaperones and remodelers. *Annu Rev Biochem* **83**: 697–725.

Johnson SA, Cubberley G, Bentley DL. 2009. Cotranscriptional recruitment of the mRNA export factor Yra1 by direct interaction with the 3' end processing factor Pcf11. *Mol Cell* **33**: 215–226.

Johnson SA, Kim H, Erickson B, Bentley DL. 2011. The export factor Yra1 modulates mRNA 3' end processing. *Nat Struct Mol Biol* **18**: 1164–1171.

Kar A, Fushimi K, Zhou X, Ray P, Shi C, Chen X, Liu Z, Chen S, Wu JY. 2011. RNA helicase p68 (DDX5) regulates tau exon 10 splicing by modulating a stem-loop structure at the 5' splice site. *Mol Cell Biol* **31**: 1812–1821.

Krebber H, Taura T, Lee MS, Silver PA. 1999. Uncoupling of the hnRNP Npl3p from mRNAs during the stress-induced block in mRNA export. *Genes Dev* **13**: 1994–2004.

Lamichhane R, Solem A, Black W, Rueda D. 2010. Single-molecule FRET of protein-nucleic acid and protein-protein complexes: Surface passivation and immobilization. *Methods* **52**: 192–200.

Laurent FX, Sureau A, Klein AF, Trouslard F, Gasnier E, Furling D, Marie J. 2012. New function for the RNA helicase p68/DDX5 as a modifier of MBNL1 activity on expanded CUG repeats. *Nucleic Acids Res* **40**: 3159–3171.

Linder P, Fuller-Pace F V. 2013. Looking back on the birth of DEAD-box RNA helicases. *Biochim Biophys Acta - Gene Regul Mech* **1829**: 750–755.

Liu F, Putnam AA, Jankowsky E. 2014. DEAD-box helicases form nucleotide-dependent, long-lived complexes with RNA. *Biochemistry* **53**: 423–433.

Liu ZR. 2002. p68 RNA helicase is an essential human splicing factor that acts at the U1 snRNA-5' splice site duplex. *Mol Cell Biol* **22**: 5443–5450.

Loh PG, Yang HS, Walsh MA, Wang Q, Wang X, Cheng Z, Liu D, Song H. 2009. Structural basis for translational inhibition by the tumour suppressor Pdcd4. *EMBO J* **28**: 274–285.

Low WK, Dang Y, Schneider-Poetsch T, Shi Z, Choi NS, Merrick WC, Romo D, Liu JO. 2005. Inhibition of eukaryotic translation initiation by the marine natural product pateamine A. *Mol Cell* **20**: 709–722.

Luo ML, Zhou Z, Magni K, Christoforides C, Rappsilber J, Mann M, Reed R. 2001. Pre-mRNA splicing and mRNA export linked by direct interactions between UAP56 and Aly. *Nature* **413**: 644–647.

Ma WK, Cloutier SC, Tran EJ. 2013. The DEAD-box protein Dbp2 functions with the RNA-binding protein Yra1 to promote mRNP assembly. *J Mol Biol* **425**: 3824–3838.

Maeder C, Kutach AK, Guthrie C. 2009. ATP-dependent unwinding of U4/U6 snRNAs by the Brr2 helicase requires the C terminus of Prp8. *Nat Struct Mol Biol* **16**: 42–48.

Mozaffari-Jovin S, Santos KF, Hsiao HH, Will CL, Urlaub H, Wahl MC, Lührmann R. 2012. The Prp8 RNase H-like domain inhibits Brr2-mediated U4/U6 snRNA unwinding by blocking Brr2 loading onto the U4 snRNA. *Genes Dev* **26**: 2422–2434.

Mozaffari-Jovin S, Wandersleben T, Santos KF, Will CL, Lührmann R, Wahl MC. 2013. Inhibition of RNA helicase Brr2 by the C-terminal tail of the spliceosomal protein Prp8. *Science* **341**: 80–4.

Mundigala H, Michaux JB, Feig AL, Ennifar E, Rueda D. 2014. HIV-1 DIS stem loop forms an obligatory bent kissing intermediate in the dimerization pathway. *Nucleic Acids Res* **42**: 7281–7289.

Nielsen KH, Chamieh H, Andersen CB, Fredslund F, Hamborg K, Le Hir H, Andersen GR. 2009. Mechanism of ATP turnover inhibition in the EJC. *RNA* **15**: 67–75.

Pan C, Russell R. 2010. Roles of DEAD-box proteins in RNA and RNP Folding. *RNA Biol* **7**: 667–676.

Pena V, Jovin SM, Fabrizio P, Orlowski J, Bujnicki JM, Lührmann R, Wahl MC. 2009. Common Design Principles in the Spliceosomal RNA Helicase Brr2 and in the Hel308 DNA Helicase. *Mol Cell* **35**: 454–466.

Putnam AA, Gao Z, Liu F, Jia H, Yang Q, Jankowsky E. 2015. Division of Labor in an Oligomer of the DEAD-Box RNA Helicase Ded1p. *Mol Cell* **59**: 541–52.

Putnam AA, Jankowsky E. 2013a. AMP sensing by DEAD-box RNA helicases. *J Mol Biol* **425**: 3839–3845.

Putnam AA, Jankowsky E. 2013b. DEAD-box helicases as integrators of RNA, nucleotide and protein binding. *Biochim Biophys Acta* **1829**: 884–893.

Ramos SB V, Laederach A. 2014. Molecular biology: A second layer of information in {RNA}. *Nature* **505**: 621–622.

Rogers Jr. GW, Richter NJ, Lima WF, Merrick WC. 2001. Modulation of the helicase activity of eIF4A by eIF4B, eIF4H, and eIF4F. *J Biol Chem* **276**: 30914–30922.

Rogers Jr. GW, Richter NJ, Merrick WC. 1999. Biochemical and kinetic characterization of the RNA helicase activity of eukaryotic initiation factor 4A. *J Biol Chem* **274**: 12236–12244.

Rouskin S, Zubradt M, Washietl S, Kellis M, Weissman JS. 2014. Genome-wide probing of RNA structure reveals active unfolding of mRNA structures in vivo. *Nature* **505**: 701–705.

Rozen F, Edery I, Meerovitch K, Dever TE, Merrick WC, Sonenberg N. 1990. Bidirectional RNA helicase activity of eucaryotic translation initiation factors 4A and 4F. *Mol Cell Biol* **10**: 1134–1144.

Rudolph MG, Klostermeier D. 2015. When core competence is not enough: functional interplay of the DEAD-box helicase core with ancillary domains and auxiliary factors in RNA binding and unwinding. *Biol Chem* **396**: 849–65.

Schutz P, Bumann M, Oberholzer AE, Bieniossek C, Trachsel H, Altmann M, Baumann U. 2008. Crystal structure of the yeast eIF4A-eIF4G complex: an RNA-helicase controlled by protein-protein interactions. *Proc Natl Acad Sci U S A* **105**: 9564–9569.

Sengoku T, Nureki O, Nakamura A, Kobayashi S, Yokoyama S. 2006. Structural Basis for RNA Unwinding by the DEAD-Box Protein Drosophila Vasa. *Cell* **125**: 287–300.

Shuda M, Kondoh N, Tanaka K, Ryo A, Wakatsuki T, Hada A, Goseki N, Igari T, Hatsuse K, Aihara T, et al. 2000. Enhanced expression of translation factor mRNAs in hepatocellular carcinoma. *Anticancer Res* **20**: 2489–2494.

Strasser K, Hurt E. 2000. Yra1p, a conserved nuclear RNA-binding protein, interacts directly with Mex67p and is required for mRNA export. *EMBO J* **19**: 410–420.

Stutz F, Bachi A, Doerks T, Braun IC, Seraphin B, Wilm M, Bork P, Izaurralde E. 2000. REF, an evolutionary conserved family of hnRNP-like proteins, interacts with TAP/Mex67p and participates in mRNA nuclear export. *RNA* **6**: 638–650.

Taniguchi I, Ohno M. 2008. ATP-dependent recruitment of export factor Aly/REF onto intronless mRNAs by RNA helicase UAP56. *Mol Cell Biol* **28**: 601–608.

Tran EJ, Zhou Y, Corbett AH, Wente SR. 2007. The DEAD-box protein Dbp5 controls mRNA export by triggering specific RNA:protein remodeling events. *Mol Cell* **28**: 850–859.

Tsu CA, Kossen K, Uhlenbeck OC. 2001. The Escherichia coli DEAD protein DbpA recognizes a small RNA hairpin in 23S rRNA. *RNA* **7**: 702–709.

Umate P, Tuteja N, Tuteja R. 2011. Genome-wide comprehensive analysis of human helicases. *Commun Integr Biol* **4**: 1–20.

Wan Y, Qu K, Zhang QC, Flynn R a, Manor O, Ouyang Z, Zhang J, Spitale RC, Snyder MP, Segal E, et al. 2014. Landscape and variation of RNA secondary structure across the human transcriptome. *Nature* **505**: 706–9.

Wen YH, Shi X, Chiriboga L, Matsahashi S, Yee H, Afonja O. 2007. Alterations in the expression of PDCD4 in ductal carcinoma of the breast. *Oncol Rep* **18**: 1387–1393.

Wood S, Ferré-D'Amaré AR, Rueda D. 2012. Allosteric tertiary interactions preorganize the c-di-GMP riboswitch and accelerate ligand binding. *ACS Chem Biol* **7**: 920–927.

Yang HS, Jansen AP, Komar AA, Zheng X, Merrick WC, Costes S, Lockett SJ, Sonenberg N, Colburn NH. 2003. The transformation suppressor Pdcd4 is a novel eukaryotic translation initiation factor 4A binding protein that inhibits translation. *Mol Cell Biol* **23**: 26–37.

Yang Q, Jankowsky E. 2005. ATP- and ADP-dependent modulation of RNA unwinding and strand annealing activities by the DEAD-box protein DED1. *Biochemistry* **44**: 13591–13601.

Young CL, Khoshnevis S, Karbstein K. 2013. Cofactor-dependent specificity of a DEAD-box protein. *Proc Natl Acad Sci U S A* **110**: E2668–76.

Zenklusen D, Vinciguerra P, Strahm Y, Stutz F. 2001. The yeast hnRNP-Like proteins Yra1p and Yra2p participate in mRNA export through interaction with Mex67p. *Mol Cell Biol* **21**: 4219–4232.

Zonta E, Bittencourt D, Samaan S, Germann S, Dutertre M, Auboeuf D. 2013. The RNA helicase DDX5/p68 is a key factor promoting c-fos expression at different levels from transcription to mRNA export. *Nucleic Acids Res* **41**: 554–564.

Zorio DA, Bentley DL. 2004. The link between mRNA processing and transcription: communication works both ways. *Exp Cell Res* **296**: 91–97.

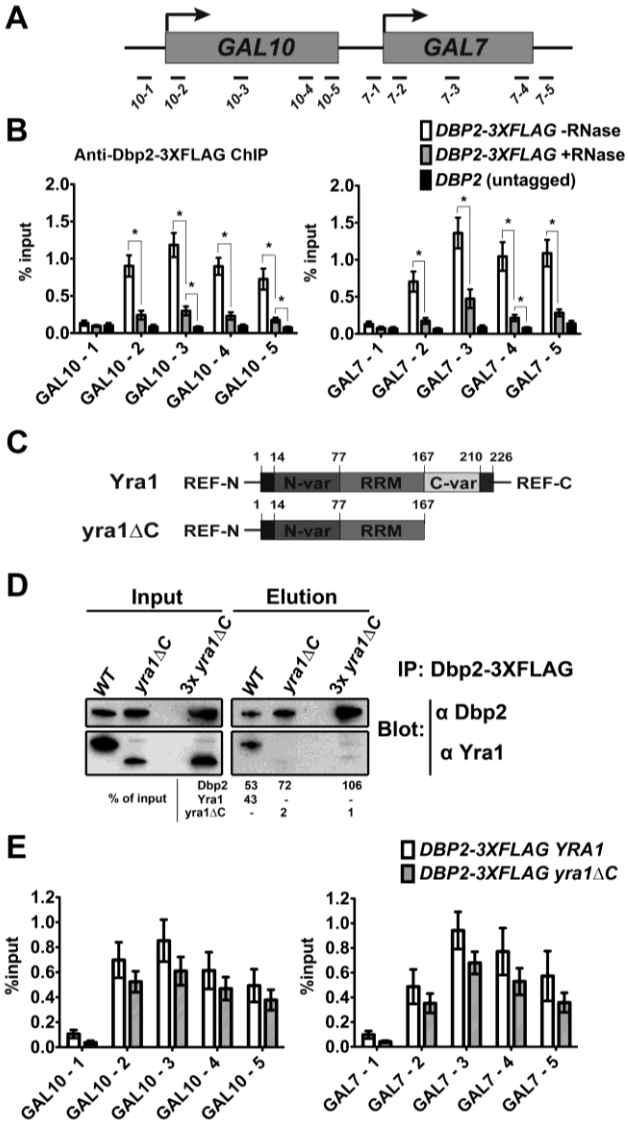

Figure 5.1. Dbp2 is recruited to chromatin via RNA. *(A) Schematic diagram of the GAL10 and GAL7 genes and the positions of qPCR amplicons*. *(B) Dbp2 is recruited to chromatin in an RNA-dependent manner*. Transcription of the *GAL* genes was induced by growing yeast cells in rich media plus glucose initially and subsequently shifting to media with galactose for 5 hours. Chromatin was then isolated, sheared by sonication, and incubated with 7.5 U RNase A and 300 U RNase I or buffer alone before being subjected to ChIP using anti-FLAG antibodies. Results are presented as the percent of precipitated DNA over input averaged across four biological replicates with SEM. Student t-test was performed between RNase untreated and treated samples or RNase treated samples and *DBP2* untagged strains in all primer sets. * indicate the difference between samples is statistically significant with a p-value < 0.05. *(C) Schematic diagram of the primary sequence and functional motifs of Yra1*(Zenklusen et al. 2001; Stutz et al. 2000; Strasser and Hurt 2000; Johnson et al. 2009). The C-terminal half of Yra1 is sufficient to interact with Dbp2 *in vitro* (Ma et al. 2013). *(D) Dbp2 interacts with the C-*

terminal half of Yra1 in vivo. Immunoprecipitation assays were conducted using anti-FLAG antibodies to isolate Dbp2-3xFLAG and associated proteins from wild type or *yra1ΔC* lysate. 10% of the lysate was used as input. Dbp2 and Yra1 were detected by Western blotting with protein-specific antibodies. Dbp2, Yra1 and yra1ΔC from elution were quantified by densitometry with respect to input. *(E) Loss of the C-terminal half of Yra1 does not affect the association of Dbp2 with the actively transcribing GAL10 (left) or GAL7 (right) gene.* WT and *yra1ΔC* strains were used for ChIP with anti-FLAG antibody against Dbp2-3xFLAG. Student t-test was performed between full-length *YRA1* and *yra1ΔC* strains in all primer sets. All the p-values > 0.05.

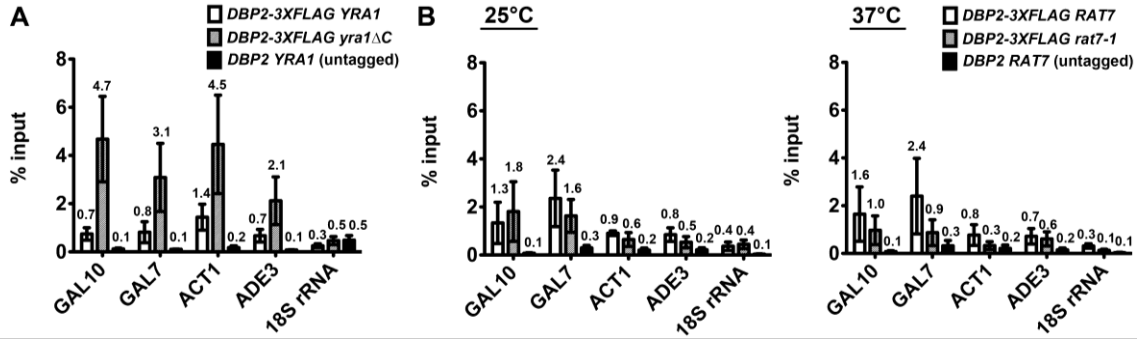

Figure 5.2. Yra1 prevents over-accumulation of Dbp2 on RNA Pol II transcripts. *(A) Dbp2 accumulates on the RNA Pol II transcripts in a yra1ΔC strain.* RNA immunoprecipitation (RIP) assays were performed to determine the level of RNA associated with Dbp2 in wild type and isogenic *yra1ΔC* cells. Cells were grown with galactose to promote expression of *GAL10* and *GAL7* genes as in Fig. 5.1 and subsequently cross-linked with formaldehyde. RNPs were isolated with anti-FLAG antibodies and transcripts were detected by RT-qPCR with primers specific to the 5' end of each mRNA (see Table 5.4). Dbp2-3xFLAG occupancy on specific transcripts is shown as the average percent of isolated RNA over input for three biological replicates. Error bars indicate the SEM. *(B) The association of Dbp2 with RNA Pol II transcripts is not altered in the mRNA export mutant strain, rat7-1*. RIP assays were performed as above with wild type cells, isogenic *rat7-1* cells (Brykailo et al. 2007), or isogenic, wild type untagged cells at both the permissive temperature (25°C, left) and the non-permissive temperature (37°C, right) for *rat7-1* (Krebber et al. 1999; Gorsch et al. 1995; Del Priore et al. 1996).

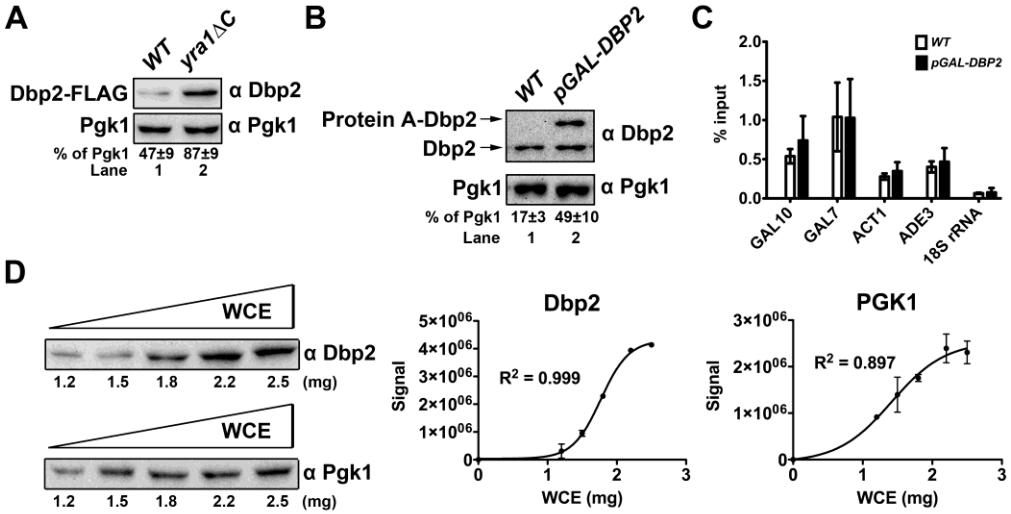

Figure 5.3. Overexpression of *DBP2* does not cause over-accumulation Dbp2 on RNA Pol II transcripts. *(A) Loss of the C-terminal half of Yra1 upregulates the protein level of DBP2-3xFLAG.* Western blotting was conducted with the indicated antibodies. Dbp2 was quantified by densitometry with respect to Pgk1. *(B) Western blotting shows that pGAL-DBP2 is expressed.* Western blotting was conducted with the indicated antibodies from strains expressing vector alone or pGAL-DBP2 as indicated. Signals from Dbp2 and Protein A-Dbp2 were combined and quantified by densitometry with respect to Pgk1. *(C) Overexpression of DBP2 does not affect the association of Dbp2 with transcripts.* RIP was performed as Fig. 5.2 with wild type strain with empty vector or with a plasmid encoding *DBP2* under the control of the galactose-inducible *pGAL* promoter. Strains were grown in selective media (-URA) + glucose followed by a 5 hour shift to galactose to induce overexpression of Dbp2. *(D) Anti-Dbp2 and anti-Pgk1 antibodies can semi-quantitatively determine the levels of Dbp2 and Pgk1, respectively, using Western blotting analysis.* The amount of whole cell extract (2 mg) that was used in the assays is within the linear range of detection for both Dbp2 and Pgk1 antibodies.

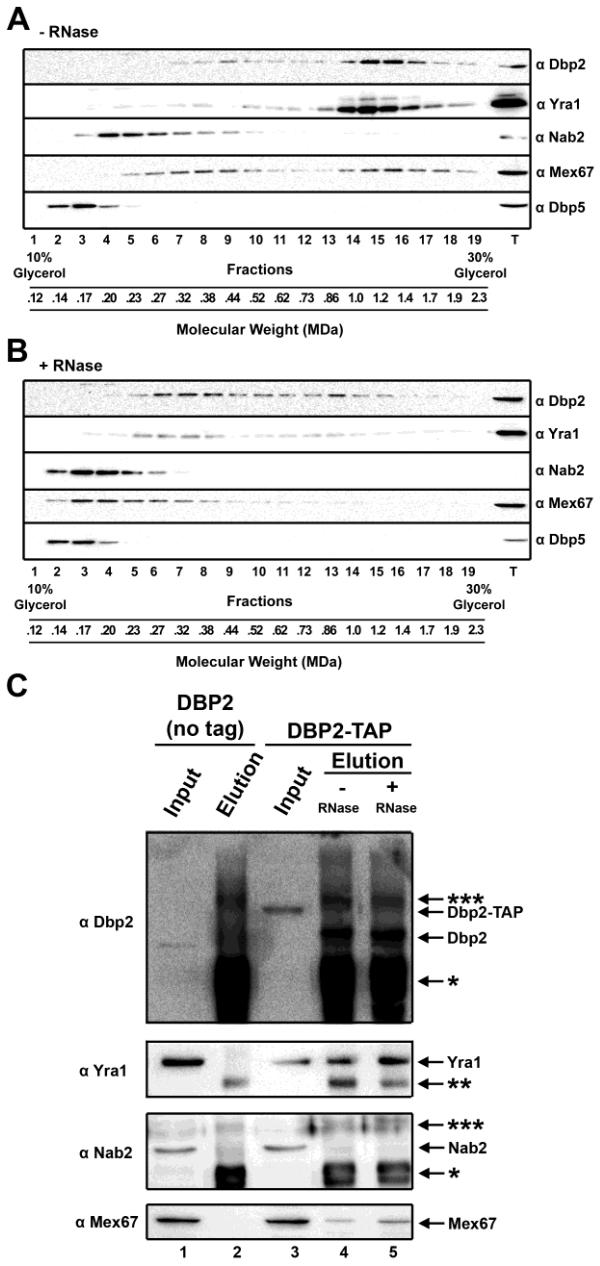

Figure 5.4. Dbp2 forms a large RNA-dependent complex with Yra1 and Mex67 *in vivo*. *(A) Dbp2, Yra1 and Mex67 co-migrate as a large complex by glycerol gradient fractionation.* Glycerol gradient (10 – 30%) were performed with yeast lysate and the isolated fractions were resolved by SDS-PAGE and proteins were detected by western blotting. Molecular weights were determined using a standard curve that was generated by resolving the molecular weight standards comprising catalase (250 kDa), apoferritin (480 kDa), and thyroglobulin (670 kDa). *(B) RNase treatment of yeast lysate prior to gradient fractionation disrupts formation of the large Dbp2-Yra1-Mex67 complex.* Glycerol gradient (10 – 30%) were performed as above but with 70 U of RNase A and 1000 U of RNase I. *(C) RNase treatment does not alter the Dbp2-Yra1-Mex67*

interaction. TAP-tag immunoprecipitation assays of Dbp2 were conducted in the presence or absence of 70 U of RNase A and 1000 U of RNase I. Input (1%) and elutions were resolved by SDS-PAGE and proteins were detected by western blotting. * indicative of heavy chains from antibody. ** indicative of light chains from antibody. *** indicative of a non-specific band.

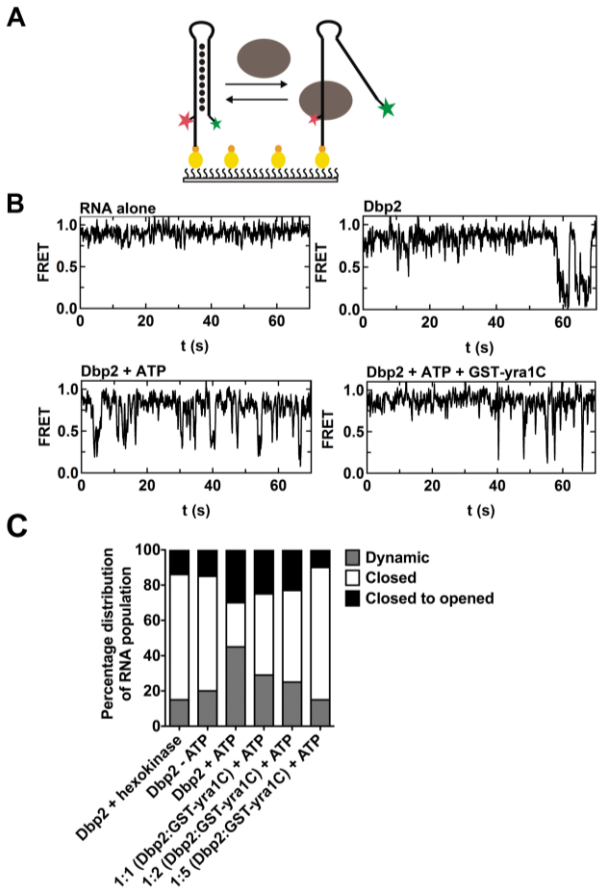

Figure 5.5. Yra1 decreases the unwinding rate and specific activity of Dbp2 in smFRET studies. *(A) Schematic representation of smFRET with a dual labeled hairpin RNA.* Dual labeled RNA (Cy3 and Cy5) was purchased from IDT and subsequently surface-immobilized on a pegylated microscope quartz slide via biotin-neutravidin bridge (Lamichhane et al. 2010). The oval represents Dbp2. The red star represents Cy5 and the green star represents Cy3. *(B) Representative FRET trajectory in the smFRET experiments.* Representative trajectories of a closed RNA hairpin alone (top left), in the presence of 10 nM Dbp2 (top right),10 nM Dbp2 and 100 μM ATP (bottom left), or in the presence of 10 nM Dbp2, 20 nM yra1C, and 100 μM ATP (bottom right) are shown. Numerous (~100) trajectories were used to build the dwell time histograms to determine the opening and closing rate constant. *(C) Yra1 decreases the number of hairpin dsRNAs unwound by Dbp2.* The distribution of closed, closed to opened (single opening events), or dynamic (multiple cycles of opening and closing) hairpin dsRNAs with 10 nM Dbp2 with or without 100 μM hexokinase and 1 mM glucose in the absence of ATP or 10 nM Dbp2 with increasing concentrations of GST-yra1C in the presence of ATP are shown. Trajectories exhibiting more than one excursion into 0.2 – 0.8 FRET are considered dynamic molecules. Trajectories exhibiting constant 0.9 or 0.1 FRET throughout the experimental time window are classified as statically closed or opened molecules, respectively.

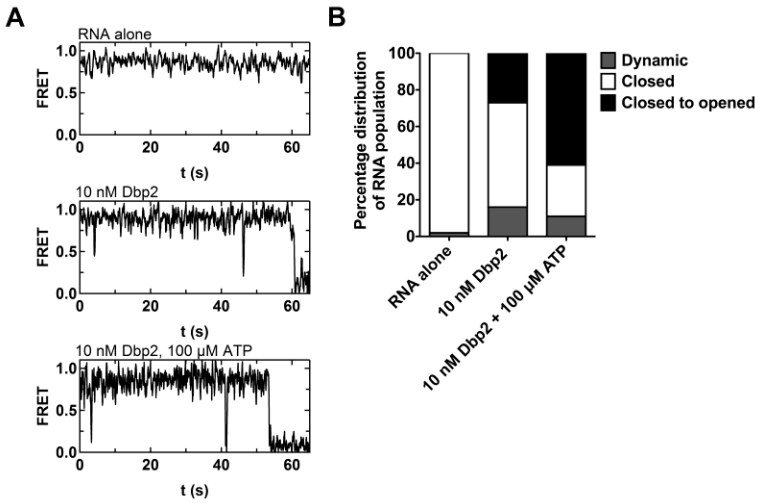

Figure 5.6. smFRET in 30 mM NaCl. *(A) Representative FRET trajectory of the smFRET experiment in 30 mM NaCl.* FRET trajectory of a closed RNA hairpin in the absence of any protein and ATP (top), in the presence of 10 nM Dbp2 (middle), or in the presence of 10 nM Dbp2 100 μM ATP (bottom). *(B) The hairpin dsRNAs show low dynamic in low salt (30 mM NaCl).* The distribution of closed, closed to opened (single opening events), or dynamic (multiple cycles of opening and closing) hairpin dsRNAs populations obtained from smFRET studies in 30 mM NaCl are shown. The molecules show very low dynamic behavior (multiple cycles).

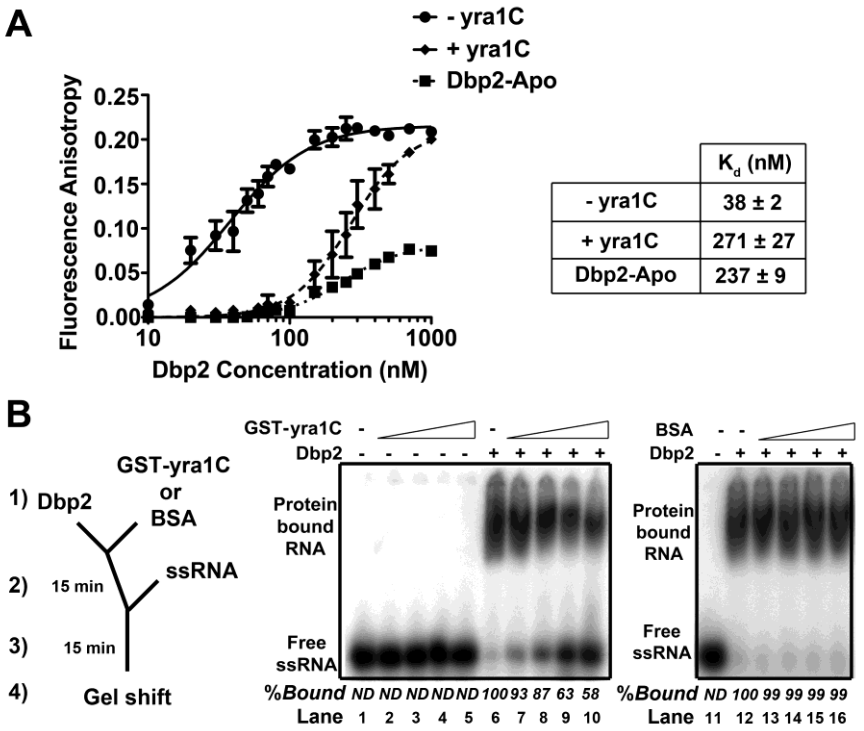

Figure 5.7. Yra1 reduces binding of Dbp2 onto ssRNA *in vitro*. *(A) Yra1 decreases the ssRNA-binding affinity of Dbp2.* Fluorescence anisotropy assays were conducted with varying amounts of Dbp2 and 10 nM of fluorescently labeled ssRNA in the presence or absence of 2 mM ADP-BeF_x under equilibrium condition. In the presence of 2 mM ADP-BeF_x, increasing amounts of Dbp2 and 10 nM labeled ssRNA were incubated with or without 150 nM of yra1C. Three technical replicated were conducted in this experiment. Error bars indicate the SEM. *(B) Yra1 decreases the association of Dbp2 with ssRNA.* Gel shift assays were conducted in the presence of 2 mM ADP-BeF_X/$MgCl_2$, 10 nM of 5'-radioactively labeled ssRNA (16 nt), with or without the Dbp2 (400 nM) and varying amounts of GST-yra1C or BSA (0 nM, 300 nM, 600 nM, 1200 nM, and 1800 nM). Complexes were assembled at 4°C as indicated in the schematic diagram followed by resolution on a 4% native PAGE and subsequent autoradiography. ND indicates the protein-bound signal was not detected.

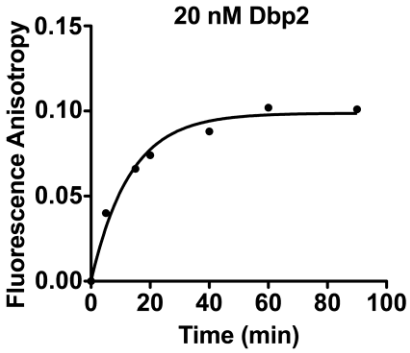

Figure 5.8. Dbp2 reaches equilibrium binding with ssRNA within 100 min. Fluorescence anisotropy assays were conducted by incubating 20 nM of Dbp2 with 10 nM of fluorescently labeled ssRNA in the presence of 2 mM ADP-BeF_x. A time course was performed to determine the time that requires for Dbp2 to reach equilibrium binding with ssRNA.

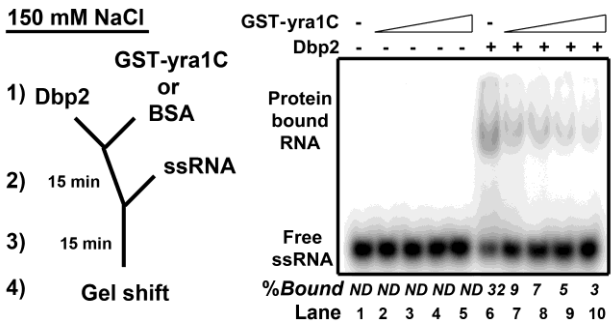

Figure 5.9. ***Yra1 reduces the affinity of Dbp2 for ssRNA at 150 mM NaCl.*** RNA-protein complexes were assembled as in Fig. 5.7B but in the presence of 150 mM NaCl.

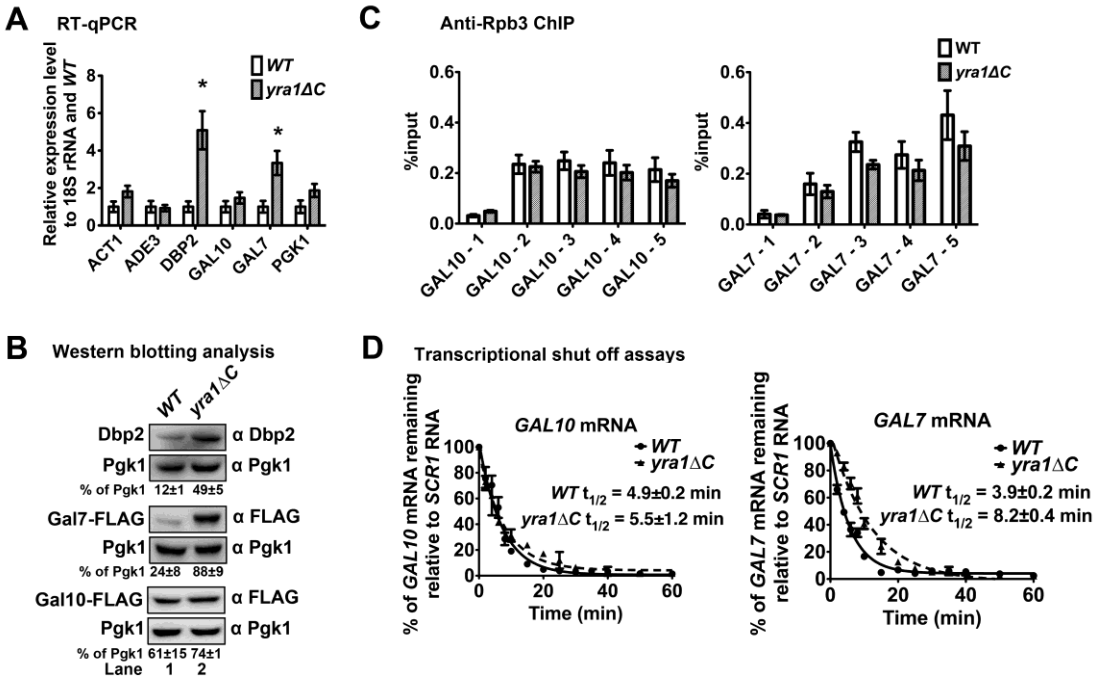

Figure 5.10. Inhibition of Dbp2 by Yra1 prevents overexpression of specific of gene products *in vivo.* *(A) Loss of the Dbp2-Yra1 interaction results in upregulation of the GAL7 and DBP2 transcript.* RT-qPCR was performed with transcripts that were extracted from wild type cells and isogenic *yra1ΔC* cells. Transcription of the *GAL* genes was induced by growing cells with galactose. Transcript levels were normalized to 18S rRNA and wild type cells. Error bars indicate the SEM from three biological replicates and * indicates a p-value <0.05 from a two tailed student t-test. *(B) Loss of the Dbp2-Yra1 interaction increases the protein levels of Gal7 and Dbp2.* C-terminally 3X-FLAG-tagged *GAL10* and *GAL7* strains were constructed in the *yra1ΔC* strain by standard yeast methods to provide an epitope for western blotting. Protein detection by western blotting was conducted using anti-Dbp2 (Beck et al. 2014) or anti-FLAG as indicated. Quantification of the protein signal is done by ImageQuant. Error indicates the SEM from three biological replicates. *(C) RNA Pol II exhibits a similar pattern of gene occupancy in both wild type and yra1ΔC strains.* ChIP was performed as above, but with anti-Rpb3 antibodies, a subunit of RNA Pol II. *(D) The GAL7 mRNA has a longer half-life in yra1ΔC strains than wild type cells.* Transcriptional shut off assays were performed by shifting indicated strains to glucose to repress transcription of *GAL* genes after a 10 hours induction with galactose. RNA was extracted at the indicated time points and transcripts were detected by Northern blotting. Transcripts were quantified by densitometry and normalized to scR1. Half-lives were calculated from three, independent biological replicates by fitting the data to an exponential decay equation.

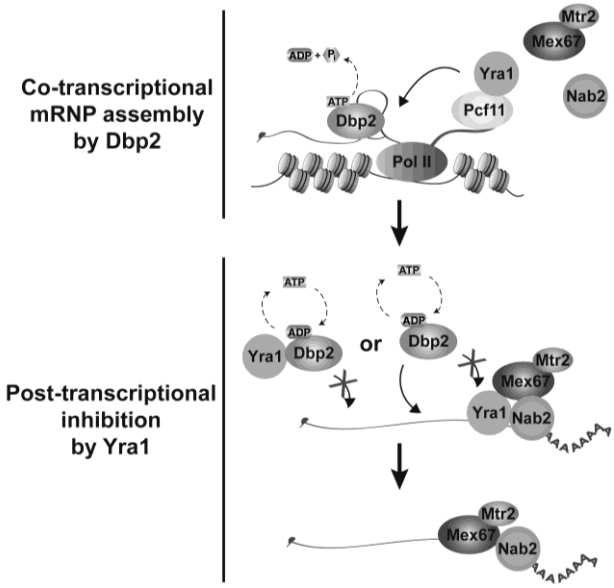

Figure 5.11. Enzymatic inhibition of Dbp2 by Yra1 restricts cycles of Dbp2-dependent mRNP remodeling *in vivo*. Dbp2 is co-transcriptionally recruited to chromatin through RNA to resolve RNA duplexes. This resolution allows co-transcriptional loading of RNA-binding proteins Yra1 and Mex67 onto the nascent RNA. Dbp2 then guides Yra1 and Mex67 to assemble onto the RNA at site where it is structure-free . After nucleotide exchange, Yra1 prevents post-transcriptional re-association by reducing the single-stranded RNA binding affinity of Dbp2. This activity likely prevents Dbp2 from accumulating on mRNA, which results in aberrant transcript stabilization and overexpression of specific gene products.

Table 5.1. Yeast and bacterial plasmids

Name	Description	Source/Reference
BTP22	pMAL-TEV-Dbp2	(Ma et al. 2013)
BTP27	GST-TEV-Yra1	(Ma et al. 2013)
GST-Yra1C	pET21GST-Yra1C (124-226)	(Johnson et al. 2009)
BTP2	pET28a-Sub2 (HIS-Sub2)	This study
HA-Yra1	YCpLac22-HA-Yra1 (pTRP-HA-Yra1)	(Zenklusen et al. 2001)
HA-Yra1 1-167	YCpLac22-HA-Yra1 1-167 (pTRP-HA-Yra1 1-167)	(Zenklusen et al. 2001)
pTRP	pRS314	(Sikorski and Hieter 1989)
pURA3	pRS316	(Sikorski and Hieter 1989)
pGAL-DBP2	pGAL-DBP2/2μ/URA3	Open Biosystems

Table 5.2. Yeast strains

Strain	Genotype	Source/Reference
yra1Δ pHA-YRA1	*MATa ade2 his3 leu2 trp1 ura3 yra1::HIS3 <pTRP-HA-Yra1>*	(Zenklusen et al. 2001)
yra1Δ pHA-yra1ΔC	*MATa ade2 his3 leu2 trp1 ura3 yra1::HIS3 <pTRP-HA-Yra1 1-167>*	(Zenklusen et al. 2001)
DBP2-3xFLAG (BTY247)	*MATα ade2-1 his3-11,15 ura3-1 leu2-1 trp1-1 can1-100 DBP2-3xFLAG:KanR*	This study
DBP2-3xFLAG yra1Δ pHA-YRA1 (BTY351)	*MATa ade2 his3 leu2 trp1 ura3 yra1::HIS3 <pTRP-HA-Yra1> DBP2-3xFLAG:KanR*	This study
DBP2-3xFLAG yra1Δ pHA-yra1ΔC (BTY339)	*MATa ade2 his3 leu2 trp1 ura3 yra1::HIS3 <pTRP-HA-yra1 1-167> DBP2-3xFLAG:KanR*	This study
Wild type (BY4742)	*MATα hisΔ1 leu2Δ0 ura3Δ0 lys2Δ0*	Open biosystems
DBP2-3xFLAG BY4742 (BTY376)	*MATα hisΔ1 leu2Δ0 ura3Δ0 lys2Δ0 DBP2-3xFLAG:KanR*	This study
DBP2-3xFLAG rat7-1 (BTY377)	*MATα his3 ura3 leu2 rat7-1 DBP2-3xFLAG:KanR*	This study
GAL10-3xFLAG yra1Δ	*MATa ade2 his3 leu2 trp1 ura3*	This study

pHA-YRA1 (BTY412)	*yra1::HIS3 <pTRP-HA-Yra1> GAL10-3xFLAG:KanR*	
GAL10-3xFLAG yra1Δ pHA-yra1ΔC (BTY414)	*MATa ade2 his3 leu2 trp1 ura3 yra1::HIS3 <pTRP-HA-Yra1 1-167> GAL10-3xFLAG:KanR*	This study
GAL7-3xFLAG yra1Δ pHA-YRA1 (BTY413)	*MATa ade2 his3 leu2 trp1 ura3 yra1::HIS3 <pTRP-HA-Yra1> GAL7-3xFLAG:KanR*	This study
GAL7-3xFLAG yra1Δ pHA-yra1ΔC (BTY415)	*MATa ade2 his3 leu2 trp1 ura3 yra1::HIS3 <pTRP-HA-Yra1 1-167> GAL7-3xFLAG:KanR*	This study
Wild type (BY4741)	*MATa hisΔ1 leu2Δ0 met15Δ0 ura3Δ0*	Open biosystems
DBP2-TAP	*MATa DBP2::TAP:HIS3 hisΔ1 leu2Δ0 met15Δ0 ura3Δ0*	Open biosystems

Table 5.3. Primetime primers for ChIP

Name	Forward	Reverse	Probe
GAL10 – 1	CTTTATTGTTCGGAGCAGTGC	GCTCATTGCTATATTGAAGTACGG	CGGTGAAGACGAGGACGCACG
GAL10 – 2	TGGTGCTGGATACATTGGTTC	AGGGAATGTGATGCTTGGTC	TGACTGTGTTGTTGCTGATAACCTGTCG
GAL10 – 3	TGAAGGTTTGTGTCGTGAGTG	TCTGCCCGTAACTTTGTATGG	CTTGGGTTCCGGTAAAGGTTCTACAGTT
GAL10 – 4	ACTCTACAAAGCCAACGGTC	GAATCGGGATGAAAAGCCTTG	TCCACCACAAAACAACAATCAAACTGGG
GAL10 – 5	GGTTTTGCAATTGAGCCTGG	GCTGGCAAATCAGGAAAATCTG	AAACGGTGAAACTTACGGGTCCAAGA
GAL7 – 1	GCGCTCGGACAACTGTTG	TTTCCGACCTGCTTTTATATCTTTG	CCGTGATCCGAAGGACTGGCTATACA
GAL7 – 2	ATCATACAATGGAGCTGTGGG	CTAGCCATTCCCATAGACGTTAC	AAGCAGCCTCCTGTTGACCTAACC
GAL7 – 3	TGCGAAACTTCACTAGGGATG	CCAGAGAAGCAAGAGAAAATCATAAG	CAACCCATGGCTGTACCTTTGTTTTCA
GAL7 – 4	GCATTTCTACCCACCTTTACTGAG	CAGCTTGTTCCGAAGTTAAATCTC	AGGCTCACCTAACAATTCAAAACCAACC
GAL7 – 5	GGACCACTCTTACATAACTAGAATAGC	TTTTCTATTAACTGCCTGGTTTCTTT	TGTCACTCCGTTCAAGTCGACAACC

Table 5.4. RT-qPCR oligos

Name	Forward	Reverse
GAL10	GAGGTCTTGACCAAGCATCACA	TTCCAGACCTTTTCGGTCACA
GAL7	CCATTCCACAAATGAAACAATCA	GGAGAGATCGTCAGTCAATGCTT
ACT1	TGGATTCCGGTGATGGTGTT	TCAAAATGGCGTGAGGTAGAGA
ADE3	CCCGTGATATCGCATCATACTTAC	GGCCGATGGCAACGACTA
18S rRNA	CGAATCGCATGGCCTTGT	CGAAAGTTGATAGGGCAGAAATTT
PGK1	GTTTTGGAACACCACCCAAGA	TCACCGTTTGGTCTACCCAAGT

Table 5.5. The opening and closing rate constants of the RNA hairpin

	$k_{opening}$ (s^{-1})	$k_{closing}$ (s^{-1})
10 nM Dbp2	4.1 ± 0.2	3.3 ± 0.3
10 nM Dbp2 and 100 μM ATP	6.3 ± 0.5	5.9 ± 0.4
10 nM Dbp2, 20 nM GST-yra1C and 100 μM ATP	4.8 ± 0.4	5.5 ± 0.3

CHAPTER 6. SUMMARY AND PERSPECTIVE

6.1 Summary of Dbp2

DEAD-box proteins have been associated with different RNA processes in cells. However, the exact role of most DEAD-box proteins is not clear. Prior to the studies from our laboratory, the DEAD-box protein Dbp2 in *Saccharomyces cerevisiae* had only been demonstrated to function in ribosome biogenesis and NMD (Bond et al. 2001). In addition, ectopically expressed DDX5 rescues the slow growth defect of *DBP2* deleted cells (Barta and Iggo 1995). Over the past years, our laboratory has made a significant contribution in elucidating the function of Dbp2 and its regulation. We showed that Dbp2 is predominantly localized in the nucleus and nucleolus, which is consistent with functioning in ribosome biogenesis (Cloutier et al. 2012). However, we also demonstrated that loss of *DBP2* results in multiple transcriptional defects including accumulation of noncoding transcripts, cryptic transcription, termination defects, loss of lncRNA-dependent gene regulation and aberrant expression of glucose-dependent genes (Cloutier et al. 2012, 2013; Beck et al. 2014). Interestingly, Dbp2 changes its localization from the nucleus to the cytoplasm upon glucose depletion (Beck et al. 2014). This change in localization partially mimicks *DBP2* deleted strains (Beck et al. 2014). These observations suggest that Dbp2 is involved in metabolic gene regulation.

To characterize the precise role of Dbp2, we found that Dbp2 is recruited to actively transcribing chromatin in an RNA-dependent manner ((Cloutier et al. 2012); unpublished data). Furthermore, Dbp2 is an active RNA-dependent ATPase and RNA helicase that unwinds RNA duplexes and anneals RNA substrates *in vitro* (Cloutier et al. 2012; Ma et al. 2013). This suggests that Dbp2 acts as a RNA chaperone to remodel RNA structures co-transcriptionally. Given that DEAD-box proteins facilitates RNA structural rearrangement to promote RNP assembly (Gosai et al. 2015; Linder and Jankowsky 2011; Liu and Cheng 2015), Dbp2 could function as a RNA chaperone to facilitate RNP assembly. Consistent with this idea, Dbp2 is required to promote efficient mRNP assembly of the mRNA export proteins, Mex67, Nab2, and Yra1 onto poly(A) mRNA (Ma et al. 2013).

Yra1 is an evolutionarily conserved mRNA-binding protein that is recruited to chromatin co-transcriptionally through RNA and the 3' end processing/termination factor Pcf11 (Stutz et al. 2000; Lei et al. 2001; Abruzzi et al. 2004; Lei and Silver 2002; Johnson et al. 2009). Furthermore, Yra1 is a multifunctional protein that is involved in mRNA export, poly(A) site choice, and DNA replication (Zenklusen et al. 2001; Iglesias et al. 2010; Johnson et al. 2011; Swaminathan et al. 2007). Consistent with the role of Yra1 in poly(A) site choice, loss of *DBP2* decreases the assembly of Yra1 on RNA and results in transcription termination defects ((Ma et al. 2013; Cloutier et al. 2012); unpublished data). Thus, Dbp2 might function in transcription termination by facilitating assembly of Yra1 on RNA. Several studies have shown that Yra1 forms a complex with Dbp2 *in vivo* (Oeffinger et al. 2007; Kashyap et al. 2005). In addition, we showed that Yra1 physically interacts with Dbp2 and inhibits its unwinding activity (Ma et al. 2013).

To determine the inhibition mechanism, we showed that Yra1 decreases the RNA binding affinity of Dbp2 (unpublished data). Interestingly, the inhibition does not decrease the ATPase activity of Dbp2 (Ma et al. 2013), suggesting that Yra1 utilizes a distinct inhibition mechanism from the Pdcd4-dependent inhibition of eIF4A (Chang et al. 2009; Loh et al. 2009). Future studies are needed to reveal the precise molecular mechanism of Yra1-dependent inhibition of Dbp2.

To elucidate the biological significance of the Yra1-dependent inhibition of Dbp2, our laboratory found that loss of the C-terminal half of Yra1 abolishes the interaction with Dbp2 and accumulates Dbp2 on Pol II transcripts (unpublished data). This is consistent with the fact that Yra1 inhibits the RNA binding affinity of Dbp2. Furthermore, the over-accumulation of Dbp2 leads to aberrant stabilization of certain transcripts (unpublished data). Taken together, our results suggest that Dbp2 is an active RNA helicase that associates nascent RNA to promote RNA structural rearrangements and assembly of RNA-binding proteins, including Yra1, Nab2, and Mex67, during transcription. Yra1 then inhibits Dbp2 to associate with ssRNA to prevent further cycles of unwinding. This regulation is critical for efficient mRNP assembly and proper gene expression. These findings shed lights on how DEAD-box proteins are regulated and provide insights on the role of the human ortholog of Dbp2, DDX5, which is often overexpressed in cancer cells

6.2 Unpublished results and future directions

6.2.1 Determine if Dbp2 is required for transcription termination

Over the past several years, we have started to gain some insights on the precise role of Dbp2 in gene expression. There are many more questions to be addressed in the future. Previously, we demonstrated that Dbp2 is required to promote efficient assembly of Yra1 onto mRNA and loss of *DBP2* results in transcription read through defects (Cloutier et al. 2012; Ma et al. 2013). Furthermore, Yra1 plays a role in mRNA 3' end processing (Johnson et al. 2011). These observations suggest that Dbp2 facilitates Yra1 to assemble onto RNA to promote proper transcription termination. To test if Dbp2 is required for proper transcription termination, we utilized a termination reporter assay. The termination reporter is composed of an intron-containing *ACT1* gene fused with *CUP1* gene and the poly(A)+ termination site of either the protein-coding *CYC1* gene or the non-coding *SNR13* gene were inserted into the intron (Fig. 6.1A). If the strain exhibits a termination defect, *CUP1* gene will be expressed. In contrast, *CUP1* gene will not be transcribed if the strain exhibits normal termination. *CUP1* is a gene that encodes metallothionein that binds copper and provides resistance for cells to grow in high concentration of copper (Winge et al. 1985). To conduct this assay, the two termination reporters show in figure 6.1A were transformed into *cup1Δ* or *cup1Δdbp2Δ* cells and grow on synthetic complete plates that have different concentration of copper. In parallel, *cup1Δsen1-E1597K* strains with the reporter plasmid were used as a positive control with the idea that *sen1-E1597K* exhibits a termination defect (Steinmetz et al. 2006). Interestingly, *cup1Δdbp2Δ* in the presence of *CYC1* termination site in the reporter

plasmid shows resistance to high copper concentration (0.5 mM) at 35°C while *cup1Δ* in the presence of *CYC1* termination does not (Fig 6.1B). Furthermore, there is no significant growth difference with the *cup1Δdbp2Δ* and *cup1Δ* strains in the presence of *SNR13* termination. This suggests that loss of *DBP2* results in transcription termination defects of protein-coding genes, but not the non-coding gene. Since loss of *DBP2* also results in cryptic transcription (Cloutier et al. 2012), Further experiments are needed to distinguish whether the copper resistance is due to a termination or cryptic initiation defect.

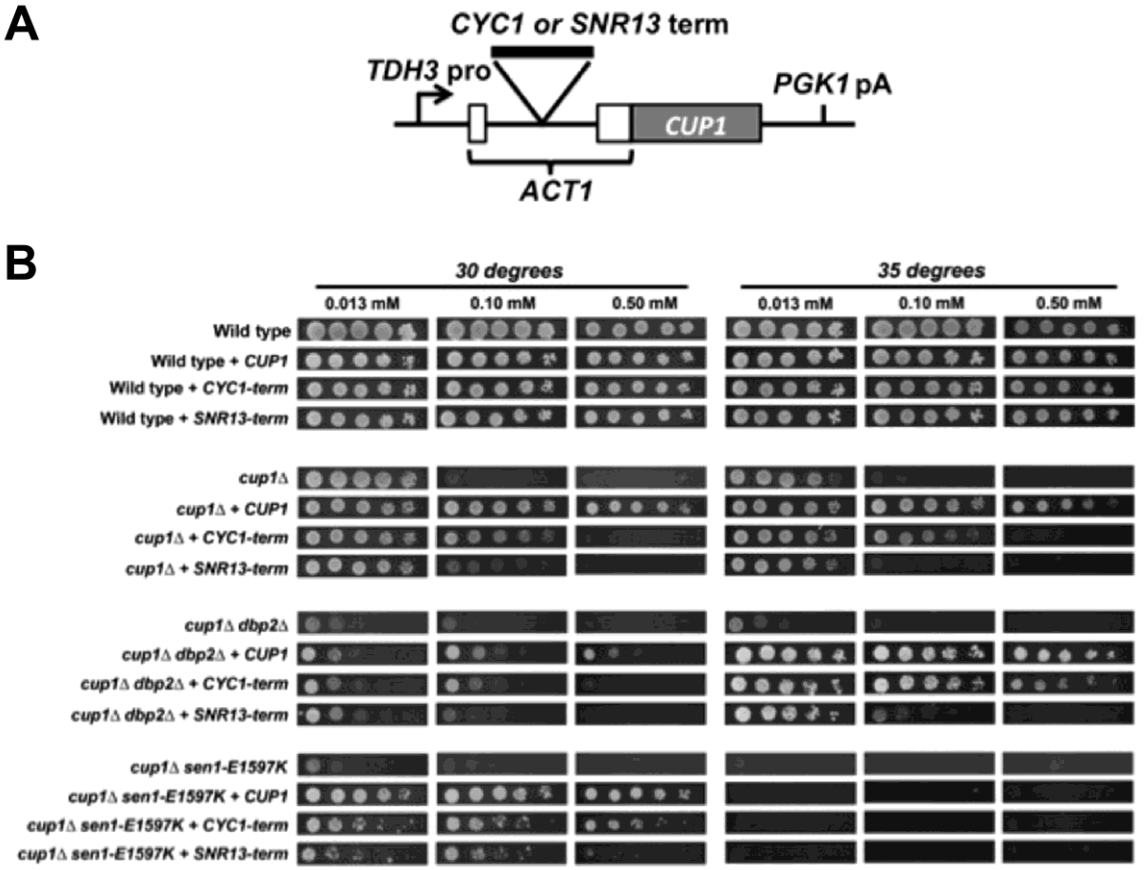

Figure 6.1. *ACT1/CUP1* termination reporter assay. (a) A schematic diagram of ACT1/CUP1 termination reporter plasmid. A plasimid containing a reporter gene that has *TDH3* promoter followed by intron-containing *ACT1* fused with *CUP1* and the *PGK1* termination site. Within the intron of *ACT1*, either the *CYC1* or *SNR13* termination site was inserted. If the cells display termination defect, *CUP1* will be expressed and provide resistance for the cells to grow in the presence of high concentration of copper. In contrast, if the cells do not exhibit termination defect, *CUP1* will not be expressed and the cells will not be able to grow in the presence of high concentration of copper. (b) Loss of DBP2 exhibits termination defects. Indicated strains were spotted in 5-fold serial dilutions onto synthetic complete plates with varying concentration of copper concentration and are grown at 30°C and 35°C because *dbp2Δ* cells are cold sensitive and *sen1-E1597K* strains are temperature sensitive.

6.2.2 Define the region of Dbp2 that is required to interact with Yra1

Yra1 inhibits the unwinding activity of Dbp2 through reducing the ssRNA-binding activity of Dbp2 (Fig 5.7). To gain some insights on how Yra1 decreases the ssRNA-binding activity, we decided to identify the region of Dbp2 that is necessary for the Dbp2-Yra1 interaction using different truncation mutants of Dbp2 (Fig 6.2A). Consistent with our previous study, full length Dbp2 is able to interact with GST-yra1C (Fig 6.2C, (Ma et al. 2013)). Strikingly, the loss of domain 1 or domain 2 of Dbp2 does not affect the interaction with GST-yra1C (Fig 6.2C). However, loss of the C-terminus of Dbp2 abolishes the interaction with GST-yra1C (Fig 6.2C). This reveals that the C-terminus of Dbp2 is necessary to interact with Yra1 and suggests that Yra1 might inhibit the ssRNA-binding activity through the C-terminus of Dbp2. However, this does not exclude the possibly that Yra1 also interacts and confers inhibition via other regions in addition to the C-terminus of Dbp2. Further studies are required to elucidate the molecular mechanism of how Yra1 inhibits the ssRNA-binding activity of Dbp2.

Next, we assayed the biochemical importance of the C-terminus of Dbp2. The C-terminus of Dbp2 consists of an RG-rich sequence, which makes up an RG-rich motif (Fig 6.2B). RG-rich motifs generally act as RNA-binding domains and/or oligomerization domains (Thandapani et al. 2013). To analyze the function of the C-terminus of Dbp2, we tested if the C-terminus plays any role in the enzymatic activity of Dbp2 using *in vitro* ATPase assays and helicase assays. Consistent with previous studies, Dbp2 exhibits ATPase activity in the presence of RNA but the activity is reduced in the absence of the C-terminus (Ma et al. 2013; Cloutier et al. 2012) (Fig 6.3A). Notably, the reduced activity is above background, which indicates that dbp2ΔC is a functional enzyme (Fig

6.3A). This suggests that the C-terminus is critical for Dbp2 to function as an ATPase. In the helicase assays, Dbp2 shows both unwinding and annealing activities with an unwinding rate (k_{obs}) of 0.28 min^{-1} on blunt end RNA duplexes (Fig 6.3B, top). Strikingly, loss of the C-terminus of Dbp2 reduces both the unwinding and annealing activities (Fig 6.3B, bottom). The decreases in the unwinding and annealing activities are also observed in overhang RNA duplexes and blunt end DNA/RNA hybrids

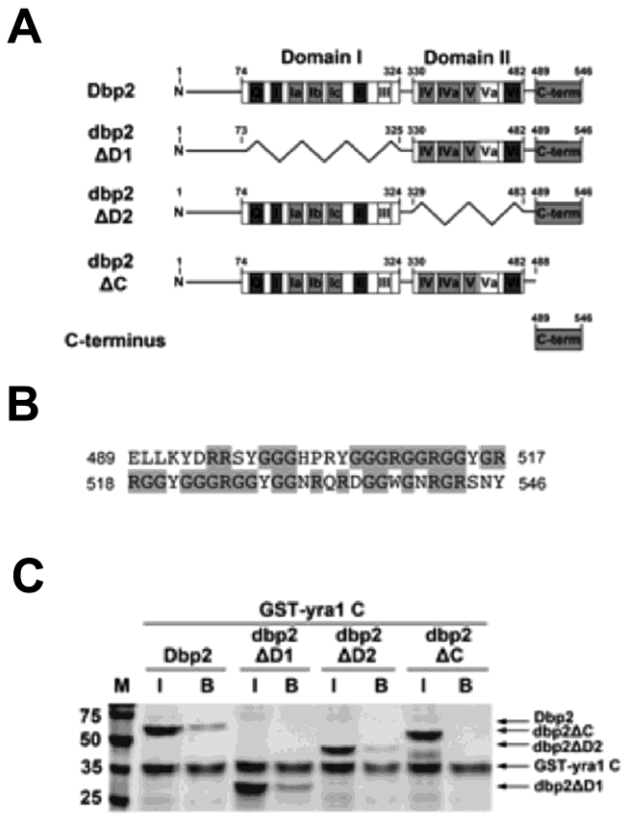

Figure 6.2. The C-terminus of Dbp2 is necessary and sufficient to interact with Yra1. (a) A schematic representation of the primary sequence of Dbp2 and truncation mutants. (b) The amino acid sequence of the C-terminus of Dbp2 contains high RG-rich sequence. The arginine and glycine are highlighted in grey. (c) *In vitro* binding assays of recombinant, purified GST-yra1C with recombinant, purified full length Dbp2 and different Dbp2 truncation mutants. 20% of the protein mix was removed as input ("I") and the bound fraction is indicated as "B".

(Fig 6.3C and 6.3D, respectively). This suggests that the C-terminus is important for the RNA remodeling activity of Dbp2.

6.2.3 Characterize the oligomeric state of Dbp2 during unwinding

It is well established that DEAD-box RNA helicases unwind RNA duplexes in a local strand separation manner that is distinct from canonical helicases. However, it is not yet clear whether all DEAD-box proteins utilize the same mechanism for unwinding. Recent studies have revealed that Mss116, Hera and YixN use different mechanisms to recognize RNA duplexes, which suggests that they have slight differences in their unwinding mechanism (Mallam et al. 2012; Samatanga and Klostermeier 2014). If different DEAD-box proteins use distinct mechanisms for unwinding, what factors determine which mechanism to use remains unclear. A previous study has shown that the DEAD-box protein Ded1 needs to oligomerize to form a trimer to promote efficient RNA unwinding (Putnam et al. 2015). Given that the human ortholog of Dbp2, termed DDX5, has been suggested to oligomerize (Ogilvie et al. 2003), we postulated that Dbp2 might also be able to oligomerize and unwind in a cooperative manner. To test this, we performed unwinding assays with varying concentrations of Dbp2. This shows that Dbp2 unwinds with a Hill coefficient of 3.9, suggesting that Dbp2 unwinds in a cooperative manner (Fig 6.4A).

As yra1C inhibits the unwinding activity of Dbp2 and yra1C reduces the association of Dbp2 with ssRNA (Ma et al. 2013), it is possible that yra1C might affect the cooperativity of Dbp2 during unwinding. To test this idea, we performed unwinding

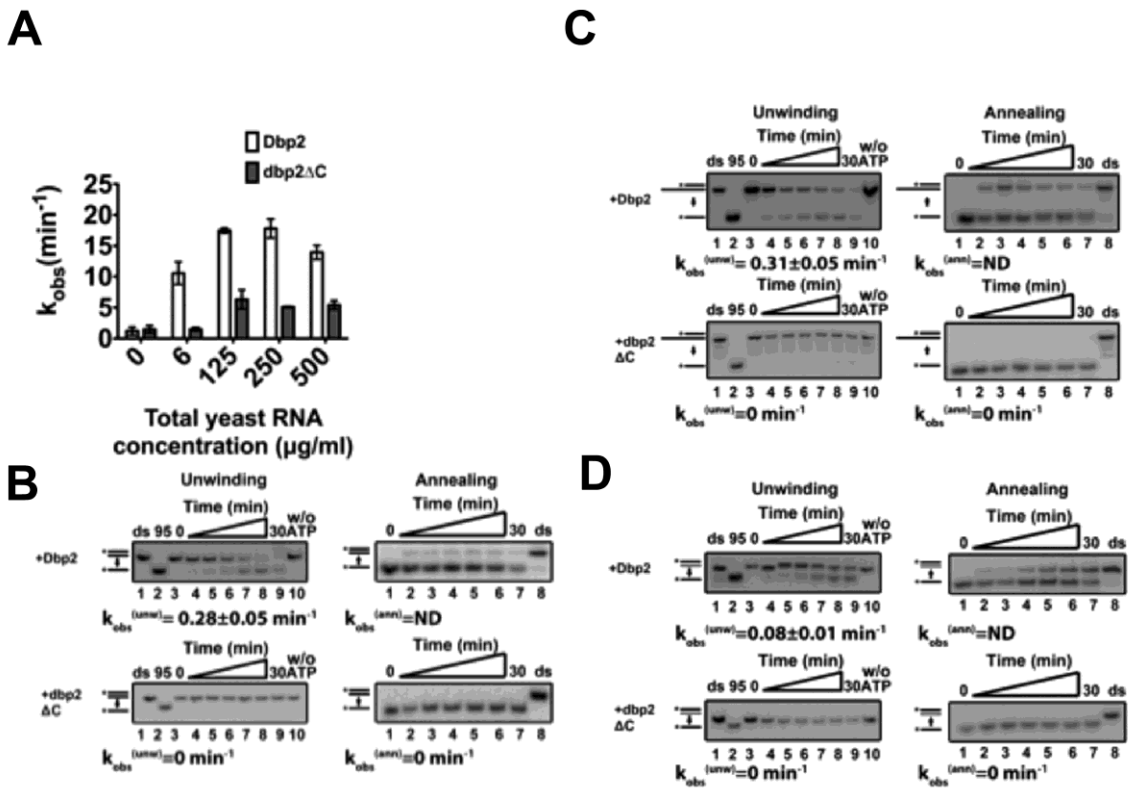

Figure 6.3. The C-terminus of Dbp2 is important for the ATPase, unwinding, and annealing activity of Dbp2. (a) Loss of the C-terminus of Dbp2 reduces the ATPase activity of Dbp2. *In vitro* ATPase assays were conducted using 200 nM of Dbp2 or dbp2ΔC in different total yeast RNA concentration as indicated. (b-d) Loss of the C-terminus of Dbp2 reduces both the unwinding and annealing activity of Dbp2 on blunt end RNA duplexes, overhang RNA duplexes, and blunt end DNA/RNA duplexes. Representative non-denaturing PAGE gels are shown and the k_{obs} is determined as described in (Linder 2006).

assays as mentioned above but in the presence of 200 nM yra1C, which is the IC_{50} of yra1C that inhibits Dbp2 unwinding (Fig 6.4B). Consistent with previous study, yra1C inhibits the unwinding activity of Dbp2 ((Ma et al. 2013); Fig 6.4A). To our surprise, yra1C does not significantly change the Hill coefficient. This indicates that yra1C inhibits the unwinding activity of Dbp2 without altering the cooperativity of Dbp2 (Fig 6.4A).

6.2.4 Analyze whether Dbp2 oligomerizes

Since Dbp2 unwinds in a cooperative manner and DDX5 self-associates *in vivo* (Ogilvie et al. 2003), this led us to test if Dbp2 interacts with itself. To analyze this, we performed *in vitro* binding assays. Lysate of bacterial cells that express recombinant MBP-Dbp2 and recombinant, purified Dbp2 were incubated in the presence or absence of RNase treatment with amylose resins. Recombinant, purified Dbp2 alone was incubated with amylose resins to serve as non-specific binding control. This reveals that Dbp2 interacts with itself independent on the presence of RNA (Fig 6.5A), suggesting that Dbp2 oligomerizes.

Given that the RG-rich motif has been implicated to facilitate oligomerization (Thandapani et al. 2013), we predicted that the RG-rich motif of Dbp2 is critical for Dbp2 oligomerization. To test this idea, we performed *in vitro* binding assays as above but with dbp2ΔC, which lost the RG-rich motif. This demonstrates that dbp2ΔC abolishes self-interaction (Fig 6.5B), suggesting that the C-terminus of Dbp2 is critical for Dbp2 oligomerization. Nonetheless, the oligomeric state of Dbp2 and whether oligomerization of Dbp2 happens *in vivo* remain to be determined.

6.2.5 Perspective/Remaining Questions

Similar to most RNA helicases, there is limited information on the cellular RNA substrates and the precise binding site of Dbp2. Identifying the RNA targets and binding site are crucial to further understand the precise role of Dbp2 in cells. Although Dbp2 is a well-characterized RNA helicase that unwinds RNA duplexes and anneal RNA substrates *in vitro*, it is not known whether Dbp2 is able to remodel RNA structures *in vivo*. This is an intriguing question because not all DEAD-box proteins function to remodel RNA structures (Putnam and Jankowsky 2013). In particular, several studies have suggested that the helicase activity of DDX5 is dispensable for its function in transcription (Endoh et al. 1999; Clark et al. 2008; Bates et al. 2005; Jensen et al. 2008). Knowing if Dbp2 unwinds in cells will provide insights on the precise role of Dbp2 in its physiological functions. Interestingly, ATPase deficient mutants of Dbp2 show slow growth defect similar to *DBP2* deleted cells (Cloutier et al. 2012). This suggests that ATP binding and/or hydrolysis is critical for the function of Dbp2. However, it is not known whether the ATP binding and/or hydrolysis activity is required for Dbp2 to remodel RNA secondary structures and promote mRNP assembly in cells. It is also not understood how over-accumulation of Dbp2 contributes to transcript stabilization. One potential hypothesis is that the over-accumulated Dbp2 actively removes factors or elements that are required for transcript destabilization. Finally, it is important to determine if the Yra1-dependent inhibition of Dbp2 is conserved in humans. The human orthologs of Yra1 and Dbp2, termed ALY and DDX5, also interact with each other (Zonta et al. 2013), suggesting that this inhibition is conserved. More studies are needed to determine the role of Dbp2 in gene expression.

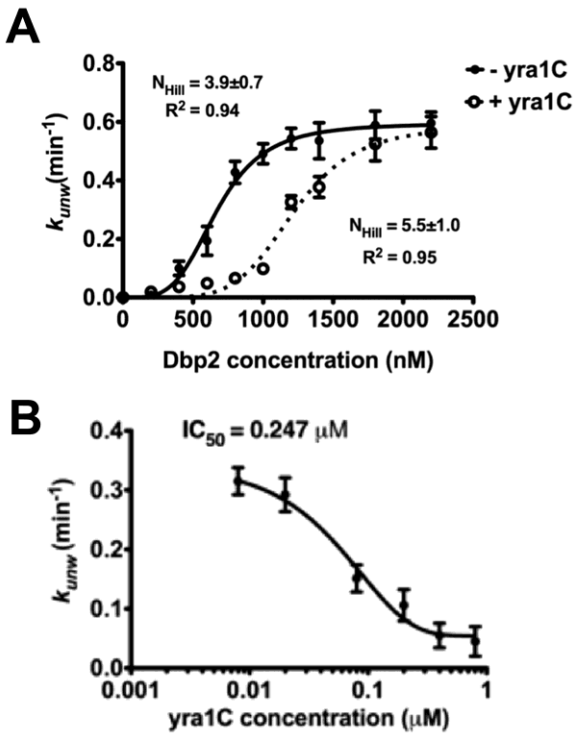

Figure 6.4. Yra1 reduces the unwinding activity, but does not alter the cooperativity of Dbp2. (a) Yra1 inhibits the unwinding activity of Dbp2. Helicase assays were performed at 19 °C water bath with varying concentrations of Dbp2, 2 mM ATP, and 0.1 nM of 16-bp blunt end dsRNA in the presence or absence of 200 nM yra1C. The k_{unw} was determined as (Yang and Jankowsky 2005). All assays were done in triplicate. The results are presented as the mean with S.E.M. of triplicates. The Hill coefficients were determined by fitting the allosteric sigmoidal equation ($Y=V_{max}*X^h/(K_{prime}+X^h)$) in Prism to the data. (b) The IC_{50} of yra1C that inhibits Dbp2 unwinding activity is determined. Helicase assays were performed as above with varying concentrations of yra1C and 800 nM of Dbp2. The log (inhibitor) VS. response – Variable slope equation ($Y=Bottom+(Top-Bottom)/(1+10^{((LogIC50-X)*HillSlope)})$) in prism was used to fit the data.

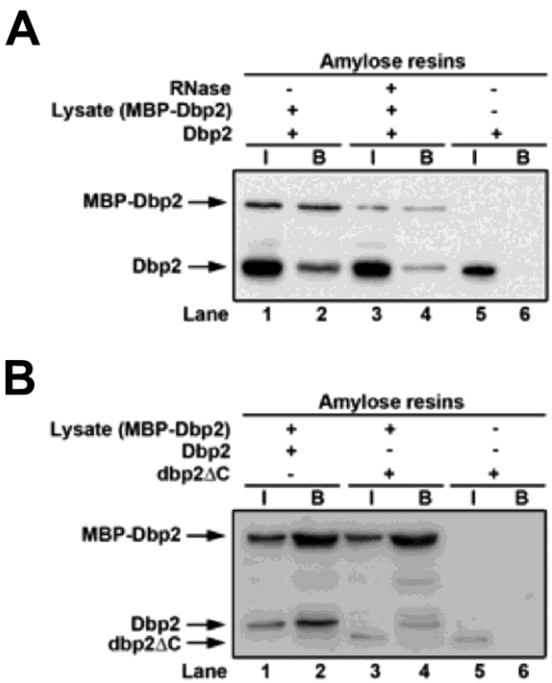

Figure 6.5. Dbp2 interacts with itself *in vitro*. (a) Full length Dbp2 associates with itself. *In vitro* binding assays were performed using lysate of bacterial cells that express recombinant MBP-Dbp2 and recombinant, purified full length Dbp2. 5% of the protein mix was removed as input "I" and the bound fraction is indicated as "B". Proteins were resolved using SDS-PAGE followed by Western blotting analysis. Anti-Dbp2 antibodies were used to specifically target Dbp2. (b) Loss of the C-terminus of Dbp2 abolishes self-association. *In vitro* binding assays were conducted as above with recombinant, purified dbp2ΔC, instead of full length Dbp2.

6.3 References

Abruzzi KC, Lacadie S, Rosbash M. 2004. Biochemical analysis of TREX complex recruitment to intronless and intron-containing yeast genes. *EMBO J* **23**: 2620–2631.

Barta I, Iggo R. 1995. Autoregulation of expression of the yeast Dbp2p "DEAD-box" protein is mediated by sequences in the conserved DBP2 intron. *EMBO J* **14**: 3800–3808.

Bates GJ, Nicol SM, Wilson BJ, Jacobs AM, Bourdon JC, Wardrop J, Gregory DJ, Lane DP, Perkins ND, Fuller-Pace F V. 2005. The DEAD box protein p68: a novel transcriptional coactivator of the p53 tumour suppressor. *EMBO J* **24**: 543–553.

Beck ZT, Cloutier SC, Schipma MJ, Petell CJ, Ma WK, Tran EJ. 2014. Regulation of Glucose-Dependent Gene Expression by the RNA Helicase Dbp2 in Saccharomyces cerevisiae. *Genetics* **198**: 1001–14.

Bond a T, Mangus D a, He F, Jacobson a. 2001. Absence of Dbp2p alters both nonsense-mediated mRNA decay and rRNA processing. *Mol Cell Biol* **21**: 7366–79.

Chang JH, Cho YH, Sohn SY, Choi JM, Kim A, Kim YC, Jang SK, Cho Y. 2009. Crystal structure of the eIF4A-PDCD4 complex. *Proc Natl Acad Sci U S A* **106**: 3148–3153.

Clark EL, Coulson A, Dalgliesh C, Rajan P, Nicol SM, Fleming S, Heer R, Gaughan L, Leung HY, Elliott DJ, et al. 2008. The RNA helicase p68 is a novel androgen receptor coactivator involved in splicing and is overexpressed in prostate cancer. *Cancer Res* **68**: 7938–7946.

Cloutier SC, Ma WK, Nguyen LT, Tran EJ. 2012. The DEAD-box RNA helicase Dbp2 connects RNA quality control with repression of aberrant transcription. *J Biol Chem* **287**: 26155–26166.

Cloutier SC, Wang S, Ma WK, Petell CJ, Tran EJ. 2013. Long Noncoding RNAs Promote Transcriptional Poising of Inducible Genes. *PLoS Biol* **11**.

Endoh H, Maruyama K, Masuhiro Y, Kobayashi Y, Goto M, Tai H, Yanagisawa J, Metzger D, Hashimoto S, Kato S. 1999. Purification and identification of p68 RNA helicase acting as a transcriptional coactivator specific for the activation function 1 of human estrogen receptor alpha. *Mol Cell Biol* **19**: 5363–72.

Gosai SJ, Foley SW, Wang D, Silverman IM, Selamoglu N, Nelson ADL, Beilstein MA, Daldal F, Deal RB, Gregory BD. 2015. Global analysis of the RNA-protein interaction and RNA secondary structure landscapes of the Arabidopsis nucleus. *Mol Cell* **57**: 376–88.

Iglesias N, Tutucci E, Gwizdek C, Vinciguerra P, Von Dach E, Corbett AH, Dargemont C, Stutz F. 2010. Ubiquitin-mediated mRNP dynamics and surveillance prior to budding yeast mRNA export. *Genes Dev* **24**: 1927–1938.

Jensen ED, Niu L, Caretti G, Nicol SM, Teplyuk N, Stein GS, Sartorelli V, van Wijnen AJ, Fuller-Pace F V, Westendorf JJ. 2008. p68 (Ddx5) interacts with Runx2 and regulates osteoblast differentiation. *J Cell Biochem* **103**: 1438–1451.

Johnson SA, Cubberley G, Bentley DL. 2009. Cotranscriptional recruitment of the mRNA export factor Yra1 by direct interaction with the 3' end processing factor Pcf11. *Mol Cell* **33**: 215–226.

Johnson SA, Kim H, Erickson B, Bentley DL. 2011. The export factor Yra1 modulates mRNA 3' end processing. *Nat Struct Mol Biol* **18**: 1164–1171.

Kashyap AK, Schieltz D, Yates 3rd J, Kellogg DR. 2005. Biochemical and genetic characterization of Yra1p in budding yeast. *Yeast* **22**: 43–56.

Lei EP, Krebber H, Silver P a. 2001. Messenger RNAs are recruited for nuclear export during transcription. *Genes Dev* **15**: 1771–1782.

Lei EP, Silver P a. 2002. Intron status and 3'-end formation control cotranscriptional export of mRNA. *Genes Dev* **16**: 2761–2766.

Linder P. 2006. Dead-box proteins: a family affair--active and passive players in RNP-remodeling. *Nucleic Acids Res* **34**: 4168–4180.

Linder P, Jankowsky E. 2011. From unwinding to clamping - the DEAD box RNA helicase family. *Nat Rev Mol Cell Biol* **12**: 505–516.

Liu Y-C, Cheng S-C. 2015. Functional roles of DExD/H-box RNA helicases in Pre-mRNA splicing. *J Biomed Sci* **22**: 54.

Loh PG, Yang HS, Walsh MA, Wang Q, Wang X, Cheng Z, Liu D, Song H. 2009. Structural basis for translational inhibition by the tumour suppressor Pdcd4. *EMBO J* **28**: 274–285.

Ma WK, Cloutier SC, Tran EJ. 2013. The DEAD-box protein Dbp2 functions with the RNA-binding protein Yra1 to promote mRNP assembly. *J Mol Biol* **425**: 3824–3838.

Mallam AL, Del Campo M, Gilman B, Sidote DJ, Lambowitz AM. 2012. Structural basis for RNA-duplex recognition and unwinding by the DEAD-box helicase Mss116p. *Nature* **490**: 121–125.

Oeffinger M, Wei KE, Rogers R, DeGrasse JA, Chait BT, Aitchison JD, Rout MP. 2007. Comprehensive analysis of diverse ribonucleoprotein complexes. *Nat Methods* **4**: 951–956.

Ogilvie VC, Wilson BJ, Nicol SM, Morrice NA, Saunders LR, Barber GN, Fuller-Pace F V. 2003. The highly related DEAD box RNA helicases p68 and p72 exist as heterodimers in cells. *Nucleic Acids Res* **31**: 1470–1480.

Putnam AA, Gao Z, Liu F, Jia H, Yang Q, Jankowsky E. 2015. Division of Labor in an Oligomer of the DEAD-Box RNA Helicase Ded1p. *Mol Cell* **59**: 541–52.

Putnam AA, Jankowsky E. 2013. DEAD-box helicases as integrators of RNA, nucleotide and protein binding. *Biochim Biophys Acta* **1829**: 884–893.

Samatanga B, Klostermeier D. 2014. DEAD-box RNA helicase domains exhibit a continuum between complete functional independence and high thermodynamic coupling in nucleotide and RNA duplex recognition. *Nucleic Acids Res* **42**: 1–11.

Steinmetz EJ, Warren CL, Kuehner JN, Panbehi B, Ansari AZ, Brow DA. 2006. Genome-wide distribution of yeast RNA polymerase II and its control by Sen1 helicase. *Mol Cell* **24**: 735–746.

Stutz F, Bachi A, Doerks T, Braun IC, Seraphin B, Wilm M, Bork P, Izaurralde E. 2000. REF, an evolutionary conserved family of hnRNP-like proteins, interacts with TAP/Mex67p and participates in mRNA nuclear export. *RNA* **6**: 638–650.

Swaminathan S, Kile AC, MacDonald EM, Koepp DM. 2007. Yra1 is required for S phase entry and affects Dia2 binding to replication origins. *Mol Cell Biol* **27**: 4674–4684.

Thandapani P, O'Connor TR, Bailey TL, Richard S. 2013. Defining the RGG/RG Motif. *Mol Cell* **50**: 613–623.

Winge DR, Nielson KB, Gray WR, Hamer DH. 1985. Yeast metallothionein. Sequence and metal-binding properties. *J Biol Chem* **260**: 14464–14470.

Yang Q, Jankowsky E. 2005. ATP- and ADP-dependent modulation of RNA unwinding and strand annealing activities by the DEAD-box protein DED1. *Biochemistry* **44**: 13591–13601.

Zenklusen D, Vinciguerra P, Strahm Y, Stutz F. 2001. The yeast hnRNP-Like proteins Yra1p and Yra2p participate in mRNA export through interaction with Mex67p. *Mol Cell Biol* **21**: 4219–4232.

Zonta E, Bittencourt D, Samaan S, Germann S, Dutertre M, Auboeuf D. 2013. The RNA helicase DDX5/p68 is a key factor promoting c-fos expression at different levels from transcription to mRNA export. *Nucleic Acids Res* **41**: 554–564.

CONTRIBUTION STATMENT

CONTRIBUTION STATEMENT

My scientific contribution to the field

In eukaryotes, gene expression is highly regulated and is crucial for normal cell growth. Proper RNA structure and ribonucleoprotein (RNP) complex formation are important for gene expression. A class of RNA helicases called DEAD-box proteins plays fundamental roles in RNA and RNP structure in every aspect of RNA metabolism. However, the precise biological roles of most of these enzymes are not fully understood. To define the biological roles of DEAD-box proteins, my work revealed that Dbp2 is an active RNA helicase that associates nascent RNA to unwind aberrant structures and promote assembly of RNA-binding proteins, including Yra1, Nab2, and Mex67, co-transcriptionally. Yra1 then reduces the single-stranded RNA binding affinity of Dbp2 to prevent further cycles of unwinding. This regulation is crucial for efficient mRNP assembly and proper gene expression. Collectively, these findings shed lights on how other DEAD-box proteins are involved in other aspects of RNA metabolism and provide insights on the role of the human ortholog of Dbp2, DDX5, which is often overexpressed in cancer cells. Thus, understanding the mechanism might provide insights to carcinogenesis.

Declaration of collaborative work

Chapter 1. Introduction

Writing: I was the writer. Dr. Elizabeth Tran provided multiple rounds of editing and comments.

Chapter 2. Introduction

Writing: Dr. Elizabeth Tran wrote the manuscript.

Experimental design: Dr. Elizabeth Tran designed the experiments.

Figures: Data from figure 2.1D, 2.3B, 2.3D, 2.3E, and 2.5 – 2.7 were provided by Sara Cloutier. Data from figure 2.3A and E were provided by Dr. Elizabeth Tran. Data from figure 2.4 were provided by Luyen Nguyen. I purified the recombinant Dbp2 from *E. coli* and conducted the ATPase assays, which generated the data for figure 2.1B, 2.1C, and 2.2.

Analysis: I analyzed all the ATPase assay data. Luyen Nguyen analyzed the ChIP data. Sara Cloutier analyzed the rest of the data.

Chapter 3. The DEAD-box protein Dbp2 functions with the RNA-binding protein Yra1 to promote mRNP assembly

Writing: I wrote the first and second drafts of the manuscript. Dr. Elizabeth Tran wrote the final version from my final draft.

Experimental design: Dr. Elizabeth Tran designed the experiments. I learned to include all the proper controls in each experiment.

Figures: I collected most of the data in this chapter with the exception of data from figure 3.3A and 3.3B were provided by Dr. Elizabeth Tran and Sara

Cloutier. Figure 3.4 was a collaborative work between Sara Cloutier and myself. Data from figure 3.5A and 3.5B were provided by Dr. Elizabeth Tran.

Analysis: I analyzed most of the data in this chapter with the exception of figure 3.3A, .3.3B, 3.5A, and 3.5B.

Chapter 4. Measuring helicase inhibition of the DEAD-box protein Dbp2 by Yra1

Writing: I wrote the first and second drafts of the manuscript. Dr. Elizabeth Tran edited significant portion of the manuscript.

Chapter 5. Recruitment, duplex unwinding and protein-mediated inhibition of the DEAD-box RNA helicase Dbp2 at actively transcribed chromatin

Writing: I wrote the first and second drafts of the manuscript. Dr. Elizabeth Tran wrote the final version of the manuscript.

Experimental design: I designed most of the experiments in this chapter with the exception of smFRET, glycerol gradient assays, TAP-tagged immunoprecipitation, and fluorescence anisotropy assays.

Figures: Data from figure 5.3 is provided by Dr. Ivan Sabath. Data from figure 5.4, supplemental figure 1 and supplemental table 1 were provided by Dr. Bishu Paudel in the laboratory of our collaborator, Dr. David Rueda (Imperial College London). Data from figure 5.5A is provided by Zheng Xing. I collected the rest of the data.

Analysis: I analyzed all of the data with the exception of smFRET, glycerol gradient assays, TAP-tagged immunoprecipitation, and fluorescence anisotropy assays.

Chapter 6. Summary and perspective

Writing: I was the writer. Dr. Elizabeth Tran provided comments.

VITA

VITA

Wai Kit Ma

Department of Biochemistry
Purdue University
175 South University St, West Lafayette, IN 47907
765-494-7672 (work)
928-814-4820 (cell)
ma81@purdue.edu

Education

2010 – present	*Purdue University, West Lafayette, IN* Ph.D. student in Department of Biochemistry (Current GPA: 3.73)
2007 – 2010	*Northern Arizona University, Flagstaff, AZ* B.S. in General Biology & General Chemistry (Overall GPA: 3.98)

Awards and Honors

2015	The Arnold Kent Balls Award, Purdue University*****
2015	Bird Stair Research Fellowship, Purdue University****
2014	Travel Fellowship for The 19th Annual Meeting of the RNA Society, The RNA Society***
2013	Henry Weiner Travel Award, Purdue University
2010 – 2011	Ross Assistantship, Purdue University**
2010	Gold Axe Award, Northern Arizona University*
2009	Slipher Award, Northern Arizona University
2009	Nancy & Henry Wettaw Organic Chemistry Award, Northern Arizona University

2008 – 2009	Hooper Undergraduate Research Award, Northern Arizona University
2008	Nancy & Henry Wettaw General Chemistry Award, Northern Arizona University

*****The Arnold Kent Balls Award honors an outstanding graduate student in the biochemistry department who exhibits significant contributions to biochemical research
****Bird Stair Research Fellowship rewards students with funds to purchase supplies and materials for research
*** Travel Fellowships is an international award that offered by The RNA Society to subsidize the expense for selected attendees to attend the meeting
** Ross Assistantship is offered by Purdue University Graduate School to award outstanding doctoral-seeking students related to their academic performance and student's teaching experience.
* Gold Axe award is offered by Northern Arizona University to honor outstanding seniors related to their contributions to university academic performance, service, and extracurricular activities.

Publications

1. **Ma, W.K.** and Tran, E. J. Characterization of recruitment of protein-mediated inhibition of the DEAD-box RNA helicase Dbp2. *In preparation.*
2. **Ma, W.K.** and Tran, E. J. (2015). Measuring helicase inhibition of the DEAD-box protein Dbp2 by Yra1. MiMB. 1259:183-97.
3. Beck, Z. T., Cloutier, S. C., Schipma, M. J., Petell, C. J., **Ma, W.K.,** and Tran, E. J. (2014). Regulation of glucose-dependent gene expression by the RNA helicase Dbp2 in Saccharomyces cerevisiae. Genetics. 198(3):1001-14.
4. Cloutier, S. C., Wang, S., **Ma, W.K.,** Petell, C. J., and Tran, E. J. (2013). Long noncoding RNAs promote transcriptional poising of inducible genes. PLoS Biol. 11(11):e1001715.
5. **Ma, W.K.,** Cloutier, S. C., and Tran, E. J. (2013). The DEAD-box protein Dbp2 functions with the RNA-binding protein Yra1 to promote mRNP assembly. J Mol Biol. 425(20):3824-38.
6. **Ma, W.K.,** Hendrix R, Stewart C, Campbell EV, Lavariase M, Morris K, Nichol S, Gage, M.J. (2013). FlgM proteins from different bacteria exhibit different structural characteristics. Biochim Biophys Acta., 1834(4):808-16.
7. Cloutier, S. C., **Ma, W.K.**, Nguyen, L. T., and Tran, E. J. (2012). The DEAD-box RNA helicase Dbp2 connects RNA quality control with repression of aberrant transcription. *J Biol Chem*., 287(31):26155-66.
8. Chin, C. F., Bennettm, A. M., **Ma, W.K.**, Hall, M. C., Yeong, F. M. (2011). Dependence of Chs2 ER export on dephosphorylation by cytoplasmic Cdc14 ensures that septum formation follows mitosis. *Mol Biol Cell.*, (1):45-58

9. Molloy, R.G., **Ma, W.K.**, Allen, A. C., Greenwood, K., Bryan, L., Sacora, R., Williams, L., Gage, M. J. (2010). Aquifex aeolicus FlgM protein exhibits a temperature-dependent disordered nature. *Biochimica et Biophysica Acta (BBA) - Proteins & Proteomics.*,1804(7): 1457-1466.
10. Webber, T. M., Allen, A. C., **Ma**, **W.K.**, Molloy, R.G., Kettelkamp, C. N., Dow, C.A., and Gage, M.J. (2009). Conformational detection of p53's oligomeric state by FlAsH Fluorescence. *Biochem Biophys Res Commun.,* 384(1): 66-70.

Presentations

1. 2014 Midwest yeast meeting, Evanston, Illinois. (Sep 27 – 28, 2014). ***Poster***
   Title: Enzymatic regulation of a DEAD-box RNA helicase promotes efficient mRNP assembly during transcription
2. 19th annual meeting of the RNA society, Quebec City, Canada. (Jun 3 – 8, 2014). ***Oral***

   Title: Enzymatic regulation of a DEAD-box RNA helicase promotes efficient mRNP assembly during transcription
3. 2014 Midwest chromatin and epigenetics meeting, Madison, Wisconsin. (May 18 – 20, 2014). ***Poster***
   Title: Enzymatic regulation of a DEAD-box RNA helicase promotes efficient mRNP assembly during transcription
4. 2013 Rustbelt RNA meeting, Cleveland, Ohio. (Oct 18 – 19, 2013). ***Poster***
   Title: Inhibition of the DEAD-box RNA helicase Dbp2 by the mRNA binding protein Yra1
5. Department of Biochemistry Annual Research Retreat, Turkey Run State Park, Indiana. (Aug 16, 2013). ***Oral***
   Title: Biochemical characterization of the function of Dbp2 in gene expression
6. 18th annual meeting of the RNA society, Davos, Switzerland. (Jun 11 – 16, 2013). ***Poster***

   Title: The DEAD-box protein Dbp2 functions with the RNA-binding protein Yra1 to promote mRNP assembly
7. PULSe recruitment reception, West Lafayette, Indiana. (Feb 28, 2013). ***Poster***
   Title: Dbp2 functions as a RNA chaperone whose enzymatic activity is regulated by Yra1
8. 2012 Rustbelt RNA meeting, Dayton, Ohio. (Oct 19 – 20, 2012). ***Poster***
   Title: Dbp2 functions as a RNA chaperone whose enzymatic activity is regulated by Yra1

9. 14th annual scientific retreat of Purdue University center for cancer research, West Lafayette, Indiana. (Sep 13, 2012). ***Poster***
   Title: Biochemical characterization of Dbp2 at the interface of RNA export and lncRNA-dependent transcription regulation
10. 17th annual meeting of the RNA society, Ann Arbor, Michigan. (May 29 – Jun 2, 2012). ***Poster***

    Title: Biochemical characterization of Dbp2 at the interface of RNA export and lncRNA-dependent transcription regulation
11. 2011 Rustbelt RNA meeting, Dayton, Ohio. (Oct 21 – 22, 2011). ***Poster***
    Title: Exploring the mechanism of DEAD-box protein Dbp2 in gene regulation

Research Experience

2011 – present	Ph.D. student in Dr. Elizabeth Tran's laboratory in the Biochemistry Department of Purdue University. My research focus is to characterize the biochemical function of the DEAD-box RNA helicase Dbp2 in gene regulation.
2007 - 2010	Undergraduate research assistant in Dr. Matthew Gage's laboratory in the Department of Chemistry and Biochemistry in Northern Arizona University, focusing on the relationship between the degree of disordered of an intrinsically disordered protein FlgM and the binding of its protein partner Sigma 28 in different bacteria.

Technical Experience

- Extraction, purification and quantification of DNA and RNA from yeast and bacteria
- Molecular cloning and transformation in yeast and bacteria
- Recombinant protein purification from *E. coli* using affinity chromatography
- Yeast genetics
- Chromatin immunoprecipitation (ChIP)
- RNA immunoprecipitation (RIP)
- Immunoprecipitation (IP)
- *In situ* hybridization for microscopy
- Reverse transcription polymerase chain reaction (RT-qPCR)
- Western blotting
- Northern blotting
- *In vitro* transcription
- Labeling RNA oligo with ^{32}P radioisotope
- Bio-layer interferometry (Octet)

- Enzymatic assays
  - ATPase assay, Helicase assay, Electrophoretic mobility shift assay, Filter-binding assay

Teaching/Job Experience

2015 – present	Teaching Assistant – Biochemistry Lab (BCHM 309 – 003)
2014 – 2015	Research mentor for Yu-Hsuan Lai, a rotation student in Tran laboratory
2013 – 2015	Research mentor for Zachary Beck, an undergraduate student in Tran laboratory
2013	Teaching Assistant – Regulation of Gene Expression (BCHM 695 – 003)
2013	Grading Teaching Assistant – Biochemistry (BCHM 307 – 001)
2012	Research mentor for Jingqun Ma, a rotation student in Tran laboratory
2011	Research mentor for Kate Alleva, an undergraduate student in Tran laboratory
2008 – 2010	Biology and chemistry tutor at the Learning Assistant Center in Northern Arizona University (Certified Tutor Level 2 from International Tutor Program Certification)

Departmental Service

2011 – 2013	Organizer for graduate student/post-doc seminars

Professional Organizations

2011 – present	Student membership in RNA Society
2009 – 2010	Student membership in Biophysical Society
2009 – 2010	National Society of Collegiate Scholars (NSCS)

References

1. Dr. Elizabeth Tran (Thesis advisor)
   Assistant Professor
   Department of Biochemistry
   Purdue University
   West Lafayette, Indiana, USA
   765-496-3889
   ejtran@purdue.edu

2. Dr. Barbara Golden (Committee member)
   Professor
   Department of Biochemistry
   Purdue University
   West Lafayette, Indiana, USA
   765-496-6165
   barbgolden@purdue.edu

3. Dr. Mark Hall (Committee member)
   Associate Professor
   Department of Biochemistry
   Purdue University
   West Lafayette, Indiana, USA
   765-494-0714
   mchall@purdue.edu

4. Dr. Matthew Gage (Undergraduate research advisor)
   Associate Professor
   Department of Chemistry
   University of Massachusetts Lowell
   Lowell, Massachusetts, USA
   978-934-3683
   matthew.gage@uml.edu

PUBLICATIONS

THE JOURNAL OF BIOLOGICAL CHEMISTRY VOL. 287, NO. 31, pp. 26155–26166, July 27, 2012

The DEAD-box RNA Helicase Dbp2 Connects RNA Quality Control with Repression of Aberrant Transcription*◆

Received for publication, May 17, 2012, and in revised form, June 6, 2012 Published, JBC Papers in Press, June 7, 2012, DOI 10.1074/jbc.M112.383075

Sara C. Cloutier, Wai Kit Ma, Luyen T. Nguyen, and Elizabeth J. Tran[1]

From the Department of Biochemistry and Purdue Cancer Center, Purdue University, West Lafayette, Indiana 47907-2063

Background: Dbp2 is a member of the DEAD-box family of RNA helicases.
Results: Dbp2 is a double-stranded RNA-specific ATPase required for repression of cryptic initiation and downstream RNA quality control.
Conclusion: Dbp2 functions in transcriptional fidelity as a cotranscriptional RNA chaperone.
Significance: Elucidation of key RNA enzymes is central to defining the mechanisms for eukaryotic gene regulation.

DEAD-box proteins are a class of RNA-dependent ATP hydrolysis enzymes that rearrange RNA and RNA-protein (ribonucleoprotein) complexes. In an effort to characterize the cellular function of individual DEAD-box proteins, our laboratory has uncovered a previously unrecognized link between the DEAD-box protein Dbp2 and the regulation of transcription in *Saccharomyces cerevisiae*. Here, we report that Dbp2 is a double-stranded RNA-specific ATPase that associates directly with chromatin and is required for transcriptional fidelity. In fact, loss of *DBP2* results in multiple gene expression defects, including accumulation of noncoding transcripts, inefficient 3′ end formation, and appearance of aberrant transcriptional initiation products. We also show that loss of *DBP2* is synthetic lethal with deletion of the nuclear RNA decay factor, *RRP6*, pointing to a global role for Dbp2 in prevention of aberrant transcriptional products. Taken together, we present a model whereby Dbp2 functions to cotranscriptionally modulate RNA structure, a process that facilitates ribonucleoprotein assembly and clearance of transcripts from genomic loci. These studies suggest that Dbp2 is a missing link in RNA quality control that functions to maintain the fidelity of transcriptional processes.

Essential cellular processes, such as growth, organ development, and differentiation, require precise spatial and temporal control of gene expression. Eukaryotic gene expression involves highly complex and coordinated events, including transcription, pre-messenger RNA (pre-mRNA) processing, mRNA transport to the cytoplasm, translation, and decay. During synthesis, RNA-binding proteins and complexes dynamically associate with the RNA to form a mature, translationally competent mRNP[2] complex (1). These factors promote proper pre-mRNA processing and transport as well as couple upstream and downstream steps in the gene expression network. In addition to protein-coding mRNAs, the eukaryotic genome also encodes numerous noncoding RNAs (2–4). These include well known members such as transfer RNAs, ribosomal RNAs, and spliceosomal RNAs, as well as a more recently recognized class of heterogeneous long noncoding RNAs (lncRNAs) (5). The latter class has recently gained importance due to the conserved nature of this widespread transcription and connections between specific members and epigenetic gene regulatory mechanisms (6).

In the budding yeast *Saccharomyces cerevisiae*, lncRNAs are very low in abundance and have been classically defined based on the inhibited RNA-decay mechanism used for detection. This has resulted in numerous names such as cryptic unstable transcripts, stable untranslated transcripts, and Xrn1-dependent transcripts (5). Whereas the precise function of these molecules is still hotly debated, it is clear that regulation is accomplished through the same mechanisms as those utilized for protein-coding mRNAs. In fact, lncRNAs are substrates for the nuclear exosome, a multiprotein complex responsible for maturation and degradation of numerous noncoding RNAs and aberrantly processed mRNAs (7). This suggests that the signature of a noncoding or aberrant mRNA lies within the targeted RNA molecule itself. Consistent with this, numerous studies have underscored the importance of RNP composition as failure to properly assemble mRNPs results in selective retention and subsequent nuclear degradation (7–10). However, the molecular basis for discrimination of aberrant *versus* mature mRNPs is not fully understood.

One class of enzymes that functions as critical regulators of RNP assembly are the DEAD-box RNA helicases. DEAD-box proteins are RNA-dependent ATPases that function in all aspects of RNA biology, including transcription, mRNA export, and ribosome biogenesis. DEAD-box proteins are the largest group within the RNA helicase superfamily with ~25 members in the budding yeast *S. cerevisiae* and ~40 in humans (11). Numerous studies have shown that DEAD-box proteins display a wide variety of biochemical activities *in vitro*, which includes RNA duplex unwinding, RNA folding, and RNP remodeling (12–14). In contrast to *in vitro* analyses, however, little is known regarding the precise biological function of individual DEAD-box protein family members.

* This work was supported, in whole or in part, by National Institutes of Health Grant R01GM097332 (to E. J. T.).
◆ This article was selected as a Paper of the Week.
[1] To whom correspondence should be addressed: Dept. of Biochemistry, Purdue University, BCHM 305, 175 S. University St., West Lafayette, IN. Tel.: 765-496-3889; Fax: 765-494-7897; E-mail: ejtran@purdue.edu.
[2] The abbreviations used are: mRNP, messenger ribonucleoprotein complex; RNP, ribonucleoprotein; dsRNA, double-stranded RNA; 6AU, 6-azauracil; RT-qPCR, reverse transcriptase-quantitative PCR; lncRNA, long noncoding RNA; 5′RACE, 5′-rapid amplification of cDNA ends.

TABLE 1
Yeast and bacterial plasmids

Name	Description	Source/Ref.
pUG6	KanMx disruption cassette plasmid	23
BTP13	pET28a-*DBP2*	This study
BTP18	pET28a-*dbp2-E268Q*	This study
BTP21	pET28a-*dbp2-K136N*	This study
pDBP2	*DBP2*-PL-ADH-P415	19
BTP24	*pdbp2-K136N/CEN/LEU2*	This study
BTP25	*pdbp2-E268Q/CEN/LEU2*	This study
pCEN/URA3	pRS316	24
pCEN/LEU2	pRS315	24
p3×FLAG	p3 × FLAG:KanMx	25
pGAL1-GAL10-GAL7	pYGPM11l14	Open Biosystems (Genomic Tiling)
pFLO8	pGAL-YER109C	Open Biosystems (Yeast ORF Collection)
pSCR1	YGPM29b01	Open Biosystems (Genomic Tiling)

TABLE 2
Yeast strains

Strain	Genotype	Source
Wild type (BY4741)	MATa *his3Δ1 leu2Δ0 met15Δ0 ura3Δ0*	Open Biosystems
DBP2-GFP	MATa *DBP2-GFP:HIS3 his3D1 leu2D0 met15D0 ura3D0*	Invitrogen
xrn1Δ	MATa *xrn1::KanMx his3D1 leu2D0 met15D0 ura3D0*	Open Biosystems
dbp2Δ (BTY115)	MATa *dbp2::KanMx ura3Δ0 leu2Δ0 his3Δ0 TRP1 met- lys?*	This study
dbp2-K136N (BTY166)	MATa *dbp2::KanMx ura3Δ0 leu2Δ0 his3Δ0 TRP1 met- lys? + pdbp2-K136N/CEN/LEU2*	This study
dbp2-E268Q (BTY180)	MATa *dbp2::KanMx ura3Δ0 leu2Δ0 his3Δ0 TRP1 met- lys? pdbp2-E268Q/CEN/LEU2*	This study
Wild type (FY120)	MATa *his4-912∂ lys2-128∂ leu2Δ1 ura3-52*	26
prGAL-FLO8:HIS3 (FY2393)	MATa *lys2-128∂ his3Δ200 ura3-52 leu2Δ1 trp1Δ63 prGAL1-FLO8-HIS3:KanR*	27
spt6-1004 (FY2139)	*MATα FLAG-spt6-1004 ura3-52 leu2Δ1 lys2-128∂*	27
spt6-1004 prGAL-FLO8:HIS3 (BTY217)	MATα *spt6-1004-FLAG prGAL-FLO8-HIS3::KanMx ura3-52 leu2Δ1 lys2-128∂ his4-912∂ trp?*	Reconstructed from Ref. 28
dbp2Δ prGAL-FLO8:HIS3 (BTY124)	MATα *dbp2::KanR prGAL1-FLO8-HIS3::KanMx ura3 leu2 his3 trp? lys? met?*	This study
rrp6Δ	MATa *rrp6::KanMx his3D1 leu2D0 met15D0 ura3D0*	Open Biosystems
DBP2-3×FLAG (BTY200)	MATa *DBP2-3×FLAG:KanMx his3Δ1 leu2Δ0 met15Δ0 ura3Δ0*	This study
Wild type *FT4* (JOU538)	*MATa ura3-52 trp1-Δ63 his3-Δ200 leu2::PET56*	29
FT4 + Reb1BSΔ (JOU811)	*MATa ura3-52 trp1-Δ63 his3-Δ200 leu2::PET56 gal10::URA3::pMV12 (EcoRI/XhoI-Reb1 BSΔ with BS2 silent)*	29
dbp2Δ FT4 (BTY219)	*MATa ura3-52 trp1-Δ63 his3-Δ200 leu2::PET56 dbp2::KanMx*	This study
dbp2Δ FT4+Reb1BSΔ (BTY220)	*MATa ura3-52 trp1-Δ63 his3-Δ200 leu2::PET56 gal10::URA3::pMV12 (EcoRI/XhoI-Reb1 BSΔ with BS2 silent) dbp2::KanMx*	This study

One largely uncharacterized DEAD-box protein in *S. cerevisiae* is Dbp2. In mammalian cells, the ortholog of Dbp2, termed p68, functions in ribosome biogenesis as well as numerous transcriptional and cotranscriptional processes with RNA polymerase II (15). Dbp2, however, has only been linked to ribosome biogenesis and non-sense-mediated decay in *S. cerevisiae* despite the fact that human p68 functionally complements loss of *DBP2* (16–18). This suggests that a role in transcriptional processes is either not conserved or that Dbp2 plays an as-of-yet uncharacterized function in budding yeast.

In this study, we undertook a directed approach to define the role of Dbp2 in budding yeast. Our studies now provide documentation that Dbp2 functions at the interface of chromatin and RNA structure to represses expression of aberrant transcripts. We suggest that Dbp2 is a missing link in the gene expression network that functions as a cotranscriptional RNA chaperone. This would provide a model RNA modulation during transcription with broad implications to other aspects of RNA biology.

EXPERIMENTAL PROCEDURES

Plasmids and Cloning—All plasmids were constructed by standard molecular biology techniques and are listed in Table 1. *DBP2* was expressed in yeast using the intronless p*DBP2*-PL-ADH-p415 (19) to avoid splicing-dependent changes in expression levels. ATPase-deficient variants were constructed by site-directed mutagenesis using *Pfu* polymerase. The pET28a-*DBP2* was generated by subcloning techniques from p*DBP2*-PL-ADH-p415.

Yeast Manipulations—Yeast strains were constructed using classical yeast genetic techniques and are listed in Table 2. *DBP2*-deletion strains (*dbp2Δ*) were constructed by PCR-based gene replacement using pUG6 as a template. *DBP2–3×FLAG* strains were constructed similarly using the p3×FLAG plasmid. 6AU studies were conducted with yeast strains grown in synthetic media −uracil (−URA) + 2% glucose and spotted onto −URA plates with or without 100 μg/ml 6-azauracil (Sigma). For all RNA analyses, yeast strains were grown in rich YPD media (YP + 2% glucose) at either 35 or 30 °C as indicated to an OD of 0.4–0.5 prior to cell harvesting and RNA isolation. Transcriptional induction was performed by shifting yeast cells from YPD to YP + 1% raffinose for 1 h, to induce a derepressed state, and then to YP-Gal (YP + 2% galactose) for 5 h prior to cell harvesting.

Recombinant Protein Purification—Expression of pET28a HIS_6-*DBP2* in Rosetta *Escherichia coli* (DE3) cells (Novagen) was induced by 0.2 mM isopropyl 1-thio-β-D-galactopyranoside overnight at 16 °C. Cells were lysed in 20 mM Tris at pH 7.9, 100 mM NaCl, 5 mM imidazole. Recombinant proteins were purified from the soluble fraction using nickel affinity chromatography according to the manufacturer's instructions (Qiagen).

In Vitro ATPase Assays—*In vitro* ATP hydrolysis assays were performed using a PK/lactate dehydrogenase enzyme-coupled absorbance assay as described previously (20) but with 440 nM

Dbp2 and total yeast RNA (Sigma) or purchased DNA or RNA oligonucleotides (IDT). k_{obs} values were calculated using the following formula: $V_0 = (A_{340}/\text{min} \times 2.5)/(6.22 \times 10^{-3}\ \mu\text{M})$, where $k_{obs}(\text{min}^{-1}) = V_0/\text{protein concentration}$, and the EC_{50} was determined using GraphPad Prism software. V_0 was normalized to background NADH loss in buffer alone for each condition. Presented data are the average of three independent experiments.

Cellular Microscopy—Wild type (BY4741) or *DBP2-GFP* strains were grown at 30 °C in YPD and were subsequently fixed with 10% formaldehyde, washed with PBS, and stained with 2 μg/ml DAPI (Sigma) for visualization of DNA. Images were collected using an Olympus BX51 fluorescent microscope and Metamorph TL software (Olympus America).

RT-qPCR and 5′RACE—RNA was isolated from cells by standard acid phenol purification. Complementary DNA (cDNA) was prepared using the Quantitect reverse transcriptase kit (Qiagen) according to manufacturer's instructions using random hexamer primers provided. Primer pairs for qPCR were designed using default parameters in Primer Express 3.0 (Invitrogen) and are listed in Table 3. PCRs were performed in the Bio-Rad CFX96 system. Fold changes were calculated using the Pfaffl method (22) and are reported as three biological replicates with three technical repeats each with mean ± S.E. 5′RACE of *GAL7* mRNA was conducted according to the manufacturer's protocol (Invitrogen). *GAL7* gene-specific primers (GSP primers) are listed in Table 4. Resulting 5′RACE products were cloned using a UA cloning kit (Qiagen), and precise 5′ ends were determined by DNA sequencing.

Chromatin Immunoprecipitation—Chromatin immunoprecipitation experiments were conducted as described previously (21) with the following changes. Input represents 2.5% of lysate. Anti-FLAG antibodies (M2, Sigma) were preincubated with protein G Dynabeads (Invitrogen) prior to incubation with cross-linked sheared lysate. Immunoprecipitated DNA was eluted with 400 μl of elution buffer (1% SDS, 0.1 M $NaHCO_3$) followed by reversal of cross-links by addition 16 μl of 5 M NaCl and a 65 °C overnight incubation. Resulting DNA was incubated with RNase A and proteinase K, phenol-extracted, and ethanol-precipitated. Samples were resuspended in 50 μl of TE, and 1:50 was used for qPCR using PrimeTime assay probes listed in Table 5 (IDT) and TaqMan qPCR mix (Invitrogen). All ChIP experiments were conducted with three biological replicates with four technical repeats and are shown as the fold increase above wild type signal relative to input.

Northern Blotting—20–50 μg of total RNA was resolved on a 1.2% formaldehyde-agarose gel followed by transfer to a nylon membrane (Brightstar Hybond N^+, Invitrogen). Northern blotting was conducted using standard methods. Radiolabeled double-stranded DNA probes were generated using PCR products from a plasmid template (see Table 6) and the Decaprime II kit according to manufacturer's instructions (Invitrogen). Transcripts were visualized using a PhosphorImager (GE Healthcare) and quantified by densitometry (ImageQuant, GE Healthcare).

TABLE 3
RT-qPCR oligonucleotides
F is forward and R is reverse.

1 F	TGAGTTCAATTCTAGCGCAAAGG
1 R	TTCTTAATTATGCTCGGGCACTT
2 F	GAGGTCTTGACCAAGCATCACA
2 R	TTCCAGACCTTTTCGGTCACA
3 F	AAATGAAGGTTTGTGTCGTGA
3 R	AAGCTTTGCAGAATGCATGA
4 F	TGAACAAGCCATATGGAGACA
4 R	CGACGATATTACCCGTAGGAA
5 F	CAAAAAGCGCTCGGACAACT
5 R	GCTTGGCTATTTTGTGAACACTGT
6 F (or GAL7 F)	CAAAAAGCGCTCGGACAACT
6R (or GAL7 R)	GCTTGGCTATTTTGTGAACACTGT
7 F	TCAACAGGAGGCTGCTTACAAG
7 R	CCAGGACATAGATAGCATTTTGGA
8 F	CCATTCCACAAATGAAACAATC
8 R	ACAACCCATGGCTGTACCTT
CLB2 F	GCGAATAATCCAGCCCTAAC
CLB2 R	CGGCTGTTGATCTTGATACG
POL1 F	CAGAAAGCGCCAGGAATTG
POL1 R	CGTAGCCTACACCATCGTCATC
RAD 14 F	CCGGCCTCTCGCAGTTACTA
RAD14 R	GCGGCTGCTGCATTATCAT
ACT1 F	TGGATTCCGGTGATGGTGTT
ACT1 R	TCAAAATGGCGTGAGGTAGAGA
ADE3 F	CCCGTGATATCGCATCATACTTAC
ADE3 R	GGCCGATGGCAACGACTA

TABLE 4
5′RACE primers

GAL7-GSP1	GTCCTCCTTCACCATTTGG
GAL7-GSP2	GGCCCAGTATGGAACAACAAC
GAL7-GSP3	CGTCAGTCAATGCTTGCCAAG

RESULTS

DBP2 Is an RNA-dependent ATPase in Vitro—Dbp2 is a member of the DEAD-box family of RNA-dependent ATPases in *S. cerevisiae* based on the presence of 10 conserved sequence motifs organized into two distinct structural domains (Fig. 1*A*) (11). Dbp2 also contains a C-terminal RGG motif and a unique N terminus implicated in high affinity RNA and protein binding *in vivo*, respectively (18, 33).

Although studies from other laboratories have utilized genetic manipulations to assess the enzymatic function of Dbp2 *in vivo* (16, 18, 33), Dbp2 has not been biochemically character-

TABLE 5
Oligonucleotides for chromatin immunoprecipitation

Name	Forward	Reverse	Probe	Relative to +1 Start	+1 Start Refs.
GAL7 P	GCGCTCGGACAACTGTTG	TTTCCGACCTGCTTTTATATCTTTG	CCGTGATCCGAAGGACTGGCTATACA	−66	30
GAL7 5′	ATCATACAATGGAGCTGTGGG	CTAGCCATTCCCATAGACGTTAC	AAGCAGCCTCCTGTTGACCTAACC	+190	30
GAL7 middle	TGCGAAACTTCACTAGGGATG	CCAGAGAAGCAAAGAAAATCATAAG	CAACCCATGGCTGTACCTTTGTTTTCA	+587	30
GAL7 3′	GCATTTCTACCCACCTTTACTGAG	CAGCTTGTTCCGAAGTTAAATCTC	AGGCTCACCTAACAATTCAAAACCAACC	+1079	30
GAL7 3′ UTR	GGACCACTCTTACATAACTAGAATAGC	TTTTCTATTAACTGCCTGGTTTCTTT	TGTCACTCCGTTCAAGTCGACAACC	+1259	30, 31
POL1 5′	AGAATACAGGGCCAGAAAGC	GTAGCCTACACCATCGTCATC	ACAACAAATCGTCATGCAGCAATTCCT	+125	31
RAD14 5′	TGTGTTTGTATTTTAACCGTGGG	GATTCAATTGGTCGCTACTCAG	TGTTAGCCTCCTGCACAGCTCATC	+211	31
CLB2 5′	TCCAGCCCTAACAAATTTCAAATC	GCTGTTGATCTTGATACGCTTTC	TCCGACTTCCCTCCTTCTTTACTGAGTT	+1634	32
ADE3 5′	TGGCTGGTCAAGTGTTGG	TGGTCTGTTGCCTACTTGAATG	TCAAAAGCATTCAAGGTCACGTGCC	+100	31

TABLE 6
Oligonucleotides for Northern blotting (dsDNA probes)
F is forward, and R is reverse.

FLO8 F	CTGTATCCAGTCCATTATCTTCAG
FLO8 R	TCAGCCTTCCCAATTAATAAAATTG
SCR1 F	GGATACGTTGAGAATTCTGGCCGAGG
SCR1 R	AATGTGCGAGTAAATCCTGATGGCACC
GAL7 F	CCTTGGTTAGGTCAACAGGAG
GAL7 R	AGTCGCATTCAAAGGAGCC

ized to date. To determine whether Dbp2 is a functional RNA-dependent ATPase, we established *in vitro* ATPase assays with recombinant purified Dbp2 and increasing amounts of total RNA as described previously (20). Consistent with other DEAD-box enzymes, our results demonstrate that Dbp2 is an active ATPase *in vitro* with a 50% effective concentration (EC_{50}) of 27 μg/ml for RNA (Fig. 1*B*). Next, we used site-directed mutagenesis to incorporate amino acid substitutions in motif I or II and assayed ATP hydrolysis of the resulting purified proteins to verify the origin of wild type Dbp2 activity (Fig. 1*A*). This revealed that both the K136N (motif I) and E268Q (motif II) substitutions abolish enzymatic activity at RNA concentrations 1- and 3-fold above the EC_{50}, consistent with mutations of other DEAD-box enzymes (Fig. 1*C*). Thus, Dbp2 is a functional RNA-dependent ATPase *in vitro*.

To determine whether the enzymatic activity of Dbp2 is required for normal cell growth, we utilized a plasmid complementation assay (Fig. 1*D*). To this end, we generated a *dbp2*Δ strain and analyzed the ability of wild type or ATPase-deficient *dbp2* alleles, p*dbp2-K136N* and p*dbp2-E268Q*, to confer cell growth as compared with vector alone. Consistent with previous reports, loss of *DBP2* results in slow growth and cold sensitivity with an optimal growing temperature of 35 °C (18, 19, 33). Importantly, neither point mutant restored wild type growth, paralleling the growth of the *dbp2*Δ strain with vector alone (Fig. 1*D*). This is in contrast to ectopic expression of the wild type *DBP2* (*pDBP2*), which enabled growth at all temperatures. Immunoblotting analysis verified that the inability of the mutant plasmids to rescue the *dbp2*Δ strain is not due to expression differences between the wild type (p*DBP2*) and mutant *dbp2* vectors (data not shown). Thus, substitutions that impair enzymatic activity also impair cell growth, underscoring a requirement for enzymatically active Dbp2 in budding yeast.

Dbp2 Is a dsRNA-directed ATPase—Given that the ATPase activity of Dbp2 is required for growth, we next asked if Dbp2 preferred specific RNAs for stimulation of ATP hydrolysis. This would indicate a preference for specific RNAs *in vivo*. To test this, we conducted *in vitro* ATPase assays as above in the presence of single-stranded RNA molecules of different lengths (16- or 37-mer) or dsRNA with a GNRA tetraloop ($\Delta G = -25$ kcal/mol; Fig. 2*A*). Strikingly, this revealed that Dbp2 strongly prefers dsRNA for activation of ATP hydrolysis with a resulting EC_{50} of $10^{-6.5}$ or ~0.3 μM (Fig. 2*B*). This is near the concentration of Dbp2 (0.2 μM), suggesting that the affinity is likely higher with the EC_{50} representing the upper limit of the dissociation constant. Strikingly, a longer 37-mer single-stranded RNA is also able to stimulate RNA-dependent ATPase activity but to a significantly lower extent that impairs affinity measurement. This was in contrast to the shorter 16-nucleotide single-stranded RNA, which was unable to activate Dbp2 at any concentration. Importantly, Dbp2 displayed no DNA-directed ATPase activity (Fig. 2*C*). This suggests that Dbp2 displays dsRNA-dependent ATPase activity, an enzymatic parameter that parallels human p68 but is not common among other DEAD-box family members (34, 35). Furthermore, preliminary studies show that Dbp2 is a functional RNA helicase.[3] This suggests that Dbp2 is a dsRNA-directed ATPase, which targets structured RNA elements *in vivo*.

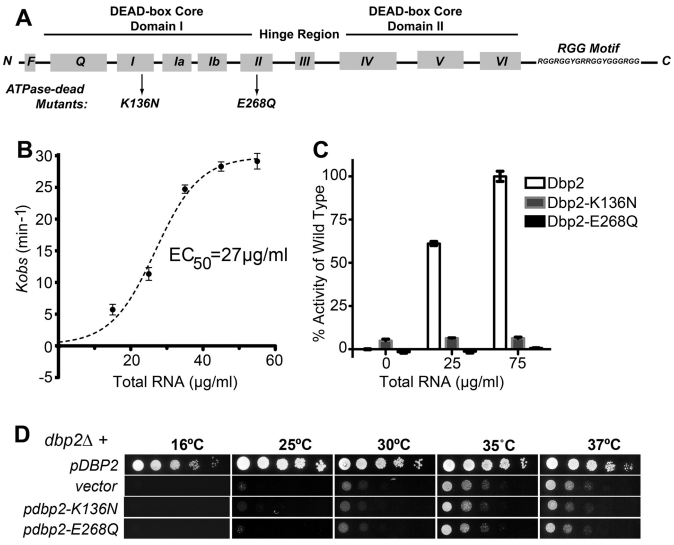

FIGURE 1. **Dbp2 is an RNA-dependent ATPase *in vitro* whose activity is required for normal cell growth.** *A,* schematic representation of Dbp2 primary sequence and conserved DEAD-box protein motifs. Core domains and the 10 sequence motifs are indicated (11). Dbp2 also contains a C-terminal RGG accessory domain predicted to enhance RNA binding activity (33). *Arrows* denote amino acid substitutions in motif I or motif II. *B,* Dbp2 is an enzymatically active, RNA-dependent ATPase *in vitro*. The ability of Dbp2 to hydrolyze ATP was assessed using an absorbance-based *in vitro* ATPase assay as described previously, which measures ATP hydrolysis indirectly through a linear depletion of NADH (20). Assays were conducted with 400 nM of recombinant purified His_6-tagged Dbp2 and increasing amounts of total yeast RNA. ATP turnover numbers (k_{obs}) were calculated from initial velocities of each assay conducted in triplicate. The EC_{50} value for RNA was determined through nonlinear regression analysis and is reflective of the concentration of RNA needed to activate ATP hydrolysis to a half-maximal rate. All data are normalized to background signals that result from very low levels of NADH depletion in buffer alone ($V_0 = 1.01 \pm 0.5$ min^{-1}). The observed ATPase rate of Dbp2 in the absence of RNA is 0.98 ± 0.4 min^{-1}, which is equivalent to buffer alone. *C,* mutation of residues within motif I and II impair enzymatic activity. Recombinant purified His_6-tagged variants Dbp2-K136N or Dbp2-E268Q were assayed for ATP hydrolysis as above using RNA concentrations equal to or 3-fold above the wild type EC_{50} concentration. Enzymatic activities are reported as a percentage of the initial velocity of ATP hydrolysis of wild type Dbp2 with 75 μg/ml RNA. *D, DBP2*-deficient strains display a slow growth and cold-sensitive phenotype. Yeast growth was analyzed using serial dilution analysis of *dbp2*Δ strains transformed with either empty vector alone or CEN plasmids encoding wild type (*pDBP2*) or ATPase-deficient mutants (*pdbp2-K136N* or *pdbp2-E268Q*) as indicated. Strains were subsequently spotted in 5-fold serial dilutions onto selective media and grown for 3–5 days at the indicated temperatures.

Dbp2 Is a Predominantly Nuclear Protein Whose Loss Is Suppressed by 6-Azauracil—Studies of Dbp2 in budding yeast have provided conflicting evidence regarding the precise localization of Dbp2 ranging from nuclear/nucleolar to predominantly cytoplasmic (16, 36). To understand the cellular function(s) of Dbp2, we asked where Dbp2 is localized at steady state by con-

[3] W. K. Ma, unpublished data.

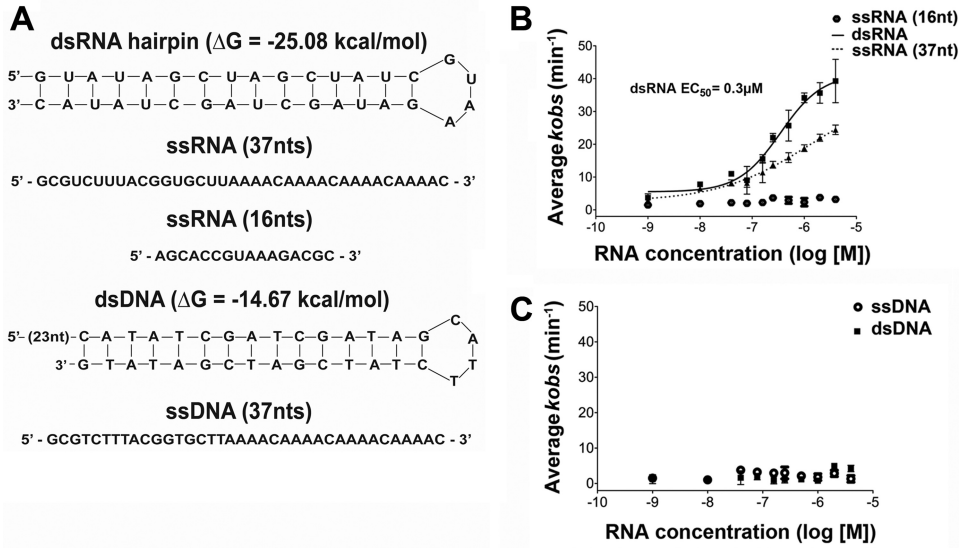

FIGURE 2. **Dbp2 is a dsRNA-directed ATPase *in vitro*.** *A,* sequence and schematic representation of RNA and DNA molecules used below. Δ*G* parameters were calculated using the MFOLD web server. *B,* Dbp2 displays a preference for dsRNA in stimulation of ATP hydrolysis. ATPase assays were conducted as above using purchased single- stranded or double-stranded RNA molecules in *A* at varying concentrations from 1 nM to 4 μM and purified Dbp2 (0.2 μM). ATP hydrolysis activity was determined in triplicate for each nucleic acid concentration and is plotted on a semi-logarithmic graph as k_{obs} *versus* log[M] concentration of RNA. The resulting EC_{50} from the dsRNA hairpin was determined through nonlinear regression analysis. EC_{50} values could not be determined for the single-stranded RNA molecules due to low levels of ATPase stimulation. *C,* ATPase activity of Dbp2 is not stimulated by DNA. *In vitro* ATPase assays were conducted as above with the DNA molecules indicated in *A* using purchased DNA molecules. *nt*, nucleotide.

ducting fluorescent microscopy of a fluorescently tagged *DBP2-GFP* strain harboring a GFP fusion at the endogenous locus. This revealed that Dbp2-GFP is a predominantly nucleoplasmic protein, colocalizing with DAPI-stained DNA, with accumulation in the nucleolus (Fig. 3*A*). This is consistent with the role of Dbp2 in ribosome biogenesis and is suggestive of an additional nuclear function.

To pinpoint a role for Dbp2 in the nucleoplasm, we subsequently asked if loss of *DBP2* renders cells sensitive to transcriptional stress by conducting growth assays of wild type and *dbp2*Δ cells with or without 100 μg/ml 6AU (Fig. 3*B*). 6AU is a transcriptional inhibitor that has been widely utilized to identify genes whose products positively regulate transcription elongation (37). Surprisingly, 6AU partially rescues the slow growth defects of the *dbp2*Δ strain at semipermissive temperatures of 30 and 32 °C, suggesting that reduction of transcription improves the growth of *DBP2*-deficient strains.

DBP2 Represses Cryptic Initiation within the FLO8 Locus—Interestingly, 6AU resistance or suppression phenotypes have been noted in only a few published reports and correlate with loss of gene products that negatively regulate transcription. This includes the transcriptional regulator/mRNA processing factor, *SSU72*, as well as chromatin-modifying enzymes like the histone methyltransferase *SET2* (38–40). To further characterize the biological role of Dbp2, we asked if *dbp2*Δ strains exhibit transcriptional defects similar to those associated with impaired repression. One type of transcriptional defect is cryptic initiation whereby failure to properly assemble chromatin results in initiation at noncognate sites either within (intragenic) or outside of (intergenic) transcribed genomic loci (28, 41, 42). To determine whether *DBP2* is required for repression of intragenic cryptic initiation, we utilized a previously characterized p*GAL-FLO8*:*HIS3* reporter construct for identification of initiation defects through a simple growth assay (28, 41). We constructed *dbp2*Δ *pGAL-FLO8*:*HIS3* strains and subsequently analyzed growth of two independent isolates with respect to wild type and *spt6-1004* strains as negative and positive controls, respectively. *SPT6* encodes a transcriptional elongation factor whose mutation results in characterized cryptic initiation defects (28, 41). Strikingly, loss of *DBP2* also results in cryptic intragenic initiation (Fig. 3*D*). Unlike *spt6-1004* strains, however, *dbp2*Δ strains require transcriptional induction for detection of cryptic initiation. This suggests that Dbp2 is needed only in the context of active transcriptional activity. Next, we conducted Northern blotting of *FLO8* transcripts from wild type, *dbp2*Δ, and *spt6-1004* strains to determine whether *dbp2*Δ strains also display cryptic initiation at the endogenous *FLO8* gene (Fig. 3*E*). This revealed a small ~4-fold increase in short *FLO8* products in the *dbp2*Δ strain as compared with wild type (4–16%). Thus, *DBP2* is required for repression of cryptic intragenic initiation in the *FLO8* reporter and within the endogenous locus.

GAL7 Transcripts Are Overabundant in the Absence of DBP2—Given that *DBP2*-deficient cells display defects associated with active transcription, we asked if *DBP2* is required for normal expression levels of endogenous genes (Fig. 3*F*). To this end, we selected a panel of genes and assessed transcript abundance in wild type and *dbp2*Δ cells using RT-qPCR. These genes were chosen based on the characterized role of the mammalian Dbp2 ortholog, p68, in cell cycle progression, cell differentiation, and response to extracellular cues (15). This revealed that *GAL7* transcripts are specifically overabundant in *dbp2*Δ cells as compared with wild type, in contrast to other gene products (Fig. 3*F*). Notably, this increase occurs under typical transcriptionally repressive conditions, suggesting that the *GAL7* gene is aberrantly derepressed in *dbp2*Δ cells. Furthermore, there was no detectable difference in *GAL7* transcript levels under

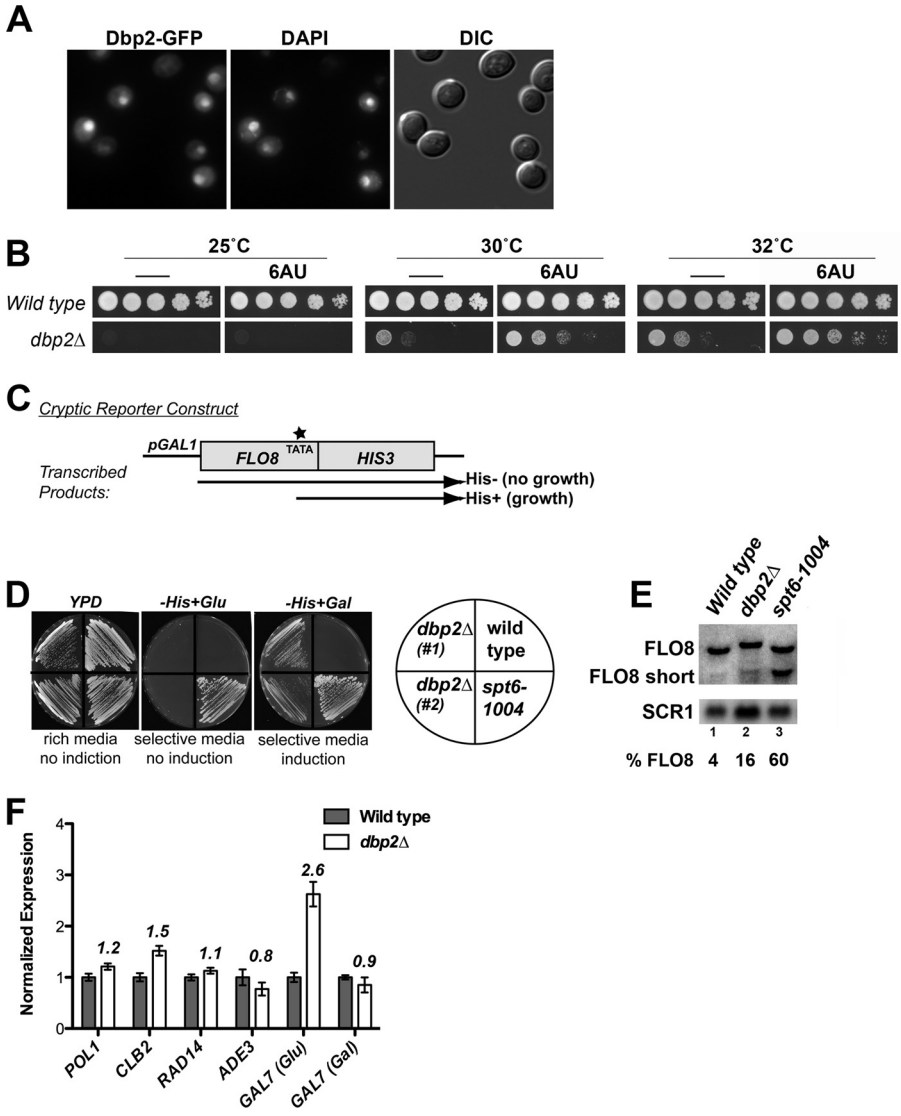

FIGURE 3. **Dbp2 is a predominantly nuclear protein required for repression of cryptic, intragenic initiation within *FLO8* and expression of *GAL7*.** *A,* live cell imaging reveals whole cell distribution of Dbp2 with a predominantly nuclear localization at steady state. Fluorescent microscopy was conducted with exponentially growing *DBP2-GFP* strains grown at 30 °C. Cells were fixed for 1 h with formaldehyde in rich growth media, washed extensively, and stained with DAPI for visualization of DNA. Differential contrast (*DIC*) images are presented in the *right-most panel*. *B,* transcriptional elongation inhibitor, 6AU, partially rescues *dbp2*Δ growth defects. Wild type (BY4741) or *dbp2*Δ strains were analyzed for 6AU sensitivity using serial dilution analysis of strains onto −URA + 2% glucose plates with or without 100 μg/ml 6AU at the indicated temperatures. *C,* schematic diagram of the *FLO8:HIS3* cryptic initiation reporter (adapted from Ref. 28). TATA (*) indicates the approximate position of the cryptic internal start site within the *FLO8* open reading frame. Following induction with galactose (+*Gal*), transcription in wild type cells proceeds through the internal TATA, resulting in out of frame *HIS3* mRNA, and failure to grow on media lacking histidine (−*His* + *Gal*). Defects in chromatin structure or assembly are correlated with aberrant initiation at the internal TATA site, which results in grown on −His media due to production of an in-frame *HIS3* mRNA. *D,* DBP2 is required for repression of cryptic intragenic initiation within the *FLO8:HIS3* reporter gene. Cryptic initiation defects were assessed following construction of *dbp2*Δ strains encoding a chromosomally integrated *pGAL-FLO8:HIS3* reporter. Two independent *dbp2*Δ strain isolates are shown compared with *DBP2* wild type and an *spt6–1004* mutant strain as negative and positive controls, respectively (27, 28). *E,* loss of DBP2 results in an ~4-fold increase in aberrant FLO8 transcripts from the endogenous *FLO8* locus. Briefly, total RNA was isolated from wild type, *dbp2*Δ, and *spt6--1004* strains and subjected to Northern blotting. 30 μg of total RNA was resolved on a 1.2% formaldehyde/agarose gel, transferred to a nylon membrane, and probed with a double-stranded, radiolabeled DNA probe corresponding to both the full-length and short 3′ transcript product. *SCR1* transcripts are shown as a loading control. *F, DBP2* is required to maintain endogenous levels of *GAL7* under transcriptionally repressive conditions (+glucose). The transcript abundance of individual gene products was determined by RT-qPCR analysis of RNA isolated from wild type or *dbp2*Δ strains grown at 35 °C. Transcript levels were determined by quantitative PCR using the Bio-Rad CFX system and SYBR Green with the indicated primer sets (Table 2). Gene product annotations are as follows: *POL1* (DNA primase 1), *CLB2* (cyclin B2), *RAD14* (DNA repair), *ADE3* (nucleotide biosynthesis), and *GAL7* (carbon source metabolism). *GAL7* primers correspond to set *6* in subsequent figures. Differences were calculated using the Pfaffl method (22) and are normalized to the level of *ACT1*. *Error bars* represent the mean ± S.E.

induced conditions (+galactose) between wild type and *dbp2*Δ cells. This suggests that Dbp2 is required for both repression of cryptic intragenic initiation and of normal promoter elements of protein-coding genes.

Dbp2 Associates Directly with Chromatin, Correlating with Transcriptional Activity—The *GAL* cluster is a well established model for dissection of gene regulatory mechanisms in *S. cerevisiae*. Briefly, the *GAL* genes are considered to have three transcriptional states as follows: active (+galactose), derepressed (+raffinose), and repressed (+glucose) (43). In the presence of galactose, transcriptional activation proceeds via the transcription factor Gal4. In the repressed state, transcriptional repressors Nrg1 and Mig1/Mig2 are responsible for promoting glucose-dependent repression (43, 44).

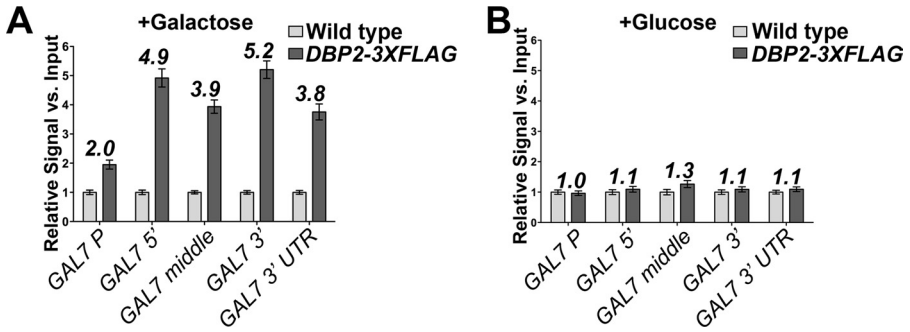

FIGURE 4. **Dbp2–3×FLAG is recruited to the *GAL7* open reading frame in a transcriptionally dependent manner.** *A,* Dbp2 associates with the *GAL7* locus, predominantly within the coding region and 3′UTR. Chromatin immunoprecipitation (*ChIP*) experiments were conducted with strains expressing untagged or C-terminally 3×FLAG-tagged Dbp2 from the endogenous locus grown in rich media after a 5-h transcriptional induction (+*galactose*). Bound DNA was detected by qPCR using primer sets corresponding to the indicated genomic locations (see Table 5). Resulting signals are reported as the relative signal above an untagged wild type strain with respect to input and are the result of three independent biological replicates with three technical repeats. *Numbers* above each bar represent the average difference above background (untagged strain). *Error bars* indicate S.E. as above. *B,* Dbp2–3×FLAG is not detectibly associated with GAL7 under transcriptionally repressive conditions. ChIP-qPCR analysis was conducted as in *A* with yeast strains grown in glucose (repressive) conditions.

Our results suggest that *DBP2* is required for proper repression of *GAL7* under transcriptionally repressive conditions, drawing parallels between Dbp2 and glucose-dependent repressors. If this is the case, this would suggest that Dbp2 functions at the *GAL7* and *FLO8* loci through distinctly different mechanisms. To test this, we utilized chromatin immunoprecipitation (ChIP) to determine whether a 3×FLAG-tagged Dbp2 is directly bound to *GAL7* under transcriptionally repressive conditions. Strikingly, this resulted in detection of Dbp2 at the *GAL7* locus under transcriptionally active conditions, in contrast to our predictions (Fig. 4*A*). Dbp2–3×FLAG associates with similar levels ~5-fold above background across the *GAL7* open reading frame with slightly lower association at the promoter region, suggesting recruitment throughout the transcriptional unit (Fig. 4*A*). We were not able to detect appreciable accumulation of Dbp2 at any tested region under repressive conditions (Fig. 4*B*, *+glucose*). Thus, Dbp2 is associated with chromatin in a transcriptionally dependent manner, suggestive of association with the transcriptional machinery and/or nascent RNAs. This also indicates the *GAL7* derepression defect in *dbp2*Δ cells may be due to either an indirect effect or to transcriptional activity, which is below the ChIP detection limit for Dbp2.

DBP2-deficient Cells Display Expression Defects across GAL10-GAL7—The *GAL7* gene is a member of the *GAL1-GAL10-GAL7* gene cluster (Fig. 5*A*). In addition to proteinaceous transcription factors, the *GAL* cluster is also associated with overlapping lncRNAs with estimated levels as low as one molecule in 14 cells (29). These include the well characterized *GAL10* lncRNA (29, 45, 46) and a recently identified, sense-oriented *GAL10s* lncRNA (termed *XUT 109-2m* in Ref. 3).

To determine the origin of the *GAL7* transcriptional product in *dbp2*Δ cells under repressive conditions, we conducted a high resolution RT-qPCR analysis by positioning qPCR primer pairs at the 5′ end of *GAL1*, 5′, middle, and 3′ end of *GAL10*, intragenic region between *GAL10* and *GAL7*, and the 5′, middle, and 3′ region of *GAL7* (Fig. 5*A*, *1–8*). Consistent with our original RT-qPCR analysis above, we detected a 2.5-fold increase at the 5′ end of *GAL7* in *dbp2*Δ (Fig. 5*B*, *6*) and similar increases across the *GAL7* open reading frame indicative of low level expression of the *GAL7* protein-coding gene. Unexpectedly, we also detected a 2-fold increase in transcript abundance upstream of *GAL7*. This is in contrast to the 5′ ends of *GAL1* and *GAL10*, which were not significantly different in wild type *versus dbp2*Δ (Fig. 5*B*, *1*). Next, we conducted RT-qPCR analysis at the *dbp2*Δ semi-permissive temperature of 30 °C with the idea that growth at lower temperatures would thermodynamically "trap" Dbp2-dependent substrates (Fig. 5*C*). Strikingly, this revealed a sharp increase in transcript abundance to ~5-fold above wild type across the same genomic region. This pattern is consistent with aberrant expression across the *GAL7* and *GAL10s* lncRNA coding regions, the latter of which is indicative of a defect in RNA quality control (3).

DBP2-deficient Cells Accumulate Aberrant GAL7 RNAs—To further characterize the role of Dbp2 at the *GAL7* locus, we conducted Northern blotting to visualize *GAL7* transcripts under repressive conditions in wild type and *dbp2*Δ cells at 30 °C (Fig. 6*A*). This revealed a weak but detectable accumulation of transcripts corresponding to both the *GAL7* protein-coding gene and a weak ~2.5-kb product in the *dbp2*Δ strain (Fig. 6*A*, *lanes 4–6*). The latter product most likely corresponds to a 3′-extended *GAL10s* lncRNA that terminates at the end of the *GAL7* gene. This is suggestive of aberrant expression of two *GAL* cluster gene products in *dbp2*Δ cells under normally repressive conditions.

Next, we analyzed the *GAL7* transcripts produced during transcriptional activation in *dbp2*Δ cells at 30 °C (Fig. 6*B*). Strikingly, in addition to abundant expression of *GAL7* mRNA transcripts, which accumulated to similar levels between wild type and *dbp2*Δ, we also detected an ~4-kb product in *DBP2*-deficient cells (Fig. 6*B*, *lanes 4–6*). The 4-kb transcript is consistent with expression of a *GAL10-GAL7* bicistronic mRNA that results from aberrant pre-mRNA processing in other mutant yeast strains (30, 47, 48). Interestingly, we did not detect defects in *dbp2*Δ cells grown at 35 °C, suggesting that higher temperatures partially bypass the requirement for Dbp2 (Fig. 3*F* and data not shown). This is consistent with a general role for Dbp2 in cotranscriptional RNA folding and/or assembly.

GAL7 Transcripts Are a Result of Cryptic Initiation in DBP2-deficient Cells—Given that *GAL7* transcription is induced by the action of a galactose-dependent transcription factor, Gal4 (43), we were surprised at our detection of *GAL7* mRNAs in

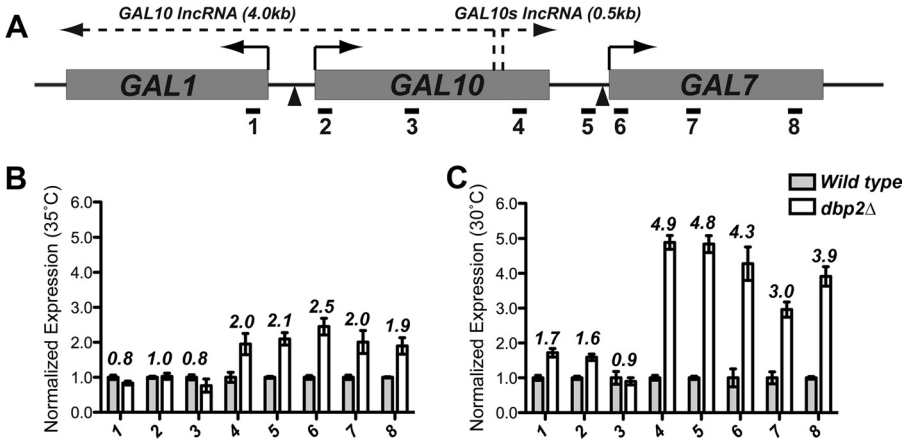

FIGURE 5. ***GAL7* expression is a result of transcriptional defects across the *GAL10-GAL7* genomic region in *DBP2*-deficient cells.** *A,* schematic representation of the GAL operon in *S. cerevisiae* denoting the three galactose-dependent genes (*GAL1*, *GAL10*, and *GAL7*) and previously identified noncoding RNAs (3, 29). *Short solid-line arrows* denote the direction of protein-coding (sense) transcription, and lncRNA transcription is represented by a *dotted line*. *Triangles below* the genes denote approximate positions of promoter elements, and *short horizontal lines* demonstrate positions of primer sets utilized in qPCR (Table 2). Set *6* is the same set used for detection of *GAL7* in Fig. 2. *B,* high resolution RT-qPCR reveals accumulation of the *GAL10s* lncRNA and transcription through the *GAL7* ORF. RT-qPCR was conducted as in Fig. 2 using higher resolution qPCR primer pairs (Table 2) with strains grown at 35 °C. *C,* growth at the *dbp2*Δ semi-permissive temperature of 30 °C exacerbates *GAL7* expression defects. High resolution RT-qPCR was conducted as above using wild type or *dbp2*Δ strains grown at 30 °C.

repressive conditions when Gal4 is inactive. To determine whether the *GAL7* transcripts originate from the normal +1 transcriptional start site, we utilized 5′RACE to map the 5′ ends of *GAL7* sense transcripts in *DBP2*-deficient cells. Strikingly, this revealed that the *GAL7* transcripts are aberrant with respect to the wild type initiation site (Fig. 6*C*). Whereas transcriptional induction in wild type cells by addition of galactose results in a single PCR product of ~500 bp, transcripts in the *dbp2*Δ cells are distinct from normal *GAL7* mRNAs (Fig. 6*C*, *lanes 1* and *2*). Sequencing of the resulting PCR products revealed the following three distinct transcriptional start sites in the *dbp2*Δ strain: one intergenic site at −50 bp upstream of the +1 start site, corresponding to two PCR products due to 5′RACE efficiency; and two intragenic sites within the open reading frame of *GAL7* (Fig. 6*D*). In contrast, 5′RACE analysis of *GAL7* mRNAs under activated conditions revealed identical transcriptional start sites between wild type and *dbp2*Δ cells (data not shown). Thus, the *GAL7* transcripts in *dbp2*Δ cells under repressive conditions are a result of cryptic intragenic initiation with respect to the *GAL10s* lncRNA, consistent with the requirement for *DBP2* at the *FLO8* locus. We speculate that the cryptic initiation defects in *DBP2*-deficient cells are an indirect result of failure to "clear" aberrant RNAs rather than a direct role in chromatin assembly, given the recent connections between RNA quality control and chromatin architecture (see "Discussion").

Simultaneous Loss of DBP2 and RRP6 Results in a Lethal Growth Phenotype—Major factors in RNA quality control are the nuclear exosome component, *RRP6,* and the cytoplasmic exonuclease, *XRN1* (2, 3). To gain further insight into the biochemical pathway for *DBP2* function, we conducted synthetic genetic analysis of *dbp2*Δ and *xrn1*Δ or *rrp6*Δ alleles using a plasmid shuffle assay (Fig. 7). This assay exploits the toxic effects of 5-fluoroorotic acid in strains that cannot grow in the absence of a plasmid encoding the uracil biosynthesis gene (*URA3*) and wild type *DBP2* (p*DBP2*). Strikingly, this revealed that *rrp6*Δ and *dbp2*Δ are synthetic lethal at all growth temperatures (Fig. 7). This genetic interaction is specific, as a *dbp2*Δ *xrn1*Δ strain grows well in the absence of the p*DBP2*. This supports a role for Dbp2 in RNA quality control steps in the nucleus. More importantly, this shows that Dbp2 is a major factor in RNA quality control that likely plays roles at multiple genes outside of the *GAL7* and *FLO8.* Taken together, we provide a model whereby the DEAD-box protein Dbp2 functions at the interface of chromatin and RNA quality control to modulate RNA structure in a manner that promotes both downstream processing steps and reassembly of chromatin in the wake of active transcription (Fig. 8). This suggests that Dbp2 is a cotranscriptional RNA chaperone, central to fidelity of the gene expression network.

DISCUSSION

A major challenge to the RNA biology field is understanding how the RNA and RNP structure contributes to cellular processes. The DEAD-box RNA helicases are central players in RNP dynamics, functioning in all aspects of RNA metabolism through ATP-dependent modulation of RNA structures (11). These include the DEAD-box proteins Sub2 and Dbp5, which are required for mRNP packing and nuclear export, respectively (49–51). Our studies now elucidate Dbp2 as a critical factor in transcriptional fidelity, adding to the complement of DEAD-box proteins associated with maintenance of the transcriptome. Furthermore, our studies provide provocative evidence that Dbp2 functions as a cotranscriptional RNA chaperone. This would be consistent with current models for DEAD-box proteins as ATP-dependent chaperones and with elegant *in vitro* studies that support this mechanism (14, 52, 53).

With elucidation of Dbp2 as a key player in this process, several tantalizing questions now emerge regarding the precise biochemical mechanism in gene regulation. Our results suggest that Dbp2 is a dsRNA-dependent ATPase recruited to chromatin during transcription. Furthermore, our studies show that *DBP2* is genetically linked to the nuclear exosome component, *RRP6*. It is well established that Rrp6-dependent decay of

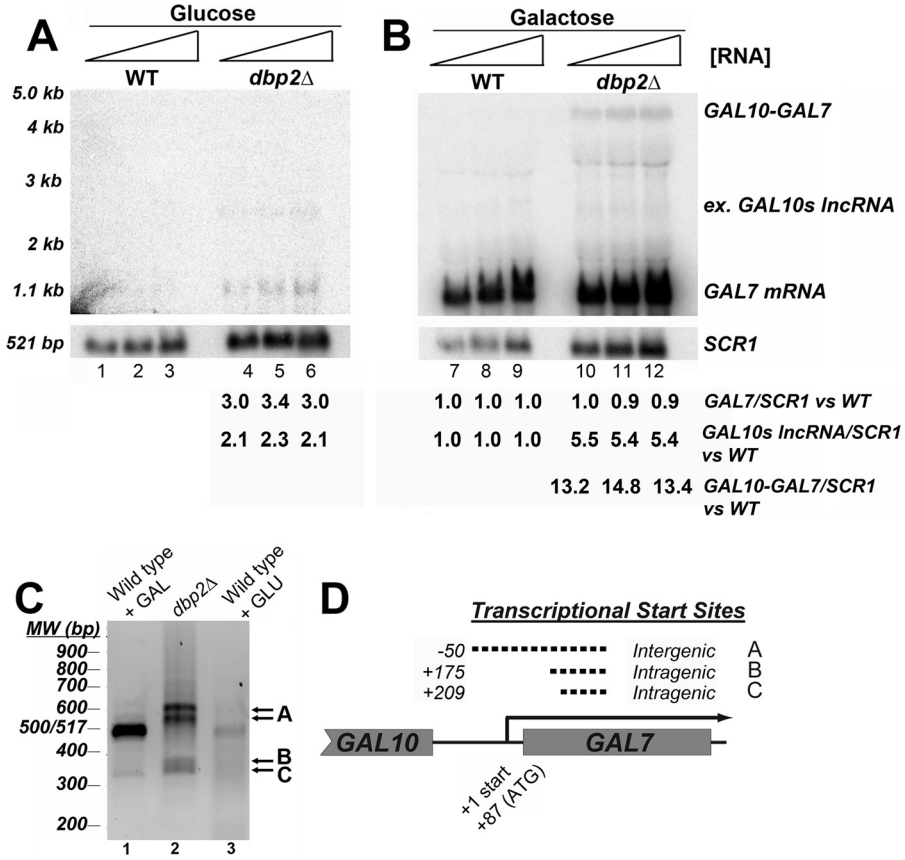

FIGURE 6. **Loss of *DBP2* results in cryptic initiation at *GAL7* and termination defects within the *GAL10-GAL7* region under repressed and activated conditions, respectively.** *A,* Northern blotting of total RNA from wild type and *dbp2*Δ cells reveals expression of *GAL7* and a 3′-extended *GAL10s* lncRNA under typically repressive conditions. Northern blotting was conducted with increasing amounts of total RNA (20–50 μg) from indicated strains grown at the semi-permissive *dbp2*Δ temperature of 30 °C in glucose (repressive) conditions (*lanes 1–6*). Accumulation of *GAL7* mRNA and a 2.5-kb transcript, likely corresponding to a 3′ extended *GAL10s* lncRNA, is evident in *lanes 4–6*. Other products at ~2 and 3.5 kb are background detection of 18 S and 25 S rRNA. Quantification is provided *below* each lane and corresponds to the quantity of the indicated transcript *versus* wild type normalized to levels of SCR1 for each lane. In lanes with no detectable product, quantities were normalized to background. *B,* transcriptional induction of the *GAL* genes results in expression of *GAL7* and appearance of a *GAL10–GAL7* transcript. Northern blotting was conducted as above following a 5-h shift to galactose-containing media. Under transcriptionally induced conditions, *GAL7* mRNA is induced along with an ~4-kb product, which most likely corresponds to a *GAL10-GAL7* bicistronic mRNA (*lanes 10–12*). *C, GAL7* mRNA transcripts in *dbp2*Δ strains are aberrant with respect to wild type *GAL7* products. Resulting 5′RACE products of aberrant *dbp2*Δ transcripts (*lane 2*) are shown with respect to the induced wild type *GAL7* transcript (*lane 1*) and basal transcriptional products (*lane 3*) shown following resolution on a 1.3% agarose gel and visualization by ethidium bromide staining. The three most prominent 5′RACE products in the *dbp2*Δ cells are denoted *A–C* to the *right* of the gel. The two A bands correspond to the same transcription initiation site (as determined by sequencing) and are likely due to differences in the cDNA "tailing" efficiency in the 5′RACE. Note that these experiments are not quantitative and do not reflect relative transcript abundance between strains or conditions. *D, GAL7* transcripts are the result of cryptic initiation events in the *dbp2*Δ strain under typically repressive conditions. Schematic representation of *GAL7* transcriptional start sites in *DBP2*-deficient cells as determined following cloning and sequencing of resulting 5′RACE products. *Dotted lines* denote cryptic transcriptional elements between (inter) or within (intra) an open reading frame with respect to the normal +1 start site in transcriptionally induced wild type cells (*solid line*) (74).

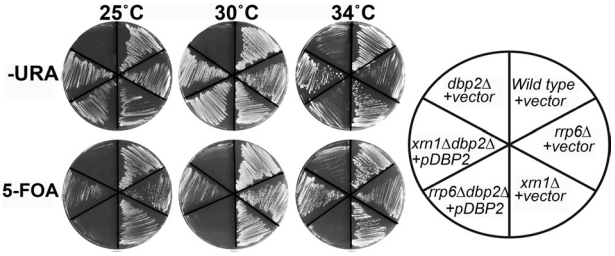

FIGURE 7. **Simultaneous loss of *DBP2* and the nuclear RNA decay factor, *RRP6*, results in synthetic lethality.** Synthetic growth defects were measured using a plasmid shuffle assay, which exploits the ability of yeast to grow in the absence of a *URA3*-encoding plasmid (vector or p*DBP2*). Indicated strains were constructed using standard yeast manipulations, and resulting transformants were streaked on either −URA or 5-fluoroorotic acid media to demonstrate growth in the presence or absence of plasmid-encoded *DBP2*, respectively.

numerous noncoding RNAs is dependent on transcription termination mechanisms (54). The primary mechanism for termination of short noncoding transcripts is through the Nrd1-Sen1 pathway whereby RNA-binding proteins, Nrd1 and Nab3, recognize specific RNA sequences in nascent RNA transcripts (55–57). Thus, it is tempting to speculate that Dbp2 promotes loading of RNA-binding proteins, such as Nrd1 and Nab3, by resolving inhibitory RNA structures. This is consistent with accumulation of a putative *GAL10-GAL7* read-through transcript in *dbp2*Δ cells and with identification of an Nrd1-dependent termination mechanism at the *GAL10* gene (47). However, given the pattern of *Dbp2* gene association and the requirement for repression of initiation, the role of Dbp2 is not likely limited to recruitment of these two factors. Interestingly, studies have also shown that the genes within the *GAL* cluster are associated with gene looping events between promoters and terminators

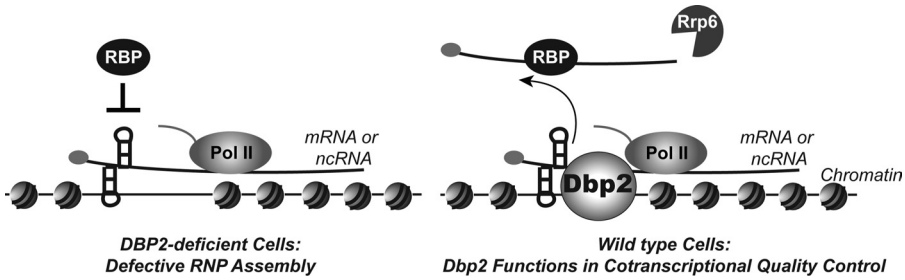

FIGURE 8. **Dbp2 is a dsRNA-directed DEAD-box enzyme that functions in cotranscriptional RNA quality control.** Our results document a previously unrecognized role for Dbp2 in transcriptional quality control. We suggest that Dbp2 is recruited during transcription to promote clearance of newly transcribed RNA from genomic loci, whose presence interferes with both chromatin and mRNP assembly. This activity may involve direct modulation of RNA or RNP structures to promote association of RNA-binding proteins (*RBPs*) such as factors required for RNA processing and/or decay. This activity would also be predicted to inhibit further synthesis of aberrant cryptic transcripts through reformation of chromatin architecture, consistent with recent studies of other cotranscriptional RNA processing/assembly factors (63, 65). *Pol II,* polymerase II.

(58–60). These gene loops have been shown to influence the rate of transcriptional reactivation in a process termed "transcriptional memory" (61). It will be interesting to determine whether Dbp2 and/or RNA folding influence higher order chromatin architecture.

Because loss of *DBP2* results in cryptic transcription indicative of aberrant chromatin architecture, we suggest that the activity of Dbp2 is necessary to promote clearance of nascent RNAs from genomic loci. Furthermore, we speculate that this requirement is due to the presence of RNA structures within nascent transcripts, which would be predicted to impair RNA processing and RNP complex assembly. In line with this model, strains deficient in cotranscriptional mRNP processing and packaging accumulate RNA:DNA hybrids in structures termed R-loops, which induce multiple defects associated with aberrant chromatin architecture (62–66). For example, simultaneous loss of the TRAMP component Trf4 and histone deacetylase Sir2 results in severe ribosomal DNA instability, underscoring an intimate connection between maintenance of the genome and transcriptome (67).

It is well understood that the activity of RNA polymerases is dependent on the chromatin environment. Moreover, loss of chromatin remodeling or histone modification machinery results in aberrant transcription, including cryptic transcriptional initiation both between and within the gene loci (28, 41, 68). To the best of our knowledge, however, no RNA decay or processing factors have been linked specifically to repression of cryptic initiation. Instead, genes encoding histones, histone-modifying enzymes, and chromatin remodeling factors as well as transcription factors have been linked to this activity, supporting the fact that aberrant transcriptional initiation is a result of altered chromatin structure (28). This suggests that either Dbp2 plays a distinct role as a bridging factor between nascent RNAs and chromatin or that roles in repressing cryptic initiation have not been defined thus far for other RNA processing factors.

In mammals, p68 has been linked to numerous cotranscriptional processing steps and has been suggested to associate with dsRNA both *in vitro* and *in vivo*, consistent with the idea that Dbp2 cotranscriptionally modulates RNA structures (34, 69, 70). Thus, the role of Dbp2 is likely evolutionarily conserved with future studies providing key insights into the biochemical mechanisms in eukaryotic gene regulation. More importantly, however, numerous studies have shown that p68 is a potent oncogene whose overexpression results in chemotherapeutic resistance (71, 72). In summary, our studies uncover a role for Dbp2 at the interface of RNA surveillance and chromatin architecture as a missing link in quality control of the transcriptome.

Acknowledgments—We thank Joe Ogas, Barb Golden, and Scott Briggs for constructive criticism regarding this manuscript. We also thank members of the Scott Briggs laboratory for assistance with experimental methods. Finally, we thank members of the Tran laboratory for scientific discussions.

REFERENCES

1. Moore, M. J., and Proudfoot, N. J. (2009) Pre-mRNA processing reaches back to transcription and ahead to translation. *Cell* **136,** 688–700
2. Neil, H., Malabat, C., d'Aubenton-Carafa, Y., Xu, Z., Steinmetz, L. M., and Jacquier, A. (2009) Widespread bidirectional promoters are the major source of cryptic transcripts in yeast. *Nature* **457,** 1038–1042
3. van Dijk, E. L., Chen, C. L., d'Aubenton-Carafa, Y., Gourvennec, S., Kwapisz, M., Roche, V., Bertrand, C., Silvain, M., Legoix-Né, P., Loeillet, S., Nicolas, A., Thermes, C., and Morillon, A. (2011) XUTs are a class of Xrn1-sensitive antisense regulatory noncoding RNA in yeast. *Nature* **475,** 114–117
4. Cabili, M. N., Trapnell, C., Goff, L., Koziol, M., Tazon-Vega, B., Regev, A., and Rinn, J. L. (2011) Integrative annotation of human large intergenic noncoding RNAs reveals global properties and specific subclasses. *Genes Dev.* **25,** 1915–1927
5. Berretta, J., and Morillon, A. (2009) Pervasive transcription constitutes a new level of eukaryotic genome regulation. *EMBO Rep.* **10,** 973–982
6. Wang, K. C., and Chang, H. Y. (2011) Molecular mechanisms of long noncoding RNAs. *Mol. Cell* **43,** 904–914
7. Schmid, M., and Jensen, T. H. (2010) Nuclear quality control of RNA polymerase II transcripts. *Wiley Interdiscip. Rev. RNA* **1,** 474–485
8. Libri, D., Dower, K., Boulay, J., Thomsen, R., Rosbash, M., and Jensen, T. H. (2002) Interactions between mRNA export commitment, 3′ end quality control, and nuclear degradation. *Mol. Cell. Biol.* **22,** 8254–8266
9. Rougemaille, M., Gudipati, R. K., Olesen, J. R., Thomsen, R., Seraphin, B., Libri, D., and Jensen, T. H. (2007) Dissecting mechanisms of nuclear mRNA surveillance in THO-sub2 complex mutants. *EMBO J.* **26,** 2317–2326
10. Galy, V., Gadal, O., Fromont-Racine, M., Romano, A., Jacquier, A., and Nehrbass, U. (2004) Nuclear retention of unspliced mRNAs in yeast is mediated by perinuclear Mlp1. *Cell* **116,** 63–73
11. Linder, P., and Jankowsky, E. (2011) From unwinding to clamping. The DEAD-box RNA helicase family. *Nat. Rev. Mol. Cell Biol.* **12,** 505–516
12. Fairman, M. E., Maroney, P. A., Wang, W., Bowers, H. A., Gollnick, P., Nilsen, T. W., and Jankowsky, E. (2004) Protein displacement by

DEX(H/D) "RNA helicases" without duplex unwinding. *Science* **304,** 730–734
13. Del Campo, M., Mohr, S., Jiang, Y., Jia, H., Jankowsky, E., and Lambowitz, A. M. (2009) Unwinding by local strand separation is critical for the function of DEAD-box proteins as RNA chaperones. *J. Mol. Biol.* **389,** 674–693
14. Bhaskaran, H., and Russell, R. (2007) Kinetic redistribution of native and misfolded RNAs by a DEAD-box chaperone. *Nature* **449,** 1014–1018
15. Janknecht, R. (2010) Multitalented DEAD-box proteins and potential tumor promoters. p68 RNA helicase (DDX5) and its paralog, p72 RNA helicase (DDX17). *Am. J. Transl. Res.* **2,** 223–234
16. Bond, A. T., Mangus, D. A., He, F., and Jacobson, A. (2001) Absence of Dbp2p alters both non-sense-mediated mRNA decay and rRNA processing. *Mol. Cell. Biol.* **21,** 7366–7379
17. Nissan, T. A., Bassler, J., Petfalski, E., Tollervey, D., and Hurt, E. (2002) 60 S pre-ribosome formation viewed from assembly in the nucleolus until export to the cytoplasm. *EMBO J.* **21,** 5539–5547
18. Barta, I., and Iggo, R. (1995) Autoregulation of expression of the yeast Dbp2p "DEAD-box" protein is mediated by sequences in the conserved DBP2 intron. *EMBO J.* **14,** 3800–3808
19. Banroques, J., Cordin, O., Doère, M., Linder, P., and Tanner, N. K. (2008) A conserved phenylalanine of motif IV in superfamily 2 helicases is required for cooperative, ATP-dependent binding of RNA substrates in DEAD-box proteins. *Mol. Cell. Biol.* **28,** 3359–3371
20. Noble, K. N., Tran, E. J., Alcázar-Román, A. R., Hodge, C. A., Cole, C. N., and Wente, S. R. (2011) The Dbp5 cycle at the nuclear pore complex during mRNA export II. Nucleotide cycling and mRNP remodeling by Dbp5 are controlled by Nup159 and Gle1. *Genes Dev.* **25,** 1065–1077
21. Johnson, S. A., Cubberley, G., and Bentley, D. L. (2009) Cotranscriptional recruitment of the mRNA export factor Yra1 by direct interaction with the 3′ end processing factor Pcf11. *Mol. Cell* **33,** 215–226
22. Pfaffl, M. W. (2001) A new mathematical model for relative quantification in real time RT-PCR. *Nucleic Acids Res.* **29,** e45
23. Güldener, U., Heck, S., Fielder, T., Beinhauer, J., and Hegemann, J. H. (1996) A new efficient gene disruption cassette for repeated use in budding yeast. *Nucleic Acids Res.* **24,** 2519–2524
24. Sikorski, R. S., and Hieter, P. (1989) A system of shuttle vectors and yeast host strains designed for efficient manipulation of DNA in *Saccharomyces cerevisiae*. *Genetics* **122,** 19–27
25. Gelbart, M. E., Rechsteiner, T., Richmond, T. J., and Tsukiyama, T. (2001) Interactions of Isw2 chromatin remodeling complex with nucleosomal arrays. Analyses using recombinant yeast histones and immobilized templates. *Mol. Cell. Biol.* **21,** 2098–2106
26. Hartzog, G. A., Wada, T., Handa, H., and Winston, F. (1998) Evidence that Spt4, Spt5, and Spt6 control transcription elongation by RNA polymerase II in *Saccharomyces cerevisiae*. *Genes Dev.* **12,** 357–369
27. Prather, D., Krogan, N. J., Emili, A., Greenblatt, J. F., and Winston, F. (2005) Identification and characterization of Elf1, a conserved transcription elongation factor in *Saccharomyces cerevisiae*. *Mol. Cell. Biol.* **25,** 10122–10135
28. Cheung, V., Chua, G., Batada, N. N., Landry, C. R., Michnick, S. W., Hughes, T. R., and Winston, F. (2008) Chromatin- and transcription-related factors repress transcription from within coding regions throughout the *Saccharomyces cerevisiae* genome. *PLoS Biol.* **6,** e277
29. Houseley, J., Rubbi, L., Grunstein, M., Tollervey, D., and Vogelauer, M. (2008) An ncRNA modulates histone modification and mRNA induction in the yeast GAL gene cluster. *Mol. Cell* **32,** 685–695
30. Greger, I. H., and Proudfoot, N. J. (1998) Poly(A) signals control both transcriptional termination and initiation between the tandem *GAL10* and *GAL7* genes of S*accharomyces cerevisiae*. *EMBO J.* **17,** 4771–4779
31. Nagalakshmi, U., Wang, Z., Waern, K., Shou, C., Raha, D., Gerstein, M., and Snyder, M. (2008) The transcriptional landscape of the yeast genome defined by RNA sequencing. *Science* **320,** 1344–1349
32. Yassour, M., Kaplan, T., Fraser, H. B., Levin, J. Z., Pfiffner, J., Adiconis, X., Schroth, G., Luo, S., Khrebtukova, I., Gnirke, A., Nusbaum, C., Thompson, D. A., Friedman, N., and Regev, A. (2009) *Ab initio* construction of a eukaryotic transcriptome by massively parallel mRNA sequencing. *Proc. Natl. Acad. Sci. U.S.A.* **106,** 3264–3269
33. Banroques, J., Cordin, O., Doère, M., Linder, P., and Tanner, N. K. (2011) Analyses of the functional regions of DEAD-box RNA "helicases" with deletion and chimera constructs tested *in vivo* and *in vitro*. *J. Mol. Biol.* **413,** 451–472
34. Huang, Y., and Liu, Z. R. (2002) The ATPase, RNA unwinding, and RNA binding activities of recombinant p68 RNA helicase. *J. Biol. Chem.* **277,** 12810–12815
35. Cordin, O., Banroques, J., Tanner, N. K., and Linder, P. (2006) The DEAD-box protein family of RNA helicases. *Gene* **367,** 17–37
36. Huh, W. K., Falvo, J. V., Gerke, L. C., Carroll, A. S., Howson, R. W., Weissman, J. S., and O'Shea, E. K. (2003) Global analysis of protein localization in budding yeast. *Nature* **425,** 686–691
37. Riles, L., Shaw, R. J., Johnston, M., and Reines, D. (2004) Large scale screening of yeast mutants for sensitivity to the IMP dehydrogenase inhibitor 6-azauracil. *Yeast* **21,** 241–248
38. Keogh, M. C., Kurdistani, S. K., Morris, S. A., Ahn, S. H., Podolny, V., Collins, S. R., Schuldiner, M., Chin, K., Punna, T., Thompson, N. J., Boone, C., Emili, A., Weissman, J. S., Hughes, T. R., Strahl, B. D., Grunstein, M., Greenblatt, J. F., Buratowski, S., and Krogan, N. J. (2005) Cotranscriptional set2 methylation of histone H3 lysine 36 recruits a repressive Rpd3 complex. *Cell* **123,** 593–605
39. Dichtl, B., Blank, D., Ohnacker, M., Friedlein, A., Roeder, D., Langen, H., and Keller, W. (2002) A role for SSU72 in balancing RNA polymerase II transcription elongation and termination. *Mol. Cell* **10,** 1139–1150
40. Du, H. N., and Briggs, S. D. (2010) A nucleosome surface formed by histone H4, H2A, and H3 residues is needed for proper histone H3 Lys-36 methylation, histone acetylation, and repression of cryptic transcription. *J. Biol. Chem.* **285,** 11704–11713
41. Kaplan, C. D., Laprade, L., and Winston, F. (2003) Transcription elongation factors repress transcription initiation from cryptic sites. *Science* **301,** 1096–1099
42. Quan, T. K., and Hartzog, G. A. (2010) Histone H3K4 and K36 methylation, Chd1 and Rpd3S oppose the functions of *Saccharomyces cerevisiae* Spt4-Spt5 in transcription. *Genetics* **184,** 321–334
43. Sellick, C. A., Campbell, R. N., and Reece, R. J. (2008) Galactose metabolism in yeast structure and regulation of the Leloir pathway enzymes and the genes encoding them. *Int. Rev. Cell Mol. Biol.* **269,** 111–150
44. Zhou, H., and Winston, F. (2001) NRG1 is required for glucose repression of the *SUC2* and *GAL* genes of *Saccharomyces cerevisiae*. *BMC Genet.* **2,** 5
45. Geisler, S., Lojek, L., Khalil, A. M., Baker, K. E., and Coller, J. (2012) Decapping of long noncoding RNAs regulates inducible genes. *Mol. Cell* **45,** 279–291
46. Pinskaya, M., Gourvennec, S., and Morillon, A. (2009) H3 lysine 4 di- and tri-methylation deposited by cryptic transcription attenuates promoter activation. *EMBO J.* **28,** 1697–1707
47. Rondón, A. G., Mischo, H. E., Kawauchi, J., and Proudfoot, N. J. (2009) Fail-safe transcriptional termination for protein-coding genes in *S. cerevisiae*. *Mol. Cell* **36,** 88–98
48. Kaplan, C. D., Holland, M. J., and Winston, F. (2005) Interaction between transcription elongation factors and mRNA 3′ end formation at the *Saccharomyces cerevisiae* GAL10-GAL7 locus. *J. Biol. Chem.* **280,** 913–922
49. Tran, E. J., Zhou, Y., Corbett, A. H., and Wente, S. R. (2007) The DEAD-box protein Dbp5 controls mRNA export by triggering specific RNA:protein remodeling events. *Mol. Cell* **28,** 850–859
50. Strässer, K., Masuda, S., Mason, P., Pfannstiel, J., Oppizzi, M., Rodriguez-Navarro, S., Rondón, A. G., Aguilera, A., Struhl, K., Reed, R., and Hurt, E. (2002) TREX is a conserved complex coupling transcription with messenger RNA export. *Nature* **417,** 304–308
51. Fasken, M. B., and Corbett, A. H. (2009) Mechanisms of nuclear mRNA quality control. *RNA Biol.* **6,** 237–241
52. Jarmoskaite, I., and Russell, R. (2011) DEAD-box proteins as RNA helicases and chaperones. *Wiley Interdiscip. Rev. RNA* **2,** 135–152
53. Sinan, S., Yuan, X., and Russell, R. (2011) The Azoarcus group I intron ribozyme misfolds and is accelerated for refolding by ATP-dependent RNA chaperone proteins. *J. Biol. Chem.* **286,** 37304–37312
54. Rougemaille, M., and Libri, D. (2011) Control of cryptic transcription in eukaryotes. *Adv. Exp. Med. Biol.* **702,** 122–131
55. Kuehner, J. N., Pearson, E. L., and Moore, C. (2011) Unraveling the means

to an end. RNA polymerase II transcription termination. *Nat. Rev. Mol. Cell Biol.* **12,** 283–294
56. Steinmetz, E. J., Warren, C. L., Kuehner, J. N., Panbehi, B., Ansari, A. Z., and Brow, D. A. (2006) Genome-wide distribution of yeast RNA polymerase II and its control by Sen1 helicase. *Mol. Cell* **24,** 735–746
57. Steinmetz, E. J., Conrad, N. K., Brow, D. A., and Corden, J. L. (2001) RNA-binding protein Nrd1 directs poly(A)-independent 3′ end formation of RNA polymerase II transcripts. *Nature* **413,** 327–331
58. O'Sullivan, J. M., Tan-Wong, S. M., Morillon, A., Lee, B., Coles, J., Mellor, J., and Proudfoot, N. J. (2004) Gene loops juxtapose promoters and terminators in yeast. *Nat. Genet.* **36,** 1014–1018
59. Lainé, J. P., Singh, B. N., Krishnamurthy, S., and Hampsey, M. (2009) A physiological role for gene loops in yeast. *Genes Dev.* **23,** 2604–2609
60. Ansari, A., and Hampsey, M. (2005) A role for the CPF 3′ end processing machinery in RNAP II-dependent gene looping. *Genes Dev.* **19,** 2969–2978
61. Brickner, J. H. (2009) Transcriptional memory at the nuclear periphery. *Curr. Opin. Cell Biol.* **21,** 127–133
62. Kim, H. D., Choe, J., and Seo, Y. S. (1999) The *sen1*$^+$ gene of *Schizosaccharomyces pombe*, a homologue of budding yeast SEN1, encodes an RNA and DNA helicase. *Biochemistry* **38,** 14697–14710
63. Mischo, H. E., Gómez-González, B., Grzechnik, P., Rondón, A. G., Wei, W., Steinmetz, L., Aguilera, A., and Proudfoot, N. J. (2011) Yeast Sen1 helicase protects the genome from transcription-associated instability. *Mol. Cell* **41,** 21–32
64. Skourti-Stathaki, K., Proudfoot, N. J., and Gromak, N. (2011) Human senataxin resolves RNA/DNA hybrids formed at transcriptional pause sites to promote Xrn2-dependent termination. *Mol. Cell* **42,** 794–805
65. Aguilera, A., and García-Muse, T. (2012) R loops. From transcription by-products to threats to genome stability. *Mol. Cell* **46,** 115–124
66. Gómez-González, B., García-Rubio, M., Bermejo, R., Gaillard, H., Shirahige, K., Marín, A., Foiani, M., and Aguilera, A. (2011) Genome-wide function of THO/TREX in active genes prevents R-loop-dependent replication obstacles. *EMBO J.* **30,** 3106–3119
67. Houseley, J., Kotovic, K., El Hage, A., and Tollervey, D. (2007) Trf4 targets ncRNAs from telomeric and rDNA spacer regions and functions in rDNA copy number control. *EMBO J.* **26,** 4996–5006
68. Yadon, A. N., Van de Mark, D., Basom, R., Delrow, J., Whitehouse, I., and Tsukiyama, T. (2010) Chromatin remodeling around nucleosome-free regions leads to repression of noncoding RNA transcription. *Mol. Cell. Biol.* **30,** 5110–5122
69. Kar, A., Fushimi, K., Zhou, X., Ray, P., Shi, C., Chen, X., Liu, Z., Chen, S., and Wu, J. Y. (2011) RNA helicase p68 (DDX5) regulates tau exon 10 splicing by modulating a stem-loop structure at the 5′ splice site. *Mol. Cell. Biol.* **31,** 1812–1821
70. Suzuki, H. I., Yamagata, K., Sugimoto, K., Iwamoto, T., Kato, S., and Miyazono, K. (2009) Modulation of microRNA processing by p53. *Nature* **460,** 529–533
71. Cohen, A. A., Geva-Zatorsky, N., Eden, E., Frenkel-Morgenstern, M., Issaeva, I., Sigal, A., Milo, R., Cohen-Saidon, C., Liron, Y., Kam, Z., Cohen, L., Danon, T., Perzov, N., and Alon, U. (2008) Dynamic proteomics of individual cancer cells in response to a drug. *Science* **322,** 1511–1516
72. Fuller-Pace, F. V., and Moore, H. C. (2011) RNA helicases p68 and p72. Multifunctional proteins with important implications for cancer development. *Future Oncol.* **7,** 239–251
73. Zuker, M. (2003) Mfold web server for nucleic acid folding and hybridization prediction. *Nucleic Acids Res.* **31,** 3406–3415
74. Tajima, M., Nogi, Y., and Fukasawa, T. (1986) Duplicate upstream activating sequences in the promoter region of the *Saccharomyces cerevisiae GAL7* gene. *Mol. Cell. Biol.* **6,** 246–256

The DEAD-box Protein Dbp2 Functions with the RNA-Binding Protein Yra1 to Promote mRNP Assembly

Wai Kit Ma, Sara C. Cloutier and Elizabeth J. Tran

Department of Biochemistry, *Purdue University, BCHM 305, 175 South University Street, West Lafayette, IN 47907-2063, USA*
Purdue University Center for Cancer Research, *Purdue University, Hansen Life Sciences Research Building, Room 141, 201 South University Street, West Lafayette, IN 47907-2064, USA*

Correspondence to Elizabeth J. Tran: *Department of Biochemistry, Purdue University, BCHM 305, 175 South University Street, West Lafayette, IN 47907-2063, USA. ejtran@purdue.edu*
http://dx.doi.org/10.1016/j.jmb.2013.05.016
Edited by A. Pyle

Abstract

Eukaryotic gene expression involves numerous biochemical steps that are dependent on RNA structure and ribonucleoprotein (RNP) complex formation. The DEAD-box class of RNA helicases plays fundamental roles in formation of RNA and RNP structure in every aspect of RNA metabolism. In an effort to explore the diversity of biological roles for DEAD-box proteins, our laboratory recently demonstrated that the DEAD-box protein Dbp2 associates with actively transcribing genes and is required for normal gene expression in *Saccharomyces cerevisiae*. We now provide evidence that Dbp2 interacts genetically and physically with the mRNA export factor Yra1. In addition, we find that Dbp2 is required for *in vivo* assembly of mRNA-binding proteins Yra1, Nab2, and Mex67 onto poly(A)+ RNA. Strikingly, we also show that Dbp2 is an efficient RNA helicase *in vitro* and that Yra1 decreases the efficiency of ATP-dependent duplex unwinding. We provide a model whereby messenger ribonucleoprotein (mRNP) assembly requires Dbp2 unwinding activity and once the mRNP is properly assembled, inhibition by Yra1 prevents further rearrangements. Both Yra1 and Dbp2 are conserved in multicellular eukaryotes, suggesting that this constitutes a broadly conserved mechanism for stepwise assembly of mature mRNPs in the nucleus.

Introduction

Over the last several decades, major advances have been made in our understanding of RNA structures and the parameters for RNA folding *in vivo* and *in vitro*.[1,2] Unlike DNA, cellular RNAs have a high propensity to form intramolecular helices and tertiary contacts that are central to the functionality of the given RNA molecule.[1,3–5] Proper folding is critical for small ribozymes not only to form active sites but also to enable highly efficient catalysis.[1,3,5] This is also the case for more complex RNAs, such as the 18 and 28S ribosomal (r)RNAs, which also assemble with RNA-binding proteins to form a fully functional translational apparatus.[6,7]

Strikingly, while it is now common knowledge that cellular RNAs such as rRNAs, transfer RNAs (tRNAs), and spliceosomal (sn)RNAs are all highly structured and intrinsically dynamic, our knowledge regarding messenger RNA (mRNA) structure has lagged behind.[8] One possible explanation for this discrepancy is that, unlike other RNAs, mRNAs are highly heterogeneous in sequence, length, and assembly with RNA-binding proteins. Moreover, both the structure and composition of a given messenger ribonucleoprotein (mRNP) complex change at different steps during synthesis, maturation, and translation.[9,10] Computational predictions and genome-wide *in vivo* analyses demonstrate that mRNAs have significant secondary structure and this characteristic is likely a critical aspect of gene regulation.[2,11,12] However, key mechanistic questions regarding the factors that are required for proper folding of mRNAs and subsequent assembly of the mRNA into an mRNP have not been fully addressed.

One class of enzymes that controls cellular RNA structure is the DEAD-box RNA helicase family.

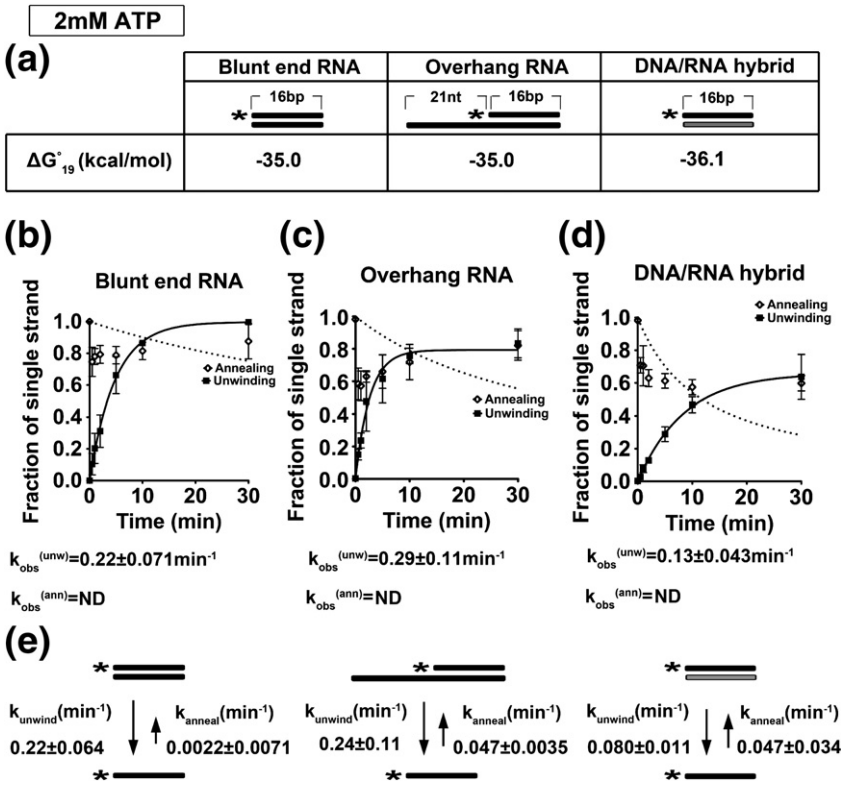

Fig. 1. Dbp2 displays ATP-dependent duplex unwinding on multiple RNA substrates at 2 mM ATP:Mg^{2+}. (a) Schematic representation and thermodynamic stability of RNA duplex substrates. All RNA substrates were designed with similar stability, which was calculated using the Nearest-Neighbor Database and converting to ΔG°_{19} using $\Delta G^{\circ} = \Delta H^{\circ} - T\Delta S^{\circ}$.[25,26] Black or gray coloring denotes RNA or DNA strands, respectively, whereas asterisks mark the position of the ^{32}P-radiolabeled 5′ end. (b) Graphical representations of unwinding and annealing assays using radiolabeled 16-bp blunt end RNA duplexes, (c) 21-nt overhang that is 3′ to the 16-bp RNA duplexes, and (d) 16-bp blunt end RNA-DNA hybrids. Reactions were performed at 19 °C with 2 mM ATP:Mg^{2+}, 0.1 nM radiolabeled duplex, and 600 nM recombinant, purified Dbp2. The fraction of the single-stranded substrate at each time point is plotted as the average of three independent reactions with standard deviations from the mean. The data were fitted to the integrated form of a homogenous first-order rate law to determine the $k_{obs}^{(unw)}$. $k_{obs}^{(ann)}$ was determined using the integrated rate law for the bimolecular annealing reaction as previously described.[27] ND, not determined. Representative non-denaturing gels are shown in Fig. S2. (e) Kinetic parameters for Dbp2 unwinding and annealing at 2 mM ATP. The rate constants for Dbp2 unwinding and annealing were calculated as previously described.[27]

DEAD-box helicases are the largest class of enzymes within the RNA helicase superfamily, functioning in all aspects of RNA metabolism from transcription to translation.[13,14] DEAD-box RNA helicases are unique among other helicase enzyme families in that they are non-directional and non-processive, with maximal unwinding on duplexes that are one to one and a half turns of an A-form RNA helix. This activity makes DEAD-box proteins well suited for cellular RNAs, which rarely contain helices longer than 12 bp in length.[14] Furthermore, DEAD-box proteins exhibit a wide array of biochemical activities including duplex unwinding, RNA-binding protein displacement from single-stranded RNA, and RNA strand annealing.[13,14] Thus, although classically defined as helicases, these enzymes are more likely to function as cellular RNA chaperones that conduct a variety of biochemically distinct steps to properly assemble RNPs *in vivo*.

Three DEAD-box proteins, namely, Sub2, Dbp5, and Dbp2, have been implicated in nuclear gene expression steps in the budding yeast *Saccharomyces cerevisiae*.[14] The least well understood DEAD-box protein, however, is Dbp2. In multicellular eukaryotes, the Dbp2 ortholog p68 functions in multiple gene expression steps including precursor messenger RNA (pre-mRNA) splicing, microRNA processing, and regulation of transcription initiation.[15–17] This factor has also recently been linked to nuclear mRNA export and RNA quality control in yeast and metazoan cells.[18–20] Moreover, recent studies from our laboratory determined that Dbp2 is directly associated with transcriptionally active chromatin.[18] This suggests that Dbp2 may function as a co-transcriptional mRNA chaperone by facilitating proper mRNA folding, and likely mRNP formation, in the nucleus.

To shed light on the mechanisms governing mRNP structure and assembly, we focused on the biological and biochemical mechanism of Dbp2. Our results now show that Dbp2 is an efficient RNA helicase that promotes assembly of the RNA-binding proteins Yra1 and Nab2 and the export receptor Mex67 onto newly synthesized mRNA. We also demonstrate that Dbp2 interacts directly with Yra1 and that Yra1 inhibits the duplex unwinding activity of Dbp2. We speculate that this may be a common mode of regulation for other DEAD-box RNA

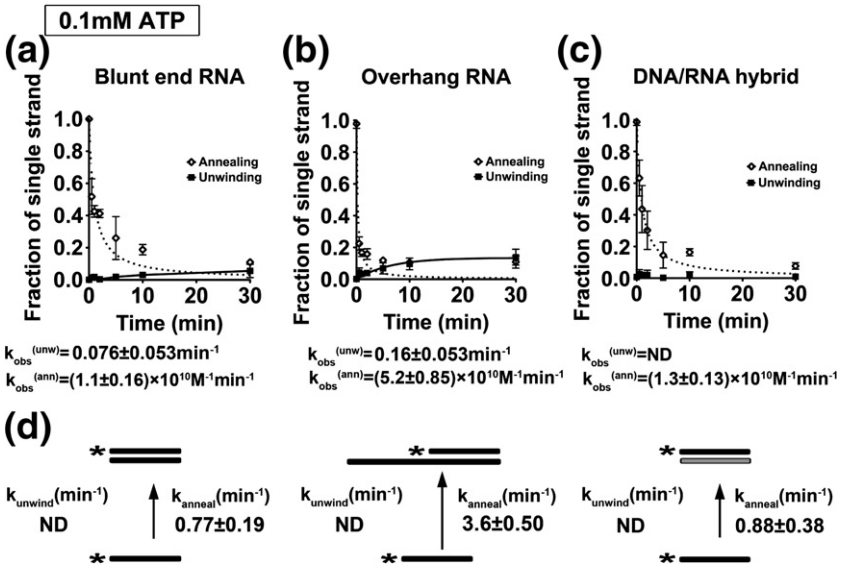

Fig. 2. Dbp2 exhibits a preference for strand annealing with single-stranded overhang RNA substrates at low ATP concentration. (a–c) Graphical representation of unwinding and annealing assays with 0.1 mM ATP using (a) the blunt end RNA duplex, (b) the RNA duplex with 3′ single-strand overhang, or (c) the blunt end RNA–DNA hybrid. Unwinding and annealing assays were conducted as above but with 0.1 mM ATP and 2 mM $MgCl_2$. Data from the unwinding and annealing assays were fitted as above. Representative non-denaturing gels are shown in Fig S3. (d) Kinetic parameters for Dbp2 unwinding at 0.1 mM ATP. Since there is little or no observable unwinding, the unwinding data cannot be fitted with the steady-state equation as mentioned above and are listed as ND (not determined). Therefore, we assumed that the $k_{obs}^{(ann)}$ is the same as k_{anneal} and converted the reported $k_{obs}^{(ann)}$ to the first-order rate constant as previously described.[27]

helicases. We provide a model whereby Dbp2 duplex unwinding and subsequent enzymatic inhibition are necessary to properly assemble mRNPs.

Results

Dbp2 catalyzes RNA duplex unwinding on blunt end and single-strand overhang substrates

Previous studies from our laboratory established that Dbp2 is an enzymatically active ATPase associated with transcribing genes.[18] Moreover, we found that loss of *DBP2* in budding yeast results in RNA quality control and termination defects, suggesting that Dbp2 may function in proper assembly of mRNPs in the nucleus. To shed light on the role of Dbp2 in gene expression, we first asked if Dbp2 is a bona fide RNA helicase *in vitro* and if this enzyme shows any preference for specific RNA duplex substrates. It is well established that DEAD-box proteins, with the exception of DbpA, show no sequence-specific association with RNA.[13] However, individual members display preferences for pure RNA duplexes and/or RNA-binding "platforms" for duplex unwinding.[21–24] To this end, we conducted an analysis of *in vitro* strand unwinding under pre-steady-state conditions with three different nucleic acid substrates and 2 mM ATP:Mg^{2+} in the presence of recombinant, purified Dbp2 (Fig. 1 and Fig. S1). These substrates include a 16-bp blunt-ended RNA duplex, a 16-bp duplex of identical sequence with a 21-nt single-stranded overhang, and a 16-bp RNA–DNA duplex with a different sequence but similar stability (Fig. 1a). The latter was chosen to account for the fact that RNA–DNA duplexes are less stable than their RNA–RNA counterparts and that the ability of DEAD-box RNA helicases to unwind a given substrate is inversely proportional to duplex stability.[28] The unwinding assays were then conducted with 600 nM of Dbp2 and preformed duplexes over a 30-min time frame (Fig. 1 and Fig. S2).

Consistent with other DEAD-box proteins, Dbp2 was able to unwind all three nucleic acid substrates with a preference for an RNA–RNA duplex (Fig. 1b–d). Importantly, we observed no ATP-independent unwinding activity, as evidenced from a lack of duplex destabilization after a 30-min incubation (Fig. S2a–c, lane 10). Unlike Ded1, which exhibits unwinding rate constants of ~0.1 min^{-1} or ~3.8 min^{-1} on blunt end or single-strand overhang duplexes, respectively,[21] Dbp2 showed no preferential unwinding of a duplexed RNA with a single-stranded region. This is evidenced by observed unwinding rates that are dependent upon the presence of Dbp2 and ATP (Fig. 1b–d, bottom; Fig. S2).

DEAD-box proteins also exhibit RNA strand annealing activity *in vitro*.[13] To measure annealing activity, we conducted the same assay as above but with the single-strand components for each substrate. This showed that the substrates have no spontaneous annealing activity whereas Dbp2 exhibits some annealing activity on all three substrates at 2 mM ATP (Fig. 1b–d; Fig. S2d–f). To determine the precise biochemical mechanism of Dbp2, we subsequently calculated rate constants for both unwinding and

annealing because the observed unwinding rate does not distinguish between these two parameters. Initial attempts to measure observed annealing rates at 2 mM ATP were complicated due to substantial unwinding activity. This resulted in a poor curve fit for annealing (open circles, Fig. 1b–d; Fig. S2). However, when this RNA strand annealing activity was taken into account according to the steady-state equation in Ref. 27, both the unwinding and annealing rate constants were accurately determined (Fig. 1e). The similar unwinding rate constants of ~0.2 min^{-1} for both blunt end and overhang substrates further demonstrated that Dbp2 does not require a single-stranded overhang for duplex destabilization (Fig. 1e). This is consistent with our previous studies demonstrating double-stranded RNA (dsRNA)-directed ATPase activity[18] and is similar to another DEAD-box protein, Mss116, whose activity is not enhanced by the presence of a single-stranded region within the RNA substrate.[22] This suggests that Dbp2 recognizes duplexed RNAs directly.

Dbp2 preferentially anneals RNA duplexes with single-stranded regions at low ATP concentrations

Studies of the human ortholog of Dbp2, termed p68, have shown that this enzyme promotes efficient annealing under ATP-limiting conditions.[29] As mentioned above, DEAD-box proteins also facilitate strand annealing and, in some cases, this activity is biologically relevant.[22,27,30–32] To determine if the annealing activity of Dbp2 is enhanced by reduced ATP concentrations, we conducted our unwinding and annealing assays again but with 20-fold less ATP (0.1 mM ATP). Consistent with previous studies

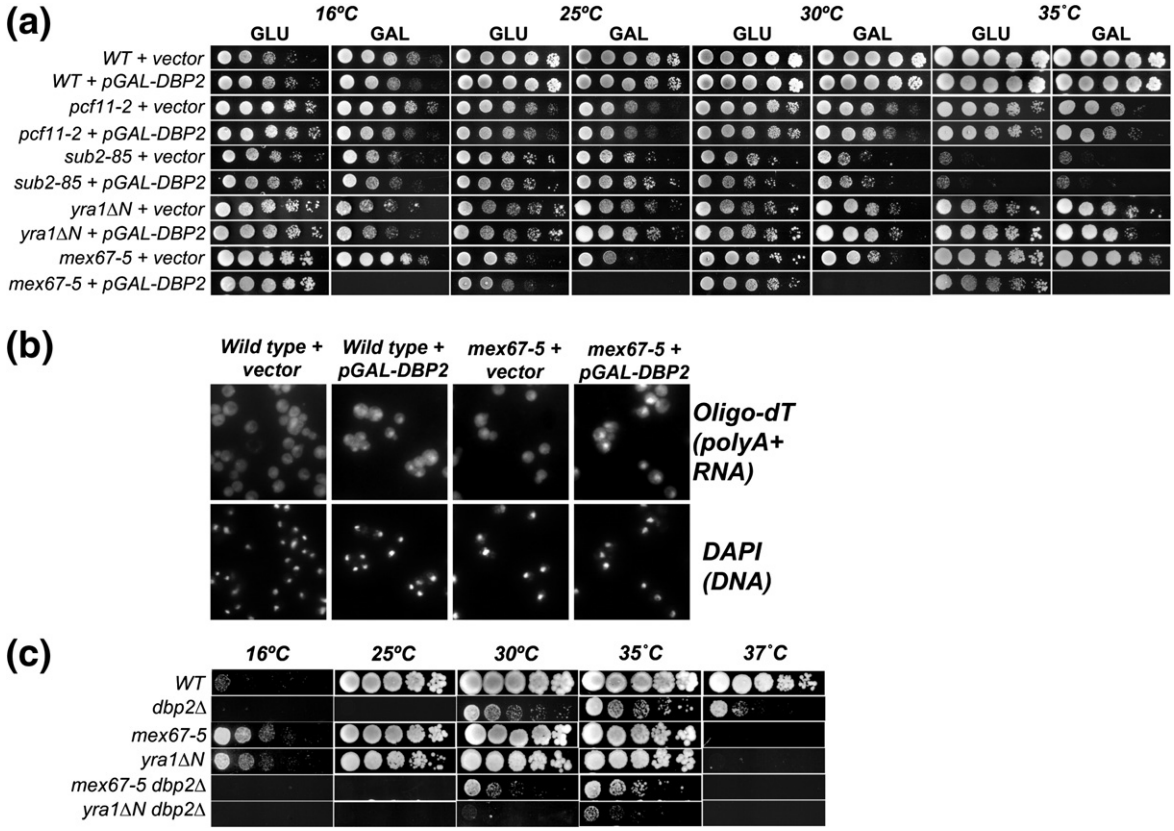

Fig. 3. *DBP2* displays genetic interactions with mRNA export factor mutants *mex67-5* and *yra1ΔN*. (a) Overexpression of *DBP2* is lethal in *mex67-5* strains. Indicated strains were transformed with empty vector or galactose-inducible pGAL-*DBP2*. Resulting transformants were then spotted in 5-fold serial dilutions onto transcriptionally repressive (glucose) or inducing (galactose) media and subsequently grown at the indicated temperatures from 16 to 35 °C. (b) Overexpression of *DBP2* in the *mex67-5* strain induces an mRNA export defect at the *mex67-5* permissive temperature. Briefly, yeast strains were grown at 25 °C to mid-log phase in selective media and then shifted to galactose-containing media for 1 h to induce *DBP2* overexpression. Cells were then harvested and *in situ* hybridization was conducted with oligodT_{30} to visualize accumulation of total poly(A)+ RNA. DAPI (4′,6-diamidino-2-phenylindole) staining of DNA shows the position of the nucleus. (c) Loss of *DBP2* in *yra1ΔN* strain results in a synthetic sick growth defect. The indicated double mutant strains were constructed using standard methods and were analyzed for growth defects as above by serial dilution analysis onto rich media. The *dbp2Δ* displays a cold-sensitive phenotype as previously described.[18]

of Ded1 and Mss116,[22,27] Dbp2 efficiently annealed all three nucleic acid substrates at low ATP concentrations with little to no detectable unwinding activity (Fig. 2a–c and Fig. S3). Moreover, Dbp2 also annealed overhang and blunt end RNA substrates in the absence of ATP (data not shown). In contrast to other DEAD-box proteins, however, Dbp2 exhibited a strong annealing preference for RNA substrates with a single-stranded overhang, resulting in a k_{anneal} of 3.60 ± 0.50 min^{-1} (Fig. 2d). This is approximately fourfold higher than the 0.8 min^{-1} rate observed for the blunt end RNA–RNA and RNA–DNA duplexes. To the best of our knowledge, this preference has not been observed for any other DEAD-box protein to date, suggesting that Dbp2 has a unique ability to preferentially anneal structured RNAs with single-stranded regions. In general, this is the type of secondary structure we expect to find in mRNAs, sporadic regions of duplex RNA flanked by single-stranded regions. We would therefore speculate that this activity might make Dbp2 a more effective chaperone for secondary-structure formation of cellular mRNAs under specific growth conditions with limited ATP (see Discussion).

DBP2 genetically interacts with mRNA export factors *YRA1* and *MEX67*

Given the biochemical activity of Dbp2, we speculated that Dbp2 functions as an RNA chaperone for newly synthesized mRNA. Previous studies from our laboratory have provided evidence that Dbp2 is required for early gene expression steps including termination and RNA quality control,[18] two processes intimately connected to mRNP assembly and export.[10,33–35] To pinpoint the precise biological role of Dbp2, we first conducted a series of genetic studies with a plasmid that overexpresses *DBP2* via a galactose-inducible promoter (*pGAL-DBP2*) and strains harboring mutations in genes linked to 3′ end formation and/or mRNA export. To this end, we selected yeast strains with mutations in the polyadenylation/cleavage factor *PCF11*,[36,37] the pre-mRNA splicing and export factor *SUB2*,[38,39] the RNA-binding protein gene *YRA1*,[40] and the mRNA export receptor *MEX67*,[41] with the idea that overexpression of *DBP2* might either rescue or enhance the growth defects of specific mutant strains. Yeast strains were transformed either with vector alone or with a *pGAL-DBP2* high-copy overexpression vector and then plated as fivefold serial dilutions onto either transcriptionally repressive (GLU) or inducing (GAL) media at multiple temperatures. Strikingly, whereas wild-type, *pcf11-2*, *sub2-85*, and *yra1ΔN* mutant strains displayed no obvious growth differences, overexpression of *DBP2* was lethal in *mex67-5* cells at all temperatures (Fig. 3a, bottom).

Because Mex67 is required for mRNA exit from the nucleus, we then asked if *DBP2* overexpression results in a perturbation of mRNA transport. This was addressed by conducting *in situ* hybridization assays to visualize the cellular localization of poly(A)+ RNAs by indirect immunofluorescence in wild-type or *mex67-5* cells with vector only or overexpressed *DBP2*. Importantly, these experiments were conducted at the permissive temperature for *mex67-5*, which does not typically result in accumulation of poly(A)+ RNAs in nucleus.[41] Whereas both wild-type and *mex67-5* cells showed diffuse, whole-cell staining in the presence of vector alone, *mex67-5* cells with overexpressed *DBP2* exhibited an accumulation of poly(A)+ RNA in the nucleus (Fig. 3b). We also observed a detectable accumulation of mRNA in the nucleus of wild-type cells upon overexpression of *DBP2* (Fig. 3b), even though we did not previously observe any growth defects in wild-type cells (Fig. 3a). It is of note that this nuclear poly(A)+ RNA accumulation is not as great as when the *mex67-5* cells are grown at the non-permissive temperature of 37 °C (Ref. 41 and data not shown), suggesting that the export block is modest or is a result of a secondary effect. Consistent with the latter, we observed no mRNA transport defects in a *dbp2Δ* strain (data not shown). Thus, *DBP2* overexpression induces a slight mRNA export defect in *mex67-5* cells, suggesting a role for this enzyme during or immediately prior to mRNA transport.

Mex67 is recruited to nascent mRNPs during transcription through protein–protein interactions with RNA-binding proteins Npl3, Yra1, and Nab2.[42–44] Interestingly, recent studies have documented an interaction between p68 and Aly, the human ortholog of Yra1.[19] This suggests that Dbp2 may be functionally connected to Mex67 recruitment through Yra1. To test this, we asked if loss of *DBP2* results in synthetic genetic interactions with *mex67-5* or *yra1ΔN* alleles by constructing double mutant strains and analyzing growth defects as above. Both the *mex67-5* and *yra1ΔN* strains failed to grow at 37 °C, whereas the *dbp2Δ* exhibits a previously documented cold-sensitive growth at 25 °C and below.[18,41,45] However, the *yra1ΔN dbp2Δ* strain displayed severely retarded growth at the permissive temperature for both single mutants alone (30 °C), suggesting that *DBP2* and *YRA1* are functionally linked (Fig. 3c). Loss of *DBP2* also results in a synthetic growth defect with *mex67-5*, albeit much weaker than with *yra1ΔN* (Fig. 3c). This suggests that Dbp2 and Yra1 function in a similar pathway and that Dbp2 is not directly required for mRNA export.

DBP2 is required for efficient association of Yra1, Nab2, and Mex67 with poly(A)+ RNA

mRNA is assembled with 12–30 different RNA-binding proteins to form co-transcriptionally assembled mRNPs.[46] Given the genetic interactions between *DBP2*, *YRA1*, and *MEX67* above, we

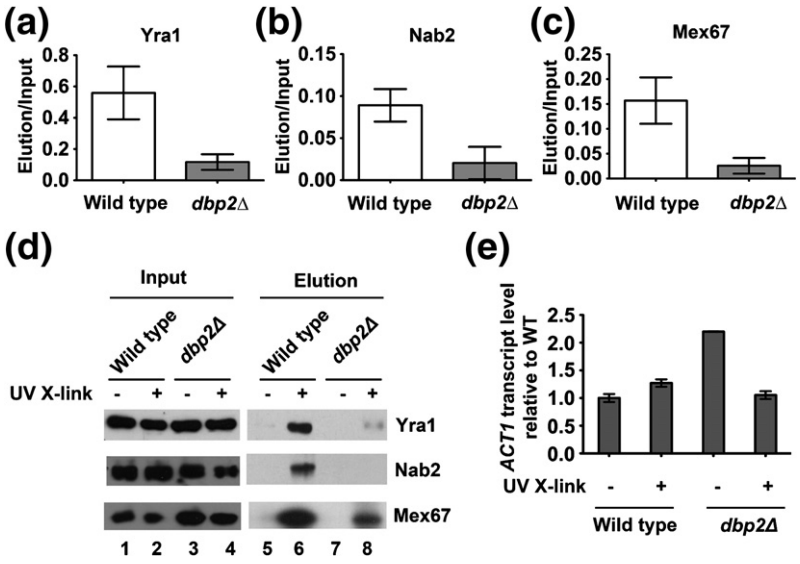

Fig. 4. Loss of *DBP2* results in reduced association of Yra1, Nab2, and Mex67 with poly(A)$^+$ RNA. *In vivo* UV cross-linking reveals reduced association of (a) Yra1, (b) Nab2, and (c) Mex67 with poly(A)$^+$ RNA in *dbp2Δ* cells. Wild-type and *dbp2Δ* cells were subjected to UV cross-linking followed by poly(A)+ RNA isolation as previously described.[48] The eluted fraction of wild-type and *dbp2Δ* cells was normalized to equal RNA concentration using equivalent A_{260nm} absorbance units. Proteins from the eluted fractions were detected by Western blotting. The relative quantity of poly(A)+ RNA-bound proteins was determined following quantification of the resulting isolated proteins from three independent biological replicates and is reported as the amount of isolated protein relative to total (input). (d) Representative Western blot of *in vivo* UV cross-linking. The total protein abundance (input) is shown along with the amount of isolated proteins with and without UV cross-linking. The latter serves as a background control to show that proteins isolated following UV cross-linking are not due to nonspecific interactions. (e) RT-qPCR shows efficient isolation of ACT1 mRNA from both wild-type and *dbp2Δ* cells following oligo-dT selection. Equal fractions of eluted RNA were reverse transcribed and subjected to qPCR with ACT1-specific primers as previously described.[18] Transcript levels were normalized by setting the wild-type elution without UV cross-linking to 1 and are a result of three technical replicates from one biological sample per strain.

asked if *DBP2* is required for efficient association of these RNA-binding proteins with mRNA. To test this, we conducted *in vivo* UV cross-linking and subsequently isolated poly(A)+ RNA from wild-type or *dbp2Δ* cells. We then analyzed the association of Yra1 and Mex67 by Western blotting the isolated fractions. We also analyzed Nab2, a nuclear poly(-A)-RNA-binding protein that interacts directly with both Yra1 and Mex67.[43,47] Strikingly, this analysis revealed that all three proteins, Yra1, Nab2, and Mex67, exhibit reduced association with poly(A)+ RNA in *dbp2Δ* cells (Fig. 4a–c). This decrease is not due to differences in UV-independent, nonspecific binding, as evidenced by a representative Western blot (Fig. 4d). Furthermore, analysis of *ACT1* transcript abundance by reverse transcription-quantitative PCR (RT-qPCR) revealed that this reduction in *dbp2Δ* cells is not due to mRNA isolation efficiency (Fig. 4e). Thus, Dbp2 is required for efficient association of Yra1, Nab2, and Mex67 with poly(A)+ RNA, consistent with a role in nuclear mRNP assembly.

Dbp2 physically interacts with Yra1 *in vivo* and *in vitro*

Many DEAD-box proteins associate with protein cofactors that either regulate the enzymatic activity or direct the biological role of a given DEAD-box enzyme.[49] Two independent studies have identified Dbp2 as a component of Yra1-bound protein complexes, suggesting that Dbp2 may interact directly with Yra1.[50,51] To test this, we first confirmed the previous interaction by asking if Yra1 copurifies with a genomically encoded, tandem affinity purification (TAP)-tagged Dbp2 in yeast cells, which consists of two IgG-binding units of Protein A, a tobacco etch virus (TEV) cleavage site and the calmodulin-binding peptide that is fused to Dbp2 (Fig. 5a). An untagged wild-type strain was utilized as a negative control for background association of Yra1 with the IgG-bound magnetic beads. Consistent with the previous studies, selection of Dbp2-TAP resulted in copurification of Yra1 (Fig. 5a). No Yra1 was detected in our background control, indicating that the interaction is Dbp2 dependent. Next, we asked if the association between Dbp2 and Yra1 is direct by conducting protein pull downs with recombinant, purified proteins expressed in *Escherichia coli*. Dbp2 and Yra1 were expressed as N-terminal His-tag or glutathione *S*-transferase (GST)-tag fusion proteins, respectively, and then purified to homogeneity by standard affinity chromatography methods. The proteins were then incubated together, selected on glutathione resin selection, resolved by SDS-PAGE electrophoresis, and visualized by Coomassie staining (Fig. 5b). Dbp5 is another DEAD-box protein that was used as negative control for nonspecific interactions. Whereas Dbp2 did not interact with beads alone or with Dbp5 (Fig. 5b, lanes 2 and 8), Dbp2 was copurified with GST-tagged Yra1 (Fig. 5b, lane 4). Dbp5, on the other hand, did not

copurify with GST-Yra1 (Fig. 5b, lane 6), further demonstrating the specificity of the interaction with Dbp2. Thus, Dbp2 interacts directly with Yra1.

Yra1 is an evolutionarily conserved RNA-binding protein and RNA export factor (REF).[40] Like other members of the REF protein family, Yra1 contains a central RNA recognition motif (RRM), two variable spacer regions, and highly conserved N- and C-termini (REF-N and REF-C, respectively) (Ref. 40 and Fig. 5c). Previous studies have shown that Mex67 interacts with the N-terminus (amino acids 1–77) and C-variable spacer region (amino acids 167–210) of Yra1, whereas the N-variable spacer region (amino acids 14–77) and C-variable spacer region (amino acids 167–210) of this protein are each sufficient to interact with RNA.[45] To determine what region of Yra1 is necessary for Dbp2 binding, we obtained bacterial expression plasmids for expression of two GST-tagged Yra1 truncation mutations that express either the RRM and C-terminal region (RRM + C) or the C-terminal region alone (yra1C) (Fig. 5c and Ref. 52). We then purified the truncation mutants and conducted pull-down assays as above. Interestingly, Dbp2 interacted with all three proteins, full-length Yra1, Yra1 RRM + C, and the C-terminus alone (Fig. 5d, lanes 6 and 8), suggesting that the C-terminus constitutes the Dbp2-binding domain. We then attempted to determine if the C-terminus is necessary for this interaction; however, we were unable to express the GST-yra1ΔC mutant in bacteria. Regardless, these studies suggest that Dbp2 interacts with the C-terminus of Yra1.

Yra1 inhibits the helicase activity of Dbp2

Many DEAD-box protein-binding factors also regulate the enzymatic activity of their respective RNA helicase. This includes the translation initiation factor eIF4A, whose helicase activity is activated by eIF4B, 4H and 4F, and eIF4AIII, whose ATPase activity is regulated by Y14 and MAGOH.[53–56] Thus, we asked if Yra1 modulates the helicase activity of Dbp2. To test this, we first conducted *in vitro* unwinding assays with Dbp2 in the presence of full-length Yra1. However, we were unable to accurately measure the unwinding activity of Dbp2 due to the previously documented strand annealing activity of Yra1 (Ref. 57 and data not shown). To resolve this problem, we then analyzed the annealing activity of the minimal Dbp2-interacting domain,

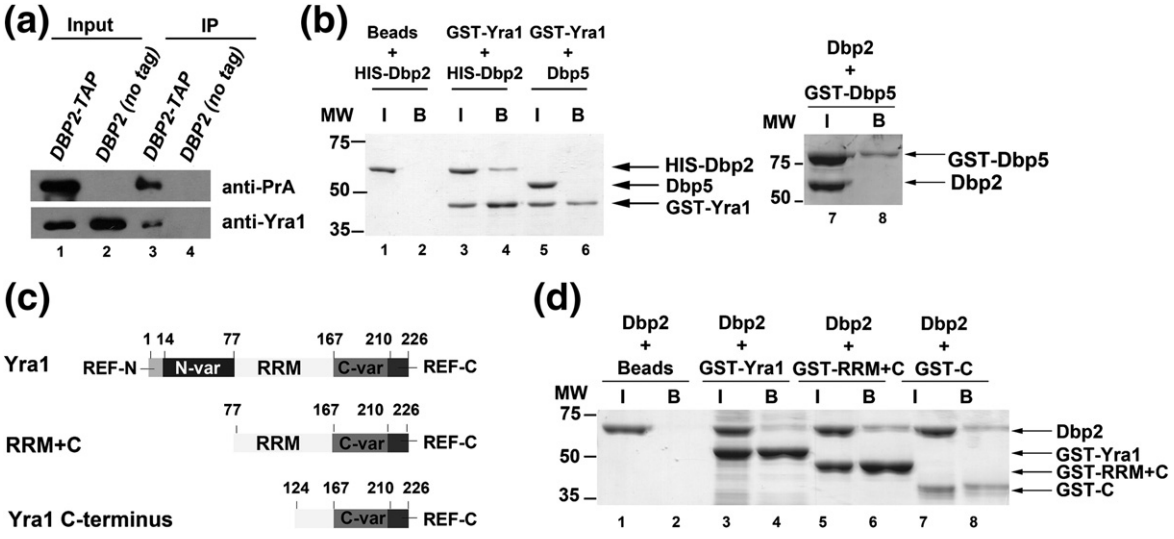

Fig. 5. Dbp2 physically interacts with Yra1 *in vivo* and *in vitro*. (a) Yra1 co-immunoprecipitates with Dbp2. Immunoprecipitation assays were performed from wild-type (*DBP2* no tag) and *DBP2-TAP* strains using IgG-conjugated dynabeads. Ten percent of the lysate was used as input. Proteins from the input and immunoprecipitated fractions were resolved by SDS-PAGE and detected by Western blotting analysis. (b) Dbp2 interacts directly with Yra1. *In vitro* pull-down assays were performed with recombinant, purified 6×His-tagged Dbp2 and GST-tagged Yra1. Briefly, recombinant, purified proteins were incubated together, 20% of the protein mix was removed as input ("I"), and interacting proteins were selected on glutathione Sepharose resin (bound "B" proteins). Proteins were resolved by SDS-PAGE electrophoresis and visualized by Coomassie staining. Neither GST-Yra1 nor Dbp2 co-elute with an unrelated DEAD-box protein Dbp5 (lanes 6 and 8), demonstrating that this interaction is specific. (c) Schematic representation of the primary sequence of Yra1, functional motifs, and truncation mutants. Yra1 is composed of evolutionarily conserved REF domains at the N- and C-terminus separated by variable regions.[40,42,45,52] Yra1 also contains a central RRM that does not appear to harbor RNA binding activity.[45] (d) The C-terminal half of Yra1 (amino acids 124–226) is sufficient to interact with Dbp2. GST-tagged Yra1 and truncation mutants were purified as recombinant proteins from *E. coli* and subjected to *in vitro* pull downs as above.

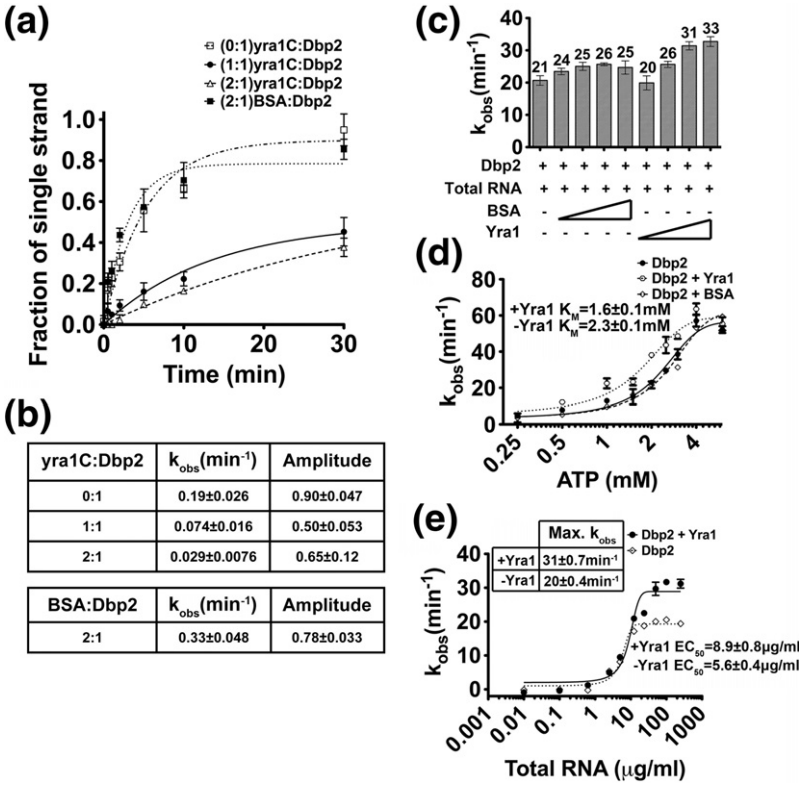

yra1C:Dbp2	k_{obs}(min^{-1})	Amplitude
0:1	0.19±0.026	0.90±0.047
1:1	0.074±0.016	0.50±0.053
2:1	0.029±0.0076	0.65±0.12

BSA:Dbp2	k_{obs}(min^{-1})	Amplitude
2:1	0.33±0.048	0.78±0.033

Fig. 6. Yra1 modulates the enzymatic activity of Dbp2. (a) Graphical representation of Dbp2 duplex unwinding with yra1C. Unwinding assays were conducted with the blunt end RNA duplex and either Dbp2 alone (600 nM) or yra1C (600 nM, 1200 nM) or BSA (1200 nM). Representative non-denaturing gels are shown in Fig. S4 and demonstrate that yra1C and BSA do not have intrinsic annealing activity. (b) The $k_{obs}^{(unw)}$ and the amplitude of the unwinding reaction. The $k_{obs}^{(unw)}$ and the amplitude are determined using the integrated rate law for a homogeneous first-order reaction as previously described.[27] (c) Full-length Yra1 moderately enhances ATP hydrolysis activity of Dbp2. *In vitro* ATPase assays were conducted with 200 nM of recombinant, purified Dbp2 and 250 μg/ml of total yeast RNA using a PK/lactate dehydrogenase enzyme-coupled absorbance-based detection method as previously described.[18] Recombinant, purified Yra1 was included where indicated at final concentrations from 100 to 600 nM. Equal concentrations of BSA were also tested to account for nonspecific interactions. The ATPase activity of Dbp2 alone is similar to previous publications and has already been characterized.[18] (d) Yra1 moderately enhances the ATP binding affinity of Dbp2. *In vitro* ATPase assays were conducted as above with constant amounts of Dbp2, Yra1, and total RNA (10 μg/ml); increasing amounts of ATP; and constant $MgCl_2$ (2 mM). Assays were also conducted with BSA in place of Yra1 to account for nonspecific effects. The K_m is indicative of the ATP binding affinity of Dbp2. (e) Yra1 slightly increases the amount of RNA necessary for activation of ATP hydrolysis. *In vitro* ATPase assays were conducted as above with 200 nM Dbp2, 400 nM Yra1, and increasing amounts of total yeast RNA. The amount of RNA necessary for 50% stimulation of maximum ATPase activity (EC_{50}) is reflective of the RNA binding affinity of Dbp2.

yra1C, which has previously been shown to have severely impaired RNA-binding activity *in vitro*.[45] Importantly, this revealed that the yra1C protein has no intrinsic annealing activity *in vitro* at the tested concentrations (Fig. S4e and f). To test the effect of yra1C on the unwinding activity of Dbp2, we conducted unwinding assays as above with the blunt end RNA duplex either with Dbp2 alone or with equimolar or twofold excess of Yra1 (Fig. 6). Strikingly, we found that yra1C decreased both the unwinding rate [$k_{obs}^{(unw)}$] and the amplitude of duplex unwinding by Dbp2 (Fig. 6a and b; Fig. S4a–c). In fact, the decreased unwinding rate is almost a full order of magnitude lower with yra1C (Fig. 6b). We also tested the unwinding activity of Dbp2 in the presence of twofold molar excess of bovine serum albumin (BSA) to show that the unwinding inhibition effect is specific to Yra1. Interestingly, this revealed a slight increase in the k_{obs} for unwinding most likely due to molecular crowding (Fig. 6a and b; Fig. S4d). This suggests that the inhibition of Dbp2 is specific to Yra1.

To elucidate the mechanism of inhibition, we then asked if Yra1 alters the ATPase activity of Dbp2 by conducting *in vitro* ATP hydrolysis assays with increasing concentrations of full-length Yra1 or BSA (Fig. 6c). Consistent with our previous studies, Dbp2 exhibited an observed ATP hydrolysis rate (k_{obs}) of 21 min^{-1} with saturating RNA (250 μg/ml of total yeast RNA) and 1 mM ATP (Fig. 6c). Whereas addition of BSA resulted in a slight enhancement of the k_{obs} from 21 to 25 min^{-1}, Yra1 gave a greater stimulation at each tested concentration. Thus, Yra1 slightly enhances the ATPase activity of Dbp2.

To determine if Yra1 enhances the ATPase rate by increasing the ATP-binding affinity of Dbp2, we measured the K_m for ATP with or without a twofold excess of Yra1 or BSA (Fig. 6d). This revealed that Yra1 reduces the K_m for ATP by ~30%, from 2.3 to 1.6 mM. This modest effect is similar to the observed increase in ATPase rate. Although moderate, this increase is specific for Yra1 as addition of BSA resulted in an ATPase curve that was superimposable with Dbp2 alone. This suggests that Yra1

stimulates the ATPase activity of Dbp2 through increasing the affinity for ATP. We suggest that this decrease in the K_m is biologically relevant because it occurs within the physiological range of cellular ATP concentrations.

Finally, we asked if Yra1 alters the effective RNA-binding activity of Dbp2. To this end, we measured the ATPase activity of Dbp2 as above but with a range of RNA concentrations from 1 ng/ml to 1 mg/ml (Fig. 6e). It is of note that the EC_{50} of Dbp2 alone is lower than our previous studies,[18] due to a more refined purification method for enzymatically active Dbp2 that increases its specific activity. Interestingly, inclusion of Yra1 increased the amount of RNA necessary for ATP hydrolysis by Dbp2 by ~50% (Fig. 6e). This suggests that Yra1 slightly reduces the RNA-binding affinity of Dbp2, while increasing the ATP binding and hydrolysis rate. We suggest that these subtle changes on the enzymatic parameters of Dbp2 result in release of Dbp2 from RNA, thereby inhibiting helicase activity *in vitro*. It is also possible that inhibition could also be due to Yra1 blocking initial association of Dbp2 with RNA. However, if this were the case, we would expect that Yra1 would reduce the RNA-dependent ATPase activity (Fig. 6c). Because we do not observe a decrease in RNA-dependent ATPase activity, this suggests that Yra1 inhibits duplex unwinding of Dbp2 through an as-of-yet uncharacterized mode distinct from other DEAD-box RNA helicase-interacting proteins.

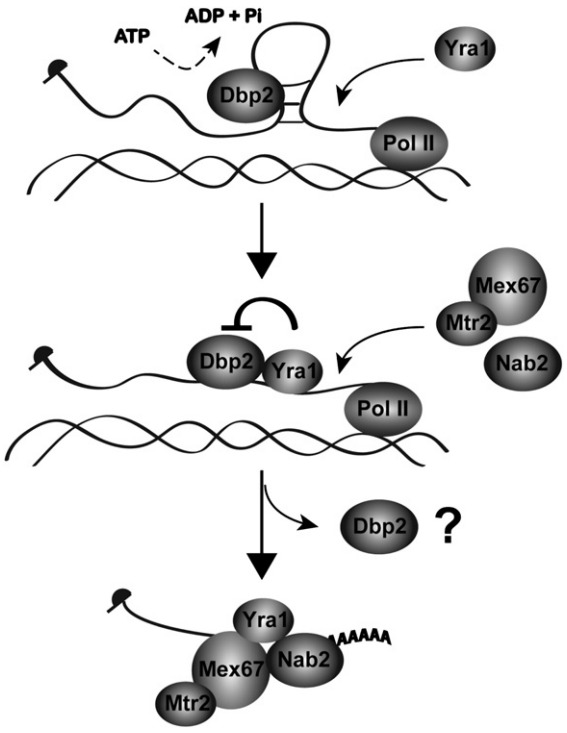

Fig. 7. Model for Dbp2-dependent loading of RNA-binding proteins onto mRNA. Yra1 is recruited to the actively transcribing loci through interacting with Sub2 or Pcf11 on the C-terminal domain of the RNA polymerase II.[52,58] However, structures of the nascent mRNA prevent association with Yra1. Dbp2 unwinds these structures co-transcriptionally in an ATP-dependent manner. This promotes mRNP assembly by facilitating loading of Yra1, Nab2, and Mex67 onto nascent mRNA. Mex67 is shown interacting with its heterodimerization partner, Mtr2.[59] Yra1 then inhibits the helicase activity of Dbp2 to prevent further remodeling of the assembled mRNP and may also promote release of Dbp2 from the RNA. This constitutes a biochemical mechanism of RNA helicase unwinding and subsequent inhibition during co-transcriptional assembly of mRNAs in the nucleus.

Taken together, we provide a model whereby Yra1 controls the enzymatic activity of Dbp2 to promote proper mRNP formation in the nucleus (Fig. 7). During transcription, Dbp2 unwinds aberrant structures on the nascent transcript that are refractory to RNA-binding protein assembly. This facilitates the loading of Yra1, Mex67, and Nab2 and likely other RNA-binding proteins onto the mRNA. The interaction of Yra1 with Dbp2 then inhibits duplex unwinding and possibly also promotes Dbp2 release. Alternatively, Dbp2 may remain bound to the mRNA as part of a Yra1–Dbp2 complex. If this were the case, Dbp2 would function similarly to eIF4AIII, which acts as an RNA clamp for a ribonucleoprotein complex.[55] With either scenario, we predict that inhibition of Dbp2 helicase activity by Yra1 prevents further remodeling of the properly assembled mRNP, as DEAD-box proteins can also efficiently remodel ribonucleoprotein complexes.[48,60,61] This constitutes a previously unknown mechanism for regulation of Dbp2 as well as the first biochemical mechanism for co-transcriptional assembly of an mRNP complex by this RNA helicase.

Discussion

Proper nuclear mRNP assembly is crucial for co-transcriptional and post-transcriptional processing steps including removal of introns by splicing, 3′ end cleavage and polyadenylation, as well as formation of a translationally competent mRNA.[10,62] During each of these steps, the evolving mRNP must assemble with a complement of RNA-binding proteins to direct the next step in the gene expression process. Our studies now provide evidence that the DEAD-box RNA helicase, Dbp2, plays a critical role in mRNP assembly in the nucleus. The human ortholog of Dbp2, termed p68, has been implicated in numerous transcriptional and post-transcriptional events, including transcriptional regulation, alternative splicing, and microRNA processing.[15,17,63,64] The fact that ectopic expression of human p68 in yeast fully complements the growth defects of *dbp2Δ* cells suggests that these roles are evolutionarily

conserved.[65] Given the multifaceted role, it is likely that p68 and Dbp2 are major players in the structural assembly of the transcriptome in all eukaryotes.

Our studies establish that Dbp2 is a bona fide RNA helicase, with efficient duplex unwinding activity on blunt-ended duplexes. This suggests that Dbp2 recognizes secondary structure directly, without the need for a single-stranded region for initial "loading" of the enzyme. This activity is consistent with a subset of DEAD-box family members with highly efficient duplex unwinding, such as CYT-19 and Mss116.[22,66–68] Moreover, it is consistent with our previous observation that Dbp2 displays dsRNA-directed ATPase activity.[18] Interestingly, whereas the core sequence is conserved among all DEAD-box protein family members, these three enzymes also contain C-terminal extensions. In fact, a recent biochemical and structural analysis of CYT-19 demonstrated that the C-terminal RGG motif of this enzyme functions as a "tether" to enable multiple rounds of duplex unwinding.[69]

Several DEAD-box proteins have been shown to utilize protein cofactors to trigger duplex unwinding by increasing the ATP binding or RNA-binding affinities of an inefficient DEAD-box enzyme.[54,70–72] Given the high duplex unwinding activity of Dbp2, however, inhibition may be the more important mode of regulation. In support of this, we find that Yra1 inhibits the helicase activity of Dbp2. The human ortholog of Dbp2, p68, was recently shown to interact with Aly, the human counterpart to Yra1,[19] suggesting that this regulation is conserved in higher eukaryotes. We speculate that *in vivo* the modulation of Dbp2 helicase activity by Yra1 is utilized to prevent further remodeling of the assembled mRNP. If this is the case, this would constitute a previously unrecognized mechanism for temporal regulation of DEAD-box enzymes *in vivo*. Although we do not know the mechanism for inhibition of duplex unwinding by Yra1, a recent study of Mss116 revealed that DEAD-box proteins are modular enzymes.[73] In fact, the C-terminal domain provides direct recognition of dsRNA duplexes whereas the N-terminal domain interacts with ATP.[73] The ability to couple ATP hydrolysis with duplex unwinding lies in the formation of a closed helicase with juxtaposed N- and C-terminal domains.[73] Because our studies suggest that Yra1 uncouples ATP hydrolysis from duplex unwinding, it will be interesting to determine the precise mechanism for Yra1-dependent inhibition of Dbp2.

Our studies show that Dbp2 is required for assembly of Yra1, Nab2, and Mex67 onto poly(A)+ RNA. It is well established that proper termination and 3′ end formation is required for mRNA export, as defects in these processes result in impaired recruitment of Mex67 to newly synthesized mRNAs and RNA decay.[35,74,75] The fact that loss of *DBP2* results in reduced association of Mex67, as well as the poly(A)+ RNA-binding protein Nab2, suggests that Dbp2 functions concert with termination and 3′ end formation. In support of this, loss of *DBP2* results in transcription of a bicistronic *GAL10–GAL7* mRNA, a characteristic phenotype of termination defects.[18] This idea is also consistent with our genetic analysis and the fact that *DBP2* overexpression resulted in lethality of *mex67-5* strains but not *sub2-85* or *pcf11-2* strains. This suggests that Dbp2 functions upstream of Mex67 but downstream or independent of Sub2 and Pcf11. Interestingly, Yra1 also interacts directly with all three of these proteins,[38,42,52] indicating that this small protein acts as a coupling factor for multiple co-transcriptional processing and assembly steps. Furthermore, recent studies from the Bentley laboratory have demonstrated that Pcf11 is required for recruitment of Yra1 to chromatin, which then functions to modulate poly(A) site selection.[52,76] Thus, the order of events for this process and role of Dbp2 in termination is an intriguing question for future studies.

In addition to canonical duplex unwinding, our studies also show that Dbp2 displays strong RNA strand annealing activity. This is not unprecedented as the DEAD-box protein Mss116 utilizes both annealing and duplex unwinding activities to promote folding of the ai5γ group II intron in mitochondria.[30–32] This would suggest that Dbp2 could function similarly; however, in contrast to Mss116, Dbp2 only displays significant annealing under ATP-limiting conditions. Interestingly, recent work from the Parker laboratory revealed that, under conditions of glucose starvation, the sub-cellular localization of numerous RNA-binding proteins is drastically altered.[77] This suggests that cellular ribonucleoprotein complexes undergo dynamic alterations in nutrient-limited conditions when cellular ATP concentrations are low. Thus, it will be interesting to determine the function of Dbp2 under specific physiological growth conditions, which may promote strand annealing.

Our studies now add Dbp2 to the complement of DEAD-box proteins that function in nuclear mRNP assembly in *S. cerevisiae*. This includes Sub2, which functions in both splicing and formation of an export-competent mRNP, and Dbp5, which promotes nuclear release of exporting transcripts.[14] When considering that rRNA biogenesis requires 21 of the 25 DEAD-box proteins in budding yeast,[14,78] one might ask why there aren't more DEAD-box RNA helicases associated with mRNP biogenesis. Unlike other cellular RNAs such as snRNAs, tRNAs, and rRNAs, mRNAs stand out as distinct as tertiary structure does not appear to play a large role in the functionality of these RNAs in eukaryotes. Given the propensity for RNAs to fold and misfold in solution,[1] the prevailing model is that co-transcriptional association of RNA-binding proteins maintains primarily linear structure of a nascent transcript.[10] Although the average length of an mRNA is 1 kb, pre-mRNA

transcripts can range from 3 kb to ~2.5 Mb, making it likely that DEAD-box helicases function as key structural modulators of the transcriptome. The challenge then will be defining the precise molecular rearrangements that require p68/Dbp2 or other members of the DEAD-box protein family given the highly coupled nature of nuclear gene expression steps. With the advancement in RNA sequence and target identification coupled with structural studies of mRNAs,[79] these questions can be addressed in the very near future.

Materials and Methods

Yeast strains, yeast plasmids, and bacterial plasmids

Corresponding data are listed in Tables 1 and 2.

Recombinant protein expression and purification

Expression of pMAL MBP-TEV-DBP2 in BL21 *E. coli* (DE3) cells (New England Bio Labs) was induced with 1 mM IPTG at 37 °C for 3 h and was subsequently purified from the soluble fraction using amylose resin according to the manufacturer's instructions (New England Bio Labs). The MBP tag was then cleaved with 50 U of TEV protease (Invitrogen) overnight at 16 °C. The cleaved Dbp2 was then subjected to cation-exchange chromatography with SP Sepharose (Sigma). Dbp2 was eluted in 50 mM Tris–HCl at pH 8 with 600 mM NaCl and 20% glycerol and stored at −80 °C until usage. Expression of pET28a His_6-*DBP2* in Rosetta *E. coli* (DE3) cells (Novagen) was induced by 0.2 mM IPTG at 16 °C and purified as previously described.[18] Two consecutive TEV sites were inserted between the GST-tag and the coding sequence of Yra1 by PCR using pFS1853 GST-Yra1 as a template, a set of primer pairs that contain the TEV sites coding sequence flanked next to the GST-tag and Yra1 coding sequence. Forward primer: 5′-GAAAACCTGTACTTCCAGGGAATGTCTGCTAACTTAGATAAATCCTTAGAC-3′; reverse primer: 5′-TCCCTGGAAGTACAGGTTTTCCTCGAGATGGTCGCCACCACCAAACGTGGC-3′. Expression of the GST-TEV-YRA1 in Rosetta *E. coli* (DE3) cells (Novagen) was induced by 0.2 mM IPTG overnight at 16 °C and was subsequently purified from the soluble fraction using glutathione Sepharose according to the manufacturer's instructions (GE Healthcare). The GST tag was then cleaved with 50 U of TEV protease (Invitrogen) overnight at 16 °C. The cleaved purified recombinant proteins were subsequently subjected to SP Sepharose (Sigma). Yra1 were eluted in 50 mM Tris–HCl at pH 8 with 600 mM NaCl and 20% glycerol and stored at −80 °C until usage. Expression of the pET21 GST-Yra1C and pET21 GST-Yra1 RRM + C in Rosetta *E. coli* (DE3) cells (Novagen) was induced by 0.2 mM IPTG overnight at 16 °C and was subsequently purified from the soluble fraction using glutathione Sepharose according to the manufacturer's instructions (GE Healthcare). The purified proteins were eluted with 20 mM glutathione, 150 mM NaCl, 20% glycerol, and 20 mM Hepes at pH 7.5 and stored at −80 °C until usage.

Table 1. Yeast and bacterial plasmids

Name	Description	Source/Reference
BTP13	pET28a-DBP2	31
pCEN/URA3	pRS316	40
pGAL1-GAL10-GAL7	pYGPM11714	Open Biosystems
BTP22	pMAL-TEV-Dbp2	This study
BTP27	GST-TEV-Yra1	This study
pSW3319	GST-Dbp5	41
pRS426	pURA3/2μ	40
pGAL-DBP2	pGAL-DBP2/2μ/URA3	Open Biosystems
GST-Yra1 C	pET21GST-Yra1 C	38
GST-Yra1 RRM+C	pET21GST-Yra1 RRM+C	38
psub2-85	psub2-85/CEN/TRP1	42

Table 2. Yeast strains

Strain	Genotype	Source
Wild type (BY4741)	MATa *his3Δ1 leu2Δ0 met15Δ0 ura3Δ0*	Open Biosystems
dbp2Δ (BTY115)	MATa dpb2::*KanMx ura3Δ0 leu2Δ0 his3Δ0 TRP1 met-lys*?	31
DBP2-TAP	Mata *DPB2::TAP:HIS3 his3Δ1 leu2Δ0 met15Δ0 ura3Δ0*	Open Biosystems
mex67-5	MATa *mex67::HIS3 ura3 ade2 his3 leu2 trp1 pTRP/CEN/mex67-5*	43
Wild type (W303)	MATa *ura3-1 ade2-1 his3-11, 15 leu2-1 trp1-1 can1-100*	R. Rothstein
yra1ΔN + Yra1	MATα *yra1::HIS3 ura3 ade2 ade3 leu2-1 trp1 pRS314-yra1ΔN +pHT4467Δ-YRA1 (with intron)*	42
pcf11-2	MATa *ura3-1 trpΔ ade2-1 leu2-3, 112 his3-11, 15 pcf11-2*	44
SUB2 shuffle	MATa *sub2:: HIS3 ade2 leu2, ura3, trp1 pCG788*	45

Unwinding assays

RNA oligonucleotides were purchased from Integrated DNA Technologies, and duplex substrates were prepared as previously described.[27,80] The blunt end RNA duplex sequences are as follows: (top strand) 5′-AGCACCGUAAAGACGC-3′ + (bottom strand) 5′-GCGUCUUUACGGUGCU-3′. The overhang RNA duplex sequences are as follows: (top strand) 5′-AGCACCGUAAAGACGC-3′ + (bottom strand) 5′-GCGUCUUUACGGUGCUUAAAACAAAACAAAACAAAAC-3′. The blunt end RNA/DNA duplex sequences are as follows: (top strand) 5′-GGCACGGUGGGGACCG-3′ + (bottom strand) 5′-CGGTCCCCACCGTGCC-3′. The top strand of the RNA duplex was 5′-end-labeled with [γ^{32}P]ATP using T4 polynucleotide kinase according to standard methods. *In vitro* unwinding assays were conducted as previously described[27] except for using 0.1 nM ^{32}P-labeled duplex in a 30-μl reaction mixture containing 40 mM Tris–HCl (pH 8), 50 mM NaCl, 2.5 mM $MgCl_2$, 2 mM DTT, 60 U Superase-in (Life Technologies), and 600 nM Dbp2 and 600 nM or 1200 nM of Yra1 where indicated. The reaction mixture was incubated in a 19 °C water bath for 10 min prior to the reaction. All reactions were performed at 19 °C. Unwinding reactions were initiated by adding ATP (2 mM or 0.1 mM as

indicated). At the times indicated, 3-μl aliquots were removed and the reaction was stopped with a buffer containing 1% SDS, 50 mM ethylenediaminetetraacetic acid (EDTA), 0.1% xylene cyanol, 0.1% bromophenol blue, and 20% glycerol. Aliquots were subsequently resolved on a 10% nondenaturing PAGE. The gels were dried and radiolabeled RNAs were quantified using ImageQuant software. The data from each time point were calculated using the following formula: fraction of single stranded = (single-stranded RNA/total RNA). The data were then fitted to the integrated form of a homogenous first-order rate law to determine the $k_{obs}^{(unw)}$.

The rate constants for unwinding k_{unw} and k_{ann} were determined using Frac ss = $k_{unw}(k_{unw} + k_{ann})_{-1}(1 - \exp(-(k_{unw} + k_{ann})t))$ as described in Ref. 27.

Annealing assays

In vitro annealing assays were performed in the presence of 2 mM or 0.1 mM ATP with the same reaction mixture as unwinding assays without the 10-min pre-incubation. The RNA duplex was denatured at 95 °C for 2 min to generate single-stranded RNAs. All the reactions were conducted in a 19 °C water bath and were initiated by addition of 0.1 nM of the denatured substrate strands. Aliquots of the reactions were treated as described in the unwinding assays. The data from each time point were calculated as described in the unwinding assays. The data were then fitted to the integrated rate law for the bimolecular annealing reaction to determine the $k_{obs}^{(ann)}$.

Cellular microscopy

In situ hybridization was performed on cells that were grown to mid-log phase at the permissive temperature (25 °C) with −URA + 2% glucose and then shifted to −URA + 2% galactose for a 1-h induction of *DBP2* overexpression. Cells were subsequently harvested, fixed with formaldehyde, and mounted on glass slides. Poly(A)+ RNA was then visualized by microscopy following hybridization with digoxigenin-conjugated oligodT_{50} and detection with fluorescein isothiocyanate-conjugated anti-digoxigenin secondary antibody (Roche) as previously described.[48] DAPI staining was utilized to visualize DNA.[48] Images were collected using an Olympus BX51 microscope using Metamorph software.

TAP-tag immunoprecipitation

Cells expressing genomically encoded Dbp2-TAP or untagged Dbp2 (BY4741) were grown in YPD at 30 °C to an OD_{600} of 0.6. Harvested cells were pelleted and injected into liquid nitrogen. The frozen cells were then lysed in the solid phase by milling, using a planetary ball mill. The lysed cells were subsequently resuspended in 15 ml of extraction buffer (20 mM Hepes at pH 7.4, 110 mM KoAc, 0.5% Triton X-100, 0.1% Tween-20, and 70 mM NaCl) in the presence of 1× protease inhibitor cocktail tablets (Roche) followed by centrifugation at 4700 rpm at 4 °C for 15 min as previously described.[81] The soluble fraction of the lysate was incubated with IgG-conjugated dynabeads at 4 °C for 30 min. The unbound protein was washed away with extraction buffer. The bound protein was eluted with 10 U of AcTEV protease (Life Technologies) followed by trichloroacetic acid precipitation. The proteins were then resolved by SDS-PAGE and detected by Western blotting analysis. Western blotting analysis was conducted with standard molecular biology techniques rabbit anti-Yra1,[52] rabbit anti-Protein A, and horseradish-peroxidase-conjugated goat anti-rabbit antibody (Sigma).

In vitro binding (pull down) assays

Twenty micrograms of recombinant, purified GST-Yra1, GST-Yra1 RRM + C, GST-Yra1 C, GST-Dbp5, His-Dbp2, Dbp5, or Dbp2 were incubated with the glutathione Sepharose in 20 mM Hepes, pH 7.5, 150 mM NaCl, and 20% glycerol at room temperature for 10 min as indicated following removal of 20% of the protein mixture for input. Bound proteins were eluted with 50 mM reduced glutathione in 20 mM Hepes, pH 7.5, 150 mM NaCl, and 20% glycerol and were resolved by SDS-PAGE followed by Coomassie staining.

In vitro ATPase assays

In vitro ATP hydrolysis assays were performed using a PK/lactate dehydrogenase enzyme-coupled absorbance assay as previously described,[18] but with 200 nM Dbp2 and increasing amounts of recombinant purified Yra1, total yeast RNA (Sigma), or ATP as indicated. Presented data are the average of three independent experiments and the error bars represent the standard deviation.

In vivo UV cross-linking assays

Wild-type and *dbp2Δ* yeast cells were grown in YPD at 30 °C. Mid-log phase cells were harvested and resuspended into 50 ml of 10 mM Tris–HCl at pH 7.5, 500 mM NaCl, and 1 mM EDTA. The resuspended cells were then subjected to UV light with 180,000 μJ/cm^2 on ice for 2.5 min using UV Stratalinker 1800. The UV treatment was conducted twice with 45-s pause in between each treatment. The cells were then centrifuged at 4000 rpm for 10 min at 4 °C. The pelleted cells were resuspended into 10 ml of 10 mM Tris–HCl at pH 7.5, 500 mM NaCl, 1 mM EDTA, 500 U of Superase-in (Life Technologies), 1 mM PMSF, and 0.5× of protease inhibitor cocktail tablets (Roche). The cells were then lysed by bead beating, cleared by centrifugation, and then subjected to poly(A)+ RNA pull down using oligo dT cellulose (Life Technologies). The RNA concentration from the eluted fraction was determined by measuring the absorbance at 260 nm. RNase treatment and trichloroacetic acid precipitation were then performed to recover bound proteins. Fractions were then resolved by SDS-PAGE and proteins were detected by Western blotting with rabbit anti-Nab2,[48] rabbit anti-Mex67,[82] rabbit anti-Yra1,[52] and horseradish-peroxidase-conjugated goat anti-rabbit antibodies (Promega).

RT-qPCR analysis

RNA was isolated from oligo dT-purified RNPs (see UV cross-linking) by standard acid phenol purification. Equal fractions from the elution were then reverse transcribed

into cDNA (Qiagen) and the quantity of *ACT1* RNA was measured by quantitative PCR using the BioRad CFX96 system. The sequences for *ACT1* primers were as follows: forward primer, 5′-TGGATTCCGGTGATGGTGTT3′; reverse primer, 5′-TCAAAATGGCGTGAGGTAGAGA-3′. The fold change of *ACT1* transcript abundance was calculated by normalizing the signal from each sample to the signal obtained from wild type without UV treatment and is reported as the average of three technical repeats with standard error from the mean.

Serial dilution growth assay

Indicated strains were grown in – URA + 2% glucose or YPD liquid cultures and then harvested at mid-log phase. Cells were then spotted in 5-fold serial dilutions onto – URA + 2% glucose, – URA + 2% galactose, or YPD plates and incubated at temperatures ranging from 16 to 37 °C as indicated.

Supplementary data to this article can be found online at http://dx.doi.org/10.1016/j.jmb.2013.05.016

Acknowledgements

We thank Barb Golden for constructive criticism regarding the manuscript. We also thank other members of the Tran laboratory for thoughtful discussions.

Received 14 March 2013;
Received in revised form 1 May 2013;
Accepted 18 May 2013
Available online 28 May 2013

Keywords:
RNA unwinding;
RNA annealing;
gene expression;
mRNP remodeling;
co-transcriptional

Abbreviations used:
pre-mRNA, precursor messenger RNA; mRNP, messenger ribonucleoprotein; TAP, tandem affinity purification; GST, glutathione *S*-transferase; RT-qPCR, reverse transcription-quantitative PCR; dsRNA, double-stranded RNA; TEV, tobacco etch virus; REF, RNA export factor; RRM, RNA recognition motif; BSA, bovine serum albumin; EDTA, ethylenediaminetetraacetic acid.

References

1. Zemora, G. & Waldsich, C. (2010). RNA folding in living cells. *RNA Biol.* **7**, 634–641.
2. Wan, Y., Qu, K., Ouyang, Z., Kertesz, M., Li, J., Tibshirani, R. *et al.* (2012). Genome-wide measurement of RNA folding energies. *Mol. Cell*, **48**, 169–181.
3. Woodson, S. A. (2010). Compact intermediates in RNA folding. *Annu. Rev. Biophys.* **39**, 61–77.
4. Treiber, D. K. & Williamson, J. R. (1999). Exposing the kinetic traps in RNA folding. *Curr. Opin. Struct. Biol.* **9**, 339–345.
5. Wilson, T. J., Nahas, M., Ha, T. & Lilley, D. M. (2005). Folding and catalysis of the hairpin ribozyme. *Biochem. Soc. Trans.* **33**, 461–465.
6. Woodson, S. A. (2008). RNA folding and ribosome assembly. *Curr. Opin. Chem. Biol.* **12**, 667–673.
7. Stern, S., Powers, T., Changchien, L. M. & Noller, H. F. (1989). RNA–protein interactions in 30S ribosomal subunits: folding and function of 16S rRNA. *Science*, **244**, 783–790.
8. Rajkowitsch, L., Chen, D., Stampfl, S., Semrad, K., Waldsich, C., Mayer, O. *et al.* (2007). RNA chaperones, RNA annealers and RNA helicases. *RNA Biol.* **4**, 118–130.
9. Moore, M. J. (2005). From birth to death: the complex lives of eukaryotic mRNAs. *Science*, **309**, 1514–1518.
10. Schmid, M. & Jensen, T. H. (2010). Nuclear quality control of RNA polymerase II transcripts. *Wiley Interdiscip. Rev. RNA*, **1**, 474–485.
11. Gaspar, P., Moura, G., Santos, M. A. & Oliveira, J. L. (2013). mRNA secondary structure optimization using a correlated stem–loop prediction. *Nucleic Acids Res.* **41**, e73.
12. Kertesz, M., Wan, Y., Mazor, E., Rinn, J. L., Nutter, R. C., Chang, H. Y. & Segal, E. (2010). Genome-wide measurement of RNA secondary structure in yeast. *Nature*, **467**, 103–107.
13. Putnam, A. A. & Jankowsky, E. (2013). DEAD-box helicases as integrators of RNA, nucleotide and protein binding. *Biochim. Biophys. Acta.* **1829**, 884–893.
14. Linder, P. & Jankowsky, E. (2011). From unwinding to clamping—the DEAD box RNA helicase family. *Nat. Rev. Mol. Cell Biol.* **12**, 505–516.
15. Janknecht, R. (2010). Multi-talented DEAD-box proteins and potential tumor promoters: p68 RNA helicase (DDX5) and its paralog, p72 RNA helicase (DDX17). *Am. J. Transl. Res.* **2**, 223–234.
16. Fukuda, T., Yamagata, K., Fujiyama, S., Matsumoto, T., Koshida, I., Yoshimura, K. *et al.* (2007). DEAD-box RNA helicase subunits of the Drosha complex are required for processing of rRNA and a subset of microRNAs. *Nat. Cell Biol.* **9**, 604–611.
17. Caretti, G., Schiltz, R. L., Dilworth, F. J., Di Padova, M., Zhao, P., Ogryzko, V. *et al.* (2006). The RNA helicases p68/p72 and the noncoding RNA SRA are coregulators of MyoD and skeletal muscle differentiation. *Dev. Cell*, **11**, 547–560.
18. Cloutier, S. C., Ma, W. K., Nguyen, L. T. & Tran, E. J. (2012). The DEAD-box RNA helicase Dbp2 connects RNA quality control with repression of aberrant transcription. *J. Biol. Chem.* **287**, 26155–26166.
19. Zonta, E., Bittencourt, D., Samaan, S., Germann, S., Dutertre, M. & Auboeuf, D. (2013). The RNA helicase DDX5/p68 is a key factor promoting c-fos expression at different levels from transcription to mRNA export. *Nucleic Acids Res.* **41**, 554–564.
20. Buszczak, M. & Spradling, A. C. (2006). The *Drosophila* P68 RNA helicase regulates transcriptional deactivation by promoting RNA release from chromatin. *Genes Dev.* **20**, 977–989.

21. Yang, Q., Del Campo, M., Lambowitz, A. M. & Jankowsky, E. (2007). DEAD-box proteins unwind duplexes by local strand separation. *Mol. Cell*, **28**, 253–263.
22. Halls, C., Mohr, S., Del Campo, M., Yang, Q., Jankowsky, E. & Lambowitz, A. M. (2007). Involvement of DEAD-box proteins in group I and group II intron splicing. Biochemical characterization of Mss116p, ATP hydrolysis-dependent and -independent mechanisms, and general RNA chaperone activity. *J. Mol. Biol.* **365**, 835–855.
23. Tijerina, P., Bhaskaran, H. & Russell, R. (2006). Nonspecific binding to structured RNA and preferential unwinding of an exposed helix by the CYT-19 protein, a DEAD-box RNA chaperone. *Proc. Natl Acad. Sci. USA*, **103**, 16698–16703.
24. Turner, A. M., Love, C. F., Alexander, R. W. & Jones, P. G. (2007). Mutational analysis of the *Escherichia coli* DEAD box protein CsdA. *J. Bacteriol.* **189**, 2769–2776.
25. Sugimoto, N., Nakano, S., Katoh, M., Matsumura, A., Nakamuta, H., Ohmichi, T. *et al.* (1995). Thermodynamic parameters to predict stability of RNA/DNA hybrid duplexes. *Biochemistry*, **34**, 11211–11216.
26. Turner, D. H. & Mathews, D. H. (2010). NNDB: the nearest neighbor parameter database for predicting stability of nucleic acid secondary structure. *Nucleic Acids Res.* **38**, D280–D282.
27. Yang, Q. & Jankowsky, E. (2005). ATP- and ADP-dependent modulation of RNA unwinding and strand annealing activities by the DEAD-box protein DED1. *Biochemistry*, **44**, 13591–13601.
28. Stampfl, S., Doetsch, M., Beich-Frandsen, M. & Schroeder, R. (2013). Characterization of the kinetics of RNA annealing and strand displacement activities of the *E. coli* DEAD-box helicase CsdA. *RNA Biol.* **10**, 149–156.
29. Rossler, O. G., Straka, A. & Stahl, H. (2001). Rearrangement of structured RNA via branch migration structures catalysed by the highly related DEAD-box proteins p68 and p72. *Nucleic Acids Res.* **29**, 2088–2096.
30. Zingler, N., Solem, A. & Pyle, A. M. (2010). Dual roles for the Mss116 cofactor during splicing of the ai5gamma group II intron. *Nucleic Acids Res.* **38**, 6602–6609.
31. Fedorova, O., Solem, A. & Pyle, A. M. (2010). Protein-facilitated folding of group II intron ribozymes. *J. Mol. Biol.* **397**, 799–813.
32. Liebeg, A., Mayer, O. & Waldsich, C. (2010). DEAD-box protein facilitated RNA folding in vivo. *RNA Biol.* **7**, 803–811.
33. Moore, M. J. & Proudfoot, N. J. (2009). Pre-mRNA processing reaches back to transcription and ahead to translation. *Cell*, **136**, 688–700.
34. Fasken, M. B. & Corbett, A. H. (2009). Mechanisms of nuclear mRNA quality control. *RNA Biol.* **6**, 237–241.
35. Qu, X., Lykke-Andersen, S., Nasser, T., Saguez, C., Bertrand, E., Jensen, T. H. & Moore, C. (2009). Assembly of an export-competent mRNP is needed for efficient release of the 3′-end processing complex after polyadenylation. *Mol. Cell. Biol.* **29**, 5327–5338.
36. Birse, C. E., Minvielle-Sebastia, L., Lee, B. A., Keller, W. & Proudfoot, N. J. (1998). Coupling termination of transcription to messenger RNA maturation in yeast. *Science*, **280**, 298–301.
37. Amrani, N., Minet, M., Wyers, F., Dufour, M. E., Aggerbeck, L. P. & Lacroute, F. (1997). PCF11 encodes a third protein component of yeast cleavage and polyadenylation factor I. *Mol. Cell. Biol.* **17**, 1102–1109.
38. Strasser, K. & Hurt, E. (2001). Splicing factor Sub2p is required for nuclear mRNA export through its interaction with Yra1p. *Nature*, **413**, 648–652.
39. Kistler, A. L. & Guthrie, C. (2001). Deletion of MUD2, the yeast homolog of U2AF65, can bypass the requirement for sub2, an essential spliceosomal ATPase. *Genes Dev.* **15**, 42–49.
40. Stutz, F., Bachi, A., Doerks, T., Braun, I. C., Seraphin, B., Wilm, M. *et al.* (2000). REF, an evolutionary conserved family of hnRNP-like proteins, interacts with TAP/Mex67p and participates in mRNA nuclear export. *RNA*, **6**, 638–650.
41. Segref, A., Sharma, K., Doye, V., Hellwig, A., Huber, J., Luhrmann, R. & Hurt, E. (1997). Mex67p, a novel factor for nuclear mRNA export, binds to both poly(A)+ RNA and nuclear pores. *EMBO J.* **16**, 3256–3271.
42. Strasser, K. & Hurt, E. (2000). Yra1p, a conserved nuclear RNA-binding protein, interacts directly with Mex67p and is required for mRNA export. *EMBO J.* **19**, 410–420.
43. Iglesias, N., Tutucci, E., Gwizdek, C., Vinciguerra, P., Von Dach, E., Corbett, A. H. *et al.* (2010). Ubiquitin-mediated mRNP dynamics and surveillance prior to budding yeast mRNA export. *Genes Dev.* **24**, 1927–1938.
44. Gilbert, W. & Guthrie, C. (2004). The Glc7p nuclear phosphatase promotes mRNA export by facilitating association of Mex67p with mRNA. *Mol. Cell*, **13**, 201–212.
45. Zenklusen, D., Vinciguerra, P., Strahm, Y. & Stutz, F. (2001). The yeast hnRNP-like proteins Yra1p and Yra2p participate in mRNA export through interaction with Mex67p. *Mol. Cell. Biol.* **21**, 4219–4232.
46. Hogan, D. J., Riordan, D. P., Gerber, A. P., Herschlag, D. & Brown, P. O. (2008). Diverse RNA-binding proteins interact with functionally related sets of RNAs, suggesting an extensive regulatory system. *PLoS Biol.* **6**, e255.
47. Anderson, J. T., Wilson, S. M., Datar, K. V. & Swanson, M. S. (1993). NAB2: a yeast nuclear polyadenylated RNA-binding protein essential for cell viability. *Mol. Cell. Biol.* **13**, 2730–2741.
48. Tran, E. J., Zhou, Y., Corbett, A. H. & Wente, S. R. (2007). The DEAD-box protein Dbp5 controls mRNA export by triggering specific RNA:protein remodeling events. *Mol. Cell*, **28**, 850–859.
49. Jankowsky, E. (2011). RNA helicases at work: binding and rearranging. *Trends Biochem. Sci.* **36**, 19–29.
50. Oeffinger, M., Wei, K. E., Rogers, R., DeGrasse, J. A., Chait, B. T., Aitchison, J. D. & Rout, M. P. (2007). Comprehensive analysis of diverse ribonucleoprotein complexes. *Nat. Methods*, **4**, 951–956.
51. Kashyap, A. K., Schieltz, D., Yates, J., 3rd & Kellogg, D. R. (2005). Biochemical and genetic characterization of Yra1p in budding yeast. *Yeast*, **22**, 43–56.
52. Johnson, S. A., Cubberley, G. & Bentley, D. L. (2009). Cotranscriptional recruitment of the mRNA export

factor Yra1 by direct interaction with the 3′ end processing factor Pcf11. *Mol. Cell*, **33**, 215–226.
53. Oberer, M., Marintchev, A. & Wagner, G. (2005). Structural basis for the enhancement of eIF4A helicase activity by eIF4G. *Genes Dev.* **19**, 2212–2223.
54. Rogers, G. W., Jr., Richter, N. J., Lima, W. F. & Merrick, W. C. (2001). Modulation of the helicase activity of eIF4A by eIF4B, eIF4H, and eIF4F. *J. Biol. Chem.* **276**, 30914–30922.
55. Ballut, L., Marchadier, B., Baguet, A., Tomasetto, C., Seraphin, B. & Le Hir, H. (2005). The exon junction core complex is locked onto RNA by inhibition of eIF4AIII ATPase activity. *Nat. Struct. Mol. Biol.* **12**, 861–869.
56. Nielsen, K. H., Chamieh, H., Andersen, C. B., Fredslund, F., Hamborg, K., Le Hir, H. & Andersen, G. R. (2009). Mechanism of ATP turnover inhibition in the EJC. *RNA*, **15**, 67–75.
57. Portman, D. S., O'Connor, J. P. & Dreyfuss, G. (1997). YRA1, an essential *Saccharomyces cerevisiae* gene, encodes a novel nuclear protein with RNA annealing activity. *RNA*, **3**, 527–537.
58. Strasser, K., Masuda, S., Mason, P., Pfannstiel, J., Oppizzi, M., Rodriguez-Navarro, S. *et al.* (2002). TREX is a conserved complex coupling transcription with messenger RNA export. *Nature*, **417**, 304–308.
59. Katahira, J., Strasser, K., Podtelejnikov, A., Mann, M., Jung, J. U. & Hurt, E. (1999). The Mex67p-mediated nuclear mRNA export pathway is conserved from yeast to human. *EMBO J.* **18**, 2593–2609.
60. Jankowsky, E., Gross, C. H., Shuman, S. & Pyle, A. M. (2001). Active disruption of an RNA-protein interactionby a DExH/D RNA helicase. *Science*, **291**, 121–125.
61. Fairman, M. E., Maroney, P. A., Wang, W., Bowers, H. A., Gollnick, P., Nilsen, T. W. & Jankowsky, E. (2004). Protein displacement by DExH/D "RNA helicases" without duplex unwinding. *Science*, **304**, 730–734.
62. Kallehauge, T. B., Robert, M. C., Bertrand, E. & Jensen, T. H. (2012). Nuclear retention prevents premature cytoplasmic appearance of mRNA. *Mol. Cell*, **48**, 145–152.
63. Kar, A., Fushimi, K., Zhou, X., Ray, P., Shi, C., Chen, X. *et al.* (2011). RNA helicase p68 (DDX5) regulates tau exon 10 splicing by modulating a stem-loop structure at the 5′ splice site. *Mol. Cell. Biol.* **31**, 1812–1821.
64. Salzman, D. W., Shubert-Coleman, J. & Furneaux, H. (2007). P68 RNA helicase unwinds the human let-7 microRNA precursor duplex and is required for let-7-directed silencing of gene expression. *J. Biol. Chem.* **282**, 32773–32779.
65. Barta, I. & Iggo, R. (1995). Autoregulation of expression of the yeast Dbp2p 'DEAD-box' protein is mediated by sequences in the conserved DBP2 intron. *EMBO J.* **14**, 3800–3808.
66. Chen, Y., Potratz, J. P., Tijerina, P., Del Campo, M., Lambowitz, A. M. & Russell, R. (2008). DEAD-box proteins can completely separate an RNA duplex using a single ATP. *Proc. Natl. Acad. Sci. USA*, **105**, 20203–20208.
67. Del Campo, M., Mohr, S., Jiang, Y., Jia, H., Jankowsky, E. & Lambowitz, A. M. (2009). Unwinding by local strand separation is critical for the function of DEAD-box proteins as RNA chaperones. *J. Mol. Biol.* **389**, 674–693.
68. Yang, Q. & Jankowsky, E. (2006). The DEAD-box protein Ded1 unwinds RNA duplexes by a mode distinct from translocating helicases. *Nat. Struct. Mol. Biol.* **13**, 981–986.
69. Mallam, A. L., Jarmoskaite, I., Tijerina, P., Del Campo, M., Seifert, S., Guo, L. *et al.* (2011). Solution structures of DEAD-box RNA chaperones reveal conformational changes and nucleic acid tethering by a basic tail. *Proc. Natl Acad. Sci. USA*, **108**, 12254–12259.
70. Granneman, S., Lin, C., Champion, E. A., Nandineni, M. R., Zorca, C. & Baserga, S. J. (2006). The nucleolar protein Esf2 interacts directly with the DExD/H box RNA helicase, Dbp8, to stimulate ATP hydrolysis. *Nucleic Acids Res.* **34**, 3189–3199.
71. Alcazar-Roman, A. R., Tran, E. J., Guo, S. & Wente, S. R. (2006). Inositol hexakisphosphate and Gle1 activate the DEAD-box protein Dbp5 for nuclear mRNA export. *Nat. Cell Biol.* **8**, 711–716.
72. Weirich, C. S., Erzberger, J. P., Flick, J. S., Berger, J. M., Thorner, J. & Weis, K. (2006). Activation of the DExD/H-box protein Dbp5 by the nuclear-pore protein Gle1 and its coactivator InsP6 is required for mRNA export. *Nat. Cell Biol.* **8**, 668–676.
73. Mallam, A. L., Del Campo, M., Gilman, B., Sidote, D. J. & Lambowitz, A. M. (2012). Structural basis for RNA-duplex recognition and unwinding by the DEAD-box helicase Mss116p. *Nature*, **490**, 121–125.
74. Schmid, M., Poulsen, M. B., Olszewski, P., Pelechano, V., Saguez, C., Gupta, I. *et al.* (2012). Rrp6p controls mRNA poly(A) tail length and its decoration with poly(A) binding proteins. *Mol. Cell*, **47**, 267–280.
75. Saguez, C., Schmid, M., Olesen, J. R., Ghazy, M. A., Qu, X., Poulsen, M. B. *et al.* (2008). Nuclear mRNA surveillance in THO/sub2 mutants is triggered by inefficient polyadenylation. *Mol. Cell*, **31**, 91–103.
76. Johnson, S. A., Kim, H., Erickson, B. & Bentley, D. L. (2011). The export factor Yra1 modulates mRNA 3′ end processing. *Nat. Struct. Mol. Biol.* **18**, 1164–1171.
77. Mitchell, S. F., Jain, S., She, M. & Parker, R. (2013). Global analysis of yeast mRNPs. *Nat. Struct. Mol. Biol.* **20**, 127–133.
78. Cordin, O., Banroques, J., Tanner, N. K. & Linder, P. (2006). The DEAD-box protein family of RNA helicases. *Gene*, **367**, 17–37.
79. Wan, Y., Kertesz, M., Spitale, R. C., Segal, E. & Chang, H. Y. (2011). Understanding the transcriptome through RNA structure. *Nat. Rev. Genet.* **12**, 641–655.
80. Jankowsky, E. & Putnam, A. (2010). Duplex unwinding with DEAD-box proteins. *Methods Mol. Biol.* **587**, 245–264.
81. Carmody, S. R., Tran, E. J., Apponi, L. H., Corbett, A. H. & Wente, S. R. (2010). The mitogen-activated protein kinase Slt2 regulates nuclear retention of non-heat shock mRNAs during heat shock-induced stress. *Mol. Cell. Biol.* **30**, 5168–5179.
82. Gwizdek, C., Iglesias, N., Rodriguez, M. S., Ossareh-Nazari, B., Hobeika, M., Divita, G. *et al.* (2006). Ubiquitin-associated domain of Mex67 synchronizes recruitment of the mRNA export machinery with transcription. *Proc. Natl Acad. Sci. USA*, **103**, 16376–16381.

Long Noncoding RNAs Promote Transcriptional Poising of Inducible Genes

Sara C. Cloutier[1☯], Siwen Wang[1☯], Wai Kit Ma[1], Christopher J. Petell[1], Elizabeth J. Tran[1,2*]

1 Department of Biochemistry, Purdue University, West Lafayette, Indiana, United States of America, **2** Purdue University Center for Cancer Research, Purdue University, West Lafayette, Indiana, United States of America

Abstract

Long noncoding RNAs (lncRNAs) are a class of molecules that impinge on the expression of protein-coding genes. Previous studies have suggested that the *GAL* cluster-associated lncRNAs of *Saccharomyces cerevisiae* repress expression of the protein-coding *GAL* genes. Herein, we demonstrate a previously unrecognized role for the *GAL* lncRNAs in activating gene expression. In yeast strains lacking the RNA helicase, *DBP2*, or the RNA decay enzyme, *XRN1*, we find that the *GAL* lncRNAs specifically accelerate gene expression from a prior repressive state. Furthermore, we provide evidence that the previously suggested repressive role is a result of specific mutant phenotypes, rather than a reflection of the normal, wild-type function of these noncoding RNAs. To shed light on the mechanism for lncRNA-dependent gene activation, we show that rapid induction of the protein-coding *GAL* genes is associated with faster recruitment of RNA polymerase II and reduced association of transcriptional repressors with *GAL* gene promoters. This suggests that the *GAL* lncRNAs enhance expression by derepressing the *GAL* genes. Consistently, the *GAL* lncRNAs enhance the kinetics of transcriptional induction, promoting faster expression of the protein-coding *GAL* genes upon the switch in carbon source. We suggest that the *GAL* lncRNAs poise inducible genes for rapid activation, enabling cells to more effectively trigger new transcriptional programs in response to cellular cues.

Citation: Cloutier SC, Wang S, Ma WK, Petell CJ, Tran EJ (2013) Long Noncoding RNAs Promote Transcriptional Poising of Inducible Genes. PLoS Biol 11(11): e1001715. doi:10.1371/journal.pbio.1001715

Academic Editor: Fred Winston, Harvard Medical School, United States of America

Received June 3, 2013; **Accepted** October 9, 2013; **Published** November 19, 2013

Funding: This work was funded through NIH R01GM097332-01 to EJT. The funders had no role in study design, data collection and analysis, decision to publish, or preparation of the manuscript.

Competing Interests: The authors have declared that no competing interests exist.

Abbreviations: ChIP, chromatin immunoprecipitation; *GAL*, galactose metabolic gene; lncRNA, long noncoding RNA; mRNA, messenger RNA; RT-qPCR, reverse transcriptase-quantitative PCR; Vi, initial velocity.

* E-mail: ejtran@purdue.edu

☯ These authors contributed equally to this work.

Introduction

Essential cellular processes, such as growth, organ development, and differentiation, require precise spatial and temporal control of gene expression. Eukaryotes have developed intricate pathways for regulating gene expression at the transcriptional level in both global and gene-specific manners [1,2]. Recent studies have provided evidence that lncRNA molecules facilitate transcriptional control of protein-coding genes [3,4]. Thus far, the most well-characterized lncRNA is *Xist*, which facilitates X chromosome inactivation in mammalian cells [5,6]. Similar to a transcription factor, *Xist* functions by directing corepressor complexes to the targeted DNA loci [7]. Other examples of repressive lncRNAs include *HOTAIR*, a 2.1 kilobase transcript that directs repression of developmental gene loci, and *PANDA*, which regulates cell-cycle–dependent gene expression [8,9]. Recruitment of transcription factors may also be a primary mechanism for lncRNAs associated with transcriptional activation [10–13], suggesting that these molecules may recruit both activators and repressors. Other lncRNAs, however, appear to function solely through their synthesis, whereby the act of transcription alters the chromatin structure of a targeted gene promoter [14–16]. This diversity of action may account for the fact that individual lncRNAs are more conserved in their position than in their nucleotide sequence [17]. Interestingly, many mammalian lncRNAs are associated with genes that require precise temporal control of initiation to facilitate proper cell growth and differentiation [9,13,18–23]. This suggests that these molecules may control the timing of gene expression in response to specific signals.

The *GAL10* lncRNA in the *S. cerevisiae* budding yeast model system is encoded within the *GAL* gene cluster, which is composed of the *GAL1*, *GAL10*, and *GAL7* metabolic genes required for utilization of galactose as a carbon source [24–26]. Budding yeast are able to utilize glucose and this catabolite is the preferential carbon source for energy production. However, yeast also has the capacity to utilize galactose when it is the sole carbon source in the media [27,28]. The transition from glucose to galactose metabolism requires an intricate switch in transcriptional programs, whereby genes repressed in the presence of glucose must be activated for production of galactose metabolizing enzymes [29–31]. The highly orchestrated series of events required to facilitate this *GAL* gene metabolic switch is well understood and involves modulation of carbon source-dependent transcriptional activators and repressors [1,29,32–34]. Interestingly, the *GAL10* lncRNA has been proposed to act additively with transcriptional repressors, to provide tighter control of this gene expression network

Author Summary

Long noncoding RNAs (lncRNAs) are a recently identified class of molecules that regulate the expression of protein-coding genes through a number of mechanisms, some of them poorly characterized. The *GAL* gene cluster of the yeast *Saccharomyces cerevisiae* encodes a series of three inducible genes that are turned on or off by the presence or absence of specific carbon sources in the environment. Previous studies have documented the presence of two lncRNAs—*GAL10* and *GAL10s*—encoded by genes that overlap the *GAL* cluster. We have now uncovered a role for both these lncRNAs in promoting the activation of the *GAL* genes when they are released from repressive conditions. This activation occurs at the kinetic level, through more rapid recruitment of RNA polymerase II and decreased association of the co-repressor, Cyc8. Under normal conditions, but also especially when they are stabilized and their levels are up-regulated, these *GAL* lncRNAs promote faster *GAL* gene activation. We suggest that these lncRNA molecules poise inducible genes for quick response to extracellular cues, triggering a faster switch in transcriptional programs.

[24,25,35,36]. The repressive role of the *GAL10* lncRNA is supported by correlative changes in histone acetylation patterns and the observation that impaired lncRNA degradation in RNA decay-deficient mutants results in defective expression of the *GAL1* and *GAL10* genes [24,25]. However, the mechanism for repression has not been established, and unlike *Xist*, there is no evidence for a direct interaction between the *GAL10* lncRNA and a transcriptional repressor.

Our laboratory recently found that loss of the RNA helicase *DBP2* results in up-regulation of another lncRNA within the *GAL* cluster, termed *GAL10s* [37,38]. To determine the role of Dbp2 in this process, we initially set out to test the hypothesis that the *GAL10s* lncRNA also functions in transcriptional repression, similar to the *GAL10* lncRNA. Surprisingly, this revealed an unexpected and uncharacterized role for both of the *GAL* lncRNAs in promoting gene activation. We suggest that these findings identify a novel role for the *GAL* lncRNAs in poising protein-coding genes for rapid induction in response to cellular and environmental cues.

Results

The *GAL7* and *GAL10* Genes Are Rapidly Induced from Repressed Conditions in *dbp2Δ* Cells as Compared to Wild Type

The *GAL* cluster is a group of gene loci that have been extensively utilized to define the mechanism and order of events in transcriptional regulation [1,27–29,39]. The cluster encodes three genes, *GAL1*, *GAL7*, and *GAL10*, which exist in three distinct transcriptional states in response to carbon sources: repressed (+glucose), derepressed (+raffinose), and activated (+galactose) (Figure 1A). This cluster also encodes the *GAL10* lncRNA, which is a 4.0 kb antisense transcript that overlaps *GAL10* and *GAL1*, and the *GAL10s* lncRNA, a 0.5 kb sense-oriented transcript upstream of *GAL7* (Figure 1A) [24,26,38]. The protein-coding *GAL* genes are regulated by carbon source-responsive repressors and activators (Figure 1A) [27,29,32]. In contrast, the *GAL* lncRNAs are expressed when the protein-coding *GAL* genes are transcriptionally inactive (+glucose or raffinose) [24–26] and are dependent on the transcription factor, Reb1 (Figure 1D) [24,26].

Previous studies from our laboratory demonstrated that loss of the RNA helicase *DBP2* results in accumulation of a 3′ extended *GAL10s* lncRNA under conditions when the protein-coding *GAL* genes are transcriptionally repressed (+glucose) [37]. Based on previous evidence that up-regulation of the *GAL10* lncRNA impairs transcriptional activation of the *GAL1* and *GAL10* genes [25], we anticipated that loss of *DBP2* would similarly delay transcriptional activation of *GAL7*. To this end, we analyzed the transcriptional induction profile of *GAL7* in wild-type and *dbp2Δ* cells following a media shift from repressed to activated conditions (glucose to galactose) by isolating RNA fractions over time at 30 min intervals from three, independent biological replicates per strain. We then conducted northern blotting of isolated RNAs and then obtained a semiquantitative estimate of the degree of repression by calculating the average lag time or time to the first appearance of *GAL7* transcripts after normalization to the *SCR1* loading control (Figure 1B). In contrast to wild-type cells, which exhibited a normal, ~2-h lag time to induction [40,41], *dbp2Δ* cells displayed detectible *GAL7* transcripts within an average of 40 min (Figure 1B). This was unexpected and suggested that loss of *DBP2* results in a rapid induction of *GAL7* expression from repressive conditions. To determine if the requirement for *DBP2* is specific to *GAL7*, we then assayed *GAL10* induction (Figure 1B, bottom). This revealed that *GAL10* is also rapidly induced in *dbp2*Δ cells (Figure 1C). In addition to full-length *GAL10* transcripts, we also observed the appearance of shorter *GAL10* products, which are likely the result of previously noted cryptic initiation defects in *dbp2*Δ cells (Figure 1C, bottom) [37]. Regardless, this reveals that the loss of *DBP2* results in rapid induction of both the *GAL7* and *GAL10* genes from repressed (+glucose) conditions.

Loss of the *GAL* lncRNAs Restores Repression in *dbp2Δ* Cells

The results above suggest that *DBP2* is required to maintain glucose-dependent repression of the protein-coding *GAL* genes. To determine if this requirement is dependent on the presence of the *GAL* lncRNAs, we constructed a *dbp2*Δ *lncRNA*Δ strain that lacks expression of both of the *GAL10* and *GAL10s* lncRNA molecules. Expression of the *GAL10* lncRNA is dependent on the Reb1 transcription factor, which has four putative binding sites within the 3′ end of the *GAL10* coding region [24,26]. Although it is not known which Reb1 site(s) is necessary for expression of the *GAL10* lncRNA, previous studies have shown that the *lncRNA*Δ strain, which harbors silent mutations of all four sites, abolishes synthesis of this lncRNA (Figure 1D) [24]. Because the *GAL10* and *GAL10s* lncRNAs arise from juxtaposed sites within the protein-coding *GAL10* gene, we speculated that the *lncRNA*Δ mutation would also abolish synthesis of the *GAL10s* lncRNA. To test this, we conducted reverse transcription-quantitative PCR (RT-qPCR) analysis to measure lncRNA abundance in isogenic wild-type, *dbp2*Δ, *lncRNA*Δ, and *dbp2*Δ *lncRNA*Δ cells grown in the presence of glucose, using primers positioned within the 5′ ends of the respective lncRNAs (nc10 and nc10s in Figure 1D). This revealed a slight increase in the *GAL10* lncRNA and greater overabundance of the *GAL10s* lncRNA in the *dbp2*Δ strain similar to previous studies [37]. More importantly, neither the *GAL10* nor the *GAL10s* lncRNA were detectible in strains harboring the *lncRNA*Δ (Figure 1D). This suggests that the *lncRNA*Δ mutation abolishes expression of both lncRNAs, consistent with our prediction.

Next, we conducted transcriptional induction analysis as above using isogenic *dbp2*Δ and *dbp2*Δ *lncRNA*Δ cells to determine if the rapid induction phenotype is linked to the presence of the *GAL* lncRNAs. Strikingly, incorporation of the *lncRNA*Δ mutation in the *DBP2*-deficient strain restored the induction kinetics of both *GAL7*

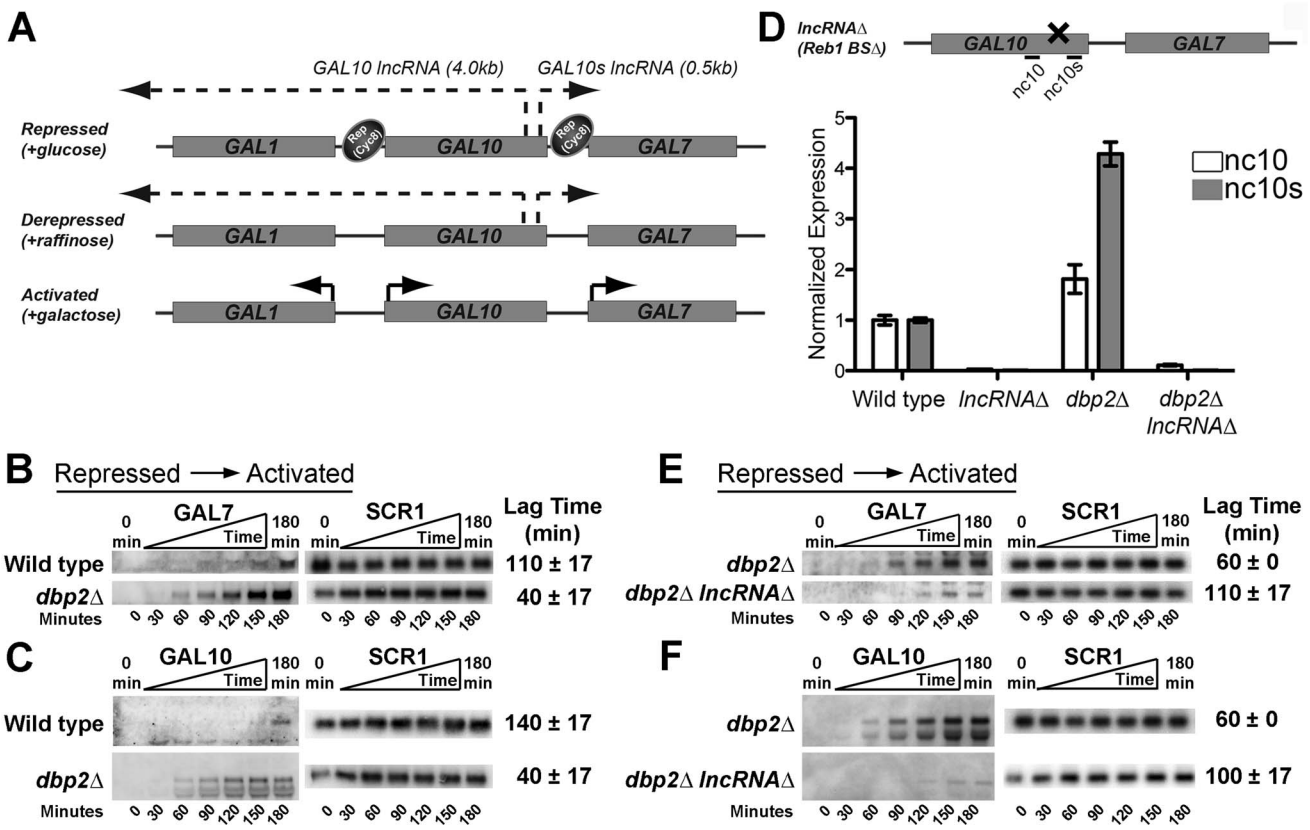

Figure 1. Loss of *DBP2* results in rapid, lncRNA-dependent induction of *GAL10* and *GAL7* from repressed conditions. (A) Simplified model for carbon-source-dependent regulation of *GAL1*, *GAL7*, and *GAL10* genes within the *GAL* cluster. Glucose-dependent repression is mediated by transcription factors (not shown), which then recruit other proteins such as the Tup1–Cyc8 co-repressor complex to promote repression [28,32,40,46,47,51]. Derepression occurs under nonrepressing, noninducing conditions when the repressors are no longer present and the *GAL* genes are not transcriptionally active [29]. Activation only occurs in the presence of galactose [1,29]. Synthesis of the *GAL10* lncRNA, and likely the *GAL10s* lncRNA, is mutually exclusive with activated expression of the *GAL* genes [24,25]. (B–C) *GAL7* (B) and *GAL10* (C) genes are rapidly induced in *dbp2Δ* cells following a switch from repressed to activated conditions. Transcriptional induction of wild-type (BY4741) and *dbp2Δ* strains was conducted by isolating RNA from cells at 30 min intervals prior to and immediately following a nutritional shift from repressive (+glucose) to activated (+galactose) conditions. Transcripts were detected by northern blotting using ^{32}P-labeled, double-stranded (ds)DNA probes corresponding to *GAL7*, *GAL10*, or *SCR1* RNA as indicated. Each time course was conducted in triplicate. Average lag times to induction are shown with the standard deviation (s.d.) for three, independent biological replicates and correspond to the first time point in a series of time points with increasing *GAL* transcript levels after normalization to *SCR1*. An s.d. of zero indicates no variation between biological samples with 30 min time points, whereas an s.d. of 17 indicates a variance of 30 min between replicates. (D, Top) Schematic diagram of the *lncRNAΔ* strain with *GAL10* and *GAL10s* lncRNAs and primer sets for RT-qPCR. The four previously identified binding sites for the Reb1 transcription factor are present within the 3′ end of the *GAL10* coding region [24]. The *lncRNA*Δ harbors silent mutations that disrupt all binding sites for the Reb1 transcription factor [24]. (D, Bottom) The *lncRNA*Δ mutation abolishes expression of both the *GAL10* and *GAL10s* lncRNA in wild-type and *dbp2*Δ cells. *GAL10* and *GAL10s* lncRNAs were detected in the indicated strains following growth in glucose using RT-qPCR as previously described with primers nc10 and nc10s [37]. Transcript levels were normalized to *ACT1*, which does not vary between these strains, and is the average of three biological replicates with respect to wild type and standard error from the mean (SEM). (E–F) Loss of *GAL10* and *GAL10s* lncRNAs restores repression at *GAL7* (E) and *GAL10* (F) loci in *DBP2*-deficient cells. Transcriptional induction assays from repressive conditions were conducted with isogenic *dbp2*Δ and *dbp2*Δ *lncRNA*Δ strains as in Figure 1B–C.
doi:10.1371/journal.pbio.1001715.g001

and *GAL10* to near wild-type profiles (Figure 1E–F). This suggests that the rapid induction of *GAL7* and *GAL10* from repressive conditions in *dbp2*Δ cells is lncRNA-dependent, indicating that the *GAL* lncRNAs play an as-of-yet uncharacterized role in gene activation. Alternatively, the delayed activation in *dbp2*Δ *lncRNA*Δ cells may be due to a role for Reb1 and/or the Reb1-binding sites in efficient expression of *GAL7* and *GAL10*.

Defects in RNA Decay and Decapping Cause Rapid Induction of the *GAL* Cluster Genes from Repressive Conditions

Previous studies have utilized mutant strains with impaired RNA decay pathways to demonstrate the roles of lncRNAs at targeted gene loci [25,38]. The 5′-3′ exonuclease, Xrn1, is required for degradation of both the *GAL10* and *GAL10s* lncRNAs [26,38,42,43]. *DCP2*-deficient cells also accumulate lncRNAs but through a defect in RNA decapping [25]. Interestingly, up-regulation of the *GAL* lncRNAs, via loss of *DCP2*, has been linked to delayed transcriptional activation of the *GAL* genes from derepressed conditions (+raffinose) [25]. This was also observed for *xrn1*Δ cells, but to a lesser extent [25]. Recent studies have shown that both Dcp2 and Xrn1 are present in the nucleus and associate with transcribed chromatin, indicative of a direct link between decay and gene expression [44,45]. However, contribution of RNA decay pathways to induction from repressed conditions (+glucose) has not been addressed.

To determine if the up-regulation of lncRNAs, via loss of RNA decay and/or decapping pathways, impacts the expression of the *GAL* genes from repressed conditions, we analyzed the transcriptional induction of *GAL7* and *GAL10* in *xrn1*Δ and *dcp2*Δ strains (Figure 2A–B). We also included *dbp2*Δ cells in this analysis for comparison to studies above. Surprisingly, and in contrast to defective expression, this revealed that *GAL7* and *GAL10* are rapidly induced in both *xrn1*Δ and *dcp2*Δ strains with overabundant lncRNAs. In fact, detectible transcripts appear 2- to 3-fold faster in these strains than in wild type, similar to the rapid induction kinetics of *dbp2*Δ cells (Figure 2A–B). Note that the *GAL10* lncRNA is also readily detectable in these RNA decay-deficient strains due to the use of a double-stranded DNA probe and consistent with the role of Xrn1 and Dcp2 in lncRNA decay (Figure 2B, asterisks) [25,26,38]. Thus, loss of genes encoding either the RNA helicase *DBP2* or the RNA decay factors *XRN1* or *DCP2* results in faster activation of the protein-coding *GAL* genes from repressive conditions. This suggests that the *GAL* lncRNAs may actually promote gene expression.

GAL1 Is Also Rapidly Activated from Repressed Conditions

In contrast to our results above, prior studies have proposed a repressive role for the *GAL10* lncRNA [24–26]. However, a major difference between our studies and past reports is that prior experiments were primarily focused on *GAL1* induction from derepressive conditions (+raffinose), rather than *GAL10* and *GAL7* from a repressive state (+glucose) [24–26]. To determine if *GAL1* exhibits a different induction profile than *GAL7* and *GAL10*, we analyzed the induction of this gene as above (Figure 2C). Northern blotting analysis of RNAs from wild-type, *dbp2*Δ, *xrn1*Δ, and *dcp2*Δ strains revealed that *GAL1* is also rapidly induced from repressive conditions in all three mutant strains with lag times of ~50 min (Figure 2C). This suggests a common mechanism for the *GAL* lncRNAs at all three *GAL* cluster genes.

Induction of the *GAL* Cluster Genes from Derepressive Conditions Occurs with Wild-Type Kinetics for *dbp2*Δ, *xrn1*Δ, and *dcp2*Δ Strains

In the presence of glucose, the *GAL* genes are repressed through several mechanisms, including the action of glucose-dependent transcriptional repressors (Figure 1A) [28,31,46–48]. However, when cells use raffinose as a carbon source, the *GAL* genes become derepressed due to environmentally induced loss of repressors (Figure 1A). To determine if the rapid induction of the *GAL* genes is specific for activation from repressive conditions (+glucose), we conducted induction analysis from the derepressed state (+raffinose). Interestingly, wild-type, *dbp2*Δ, *xrn1*Δ, and *dcp2*Δ strains all

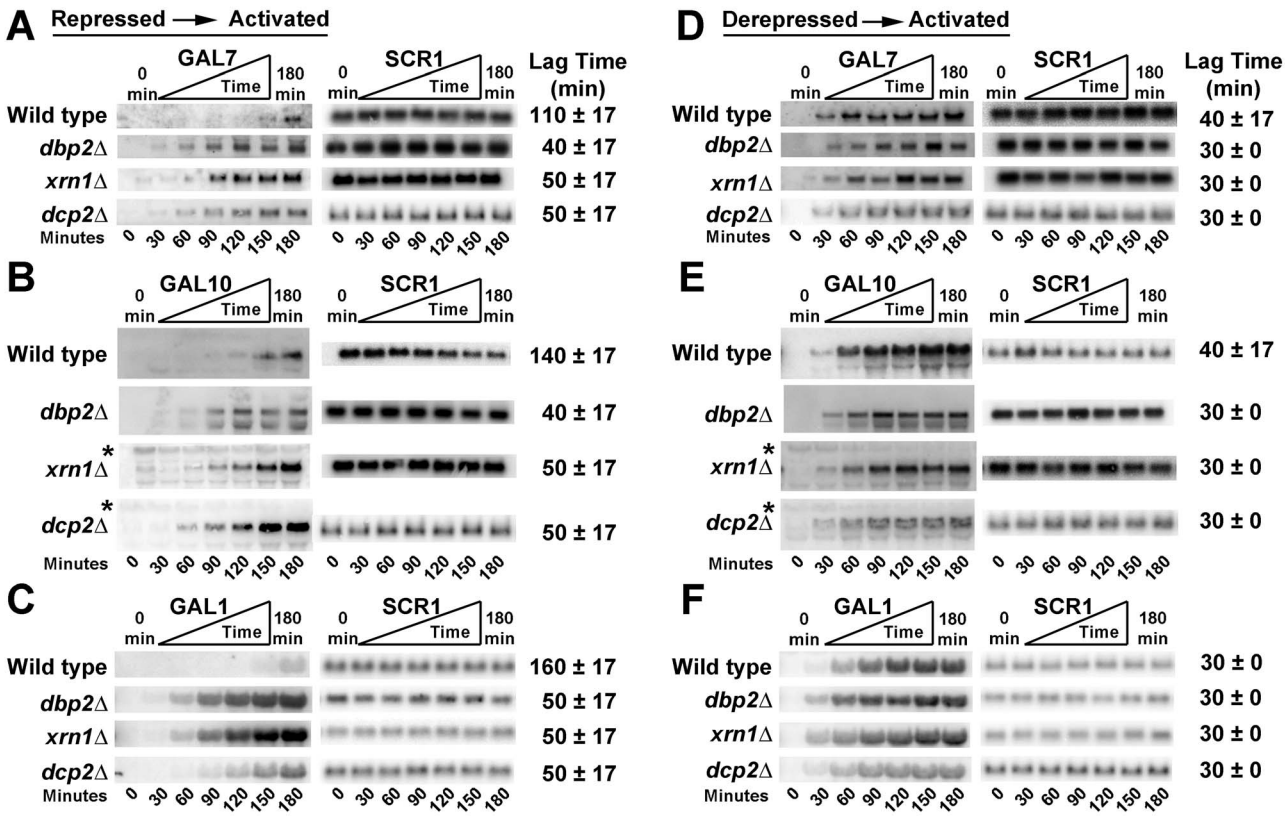

Figure 2. All three *GAL* cluster genes are rapidly induced from repressed conditions upon loss of *DBP2* or the RNA decay factors *XRN1* and *DCP2*. (A–C) *GAL7* (A), *GAL10* (B), and *GAL1* (C) are rapidly induced from repressed conditions in *dbp2*Δ, *xrn1*Δ, and *dcp2*Δ strains. Induction assays were conducted as in Figure 1 with isogenic *xrn1*Δ, *dbp2*Δ, *dcp2*Δ, and wild-type strains. Asterisks mark the *GAL10* lncRNA transcripts, which are visible in the *xrn1*Δ and *dcp2*Δ strains due to high abundance and the use of dsDNA probes (most visible from 0–90 min). Lag times represent the average of three biological replicates and the s.d. as in Figure 1. (D–F) Induction of *GAL7* (D), *GAL10* (E), and *GAL1* (F) from derepressed (+raffinose) conditions in *dbp2Δ*, *xrn1*Δ, and *dcp2*Δ cells occurs with wild-type kinetics. Transcriptional induction was measured as above following a nutritional shift from derepressed (+raffinose) to activated (+galactose) conditions.
doi:10.1371/journal.pbio.1001715.g002

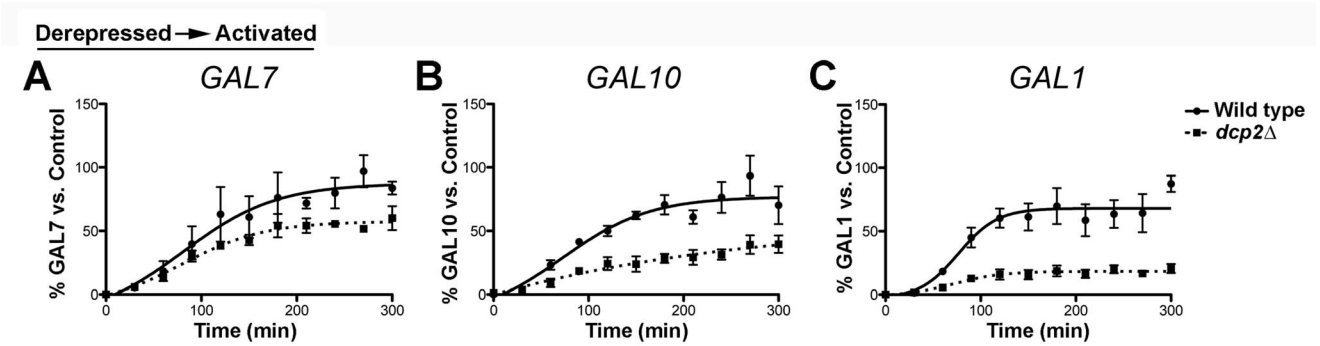

Figure 3. Loss of *DCP2* impairs *GAL1* transcript accumulation when induced from derepressive conditions. (A–C) Extended time course for analysis of *GAL7* (A), *GAL10* (B), and *GAL1* (C) induction from derepressed conditions in *dcp2*Δ cells. Wild-type and *dcp2*Δ cells were grown in raffinose as above and were shifted to galactose to induce transcription of the *GAL* cluster genes. RNA fractions were isolated at 30 min intervals over a 300 min time frame. Resulting transcript profiles from three biological replicates were normalized to *scR1* and plotted over time as a percentage of the average transcript levels with respect to a fully induced, wild-type "control" RNA for normalization between replicates. The "control" corresponds to total RNA isolated from wild-type cells after 5 h in galactose media following initial growth in raffinose for maximal expression. Error bars indicate the SEM. Statistical significance was calculated using a two-tailed *t* test. Time points with significantly different transcript levels ($p<0.05$) between wild-type and dcp2Δ cells for each gene are as follows: *GAL10*, 60–120 min time points; *GAL1*, 90–150, 240, 300 min time points. The 210 and 270 min time points for *GAL7* correspond to $p<0.10$, whereas no other time points in the *GAL7* analysis displayed significantly different transcript levels between wild-type and *dcp2*Δ cells.
doi:10.1371/journal.pbio.1001715.g003

exhibited similar induction kinetics from derepressed to activated conditions with the appearance of transcripts within ~30 min for all three *GAL* cluster genes (Figure 2D–F). This is consistent with a recent study showing that *xrn1*Δ cells accumulate *GAL7* and *GAL10* transcripts at the same rate as wild-type cells when induced from raffinose [45]. *DCP2*-deficient cells also displayed detectible transcripts at 30 min postinduction for all three *GAL* genes, albeit with an apparent reduction of transcript levels for *GAL1* as compared to wild type (Figure 2D–F, bottom). This demonstrates that the rapid induction of *GAL7*, *GAL10*, and *GAL1* is specific for the environmental switch from repressive (+glucose) to activating (+galactose) conditions. Moreover, it suggests that the loss of the RNA decay machinery does not necessarily result in lncRNA-dependent repression [25,36].

RNA Decapping Deficiencies Impair *GAL1* Transcript Accumulation

Prior studies suggested that *GAL* lncRNAs are repressive based on defective induction of the *GAL* genes in RNA decapping and decay-deficient strains [25]. However, our results suggest that this is not the case for *xrn1*Δ cells with defective RNA decay. To determine if the apparent reduction in mRNA levels in *dcp2*Δ cells above indicates a specific requirement for decapping in *GAL* gene induction, we conducted longer induction analyses from derepressive conditions for three, independent biological replicates. We then graphed the resulting transcript levels over time as the fraction of a fully induced wild-type RNA sample ("Control") following normalization to the *SCR1* loading control (Figure 3A–C). Consistent with previous studies, *dcp2*Δ cells displayed severe *GAL1* expression defects, with levels reaching only 20% of wild type after 5 h of induction (Figure 3C) [25]. *GAL10*, on the other hand, showed more moderate defects more in line with defective transcript accumulation than impaired initiation, whereas the *GAL7* induction profile was similar between wild-type and *dcp2*Δ cells (Figure 3A–B). This suggests that the decapping requirement for robust expression of lncRNA-targeted, inducible genes may be specific to *GAL1* [25,36]. Furthermore, the fact that *dcp2*Δ cells show enhanced induction from repressed conditions (Figure 2A–C) argues against a generally repressive role for the *GAL* lncRNAs. Thus, the previously described lncRNA-dependent repression at the *GAL* cluster in RNA decay-deficient strains may reflect a requirement for decapping in the accumulation of *GAL1* transcripts, and especially *GAL1*, rather than a repressive role for the *GAL* lncRNAs.

DBP2- and *XRN1*-Deficient Cells Display Faster Recruitment of RNA Polymerase II to *GAL7* and *GAL10* Genes

Our results above provide evidence that the *GAL* lncRNAs may act in a positive manner by stimulating induction of the protein-coding *GAL* genes from repressed conditions. However, it is also possible that the increase in transcript abundance over time is due to a decrease in mRNA decay rather than an increase in transcriptional activity. To determine if the rapid induction correlates with an increased rate of transcriptional induction in *dbp2*Δ and *xrn1*Δ cells as compared to wild type, we asked if RNA polymerase II (RNAPII) is recruited faster to the *GAL7* and *GAL10* gene promoters [39,49]. RNAPII recruitment was measured by conducting chromatin immunoprecipitation (ChIP) over a 300-min time course following induction from repressed conditions with an antibody to a RNAPII core subunit (anti-Rpb3) (Figure 4A). Suggestive of a transcriptional effect, this revealed that RNAPII is recruited to the *GAL7* and *GAL10* promoters more rapidly in both *dbp2*Δ and *xrn1*Δ cells (Figure 4A). This faster recruitment was most evident at 120 min postinduction, with ~4-fold and ~6- to 9-fold higher levels of RNAPII at *GAL7* and *GAL10*, respectively (Figure 4A). This suggests that loss of *DBP2* or *XRN1*, and the resulting accumulation of the *GAL* lncRNAs, results in a direct effect on transcription initiation. In contrast, analysis of the galactose-inducible *GAL6* gene revealed similar RNAPII recruitment rates for all three strains with a slightly lower RNAPII signal for *xrn1*Δ and *dbp2*Δ cells at the 300 min time point (Figure 4B) [50]. The latter is consistent with recent studies showing that *xrn1*Δ cells have reduced steady-state transcription levels [45]. Furthermore, it demonstrates that the rapid recruitment of RNAPII is specific for the *GAL* lncRNA-targeted genes within the *GAL* cluster.

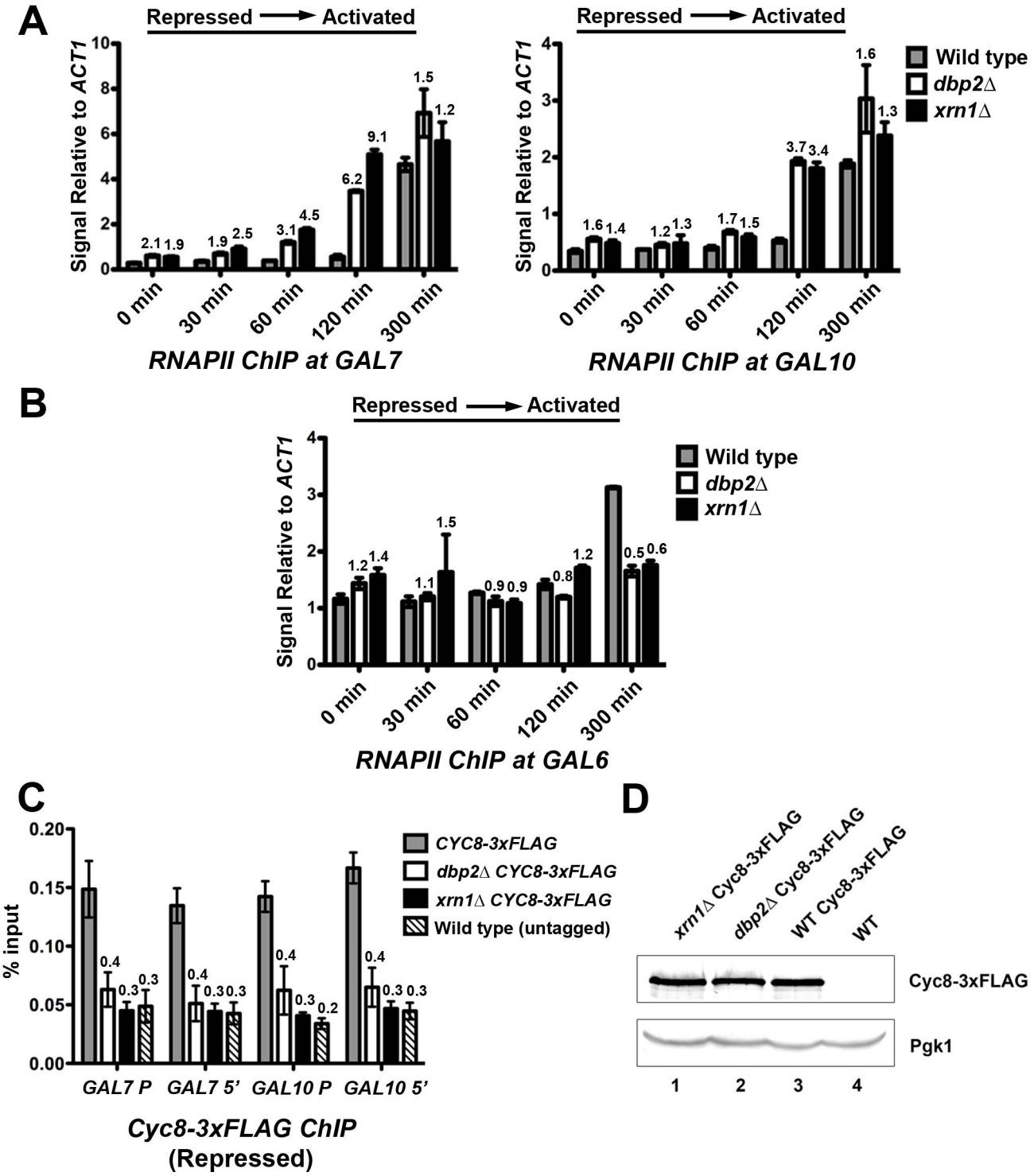

Figure 4. Rapid induction of the *GAL* genes correlates with faster recruitment of RNAPII and reduced corepressor binding to chromatin. (A) RNAPII is recruited faster to *GAL7* (left) and *GAL10* (right) promoters following a shift from repressive to activating conditions in *XRN1*- and *DBP2*-deficient cells. Wild-type, *dbp2*Δ, and *xrn1*Δ cells were shifted from transcriptionally repressive conditions (+glucose) to transcriptionally active conditions (+galactose). Cells were collected before (0 min) and at 30 min, 60 min, 120 min, and 300 min time points following a shift to galactose media. ChIP was conducted using an anti-Rpb3 antibody followed by qPCR. Results are presented as the relative Rpb3 occupancy at the *GAL10* or *GAL7* promoter with respect to the constitutively activated *ACT1* gene. Numbers above each bar represent the fold above wild type at the same time point postinduction for both *dbp2*Δ and *xrn1*Δ cells. (B) The galactose-dependent *GAL6* gene does not show increased RNAPII recruitment in *dbp2*Δ or *xrn1*Δ cells. ChIP was conducted as above followed by qPCR at *GAL6* promoter. Results are represented as the relative Rpb3 occupancy at the *GAL6* promoter with respect to the *ACT1* gene. (C) Both *dbp2*Δ and *xrn1*Δ cells display reduced association of the Cyc8 component of the Tup1–Cyc8 co-repressor complex at *GAL* genes under repressive conditions. Briefly, wild-type, *dbp2*Δ, and *xrn1*Δ cells harboring a *3×FLAG*-tagged *CYC8* at the endogenous locus as well as a wild-type strain with untagged *CYC8* were grown under transcriptionally repressive conditions (+glucose),

representing the 0 min time point for the induction time courses above, and were then subjected to ChIP with anti-FLAG antibodies. Cyc8–3×FLAG occupancy is presented as the percentage of isolated DNA over input. Numbers above each bar represent the fraction of bound DNA in each strain versus that in the wild-type strain harboring the *3×FLAG-tagged CYC8*. (D) Cyc8–3×FLAG is expressed at similar levels in wild-type, *dbp2*Δ, and *xrn1*Δ strains. Western blotting was conducted with whole cell lysates from the indicated strains and Cyc8–3×Flag was detected with polyclonal anti-FLAG antibodies. Pgk1 serves as a loading control, whereas wild type with an untagged Cyc8 (lane 4) demonstrates antibody specificity.
doi:10.1371/journal.pbio.1001715.g004

Derepression of *GAL7* and *GAL10* Correlates with Reduced Binding of the Cyc8 Corepressor

Glucose-dependent repression is accomplished by transcription factors Mig1, Mig2, and Nrg1, which recognize specific DNA sequences and subsequently recruit co-repressor complexes like the Tup1–Cyc8 complex [28,40,46–48,51,52]. To determine why *dbp2*Δ and *xrn1*Δ cells exhibit faster recruitment of RNAPII, we asked if these strains display lower levels of bound co-repressors. To test this, we conducted ChIP assays to measure the association of Cyc8 at *GAL7* and *GAL10* at the 0 min time point when the *GAL* genes are repressed. We tested both the promoter and 5′ end of *GAL7* and *GAL10* as Tup1 has been shown to associate with the ORF and the promoter of specific gene loci [53]. Consistent with the more rapid recruitment of RNAPII, both *DBP2*- and *XRN1*-deficient cells exhibited severely reduced Cyc8 binding at both the promoter and 5′-end of the open reading frame (ORF), with levels equivalent to background ChIP signal (Figure 4C). Western blotting revealed that *CYC8–3×FLAG* is expressed at similar levels in all three strains, indicating that reduced binding is not due to different protein levels (Figure 4D). Thus, the rapid induction of *GAL7* and *GAL10* in *xrn1*Δ and *dbp2*Δ cells correlates with reduced association of Cyc8 corepressor. This provides an explanation for the rapid induction of *GAL* gene expression from the repressed (+glucose) but not derepressed (+raffinose) conditions (Figures 1 and 2); the *GAL* genes are derepressed in the *dbp2*Δ and *xrn1*Δ strains.

The *GAL* lncRNAs Do Not Alter the Transcriptional Induction Profiles of *GAL7* or *GAL10* from Derepressed Conditions in *XRN1*-Deficient Cells

If derepression is caused by the *GAL* lncRNAs, then deletion of these noncoding RNA molecules should have no effect on the induction or final levels of *GAL7* and *GAL10*. To determine if this is the case, we constructed *xrn1*Δ and *xrn1*Δ *lncRNA*Δ cells, as *xrn1*Δ and *dbp2*Δ cells exhibit similar induction profiles. We then conducted extended time courses of wild-type, *xrn1*Δ, *lncRNA*Δ, and *xrn1*Δ *lncRNA*Δ strains to measure both the induction kinetics and steady-state transcript levels of the *GAL* genes from the derepressed (+raffinose) condition (Figure S1, representative northern blot). Resulting induction profiles were then graphed for each condition, lag times were determined as above, and the velocity of transcript accumulation and final steady-state levels were determined after normalization to *SCR1* and with respect to a fully induced, wild-type strain (“control”) (Figure 5).

Consistent with our shorter time course analysis (Figure 2), both wild-type and *xrn1*Δ cells displayed similar lag times for induction and final steady-state transcript levels for both *GAL7* and *GAL10* when induced from derepressive conditions (+raffinose)

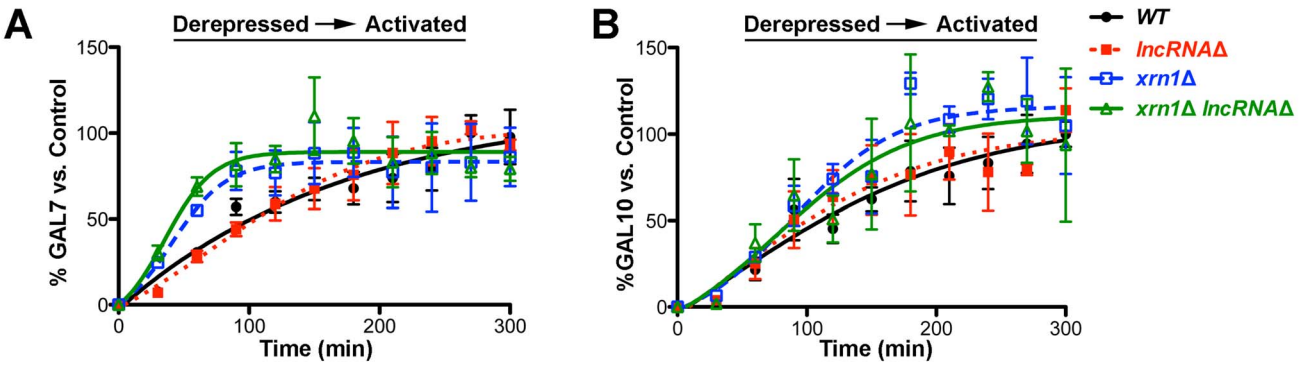

C

GAL7	Estimated Lag Time (min)	V_i (% ctl/min)	$T_{1/2}$ (min)	T_{max} (min)
Wild type	30±0	0.3±0.0	110±10	250±17
*lncRNA*Δ	30±0	0.4±0.0	110±8	240±30
*xrn1*Δ	30±0	0.9±0.1	52±9	120±30
*xrn1*Δ *lncRNA*Δ	30±0	0.9±0.1	42±6	110±17

D

GAL10	Estimated Lag Time (min)	V_i (% ctl/min)	$T_{1/2}$ (min)	T_{max} (min)
Wild type	30±0	0.3±0.0	130±11	290±17
*lncRNA*Δ	30±0	0.3±0.1	130±14	290±17
*xrn1*Δ	30±0	0.9±0.2	110±9	210±30
*xrn1*Δ *lncRNA*Δ	30±0	1.0±0.3	120±15	180±0

Figure 5. The *GAL* lncRNAs do not alter the *GAL7* or *GAL10* transcription profile in *xrn1*Δ cells when induced from derepressed conditions. (A–B) The *xrn1*Δ and *xrn1*Δ *lncRNA*Δ strains display superimposable transcriptional induction profiles of *GAL7* (A) and *GAL10* (B) from derepressed conditions. Isogenic wild-type (closed black circle), *lncRNA*Δ (closed red square), *xrn1*Δ (open blue square), and *xrn1*Δ *lncRNA*Δ (open green triangle) strains were analyzed for both rapid induction from derepressive conditions (+raffinose) and final, steady-state transcript levels by conducting time courses as above up to 300 min. Resulting induction profiles were plotted as in Figure 3 following normalization to a fully induced *GAL* “control” and to *SCR1*. Representative northern blots are shown in Figure S1. (C–D) *GAL7* (C) and *GAL10* (D) transcriptional induction kinetic profiles are similar between *xrn1*Δ and *xrn1*Δ *lncRNA*Δ cells. The lag times were calculated as above for each individual biological replicate following normalization to *SCR1* and are reported as the average with s.d. The T_{max} and $T_{1/2}$ correspond to the time point when transcript levels plateau and the half-time to T_{max}, respectively. Initial velocities were calculated as the slope of the straight line from the lag time to T_{max}, with increases most likely reflecting greater transcript production in a given cell population over time. All kinetic parameters were calculated independently for each biological replicate after graphical analysis, after normalization to *SCR1* and the control RNA, and are the average of the three replicates with the s.d.
doi:10.1371/journal.pbio.1001715.g005

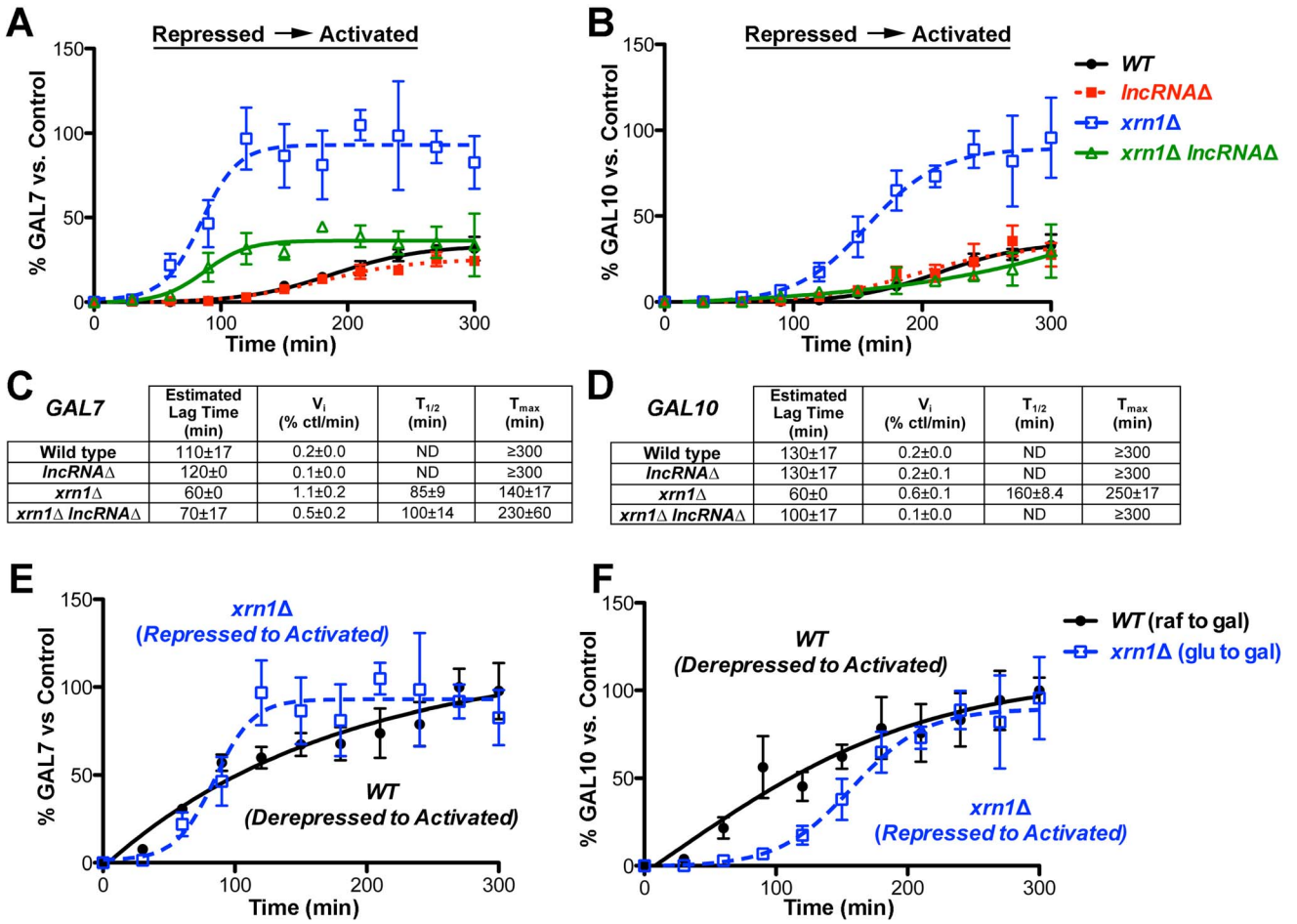

C

GAL7	Estimated Lag Time (min)	V_i (% ctl/min)	$T_{1/2}$ (min)	T_{max} (min)
Wild type	110±17	0.2±0.0	ND	≥300
*lncRNA*Δ	120±0	0.1±0.0	ND	≥300
*xrn1*Δ	60±0	1.1±0.2	85±9	140±17
*xrn1*Δ *lncRNA*Δ	70±17	0.5±0.2	100±14	230±60

D

GAL10	Estimated Lag Time (min)	V_i (% ctl/min)	$T_{1/2}$ (min)	T_{max} (min)
Wild type	130±17	0.2±0.0	ND	≥300
*lncRNA*Δ	130±17	0.2±0.1	ND	≥300
*xrn1*Δ	60±0	0.6±0.1	160±8.4	250±17
*xrn1*Δ *lncRNA*Δ	100±17	0.1±0.0	ND	≥300

Figure 6. The *GAL* lncRNAs enhance the kinetics of transcriptional induction from repressed conditions in *xrn1*Δ cells. (A–B) Rapid induction of *GAL7* (A) and *GAL10* (B) transcripts in *xrn1*Δ cells is lncRNA-dependent. Transcriptional induction of isogenic wild-type (closed black circle), *lncRNAΔ* (closed red square), *xrn1*Δ (open blue square), and *xrn1*Δ *lncRNA*Δ (open green triangle) strains induced from repressed conditions (+glucose) was analyzed as above to determine lag times, initial velocities, and final levels. Note that the transcript abundance is reported as a percentage of the fully induced "control" as in Figure 5, illustrating that wild-type cells are not fully induced at the end of this time course. Representative northern blots are shown in Figure S2. (C–D) *GAL7* (C) and *GAL10* (D) transcriptional induction kinetic profiles illustrate lncRNA-dependent kinetic enhancement from repressed conditions. Kinetic parameters were determined as in Figure 5. Strains that did not reach an induction plateau within the 300 min time frame display T_{max} values that are equal to or greater than 300 min. In these cases, half-times ($T_{1/2}$) were not determined (ND). (E–F) The lncRNA-dependent enhanced induction in *xrn1*Δ cells parallels wild-type induction from a derepressed state. Transcriptional profile overlay of *GAL7* (E) and *GAL10* (F) induction in wild-type cells (closed black circle) from derepressed to activated conditions as compared to *xrn1*Δ cells (opened blue square) from repressive conditions.
doi:10.1371/journal.pbio.1001715.g006

(Figure 5A–B). This is in line with other studies demonstrating identical induction profiles from derepressive conditions between wild-type and *xrn1*Δ cells [26,45]. Moreover, this further illustrates that *GAL* lncRNA-dependent repression is not a general phenotype of RNA decay-deficient strains. *XRN1*-deficient cells did, however, show increased transcript levels at early time points within the induction profile of both genes, as evidenced by the higher "shoulder" in the graphical analysis (Figure 5A–B) and increased initial velocities of transcript accumulation (Figure 5C–D). These increases are not due to the *GAL* lncRNAs though, as the induction profiles of *GAL7* and *GAL10* in the *xrn1*Δ strain are superimposable with the *xrn1*Δ *lncRNA*Δ strain. This also demonstrates that the *lncRNA*Δ mutation itself, and resulting loss of Reb1 binding, does not impair the transcriptional activity of *GAL7* or *GAL10*. Consistently, both the *xrn1*Δ and *xrn1*Δ *lncRNA*Δ strains have similar kinetic parameters for transcriptional induction. This includes identical initial velocities as well as half time ($T_{1/2}$) and time to maximum transcript levels (T_{max}) between *xrn1*Δ strains regardless of the presence or absence of the *GAL* lncRNAs (Figure 5C–D). Thus, the *GAL* lncRNAs do not alter the transcriptional induction of the *GAL* genes in *XRN1*-deficient cells from derepressive conditions.

The *GAL* lncRNAs Alter the Kinetics of Induction from Repressed Conditions in *xrn1*Δ Cells

We then analyzed the transcriptional induction kinetics of *xrn1*Δ cells from repressed (+glucose) to activated conditions to determine the role of the *GAL* lncRNAs during this specific transcriptional switch (Figure S2, representative northern blot). Resulting *GAL7* and *GAL10* profiles were plotted as above with respect to the same, fully induced wild-type control. In contrast to induction from derepressed conditions, this analysis revealed sharply different

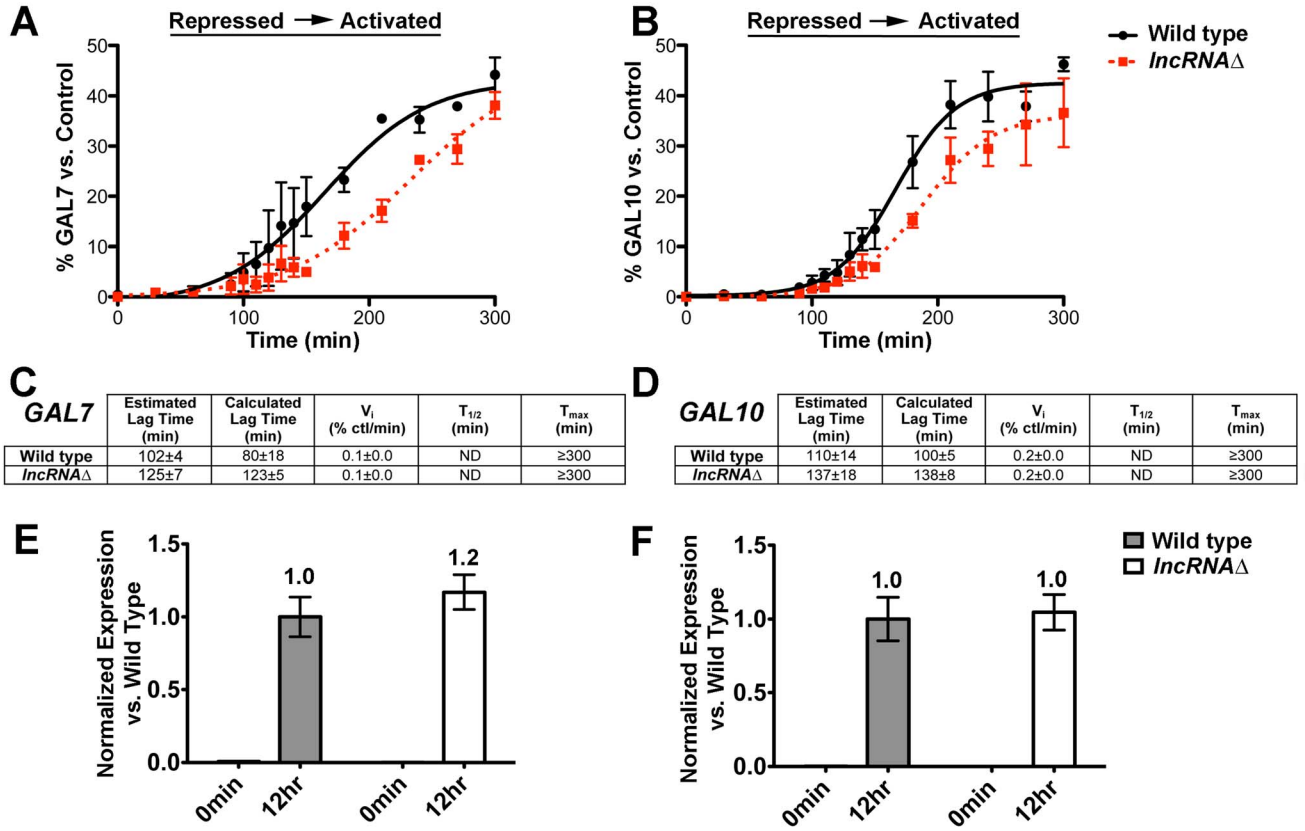

C

GAL7	Estimated Lag Time (min)	Calculated Lag Time (min)	V_i (% ctl/min)	$T_{1/2}$ (min)	T_{max} (min)
Wild type	102±4	80±18	0.1±0.0	ND	≥300
*lncRNA*Δ	125±7	123±5	0.1±0.0	ND	≥300

D

GAL10	Estimated Lag Time (min)	Calculated Lag Time (min)	V_i (% ctl/min)	$T_{1/2}$ (min)	T_{max} (min)
Wild type	110±14	100±5	0.2±0.0	ND	≥300
*lncRNA*Δ	137±18	138±8	0.2±0.0	ND	≥300

Figure 7. The *GAL* lncRNAs kinetically enhance *GAL* gene induction from repressed conditions in wild-type cells. (A–B) The *GAL* lncRNAs increase the rate of *GAL7* and *GAL10* activation in wild-type cells. Graphical representation of transcriptional induction of *GAL7* (A) and *GAL10* (B) in wild-type (closed black circle) and *lncRNAΔ* (closed red square) strains from repressed to activated conditions. High-resolution transcriptional analysis was conducted with wild-type or *lncRNA*Δ cells from repressed conditions from 0 to 300 min by including 10 additional 10-min time points between 90 and 150 min. Transcript abundance is reported as a percentage of the control as previously described. The differences in final *GAL7* or *GAL10* transcript levels at the 300 min time point are not statistically significant (p value>0.2). Representative northern blots are shown in Figure S3. (C–D) The GAL lncRNAs increase the kinetics of transcriptional activation from repressive conditions. Transcription induction parameters for the wild-type and *lncRNA*Δ strains were determined as above for three independent biological replicates. Calculated lag times were determined using curve-fitting analysis (DM Fit v. 2.0) [54], which facilitates quantitative assessment of lag from the curve fit (Figure S4). Lag times assessed from the data points as in prior figures are denoted as "estimated" lag times for differentiation from the curve fitting values. The estimated lag times result in p values from a two-tailed t test of 0.12 and 0.09 for *GAL7* and *GAL10*, respectively, whereas calculated lag times are significantly different between wild-type and *lncRNA*Δ strains (*GAL7* lag p value = 0.01; *GAL10* lag p value = 0.07). The initial velocities of transcript accumulation are not significantly different. (E–F) The presence of *GAL* lncRNAs does not alter the final levels of *GAL7* and *GAL10* transcripts at longer time points postactivation. *GAL7* (E) and *GAL10* (F) transcript levels were measured by RT-qPCR under repressed conditions (0 min time point) and after a 12-h shift to activated conditions (12-h time point) from repressed to activating conditions. *GAL7* and *GAL10* transcripts were measured from three biological replicates and normalized to *ACT1*. Normalized expression is presented as the average fold change from the first wild-type biological replicate with error bars representing the SEM. Note that the *GAL10* lncRNA, which is also recognized by the *GAL10* primers, is not evident at the 0 min time point due to the high expression levels of *GAL7* and *GAL10* after 12 h and necessary scaling of the bar graph.
doi:10.1371/journal.pbio.1001715.g007

transcriptional profiles between *xrn1*Δ and wild-type cells (Figure 6). In fact, *xrn1*Δ cells showed shorter lag times as well as ~3-fold higher levels of *GAL7* and *GAL10* transcripts as compared to wild type (Figure 6A–B). Kinetic analysis revealed that *xrn1*Δ cells have a more rapid approach to steady state than wild-type cells when induced from repressive conditions, as evidenced by the reduced lag time and 3- to 6-fold increase in the initial rate (V_i) of transcript accumulation for both *GAL7* and *GAL10* (Figure 6C–D). This is also illustrated by the fact that *xrn1*Δ cells reach 100% of the fully induced "control" within the 300 min time frame, while wild-type cells do not (Figure 6A–B). This rapid, high-level induction in *xrn1*Δ cells during the switch from repressed to activated conditions is consistent with the reduced association of Cyc8 and faster recruitment of RNAPII (see Figure 4).

Strikingly, removal of the *GAL* lncRNAs abolished both the rapid induction and high transcript levels in the *xrn1*Δ strain, resulting in profiles more similar to wild type (Figure 6A–B). In fact, the *GAL10* induction profile of *xrn1*Δ *lncRNA*Δ cells is superimposable with that of wild-type cells, demonstrating that the rapid induction of this gene in *xrn1*Δ cells is fully dependent on the *GAL* lncRNAs (Figure 6B,D). The induction profile of *GAL7* was also restored by incorporation of the *lncRNA*Δ mutation into the *xrn1*Δ strain, but to a lesser extent (Figure 6A,C). This partial reduction may be due to the contribution of another lncRNA that overlaps *GAL7*, as prior studies have indicated the presence of a *GAL7* antisense transcript that originates outside of the *lncRNA*Δ mutation [24]. Interestingly, removal of the *GAL* lncRNAs resulted in both a longer lag time as well as decreased initial velocity in *XRN1*-deficient cells (Figure 6C–D). This suggests that the *GAL*

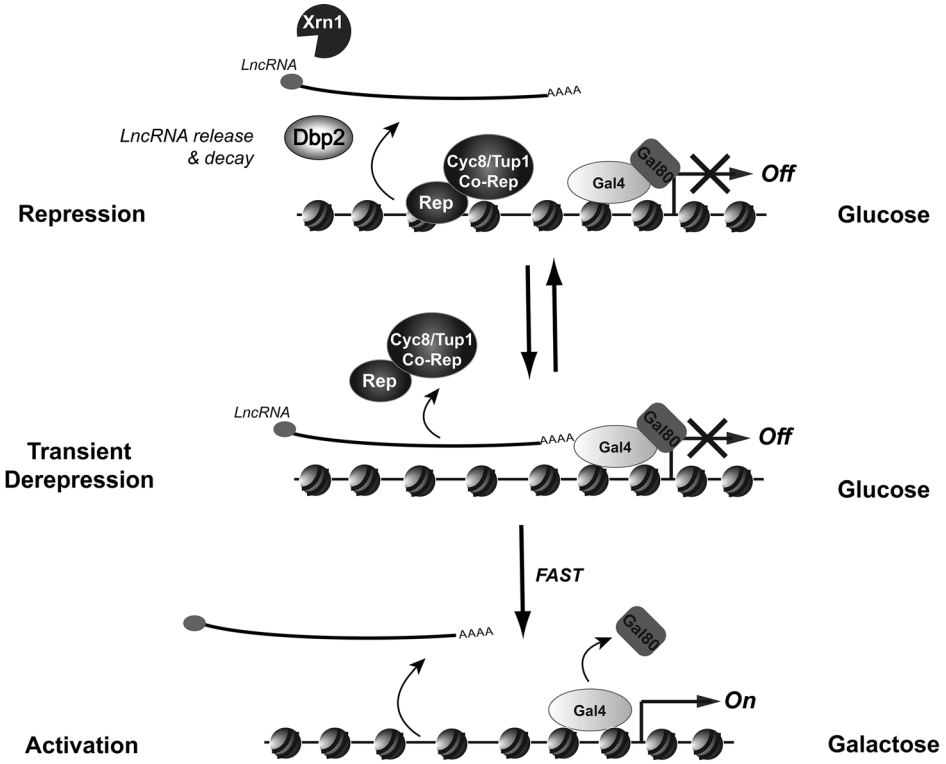

Figure 8. The *GAL* cluster lncRNAs poise the protein-coding *GAL* genes for rapid induction from repressive conditions. Transcriptional repression of the protein-coding *GAL* genes occurs through binding of glucose-responsive transcriptional repressors (Rep) and subsequent recruitment of co-repressors Tup1–Cyc8 to gene promoters (repression) [28,32,46–48,51]. Derepression is accomplished through lncRNA-dependent displacement of these repressors from chromatin. Displacement may occur through transcriptional interference and/or formation of RNA–DNA hybrids between the lncRNA and targeted, protein-coding gene. Derepression is transient, however, due to the action of Dbp2 and Xrn1, which facilitate lncRNA release from chromatin and RNA decay, respectively. This equilibrium between repressed and derepressed states allows for faster transcriptional activation in the presence of galactose. Activation then requires release of the Gal80 inhibitor protein from the Gal4 activator and subsequent recruitment of coactivating complexes and RNAPII (not pictured) [29]. Thus, the *GAL* lncRNAs function at the temporal level of gene regulation by enhancing the kinetics of *GAL* gene induction from transcriptionally repressive conditions.
doi:10.1371/journal.pbio.1001715.g008

lncRNAs function at the kinetic level by enhancing the approach to steady state. It also indicates that the *GAL* lncRNA molecules have the largest impact at the point of induction of the protein-coding *GAL* genes.

Next, we asked if the induction of *xrn1*Δ cells from repressed conditions (+glucose) is similar to that of wild-type cells from derepressed conditions (+raffinose), with the idea that lncRNA-dependent derepression in *XRN1*-deficient cells should mimic the derepressed transcriptional state in wild-type cells. Overlaying the *GAL7* and *GAL10* induction profiles revealed that *xrn1*Δ cells exhibit a similar induction trend from repressed conditions as wild-type cells induced from derepressed conditions (Figure 6E–F). This is consistent with the fact that *xrn1*Δ cells have reduced association of Cyc8 (Figure 4) and the idea that the *GAL* lncRNAs promote derepression of the protein-coding *GAL* genes in *xrn1*Δ cells. The difference in shape of the two curves between wild type and *xrn1*Δ may reflect the activity of other, glucose-dependent repression mechanisms (see Discussion) or the presence of low levels of Cyc8 at the *GAL* gene promoters that are below our detection by ChIP. Regardless, this is consistent with a model whereby the *GAL* lncRNAs activate gene expression by promoting derepression.

The *GAL* LncRNAs Promote Induction of *GAL7* and *GAL10* Genes from Repressed Conditions in Wild-Type Cells

Our results above demonstrate a positive role for the *GAL* lncRNAs in promoting gene expression. Furthermore, our studies suggest that these noncoding RNAs impact the timing of transcriptional activation by stimulating the kinetics of induction. Given this knowledge, we then asked if the *GAL* lncRNAs have any effect in wild-type cells, which were not initially evident due to the analysis of induction with 30 min time points. To this end, we conducted a higher time-resolved analysis of *GAL7* and *GAL10* induction from repressed conditions in wild-type and *lncRNA*Δ cells by including additional 10 min time points at the induction point, immediately prior to and following recruitment of RNAPII (Figure 4A). Strikingly, this revealed distinct *GAL7* and *GAL10* induction profiles between wild-type and *lncRNA*Δ strains (Figure 7A–B; Figure S3). More specifically, wild-type cells expressing the *GAL* lncRNAs induced both *GAL7* and *GAL10* faster than the *lncRNA*Δ cells, resulting in a clear separation of the transcriptional profiles between the two strains along the *x*-axis (Figure 7A–B). Lag time calculation revealed that *lncRNA*Δ cells lacking the *GAL* lncRNAs exhibit transcriptional lags of ~125–137 min, and wild-type cells induced both *GAL7* and *GAL10* ~30 min faster (Figure 7C–D, estimated lag time). This suggests that the *GAL* lncRNAs promote induction in wild-type cells. To more quantitatively assess lag times between wild-type and *lncRNA*Δ strains, we then utilized a curve fitting method for mathematical assignment of lag times (DM fit v2.0 Excel Macro) [54], which was only possible with higher time-resolved analysis (Figure S4). The calculated lag times, although similar in magnitude to the estimates, resulted in more statistically significant

differences between wild-type and *lncRNAΔ* strains (Figure 7C–D; p values<0.1 for both genes). This suggests that curve fitting may be a more accurate assessment of lag times from biological data sets. More importantly, however, this demonstrates that the *GAL* lncRNAs promote a subtle but reproducible acceleration of induction in wild-type cells. In contrast to the lncRNA-dependent reduction of lag times, we did not observe a significant difference in the initial velocity of transcript accumulation between strains, however (Figure 7C–D). This indicates that either the *GAL* lncRNAs do not alter transcript accumulation rates in wild-type cells or that this effect is not evident by analysis across a cell population when the lncRNA levels are low (est. 1 in 14 cells in [24]). Regardless, the statistically significant shift in lag times suggests that the *GAL* lncRNAs enhance the induction of the *GAL7* and *GAL10* genes in wild-type cells, consistent with an effect on induction kinetics rather than steady-state levels. Moreover, the final levels of *GAL7* and *GAL10* within the 5-h time course (Figure 7A–B) or after 12 h postinduction were not significantly different between wild-type and *lncRNA*Δ strains (Figure 7E–F). This indicates that the *GAL* lncRNAs promote transcriptional induction in wild-type cells without altering the final transcript abundance of the targeted protein-coding genes. We propose that the *GAL* lncRNAs poise the protein-coding *GAL* genes for rapid induction, thereby enhancing the transcriptional switch from repressed to activated conditions.

Taken together, our studies demonstrate that the *GAL* lncRNAs enhance the activation kinetics of the inducible *GAL* genes from repressed conditions. Based on these observations, we present a model whereby the *GAL* lncRNAs displace glucose-dependent repressors from the *GAL* gene promoters under typically repressive conditions (Figure 8). Because this role does not result in full derepression in wild-type cells, we suggest that this displacement is transient due to the action of Dbp2 and Xrn1, which promote lncRNA release and decay, respectively [37,38,43,55]. If this is the case, this suggests that the *GAL* lncRNAs complement the roles of proteinaceous factors to increase the efficiency of the *GAL* gene transcriptional switch [29,39,56]. Moreover, these studies indicate that the *GAL* lncRNAs promote formation of a dynamic chromatin template. These dynamics facilitate faster activation by poising the *GAL* genes for induction in response to galactose, which may provide a selective advantage for cells responding to changing environmental conditions. This indicates that the *GAL* lncRNAs temporally regulate gene expression by influencing the rate of transcriptional responses to extracellular stimuli.

Discussion

In an effort to define the role of the *GAL10s* lncRNA at the *GAL* cluster, our studies uncovered an important new role for both this lncRNA and the previously characterized *GAL10* lncRNA in activating gene expression from repressed conditions [24–26]. Glucose-dependent repression of the *GAL* genes is accomplished through several, mechanistically distinct processes including inhibition of the Gal4 activator, reduction of intracellular galactose uptake, and transcriptional repression of *GAL* promoters [28,31,34,40,46,48,51,56]. Our studies suggest that the *GAL* lncRNAs act on the latter mechanism by transiently displacing repressors from bound promoters, eliciting a dynamic equilibrium between derepressed and repressed states (Figure 8). We predict that this equilibrium poises the *GAL* genes for rapid induction, enhancing the transcriptional switch in response to extracellular signals.

The role of the *GAL* lncRNAs in enhancing induction is distinctly different from a true role in transcriptional activation, as has been documented for the roX RNAs in Drosophila or the activating ncRNAs (ncRNA-a) in mammalian cells [10,57]. Instead, our studies are more consistent with an interference-based model, whereby the *GAL* lncRNAs prevent the association of transcription factors with targeted gene promoters. This is supported by our observation that the *GAL* lncRNAs promote derepression by reducing the association of Cyc8 with the *GAL* genes. It is also in line with the fact that the *GAL* genes are not activated by the *GAL* lncRNAs per se but that the rate of induction is faster. It is also important to note that the kinetics reported here reflect the average transcriptional profile across a cell population and not the profile of individual cells. Because the abundance of the *GAL* mRNAs varies widely across single cells during early induction [58], it is possible that the lncRNA-dependent derepression proposed here facilitates a more robust mRNA accumulation in individual cells. Alternatively, the *GAL* lncRNAs may allow a larger population of cells to rapidly "switch" from repression to activation. Recent studies of the antisense *PHO84* lncRNA have proposed such a model whereby synthesis of this lncRNA results in cellular heterogeneity within a culture, with a fraction of cells exhibiting lncRNA-dependent repression of sense *PHO84* expression [59].

One of the most surprising aspects of our findings is that the *GAL10* lncRNA was thought to be exclusively repressive [24,25]. Although our studies show that both the *GAL10* and *GAL10s* lncRNAs promote gene expression, this is not necessarily mutually exclusive with a repressive role under specific conditions. However, it should be noted that the mechanism by which *GAL* lncRNAs induce transcriptional repression is still unknown. Early analysis of the *GAL10* lncRNA reported a delay of induction in a mixed glucose/galactose carbon source, making mechanistic insight difficult due to simultaneous presence of repressors and activators [24]. Subsequent studies then suggested that the *GAL* lncRNAs are repressive based on defective induction of the *GAL* genes in RNA decapping and decay-deficient strains [25]. While our studies corroborate the requirement for decapping for normal expression of the *GAL1*, and to a lesser extent *GAL10*, the fact that *xrn1*Δ cells do not show expression deficiencies and that both *xrn1*Δ and *dcp2*Δ cells show enhanced induction from repressed conditions argues against a repressive model. Instead, it is more likely that both the apparent expression defects in *dcp2*Δ cells and enhanced transcriptional induction occur through a common mechanism, whereby the *GAL* lncRNAs simply occlude transcription-factor binding sites at the targeted promoters. These transcription factors include glucose-dependent repressors when the *GAL* genes are induced from repressive conditions. However, the high level of the *GAL* lncRNAs in *dcp2*Δ cells may also cause interference with Gal4 or transcriptional coactivators such as SAGA and/or Mediator. This model would account for both the decreased transcriptional activity and histone acetylation at targeted chromatin (Figure 3) [25]. It is not clear, however, why *GAL1* is more sensitive to loss of decapping than other genes within the *GAL* cluster. Alternatively, the decreased transcriptional activity in *dcp2*Δ cells may be due to the recently proposed, and as-of-yet uncharacterized, role for decapping and decay factors in transcription [45]. Nevertheless, the fact that ablation of the *GAL10* lncRNA rescues *GAL1* transcriptional delays indicates that at least some part of the expression defect in *dcp2*Δ cells is dependent on the lncRNA [25]. Interestingly, the Set3C histone deactylase complex has also been shown to influence the kinetics of inducible genes [60], suggesting that lncRNA-dependent gene expression involves a complex interplay between histone modifications, lncRNAs, and metabolic genes.

One mechanism for promoter occlusion by lncRNAs is the formation of transient lncRNA–DNA hybrids at the *GAL* gene promoters. RNA–DNA hybrids, or R loops, are found in all organisms from yeast to humans and have been recently linked to regulation of chromatin architecture [61–63]. These structures form during transcription and have historically been associated with defects in termination and/or mRNP assembly (for review, see [63]). However, recent studies have found widespread formation of RNA–DNA hybrids at multiple gene loci in normal cells, with roles linked to transcriptional regulation, termination replication, and recombination [63–65]. Interestingly, the mammalian *DHFR* lncRNA forms an RNA–DNA triplex at the *DHFR* promoter [23]. This lncRNA represses transcription of the *DHFR* gene by interfering with the association of the TFIIB basal transcription factor, demonstrating that formation of this RNA–DNA hybrid occludes the binding site for the transcriptional apparatus. Although not an R loop, this study is consistent with the idea that lncRNAs may act through base pairing with target DNA. Recent studies implicating Dbp2 in both co-transcriptional mRNP assembly and in termination of coding and noncoding RNAs [37,55], two processes that prevent RNA–DNA hybrid formation, is also suggestive of a role for these nucleic acid structures in *GAL* gene induction. This model may even account for transcriptional interference of *GAL7*, and reduced association of the Gal4 activator, in strains with defects in *GAL10* transcriptional termination [66,67]. Moreover, recent work from the Tollervey lab has revealed striking differences in the termination/3′-end formation pathways and assembly of mRNA export factors between the majority of lncRNAs as compared to mRNAs, suggesting that the function of a transcript may be largely determined at late maturation steps [68]. The fact that p68, the human ortholog of Dbp2, also functions in lncRNA-dependent gene regulation suggests that the role for Dbp2 in RNA-mediated transcriptional control may be conserved between yeast and multicellular eukaryotes [69,70].

Due to predominantly cytoplasmic localization [71–73], both Xrn1 and Dcp2 were long thought to function solely in cytoplasmic RNA decay. However, studies of noncoding RNAs implicated both of these factors in nuclear RNA decay, as loss of either gene product elicited transcriptional defects [25,38,74]. The Choder laboratory has now provided evidence that both of these RNA decay factors are present in the nucleus and associate with chromatin [45]. Although it was suggested that these RNA decay factors promote transcription through an as-of-yet uncharacterized mechanism, it is possible that Xrn1 and Dcp2 function in co-transcriptional RNA decay. If this is the case, RNA–DNA hybrids may accumulate in *xrn1*Δ and *dcp2*Δ strains as a result of failure to "clear" aberrant transcriptional products. This would be consistent with prior studies showing that the *GAL10* lncRNA functions in *cis* by suggesting that these decay enzymes also function at the site of synthesis [24].

Given that the *GAL* lncRNAs promote induction, one might ask why we do not observe a net increase in steady-state transcript levels. This is consistent with studies of the Set3C complex, whose loss results in altered *GAL* gene induction kinetics with no effect on the final transcript levels [60]. Moreover, this is a well-known phenomenon in pre–steady state enzyme kinetics, which depends on different mechanisms than steady state [75]. In the case of *GAL7* and *GAL10* expression, steady state is the period when the rate of RNA synthesis and decay are matched. Pre–steady state, however, is governed by release of transcriptional repressors and recruitment of RNAPII. Our data strongly suggest that it is these latter two processes that are likely accelerated by the *GAL* lncRNAs.

The idea that lncRNAs play a kinetic role was initially put forth by studies of the *PHO5* lncRNA, which promotes transcriptional activation of the *PHO5* gene by altering the rate of chromatin remodeling [15]. It is well established that the protein-coding genes within the *GAL* cluster are highly regulated through carbon-source-specific transcription factors [27,29,32,40]. Upon a switch to galactose, glucose-dependent transcription factors are shunted to the cytoplasm, and the transcriptional activator Gal4 is released from the Gal80 inhibitor (Figure 7) [28,32,56,76]. Our studies now show that the *GAL* lncRNAs add to this mechanism by promoting this transcriptional switch. This suggests that lncRNAs promote "kinetic synergism," which is a model stating that kinetic alterations can have greater, combined effects on transcription than thermodynamics alone [77]. Kinetic synergism describes how the combination of multiple slow steps in transcriptional induction results in a more rapid and effective transcriptional activation. The *GAL* lncRNAs would function by promoting a more dynamic chromatin template, which synergistically enhances the activity of transcription factors by allowing transient access to DNA.

Our studies now complement the current knowledge regarding the function of lncRNAs by demonstrating that lncRNAs can influence the rate of transcriptional responses to extracellular cues. This is an exciting possibility because it suggests that the presence of lncRNAs may confer a selective advantage for a given organism to rapidly adapt to changing conditions. For example, wild-type cells could begin utilizing galactose as a carbon source at least 30 min earlier than cells without the *GAL* lncRNAs (Figure 7). This ability to influence the timing of a transcriptional switch would provide a rationale for the presence of lncRNAs in all eukaryotes and the conservation of these molecules near developmentally regulated genes in multicellular organisms [13,17,18,21,22]. Moreover, the ability of lncRNAs to alter chromatin dynamics may provide a more universal, functional role for widespread transcription of these noncoding molecules. Analysis of temporal effects of lncRNAs in multicellular organisms represents a future challenge in deciphering the role of these multifunctional regulators of the eukaryotic genome.

Materials and Methods

Plasmids and Strains

All plasmids were constructed by standard molecular biology techniques and are listed in Table 1. Yeast strains were constructed using classical yeast genetic techniques and are listed in Table 2. Oligos for PCR-mediated homologous recombination are listed in Table 3.

Table 1. Template plasmids for northern blot probes and strain construction.

Name	Description	Source/ Reference
pGAL1-GAL10-GAL7	pYGPM11l14	Open Biosystems
pSCR1	pYGPM29b01	Open Biosystems
pUG6	KanMx disruption cassette plasmid	[78]
pAG32	HygB disruption cassette plasmid	[79]
p3×FLAG	p3×FLAG:KanMX	[80]

doi:10.1371/journal.pbio.1001715.t001

Table 2. Yeast strains.

Strain	Genotype	Source
Wild type (BY4741)	*MATa his3Δ1 leu2Δ0 met15Δ0 ura3Δ0*	Open Biosystems
xrn1Δ	*MATa xrn1::KanR his3Δ1 leu2Δ0 met15Δ0 ura3Δ0*	Open Biosystems
dbp2Δ (BTY115)	*MATa dbp2::KanR ura3Δ0 leu2Δ0 his3Δ0 met15Δ0 lys?*	[37]
dcp2Δ (BTY289)	*MATa dcp2::HygR his3Δ1 leu2Δ0 met15Δ0 ura3Δ0*	This study
Wild type (FT4)	*MATa ura3–52 trp1-Δ63 his3-Δ200 leu2::PET56*	[24]
FT4+Reb1BSΔ	*MATa ura3–52 trp1-Δ63 his3-Δ200 leu2::PET56 gal10::URA3::pMV12 (EcoRI/XhoI-Reb1 BSΔ with BS2 silent)*	[24]
FT4 dbp2Δ (BTY219)	*MATa ura3–52 trp1-Δ63 his3-Δ200 leu2::PET56 dbp2::KanR*	This study
FT4+Reb1BSΔ dbp2Δ (BTY220)	*MATa ura3–52 trp1-Δ63 his3-Δ200 leu2::PET56 gal10::URA3::pMV12 (EcoRI/XhoI-Reb1 BSΔ with BS2 silent) dbp2::KanR*	This study
FT4 xrn1Δ (BTY226)	*MATa, ura3–52, trp1-Δ63, his3-Δ200, leu2::PET56 xrn1::HygR*	This study
FT4+Reb1BSΔ xrn1Δ (BTY227)	*MATa, ura3-52, trp1-Δ63, his3-Δ200, leu2::PET56 gal10::URA3::pMV12 (EcoRI/XhoI-Reb1 BSΔ with BS2 silent) xrn1::HygR*	This study
CYC8-3×FLAG (BTY234)	*MATa his3D1 leu2D0 met15D0 ura3D0 CYC8–3×FLAG (kanR)*	This study
dbp2Δ CYC8–3×FLAG (BTY248)	*MATa dbp2::HygB his3D1 leu2D0 met15D0 ura3D0 CYC8–3×FLAG (kanR)*	This study
xrn1Δ CYC8–3×FLAG (BTY249)	*MATa xrn1::HygB his3D1 leu2D0 met15D0 ura3D0 CYC8–3×FLAG (kanR)*	This study

All strains in the BY4741 background unless otherwise noted.
doi:10.1371/journal.pbio.1001715.t002

GAL Induction Analyses

Time courses were performed by growing strains at 30°C to an OD_{600} of 0.4 in YP 2% glucose or raffinose when indicated and shifting to 2% galactose media. 3OD units were harvested at 30 min time points from 0–180 min. Kinetic studies were conducted over a 300 min induction with 30 min time points with the inclusion of additional 10 min time points for higher resolution analysis of wild-type cells where indicated. Lag times, rates, and half times were calculated following autoradiography and quantification of abundance with respect to the *SCR1* loading control and a *GAL* control RNA when indicated. The *GAL* control RNA corresponds to RNA isolated from an isogenic wild-type strain following a 300 min induction from raffinose and is utilized as a control for full induction. Estimated lag times are independent of final, steady-state levels and correspond to the first time point in a series with increasing *GAL* mRNA signal above background after normalization to *SCR1*. Lag time error between biological replicates is reported as the standard deviation to illustrate the range of variation. Transcript levels were determined as the percentage of a wild-type control using the following equation: (*GAL* Transcript Signal/*SCR1* signal)÷(*GAL* Control/*SCR1* Control)×100%, whereby *GAL* positive corresponds to total RNA from a wild-type culture following a 300-min induction from derepressive (+raffinose) conditions. Transcriptional profiles were fitted to a dose response curve with variable slope in GraphPad Prism using the following equation: Y = lowest level+(highest level−lowest level)÷(1+10^((T$_{1/2}$−X)×HillSlope)). T_{max} corresponds to the first time point in a series when the *GAL* mRNA signal reaches a steady-state plateau, whereas initial velocities were determined by calculating the slope of a straight

Table 3. Oligos for strain construction.

DBP2 KO F	CAACAACCTGTAACAGAATTAAGCACTATTAAGGCAAATTTAGAGCAAA TATGCAGCTGAAGCTTCGTACGC
DBP2 KO R	GCAGTCAACTTATATAATTATTATTAATAGAGATGAATGAATTGAATCA CTTTGGCATAGGCGACTAGTGGATCTG
XRN1 KO F	ATGGGTATTCCAAAATTTTTCAGGTACATCTCAGAAAGATGGCCCATG ATTTTACAGCTTTGCAGCTGAAGCTTCGTACGC
XRN1 KO R	CTAAGTAGATTCGTCTTTTTTATTATCACGGTCAGCAGCATTGCTTTGT GACTTTGGCGAGCATAGGCGACTAGTGGATCTG
DCP2 KO F	ATAATATTGCTTTGAATCTGAAAAAAATAAAAGTACCTTCGCATT AGACAATGCAGCTGAAGCTTCGTACGC
DCP2 KO R	GGCTGCCTTCATTTACAGTGTGTCTATAAAACGTATAACACTTATT CTTTGCATAGGCGACTAGTGGATCTG
CYC8-3×FLAG F	TGTAGTAAGGCAAGTGGAAGAAGATGAAAACTACGACGACAGGGA ACAAAAGCTGGAG
CYC8-3×FLAG R	GATTATAAATTAGTAGATTAATTTTTTGAATGCAAACTTTCTATAGGGC GAATTGGGT

doi:10.1371/journal.pbio.1001715.t003

Table 4. RT-qPCR oligos.

nc10 F	GAGGTCTTGACCAAGCATCACA
nc10 R	TTCCAGACCTTTTCGGTCACA
nc7 F	TGAACAAGCCATATGGAGACA
nc7 R	CGACGATATTACCCGTAGGAA
GAL10 5′ F	GAGGTCTTGACCAAGCATCACA
GAL10 5′ R	TTCCAGACCTTTTCGGTCACA
GAL7 5′ F	CAAAAAGCGCTCGGACAACT
GAL7 5′ R	GCTTGGCTATTTTGTGAACACTGT
ACT1 F	TGGATTCCGGTGATGGTGTT
ACT1 R	TCAAAATGGCGTGAGGTAGAGA

doi:10.1371/journal.pbio.1001715.t004

Table 5. Oligos for northern blotting (dsDNA probes).

SCR1 F	GGATACGTTGAGAATTCTGGCCGAGG
SCR1 R	AATGTGCGAGTAAATCCTGATGGCACC
GAL7 F	CCTTGGTTAGGTCAACAGGAG
GAL7 R	AGTCGCATTCAAAGGAGCC
GAL10 F	GCATCACATTCCCTTCTATGAG
GAL10 R	ACGATTAGCATACCTGCCG
GAL1 F	TTGGACGGTTCTTATGTCAC
GAL1 R	GAGACTCGTTCATCAAGGC

doi:10.1371/journal.pbio.1001715.t005

line from the lag time to the T_{max}. $T_{1/2}$ times correspond to the average time to reach 50% maximum transcript levels within the cell population. Calculated lag times in Figure 7 were determined by fitting transcriptional induction data points for each biological replicate to a multivariable, exponential growth curve (DM Fit v. 2.0) [54] and are reported as the average with the s.d. All experiments were conducted with three biological replicates with error between transcript levels as SEM.

RNA Isolation and Quantitation

RNA extraction, northern blotting, and RT-qPCR were performed as in [37]. Probes were made from PCR products using the DNA plasmid templates listed in Table 1. RT-qPCR primers are listed in Table 4. Primers for Northern blotting probes are listed in Table 5.

ChIP Analysis

ChIP was performed as described previously [37], with the following modifications. After formaldehyde fixation, cells were pelleted and washed twice with cold wash buffer (50 mM HEPES•KOH, 140 mM NaCl, and 1 mM EDTA) and frozen in liquid nitrogen. Cells were then lysed cryogenically using a Retsch Oscillating Mill MM400. Cell lysates were then resuspended in cold Lysis Buffer (50 mM HEPES•KOH, 140 mM NaCl, 1 mM EDTA, 1% Triton X-100, 0.1% sodium deoxycholate, 1 mM PMSF and 1× protease inhibitor (complete, ETDA-free, Roche)), and chromatin was sheared by sonication. For Cyc8–3×flag ChIP, chromatin from $\sim 1.4\times10^8$ cells was immunoprecipitated with 1 µL of FLAG M2 monoclonal antibody (F3165, Sigma) and 12 µL of Protein G Dynabeads (30 mg/mL, Invitrogen) at 4°C for 2 h. For PolII ChIP, chromatin from $2–3\times10^8$ cells was immunoprecipitated with 1 µL of Rpb3 monoclonal antibody (WP012, Neoclone) and 12 µL of Protein G Dynabeads (30 mg/mL, Invitrogen) at 4°C for 2 h. Immunoprecipitated DNA was isolated as described previously [37]. Quantitative PCR was performed using Bio-Rad CFX96 Real-time system using PrimeTime Assay primers purchased from IDT (Table 6). All ChIP experiments were performed with three biological replicates and three technical repeats. Error bars represent the SEM of three biological replicates.

Yeast Cell Lysate Preparation and Western Blotting

Yeast cells were grown in YP 2% glucose to an O.D. of 0.4–0.6. We harvested 30 mg of yeast cells and lysed them with 1.85 M NaOH and 7.4% β-mercaptoethanol on ice for 10 min. Proteins were precipitated with 50% TCA on ice for 10 min and resuspended into 300 µl 1×SDS-PAGE loading dye. We then resolved 1–1.5 mg proteins by SDS-PAGE and transferred them to a nitrocellulose membrane. FLAG-tagged Cyc8 and Pgk1 were detected by rabbit anti-3×FLAG (F7425, Sigma) and monoclonal mouse anti-yeast Pgk1 (459250, Invitrogen), respectively. Proteins were visualized by alkaline phosphatase-based detection using AP-conjugated anti-rabbit secondary antibody and AP-conjugated anti-mouse secondary antibody, respectively, followed by a BCIP/NBT chemistry (S3771, Promega).

Supporting Information

Figure S1 Representative northern blots for *GAL7* and *GAL10* induction from derepressed conditions in *XRN1*-deficient cells. (A–B) *GAL7* (A) and *GAL10* (B) induction profile of one biological replicate for wild -type, *lncRNAΔ*, *xrn1Δ*, and *xrn1Δ lncRNAΔ* strains from derepressed conditions. Transcriptional induction assays were conducted from cells grown in derepressive (+raffinose) to activated (+galactose) conditions. *GAL7* and *GAL10* transcripts were detected by northern blotting using a

Table 6. Primetime assays for ChIP.

Name	Forward	Reverse	Probe
GAL10 promoter	CTTTATTGTTCGGAGCAGTGC	GCTCATTGCTATATTGAAGTACGG	CGGTGAAGACGAGGACGCACG
GAL10 5′	TGGTGCTGGATACATTGGTTC	AGGGAATGTGATGCTTGGTC	TGACTGTGTTGTTGCTGATAACCTGTCG
GAL7 promoter	GCGCTCGGACAACTGTTG	TTTCCGACCTGCTTTTATATCTTTG	CCGTGATCCGAAGGACTGGCTATACA
GAL7 5′	ATCATACAATGGAGCTGTGGG	CTAGCCATTCCCATAGACGTTAC	AAGCAGCCTCCTGTTGACCTAACC
GAL6 promoter	CCAGAAAGTCACCTGCTCTC	GCATGTAACAAAAGAGCAAGGG	CGCCGACGGGCACCCATAA
ACT1 middle	ATTGAGAGTTGCCCCAGAAG	ATGGAAACGTAGAAGGCTGG	ACACCC TGTTCTTTTGACTGAAGCTCC

doi:10.1371/journal.pbio.1001715.t006

^{32}P-labeled double-stranded DNA probe as in Figure 1. *SCR1* was detected similarly and serves as a loading control. Lag times correspond to the average time to detection of *GAL* transcripts for the three independent biological replicates shown in Figure 5 following normalization to *SCR1* and the control RNA (not pictured). Note that bands are detectible in wild-type and *lncRNA*Δ strains in (B) at the 30 min time point (yielding similar lag times for all strains), but appear weaker than in *xrn1*Δ strains due to loading differences between blots.
(TIF)

Figure S2 Representative northern blots for *GAL7* and *GAL10* induction from repressed conditions in *XRN1*-deficent cells. (A–B) *GAL7* (A) and *GAL10* (B) induction profile of one biological replicate for wild-type, *lncRNAΔ*, *xrn1Δ*, and *xrn1Δ lncRNAΔ* strains from repressed conditions. Transcriptional induction assays were conducted as above during the switch from repressed (+glucose) to activated (+galactose) conditions. Lag times correspond to the average time to detection of *GAL* transcripts for the three, independent biological replicates shown in Figure 6 and are calculated following normalization to *SCR1* and the *GAL* control.
(TIF)

Figure S3 Transcriptional induction assays for wild-type and *lncRNA*Δ strains from repressed to activated conditions. (A–B) High-resolution analysis of transcriptional induction in wild-type and *lncRNAΔ* cells. Transcription induction was measured in wild-type or *lncRNA*Δ cells from repressed conditions as above with the inclusion of additional 10 min time points from 90–150 min immediately prior to recruitment of RNAPII (see Figure 4). Lag times are not determined visually from the blots but were calculated as the average across three biological replicates after normalization to the *SCR1* loading control.
(TIF)

Figure S4 Individual transcriptional induction profiles following curve fitting analysis. Individual biological replicates of induction profiles of wild-type and *lncRNAΔ* strains from repressed to activated conditions. Transcript levels were normalized to *SCR1* and the *GAL* "control" RNA as above. Resulting data points were then fit to a dynamic exponential growth curve (DM fit v. 2.0) [54]. R^2 values and lag times are shown for each individual profile. Calculated lag times are reported in Figure 7 (C and D) and correspond to the average lag time and s.d. for induction of *GAL7* and *GAL10* after curve fitting for wild-type and *lncRNA*Δ strains.
(TIF)

Acknowledgments

Special thanks to Scott Briggs, Joe Ogas, Barb Golden, and Joe Kappock for advice and critical reading of this manuscript.

Author Contributions

The author(s) have made the following declarations about their contributions: Conceived and designed the experiments: SW SCC CJP EJT. Performed the experiments: WKM SW SCC CJP EJT. Analyzed the data: WKM SW SCC CJP. Contributed reagents/materials/analysis tools: WKM SW SCC. Wrote the paper: EJT.

References

1. Weake VM, Workman JL (2010) Inducible gene expression: diverse regulatory mechanisms. Nat Rev Gen 11: 426–437.
2. Hahn S, Young ET (2011) Transcriptional regulation in Saccharomyces cerevisiae: transcription factor regulation and function, mechanisms of initiation, and roles of activators and coactivators. Genetics 189: 705–736.
3. Hu W, Alvarez-Dominguez JR, Lodish HF (2012) Regulation of mammalian cell differentiation by long non-coding RNAs. EMBO Rep 13: 971–983.
4. Rinn JL, Chang HY (2012) Genome regulation by long noncoding RNAs. Annu Rev Biochem 81: 145–166.
5. Pontier DB, Gribnau J (2011) Xist regulation and function explored. Human Genetics 130: 223–236.
6. Lee JT (2011) Gracefully ageing at 50, X-chromosome inactivation becomes a paradigm for RNA and chromatin control. Nat Rev Mol Cell Biol 12: 815–826.
7. Zhao J, Sun BK, Erwin JA, Song JJ, Lee JT (2008) Polycomb proteins targeted by a short repeat RNA to the mouse X chromosome. Science 322: 750–756.
8. Tsai MC, Manor O, Wan Y, Mosammaparast N, Wang JK, et al. (2010) Long noncoding RNA as modular scaffold of histone modification complexes. Science 329: 689–693.
9. Hung T, Wang Y, Lin MF, Koegel AK, Kotake Y, et al. (2011) Extensive and coordinated transcription of noncoding RNAs within cell-cycle promoters. Nat Gen 43: 621–629.
10. Lai F, Orom UA, Cesaroni M, Beringer M, Taatjes DJ, et al. (2013) Activating RNAs associate with Mediator to enhance chromatin architecture and transcription. Nature 494: 497–501.
11. Feng J, Bi C, Clark BS, Mady R, Shah P, et al. (2006) The Evf-2 noncoding RNA is transcribed from the Dlx-5/6 ultraconserved region and functions as a Dlx-2 transcriptional coactivator. Genes Dev 20: 1470–1484.
12. Natoli G, Andrau JC (2012) Noncoding transcription at enhancers: general principles and functional models. Annu Rev Genet 46: 1–19.
13. Orom UA, Derrien T, Beringer M, Gumireddy K, Gardini A, et al. (2010) Long noncoding RNAs with enhancer-like function in human cells. Cell 143: 46–58.
14. Hainer SJ, Pruneski JA, Mitchell RD, Monteverde RM, Martens JA (2011) Intergenic transcription causes repression by directing nucleosome assembly. Genes Dev 25: 29–40.
15. Uhler JP, Hertel C, Svejstrup JQ (2007) A role for noncoding transcription in activation of the yeast PHO5 gene. Proc Natl Acad Sci U S A 104: 8011–8016.
16. Latos PA, Pauler FM, Koerner MV, Senergin HB, Hudson QJ, et al. (2012) Airn transcriptional overlap, but not its lncRNA products, induces imprinted Igf2r silencing. Science 338: 1469–1472.
17. Ulitsky I, Shkumatava A, Jan CH, Sive H, Bartel DP (2011) Conserved function of lincRNAs in vertebrate embryonic development despite rapid sequence evolution. Cell 147: 1537–1550.
18. Ghosal S, Das S, Chakrabarti J (2013) Long noncoding RNAs: new players in the molecular mechanism for maintenance and differentiation of pluripotent stem cells. Stem Cells Dev 22: 2240–2253.
19. Kitagawa M, Kotake Y, Ohhata T (2012) Long non-coding RNAs involved in cancer development and cell fate determination. Curr Drug Targets 13: 1616–1621.
20. Santoro F, Mayer D, Klement RM, Warczok KE, Stukalov A, et al. (2013) Imprinted Igf2r silencing depends on continuous Airn lncRNA expression and is not restricted to a developmental window. Development 140: 1184–1195.
21. Guttman M, Donaghey J, Carey BW, Garber M, Grenier JK, et al. (2011) lincRNAs act in the circuitry controlling pluripotency and differentiation. Nature 477: 295–300.
22. Moran VA, Perera RJ, Khalil AM (2012) Emerging functional and mechanistic paradigms of mammalian long non-coding RNAs. Nucleic Acids Res 40: 6391–6400.
23. Martianov I, Ramadass A, Serra Barros A, Chow N, Akoulitchev A (2007) Repression of the human dihydrofolate reductase gene by a non-coding interfering transcript. Nature 445: 666–670.
24. Houseley J, Rubbi L, Grunstein M, Tollervey D, Vogelauer M (2008) A ncRNA modulates histone modification and mRNA induction in the yeast GAL gene cluster. Mol Cell 32: 685–695.
25. Geisler S, Lojek L, Khalil AM, Baker KE, Coller J (2012) Decapping of long noncoding RNAs regulates inducible genes. Mol Cell 45: 279–291.
26. Pinskaya M, Gourvennec S, Morillon A (2009) H3 lysine 4 di- and trimethylation deposited by cryptic transcription attenuates promoter activation. EMBO J 28: 1697–1707.
27. Sellick CA, Campbell RN, Reece RJ (2008) Galactose metabolism in yeast-structure and regulation of the leloir pathway enzymes and the genes encoding them. Int Rev Cell Mol Biol 269: 111–150.
28. Gancedo JM (1998) Yeast carbon catabolite repression. MMBR 62: 334–361.
29. Traven A, Jelicic B, Sopta M (2006) Yeast Gal4: a transcriptional paradigm revisited. EMBO Rep 7: 496–499.
30. Yano K, Fukasawa T (1997) Galactose-dependent reversible interaction of Gal3p with Gal80p in the induction pathway of Gal4p-activated genes of Saccharomyces cerevisiae. Proc Natl Acad Sci U S A 94: 1721–1726.
31. Platt A, Reece RJ (1998) The yeast galactose genetic switch is mediated by the formation of a Gal4p-Gal80p-Gal3p complex. EMBO J 17: 4086–4091.
32. Bhat PJ, Murthy TV (2001) Transcriptional control of the GAL/MEL regulon of yeast Saccharomyces cerevisiae: mechanism of galactose-mediated signal transduction. Mol Microbiol 40: 1059–1066.
33. Lohr D, Venkov P, Zlatanova J (1995) Transcriptional regulation in the yeast GAL gene family: a complex genetic network. FASEB J 9: 777–787.

34. Johnston M (1987) A model fungal gene regulatory mechanism: the GAL genes of Saccharomyces cerevisiae. Microbiol Rev 51: 458–476.
35. Costa FF (2010) Non-coding RNAs: meet thy masters. Bioessays 32: 599–608.
36. Ramaiah M, Shum EY, Wilkinson MF (2012) How to activate a gene: decap its associated noncoding RNA. Mol Cell 45: 271–273.
37. Cloutier SC, Ma WK, Nguyen LT, Tran EJ (2012) The DEAD-box RNA helicase Dbp2 connects RNA quality control with repression of aberrant transcription. J Biol Chem 287: 26155–26166.
38. van Dijk EL, Chen CL, d'Aubenton-Carafa Y, Gourvennec S, Kwapisz M, et al. (2011) XUTs are a class of Xrn1-sensitive antisense regulatory non-coding RNA in yeast. Nature 475: 114–117.
39. Bryant GO, Ptashne M (2003) Independent recruitment in vivo by Gal4 of two complexes required for transcription. Mol Cell 11: 1301–1309.
40. Johnston M, Flick JS, Pexton T (1994) Multiple mechanisms provide rapid and stringent glucose repression of GAL gene expression in Saccharomyces cerevisiae. Mol Cell Biol 14: 3834–3841.
41. Adams BG (1972) Induction of galactokinase in Saccharomyces cerevisiae: kinetics of induction and glucose effects. J Bacteriol 111: 308–315.
42. Amberg DC, Goldstein AL, Cole CN (1992) Isolation and characterization of RAT1: an essential gene of Saccharomyces cerevisiae required for the efficient nucleocytoplasmic trafficking of mRNA. Genes Dev 6: 1173–1189.
43. Larimer FW, Stevens A (1990) Disruption of the gene XRN1, coding for a 5′-3′ exoribonuclease, restricts yeast cell growth. Gene 95: 85–90.
44. Grousl T, Ivanov P, Frydlova I, Vasicova P, Janda F, et al. (2009) Robust heat shock induces eIF2alpha-phosphorylation-independent assembly of stress granules containing eIF3 and 40S ribosomal subunits in budding yeast, Saccharomyces cerevisiae. J Cell Sci 122: 2078–2088.
45. Haimovich G, Medina DA, Causse SZ, Garber M, Millan-Zambrano G, et al. (2013) Gene expression is circular: factors for mRNA degradation also foster mRNA synthesis. Cell 153: 1000–1011.
46. Papamichos-Chronakis M, Gligoris T, Tzamarias D (2004) The Snf1 kinase controls glucose repression in yeast by modulating interactions between the Mig1 repressor and the Cyc8-Tup1 co-repressor. EMBO Rep 5: 368–372.
47. Zhou H, Winston F (2001) NRG1 is required for glucose repression of the SUC2 and GAL genes of Saccharomyces cerevisiae. BMC Genetics 2: 5.
48. Trumbly RJ (1992) Glucose repression in the yeast Saccharomyces cerevisiae. Mol Microbiol 6: 15–21.
49. Farrell S, Simkovich N, Wu Y, Barberis A, Ptashne M (1996) Gene activation by recruitment of the RNA polymerase II holoenzyme. Genes Dev 10: 2359–2367.
50. Zheng W, Xu HE, Johnston SA (1997) The cysteine-peptidase bleomycin hydrolase is a member of the galactose regulon in yeast. J Biol Chem 272: 30350–30355.
51. Lutfiyya LL, Iyer VR, DeRisi J, DeVit MJ, Brown PO, et al. (1998) Characterization of three related glucose repressors and genes they regulate in Saccharomyces cerevisiae. Genetics 150: 1377–1391.
52. Wong KH, Struhl K (2011) The Cyc8-Tup1 complex inhibits transcription primarily by masking the activation domain of the recruiting protein. Genes Dev 25: 2525–2539.
53. Ducker CE, Simpson RT (2000) The organized chromatin domain of the repressed yeast a cell-specific gene STE6 contains two molecules of the corepressor Tup1p per nucleosome. EMBO J 19: 400–409.
54. Baranyi J, Roberts TA (1994) A dynamic approach to predicting bacterial growth in food. Int J Food Microbiol 23: 277–294.
55. Ma WK, Cloutier SC, Tran EJ (2013) The DEAD-box protein Dbp2 functions with the RNA-binding protein Yra1 to promote mRNP assembly. J Mol Biol: doi: 10.1016/j.jmb.2013.1005.1016. [Epub ahead of print].
56. Egriboz O, Jiang F, Hopper JE (2011) Rapid GAL gene switch of Saccharomyces cerevisiae depends on nuclear Gal3, not nucleocytoplasmic trafficking of Gal3 and Gal80. Genetics 189: 825–836.
57. Maenner S, Muller M, Frohlich J, Langer D, Becker PB (2013) ATP-dependent roX RNA remodeling by the helicase maleless enables specific association of MSL proteins. Mol Cell 51: 174–184.
58. Gandhi SJ, Zenklusen D, Lionnet T, Singer RH (2011) Transcription of functionally related constitutive genes is not coordinated. Nat Struct Mol Biol 18: 27–34.
59. Castelnuovo M, Rahman S, Guffanti E, Infantino V, Stutz F, et al. (2013) Bimodal expression of PHO84 is modulated by early termination of antisense transcription. Nat Struct Mol Biol 20: 851–858.
60. Kim T, Xu Z, Clauder-Munster S, Steinmetz LM, Buratowski S (2012) Set3 HDAC mediates effects of overlapping noncoding transcription on gene induction kinetics. Cell 150: 1158–1169.
61. Skourti-Stathaki K, Proudfoot NJ, Gromak N (2011) Human senataxin resolves RNA/DNA hybrids formed at transcriptional pause sites to promote Xrn2-dependent termination. Mol Cell 42: 794–805.
62. Stirling PC, Chan YA, Minaker SW, Aristizabal MJ, Barrett I, et al. (2012) R-loop-mediated genome instability in mRNA cleavage and polyadenylation mutants. Genes Dev 26: 163–175.
63. Aguilera A, Garcia-Muse T (2012) R loops: from transcription byproducts to threats to genome stability. Mol Cell 46: 115–124.
64. Sun Q, Csorba T, Skourti-Stathaki K, Proudfoot NJ, Dean C (2013) R-loop stabilization represses antisense transcription at the Arabidopsis FLC locus. Science 340: 619–621.
65. El Hage A, French SL, Beyer AL, Tollervey D (2010) Loss of topoisomerase I leads to R-loop-mediated transcriptional blocks during ribosomal RNA synthesis. Genes Dev 24: 1546–1558.
66. Greger IH, Aranda A, Proudfoot N (2000) Balancing transcriptional interference and initiation on the GAL7 promoter of Saccharomyces cerevisiae. Proc Natl Acad Sci U S A 97: 8415–8420.
67. Greger IH, Proudfoot NJ (1998) Poly(A) signals control both transcriptional termination and initiation between the tandem GAL10 and GAL7 genes of Saccharomyces cerevisiae. EMBO J 17: 4771–4779.
68. Tuck AC, Tollervey D (2013) A transcriptome-wide atlas of RNP composition reveals diverse classes of mRNAs and lncRNAs. Cell 154: 996–1009.
69. Arun G, Akhade VS, Donakonda S, Rao MR (2012) mrhl RNA, a long noncoding RNA, negatively regulates Wnt signaling through its protein partner Ddx5/p68 in mouse spermatogonial cells. Mol Cell Biol 32: 3140–3152.
70. Caretti G, Schiltz RL, Dilworth FJ, Di Padova M, Zhao P, et al. (2006) The RNA helicases p68/p72 and the noncoding RNA SRA are coregulators of MyoD and skeletal muscle differentiation. Dev Cell 11: 547–560.
71. van Dijk E, Cougot N, Meyer S, Babajko S, Wahle E, et al. (2002) Human Dcp2: a catalytically active mRNA decapping enzyme located in specific cytoplasmic structures. EMBO J 21: 6915–6924.
72. Sheth U, Parker R (2003) Decapping and decay of messenger RNA occur in cytoplasmic processing bodies. Science 300: 805–808.
73. Johnson AW (1997) Rat1p and Xrn1p are functionally interchangeable exoribonucleases that are restricted to and required in the nucleus and cytoplasm, respectively. Mol Cell Biol 17: 6122–6130.
74. Berretta J, Pinskaya M, Morillon A (2008) A cryptic unstable transcript mediates transcriptional trans-silencing of the Ty1 retrotransposon in S. cerevisiae. Genes Dev 22: 615–626.
75. Gutfreund H (1972) Enzymes: physical principles. London-New York-Sydney-Toronto: Wiley-Interscience.
76. De Vit MJ, Waddle JA, Johnston M (1997) Regulated nuclear translocation of the Mig1 glucose repressor. Mol Biol Cell 8: 1603–1618.
77. Herschlag D, Johnson FB (1993) Synergism in transcriptional activation: a kinetic view. Genes Dev 7: 173–179.
78. Guldener U, Heck S, Fielder T, Beinhauer J, Hegemann JH (1996) A new efficient gene disruption cassette for repeated use in budding yeast. Nucleic Acids Res 24: 2519–2524.
79. Goldstein AL, McCusker JH (1999) Three new dominant drug resistance cassettes for gene disruption in Saccharomyces cerevisiae. Yeast 15: 1541–1553.
80. Gelbart ME, Rechsteiner T, Richmond TJ, Tsukiyama T (2001) Interactions of Isw2 chromatin remodeling complex with nucleosomal arrays: analyses using recombinant yeast histones and immobilized templates. Mol Cell Biol 21: 2098–2106.

Regulation of Glucose-Dependent Gene Expression by the RNA Helicase Dbp2 in *Saccharomyces cerevisiae*

Zachary T. Beck,*,[1] Sara C. Cloutier,*,[1] Matthew J. Schipma,[†] Christopher J. Petell,* Wai Kit Ma,* and Elizabeth J. Tran*,[‡,2]

*Department of Biochemistry, Purdue University, West Lafayette, Indiana 47907-2063, [‡]Purdue University Center for Cancer Research, Purdue University, West Lafayette, Indiana 47907-2064, and [†]Next Generation Sequencing Core Facility, Feinberg School of Medicine, Northwestern University, Chicago, Illinois 60611

ABSTRACT Cellular homeostasis requires a fine balance between energy uptake, utilization, and growth. Dbp2 is a member of the DEAD-box protein family in *Saccharomyces cerevisiae* with characterized ATPase and helicase activity *in vitro*. DEAD-box RNA helicases are a class of enzymes that utilize ATP hydrolysis to remodel RNA and/or RNA–protein (RNP) composition. Dbp2 has been proposed to utilize its helicase activity *in vivo* to promote RNA–protein complex assembly of both messenger (m)RNAs and long noncoding (lnc)RNAs. Previous work from our laboratory demonstrated that loss of *DBP2* enhances the lncRNA-dependent transcriptional induction of the *GAL* genes by abolishing glucose-dependent repression. Herein, we report that either a carbon source switch or glucose deprivation results in rapid export of Dbp2 to the cytoplasm. Genome-wide RNA sequencing identified a new class of antisense hexose transporter transcripts that are specifically upregulated upon loss of *DBP2*. Further investigation revealed that both sense and antisense hexose transporter (*HXT*) transcripts are aberrantly expressed in *DBP2*-deficient cells and that this expression pathway can be partially mimicked in wild-type cells by glucose depletion. We also find that Dbp2 promotes ribosome biogenesis and represses alternative ATP-producing pathways, as loss of *DBP2* alters the transcript levels of ribosome biosynthesis (snoRNAs and associated proteins) and respiration gene products. This suggests that Dbp2 is a key integrator of nutritional status and gene expression programs required for energy homeostasis.

CELL growth and division is intimately coupled to cell mass, with the nutrient availability and ribosome content playing a key role in dictating growth rate (Lempiainen and Shore 2009). This involves phosphorylation cascades such as the TOR (target of rapamycin) and the Ras–cAMP–protein kinase A signaling pathways to transmit information regarding the availability of nutrients to essential processes for cell growth (Powers and Walter 1999; Warner 1999; Lempiainen and Shore 2009; Broach 2012).

Dbp2 is a member of the DEAD-box RNA helicase family in the budding yeast *Saccharomyces cerevisiae*. DEAD-box proteins are RNA-dependent ATPases that utilize ATP hydrolysis to catalyze structural rearrangements to RNA and RNA–protein (RNP) complexes (Bowers *et al.* 2006; Bhaskaran and Russell 2007; Del Campo *et al.* 2009; Jankowsky 2011; Putnam and Jankowsky 2013b). The metazoan ortholog of Dbp2, hDDX5, or p68 has been linked to ribosome biogenesis as well as a variety of gene regulatory processes including transcriptional regulation, alternative splicing, and mRNA export (Wilson *et al.* 2004; Buszczak and Spradling 2006; Caretti *et al.* 2006; Jalal *et al.* 2007; Salzman *et al.* 2007; Camats *et al.* 2008; Clark *et al.* 2008; Fuller-Pace and Moore 2011). Budding yeast Dbp2 is also required for ribosome biogenesis and numerous processes linked to transcriptional fidelity (Barta and Iggo 1995; Bond *et al.* 2001; Bohnsack *et al.* 2009; Cloutier *et al.* 2012; Cloutier *et al.* 2013; Ma *et al.* 2013).

Biochemical characterization has established that Dbp2 is a *bona fide* helicase and ATPase *in vitro*, with robust duplex unwinding in line with other DEAD-box proteins (Cloutier *et al.* 2012; Kovalev *et al.* 2012; Ma *et al.* 2013). Dbp2 associates directly with actively transcribed chromatin, suggestive of a cotranscriptional role (Cloutier *et al.* 2012). Moreover,

doi: 10.1534/genetics.114.170019
Manuscript received June 9, 2014; accepted for publication August 20, 2014; published Early Online August 27, 2014.
Supporting information is available online at http://www.genetics.org/lookup/suppl/doi:10.1534/genetics.114.170019/-/DC1.
[1]These authors contributed equally to this work.
[2]Corresponding author: Department of Biochemistry, Purdue University, BCHM 305, 175 S. University St., West Lafayette, IN 47907. E-mail: ejtran@purdue.edu

loss of *DBP2* results in decreased association of mRNA-binding proteins and nuclear export factors Yra1, Nab2, and Mex67 to mRNA (Ma *et al.* 2013). This has led to the model that Dbp2 promotes mRNP assembly by modulating nascent RNA structure during transcription.

Recent work from our laboratory connected the RNA helicase Dbp2 to long noncoding RNA (lncRNA)-dependent gene regulation (Cloutier *et al.* 2013). Although the precise molecular role(s) for the >30,000 eukaryotic lncRNAs identified thus far is not well defined, an emerging theme is that lncRNAs fine tune transcriptional switches in gene expression (Fatica and Bozzoni 2014). The *GAL* cluster genes are part of the galactose metabolic switch that allows budding yeast to rapidly adapt to the availability of galactose as an alternative to glucose as a carbon source (Lohr *et al.* 1995; Sellick *et al.* 2008). This switch involves a number of carbon source sensors, sugar transporters, signaling cascades, and transcriptional effectors to globally alter the metabolic program for energy production (Gancedo 1998; Johnston and Kim 2005; Traven *et al.* 2006; Broach 2012). Interestingly, our work revealed that the *GAL* lncRNAs function in this switch by enhancing the transcriptional response rate to the carbon source switch (Cloutier *et al.* 2013). Dbp2 antagonizes this role by maintaining glucose-dependent repression of the *GAL* genes, with loss of *DBP2* enhancing transcriptional induction in an lncRNA-dependent manner (Cloutier *et al.* 2013). This suggests that Dbp2 may be fundamentally integrated into gene regulatory programs that are responsive to nutritional status of the cell.

Herein, we show that Dbp2 plays a global role in glucose-dependent repression. Our results suggest that this RNA helicase is both regulated by carbon source availability and controls expression of energy-producing and -consuming gene expression networks. We also document a class of lncRNAs that are antisense to hexose transporter genes and show that the levels of these lncRNAs are dependent on Dbp2. These results are intriguing because glucose-dependent repression is primarily maintained by transcription factors whose activity is controlled by cellular signaling cascades. Our work now establishes a role for an RNA helicase in this process, indicating that gene expression networks may also be regulated by modulation of RNA structure.

Materials and Methods

Yeast strains

The strains used in this study include: *DBP2–GFP*, MAT**a** *DBP2–GFP:HIS3 his3Δ1 leu2Δ0 met15Δ0 ura3Δ0*; wild type, MAT**a** *his3Δ1 leu2Δ0 met15Δ0 ura3Δ0* dbp2Δ (BTY115), MAT**a** *dbp2::KanMx6 his3Δ1 leu2Δ0 met15Δ0 ura3Δ0*; *msn5Δ DBP2–GFP* MAT**a** *msn5::KanMx6 DBP2–GFP:HIS3 his3Δ1 leu2Δ0 met15Δ0 ura3Δ0; snf1Δ DBP2–GFP* MAT**a** *snf1::KanMx6 DBP2–GFP:HIS3 his3Δ1 leu2Δ0 met15Δ0 ura3Δ0*; *hog1Δ DBP2–GFP*, MAT**a** *hog1::KanMx6 DBP2–GFP:HIS3 his3Δ1 leu2Δ0 met15Δ0 ura3Δ0*; *DBP2–FLAG* MAT**a** *his3Δ1 leu2Δ0 met15Δ0 ura3Δ0 DBP2–3xFLAG:KanMx6*. All strains are in the BY4741 strain background. *DBP2–GFP* is available from Invitrogen whereas wild type is available from Open Biosystems. The *dbp2*Δ strain was constructed by PCR-mediated gene replacement as previously described (Cloutier *et al.* 2012).The *msn5Δ DBP2–GFP* and *snf1Δ DBP2–GFP* strains were constructed by PCR-mediated integration of a GFP tag into *DBP2* genomic locus in the the *msn5Δ*, *snf1Δ*, and *hog1Δ* strains available from Open Biosystems.

Table 1 Oligonucleotides for qPCR

ACT1 forward	TGGATTCCGGTGATGGTGTT
ACT1 reverse*	TCAAAATGGCGTGAGGTAGAGA
HXT1 forward**	GAATTGGAATCTGGTCGTTC
HXT1 reverse*	TAGACACCTTTTCCGGTGTT
HXT4 forward**	CCGCCTACGTTACAGTTTCC
HXT4 reverse*	ACAAAACCACCGAAAGCAAC
HXT5 sense forward	GCCGGTTACAACGATAATTTGG
HXT5 sense reverse*	GGCCTTCATGGGAAATGTAACT
HXT5 antisense forward**	TTTCTGCCCACTTCTCTCTTACAA
HXT5 antisense reverse	CCGTCCTCACTGTTTTATTACCAA
HXT8 forward**	TTTCCATTAAGGGTGAGATCCAA
HXT8 reverse	CGATTAGGAACCCCCACAATAA

Oligonucleotides for quantitative PCR after reverse transcription (RT–qPCR). Oligonucleotides for RT–qPCR are listed as forward and reverse pairs for each transcript tested. Primers used for strand-specific cDNA preparation are indicated with one asterisk corresponding to a primer for sense and two asterisks for antisense. QPCR was conducted with both forward and reverse primer pairs.

Preparation and purification of anti-Dbp2

Polyclonal rabbit anti-Dbp2 antibodies were generated by Cocalico Biologicals, Inc., using full-length, recombinant purified Dbp2 expressed in bacteria (Cloutier *et al.* 2012). Resulting immunosera was dialyzed against PBS and subjected to affinity purification using Dbp2-conjugated CNBr–sepharose according to manufacturer's instructions (Sigma). The eluted, purified anti-Dbp2 antibody was stored at 4° in the presence of 0.05% sodium azide. Western blotting was conducted with a 1:5000 dilution of anti-Dbp2.

Fluorescent cell microscopy

Cells were initially grown to an $OD_{600\ nm}$ of 0.1 at 30° in YP + 2% Glucose (YPD). Cells were washed twice with YP + 0% Glucose (YP) and then resuspended in YP + different concentrations of glucose as indicated. Cells were harvested by centrifugation at the indicated time points and were visualized using an Olympus BX-51 fluorescent microscope. For translational shut-off assays, cells grown in YPD were shifted to YP and then back to YPD with or without 300 μg/ml cycloheximide for 30 min before visualization. Where indicated, 10 μg/ml rapamycin was included. Images were captured with a Hamamatsu Orca R2 camera and MetaMorph software (Molecular Devices, Sunnyvale, CA).

Quantitative Western blotting

Protein stability was assayed following addition of cycloheximide to the media as above, but with 20 μg/ml of cycloheximide. Yeast cell lysates were prepared as described previously (Cloutier *et al.* 2013). Dbp2, Upf1, and Pgk1 were detected using

Table 2 Oligonucleotides for Chromatin Immunoprecipitation (ChIP)

Name	Forward primer	Reverse primer	Probe
HXT1 antisense	TTCCAGGCTGTCGGTTTAAG	AGCACCCCACATCAAACAG	CCAAAACGGTCAACGGTGTAC
HXT1 sense	GGCCATGAATACTCCAGAAGG	CACCGAAAGCAACCATAACAC	AGTGAAAGTCAAGTGCAACCCGC
HXT4 sense	GTTGGTGTTACAAGATTGTGGC	CAGGTAGTGGCAAAACAGAATAAG	AACGGGTCTTCTAAGGGTGCTGG
HXT5 antisense	TTACTCGAGGTTTCAACAGGG	AGGTAGCGGAGTTTTCAGTTC	AATCAAGAGCCCCGTTCTTTTACCGT
HXT5 sense	CGGAACTTGAAAACGCTCATC	TGAGACGGGTTTAGCTTGTG	CCTTGGAAGGGTCTGCTACTGTGA
HXT8 antisense	TCTGTTGATAAGTTGGGCCG	GTAAATAACCATGCACGCCG	TCTTTTACTTGGAGCAGCCACCATGA
HXT8 sense	TTAGTGTTCTTGCCCCGATG	CGAAAGTCACCATCAATTGCC	ACTGCGCCAAAGCATATCAGAGGT

Oligonucleotides for ChIP are Primetime qPCR assays (IDT) and are listed as forward and reverse primers and probe for each gene tested.

rabbit anti-Dbp2 (this study), rabbit anti-Upf1 (Bond *et al.* 2001), or mouse anti-Pgk1 (459250, Invitrogen) respectively. Proteins were visualized using Luminata Crescendo Western HRP Substrate (Millipore) according to manufacturer's instructions. Bands were quantified using ImageQuant TL software (GE Life Sciences).

RNA sequencing sample preparation

Wild-type and *dbp2Δ* cells were grown in YPD at 30° to an $OD_{600\ nm}$ of 0.4 before being harvested by centrifugation, flash frozen in liquid nitrogen, and stored at −80°. Total RNA isolation was performed using a standard acid phenol: chloroform purification as previously described (Cloutier *et al.* 2012). DNase treatment was performed using 1 U TurboDNase (Life Technologies) per 10 μg of RNA for 30 min at 37°. RNA was analyzed with a DU-730 Beckman-Coulter spectrophotometer. RNA purity was considered suitable for qPCR if the $A_{260/280}$ was ∼2.0 and the yield was ∼80% after DNase treatment.

Ribosomal RNA depletion was performed prior to library generation (Ribominus Eukaryote kit, Life Technologies). A strand-specific RNA sequencing library was generated using paired-end reads and SOLiD sequencing on the 5500 XL platform (Life Technologies) by the Northwestern University Genomics Core Facility. Forward sequences were generated using the F3 tag and were 75 bp in length; reverse sequences were generated with the F5 tag and were 35 bp in length.

RNA sequencing data analysis

RNA sequencing generated ∼60 million and 40 million mappable reads in wild type and *dbp2*Δ, respectively, per replicate. Raw data quality was evaluated by FastQC software with Illumina 1.9 encoding. Reads were aligned by position and orientation to the reference *S. cerevisiae* genome sacCer3 (http://www. http://genome.ucsc.edu) using LifeScope v. 2.5.1. Gene expression (in RPKM), statistical analysis, and fold change between strains were determined using Cufflinks 2.0 software. Those genes with a statistically significant increase in transcripts in *dbp2*Δ were analyzed for GO-term enrichment for similar processes using FuncAssociate 2.0 (http://llama.mshri.on.ca/funcassociate/) (Berriz *et al.* 2009). RNA sequencing data are deposited in the NCBI GEO database no. GSE58097.

Strand-specific RT-qPCR

Primers for RT–qPCR were designed using Primer Express 3.0 software. Strand-specific reverse transcription was performed using the Quantitect reverse transcription kit (Qiagen) with the following modifications: A total amount of 2 μg of RNA was prepared for a 20μl reaction. Primers specific to one strand of the target gene and the sense strand of a reference gene, *ACT1*, were added to a final concentration of 5 μM. Actinomycin D was included in the reverse transcription reaction to a final concentration of 6 ng/μl to prevent second-strand synthesis. Following heat inactivation, unincorporated primers were removed using the QiaQuick PCR Purification Kit (Qiagen) according to the manufacturer's instructions. Quantitative PCR was performed as previously described (Cloutier *et al.* 2012). Fold changes were calculated using the Pfaffl method (Pfaffl 2001), with results reported as the mean ±SE of three biological replicates with three technical repeats. See Table 1 for a listing of primers used for strand-specific reverse transcription.

Chromatin immunoprecipitation

Chromatin immunoprecipitation (ChIP) was performed as described previously (Cloutier *et al.* 2012). Primer-probe sets were designed to amplify DNA corresponding to the genomic regions to the 5′ ends of the sense and antisense transcripts of *HXT1*, *HXT5*, and *HXT8* and the region corresponding to the sense transcript of *HXT4*. Results represent three biological replicates with three technical replicates shown as the mean percentage signal above input and SEM. Primetime assay primer-probe sets (IDT) are listed in Table 2.

Results

The cellular localization of Dbp2 is responsive to extracellular glucose

Many glucose-dependent repressors are regulated at the level of cellular localization, protein stability, and/or synthesis in response to nutrient availability (Gancedo 1998). Moreover, recent global analyses of mRNP complexes in budding yeast revealed that the subcellular distribution of a large proportion of RNA-binding proteins is dictated by environmental growth conditions (Mitchell *et al.* 2013). To determine if Dbp2 is regulated similarly, we first examined the localization of a C-terminally GFP-tagged Dbp2 in *S. cerevisiae* during the shift from glucose to galactose (Figure 1A). Briefly, strains expressing a genomically encoded *DBP2–GFP* were grown to early log phase ($OD_{600\ nm}$ of 0.1) in standard, rich media

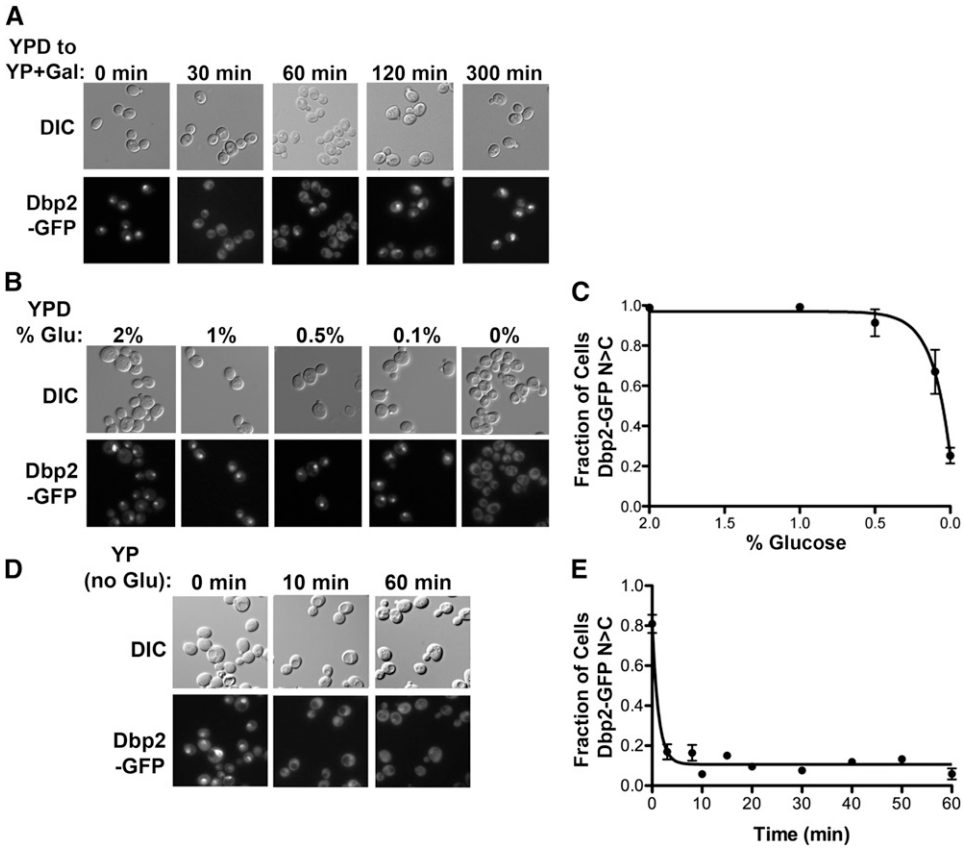

Figure 1 Dbp2 is redistributed to the cytosol upon glucose deprivation. (A) The nuclear Dbp2–GFP signal is rapidly lost during a shift from glucose to galactose media. Dbp2–GFP cells were grown in the presence of 2% glucose (YPD) and shifted to media with 2% galactose (YP + Gal). Fluorescent images were collected by microscopy at the indicated time points following the shift. (B) Nuclear Dbp2–GFP signal decreases with lower glucose concentrations. Yeast cells expressing a C-terminally GFP-tagged Dbp2 encoded within the endogenous *DBP2* locus were grown to early log phase (0.1 OD at 600 nm) at 30° in rich media + 2% glucose (YPD) and then shifted to media with the indicated glucose concentrations for 30 min. The localization of Dbp2–GFP was determined by fluorescent microscopy (bottom) with corresponding DIC images (top). All images were collected with the same exposure time and are scaled equivalently. (C) Graphical representation of glucose-dependent nuclear localization of Dbp2. Dbp2–GFP localization was determined as above over a range of glucose concentrations. The fraction of cells with a predominantly nuclear Dbp2–GFP signal is reported for each glucose concentration tested. Graphical points represent the average of three biological replicates with >100 cells per replicate counted and scored. Error bars represent the SEM. (D) Dbp2 is rapidly lost from the nucleus after glucose removal. Fluorescence microscopy images of Dbp2–GFP localization at the indicated time points following depletion of glucose (YP) are shown. DIC and fluorescent microscopy images were collected as above following growth of Dbp2–GFP-expressing yeast cells in rich media with glucose to early log phase and subsequent removal by centrifugation and resuspension in media lacking glucose. (E) Graphical analysis of the rate of nuclear Dbp2–GFP loss following removal of glucose. The time for Dbp2–GFP relocalization following glucose depletion was determined by growing Dbp2–GFP-expressing cells in YP+2% glucose as above, rapidly shifting the cells to YP lacking glucose and collecting images by fluorescence microscopy at the indicated time points before (0 min) and immediately following glucose depletion. The fraction of cells with nuclear signal was determined as in C.

(YP) plus 2% glucose and then shifted to rich media plus 2% galactose. The cellular localization of Dbp2–GFP was determined by epifluorescent microscopy of samples before (0 min) or at different time points following readdition of galactose.

Consistent with previous studies, Dbp2–GFP displayed a predominantly nuclear localization when cells were grown in the presence of glucose (Figure 1A, 0 min, Cloutier *et al.* 2012). However, Dbp2–GFP redistributed to the cytosol after the carbon source shift (Figure 1A, 30 and 60 min). Interestingly, the nuclear localization was restored by 300 min, suggesting that the cellular redistribution of Dbp2–GFP is due to the removal of glucose, not the presence of galactose. To test this, we asked if reduction of glucose concentrations in the media would also render Dbp2 cytoplasmic. Interestingly, Dbp2 exhibited cytosolic localization only upon full glucose deprivation (0%), whereas Dbp2 is largely nuclear at all tested concentrations (Figure 1, B and C). Next, we asked how quickly cytoplasmic redistribution occurs by conducting a microscopy time course immediately prior to and following removal of glucose from the media (Figure 1, D and E). This revealed that Dbp2–GFP is redistributed to the cytosol within 2 min following glucose removal, indicating a rapid alteration of cellular localization (Figure 1E). Moreover, the cytosolic localization persisted over a 1-hr time frame (Figure 1, D and E), indicating that the redistribution is both rapid and stable.

The change in Dbp2 localization is due to nuclear transport not protein turnover

The apparent cellular redistribution of Dbp2 could be due to active nuclear export and/or protein turnover. To test this, we measured Dbp2 protein stability by quantitative Western blotting over time following addition of the translational inhibitor cycloheximide. Dbp2 levels were then plotted with respect to the loading control Pgk1 (Figure 2, A and B). Consistent with prior data stating that Dbp2 is exceptionally stable with an estimated half-life of ~250 min (Laxman *et al.* 2010), we did not observe an appreciable decrease within the 1-hr time frame of our analysis. This was not due to an incomplete translational block, as the levels of another RNA helicase, Upf1, was degraded with a half-life within the range of other studies (Figure 2A, red; Ruiz-Echevarria *et al.* 1998). Furthermore, the stability of Dbp2 did not change upon removal of glucose within 1 hr (Figure 2B). This suggests that protein turnover is not a major mechanism for the observed relocalization.

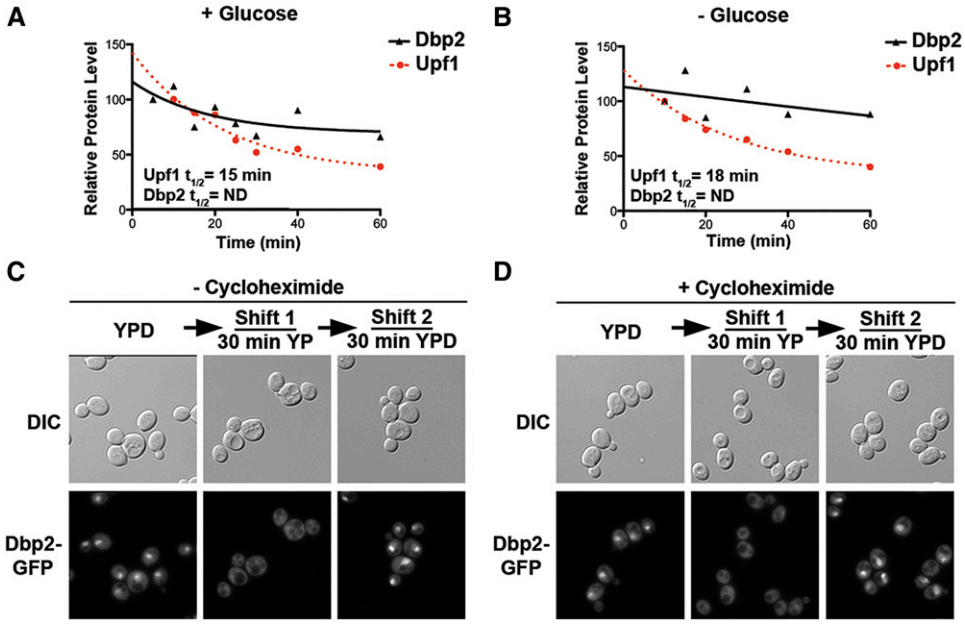

Figure 2 The change in cellular localization of Dbp2 is due to nuclear transport, not protein turnover. (A and B) Dbp2 protein exhibits similar stability irrespective of the presence of glucose in the media. The stability of Dbp2 protein in the presence of glucose (A) or following glucose deprivation (B) by adding cycloheximide, as previously described to prevent new protein synthesis (Castoralova *et al.* 2012). Samples were removed at 5-, 10-, 20-, 30-, 40-, and 60-min increments and subjected to Western blotting with rabbit polyclonal anti-Dbp2. Dbp2 levels were quantified with respect to Pgk1 and are presented graphically. Upf1, another RNA helicase, has a reported half-life of ~16 min (Ruiz-Echevarria *et al.* 1998) and is included as a control for efficient translational shutoff. Dbp2 half-lives could not be determined for either growth conditions because they do not decrease substantially within a 1-hr time frame. (C) Readdition of glucose to glucose-deprived cells restores nuclear Dbp2 signal. Dbp2–GFP-expressing cells were subjected to a 30-min glucose deprivation, to ensure complete cytosolic redistribution, and were then resuspended in fresh media with saturating glucose (2%). Dbp2–GFP was visualized before glucose removal (0 min), following deprivation, and after 30 min incubation with fresh, glucose-containing media. Dbp2 localization was visualized by fluorescent microscopy as above. Note that Dbp2–GFP-expressing strains show reduced signal in the absence of glucose (middle). However, this is not due to a change in Dbp2 protein levels (see Figure 2A). (D) New protein synthesis is not necessary for restoration of nuclear signal upon glucose readdition. Dbp2–GFP localization was determined as in C, but in the presence of cyclohexamide to block translation.

We then asked if nuclear signal could be restored upon readdition of glucose (Figure 2C). To this end, we subjected cells to a 30-min glucose depletion followed by a 30-min incubation in the presence of glucose (2%). Fluorescent microscopy revealed that the predominantly nuclear localization of Dbp2 was fully restored by adding back glucose (Figure 2C). Moreover, the addition of cyclohexamide had no effect on this nuclear accumulation (Figure 2D). This is similar to the regulated localization of the glucose-dependent repressor Mig1 (De Vit *et al.* 1997) and suggests that relocalization of Dbp2 upon glucose deprivation occurs through regulated nucleocytoplasmic transport.

Transport of Dbp2 is not dependent on the Snf1/Msn5, Hog1, or TOR signaling pathways

Upon reduction in extracellular glucose, Mig1 is exported to the cytoplasm through the activity of Snf1, the budding yeast ortholog of the human AMP-activated protein kinase AMPK (Woods *et al.* 1994; De Vit *et al.* 1997; Hardie *et al.* 2012), and the export receptor Msn5 (DeVit and Johnston 1999). To determine if the Snf1 signaling pathway is involved in Dbp2 relocalization, we constructed *DBP2–GFP snf1*Δ cells through standard yeast genetic methods and conducted cellular microscopy following glucose deprivation as above. In contrast to Mig1, Dbp2–GFP was still localized to the cytoplasm following glucose removal in *SNF1*-deficient strains (Figure 3A, left and middle). Moreover, loss of *MSN5* had no effect on relocalization of Dbp2–GFP to the cytoplasm (Figure 3A, right). This suggests that export of Dbp2 upon glucose deprivation is not dependent on the Snf1 signaling pathway. We also observed efficient cytoplasmic relocalization of Dbp2–GFP in the absence of *HOG1*, a mitogen-activated protein kinase involved in osmolaric stress responses that has recently been linked to glucose deprivation (Westfall *et al.* 2004; Piao *et al.* 2012; Figure 3B).

We then asked if the glucose-dependent cellular localization of Dbp2 is an effect of inhibited reimport rather than stimulated export. The TOR signaling pathway promotes anabolic processes that promote cell growth (Wullschleger *et al.* 2006). To determine if the localization of Dbp2–GFP requires TOR signaling, we performed cellular microscopy following glucose removal and readdition in the presence of the TOR inhibitor, rapamycin. The translational inhibitor, cycloheximide, was also included to ensure that perceived changes in cellular localization were not due to new protein synthesis. Dbp2–GFP, however, was efficiently reimported upon addition of glucose regardless of the presence of rapamycin (Figure 3C, compare to Figure 2, C and D). Thus, the cytoplasmic relocalization of Dbp2 is not dependent upon Snf1 or Hog1 signaling and neither import nor export of Dbp2 requires TOR. This suggests that the cellular localization of Dbp2 is dependent on another, as-of-yet unidentified signaling pathway or that multiple pathways dictate the glucose-dependent localization of Dbp2 (see *Discussion*).

DBP2 facilitates glucose-dependent regulation of multiple gene expression networks

Dbp2 is a *bona fide* RNA helicase that associates directly with transcribed chromatin (Cloutier *et al.* 2012; Ma *et al.* 2013). However, our data above suggest that this enzyme

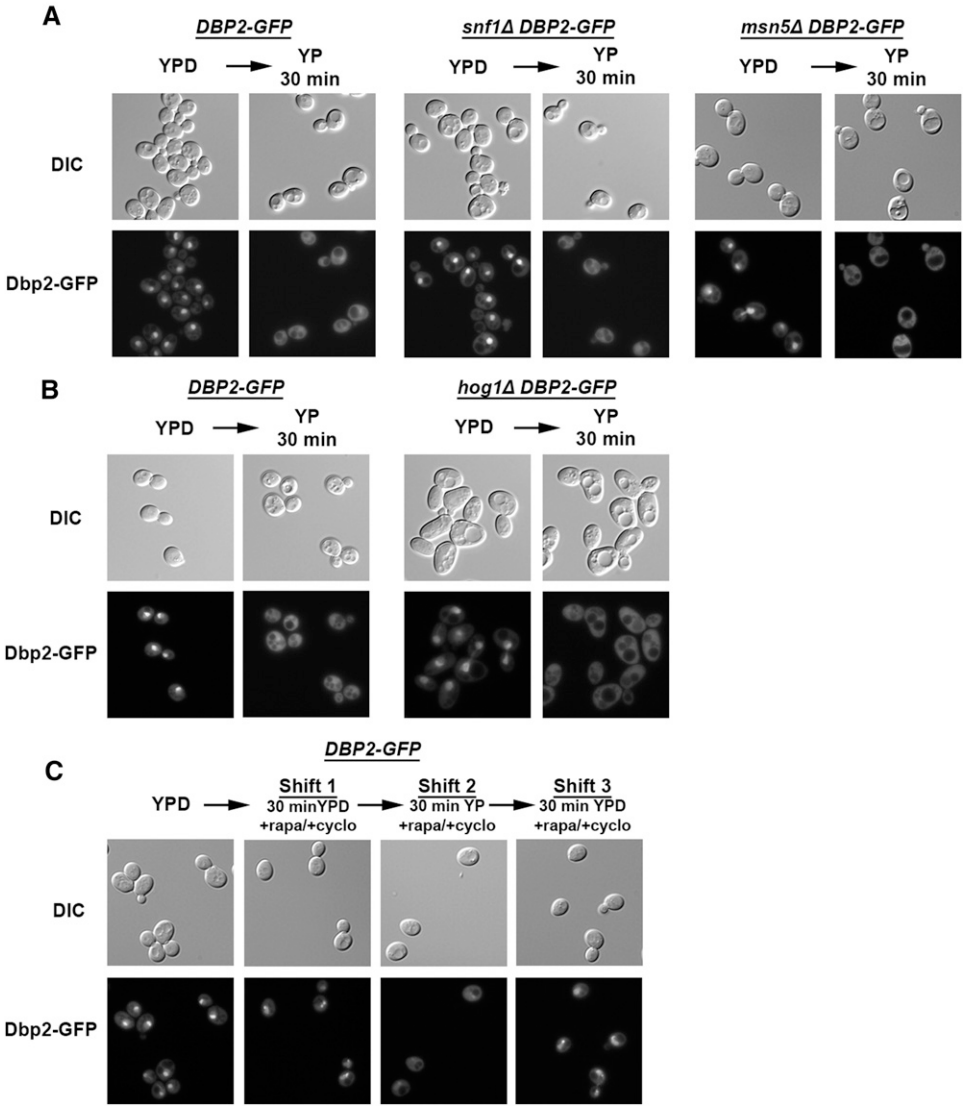

Figure 3 The cellular redistribution of Dbp2 upon glucose deprivation does not depend on the Snf1 pathway, Hog1 pathway, or TOR signaling. (A) Dbp2–GFP signal relocalization is not dependent on the Snf1 kinase pathway. Wild-type, *snf1*Δ, and *msn5*Δ cells harboring genomically encoded *DBP2–GFP* constructs were visualized for Dbp2 localization in the presence of glucose (YPD) or after a 30-min deprivation (YP 30 min). Dbp2–GFP was visualized by epifluorescent microscopy and images are representative of three biological replicates. (B) Dbp2–GFP signal is not redistributed to the cytoplasm via the HOG1 osmolaric stress response pathway. Dbp2–GFP localization in wild-type and *hog1*Δ cells was visualized in both the presence of glucose (YPD) and following a 30-min glucose deprivation (YP 30 min) as above. (C) Glucose-dependent localization of Dbp2–GFP is not dependent on the TOR pathway. Dbp2–GFP cells were grown in the presence of glucose (YPD) and then shifted to YPD supplemented with rapamycin for 30 min to inhibit the TOR pathway and cycloheximide to inhibit *de novo* protein synthesis (Shift 1). Cells were then subjected to a 30-min glucose deprivation (YP 30 min) in the presence of rapamycin and cycloheximide (Shift 2). After glucose deprivation, cells were given access to glucose (YPD) supplemented with rapamycin and cycloheximide (Shift 3). Fluorescent images were collected as above.

may function more like a carbon-source-regulated transcription factor. Consistent with this, Dbp2 is required for glucose-dependent repression of the *GAL* cluster genes through modulation of associated long noncoding RNAs (Cloutier *et al.* 2013). To determine if Dbp2 plays a more widespread role in nutrient-dependent gene expression, we conducted RNA sequencing of wild-type and *dbp2*Δ cells using SOLiD NextGen technology to reveal the entire complement of transcripts whose levels depend on *DBP2*. This resulted in ~50 million mappable reads per strain per replicate, which were then subjected to bioinformatics analysis and alignment to the *S. cerevisiae* genome (Supporting Information, Table S1). Transcripts were separated by sense *vs.* antisense orientation with respect to the protein-coding gene and fold change from wild type was determined using Cufflinks 2.0 (Table S2 and Table S3, respectively).

RNA seq identified ~3000 coding and noncoding (nonribosomal) transcripts that are either over- or underrepresented in *DBP2*-deficient cells as compared to wild type. To determine if these differentially expressed transcripts fall into common functional categories, we then conducted GO term analysis using FuncAssociate 2.0 (Berriz *et al.* 2009). Consistent with the link between Dbp2 and carbon source availability, GO classification revealed a robust overaccumulation of transcripts encoding mitochondrial respiration components (Table 3). *S. cerevisiae* preferentially utilize aerobic fermentation over oxidative respiration for energy production until fermentable carbon sources, such as glucose, become limiting (Broach 2012). These genes are typically repressed in wild-type cells to promote fermentation over oxidation in the presence of glucose. Conversely, transcripts encoding ribosome biogenesis factors, whose expression is activated by glucose, were underrepresented in *dbp2*Δ cells (Table 4). Ribosome biogenesis is also dictated by nutrient availability, balancing energy production with consumption (Warner 1999; Broach 2012). Taken together, this indicates that *DBP2* links nutrient availability to the energy status of the cell.

Unexpectedly, our analysis also revealed accumulation of antisense transcripts overlapping hexose transporter genes (Table 5). Hexose transport constitutes an essential and

Table 3 Upregulated Sense Transcripts (895)

N	LOD	*P*	*P*_adj	attrib ID	attrib name
9	1.278165325	4.12*E*-06	0.001	GO:0006122	Mitochondrial electron transport, ubiquinol to cytochrome c
8	1.229371024	2.03*E*-05	0.012	GO:0005750	Mitochondrial respiratory chain complex III
8	1.229371024	2.03*E*-05	0.012	GO:0045275	Respiratory chain complex III
8	1.083144865	6.35*E*-05	0.043	GO:0005991	Trehalose metabolic process
10	1.066652419	9.00*E*-06	0.006	GO:0005199	Structural constituent of cell wall
12	1.056106801	1.29*E*-06	<0.001	GO:0070469	Respiratory chain
20	0.953976428	3.53*E*-09	<0.001	GO:0022904	Respiratory electron transport chain
24	0.580122409	3.65*E*-06	0.001	GO:0015078	Hydrogen ion transmembrane transporter activity
25	0.571861779	2.95*E*-06	<0.001	GO:0022900	Electron transport chain
24	0.483759772	5.38*E*-05	0.033	GO:0015077	Monovalent inorganic cation transmembrane transporter activity
49	0.4055929	6.90*E*-07	<0.001	GO:0001071	Nucleic acid binding transcription factor activity
49	0.4055929	6.90*E*-07	<0.001	GO:0003700	Sequence-specific DNA binding transcription factor activity
50	0.30780812	6.48*E*-05	0.043	GO:0006091	Generation of precursor metabolites and energy
60	0.27626111	7.13*E*-05	0.046	GO:0043565	Sequence-specific DNA binding

Transcripts encoding respiration and energy production factors are upregulated in *dbp2*Δ cells. RNA sequencing was conducted for wild-type and *dbp2*Δ cells grown at 30° in YP + 2%D using a SOLiD platform and pairwise analysis. Sense and antisense reads were differentiated using Cufflinks 2.0. Resulting transcripts were analyzed as separate data sets depending on over- or underrepresentation and sense *vs.* antisense orientation with respect to the gene. Genes with sense transcripts that were overrepresented in *dbp2*Δ cells as compared to wild type were selected from the RNA sequencing data set. Gene ontology (GO) terms for functional processes were determined using FuncAssociate 2.0 (http://llama.mshri.on.ca/funcassociate/) (Berriz *et al.* 2009). The columns are as follows: *N*, no. of entries in the category; LOD, Log_{10} of the odds ratio; *P*, one-sided *P*-value of the association of attribute and query; *P*_adj, adjusted *P*-value as a fraction of 1000 null-hypothesis simulations; attrib ID, GO term identification number for attribution category; attrib name, category name for functional processes. RNA sequencing data are deposited in GEO, no. GSE58097.

rate-limiting step in sugar catabolism, with hexose transporters providing the sole portal for cellular import of fructose, mannose, and glucose (Johnston and Kim 2005; Horak 2013). Although the function of the hexose transporter (*HXT*) antisense transcripts is not known, this strong GO term enrichment suggests that Dbp2 may regulate expression of the *HXT* genes via lncRNAs. This would be consistent with prior studies of Dbp2 and the *GAL* cluster lncRNAs (Cloutier *et al.* 2013). We did not observe antisense transcripts at the ribosome biogenesis snoRNA or mitochondrial respiratory genes, suggesting that this is specific for the HXT antisense transcripts.

Loss of DBP2 affects both sense and antisense hexose transporter transcript levels

The vast majority of antisense transcriptional events correlate with decreased expression of overlapping, protein-coding genes. To determine if there is a general trend between the misregulated antisense transcripts and their corresponding sense targets in *dbp2*Δ cells, we manually selected all transcript pairs whose sense or antisense transcript was differentially expressed with respect to wild type (log_2-fold change greater or less than ± 0.5). We then generated a scatter plot of the change in abundance of antisense *vs.* the sense transcripts for all misregulated genes in *dbp2*Δ cells (Figure 4, gray dots). This revealed no correlation between the upregulated antisense transcripts in *dbp2*Δ cells and the level of the corresponding sense RNA, suggesting that the absence of *DBP2* does not result in a general, genome-wide downregulation of antisense-targeted genes.

Budding yeast encode 17 *HXT* genes whose expression and function constitute the rate-limiting step for glycolysis (Horak 2013). Given the striking enrichment in antisense hexose transporter transcripts in *dbp2*Δ cells (Table 5), we then asked if there was a correlation between sense and antisense *HXT* transcript levels. This revealed a slight positive correlation between the levels of sense and antisense transcripts corresponding to the *HXT* protein-coding gene products (Figure 4, red dots). In fact, 50% of the *HXT* genes displayed higher sense and antisense *HXT* transcript levels in *dbp2*Δ cells as evidenced by localization in the top, rightmost quadrant. This could occur by simultaneous expression of both, overlapping transcripts in a given cell or by mutually exclusive expression of individual RNAs in different cells within a population. Regardless, this suggests that Dbp2 regulates the levels of both sense and antisense *HXT* transcripts.

Strand-specific reverse transcriptase-quantitative PCR provides independent validation of differentially expressed HXT genes in dbp2Δ cells

To independently verify that both sense and antisense *HXT* transcripts are overabundant in *dbp2*Δ cells, we first modified a standard reverse transcriptase-quantitative PCR (RT–qPCR) method to quantify cellular RNAs transcribed from overlapping gene products (Figure 5A). This was necessary as analysis of overlapping transcriptional products is not always straightforward due to vastly different expression levels and the second-strand synthesis activity of reverse transcriptase (Perocchi *et al.* 2007). Strand-specific complementary (c) DNAs were generated using reverse transcription with gene-specific primers (GSPs) to the targeted sequence of interest, and to actin mRNA (*ACT1*) as an internal control, in the presence of actinomycin D (ActD) (Figure 5A). ActD efficiently inhibits second-strand synthesis by reverse transcriptase (data not shown), which has been noted to cause an overrepresentation of antisense transcripts in genome-wide transcriptional studies (Johnson *et al.* 2005; Perocchi *et al.* 2007). Unincorporated GSPs were then removed from the cDNA preparation by standard column chromatography. We selected the *GAL10* sense and antisense RNAs for method validation because the sense and antisense products can be

Table 4 Downregulated Sense Transcripts (700)

N	LOD	*P*	*P*_adj	attrib ID	attrib name
5	1.84052114	1.93*E*-06	0.026	GO:0004169	Dolichyl-phosphate-mannose-protein mannosyltransferase activity
18	0.711054338	1.45*E*-06	0.02	GO:0030561	RNA 2′-O-ribose methylation guide activity
18	0.711054338	1.45*E*-06	0.02	GO:0030562	rRNA 2′-O-ribose methylation guide activity
20	0.693317905	6.13*E*-07	0.006	GO:0031167	rRNA methylation
21	0.685997034	3.97*E*-07	0.005	GO:0031428	Box C/D snoRNP complex
29	0.673647597	4.46*E*-09	0	GO:0000944	Base pairing with rRNA
28	0.667960766	1.00*E*-08	0	GO:0030555	RNA modification guide activity
28	0.667960766	1.00*E*-08	0	GO:0030556	rRNA modification guide activity
31	0.606510897	2.03*E*-08	0	GO:0000154	rRNA modification
40	0.563435455	1.89*E*-09	0	GO:0000496	Base pairing
39	0.551890352	5.25*E*-09	0	GO:0000498	Base pairing with RNA
39	0.535516237	1.17*E*-08	0	GO:0019843	rRNA binding
34	0.530391432	1.18*E*-07	0.002	GO:0005732	Small nucleolar ribonucleoprotein complex
58	0.364279682	3.87*E*-07	0.005	GO:0006520	Cellular amino acid metabolic process
60	0.351442841	5.69*E*-07	0.006	GO:0044106	Cellular amine metabolic process
62	0.346800579	4.52*E*-07	0.006	GO:0006412	Translation
63	0.321570613	2.12*E*-06	0.028	GO:0009308	Amine metabolic process
77	0.313115978	3.93*E*-07	0.005	GO:0044283	Small molecule biosynthetic process

Transcripts linked to ribosome biosynthesis, primarily corresponding to small nucleolar RNAs, are downregulated in *dbp2*Δ cells. Genes with sense transcripts that were significantly underrepresented in *dbp2*Δ cells as compared to wild type were selected from the RNA sequencing data set. GO term analysis was conducted using FuncAssociate 2.0 as above. The columns are as follows: **N**, no. of entries in the category; LOD, Log10 of the odds ratio; **P**, one-sided ***P***-value of the association of attribute and query; **P**_adj, adjusted ***P***-value as a fraction of 1000 null-hypothesis simulations; attrib ID, GO term 8 identification number for attribution category; attrib name, category name for functional processes. There was no enrichment of GO terms for downregulated antisense transcripts in *DBP2*-deficient cells.

toggled by growth condition (Houseley *et al.* 2008; Pinskaya *et al.* 2009; Geisler *et al.* 2012). Measurement of *GAL10* transcripts revealed robust expression of sense mRNA above antisense levels in galactose-grown cells and the converse expression pattern in the presence of glucose, consistent with prior studies (Houseley *et al.* 2008; Pinskaya *et al.* 2009; Geisler *et al.* 2012; Figure 5B).

We then utilized strand-specific RT–qPCR to measure the levels of sense and antisense transcripts from four candidate *HXT* genes, *HXT1*, *HXT4*, *HXT5*, and *HXT8*. This revealed over-accumulation of sense transcripts of all four *HXT* genes in *dbp2*Δ cells, with levels ranging from 7- to 17-fold higher than wild type (Figure 5C). *HXT5* exhibits the largest increase, most likely because this moderate affinity hexose transporter is also induced by slow growth rate (Verwaal *et al.* 2002), which is a phenotype of *dbp2*Δ cells (Cloutier *et al.* 2012). Antisense *HXT1*, *HXT5*, and *HXT8* transcripts also accumulate in *dbp2*Δ cells but to a lesser extent than sense gene products (Figure 5D). In contrast, we were unable to detect *HXT4* antisense transcripts in *dbp2*Δ cells (Figure 5D, N.D.), suggesting that some *HXT* antisense lncRNAs are downregulated in the absence of *DBP2*. These measurements by strand-specific RT–qPCR are in line with RNA sequencing quantification, as evidenced by comparison to the RPKM values from wild-type and *dbp2*Δ cells for each *HXT* transcript (Table S2 and Table S3). The absolute fold change in expression between wild-type and *dbp2*Δ cells, however, is different between the two techniques. This is most likely due to normalization differences between these methods; *i.e.*, RT–qPCR is normalized to *ACT1* levels whereas RPKMs are normalized across the length of a transcribed unit. Regardless, this shows that loss of *DBP2* results in simultaneous accumulation of both sense and antisense *HXT* transcripts within a population of cells.

To determine if Dbp2 plays a direct role in regulation of hexose transporter expression, we then utilized ChIP to ask if Dbp2 is associated with the genomic regions corresponding to sense and antisense *HXT* transcripts (Figure 5, E and F). ChIP was conducted using a genomically encoded, 3X-FLAG-tagged *DBP2* strain and primer sets corresponding to 5′ ends of the *HXT* transcription units, based on the characterized occupancy of Dbp2 at other genomic loci (Table 2 and Cloutier *et al.* 2012). This revealed that Dbp2 is associated with chromatin encoding the sense and antisense *HXT1*, *HXT5*, and *HXT8* transcripts (Figure 5, E and F, respectively). Dbp2 also associates with the 5′ end of the *HXT4* sense-coding region (Figure 5E); however, we were unable to test the 5′ side of the *HXT4* antisense region due to the lack of unique primer sets for qPCR (Figure 5F). Because each of these genes exhibited aberrant transcript accumulation in *DBP2*-deficient cells, this suggests that Dbp2 plays a direct role at the *HXT* genes.

Misregulated HXT transcripts in DBP2-deficient cells are products of normal gene expression

To determine if the expressed *HXT* sense and antisense transcripts in *DBP2*-deficient cells map to the same genomic location as wild-type cells, we utilized the University of California—Santa Cruz (UCSC) genome browser (http://genome.ucsc.edu/) to generate representative mapped reads of the *HXT* transcriptional products for both strains (Figure 6, A and B). Consistent with expression of the *HXT* genes, sense-oriented reads fully mapped to the annotated protein coding genes for *HXT1*, *HXT4*,and *HXT5* (Figure 6A). In contrast, however, *HXT8* sequences aligned to an ∼1.5-kb region originating within the 3′ end of the *HXT8* ORF in both wild-type and *dbp2*Δ cells (Figure 6A, bottom). Interestingly, this transcript

Table 5 Upregulated Antisense Transcripts (382)

N	LOD	*P*	*P*_adj	attrib ID	attrib name
9	1.570899749	7.66*E*-10	0	GO:0005353	Fructose transmembrane transporter activity
9	1.570899749	7.66*E*-10	0	GO:0015578	Mannose transmembrane transporter activity
9	1.508665946	1.69*E*-09	0	GO:0005355	Glucose transmembrane transporter activity
9	1.454222369	3.47*E*-09	0	GO:0015145	Monosaccharide transmembrane transporter activity
9	1.454222369	3.47*E*-09	0	GO:0015149	Hexose transmembrane transporter activity
11	1.340249894	4.22*E*-10	0	GO:0051119	Sugar transmembrane transporter activity
10	1.298536807	5.17*E*-09	0	GO:0008645	Hexose transport
10	1.298536807	5.17*E*-09	0	GO:0015749	Monosaccharide transport
11	1.180032699	7.49*E*-09	0	GO:0015144	Carbohydrate transmembrane transporter activity
13	1.031860845	9.38*E*-09	0	GO:0008643	Carbohydrate transport
36	0.41867088	3.33*E*-06	0.047	GO:0022891	Substrate-specific *trans*-membrane transporter activity

GO term enrichment reveals an overrepresentation of antisense hexose transporter transcripts in *DBP2*-deficient cells. Genes with overlapping, antisense transcripts that were significantly overrepresented in *dbp2*Δ cells as compared to wild type were selected from the RNA sequencing data set. GO term analysis was conducted using FuncAssociate 2.0 as above. The columns are as follows: **N**, no. of entries in the category; LOD, Log10 of the odds ratio; **P**, one-sided ***P***-value of the association of attribute and query; **P**_adj, adjusted ***P***-value as a fraction of 1000 null-hypothesis simulations; attrib ID, GO term 8 identification number for attribution category; attrib name, category name for functional processes.

was also identified in another genome-wide study, indicating that budding yeast predominantly express this 1.5-kb intergenic product instead of *HXT8* ORF mRNAs (Xu *et al.* 2009). Because this study demonstrated accumulation of this transcript under a variety of conditions (varying carbon sources, haploid, diploid), it is currently unknown what, or if any, conditions result in accumulation of a full-length *HXT8* gene product.

Representative reads were also mapped for antisense transcripts corresponding to *HXT1*, *5 and 8* genes in wild-type and *dbp2*Δ cells (Figure 6B). Importantly, the antisense products of *HXT1* and *HXT5* map to the same location as antisense transcripts identified in prior genome-wide transcriptional profiling of wild-type and RNA decay-deficient strains (Xu *et al.* 2009; Van Dijk *et al.* 2011). This suggests that loss of *dbp2*Δ results in upregulation of antisense *HXT1* and *HXT5* gene products that are normally expressed at lower levels in wild-type cells. Antisense *HXT8* transcripts are also present in wild-type cells, albeit at very low levels. Antisense *HXT8* transcription may arise from RNA synthesis within the *HXT8* gene locus or from alternative, upstream initiation of the *YJL215C* locus as noted in prior studies (Xu *et al.* 2009). Regardless, this suggests that antisense transcription is prevalent at *HXT* gene loci and that both sense and antisense transcripts accumulate in *dbp2*Δ cells.

Sense and antisense HXT transcripts accumulate in wild-type cells upon glucose deprivation

Given that Dbp2 is rapidly depleted from the nucleus upon glucose deprivation and that loss of *DBP2* correlates with altered expression of metabolic genes, we asked if regulation of Dbp2 localization could be an unrecognized mechanism to control gene expression. If this is the case, we proposed that wild-type cells would show a similar expression pattern of *HXT* transcripts as *dbp2*Δ cells when depleted of glucose. To test this, we grew wild-type cells in rich media with glucose (2%) and then subjected the cells to glucose deprivation for 10 min to induce nuclear loss of Dbp2 (see Figure 1). We then conducted strand-specific RT–qPCR to measure the levels of sense and antisense *HXT* transcripts (Figure 7, A and B, respectively). Interestingly, this revealed a robust accumulation of *HXT4* and *HXT5* sense transcripts upon glucose deprivation (Figure 7A), reaching levels much higher than those seen in glucose-grown *dbp2*Δ cells (Figure 5, C and D). This difference in expression levels is most likely due to the activity of other nutrient responsive pathways, such as AMPK and PKA/Ras, in addition to Dbp2-dependent regulation (Broach 2012). *HXT8* sense transcripts, however, accumulated to similar levels upon glucose deprivation in wild-type cells or deletion of *DBP2*, with a four- to sevenfold increase

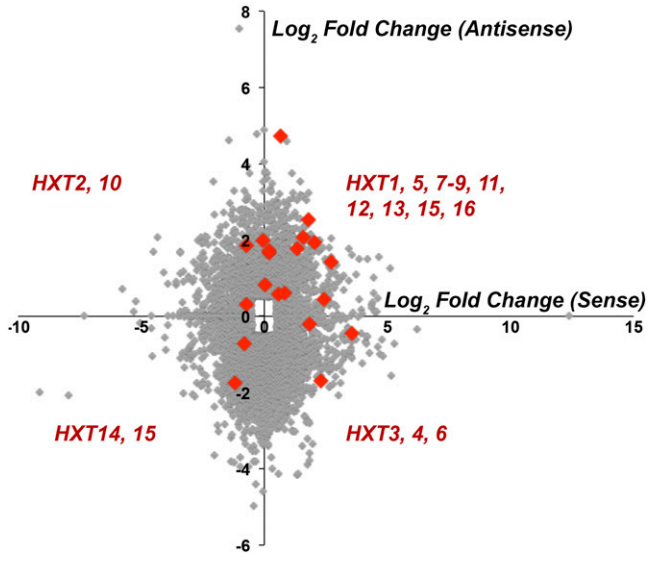

Figure 4 Loss of *DBP2* results in enrichment of sense and antisense hexose transporter gene transcripts. A scatter plot was generated to determine the correlation of sense and antisense transcript pair enrichment in DBP2-deficient cells over wild type. Log_2-fold change of transcript abundance is shown for sense transcripts *vs.* antisense transcripts with substantially increased or decreased transcript levels. Genes that had either sense or antisense transcript reads that were $>Log_2$ 0.5 or <-0.5 as compared to wild type were selected. Sense and antisense hexose transporter transcript genes *(HXTs)* are shown in red.

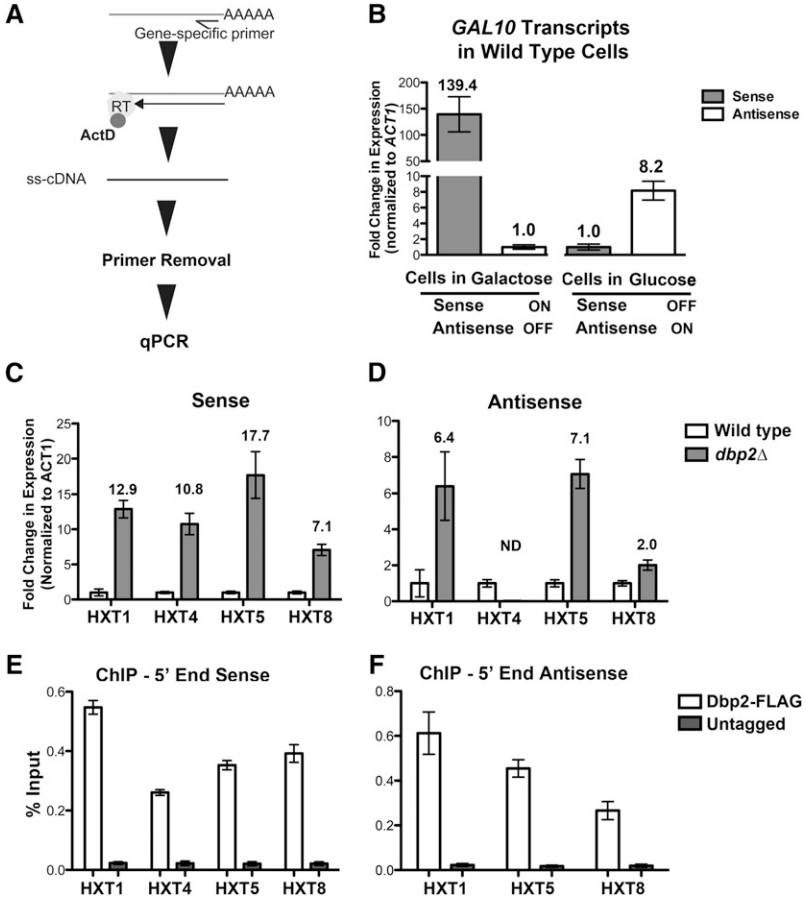

Figure 5 Strand-specific RT-qPCR confirms aberrant *HXT* transcript accumulation in *dbp2*Δ cells, correlating with presence of Dbp2 at genomic *HXT* loci. (A) Stepwise diagram of the strand-specific RT–qPCR method. Reverse transcription is conducted with a gene-specific primer that is complementary to either the sense or antisense strand. Single-stranded cDNA is produced using reverse transcriptase in the presence of actinomycin D (ActD), the latter of which prevents second-strand synthesis (Perocchi *et al.* 2007). Half arrow denotes primer positioning on targeted RNAs whereas complete arrow indicates reverse transcriptase activity. Unincorporated primers are removed using column chromatography and the resulting cDNA is quantified using PCR and SYBR green detection. (B) Single-stranded RT–qPCR measures expression of mutually exclusive GAL10 sense and antisense transcripts. Total RNA was isolated from wild-type cells grown in triplicate in either glucose or galactose media (for expression of antisense or sense *GAL10* transcripts, respectively) and subjected to transcript-specific cDNA preparation. Gene-specific primers for *ACT1* were also included in the reverse transcription reaction as an internal control for downstream quantification. Fold change in expression was calculated for each growth condition independently and is shown relative to the minority transcript (*i.e.*, transcripts from cells grown in galactose are normalized to antisense *GAL10* and to sense *GAL10* for glucose-cultured cells), which is set to 1 for representation. Numbers above each bar show the average fold change with error bars reflecting the SE.M. (C and D) Independent validation of HXT sense and antisense transcript abundance using strand-specific RT–qPCR. The fold enrichment of representative *HXT* sense and antisense transcripts in *dbp2*Δ cells over wild type was determined using strand-specific RT–qPCR as above. Transcript abundance was normalized with respect to *ACT1* transcript levels, a transcript whose levels do not vary between wild-type and *dbp2*Δ cells (Cloutier *et al.* 2012), and is the average of three independent biological replicates and the SEM. ND, not detectible. (E) Dbp2 interacts directly with 5′ region of HXT genes, with respect to the sense transcript. Chromatin immunoprecipitation of 3X-FLAG-tagged Dbp2 *vs.* and untagged control strain. Primer-probe sets (Table 2) were designed for sites on genomic DNA corresponding to the 5′ regions of the sense transcripts of *HXT1*, *HXT4*, *HXT5*, *HXT8*. (F) Dbp2 interacts directly with the genomic region encoding HXT antisense transcripts. Chromatin immunoprecipitation of 3X-FLAG-tagged Dbp2 *vs.* and untagged control strain. Primer-probe sets (Table 2) were designed for sites on genomic DNA corresponding to the 5′ regions of the antisense transcripts of *HXT1*, *HXT5*, *HXT8*. Results are presented as percentage input and are the average of three biological replicates with three technical replicates and the SEM.

in transcript abundance as compared to the control strain (Figure 5 and 7). Antisense *HXT8* transcripts also accumulated in wild-type cells upon glucose depletion (Figure 7B), suggesting that *HXT8* gene expression may be most responsive to glucose-dependent changes in Dbp2 localization. In contrast, we did not observe induction of either sense or antisense *HXT1* transcripts under these conditions, suggesting that altered *HXT1* expression in *dbp2*Δ cells is due to a different mechanism or that Dbp2 may not be fully lost from the *HXT1* locus upon glucose deprivation (Figure 7, A and B). Regardless, loss of *DBP2*, either by genomic mutation or by glucose deprivation, alters the cellular abundance of transcripts corresponding to *HXT* gene loci. Taken together, we suggest that cellular energy homeostasis is dependent on regulation of the RNA helicase Dbp2 and resulting changes in metabolic gene expression.

Discussion

Cellular life requires a fine balance between energy generation and consumption to maximize the potential for growth. The ability to drastically alter the metabolic state of the cell is a hallmark feature of tumor cells called the *Warburg effect*, as well as exercising muscle cells, red blood cells, and activated macrophages and stem cells (Ochocki and Simon 2013; Palsson-Mcdermott and O'Neill 2013). Thus, defining the mechanism(s) governing metabolic control has widespread implications in normal mammalian cell growth and human disease states.

Our results demonstrate that the RNA helicase Dbp2 is a key integrator of nutritional status and gene expression programs required for energy homeostasis. Dbp2 is a canonical member of the DEAD-box family of RNA helicases. Prior work from our laboratory has established that Dbp2 is an RNA-dependent ATPase *in vitro* capable of unwinding a variety of RNA duplex substrates (Cloutier *et al.* 2012; Ma *et al.* 2013). Dbp2 appears to function in multiple aspects of RNA biology including ribosome biogenesis, mRNP assembly, and transcription initiation (Barta and Iggo 1995; Bond *et al.* 2001; Cloutier *et al.* 2012; Ma *et al.* 2013), suggestive of a general role in RNA structure modulation.

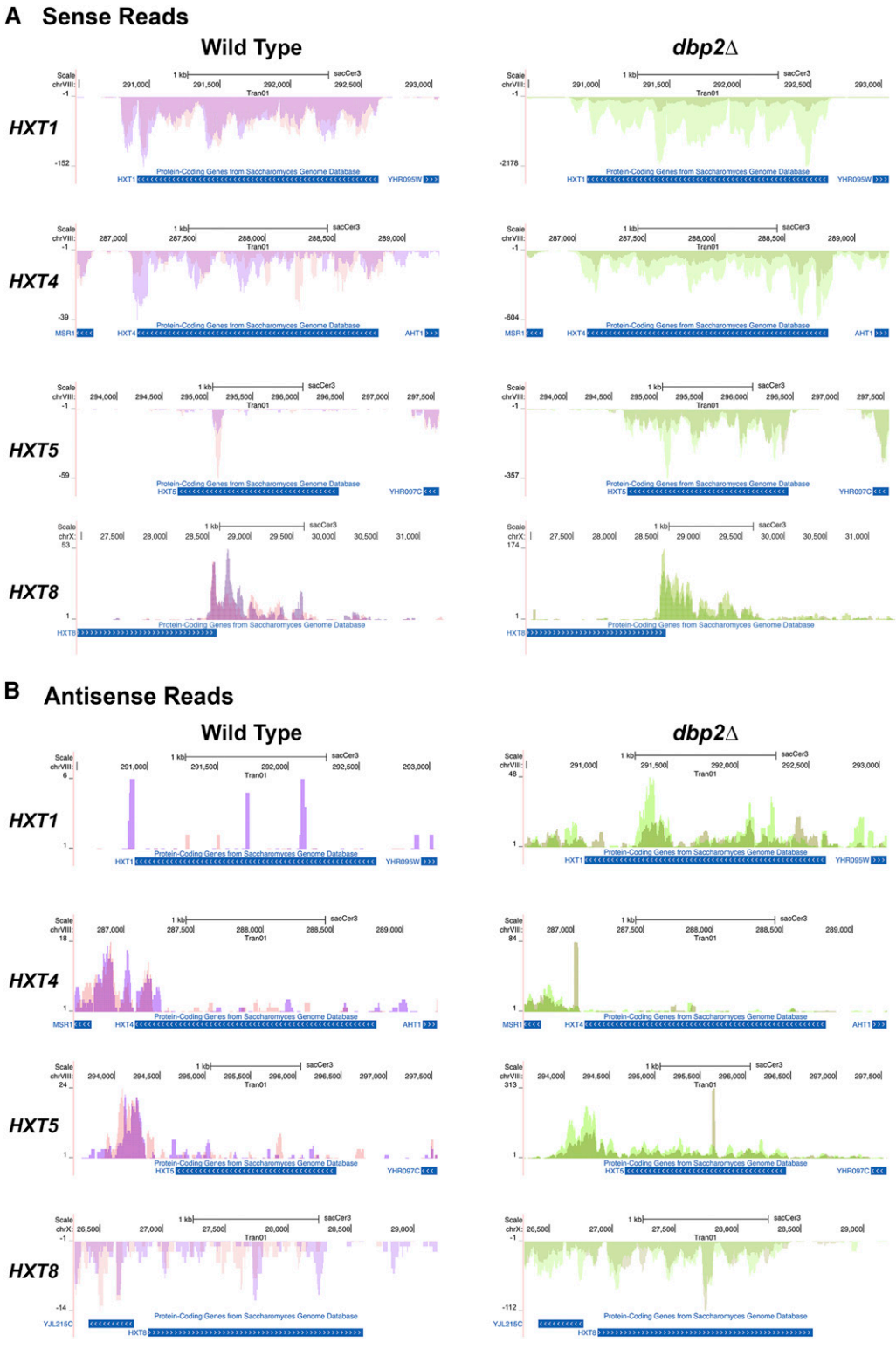

Figure 6 Mapped RNA seq reads across representative HXT genes. Alignment of mapped RNA sequencing reads shows similar (A) sense and (B) antisense expression patterns in wild-type and dbp2Δ cells. Reads were aligned to the *S. cerevisiae* genome using the UCSC genome browser. Images were generated directly through the UCSC website and show reads that correspond to the annotated, protein-coding gene. Reads on the top correspond to Watson strand-encoded transcript whereas reads on the bottom of each graph align to a gene encoded on the Crick strand. Arrows within the gene ORF rectangle indicate orientation of the sense transcript within the genome. Sense and antisense transcripts are displayed on different graphs due to differences in abundance and resulting graphical scaling. Note that the y-axis is different between wild-type and dbp2Δ cells due to expression level differences between these two strains.

Dbp2 has also been shown to associate with chromatin actively transcribed by RNA polymerase II, indicative of a cotranscriptional role. This is supported by the fact that loss of *DBP2* results in reduced association of mRNA binding proteins and inefficient transcription termination (Cloutier *et al.* 2012; Ma *et al.* 2013). Thus, our work suggests that RNA structure and/or composition may be central to the metabolic state of the cell.

The ability to match nutrient availability to cellular growth is largely accomplished through the glucose-sensing Rgt1–Snf3, the TOR, and the AMP-dependent protein kinase (Snf1 in budding yeast) pathways (Woods *et al.* 1994; Broach

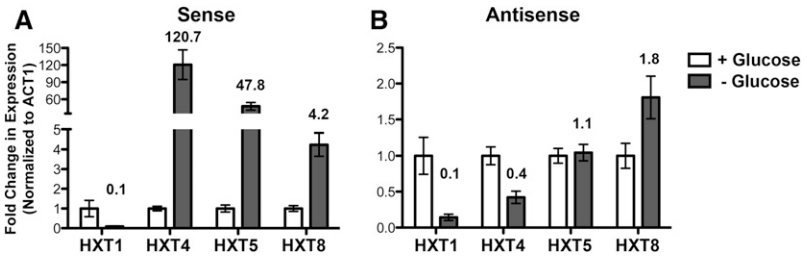

Figure 7 Glucose deprivation alters the levels of sense and antisense hexose transporter transcripts in wild-type cells. HXT sense and antisense transcript abundance using strand-specific RT–qPCR in wild-type cells grown in glucose or after glucose depletion. Wild-type cells were isolated following growth in glucose (2%) or after a 10-min shift to glucose-depleted media. The levels of (A) sense and (B) antisense hexose transporter transcripts were determined by strand-specific RT–qPCR as in Figure 4 and are reported as the average of three biological replicates with the SEM.

2012; Hardie *et al.* 2012; Horak 2013). These signaling programs communicate the presence and concentration of glucose to the energy producing metabolic gene networks and energy-consuming ribosome biogenesis and translational processes. Snf1 and TOR play opposing roles in cellular homeostasis, with the former increasing energy availability when nutrients are limiting and the latter promoting biogenesis when nutrients are abundant. Snf1-dependent relocalization of Dbp2 to the cytoplasm would be reminiscent of regulated transport of the glucose-dependent repressor Mig1 whereas TOR signaling would be required to maintain the nuclear pool of Dbp2 in the presence of glucose. The latter would be similar to glucose-dependent regulation of the transcription factor Sfp1, whose nuclear localization is dependent on active TOR and Ras/PKA pathways (Jorgensen *et al.* 2004). However, our results suggest that neither Snf1 nor TOR signaling play major roles in regulation of Dbp2 localization in response to glucose availability.

Another possibility is that Dbp2 directly senses AMP/ATP ratios in the cell. Accumulation of AMP correlates with a decrease in the cellular energy status and occurs upon decreased glucose availability (Boer *et al.* 2010). The AMP-activated protein kinase AMPK is the major energy sensor in eukaryotic cells and is directly regulated by increasing AMP concentrations (Wilson *et al.* 1996; Hardie *et al.* 2012). Interestingly, recent work from the Jankowsky laboratory shows that several DEAD-box RNA helicases are enzymatically inhibited by AMP binding *in vitro*, even though AMP is not a product of ATP hydrolysis (Putnam and Jankowsky 2013a). This included Mss116 and Ded1, which exhibit similar RNA duplex unwinding activities to Dbp2 (Yang and Jankowsky 2005; Yang *et al.* 2007; Ma *et al.* 2013). Thus, it is tempting to speculate that cellular AMP may directly regulate the helicase activity of Dbp2. This is an intriguing possibility, as Snf1, the AMPK ortholog in budding yeast, does not directly sense AMP/ATP ratios but is, instead, activated by phosphorylation (Wilson *et al.* 1996; Hardie *et al.* 2012). Further work is necessary to determine if Dbp2 can act as an AMP sensor to maintain cellular energy homeostasis.

It is currently unknown how Dbp2 affects cellular RNA levels. Interestingly, rapid changes in carbon sources cause drastic changes in mRNP stability, with ribosomal protein mRNAs undergoing rapid decay upon a glucose to galactose media switch (Munchel *et al.* 2011). It is possible that loss of Dbp2 results in widespread changes in mRNP/lncRNP composition that alter RNA stability. If this were the case, we would speculate that these compositional changes occur in the nucleus due to the direct association of Dbp2 with chromatin (Cloutier *et al.* 2012). Moreover, the similarity between misregulated antisense transcripts in *dbp2*Δ cells and glucose-deprived wild-type cells, when Dbp2 is cytoplasmic, is consistent with loss of a nuclear role.

In addition to well-known pathways that are glucose dependent, loss of *DBP2* also resulted in upregulation of both sense and antisense *HXT* transcripts. Yeasts in nature encounter a wide range of sugar concentrations that differ by 6 orders of magnitude (from micromolar to molar concentrations) (Johnston and Kim 2005; Horak 2013). A major mechanism to promote growth under these vastly different nutritional conditions is through tight regulation of hexose transporter activity. Although the mechanism(s) that govern transcriptional control of the *HXT* genes are largely established, a role for lncRNAs in this process has not been explored. Previous studies from our laboratory established a role for the *GAL* cluster-associated lncRNAs in facilitating transcriptional switches, enhancing the rate at which the transcriptional activation is stimulated or repressed in response to extracellular cues (Cloutier *et al.* 2013). We would speculate that the antisense *HXT* lncRNAs function similarly, maintaining the activation potential of the *HXT* genes for future restoration of hexose availability. This model is similar to a recently identified Ajar pathway for *HXT5* and recognition of the rapid response rate of yeast upon restoration of nutrients after glucose depletion (Kresnowati *et al.* 2006; Bermejo *et al.* 2010). In fact, upregulation of *HXT5* upon glucose deprivation is specifically required for the rapid restoration of normal growth, suggesting that this pathway allows this single-cell eukaryote to be "optimistic" regarding the return of nutrients in the environment.

An alternative explanation is that the sense and antisense *HXT* transcripts are expressed in different cells within the population, with the antisense transcripts promoting transcriptional repression. If this were the case, the *HXT* lncRNAs may function similarly to *PHO84* lncRNA that functions as a "bimodal" switch to promote different cell fates within a genetically identical population (Castelnuovo *et al.* 2013). A third possibility is that the antisense *HXT* transcripts function in the cytoplasm, controlling translational efficiency to stability of the corresponding sense mRNA (Carrieri *et al.* 2012; Pelechano and Steinmetz 2013; Wang *et al.* 2013). Additional experiments are necessary to uncover potential mechanisms for these antisense lncRNAs in cellular homeostasis. These and future endeavors offer the exciting possibility that lncRNAs, RNA structure,

and/or RNA helicases play specific roles in cellular metabolism.

Acknowledgments

Special thanks go to members of the Tran laboratory for advice and critical reading of this manuscript, to Nadereh Jafari (Northwestern) for assistance with RNA sequencing and bioinformatics, and to Vikki Weake (Purdue) for thoughtful discussion. This work was supported by National Institutes of Health (NIH) R01GM097332-01 to E.J.T.

Literature Cited

Barta, I., and R. Iggo, 1995 Autoregulation of expression of the yeast Dbp2p 'DEAD-box' protein is mediated by sequences in the conserved DBP2 intron. EMBO J. 14: 3800–3808.

Bermejo, C., F. Haerizadeh, H. Takanaga, D. Chermak, and W. B. Frommer, 2010 Dynamic analysis of cytosolic glucose and ATP levels in yeast using optical sensors. Biochem. J. 432: 399–406.

Berriz, G. F., J. E. Beaver, C. Cenik, M. Tasan, and F. P. Roth, 2009 Next generation software for functional trend analysis. Bioinformatics 25: 3043–3044.

Bhaskaran, H., and R. Russell, 2007 Kinetic redistribution of native and misfolded RNAs by a DEAD-box chaperone. Nature 449: 1014–1018.

Boer, V. M., C. A. Crutchfield, P. H. Bradley, D. Botstein, and J. D. Rabinowitz, 2010 Growth-limiting intracellular metabolites in yeast growing under diverse nutrient limitations. Mol. Biol. Cell 21: 198–211.

Bohnsack, M. T., R. Martin, S. Granneman, M. Ruprecht, E. Schleiff *et al.*, 2009 Prp43 bound at different sites on the pre-rRNA performs distinct functions in ribosome synthesis. Mol. Cell 36: 583–592.

Bond, A. T., D. A. Mangus, F. He, and A. Jacobson, 2001 Absence of Dbp2p alters both nonsense-mediated mRNA decay and rRNA processing. Mol. Cell. Biol. 21: 7366–7379.

Bowers, H. A., P. A. Maroney, M. E. Fairman, B. Kastner, R. Luhrmann *et al.*, 2006 Discriminatory RNP remodeling by the DEAD-box protein DED1. RNA 12: 903–912.

Broach, J. R., 2012 Nutritional control of growth and development in yeast. Genetics 192: 73–105.

Buszczak, M., and A. C. Spradling, 2006 The Drosophila P68 RNA helicase regulates transcriptional deactivation by promoting RNA release from chromatin. Genes Dev. 20: 977–989.

Camats, M., S. Guil, M. Kokolo, and M. Bach-Elias, 2008 P68 RNA helicase (DDX5) alters activity of cis- and trans-acting factors of the alternative splicing of H-Ras. PLoS ONE 3: e2926.

Caretti, G., R. L. Schiltz, F. J. Dilworth, M. Di Padova, P. Zhao *et al.*, 2006 The RNA helicases p68/p72 and the noncoding RNA SRA are coregulators of MyoD and skeletal muscle differentiation. Dev. Cell 11: 547–560.

Carrieri, C., L. Cimatti, M. Biagioli, A. Beugnet, S. Zucchelli *et al.*, 2012 Long non-coding antisense RNA controls Uchl1 translation through an embedded SINEB2 repeat. Nature 491: 454–457.

Castelnuovo, M., S. Rahman, E. Guffanti, V. Infantino, F. Stutz *et al.*, 2013 Bimodal expression of PHO84 is modulated by early termination of antisense transcription. Nat. Struct. Mol. Biol. 20: 851–858.

Castoralova, M., D. Brezinova, M. Sveda, J. Lipov, T. Ruml *et al.*, 2012 SUMO-2/3 conjugates accumulating under heat shock or MG132 treatment result largely from new protein synthesis. Biochim. Biophys. Acta 1823: 911–919.

Clark, E. L., A. Coulson, C. Dalgliesh, P. Rajan, S. M. Nicol *et al.*, 2008 The RNA helicase p68 is a novel androgen receptor co-activator involved in splicing and is overexpressed in prostate cancer. Cancer Res. 68: 7938–7946.

Cloutier, S. C., W. K. Ma, L. T. Nguyen, and E. J. Tran, 2012 The DEAD-box RNA helicase Dbp2 connects RNA quality control with repression of aberrant transcription. J. Biol. Chem. 287: 26155–26166.

Cloutier, S. C., S. Wang, W. K. Ma, C. J. Petell, and E. J. Tran, 2013 Long noncoding RNAs promote transcriptional poising of inducible genes. PLoS Biol. 11: e1001715.

Del Campo, M., S. Mohr, Y. Jiang, H. Jia, E. Jankowsky *et al.*, 2009 Unwinding by local strand separation is critical for the function of DEAD-box proteins as RNA chaperones. J. Mol. Biol. 389: 674–693.

De Vit, M. J., J. A. Waddle, and M. Johnston, 1997 Regulated nuclear translocation of the Mig1 glucose repressor. Mol. Biol. Cell 8: 1603–1618.

DeVit, M. J., and M. Johnston, 1999 The nuclear exportin Msn5 is required for nuclear export of the Mig1 glucose repressor of *Saccharomyces cerevisiae*. Curr. Biol. 9: 1231–1241.

Fatica, A., and I. Bozzoni, 2014 Long non-coding RNAs: new players in cell differentiation and development. Nat. Rev. Genet. 15: 7–21.

Fuller-Pace, F. V., and H. C. Moore, 2011 RNA helicases p68 and p72: multifunctional proteins with important implications for cancer development. Future Oncol. 7: 239–251.

Gancedo, J. M., 1998 Yeast carbon catabolite repression. Microbiol. Mol. Biol. Rev. 62: 334–361.

Geisler, S., L. Lojek, A. M. Khalil, K. E. Baker, and J. Coller, 2012 Decapping of long noncoding RNAs regulates inducible genes. Mol. Cell 45: 279–291.

Hardie, D. G., F. A. Ross, and S. A. Hawley, 2012 AMP-activated protein kinase: a target for drugs both ancient and modern. Chem. Biol. 19: 1222–1236.

Horak, J., 2013 Regulations of sugar transporters: insights from yeast. Curr. Genet. 59: 1–31.

Houseley, J., L. Rubbi, M. Grunstein, D. Tollervey, and M. Vogelauer, 2008 A ncRNA modulates histone modification and mRNA induction in the yeast GAL gene cluster. Mol. Cell 32: 685–695.

Jalal, C., H. Uhlmann-Schiffler, and H. Stahl, 2007 Redundant role of DEAD box proteins p68 (Ddx5) and p72/p82 (Ddx17) in ribosome biogenesis and cell proliferation. Nucleic Acids Res. 35: 3590–3601.

Jankowsky, E., 2011 RNA helicases at work: binding and rearranging. Trends Biochem. Sci. 36: 19–29.

Johnson, J. M., S. Edwards, D. Shoemaker, and E. E. Schadt, 2005 Dark matter in the genome: evidence of widespread transcription detected by microarray tiling experiments. Trends Genet. 21: 93–102.

Johnston, M., and J. H. Kim, 2005 Glucose as a hormone: receptor-mediated glucose sensing in the yeast *Saccharomyces cerevisiae*. Biochem. Soc. Trans. 33: 247–252.

Jorgensen, P., I. Rupes, J. R. Sharom, L. Schneper, J. R. Broach *et al.*, 2004 A dynamic transcriptional network communicates growth potential to ribosome synthesis and critical cell size. Genes Dev. 18: 2491–2505.

Kovalev, N., D. Barajas, and P. D. Nagy, 2012 Similar roles for yeast Dbp2 and Arabidopsis RH20 DEAD-box RNA helicases to Ded1 helicase in tombusvirus plus-strand synthesis. Virology 432: 470–484.

Kresnowati, M. T., W. A. van Winden, M. J. Almering, A. ten Pierick, C. Ras *et al.*, 2006 When transcriptome meets metabolome: fast cellular responses of yeast to sudden relief of glucose limitation. Mol. Syst. Biol. 2: 49.

Laxman, S., B. M. Sutter, and B. P. Tu, 2010 Behavior of a metabolic cycling population at the single cell level as visualized by fluorescent gene expression reporters. PLoS ONE 5: e12595.

Lempiainen, H., and D. Shore, 2009 Growth control and ribosome biogenesis. Curr. Opin. Cell Biol. 21: 855–863.

Lohr, D., P. Venkov, and J. Zlatanova, 1995 Transcriptional regulation in the yeast GAL gene family: a complex genetic network. FASEB J. 9: 777–787.

Ma, W. K., S. C. Cloutier, and E. J. Tran, 2013 The DEAD-box protein Dbp2 functions with the RNA-binding protein Yra1 to promote mRNP assembly. J. Mol. Biol. 425: 3824–3838.

Mitchell, S. F., S. Jain, M. She, and R. Parker, 2013 Global analysis of yeast mRNPs. Nat. Struct. Mol. Biol. 20: 127–133.

Munchel, S. E., R. K. Shultzaberger, N. Takizawa, and K. Weis, 2011 Dynamic profiling of mRNA turnover reveals gene-specific and system-wide regulation of mRNA decay. Mol. Biol. Cell 22: 2787–2795.

Ochocki, J. D., and M. C. Simon, 2013 Nutrient-sensing pathways and metabolic regulation in stem cells. J. Cell Biol. 203: 23–33.

Palsson-McDermott, E. M., and L. A. O'Neill, 2013 The Warburg effect then and now: from cancer to inflammatory diseases. BioEssays 35: 965–973.

Pelechano, V., and L. M. Steinmetz, 2013 Gene regulation by antisense transcription. Nat. Rev. Genet. 14: 880–893.

Perocchi, F., Z. Xu, S. Clauder-Munster, and L. M. Steinmetz, 2007 Antisense artifacts in transcriptome microarray experiments are resolved by actinomycin D. Nucleic Acids Res. 35: e128.

Pfaffl, M. W., 2001 A new mathematical model for relative quantification in real-time RT-PCR. Nucleic Acids Res. 29: e45.

Piao, H., J. MacLean Freed, and P. Mayinger, 2012 Metabolic activation of the HOG MAP kinase pathway by Snf1/AMPK regulates lipid signaling at the Golgi. Traffic 13: 1522–1531.

Pinskaya, M., S. Gourvennec, and A. Morillon, 2009 H3 lysine 4-di- and tri-methylation deposited by cryptic transcription attenuates promoter activation. EMBO J. 28: 1697–1707.

Powers, T., and P. Walter, 1999 Regulation of ribosome biogenesis by the rapamycin-sensitive TOR-signaling pathway in *Saccharomyces cerevisiae*. Mol. Biol. Cell 10: 987–1000.

Putnam, A. A., and E. Jankowsky, 2013a AMP sensing by DEAD-box RNA helicases. J. Mol. Biol. 425: 3839–3845.

Putnam, A. A., and E. Jankowsky, 2013b DEAD-box helicases as integrators of RNA, nucleotide and protein binding. Biochim. Biophys. Acta 1829: 884–893.

Ruiz-Echevarria, M. J., C. I. Gonzalez, and S. W. Peltz, 1998 Identifying the right stop: determining how the surveillance complex recognizes and degrades an aberrant mRNA. EMBO J. 17: 575–589.

Salzman, D. W., J. Shubert-Coleman, and H. Furneaux, 2007 P68 RNA helicase unwinds the human let-7 microRNA precursor duplex and is required for let-7-directed silencing of gene expression. J. Biol. Chem. 282: 32773–32779.

Sellick, C. A., R. N. Campbell and R. J. Reece, 2008 Galactose metabolism in yeast-structure and regulation of the leloir pathway enzymes and the genes encoding them. Int. Rev. Cell Mol. Biol. 269: 111–150.

Traven, A., B. Jelicic, and M. Sopta, 2006 Yeast Gal4: a transcriptional paradigm revisited. EMBO Rep. 7: 496–499.

van Dijk, E. L., C. L. Chen, Y. d'Aubenton-Carafa, S. Gourvennec, M. Kwapisz *et al.*, 2011 XUTs are a class of Xrn1-sensitive antisense regulatory non-coding RNA in yeast. Nature 475: 114–117.

Verwaal, R., J. W. Paalman, A. Hogenkamp, A. J. Verkleij, C. T. Verrips *et al.*, 2002 HXT5 expression is determined by growth rates in *Saccharomyces cerevisiae*. Yeast 19: 1029–1038.

Wang, J., C. Gong, and L. E. Maquat, 2013 Control of myogenesis by rodent SINE-containing lncRNAs. Genes Dev. 27: 793–804.

Warner, J. R., 1999 The economics of ribosome biosynthesis in yeast. Trends Biochem. Sci. 24: 437–440.

Westfall, P. J., D. R. Ballon, and J. Thorner, 2004 When the stress of your environment makes you go HOG wild. Science 306: 1511–1512.

Wilson, B. J., G. J. Bates, S. M. Nicol, D. J. Gregory, N. D. Perkins *et al.*, 2004 The p68 and p72 DEAD box RNA helicases interact with HDAC1 and repress transcription in a promoter-specific manner. BMC Mol. Biol. 5: 11.

Wilson, W. A., S. A. Hawley, and D. G. Hardie, 1996 Glucose repression/derepression in budding yeast: SNF1 protein kinase is activated by phosphorylation under derepressing conditions, and this correlates with a high AMP:ATP ratio. Curr. Biol. 6: 1426–1434.

Woods, A., M. R. Munday, J. Scott, X. Yang, M. Carlson *et al.*, 1994 Yeast SNF1 is functionally related to mammalian AMP-activated protein kinase and regulates acetyl-CoA carboxylase in vivo. J. Biol. Chem. 269: 19509–19515.

Wullschleger, S., R. Loewith, and M. N. Hall, 2006 TOR signaling in growth and metabolism. Cell 124: 471–484.

Xu, Z., W. Wei, J. Gagneur, F. Perocchi, S. Clauder-Munster *et al.*, 2009 Bidirectional promoters generate pervasive transcription in yeast. Nature 457: 1033–1037.

Yang, Q., M. Del Campo, A. M. Lambowitz, and E. Jankowsky, 2007 DEAD-box proteins unwind duplexes by local strand separation. Mol. Cell 28: 253–263.

Yang, Q., and E. Jankowsky, 2005 ATP- and ADP-dependent modulation of RNA unwinding and strand annealing activities by the DEAD-box protein DED1. Biochemistry 44: 13591–13601.

Communicating editor: M. Hampsey

GENETICS

Supporting Information
http://www.genetics.org/lookup/suppl/doi:10.1534/genetics.114.170019/-/DC1

Regulation of Glucose-Dependent Gene Expression by the RNA Helicase Dbp2 in *Saccharomyces cerevisiae*

Zachary T. Beck, Sara C. Cloutier, Matthew J. Schipma, Christopher J. Petell, Wai Kit Ma, and Elizabeth J. Tran

DOI: 10.1534/genetics.114.170019

Tables S1-S3

Available for download as Excel files at http://www.genetics.org/lookup/suppl/doi:10.1534/genetics.114.170019/-/DC1

Table S1 Excel spreadsheet of all annotated *S. cerevisiae* genes with UCSC hyperlinks to the RNA sequencing data set.
Hyperlinks are included that direct to the Saccharomyces Genome Database (yeastgenome.org) or UCSC genome browser (genome.ucsc.org) by clicking on the gene name or the chromosomal location, respectively.

Table S2 Excel spreadsheet of differentially expressed sense transcripts.
The complete list of sense transcripts resulting from RNA sequencing that are differentially expressed (up or down) with respect to wild type following data analysis by Cufflinks 2.0.

Table S3 Excel spreadsheet of differentially expressed antisense transcripts.
The complete list of antisense transcripts resulting from RNA sequencing that are differentially expressed (up or down) with respect to wild type following data analysis by Cufflinks 2.0.

Metadata of the chapter that will be visualized online

Chapter Title	Measuring Helicase Inhibition of the DEAD-Box Protein Dbp2 by Yra1	
Copyright Year	2015	
Copyright Holder	Springer Science+Business Media New York	
Author	Family Name	**Ma**
	Particle	
	Given Name	**Wai Kit**
	Suffix	
	Division	Department of Biochemistry
	Organization	Purdue University
	Address	BCHM 305, 175 S. University Street, West Lafayette, IN, 47907-2063, USA
Corresponding Author	Family Name	**Tran**
	Particle	
	Given Name	**Elizabeth J.**
	Suffix	
	Division	Department of Biochemistry
	Organization	Purdue University
	Address	BCHM 305, 175 S. University Street, West Lafayette, IN, 47907-2063, USA
	Division	Purdue University Center for Cancer Research
	Organization	Purdue University
	Address	Hansen Life Sciences Research Building, Room 141, 201 S. University Street, West Lafayette, IN, 47907-2064, USA
	Email	ejtran@purdue.edu
Abstract	Despite the highly conserved helicase core, individual DEAD-box proteins are specialized in diverse RNA metabolic processes. One mechanism that determines DEAD-box protein specificity is enzymatic regulation by other protein cofactors. In this chapter, we describe a protocol for purifying the *Saccharomyces cerevisiae* DEAD-box RNA helicase Dbp2 and RNA-binding protein Yra1 and subsequent analysis of helicase regulation. The experiments described here can be adapted to other RNA helicases and their purified cofactor(s).	
Keywords (separated by "-")	DEAD-box - RNA - Helicase - Unwinding - Annealing - Duplex - Yeast	

Chapter 12

Measuring Helicase Inhibition of the DEAD-Box Protein Dbp2 by Yra1

[AU1] Wai Kit Ma and Elizabeth J. Tran

Abstract

Despite the highly conserved helicase core, individual DEAD-box proteins are specialized in diverse RNA metabolic processes. One mechanism that determines DEAD-box protein specificity is enzymatic regulation by other protein cofactors. In this chapter, we describe a protocol for purifying the *Saccharomyces cerevisiae* DEAD-box RNA helicase Dbp2 and RNA-binding protein Yra1 and subsequent analysis of helicase regulation. The experiments described here can be adapted to other RNA helicases and their purified cofactor(s).

Key words DEAD-box, RNA, Helicase, Unwinding, Annealing, Duplex, Yeast

1 Introduction

[AU2] DEAD-box RNA helicases are the largest class of enzymes within the helicase family and can be found in all domains of life [1]. All DEAD-box proteins share at least 12 conserved motifs in the helicase core spread throughout two RecA-like domains, including the eponymic Asp-Glu-Ala-Asp (D-E-A-D) sequence in the Walker B motif [2].

Several studies have revealed that individual DEAD-box proteins display diverse biochemical activities in vitro, including RNA-protein complex (RNP) remodeling, RNA-dependent ATP hydrolysis, and ATP-dependent unwinding of RNA duplexes [3, 4]. A major question in the field is how this diversity of function is achieved among the ~25 different DEAD-box proteins in yeast (40 in humans), given the high degree of sequence and structural identity in the helicase core. Studies have shown that unique N- and/or C-terminus extensions can provide substrate specificity to individual family members [5, 6]. For example, the C-terminus of DbpA provides specificity to target 23S rRNA [7–9]. Moreover, the flanking regions can also provide nonspecific RNA tethers. This has been described for Mss116 and CYT-19 [10, 11].

Marc Boudvillain (ed.), *RNA Remodeling Proteins: Methods and Protocols*, Methods in Molecular Biology, vol. 1259, DOI 10.1007/978-1-4939-2214-7_12, © Springer Science+Business Media New York 2015

In addition to unique flanking regions, specificity can also be conferred by protein cofactors that regulate the enzymatic activity of individual DEAD-box proteins [12, 13]. For instance, the translation initiation factor eIF4G stimulates the weak ATPase activity of eIF4A [14]. This is believed to allow eIF4A to unwind secondary structures in 5′UTR and facilitate the small ribosomal subunit to scan for the start codon during translation. Recently, our laboratory showed that the *S. cerevisiae* DEAD-box protein Dbp2 interacts directly with the mRNA-binding protein Yra1 [15]. Furthermore, we found that Yra1 inhibits the unwinding activity of Dbp2 without significantly altering the ATPase activity, suggesting specific regulation of duplex unwinding [15]. Here, we describe a method to evaluate the effect of Yra1 on the unwinding activity of Dbp2. This method is widely applicable to the analysis of other protein-binding cofactors for RNA helicases.

2 Materials

2.1 Expression and Purification of Recombinant Dbp2 and Yra1 (C-Terminus Domain) in E. coli

1. LB Broth: 10 g bacto tryptone, 5 g yeast extract, and 10 g NaCl. Adjust the pH to ~7.0. Bring up to a final volume of 1 L with water. Autoclave the media.
2. LB agar: 10 g bacto tryptone, 5 g yeast extract, 10 g NaCl, and 20 g agar. Adjust the pH to ~7.0. Bring up to a final volume of 1 L with water. Autoclave the media and pour the plate after adding appropriate antibiotic.
3. LB Broth + 1 % glucose: 10 g bacto tryptone, 5 g yeast extract, 10 g NaCl, and 10 g glucose. Adjust the pH to ~7.0. Bring up to a final volume of 1 L with water. Autoclave the media.
4. Ampicillin: Dissolve ampicillin sodium salt in water to a final concentration of 75 mg/mL. Filter sterilize with a 0.2 μm syringe filter and store at −20 °C in 1 mL aliquots.
5. Chloramphenicol: Dissolve chloramphenicol in 100 % ethanol to a final concentration of 34 mg/mL and store at −20 °C in 1 mL aliquots.
6. 20 % Glycerol stock of *Escherichia coli* Rosetta (DE3): Store at −80 °C.
7. 20 % Glycerol stock of *Escherichia coli* BL21 (DE3): Store at −80 °C.
8. pMAL-TEV-Dbp2 plasmid [15].
9. pET21GST-yra1C plasmid [16].
10. IPTG solution: Dissolve isopropyl β-D-thiogalactopyranoside (Amresco) in water to a final concentration of 1 M and store at −20 °C.

11. Protease inhibitors that inhibit serine and cysteine proteases in bacterial extracts. Ad hoc inhibitor cocktails can be obtained from various commercial sources.
12. 7,000 units/mL of RNase A.
13. 100 U/μL of RNase I (*see* **Note 1**).
14. Empty 0.7 × 15 cm and 1.5 × 10 cm chromatography columns for gravity flow separations.
15. Lysis buffer (Dbp2): 50 mM CHES, 100 mM NaCl, pH 9.0.
16. Wash buffer (Dbp2): 50 mM CHES, 500 mM NaCl, pH 9.0.
17. Elution buffer (Dbp2): 50 mM Tris–HCl, 10 mM maltose, 0.5 mM EDTA, 1 mM DTT, pH 8.0.
18. Lysis buffer (yra1C): 20 mM HEPES, 1 mM EDTA, 20 % (v/v) glycerol, pH 7.5.
19. Wash buffer I (yra1C): 20 mM HEPES, 150 mM NaCl, 20 % (v/v) glycerol, pH 7.5.
20. Wash buffer II (yra1C): 20 mM HEPES, 500 mM NaCl, 20 % (v/v) glycerol, pH 7.5.
21. Elution buffer (yra1C): 20 mM HEPES, 20 mM glutathione, 150 mM NaCl, 20 % (v/v) glycerol, pH 7.5 (*see* **Note 2**).
22. 10 U/μL of TEV protease.
23. Amylose resin.
24. Glutathione sepharose resin (GE Healthcare).
25. SP sepharose resin.
26. SP equilibration buffer: 50 mM Tris–HCl, pH 8.0.
27. SP wash buffer: 50 mM Tris–HCl, 200 mM NaCl, pH 8.0.
28. SP elution buffer: 50 mM Tris–HCl, 600 mM NaCl, 20 % (v/v) glycerol, pH 8.0.

2.2 Preparation of RNA Duplexes

1. Adjustable height electrophoresis sequencer, 20 cm wide.
2. RNA oligo: Top strand (5′-AGCACCGUAAAGACGC-3′), bottom strand (5′-GCGUCUUUACGGUGCU-3′) [17].
3. 3,000 Ci/mmol, 10 mCi/mL of γ^{32}P-ATP.
4. 10,000 units/mL of T4 Polynucleotide Kinase (PNK).
5. 10× T4 Polynucleotide Kinase buffer.
6. 10× TBE: 890 mM Tris base, 890 mM boric acid, 20 mM EDTA.
7. Denaturing polyacrylamide gel: 20 % acrylamide:bisacrylamide [19:1], 7 M urea, 1× TBE.
8. Non-denaturing polyacrylamide gel: 15 % acrylamide: bisacrylamide [19:1], 0.5× TBE.

9. 5× Denaturing gel loading dye: 80 % formamide, 0.1 % bromophenol blue (BPB), 0.1 % xylene cyanol (XC).
10. 5× Non-denaturing gel loading dye: 50 % glycerol, 0.1 % BPB, 0.1 % XC.
11. X-ray films for autoradiography (e.g., Kodak X-OMAT LS, Fuji RX).
12. 20 mg/mL glycogen.
13. Gel elution buffer: 1 mM EDTA, 0.5 % SDS, 300 mM NaOAc, pH 5.2.
14. 10× duplex annealing buffer: 100 mM MOPS, 10 mM EDTA, 0.5 M KCl, pH 6.5.
15. RNA substrate storage buffer: 50 mM MOPS, 50 mM KCl, pH 6.0.

2.3 Unwinding and Annealing Assays

1. 10× Helicase reaction buffer (10× HRB): 400 mM Tris–HCl, 5 mM $MgCl_2$, 0.1 % NP-40, 20 mM DTT, pH 8.0.
2. 20 U/μL of Superase-in (Ambion).
3. 20 mM equimolar ATP/$MgCl_2$ (prepare from 100 mM ATP).
4. Purified DEAD-box proteins and protein-binding cofactors (*see* Subheading 3.1).
5. 1 nM radiolabeled RNA duplex.
6. 12 % Non-denaturing polyacrylamide gel: 12 % acrylamide: bisacrylamide [19:1], 0.5× TBE, 3 % glycerol.
7. 2× Helicase reaction stop buffer (2× HRSB): 50 mM EDTA, 1 % SDS, 0.1 % BPB, 0.1 % XC, 20 % glycerol.
8. Whatman chromatography paper.
9. Gel dryer.
10. PhosphorImager screen/PhosphorImager.

3 Methods

3.1 Preparation of Active Purified Dbp2 and yra1C

Dbp2 can bind *E. coli* RNA during expression of recombinant protein, resulting in copurification of contaminating RNA. To solve this problem, a high-salt wash step and two RNase treatments are utilized during purification. Ion-exchange chromatography is needed to remove the RNases and the affinity tags after TEV cleavage. The resulting protein preparations should be tested for RNase contamination by incubating the proteins with a radioactively labeled single-stranded RNA (ssRNA) and then resolving the RNA onto a non-denaturing polyacrylamide gel. A non-incubated, labeled RNA should be run in an adjacent well for comparison. The presence of RNA in the purified protein preparation can be determined by the ratio of A_{260nm}:A_{280nm} (*see* **Note 3**).

3.1.1 Expression of Dbp2 and Production of Cell Paste

1. Transform the pMAL-TEV-Dbp2 plasmid into BL21 (DE3) and plate onto LB agar + ampicillin (75 μg/mL). Incubate the plate at 37 °C overnight.
2. Inoculate a single colony into a 4 mL LB + ampicillin (75 μg/mL) culture and incubate at 37 °C with shaking at 200 RPM overnight.
3. Inoculate a 1 L LB + 1 % glucose + ampicillin (75 μg/mL) with all of the 4 mL culture and grow the bacteria at 37 °C with shaking at 200 RPM to an OD_{600nm} of 0.4–0.5 (*see* **Note 4**).
4. Induce MBP-TEV-Dbp2 expression by adding a final concentration of 1 mM IPTG to the culture. Express for 3 h at 37 °C with 200 RPM shaking.
5. Pellet cells at 11,100 × *g* for 15 min at 4 °C in pre-weighed bottles and then weigh the cell pellet by subtracting the empty bottle weight.
6. Store cell pellet at −20 °C or proceed to purification.

3.1.2 Purification of Dbp2

1. Resuspend the cell pellet with 6 mL of ice-cold lysis buffer (Dbp2) per gram of cell pellet and put on ice during preparation.
2. Add protease inhibitor, RNase A, and RNase I to a final concentration of 1×, 7 U/mL, and 10 U/mL, respectively.
3. Lyse cells with a probe sonicator (Branson digital sonifier) on an ice bath three times for 30 s using 30 % amplitude with 1-min cooling in between rounds. Utilization of a distinct sonifier may require re-optimization of these parameters.
4. Clear the lysate by centrifugation at 13,300 × *g* for 30 min at 4 °C. **Steps 5–13** are all performed at 4 °C.
5. Equilibrate 4 mL of 50 % slurry amylose resin (2 mL final packed volume) in a 1.5 × 10 cm chromatography column with 20 mL of lysis buffer (Dbp2).
6. Incubate the cleared lysate with the equilibrated resin in a capped chromatography column for 1 h at 4 °C with gentle rocking.
7. Wash the column with 25 mL of lysis buffer (Dbp2) followed by washing with 25 mL of wash buffer (Dbp2).
8. Shut off the column when wash buffer has flowed through but column is still wet.
9. Add 5 mL of wash buffer (Dbp2) to the column along with 35 U RNase A and 50 U RNase I.
10. Mix the resin by pipetting and incubate for at least 10 min at 4 °C.
11. Let the remaining buffer flow through and wash the column with 25 mL of lysis buffer (Dbp2).

12. Elute MBP-TEV-Dbp2 with elution buffer (Dbp2) in a 15 mL RNase-free conical tube until the A_{280nm} ~0.3 O.D (*see* **Note 5**).
13. Add 50 U of TEV protease per 1 mL of MBP-TEV-Dbp2 elution to the eluted fraction and mix it by inverting the conical tube gently several times.
14. Incubate at 16 °C for 12 h (*see* **Note 6**).
15. Equilibrate 400 µL of 50 % slurry SP sepharose (200 µL packed) with 5 mL SP equilibration buffer in a 0.7×15 cm chromatography column. The following purification steps (**steps 17–19**) are all performed at 4 °C.
16. Apply the cleaved sample to the column at 4 °C. Let the unbound sample flow through.
17. Wash the column with 10 mL of SP equilibration buffer and then 10 mL of SP wash buffer.
18. Elute with 3–5 column volumes of SP elution buffer. Store the purified Dbp2 protein at −80 °C in small aliquots as Dbp2 is not compatible with multiple freeze-thaw cycles. The purified protein can be stored at −80 °C for up to 4 months.

3.1.3 Expression of yra1C and Purification of yra1C

1. Expression and preparation of the cell pellet are as in Subheading 3.1.1 with the following exceptions: Transform the pET21GST-yra1C plasmid into Rosetta (DE3) cells, select with ampicillin (75 µg/mL) + chloramphenicol (34 µg/mL), and induce yra1C expression at 16 °C overnight (*see* **Note 7**).
2. GST-yra1C lysate is prepared as in **steps 1–4** from Subheading 3.1.2 except using lysis buffer (yra1C). **Steps 5–13** are all performed at 4 °C.
3. Equilibrate 6 mL of 50 % slurry glutathione sepharose (3 mL final packed volume) in a 1.5×10 cm chromatography column with 20 mL of lysis buffer (yra1C).
4. Incubate the cleared lysate with the equilibrated resin in a capped chromatography column for 1.5 h at 4 °C with gentle rocking (*see* **Note 8**).
5. Wash the column with 25 mL of wash buffer I (yra1C) and then 25 mL of wash buffer II (yra1C).
6. Shut off the column when vast majority of the wash buffer has flowed through but the column is still wet.
7. Add 5 mL of wash buffer II (yra1C) along with 35 U RNase A and 50 U RNase I.
8. Mix the resin with pipet and incubate for at least 10 min at 4 °C.
9. Let the remaining buffer flow through and wash the column with 50 mL of wash buffer I (yra1C).

10. Elute the GST-yra1C protein with 9 mL elution buffer (yra1C). Store the protein at −80 °C in small aliquots to avoid freeze-thaw cycles. The purified protein is stable for up to 4 months at −80 °C.

3.2 Preparation of RNA Duplexes for Unwinding and Annealing Assays

DEAD-box proteins can only unwind one to one-and-a-half turns of an RNA duplex [17, 18]; therefore, the RNA duplexes that are used in the assays are relatively short. Here, the 5′ end of the top strand of the RNA duplex is labeled with γ^{32}P-ATP using T4 polynucleotide kinase. Alternatively, the substrate can also be labeled with a fluorophore, either internally or at the 5′ or 3′ end. Because some fluorophore dyes affect duplex stability, it is critical to define differences between radiolabeled and fluorescently labeled duplexes prior to analysis [19].

3.2.1 Labeling and Isolation of RNA Duplexes

1. Mix 1 µL of 100 µM top strand RNA, 1 µL of 10× T4 PNK buffer, 1.5 µL of T4 PNK, 6 µL of 10 mCi/mL γ^{32}P-ATP, and 1.5 µL of water.
2. Incubate the mixture at 37 °C for 1 h.
3. Inactivate the kinase by adding 2 µL of denaturing gel loading dye and heating at 95 °C for 2 min (*see* **Note 9**).
4. Pre-run a denaturing 20 % polyacrylamide gel for 30 min at 30 V/cm in 1× TBE running buffer.
5. Load the labeled, top strand RNA and run at 30 V/cm for 2 h at room temperature.
6. Expose the gel to film or a phosphorimager screen to localize the labeled RNA (*see* **Note 10**).
7. Cut out the labeled strand with a razor blade and crush the gel slice into smaller pieces by passing through a 3 mL syringe into a 1.5 mL Eppendorf tube.
8. Add 600 µL of gel elution buffer to the gel pieces and incubate the sample overnight at 4 °C with gentle shaking.
9. Spin down the gel debris for 1 min at room temperature at 3,000 × *g*.
10. Transfer the aqueous fraction into two 1.5 mL tubes and add 3× volume of 100 % ethanol and 1 µL of 20 mg/mL glycogen to each tube (*see* **Note 11**).
11. Precipitate the labeled RNA for 1 h at −20 °C and centrifuge at 14,000 × *g* for 30 min at 4 °C.
12. Remove the supernatant and dry the pellet on the bench or in a speed vacuum.
13. Resuspend the two RNA pellets into a combined volume of 16 µL of water.

14. Add 2 μL of 100 μM unlabeled bottom strand RNA and 2 μL of 10× duplex annealing buffer to the 16 μL of labeled top strand RNA.
15. Heat the mixture at 95 °C for 2 min and cool the substrate at room temperature for 30 min.
16. Pre-run a 15 % non-denaturing gel for 30 min at 20 V/cm in 0.5× TBE running buffer.
17. Add 5 μL of non-denaturing gel loading dye to the labeled duplex mixture and load the labeled duplex on a 15 % non-denaturing gel.
18. Run the gel at 20 V/cm for 1 h with a cold water, cooling system or in a cold room to prevent duplex from denaturing.
19. Repeat **steps 6–12** to extract the labeled duplex RNA from the gel.
20. Dissolve the pellet in 30 μL of RNA substrate storage buffer.
21. Measure the cpm of the labeled duplex by scintillation counting. It should be around 150,000 cpm/μL.
22. Use the cpm measured from scintillation counting and calculate the RNA duplex using an equation as described [20]:

$$\frac{X\,\text{cpm}}{1.\text{L}} \times \frac{3\text{dpm}}{1\text{cpm}} \times \frac{1\mu\text{Ci}}{2220000\text{dpm}} \times \frac{0.0000\mu\text{Ci}}{1\mu\text{Ci}} \times \frac{1\text{mmol}}{Z\,\text{Ci}} \times \frac{10000000\mu\text{L}}{1\text{L}} = Y\,\text{mM}$$

where Z= the specific activity of γ^{32}P-ATP.

23. Aliquot the isolated, labeled RNA duplex into 10 μL aliquots and store at −20 °C for up to a month (*see* **Note 12**).

3.3 Unwinding and Annealing Assays

To study the effect of a protein cofactor on the unwinding activity of a DEAD-box protein, proper experimental controls are required. For instance, any unwinding and annealing activities of the cofactor in the absence of the helicase must be determined. If the protein cofactor can unwind and/or anneal an RNA substrate in vitro, these activities would need to be taken into account when assaying in the presence of an RNA helicase. Yra1 exhibits annealing activity in vitro [21], complicating analysis of Dbp2 helicase inhibition. However, deletion of the N-terminus abolishes annealing activity but preserves interaction with Dbp2 (Fig. 1d–e, [15]).

Thus, we measured the inhibition of Dbp2 in the presence of the C-terminal Yra1 domain (yra1C) (Fig. 1a–c). Bovine serum albumin (BSA) is used as a control to show specificity (Fig. 2). A step-by-step schematic diagram for analysis of protein cofactors on a helicase is provided (Fig. 3).

3.3.1 Unwinding Assays

1. Mix 3.3 μL of 10× helicase reaction buffer (HRB), 3.3 μL of 20 U/μL Superase-in, helicase and/or protein-binding cofactor

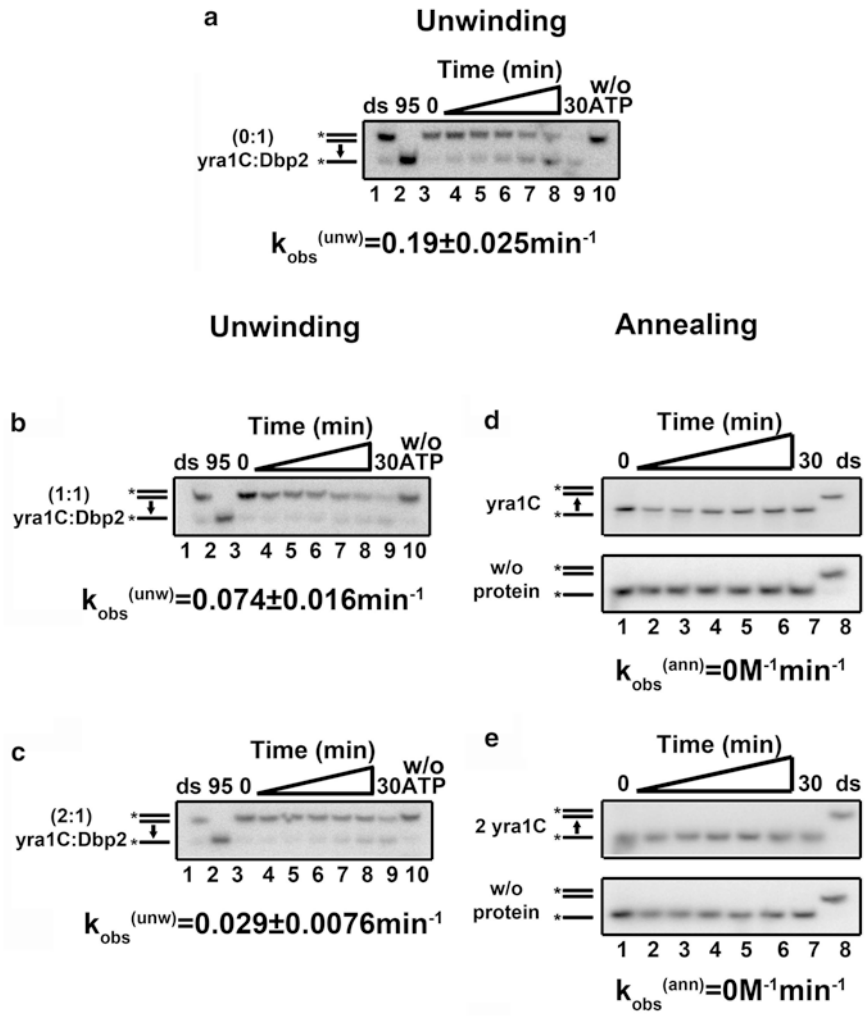

Fig. 1 The C-terminus of Yra1, yra1C, inhibits the unwinding activity of Dbp2. (**a**–**c**) Representative non-denaturing polyacrylamide gels of RNA unwinding assays using 600 nM Dbp2 alone (**a**) or with equimolar (**b**) or twofold excess of yra1C (**c**). (**d**–**e**) Representative non-denaturing polyacrylamide gels of RNA annealing assays using 600 nM (**d**) or 1,200 nM yra1C alone (**e**). This figure is reproduced from [15], with permission from Elsevier

(dilute with protein storage buffer) to desired protein concentration (600 nM for Dbp2 and 1,200 nM for yra1C), labeled RNA duplex to final concentration of 0.1 nM, and water to a final volume of 33 μL (*see* **Note 13**).

2. Incubate the mixture at 19 °C for 5 min to facilitate Dbp2 binding to the RNA duplex (*see* **Note 14**).
3. Aliquot 3 μL of the reaction mixture into 3 μL 2× helicase reaction stop buffer (HRSB) for the zero time point (Fig. 1a–c, lane 3) and place the sample on ice.

a

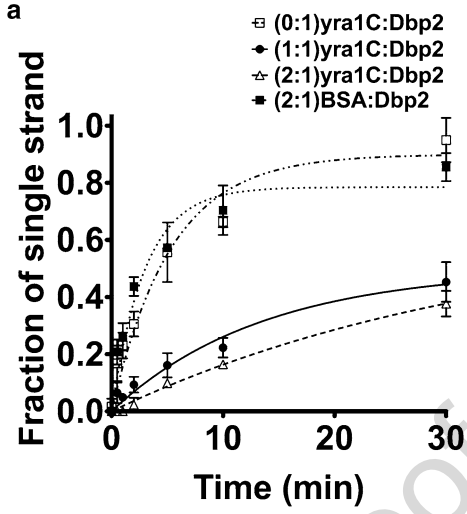

b

yra1C:Dbp2	k_{obs}(min^{-1})	Amplitude
0:1	0.19±0.026	0.90±0.047
1:1	0.074±0.016	0.50±0.053
2:1	0.029±0.0076	0.65±0.12

BSA:Dbp2	k_{obs}(min^{-1})	Amplitude
2:1	0.33±0.048	0.78±0.033

Fig. 2 Yra1 inhibits the unwinding activity of Dbp2. (**a**) A graphical representation of Dbp2 unwinding time course in the presence or absence of the C-terminus of Yra1 (yra1C). The unwinding assays were performed with 0.1 nM blunt end RNA duplex and either Dbp2 alone (600 nM) or in the presence of a 1:1 or 1:2 ratio of yra1C (600 nM, 1,200 nM) or in the presence of BSA (1,200 nM) at 19 °C. (**b**) The kinetic parameters of the unwinding reaction. The $k_{obs}^{(unw)}$ and the amplitude of the unwinding reaction were determined using the integrated rate law for a homogenous first-order reaction as described [25]. This figure is reproduced from [15], with permission from Elsevier

4. Aliquot another 3 μL of the reaction mixture to an empty tube and incubate at 19 °C for 30 min. After 30 min, add 3 μL 2× HRSB to the reaction. This is the reaction without ATP (Fig. 1a–c, lane 10).
5. Add 3 μL of 20 mM ATP/$MgCl_2$ to initiate the unwinding reaction.
6. Aliquot 3 μL of the reaction mixture into 3 μL 2× HRSB at the desired time points and place on ice.
7. Mix 3 μL of 0.1 nM labeled RNA duplex with 3 μL 2× HRSB as a dsRNA loading marker (Fig. 1a–c, lane 1).

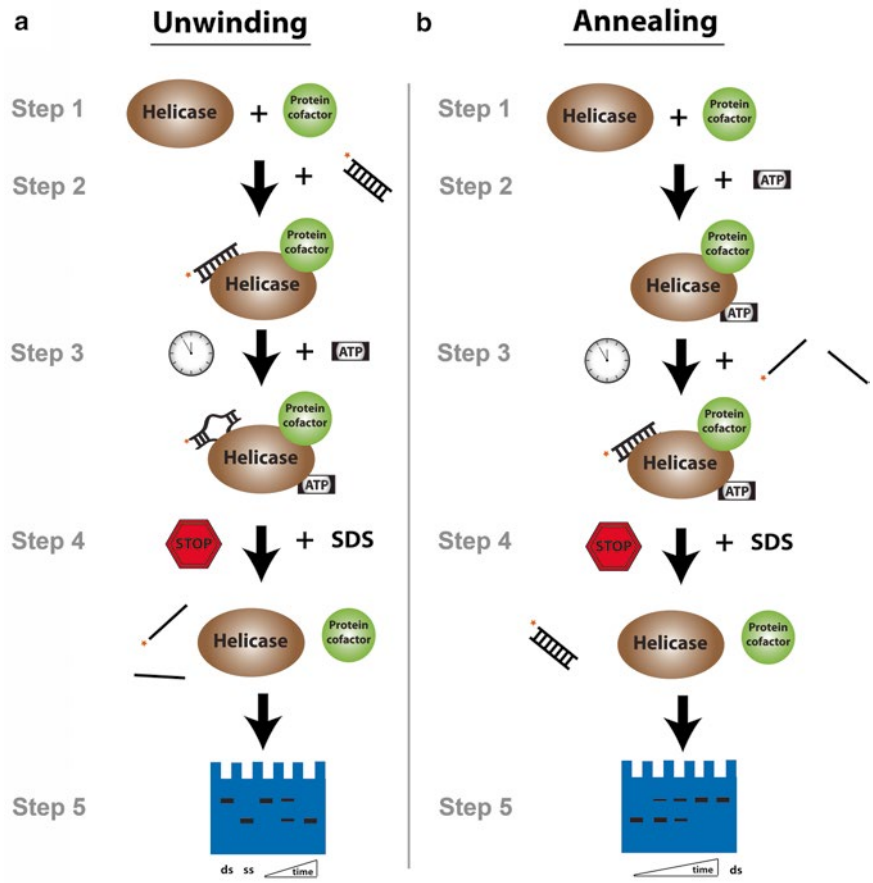

Fig. 3 Schematic flowchart of the unwinding and annealing assays. (**a**) For unwinding assays, Step 1: incubate the helicase and the protein cofactor at room temperature for 5 min. Step 2: add the radiolabeled dsRNA and incubate at the appropriate reaction temperature for 5 min. Step 3: start the reaction with equimolar concentration of ATP and $MgCl_2$. Step 4: remove aliquots at different time points and mix with SDS and EDTA to stop the reaction. Step 5: resolve the labeled RNA on a non-denaturing gel and visualize the products by autoradiography. (**b**) For annealing assays, Step 1: incubate the helicase and the protein cofactor at room temperature for 5 min. Step 2: add an equimolar concentration of ATP and $MgCl_2$ and incubate at reaction temperature for at least 5 min. Step 3: denature the labeled dsRNA at 95 °C before adding to the reaction mixture to start the reaction. Steps 4 and 5: remove aliquots over time, resolve and visualize product as above

8. Prepare the ssRNA loading marker (Fig. 1a–c, lane 2) by mixing 3 μL of 0.1 nM labeled RNA duplex with 3 μL 2× HRSB and heating the mixture at 95 °C for 2 min. 339 340 341
9. Pre-run a 12 % non-denaturing polyacrylamide gel for 30 min at 10 V/cm in 0.5× TBE running buffer and rinse the wells with the running buffer. 342 343 344
10. Load fractions on the gel and run for 1 h at 10 V/cm as in **step 18** from Subheading 3.2.1. 345 346

11. Remove the glass plates, put the gel on Whatman chromatography paper and dry gel on a gel dryer.
12. Expose gel to a PhosphorImager screen or film.
13. Quantify the intensity of radioactivity in dsRNA (I^{ds}) and intensity of radioactivity in ssRNA (I^{ss}) of each time point using a PhosphorImager and ImageQuant software.
14. The fraction of ssRNA at each time point is calculated using: Fraction of ssRNA = $I^{ss}/(I^{ss}+I^{ds})$. The representative gels are shown in (Fig. 1a–c).
15. Plot the fraction of ssRNA as a function of time and fit the data with the integrated form of a homogenous first-order rate law using the equation as described (Fig. 2 and Yang and Jankowsky [22]): Fraction of ssRNA = $\text{Amplitude} \times \left(1 - e^{-k_{obs} \times \text{time}}\right)$, where k_{obs} is the observed rate for the unwinding reaction.

3.3.2 Annealing Assays

1. Mix 3 μL of 10× HRB, 3 μL of 20 U/μL Superase-in, 3 μL of ATP/$MgCl_2$, helicase and/or protein binding cofactor (dilute with protein storage buffer) to desired protein concentration (600 nM for Dbp2 and 1,200 nM for yra1C), and water to a final volume of 28.5 μL.
2. At the same time, prepare another mixture as in **step 1** except in the absence of any protein.
3. Incubate the two individual mixtures at 19 °C for 5 min.
4. Denature 10 μL of 2 nM labeled RNA duplex at 95 °C for 2 min to generate substrates for the annealing assays (*see* **Note 15**).
5. Add 1.5 μL of the denatured, labeled RNA into a 28.5 μL mixture prepared in **step 2**.
6. Aliquot 3 μL of the mixture from **step 5** into 3 μL 2× HRSB for a zero time point (Fig. 1d–e, lane 1). Place on ice.
7. Initiate the annealing reaction by adding 1.5 μL of the denatured RNA into the mixture prepared in **step 1**.
8. Aliquot 3 μL of the reaction mixture into 3 μL 2× HRSB at desired time points and place on ice.
9. Mix 3 μL of 0.1 nM labeled RNA duplex with 3 μL 2× HRSB for dsRNA loading marker (Fig. 1d–e, lane 8) as in **step 7** from Subheading 3.3.1.
10. Follow **steps 9–15** in Subheading 3.3.1 to visualize and quantify the fraction of ssRNA in the annealing assay. The representative gels are shown in (Fig. 1d–e).
11. Plot the fraction of ssRNA over time and fit the data with integrated form of a bimolecular annealing reaction [22]: Fraction of ssRNA = $1/(1 + \text{RNA concentration at time } 0 \times k_{obs}^{(ann)} \times \text{time})$.

4 Notes

1. RNase I cleaves after all four bases of ssRNA efficiently, whereas, RNase A only cleaves after C and U bases [23, 24].
2. Adding glutathione decreases the pH of the buffer. Check the pH of the buffer again after the glutathione is fully dissolved and adjust the pH with a solution of 10 M NaOH.
3. An A_{260nm}:A_{280nm} ratio of less than 0.5 suggests that there is no significant RNA contamination. This can be further verified by conducting ATPase assays in the absence of RNA.
4. Addition of glucose to the media can reduce basal expression level in the pET system. This is important if the protein is toxic in *E. coli* [24].
5. Elute the MBP-TEV-Dbp2 protein until A_{280nm} reaches 0.3 O.D. Do not exceed this O.D. because Dbp2 will precipitate during TEV cleavage if the concentration exceeds 30 μM.
6. Vigorous rocking during the incubation with TEV protease will cause Dbp2 to precipitate.
7. yra1C expression is induced at 16 °C overnight to promote soluble protein production.
8. Since the binding kinetics between GST and glutathione are relatively slow, it is necessary to allow sufficient time to obtain maximum binding capacity.
9. Denaturing gel-loading dye contains EDTA, which chelates magnesium ions and prevents heat-induced degradation of RNA.
10. Spotting radioactive ink (or sticking phosphorescent label) onto the gel for film orientation prior to gel slicing is highly recommended.
11. Glycogen acts as a carrier to increase the efficiency of nucleic acid precipitation.
12. ^{32}P has a half-life of around 14 days. Furthermore, RNA is subjected to radiolysis over time.
13. The protein concentration should be empirically determined using a Bradford assay for protein stocks.
14. Reaction temperatures may vary for different helicases and need to be determined experimentally.
15. Experimentally verify that the denatured substrate does not spontaneously anneal during the reaction (bottom panel, Fig. 1d–e).

Acknowledgements

We thank members of the Tran lab for constructive criticism and detailed analysis of experimental methods. This work was supported by NIH grant R01GM097332 to E.J.T.

[AU3]

References

1. Linder P, Fuller-Pace FV (2013) Looking back on the birth of DEAD-box RNA helicases. Biochim Biophys Acta 1829:750–755
2. Putnam AA, Jankowsky E (2013) DEAD-box helicases as integrators of RNA, nucleotide and protein binding. Biochim Biophys Acta 1829:884–893
3. Jankowsky E (2011) RNA helicases at work: binding and rearranging. Trends Biochem Sci 36:19–29
4. Jarmoskaite I, Russell R (2011) DEAD-box proteins as RNA helicases and chaperones. Wiley Interdiscip Rev RNA 2:135–152
5. Klostermeier D, Rudolph MG (2009) A novel dimerization motif in the C-terminal domain of the Thermus thermophilus DEAD box helicase Hera confers substantial flexibility. Nucleic Acids Res 37:421–430
6. Tsu CA, Kossen K, Uhlenbeck OC (2001) The Escherichia coli DEAD protein DbpA recognizes a small RNA hairpin in 23S rRNA. RNA 7:702–709
7. Fuller-Pace FV, Nicol SM, Reid AD et al (1993) DbpA: a DEAD box protein specifically activated by 23s rRNA. EMBO J 12:3619–3626
8. Nicol SM, Fuller-Pace FV (1995) The "DEAD box" protein DbpA interacts specifically with the peptidyltransferase center in 23S rRNA. Proc Natl Acad Sci U S A 92:11681–11685
9. Hardin JW, Hu YX, McKay DB (2010) Structure of the RNA binding domain of a DEAD-box helicase bound to its ribosomal RNA target reveals a novel mode of recognition by an RNA recognition motif. J Mol Biol 402:412–427
10. Mohr G, Del Campo M, Mohr S et al (2008) Function of the C-terminal domain of the DEAD-box protein Mss116p analyzed in vivo and in vitro. J Mol Biol 375:1344–1364
11. Mallam AL, Jarmoskaite I, Tijerina P et al (2011) Solution structures of DEAD-box RNA chaperones reveal conformational changes and nucleic acid tethering by a basic tail. Proc Natl Acad Sci U S A 108:12254–12259
12. Bolger TA, Wente SR (2011) Gle1 is a multifunctional DEAD-box protein regulator that modulates Ded1 in translation initiation. J Biol Chem 286:39750–39759
13. Granneman S, Lin C, Champion EA et al (2006) The nucleolar protein Esf2 interacts directly with the DExD/H box RNA helicase, Dbp8, to stimulate ATP hydrolysis. Nucleic Acids Res 34:3189–3199
14. Hilbert M, Kebbel F, Gubaev A et al (2011) eIF4G stimulates the activity of the DEAD box protein eIF4A by a conformational guidance mechanism. Nucleic Acids Res 39:2260–2270
15. Ma WK, Cloutier SC, Tran EJ (2013) The DEAD-box protein Dbp2 functions with the RNA-binding protein Yra1 to promote mRNP assembly. J Mol Biol 425:3824–3838
16. Johnson SA, Cubberley G, Bentley DL (2009) Cotranscriptional recruitment of the mRNA export factor Yra1 by direct interaction with the 3′ end processing factor Pcf11. Mol Cell 33:215–226
17. Yang Q, Del Campo M, Lambowitz AM et al (2007) DEAD-box proteins unwind duplexes by local strand separation. Mol Cell 28: 253–263
18. Chen Y, Potratz JP, Tijerina P et al (2008) DEAD-box proteins can completely separate an RNA duplex using a single ATP. Proc Natl Acad Sci U S A 105:20203–20208
19. Moreira BG, You Y, Behlke MA et al (2005) Effects of fluorescent dyes, quenchers, and dangling ends on DNA duplex stability. Biochem Biophys Res Commun 327:473–484
20. Young C, Karbstein K (2012) Analysis of cofactor effects on RNA helicases. Methods Enzymol 511:213–237
21. Portman DS, O'Connor JP, Dreyfuss G (1997) YRA1, an essential Saccharomyces cerevisiae gene, encodes a novel nuclear protein with RNA annealing activity. RNA 3:527–537
22. Yang Q, Jankowsky E (2005) ATP- and ADP-dependent modulation of RNA unwinding and strand annealing activities by the DEAD-box protein DED1. Biochemistry 44:13591–13601
23. Spahr PF, Hollingworth BR (1961) Purification and mechanism of action of ribo-

nuclease from Escherichia Coli ribosomes. J Biol Chem 236:823–831

24. Grossman TH, Kawasaki ES, Punreddy SR et al (1998) Spontaneous cAMP-dependent derepression of gene expression in stationary phase plays a role in recombinant expression instability. Gene 209:95–103

25. Jankowsky E, Putnam A (2010) Duplex unwinding with DEAD-box proteins. Methods Mol Biol 587:245–264

Author Queries

Chapter No.: 12 0002226706

Queries	Details Required	Author's Response
AU1	Please check whether the affiliations are appropriate as typeset.	
AU2	Please check whether the edit made to hierarchy of heading levels is appropriate.	
AU3	The reference [25] is duplicate of reference [15]. Therefore it has been deleted and subsequent references and citations are renumbered. Please check.	